FRACTURE TOUGHNESS TESTING AND ITS APPLICATIONS

Published by the
AMERICAN SOCIETY FOR TESTING AND MATERIALS
in cooperation with the
NATIONAL AERONAUTICS AND SPACE ADMINISTRATION

FRACTURE TOUGHNESS TESTING AND ITS APPLICATIONS

A symposium presented at the

SIXTY-SEVENTH ANNUAL MEETING

AMERICAN SOCIETY FOR TESTING AND MATERIALS

Chicago, Ill., June 21–26, 1964

ASTM Special Technical Publication No. 381

Published by the
AMERICAN SOCIETY FOR TESTING AND MATERIALS
1916 Race St., Philadelphia 3, Pa.
in cooperation with the
NATIONAL AERONAUTICS AND SPACE ADMINISTRATION

Library of Congress Catalog Card Number: 65-16811

Printed in Baltimore, Md.
April, 1965
Second Printing, May 1970
Third Printing, January 1975
Fourth Printing, October 1981

FOREWORD

The development of various new high-strength alloys and the broadening range of their applications, particularly in aerospace and in cryogenics, has brought about increased emphasis on the study of fracture characteristics. As a result, the technology of testing for fracture toughness and crack propagation has grown rapidly in recent years. So, too, has understanding of how to apply this testing technology to design problems such as selection of materials, heat treatment, welding procedures, structural shape and size, and effects of environment.

This collection of papers constitutes an authoritative and reasonably complete statement of the current procedure and concepts in the field of fracture mechanics. It should thus be of primary value to those concerned with fracture testing and with applications of test data.

This publication is a cooperative effort of the American Society for Testing and Materials and the National Aeronautics and Space Administration. It helps to fulfill the obligation of the ASTM to provide the technical community with test methods, and with a sound understanding of their usefulness and their limitations. Through its Special Committee on Fracture Testing of High-Strength Materials (now ASTM Committee E-24 on Fracture Testing of Metallic Materials), ASTM has provided important technical leadership. This volume is the latest in a series of valuable publications on fracture testing and its application sponsored by this committee.

By cooperation with the ASTM, NASA is helping to fulfill its obligation to provide for the widest practicable and appropriate dissemination of results from its activities. Not only have aerospace problems directly furthered activity on fracture mechanics, but NASA scientists and engineers have directly contributed much to this new technology. It is the purpose of this publication to make the information in this important field as widely available as possible.

The Symposium on Fracture Toughness Testing and Its Applications was held at the Sixty-seventh ASTM Annual Meeting, in Chicago, Ill., June 21–26, 1964. It was sponsored by the ASTM Special Committee on Fracture Testing of High-Strength Materials. Chairman of the committee is J. R. Low, General Electric Co. Symposium chairman was W. F. Brown, Jr., National Aeronautics and Space Administration.

The symposium comprised three papers sessions and a panel discussion. Co-chairmen of the first session, on basic aspects of fracture mechanics, were T. J. Dolan, University of Illinois, and Harold Liebowitz, Office of Naval Research. Co-chairmen of the second session, on test methods, were Edward Steigerwald, Thompson Ramo Wooldridge, and Z. P. Saperstein, Douglas Aircraft Co. Co-chairmen of the third session, on practical applications, were B. M. Wundt, General Electric Co., and C. M. Carman, U. S. Army Ordnance. Mr. Brown was chairman of the panel discussion, and the other panelists were V. Weiss, S. Yukawa, P. Paris, J. E. Srawley, C. F. Tiffany, G. R. Irwin, T. J. Dolan, J. A. Kies, and W. F. Payne.

CONTENTS

PAGE

Basic Aspects of Fracture Mechanics

Test Methods

Practical Applications

FRACTURE TOUGHNESS TESTING AND ITS APPLICATION

INTRODUCTION

By W. F. Brown, Jr.[1]

The phenomenon of structural failure by catastrophic crack propagation at average stresses well below the yield strength has been known for many years. Rashes of such brittle failures have occurred with increasing frequency as the strength and size of our engineering structures have increased. In the past, each series of failures has given rise to a set of empirical tests and procedures that sometimes provided a solution to the specific problem at hand but did not result in a generally useful approach that would permit avoiding future failures.

Recent military and aerospace requirements for very-high-strength, lightweight hardware have given added importance to the problem of brittle fracture and greatly emphasized the need for a quantitative approach to the general problem of crack tolerance in structures. This need was dramatically highlighted several years ago by the repeated failures of early Polaris rocket motor cases at stresses well below the design value. The ASTM Special Committee on Fracture Testing of High Strength Materials was formed at the request of the Office of the Secretary of Defense to assist in providing a solution to this and related problems.

Over a period of the last five years this committee has been concerned with the question of how to evaluate the strength of metals in the presence of cracks or crack-like defects. The goal has been to provide laboratory tests and analytical techniques which will permit a quantitative measure of crack tolerance useful not only in evaluating materials for a given application but also in development of rational procedure for design against fracture. To achieve this goal requires the development of an essentially new branch of engineering science, and this, of course, is an evolutionary process which will take considerable time to complete. However, with the Irwin linear elastic fracture mechanics as a basis, considerable progess has been made in the desired direction, and today there are available reliable if somewhat overconservative procedures for avoiding failure by fracture in a new structure.

The primary purpose of this symposium was to review the methods for fracture toughness testing as proposed by the ASTM Special Committee on Fracture Testing of High Strength Materials, with a view toward defining their limitations and the extent to which they can be applied in structural design and alloy development. With this in mind the authors were asked to direct attention more toward clarification of concepts and procedures rather than toward presentation of new information. In order to further assist in this review function, the last session of the symposium consisted of a panel discussion

[1] Chairman of the symposium committee, NASA-Lewis Research Center, Cleveland, Ohio.

which gave those concerned with fracture testing an opportunity to put questions to a group of persons who have been active in the work of the ASTM Fracture Testing Committee.

There are, of course, many fracture test methods other than those discussed in this volume. Some of these often provide useful information regarding the fracture behavior of metallic materials. The pre-cracked Charpy impact test is a recent example of such a test which is easy to perform and uses only small specimens. Some efforts have been made to demonstrate a correlation between the results of pre-cracked Charpy tests and fracture toughness tests on larger specimens. A paper by G. M. Orner and C. E. Hartbower on this topic was presented at the symposium meeting, but because of space limitations does not appear in this volume. However, the reader should note that the panel discussion contains a considerable amount of information regarding the use of the pre-cracked Charpy test and references to investigations in this area.

Basic Aspects of Fracture Mechanics

STP381-EB/Apr. 1965

CRITICAL APPRAISAL OF FRACTURE MECHANICS

By V. Weiss[1] and S. Yukawa[2]

Synopsis

A critical review of the basic premises of fracture mechanics is presented. The applicability of the theoretical concepts developed by Griffith and considerably expanded by Irwin and co-workers to materials testing and the determination of a unique and characteristic value of "fracture toughness" is examined. Finally, the usefulness and limitations of sharp crack fracture mechanics to the solution of engineering design problems are discussed.

The present symposium is devoted to an evaluation of fracture testing and its applications. It is devoted to a discussion of the question concerning the condition under which a sharp crack propagates to failure in a cataclysmic fashion, in terms of what is now referred to as sharp crack fracture mechanics or fracture mechanics. It is not a symposium devoted to a discussion of fracture per se, ductile or brittle, but a symposium on the engineering aspects of fracture, fracture testing, and utilization of results from fracture testing in design applications for avoiding fracture.

Sharp crack fracture mechanics originated from a crack-propagation concept proposed some 44 years ago by A. A. Griffith (**1**)[3] which states that an existing crack will propagate in a cataclysmic fashion if the available elastic strain energy release rate exceeds the increase in surface energy of the crack. The reaction to this concept has ranged from complete acceptance to total rejection over the past 44 years. The proponents of the concept have endorsed it primarily because: (1) it yields the correct functional relationship between stress at fracture and flaw size as evidenced by many results on brittle-behaving materials including those obtained originally by Griffith (**2,3**); and (2) because it predicts a theoretical cohesive strength of the defect-free material of the right order of magnitude (0.1 E) which has also been verified approximately on single-crystal whiskers (**4**).

The principal argument against accepting the Griffith concept is the elusiveness of the value for surface tension which figures so dominantly in the concept (**5,6**). Others object to it on experimental grounds, mostly on the basis of data obtained with ductile materials where no appreciable crack-length effect, as predicted by the Griffith concept, was observed (**7**); or on the grounds that in addition to surface energy and elastic strain energy, the possibility of an energy barrier to crack initiation must be admitted. One last

[1] Associate professor of metallurgy, Syracuse University, Syracuse, N. Y.

[2] Manager, Metallurgy, Materials and Processes Laboratory, Large Steam Turbine-Generator Department, General Electric Co., Schenectady, N. Y.

[3] The boldface numbers in parentheses refer to the list of references appended to this paper.

and perhaps most serious objection to the application of the Griffith concept to structural materials may be that it represents an oversimplification (8) of a series of much more complicated phenomena in an age where there is no need to resort to such gross oversimplification, because of the development of science and the availability of computers, etc. Yet, the very simplicity of the fracture-mechanics approach, a one-parameter design concept of great potential, is to a large extent responsible for the recent progress in design against brittle fracture.

To adopt either of these two extreme positions would be unrealistic; to ignore the arguments would be folly. As engineers we must attempt to solve the problems put before us. The wealth of experimental data on sharp crack fracture mechanics in itself attests to serious consideration or acceptance of the proposed analysis by a good portion of the engineering community. The present appraisal should, therefore, be aimed at inspiring the necessary caution in applying the recommended concepts by delineating the limitations of sharp crack fracture mechanics on the basis of the applicability of the fundamental premises utilized. The emphasis has to be placed on the engineering usefulness of the approach rather than on its scientific and philosophical accuracy.

The symposium reflects this orientation towards the use of sharp crack fracture mechanics for the solution of engineering problems. The basic mathematical model, its physical implications, and limitations are discussed in the first section; in the second section, test methods to obtain the "design numbers" suggested by the mathematical model are discussed; the third section is devoted to a discussion of the use of the results of these tests and the mathematical analysis of sharp crack fracture mechanics for the solution of actual design problems. In this fashion, the symposium hopes to show that the engineering approach to the solution of problems—the theoretical (mathematical) model → testing → design-application sequence—is also applicable toward a solution of the problem of designing against fracture. The final section is a panel discussion. In addition to providing an over-all summary, the panel discussion provides for further clarification of the various problem areas, for the establishment of various interdisciplinary connections that have not already been clearly established during the first three sections, and for extended discussion of the current status and urgent research requirements.

This introductory paper has the same, if somewhat more mixed, organization and is, therefore, a broad preview of what is to follow. After a brief historical review of the developments of fracture mechanics since Griffith, the surface-energy – plastic-work analogy and its consequences will be discussed. This will be followed by comments on the aspects of initiation, propagation, and reinitiation of cracks which are intimately related to plasticity and the various plasticity-correction procedures. An attempt will also be made to relate the observed section-size effects to the stress-concentration effects as predicted by fracture mechanics, taking into consideration the influence of inhomogeneities on the mechanical behavior of the material. Finally, an outlook is given on the potential of the fracture-mechanics analysis to fatigue, stress-corrosion cracking, liquid-metal embrittlement, and fracture of nonmetals.

HISTORICAL REVIEW

Our present view of fracture certainly started with the Griffith concept of crack propagation which was presented on February 26, 1920 (1). The now well-known concept essentially states that an existing crack will propagate if thereby the total energy of the system is lowered. The stress analysis used to calculate the stored elastic energy was taken from Inglis's work (9) published in 1913 and was also based on the work of Taylor and Griffith (10) dated 1917. In his paper Griffith states that "the general conclusion may be drawn that the weakness of isotropic solids, as ordinarily met with, is due to the presence of discontinuities, or flaws, as they may be more correctly called, whose ruling dimensions are large compared with molecular distances. The effective strength of technical materials might increase ten or twenty times at least if these flaws can be eliminated." His theory provides a means of estimating the theoretical strength of solids. It also gives, for brittle materials, the correct relationship between fracture strength and defect size. There is no evidence that the advent of dislocation theory in 1934 has influenced fracture research along the lines proposed by Griffith or stimulated the application of Griffith's concept to solids other than glasses. Smekal has published a number of papers (11–17) on the brittle fracture of glasses in which he recognizes the need to consider other material inhomogeneities in addition to the starting cracks. This concern was shared by Weibull who in 1939 published his statistical theory of fracture (18). In 1944, Zener and Hollomon (19) connected the Griffith crack-propagation concept with the brittle fracture of metallic materials for the first time. Orowan referred to X ray work in 1945 (20) which showed extensive plastic deformation on the fracture surfaces of materials which had failed in a "brittle" fashion. In 1948, Irwin (21) pointed out that the Griffith-type energy balance must be between the strain energy stored in the specimen and the surface energy plus the work done in plastic deformation. He also recognized that for relatively ductile materials the work done against surface tension is generally not significant in comparison with the work done against plastic deformation. The same arguments were also stated independently at that time by Orowan (22) who in 1955 demonstrated that the modified Griffith condition for brittle fracture is not only a necessary but also a sufficient condition for crack propagation. In 1955, Irwin indicated (23) and in 1957, showed (24) that the energy approach is equivalent to a stress-intensity approach according to which fracture occurs when a critical stress distribution, characteristic of the material, is reached. In 1959, the ASTM Special Committee on Fracture Testing of High-Strength Metallic Materials was formed to launch a broad assault on fracture, based on the by-then called Griffith-Irwin concept or sharp crack fracture mechanics. The need to design specimens with a most severe artificial flaw and to test these specimens under the most severe condition was recognized and advocated by 1959 (25,26). Subsequently, the demand for plane-strain fracture toughness values was voiced and pop-in reactions were observed (27). Recent work at the Lewis Research Center of NASA with highly sensitive acoustical devices (28) indicates the need to study plane-strain crack extension instability in greater detail.

Plasticity treatments of the stress and strain fields of notches were given by Hill (29), Allen and Southwell (30), Lee (31), and Neuber (32,33). In 1956, Hult and McClintock (34) presented, for the first time, a plasticity analysis of the stress and strain fields of sharp cracks in shear; McClintock subsequently applied this analysis to ductile fracture (35). A nonlinear solution for loading without growth was presented by Neuber in 1961 (33). The conditions for the dynamics of a propagating crack were first formulated by Mott (36) in 1948 and a specific aspect of it was treated later by Yoffe (37). A good review is given by Schardin (38). Dynamic loading problems are now being studied by Krafft et al (39) in relation to strain rate sensitive materials.

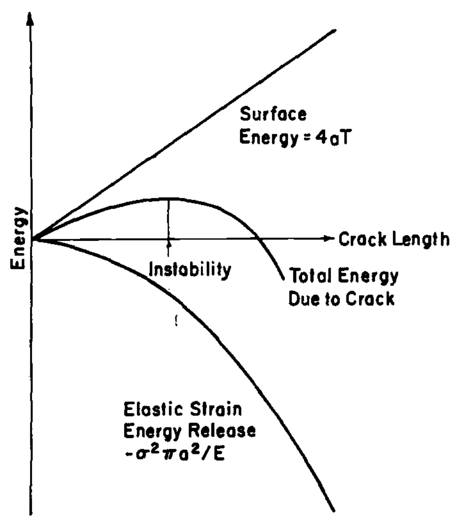

FIG. 1—Energy Balance of Crack in Infinite Plate.

There have been a number of important symposia which devoted major attention to this approach starting with an ASM symposium in 1947 (40), an MIT symposium on fatigue and fracture of metals (41), the First (42) and Second (43) Symposium (1958 and 1960) on Naval Structural Mechanics, the 1959 International Conference on the Atomic Mechanism of Fracture held in Swampscott (44) and, most recently, the 1962 AIME conference held at Maple Valley, Washington (45). The present symposium is perhaps unique in its relation to the symposia mentioned, in that it is the first symposium devoted solely to sharp crack fracture mechanics in relation to engineering and design applications.

THE SURFACE-ENERGY – PLASTIC-WORK ANALOGY

According to Griffith (1) crack growth under plane-stress conditions will occur if

$$\frac{d}{da}\left(-\frac{\sigma^2\pi a^2}{E} + 4aT\right) = 0 \ldots\ldots (1)$$

where the first term inside parentheses represents the elastic energy loss of a plate of unit thickness under a stress, σ, measured far away from the crack, if a crack of length $2a$ were suddenly cut into the plate at right angles to the direction of σ. The second term represents the energy gain of the plate due to the creation of the new surface having a surface tension, T. This is illustrated in Fig. 1 which is a schematic representation of the two energy terms and their sum as a function of crack length. When the elastic energy release due to an increment of crack growth, da, outweighs the demand for surface energy for the same crack growth, the crack will become unstable. One can define a gross fracture stress from this instability condition as

$$\sigma = (2ET/\pi a)^{1/2} \ldots\ldots\ldots\ldots (2)$$

which has, in the form $\sigma\sqrt{a}$ = constant, been shown to hold quite well for brittle and semibrittle metals. However, application of this analysis to such brittle and semibrittle metals has also shown that the data extrapolate, for $2a$ values of atomic dimensions, to T values considerably above most realistic estimates. This, together with experimental X ray evidence of cleavage facets, etc. (20,46), led to the conclusion (2,3) that in the fracture of metals the energy balance is primarily between the elastic energy release and the plastic work in crack propagation, which overshadows the energy requirements for the creation of new surfaces. Since the predicted functional relationship between the stress and the crack length was in good agreement with experimental evidence, it was suggested (2,20) simply to add a plastic-work factor, P, to the surface tension, T, in Eq 2.

The implications of this assumption together with the fact that $\sigma\sqrt{a}$ = constant holds for a great variety of

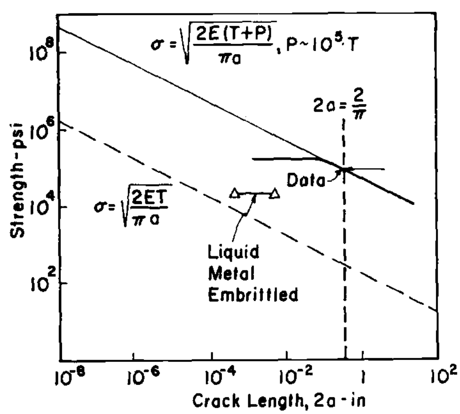

FIG. 2—Schematic Illustration of Observed and Predicted Strength–Crack Length Relationship, the Plastic Work Term, and the Effect of Liquid Metal Embrittlement.

test conditions (plane strain, plane stress, circumferential cracks, etc.) are quite astonishing. If the elastic energy release due to the crack has the form, $A\sigma^m a^n$, then the plastic-work term must have the form, $B\sigma^{m-2}a^{n-1}$. Since theory of elasticity dictates $m = 2$, the plastic-work term must be independent of stress. The elastic strain energy of a cracked plate per unit thickness is proportional to a^2 (that is, $n = 2$) and, therefore, the plastic-work term should be proportional to a. However, one might expect it to depend on the plastic volume per unit thickness which is proportional to a^2.[4] The calculations of Goodier and Field (47), which are based on Dugdale's hypothesis (48), confirm this. Other calculations show at least terms of the type, log a, to be present after differentiation.

The inadequacy of the energy, and in particular surface-energy, approach is further illuminated by a consideration of fracture results obtained under conditions of liquid-metal embrittlement (49), or other environmental effects which affect the crack-fracture strength. At first glance these effects would tend to confirm the predicted influence of surface energy on fracture strength. As a matter of fact, the Griffith-type fracture analysis is unique in this respect as it is the only crack- or notch-fracture analysis of the many proposed which seems to provide an understanding of environmental effects. However, Fig. 2 and Eq 2 clearly show the inapplicability of the type of reasoning whereby the loss in fracture strength in the presence of liquid metals is due to a reduced surface energy. If surface energy alone were responsible for fracture, the fracture toughness, K_c, would be somewhere around $10^{-5}E$ psi × in.$^{1/2}$, where E is Young's modulus. Even quite brittle materials have K_c values near 10^{-3} to 10^{-2} E psi × in.$^{1/2}$. Thus, the plastic-work factor, P, is 10^4 to 10^6 times the surface energy and any change in T due to environmental effects, even if T is reduced to zero, would have negligible effect on the fracture strength. The experimental results in this area must, therefore, lead to the conclusion that the influence of the environment, if it affects the fracture strength and the fracture toughness, is on the material's ability to deform plastically rather than on a change in surface energy. This may indeed be accomplished by such phenomena as slow crack growth (50) or

[4] See also: H. W. Liu, "Fracture Criterion of a Cracked Plate," *GALCIT SM63-29*, July, 1963.

other microscopic diffusion phenomena, which lock dislocations and thus impede plastic flow. Allen (51), however, points out that the surface-energy term may be important during the early stages of crack formation, when it is large compared to the elastic-energy term.

The plasticity question raised above is not yet resolved. It obviously bears on the generality of fracture mechanics and, therefore, merits urgent experimental and theoretical attention. The paper by Irwin and McClintock in this symposium will show another attack on the same question.

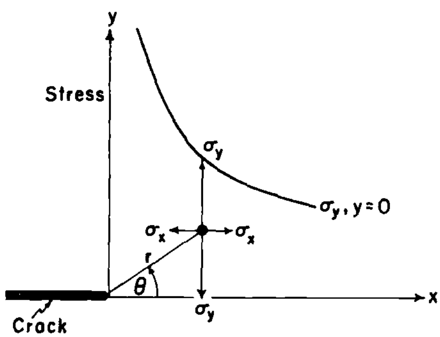

$$\sigma_x = K \frac{\cos \theta/2}{\sqrt{2r\pi}} (1 - \sin \theta/2 \sin 3\theta/2)$$

$$\sigma_y = K \frac{\cos \theta/2}{\sqrt{2r\pi}} (1 + \sin \theta/2 \sin 3\theta/2)$$

$$\tau_{xy} = K \frac{\cos \theta/2}{\sqrt{2r\pi}} \sin \theta/2 \cos 3\theta/2$$

FIG. 3—Schematic Illustration of the Elastic Stress Distribution near the Tip of a Crack.

Linear theory of elasticity provides unique and single-valued relationships among stress, strain, and energy. Therefore, a fracture criterion expressed in terms of an energy concept has its equivalent stress and strain criteria, all of which are mathematically indistinguishable.

While a stress rather than an energy criterion for fracture may not resolve the energy-balance dilemma, it can serve to assert the reasonableness of fracture mechanics by not requiring a statement concerning the use of the released elastic energy. The statement that "fracture occurs when the stress condition in a sufficiently large volume exceeds a critical value" (52–54) may readily be converted into a mathematical model with the help of Westergaard's stress field equations for cracks

$$\left.\begin{aligned} \sigma_x &= \frac{K}{(2\pi r)^{1/2}} \cos \frac{\theta}{2} \left(1 - \sin \frac{\theta}{2} \sin \frac{3\theta}{2}\right) \\ \sigma_y &= \frac{K}{(2\pi r)^{1/2}} \cos \frac{\theta}{2} \left(1 + \sin \frac{\theta}{2} \sin \frac{3\theta}{2}\right) \\ \tau_{xy} &= \frac{K}{(2\pi r)^{1/2}} \cos \frac{\theta}{2} \sin \frac{\theta}{2} \cos \frac{3\theta}{2} \end{aligned}\right\} \ldots (3)$$

which indicate that identical stress fields are obtained for identical K values. The coordinate system is shown in Fig. 3. The stress-intensity factor, K, is a function of applied stress and crack geometry and, for a crack of length $2a$ in an infinite plate, is given by $K = \sigma(\pi a)^{1/2}$. If the critical stress system under which failure occurs is characterized by a stress-intensity factor, K_c, which in itself is a material characteristic (fracture toughness), then a Griffith-type relationship results without consideration of any energy-dissipation processes involved. Primarily because of the straightforwardness of the fracture assumption and the ability to ignore the little-understood surface-energy and plastic-work phenomena accompanying fracture development, the stress-intensity approach is now preferred to the energy approach.

The dilemma is, however, not resolved by choosing the stress-intensity factor approach. Our ignorance concerning the plasticity problem is just as detrimental here as it was in the energy-balance model. An elastic stress distribution, with a singularity at the crack tip, is assumed to describe the stress field ahead of the crack, where plastic yielding has certainly taken place during loading. In either case, the mathematical model chosen to describe the event of fracture fails to describe this event realistically enough and causes some error in the prediction of the event in question. This error is due solely to plasticity phenomena. Thus, if these plasticity phenomena are negligible in relation to the phenomena occurring in the elastically stressed region of the structure, the error will be negligible. As circumstances develop which increase the ratio of volume subjected to plastic flow versus volume under elastic conditions, the error will increase. When it will reach an intolerable level depends on the design or analysis problem; however, because of the nature of the error, it may be safe to assume that it will increase gradually rather than abruptly.

As fracture mechanics provides a method to measure the "brittle" strength of a material, it is necessary to insure that the errors introduced by plastic flow are minor or adequately corrected. This demand is readily met if plasticity effects are negligible, that is, if the plastic-zone size is small in comparison with the crack length as well as the net remaining cross section. In this case, the stress field will be adequately described by linear elasticity theory. A plastic-zone correction factor, r_Y, can be estimated from Eq 3 by setting $\sigma_y = \sigma_{YS}$, the yield strength of the material, which results in

$$r_Y = \frac{1}{2\pi}\left(\frac{K}{\bar{\sigma}_{YS}}\right)^2 \quad \text{..........(4)}$$

At the onset of fracture, where $K = K_c$, one may estimate the error introduced by plastic flow from the ratio $(r_y/a) = (1/2\pi a)(K/\sigma_{YS})^2$ which is equal to $\frac{1}{2}$ $(\sigma_c/\sigma_{YS})^2$, where σ_c is the gross fracture strength. Thus, fracture mechanics represents a good mathematical model as long as the gross fracture stress is small compared to the yield strength of the material. As a refinement to this statement, one must consider that the error will not only depend on the ratio of plastic-zone size to crack length or of fracture strength to yield strength, but also on the load-carrying capacity, that is, the stresses and strains inside the plastic zone (55) which in turn depend on the strain-hardening characteristics of the material (55–58).

A fracture mode change, from plane stress to plane strain, on the other hand, may be accompanied by a more drastic change in plastic-zone size (55,59–61) and a fracture-mechanics analysis may well apply to the severe plane-strain condition but not to the plane-stress condition. Such a mode change can be caused by a change in the test-section geometry. The problem is particularly bothersome because: (1) it is connected with a rather abrupt change in fracture behavior; and (2) there exists no method to predict whether the fracture mode will be plane-stress or plane-strain.

An answer to the second problem may be attempted, based on our knowledge of the stress state of mild notches. There Weiss and Sessler (62–64) have shown that plane-strain conditions prevail at mid-thickness of the notch root if $B/\rho \geq 10$, where B is the specimen thickness and ρ the notch-root radius. Since the plastic-zone size of a sharp crack may be related to the root radius of a mild notch, the ratio of specimen thickness to plastic-zone size may be assumed to determine the fracture state (60). Thus, a condition of plane strain would obtain if $(2B/a)/(\sigma_c/\sigma_{YS})^2 \geq 10$, which again shows the need for small σ_c/σ_{YS} values, since there normally exists a limit on specimen thickness.

The problem is further complicated by the difference in response of different materials to a change in stress state. In most cases, the yield strength increases and the fracture ductility decreases on changing from plane-stress to plane-strain conditions; however, the relative changes vary from material to material. This is illustrated in Fig. 4, where the fracture-toughness value, K_c, is plotted

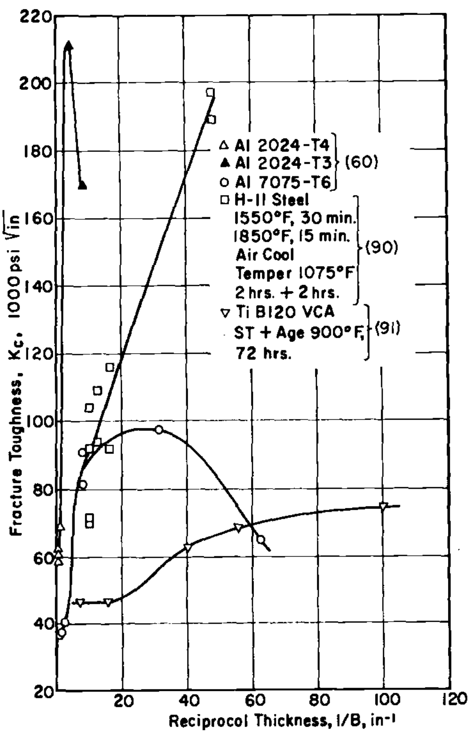

FIG. 4—Variation of Fracture Toughness with Thickness for Various Materials.

as a function of specimen thickness. As the plane-strain case is obviously the most severe, one is tempted to rate materials in accordance with their plane-strain fracture toughness, K_{Ic}. This is readily justifiable for rather similar materials. It may, however, penalize rather ductile materials, where the section sizes required to determine K_{Ic} are much larger than those considered for service.

A comment is in order on the various methods proposed for the determination of plane-strain fracture toughness, K_{Ic}, with specimens which do not necessarily lead to plane-strain fracture. Reference is made to the various pop-in determinations by compliance gauge or acoustical methods (**27,28,65**) of the first onset of crack growth. In order to retain the technical usefulness of sharp crack fracture mechanics, K_{Ic} must be defined in terms of load and crack length for which the first *significant* crack growth occurs. Individual microscopic fractures may and do occur at some lower stress, but little would be gained by ascribing an individual K_{Ic} value to each "ping" representative of the fracture of a microscopic region. Actually, since the engineering materials of concern are complex aggregates of grains, grain boundaries, inclusions, defects, etc., each of which may be highly anisotropic, one must not expect a fracture behavior which was predicted for continuous homogeneous isotropic solids. While the weakest link fracture analogy may hold, a weakest spot analogy certainly does not. For engineering purposes, a K_{Ic} value based on the first "ping" would certainly provide a careful and safe design value. However, since the damage to the structure from the fracture of a low load-bearing inclusion may be negligible, a somewhat higher K_{Ic} value may be more realistic and economical. Long time tests at these low load levels may provide the necessary clues to assess the damage of these early localized fractures.

Although it has been tentatively concluded that plasticity effects will cause gradually developing errors in the sharp crack fracture mechanics analysis, quite abrupt changes in behavior, with perhaps catastrophic consequences in service, are not altogether precluded. The change from plane-stress to plane-strain conditions is a case in point. Temperature, shape, metallurgical effects, and crack-orientation effects may precipitate such an abrupt change.

Thus, the applicability of sharp crack fracture mechanics is basically limited by plasticity phenomena. In a given technical material, fracture mechanics will not be applicable below a certain minimum size (23,26) where the material is essentially "notch- or crack-insensitive." K_c values calculated from tests in this region would be too low. With an increasing ratio of specimen width to plastic-zone size, the fracture-mechanics analysis becomes more and more accurate. For thicker specimens, this may occur earlier due to the smaller plastic-zone size in plane strain. By the same token, a gradual increase in specimen size (including thickness) may also cause an abrupt change from the K_c to the K_{Ic} portion of the curve (see Fig. 5). Once the plane-strain fracture toughness, K_{Ic}, has been suitably established, it should provide an accurate fracture analysis for specimens beyond a limiting size, save for certain material conditions which will be discussed later under "Inhomogeneities, Scatter, and Size Effects."

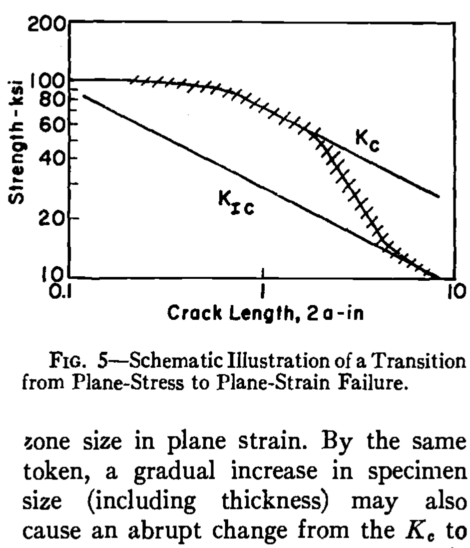

FIG. 5—Schematic Illustration of a Transition from Plane-Stress to Plane-Strain Failure.

INTERPRETATION OF FRACTURE TOUGHNESS

Since the aim of sharp crack fracture testing is to obtain a fracture-toughness value (K_c, K_{Ic} or $\mathcal{G}_c$, $\mathcal{G}_{Ic}$) useful for describing the fracture behavior of a material, it is useful to consider some factors bearing on the interpretation of this quantity.

A pertinent starting point concerns the elastic strain energy input term in the energy-balance picture of the fracture process and particularly, the relationship between the strain energy release rate, $\mathcal{G}$, and the notch- or crack-tip geometry. Experimental measurements of $\mathcal{G}$ have been determined for several specimen geometries via the compliance measurement technique (59, 65,66). These are made using specimens with relatively mild root radii, such as 0.005 or 0.010 in. In nearly all cases where this technique has been used, the functional relationship between $\mathcal{G}$ and crack dimensions obtained agrees very closely with that calculated from a sharp-crack model assuming linear elastic behavior. Thus, experimental evidence indicates that the elastic strain energy release rate is relatively insensitive to tip-root radius in the range from a mathematical "sharp" crack to macroscopic finite root radii.

This is also to be expected on theoretical or analytical grounds. For example, from Griffith's original work on a center-slotted infinite plate model, it can be shown that the release rate decreases by only about two per cent in going from a sharp crack to a root radius equal to one tenth of the crack length (67). The same thing can be seen by examining the stress-intensity factor formulation for fracture mechanics. As noted by Irwin and others, the stress-intensity factor, K, is directly related to the energy-release rate in the fully linear elastic situation:

$$K = (E\mathcal{G})^{1/2} \text{ (for plane stress)} \quad \ldots\ldots (5)$$

Irwin (68) has further noted a relation between K and elastic stress concentration analysis:

$$K = \lim_{\rho \to 0} \tfrac{1}{2} \sigma_m (\pi\rho)^{1/2} \quad \text{.........(6)}$$

where:

σ_m = maximum stress at notch root
ρ = notch-root radius.

In this relationship, K will become insensitive to root radius whenever σ_m is inversely proportional to $\rho^{1/2}$. This is the case when the root radii are small be significantly lower for a fatigue-cracked specimen than for a small but finite root-radius specimen (69). Other data show that above a certain minimum root radius, the apparent K_c increases in proportion to the square root of the radius. This minimum radius is evidently dependent either on material or strength, or both. Values ranging from 0.00025 in. for H-11 steels at high-

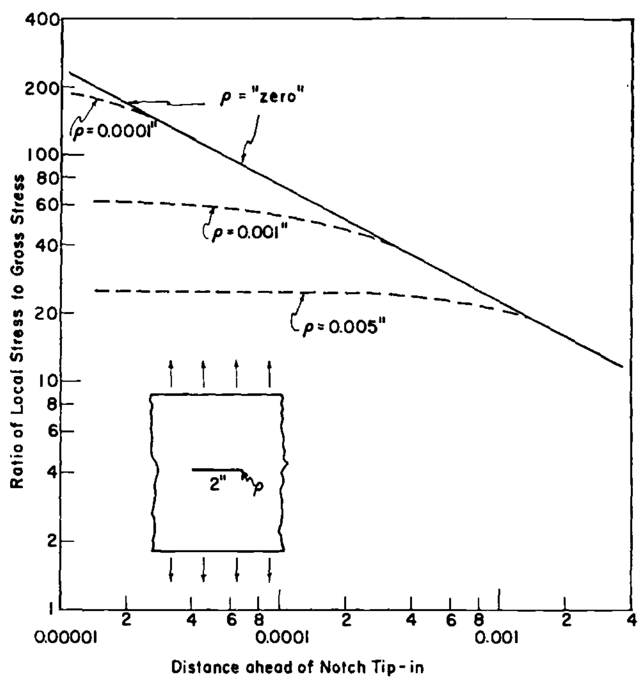

FIG. 6—Comparison of Local Stresses in the Vicinity of the Notch Tip.

compared to the notch depth or the slit length.

If the viewpoint is adopted that unstable fracturing is solely dependent on attaining a critical value of the strain energy release rate, the preceding would indicate that fracture strength and fracture toughness should be relatively insensitive to root radius in the small radius range. However, experimental fracture data show that this is not always the case. Fracture-toughness values can strength levels to 0.010 in. for 7075-T6 aluminum have been observed (70,71). These observations show that, in a finite radius specimen, it is possible to reach and exceed a value of strain energy release rate that is sufficient to satisfy the condition for unstable fracture and yet not have fracture ensue.

It is evident that more than just the attainment of a critical value of $\mathcal{G}$ (or its equivalent as K) is involved in unstable fracture. This forces attention on the small region immediately surrounding the crack or notch tip and it is pertinent to examine how small this region actually is. For example, Fig. 6 shows the distribution under elastic conditions of the longitudinal stress ahead of a crack or elliptical slots of various radii for the classical slotted infinite plate geometry. The distribution for a crack is derived from the stress-intensity factor formulation; the finite radius cases are from Neuber's analysis as recently calculated by Jackson (72). The curves for a finite radius differ from that for a crack only in the region ahead of the tip over a distance approximately equal to one fourth the respective root radius. Beyond this region, the elastic stress distributions for an infinitely sharp crack and a small but finite root radius are virtually identical. The one-fourth factor shown by the curves agrees with Weiss's analytical treatment of this subject (73). For the specimen geometry considered, this means that for a root radius of 0.005 in., the difference in stress distribution compared with a sharp crack occurs only in about the first 0.001 in. of the distance ahead of the tip.

Therefore, one must conclude that whatever happens in this small region ahead of the crack is crucial to the fracture process, especially the plastic deformation which occurs in this nearly microvolume. Furthermore, it may be that the magnitude of the plastic deformation within this region is more important than its spatial extent. It would seem that the spatial extent of plastic deformation should not differ appreciably between a crack and some small but finite radius, such as 0.005 in. However, the magnitude of the strains close to the notch tip would be expected to be quite different.

These considerations indicate that apparently two conditions have to be prescribed to characterize fully the unstable fracturing of metallic materials. One of these pertains to the conditions in a very small localized region near the crack tip which are necessary to initiate unstable fracturing. The other involves conditions more remote from the crack tip which are necessary to sustain unstable crack motion once the initiation condition has been fulfilled. The material, in turn, offers resistance to each of these conditions. The problem in fracture testing is to determine which of these resistances is controlling and being measured in any particular test. For example, if the notch tip is not extremely sharp, it is the initiation resistance which is controlling and consequently being measured.

Ideally, then, in sharp crack fracture testing, it is desirable to perform the test under conditions where the material's resistance to the initiation stage has been reduced as low as possible. From a practical testing and application viewpoint, indications are that this is easier to achieve in relatively higher-strength materials. This may explain the greater success of sharp crack fracture mechanics in higher-strength steels than in lower-strength steels.

With regard to sustaining unstable fracture, it appears that fracture mechanics provides an adequate tool for describing the necessary conditions. It is reasonable to presume that an energy-balance condition must be fulfilled and this is equivalent to having a unique distribution of elastic stresses in regions remote from, but surrounding, the crack tip. Fracture mechanics provides a description of these elastic stresses.

In contrast, the conditions important to the initiation stage are not well understood. Possibly, some limiting state of plastic strain needs to be attained to initiate the process of unstable fracture. With some differences in the assumptions regarding the limiting strain, this is essentially the viewpoint followed by McClintock (35), Krafft (74), and others who have attacked this problem. Whatever the specific details, if the conditions for initiating unstable fracture are to be handled within the present framework of fracture mechanics, an implicit assumption is necessary. The strains within the plastic zone must depend only on the stress-intensity factor and be independent of crack and specimen geometries and loading conditions. This is identical to assuming that the elastic stresses surrounding the plastic zone fully specify the strains within the zone.

The above considerations indicate that fracture toughness as derived from fracture-mechanics tests combines the two aspects of the fracture process into a single value. The successful application of fracture mechanics, then, depends on how closely these two aspects of initiation and sustained propagation are related to each other.

The complexities involved in this distinction between these two aspects of fracture can be seen by considering the effect of plane-stress and plane-strain conditions. As noted in the next section, the plastic zone is smaller under plane-strain conditions than under plane-stress conditions. Presumably, this means that the magnitude of plastic strain is smaller within the plastic zone. However, there is a region ahead of the crack which is outside of the plane-strain zone but which would be within the plastic zone if plane-stress conditions existed. Within this region, the stress normal to the crack (and the actual stress intensity) is higher in the plane-strain situation because it has not been relaxed by plastic flow as in the plane-stress situation. These higher elastic stresses would presumably enhance the initiation of fracture. At the same time, the limiting plastic strain for fracture initiation could be less under plane-strain conditions. The presently unanswered question is which of these predominates in lowering the fracture toughness as plane-strain conditions are approached.

An interpretation of the pop-in phenomenon can be made in relation to the difference in initiating and sustaining the fracture under plane-strain and plane-stress conditions. In the mid-thickness region along the crack front, plane-strain conditions occur and resistance to fracture initiation is relatively low. When this region fractures, the load carried there shifts to regions closer to the side surfaces. These regions, however, are in a state of plane stress and have higher resistance to fracture initiation. Therefore, sustained fracture is arrested after only a small region has fractured and further loading is needed for reinitiation under the changed conditions. It would seem, on this basis, that pop-in is most likely to occur in crack-notched, sheet-type specimens within some restricted range of thickness. On the thicker side of this range, pop-in and unstable fracture propagation tend to become simultaneous events. On the thinner side, it becomes more difficult to develop plane-strain conditions to induce pop-in.

Recognition of the need to determine plane-strain fracture toughness values and to determine the earliest event in the over-all unstable fracturing process has led to several evolutionary modifications in sharp-crack testing. The round notched tension and the embedded surface crack specimens provide two means of attaining plane-strain conditions at the crack-notch front. As discussed above, the pop-in determination is an attempt to measure the fracture event that occurs under plane-strain conditions in a specimen that otherwise is generally under plane stress.

Sharply notched specimens tested in a

Charpy impact machine have been suggested as another procedure for obtaining fracture toughness values by calculating the energy absorbed per unit area. It should be recognized that all the difficulties associated with resistance-to-fracture initiation, with pop-in, and with the transition from plane strain to plane stress are also present in this method. Furthermore, the absorbed energy per unit area will be an integrated value across the fracture area. Thus, it would seem more difficult to distinguish between the separate events, and interpretation of the values obtained requires careful analysis.

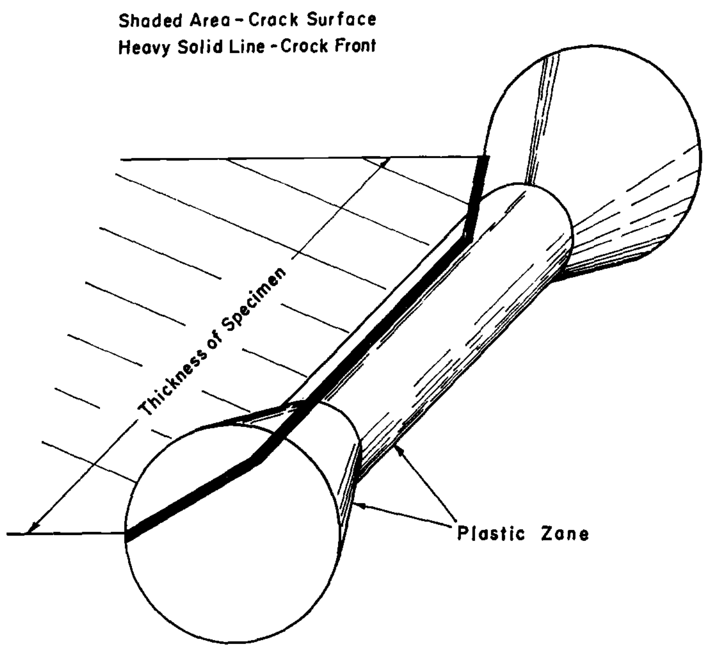

FIG. 7—Three-Dimensional Schematic Diagram of the Crack Surface, the Crack Front and the Plastic Zone.

PLASTICITY ANALYSIS AND EFFECTS

A full understanding of the localized plastic deformations around the crack or notch tip is essential if all aspects of the fracture process are to be understood. Some reasons for this have already been discussed. In addition, procedures for adjusting for plasticity effects are a part of the current treatment of sharp crack fracture testing and the suitability of the procedures needs to be examined. Calculation and experimental verification of localized plastic deformations are exceedingly difficult problems, but it is useful to consider some aspects of the present knowledge.

Most analytical calculations of the early stages of tensile deformation from a sharp notch predict that the deformation should occur in a double lobe-shaped region extending outward from the notch tip. The lobe tends to be constricted in a direction directly ahead of the crack. Observations (for example, Knott and Cottrell (75) and Gerberich (76)) indicate that the deformation zone roughly has this shape. However, Gerberich has also shown that material properties and the extent of deformation strongly influence the shape and orientation of the plastic zone, as well as its size and the strain distribution within it. The zone is more pinched and distended in low strain-hardening materials. These observations indicate one challenging area in which further refinements of plasticity analyses are needed.

It should be noted that other shapes have been postulated for the shape of the plastic zone. Dugdale's model (**48**) for example, assumes a thin zone extending directly ahead of the notch. He notes that this occurs when the slit length is small in relation to the width in a center-slotted plate specimen. This suggests that the plastic deformation behavior near a crack can be influenced by specimen dimensions and boundary condition, and that analysis only in terms of local conditions (as in elasticity analysis) may be inadequate.

A very important question concerns the effect of plane-stress versus plane-strain conditions on the shape and extent of the plastic zone. The details of this question will be covered by others in this symposium. Qualitatively, there is good basis for expecting that the deformation zone will be smaller and more constricted directly ahead of the notch in plane strain than in plane stress. Nearly all experimental studies have been limited to specimen-surface observations where plane-stress conditions exist. Ingenious experimental techniques are needed to provide more information on plane-strain deformation behavior. A related question concerns the abruptness of change in plastic behavior between plane stress and plane strain. Figure 7 shows Liu's (**77**) schematic visualization of this change across the specimen thickness, but virtually nothing is known about the specific details of this problem.

With this background, current usage of plasticity analysis in fracture mechanics can be considered. Based on suggestions originally made by Irwin, the current procedure corrects for crack-tip plasticity by adding an extra increment to the initial crack length. The adjustment is made as follows:

$$a = a_0 + r_Y \qquad (7)$$

where a_0 and a are the initial and the adjusted crack half-lengths and r_Y is as defined by Eq 4.

The net effect of this adjustment procedure is to increase the calculated fracture-toughness value for a given test. Although empirical in nature, the procedure does adjust the fracture-toughness values in the direction of trends observed experimentally. When a series of increasingly larger specimens is tested, the uncorrected fracture-toughness values tend to be low for small specimen sizes and to increase toward an asymptotic value for larger sizes. Based on present concepts of fracture mechanics, the toughness values for large specimen sizes are more truly representative of actual material behavior. For the larger sizes, the plastic-zone size tends to become smaller, both absolutely and relatively, with respect to over-all specimen dimensions. Thus, a procedure which has the effect of increasing the fracture-toughness values to adjust or correct for plasticity effects seems intuitively and empirically proper.

In using this present form of the plasticity-correction procedure, one must recognize its approximate nature and limitations. For example, the procedure is not intended to handle situations where general yielding precedes the fracture. For this reason, the recommended procedures for sharp crack fracture testing include definite limitations on the ratios of fracture stress to yield strength necessary to obtain meaningful values of K_c and K_{Ic} in various specimen configurations (**78**).

It should also be recognized that the

present plasticity correction was not intended to account for the notch-blunting effect which can become a factor with extensive plastic deformation. This refers to the change in the geometrical shape of the crack tip. Based on the earlier discussion of the notch-radius effect, such blunting could have the effect of increasing the resistance to initiation if it were the sole factor considered. However, at this point, significant redistribution of the stresses and strains has occurred and must be taken into account.

In the strictest sense, localized plastic deformation cannot be eliminated in fracture tests of structural alloys of engineering interest. However, there is ample evidence that if plastic deformation is restricted to a region small in comparison with test-specimen dimensions, the present procedures of fracture mechanics are adequately applicable currently, the future extensions of fracture mechanics will be largely determined by the progress made in characterizing the plasticity effects as affected by plane-stress and plane-strain conditions, by the material deformation behavior, and by changes in specimen geometry and loading conditions.

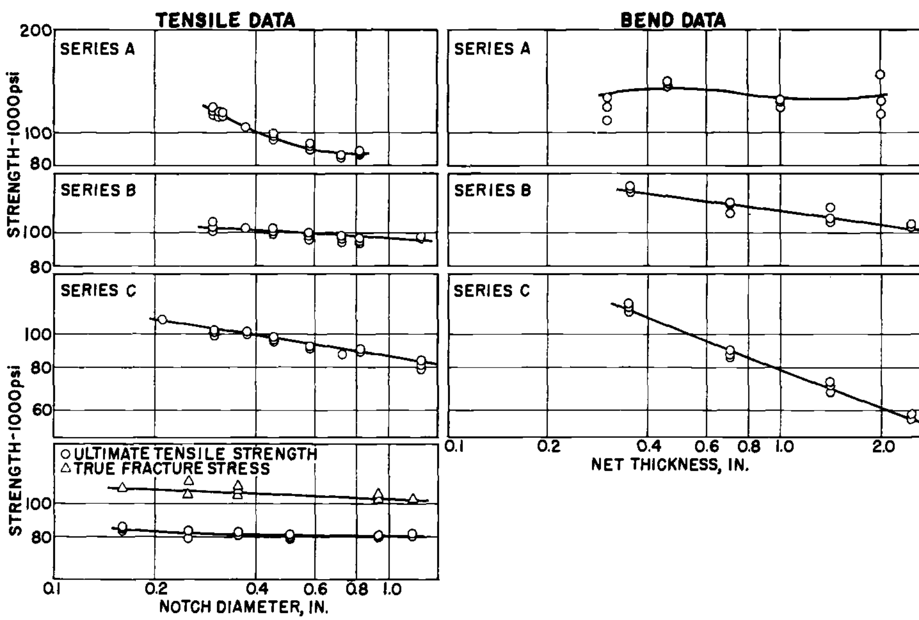

Series A: Constant stress-concentration factor, $K_t = 6$, constant stress gradient, $\rho = 0.004$ in.
Series B: Constant stress-concentration factor, $K_t = 6$, constant percentage of notch depth (50 per cent for tensile data, 30 per cent for bend data)
Series C: Constant root radius, $\rho \leqq 0.001$, constant notch depth (50 per cent, 30 per cent)

FIG. 8—Effect of Section Size on the Tensile, Notch-Tensile, Bend, and Notch-Bend Strength of 7075-T6 Aluminum.

INHOMOGENEITIES, SCATTER, AND SIZE EFFECTS

One of the most important and useful features of fracture mechanics is the prediction of a geometric section-size effect on strength. This prediction "allows" the designer to estimate the fracture strength of a large part on the basis of laboratory tests obtained on small specimens. Such a design concept takes

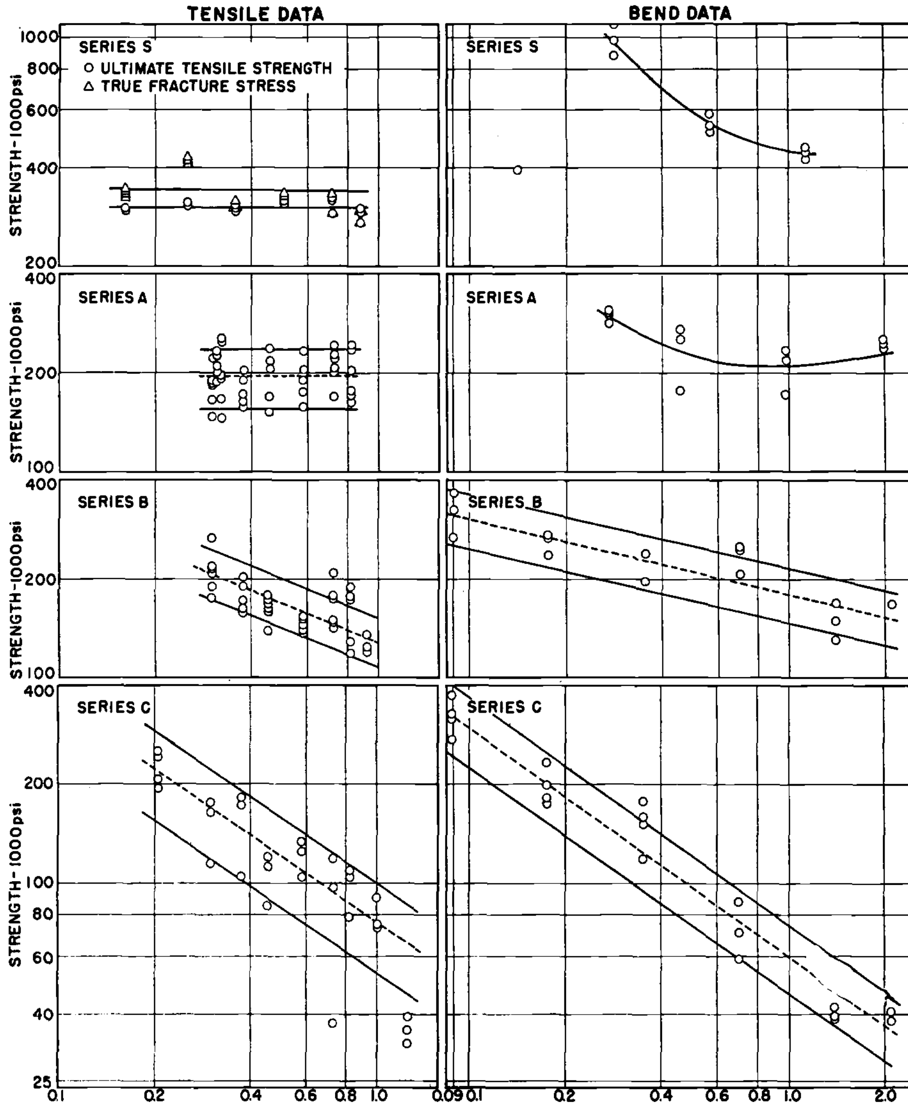

Series S: Smooth specimens
Series A: $K_t = 6$, percentage notch depth = 50 per cent for tensile, 30 per cent for bend
Series C: Constant root radius, $\rho \leqq 0.001$, constant percentage of notch depth, 50 per cent and 30 per cent

FIG. 9—Effect of Section Size on the Tensile, Bend, Notch-Tensile, and Notch-Bend Strength of H-11 Steel.

the form, K_c = constant, or, for the specific case of a finite specimen (width = W) with a center crack (length, $2a$):

$$K_c = \sigma_c[W \tan (\pi a/W)]^{1/2} = \text{constant} \quad \ldots\ldots (8)$$

If the crack length increases in proportion to W, then a/W = constant, and the relationship, $\sigma_c (W)^{1/2}$ = constant, is obtained. Since these considerations are entirely elastic and, therefore, represent the most severe case (namely, totally brittle fracture), one may consider the relationship, K_c = constant, a safe design criterion—as is, indeed, the case for the 7075-T6 aluminum alloy data shown in Fig. 8 (79). In this case, of course, the material is not truly brittle and any inhomogeneities present will be homogenized by plastic flow. In such a material, the tensile strength will be independent of section size, provided that very small samples (wire, etc.) and metallurgical variations are excluded.

Weibull (18) has shown, however, that

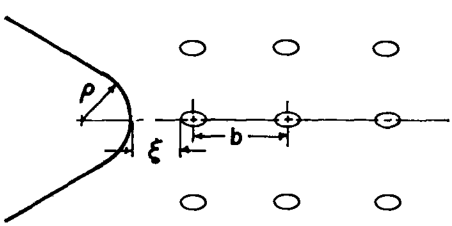

FIG. 10—"Model" of an Inhomogeneous Material Containing Flaws in Uniform Spacing.

a section-size effect exists in inhomogeneous smooth specimens which may be expressed as

$$\sigma_2/\sigma_1 = (V_2/V_1)^{-1/m} \qquad \text{.........(9)}$$

where σ is the fracture strength of a specimen having a test volume, V, and m is Weibull's statistical exponent. Thus, a large size effect is predicted for low m values (inhomogeneous materials), while none is predicted for $m = \infty$ (homogeneous materials). Unfortunately, the physical meaning of m is not clearly established, other than that a high m value indicates many small inhomogeneities and a low m value indicates few larger ones.

From these considerations (which have also been verified for ceramics (73,80)), one may suspect the possibility of a superposition of the statistical size effect, expressed in Eq 9, and the geometrical size effect, predicted by fracture mechanics as K_c = constant, for the case of relatively brittle inhomogeneous materials. This has, indeed, been observed in sharp notch tension and bend tests on H-11 steel, as shown in Fig. 9 for both tension and bend tests on specimens having a notch-root radius, $r \leqq 0.001$ in. The slope of the log σ_N versus log size curve exceeds $-\frac{1}{2}$. The existence of these inhomogeneities is further manifested by the unusual scatter of the test results which is in agreement with Weibull's predictions. However, tension tests on smooth specimens over the same section-size ranges did not show a noticeable size effect.

In order to resolve this question and get a better insight into the physical meaning of Weibull's m value, Weiss and Schaeffer (79) have proposed a simplified model of an inhomogeneous material containing an elliptical hole, as shown in Fig. 10. The inhomogeneities are spaced a distance b apart and are characterized by a stress-concentration factor, K_b. The average net-section strength of such a model is given by:

$$\bar{\sigma}_N = \frac{(1 + 4b/\rho)^{3/2} - 1}{6b/\rho} \times \sigma_{N,\,\min} \qquad \text{..(10)}$$

where ρ is the root radius of the elliptical hole, and $\sigma_{N,\,\min}$ is the minimum net-section strength which is obtained from a model where the stress-intensifying inhomogeneity is located at the root of the flaw. Accordingly, a size effect is predicted for such a material if the test specimens are geometrically similar, that is, having a constant geometrical stress-concentration factor; none is expected in sharp crack specimens since, in them, ρ = constant. Thus, the sharp crack fracture mechanics approach takes care of two dimensions with regard to the volumetric size effect, x and y in Fig. 3

but not of the third, that is, the crack-front length. As the size increases, this length and, therefore, the volume subjected to a critical stress also increase; hence, the chance of finding an inhomogeneity closer to the crack tip or of finding a more severe inhomogeneity (increased K_b or decreased $\sigma_{N,\ \min}$) increases, and thus the strength decreases. The experimental scatter reflects the degree of inhomogeneity and it is evident that it should depend on the volume subjected to a high stress, as is indeed observed on comparing the notch and smooth H-11 data of Fig. 9.

From the model of Fig. 10, one obtains an expression for the net-section strength as a function of the root radius and the distance ξ between notch root and nearest inhomogeneity

$$\sigma_N = \sigma_{N,\ \min}[(\rho + 4\xi)/\rho]^{1/2} \quad \text{.....(11)}$$

which reduces to $\sigma_{N,\ \min}$ as $\rho \rightarrow \infty$, that is, for smooth specimens. It can be shown that the scatter likewise depends only on b/ρ and either vanishes for smooth specimens or reduces to the scatter of $\sigma_{N,\ \min}$.

A direct application of the Weibull analysis as above leads to the following results. If there exists a relationship between m and the standard deviation as Weibull indicates, then the "apparent" value of m is not a material constant but depends on the "critically stressed volume." It will decrease with increasing notch sharpness. Consequently, the statistical size effect according to Eq 9 will also increase with increasing notch sharpness. The importance of these considerations lies in the fact that because of the possibility of superposition of statistical and geometric size effect, the use of the relationship, K_c = constant, may not be conservative for very large cracks in large components. While more research is required in this area to clarify the problem of inhomogeneity effects, especially with respect to the applicability of fracture mechanics to ceramics, a knowledge of the experimental scatter may indicate whether such a problem may develop.

OUTLOOK

There are many aspects of the failure of solids to which the sharp crack fracture mechanics analysis has been successfully applied. Among these are the already mentioned embrittlement by liquid metals (49) and delayed failures such as hydrogen embrittlement and stress-corrosion cracking (81,82). Such analysis has also served to explain failures in nonmetals such as glass, Plexiglas, and ceramics (1,79,83), and in the strength of adhesive joints (84).

A particularly interesting application concerns an analysis of crack propagation under alternating loads. As the stress distribution in the vicinity of a sharp crack is uniquely defined by the stress-intensity factor, K, and the stress at a finite distance from the crack tip is proportional to K, one may expect the crack-growth rate in fatigue to be related to the stress-intensity factor. From dimensional analysis considerations, Liu (85) postulates

$$\frac{da}{dN} \propto K^2 \quad \text{............(12)}$$

while Paris (86) finds better agreement with experimental results for

$$\frac{da}{dN} \propto K^4 \quad \text{............(13)}$$

Other researchers (87,88) obtain different values of the exponent.

While a good fit of a great variety of experimental data is indeed observed with Eq 13 (proposed by Paris), no satisfactory physical model can be postulated for this case. The dimensional model for Eq 12 is quite satisfying and Liu (89) has pointed out that thickness effects may be expected to influence the crack-growth rate and change the exponent.

An estimate of fatigue-crack growth in technical materials following a stress-strain relationship of the type $\sigma = K\epsilon^n$ has been proposed by Weiss and Sessler (92). With the help of Neuber's plasticity analysis for cracks (33) they obtain

$$\frac{da}{dN} \propto a \left(\frac{\sigma}{\sigma^*}\right)^{1+1/n} \quad \ldots\ldots\ldots(14)$$

for stress-controlled fracture or

$$\frac{da}{dN} \propto a \left(\frac{\epsilon}{\epsilon^*}\right)^{n+1} \quad \ldots\ldots\ldots\ldots(15)$$

for strain-controlled fracture. Here σ^* and ϵ^* are the stress or strain values causing fracture, and σ and ϵ are the alternating stresses or strains. The above analysis is in agreement with Liu's (85) formulation of the fatigue-crack growth problem insofar as crack length is concerned; however, it disagrees with the theoretical results of both Paris and Liu insofar as whether the stress or strain amplitude dependence should enter the fatigue-crack growth law under some exponent which is related to the strain-hardening exponent. Insufficient experimental evidence is available to check the validity of these relationships. A more exhaustive plasticity treatment was given by McClintock (93) in 1962. In view of the fact that an incremental fatigue-crack growth is of the order of magnitude of the plastic-zone size, a strict elastic fracture mechanics analysis of the problem may not be as applicable as an analysis which incorporates plasticity effects.

REFERENCES

(1) A. A. Griffith, "The Phenomena of Rupture and Flow in Solids," *Philosophical Transactions*, Royal Soc. (London), Series A., Vol. 221, 1920, pp. 163–198.

(2) G. R. Irwin, "Fracture," *Encyclopedia of Physics*, Springer, Vol. VI, 1958, pp. 551–590.

(3) E. Orowan, "Fracture and Strength of Solids," *Report on Progress in Physics*, Physical Soc. London, Vol. 12, 1949, p. 185.

(4) A. H. Cottrell, "Theoretical Aspects of Fracture," *Fracture*, Technology Press, New York, N. Y., 1959, pp. 20–53.

(5) N. P. Allen, "The Mechanism of the Brittle Fracture of Metals," *Fracture*, Technology Press, New York, N. Y., 1959, pp. 123–146.

(6) A. M. Bueche and J. P. Berry, "The Mechanisms of Polymer Failure," *Fracture*, Technology Press, New York, N. Y., 1959, pp. 265–280.

(7) D. C. Drucker, "A Continuum Approach to the Fracture of Metals," *Fracture of Solids*, AIME Metallurgical Society Conferences, Maple Valley, Washington, D.C., Interscience Publishers, New York, N. Y., Vol. 20, 1962, pp. 3–250.

(8) G. Sachs, discussion to V. Weiss, "Current Views and Theories on Fracture, Crack Initiation and Propagation," *Proceedings*, Seventh Sagamore Ordnance Materials Research Conference, Syracuse University, *MET. E. 661-611/F*, 1960.

(9) C. E. Inglis, "Stresses in a Plate due to the Presence of Cracks and Sharp Corners," *Transactions*, Inst. Naval Architects, Vol. 60, 1913, p. 219.

(10) G. I. Taylor and A. A. Griffith, *Proceedings*, Inst. Mechanical Engrs., 1917, pp. 755–809.

(11) A. Smekal, "The Strength Properties of Brittle Materials," (German) *Ergeb. Exact. Naturwiss*, Vol. 15.

(12) A. Smekal, *Naturwiss*, Vol. 10, 1922, p. 799.

(13) A. Smekal, II International Glass Congress, London, Sheffield, July, 1936.

(14) A. Smekal, "Fracture Theory of Brittle Materials," *Zeitschrift fuer Physik*, Vol. 103, 1936.

(15) A. Smekal, "Cohasion der Festkorper," *Handbuch d. Physc. und Techn. Mechanik*, Vol. 6, No. 2, 1931.

(16) A. Smekal, "Festigkeitsmindernde Struk-

tureigenschaften der Glaser," *Glastechnische Berichte*, Vol. 13, 1935.
(17) A. Smekal, "Ueber die Natur der Mechanischen Festigkeitseigenschaften der Glaser," *Glastechnische Berichte*, Vol. 15, 1937, pp. 259–270.
(18) W. Weibull, "A Statistical Theory of Strength of Metals," *Proceedings*, Royal Swedish Inst. Engr. Research, Vol. 193, 1939, No. 151.
(19) C. Zener and J. H. Hollomon, "Plastic Flow and Rupture of Metals," *Transactions*, Am. Soc. Metals, Vol. 33, 1944, pp. 163–235.
(20) E. Orowan, *Transactions*, Inst. Engrs. Shipbuild., Scotland, 1945, p. 165.
(21) G. R. Irwin, "Fracture Dynamics," *Fracturing of Metals*, Am. Soc. Metals, Cleveland, 1948, pp. 147–166.
(22) E. Orowan, "Energy Criteria of Fracture," *Welding Research Supplement*, Vol. 20, 1955, p. 157s.
(23) G. R. Irwin, "Onset of Fast Crack Propagation in High Strength Steel and Aluminum Alloys," *NRL Report 4763*, *Proceedings*, 1955 Sagamore Conference on Ordnance Materials, Vol. II, Syracuse University Press, Syracuse, N. Y., 1956.
(24) G. R. Irwin, "Analysis of Stresses and Strains near the End of a Crack," *Journal of Applied Mechanics*, Vol. 24, 1957, p. 361.
(25) G. B. Espey, M. H. Jones, and W. F. Brown, Jr., "The Sharp Notch Tensile Strength of Several High Strength Sheet Alloys," *Proceedings*, Am. Soc. Testing Mats., Vol. 59, Part II, 1959.
(26) B. M. Wundt, "A Unified Interpretation of Room-Temperature Strength of Notched Specimens as Influenced by Their Size," Am. Soc. Mechanical Engrs., *Paper No. 59-MET-9*, 1959.
(27) R. W. Boyle, A. M. Sullivan, and J. M. Krafft, "Determination of Plane Strain Fracture Toughness with Sharply Notched Sheets," *Welding Research Supplement*, Vol. 41, 1962, pp. 428s–432s.
(28) M. H. Jones and W. F. Brown, Jr., "Acoustic Detection of Crack Initiation in Sharply Notched Specimens," *Materials Research & Standards*, Vol. 4, No. 3, March 1964, pp. 120–129.
(29) R. Hill, "The Mathematical Theory of Plasticity," *The Oxford Engineering Science* Series, Oxford at the Clarendon Press, London, 1956.
(30) D. N. de G. Allen and R. Southwell, "Plastic Straining in Two-Dimensional Stress-Systems," *Philosophical Transactions*, Royal Soc., Series A, Vol. 242, 1950, pp. 379–414.
(31) E. H. Lee, "Plastic Flow in V-Notched Bar Pulled in Tension," *Journal of Applied Mechanics*, Vol. 19, 1952, p. 331.
(32) H. Neuber, *Kerbspannungslehre*, Springer Verlag, Berlin, 1958.
(33) H. Neuber, "Theory of Stress Concentration for Shear-Strained Prismatical Bodies with Arbitrary Non-Linear Stress Strain Law," *Transactions*, Am. Soc. Mechanical Engrs., Series E, *Journal of Applied Mechanics*, Vol. 28, 1961, pp. 544–550.
(34) J. A. H. Hult and F. A. McClintock, "Elastic-Plastic Stress and Strain Distribution Around Sharp Notches in Repeated Shear," Ninth International Congress of Applied Mechanics, Brussels, 1956.
(35) F. A. McClintock, "Ductile Fracture Instability in Shear," *Journal of Applied Mechanics*, Vol. 25, 1958, pp. 582–588.
(36) N. F. Mott, "Fracture of Metals: Theoretical Considerations," *Engineering*, Vol. 165, 1948, pp. 16–18.
(37) E. H. Yoffe, "The Moving Griffith Crack," *Philosophical Magazine*, Vol. 42, 1951, p. 739.
(38) H. Schardin, "Velocity Effects in Fracture," *Fracture*, Technology Press, New York, N. Y., 1959, pp. 297–330.
(39) J. M. Krafft and A. M. Sullivan, "Effects of Speed and Temperature upon Crack Toughness and Yield Strength in Mild Steel," *Transactions*, Am. Soc. Metals, Vol. 56, 1963, p. 160.
(40) F. Jonassen, W. P. Roop, and R. T. Bayless, editors, *Fracturing of Metals*, Am. Soc. Metals, Cleveland, 1948.
(41) M. M. Murray, *Fatigue and Fracture of Metals*, Symposium held at MIT, June 19–22, 1950, Technology Press and John Wiley & Sons, Inc., New York, N. Y., 1952.
(42) J. N. Goodier and N. J. Hoff, editors, *Structural Mechanics*, Proceedings of First Symposium on Naval Structural Mechanics, Pergamon Press, London and New York, N. Y., 1960.
(43) E. H. Lee and P. S. Symonds, editors, *Plasticity*, Proceedings of Second Symposium on Naval Structural Mechanics, Pergamon Press, London and New York, N. Y., 1960.
(44) B. L. Averback, D. K. Felbeck, G. T. Hahn, and D. A. Thomas, editors, *Fracture*, Proceedings of International Conference on Atomic Mechanisms of Fracture, Swampscott, Massachusetts, Technology Press and John Wiley & Sons, New York, N. Y., 1959.
(45) D. C. Drucker and J. J. Gilman, editors, *Fracture of Solids*, Proceedings of International Conference, Maple Valley, Wash-

ington, August, 1962, AIME Metals Soc. Conference, Vol. 20, Interscience Publishers, New York and London, 1963.

(46) E. P. Klier et al, "The Structure at a Cleavage Surface in Ferrite," *Metals Technology*, Vol. 15, December, 1948.

(47) J. N. Goodier and F. A. Field, "Plastic Energy Dissipation in Crack Propagation," in *Fracture of Solids*, edited by D. C. Drucker and J. J. Gilman, Proceedings of International Conference, Maple Valley, Washington, August, 1962, AIME Metals Soc. Conference, Vol. 20, Interscience Publishers, New York and London, 1963, p. 103.

(48) D. S. Dugdale, "Yielding of Steel Sheets Containing Slits," *Journal of the Mechanics and Physics of Solids*, Vol. 8, 1960, p. 100.

(49) W. Rostoker, J. W. McCaughey, and H. Markus, *Embrittlement by Liquid Metals*, Reinhold Publishing Co., New York, N. Y., 1960.

(50) W. A. Van Der Sluys, "Effects of Repeated Loading and Moisture on the Fracture Toughness of S.A.E. 4340 Steel," NRL Project 62R 19-05 Technical Memorandum, *T and A M Report No. 245*, University of Illinois, May, 1963.

(51) N. P. Allen, "The Mechanism of the Brittle Fracture of Metals," in *Fracture*, edited by B. L. Averback et al, Proceedings of International Conference on Atomic Mechanisms of Fracture, Swampscott, Massachusetts, Technology Press and John Wiley & Sons, Inc., New York, N. Y., 1959, p. 123.

(52) P. Ludwik, *Elements der Technologischen Mechanik*, Berlin, 1909.

(53) G. Sachs, "On the Applicability of Notch Tensile Data to Strength Criteria in Engineering Design," *Transactions*, Am. Soc. Mechanical Engrs., Vol. 79, 1957, p. 111.

(54) J. D. Lubahn, "Correlation of Tests Using the Congruency Principle," *Proceedings*, Am. Soc. Testing Mats., Vol. 58, 1958, p. 678.

(55) H. W. Liu, "Fracture Criterion of Cracked Metallic Plate," *GALCIT SM 63-29*, California Inst. Technology, July, 1963.

(56) J. M. Krafft, "Fracture Toughness of Mild Steel," Note for ASTM Special Committee on Fracture Toughness of High-Strength Metallic Materials, Committee Meeting, Washington, D. C., Dec. 17, 1963.

(57) V. Weiss, J. Sessler, K. Grewal, and R. Chait, "The Effect of Stress Concentration on the Fracture and Deformation Characteristics of Ceramics and Metals," *ASD-TDR-63-380*, April, 1963.

(58) V. Weiss, "Analysis of Crack Propagation in Strain Cycling Fatigue," in *Proceedings*, Tenth Sagamore Army Materials Research Conference, August 13–16, 1963, Syracuse University Press, 1964.

(59) G. R. Irwin, J. A. Kies, and H. L. Smith, "Fracture Strengths Relative to Onset and Arrest of Crack Propagation," *Proceedings*, Am. Soc. Testing Mats., Vol. 58, 1958, p. 640.

(60) G. R. Irwin, "Fracture Mode Transition for a Crack Traversing a Plate," *Transactions*, Am. Soc. Mechanical Engrs., Vol. 82, Series D, 1960, p. 417.

(61) G. R. Irwin, "Plastic Zone Near a Crack and Fracture Toughness," in *Proceedings*, Seventh Sagamore Ordnance Materials Research Conference, August, 1960, Syracuse University Press, *MET.E. 661-611/F.*

(62) V. Weiss and J. G. Sessler, "Analysis of the Effects of Test Temperature on the Notch Strength of High-Strength Sheet Alloys," *Symposium on Evaluation of Metallic Materials in Design for Low Temperature Service, ASTM STP No. 302*, Am. Soc. Testing Mats., 1962, pp. 3–20.

(63) V. Weiss, "Current Views and Theories on Fracture, Crack Initiation and Propagation," in *Proceedings*, Seventh Sagamore Ordnance Materials Research Conference, August, 1960, Syracuse University Press, *MET.E. 661-611/F.*

(64) V. Weiss, J. G. Sessler, and G. Sachs, "Analysis of Brittle Fracture in Sheet Materials," in *Design with Materials That Exhibit Brittle Behavior*, Materials Advisory Board Symposium *MAB-175-M*, Vol. 1, 1961, pp. 87–111.

(65) J. E. Srawley, M. H. Jones, and B. Gross, "Experimental Determination of the Dependence of Crack Extension Force on Crack Length for a Single-Edge-Notch Tension Specimen," unpublished report, NASA Lewis Research Center.

(66) J. D. Lubahn, "Experimental Determination of Energy Release Rates for Notch Bending and Notch Tension," *Proceedings*, Am. Soc. Testing Mats., Vol. 59, 1959, p. 885.

(67) J. P. Berry, "General Theory of Brittle Fracture," *Research Laboratory Report 63-RL-3284C*, General Electric Co., April, 1963.

(68) G. R. Irwin, "Fracture Mechanics in Structural Mechanics," in *Proceedings*, First Symposium on Naval Structural Mechanics, Pergamon Press, London and New York, N. Y., 1960.

(69) S. Yukawa and J. G. McMullin, "Effects of Specimen Size and Notch Acuity on the

Brittle Fracture Strength of a Heat Treated Steel," *Transactions*, Am. Soc. Mechanical Engrs., *Journal of Basic Engineering*, Vol. 83, 1961, p. 451.

(70) Third Report of the Special ASTM Committee, "Fracture Testing of High-Strength Sheet Materials," *Materials Research & Standards*, November, 1961, p. 877.

(71) J. H. Mulherin, D. F. Armiento, and H. Markus, "The Relationship Between Fracture Toughness and Stress Concentration Factors for Several High-Strength Aluminum Alloys," *Preprint 63-WA-306*, Am. Soc. Mechanical Engrs.

(72) L. R. Jackson, "Some Observations on the Distribution of Stress in the Vicinity of a Crack in the Center of a Plate," *DMIC Memo 178*, Battelle Memorial Inst., Columbus, Ohio, September, 1963.

(73) V. Weiss, "Application of Weibull's Statistical Theory of Fracture to Sheet Specimens," *Preprint 62-WA-270*, Am. Soc. Mechanical Engrs.

(74) K. M. Krafft, "Fracture Toughness of Metals," Progress Report, U.S. Naval Research Labs., November, 1964.

(75) J. F. Knott and A. H. Cottrell, "Notch Brittleness in Mild Steel," *Journal of Iron and Steel Institute*, Vol. 201, 1963, p. 249.

(76) W. W. Gerberich, "Plastic Strains and Energy Density in Cracked Plates," *Publication No. U-2238*, Philco-Aeronutronic Division, Newport Beach, Calif., June, 1963.

(77) H. W. Liu, "Qualitative Discussion on the Effects of Strains Within Plastic Enclave on Fracture Criterion," *GALCIT SM 63-32*, Graduate Aeronautical Labs., California Inst. of Technology, September, 1963.

(78) Fifth Report of the Special ASTM Committee, "Progress in Measuring Fracture Toughness and Using Fracture Mechanics," *Materials Research & Standards*, Vol. 4, No. 3, March, 1964, pp. 107–119.

(79) V. Weiss and G. Schaeffer, "Effect of Section Size on Notch Strength," *MET.E. 1078-1064-FR*, Syracuse University, October, 1964.

(80) I. M. Daniel and N. A. Weil, "The Influence of Stress Gradient upon Fracture of Brittle Materials," *Paper No. 63-WA-228*, Am. Soc. Mechanical Engrs., 1963.

(81) E. A. Steigerwals, "Delayed Failure of High-Strength Steels in Aqueous Environments," *Proceedings*, Am. Soc. Testing Mats., Vol. 60, 1960, p. 750.

(82) E. A. Steigerwals and C. J. Guarnieri, "Influence of Surface Oxidation on the Brittle-to-Ductile Transition of Tungsten," *Transactions*, Am. Soc. Metals, Quarterly, Vol. 55, No. 2, 1962.

(83) J. J. Gilman, "Cleavage, Ductility and Tenacity in Crystals," in *Fracture*, edited by B. L. Averback et al, Proceedings of International Conference on Atomic Mechanisms of Fracture, Swampscott, Massachusetts, Technology Press and John Wiley & Sons, Inc., New York, N. Y., 1959.

(84) E. J. Ripling, S. Mostovoy, and R. L. Patrick, "Measuring Fracture Toughness of Adhesive Joints," *Materials Research & Standards*, Vol. 4, No. 3, March, 1964.

(85) H. W. Liu, "Crack Propagation in Thin Metal Sheet Under Repeated Loading," *Transactions*, Am. Soc. Mechanical Engrs., Vol. 83, 1961, pp. 23–31.

(86) P. C. Paris, "The Fracture Mechanics Approach to Fatigue," *Proceedings*, Tenth Sagamore Army Materials Research Conference, August 13–16, 1963, Syracuse University Press, 1964.

(87) W. Weibull, "Theory of Fatigue Crack Propagation in Sheet Specimens," *Acta Metallurgica*, Vol. 11, 1963, pp. 745–752.

(88) A. K. Head, "The Propagation of Fatigue Cracks," *Journal of Applied Mechanics*, Vol. 23, 1956, pp. 407–410.

(89) H. W. Liu, discussion to "The Fracture Mechanics Approach to Fatigue," by P. C. Paris, *Proceedings*, Tenth Sagamore Army Materials Research Conference, August 13–16, 1963, Syracuse University Press, 1964.

(90) J. L. Slinery, Jr., "Notch Properties of Five Per Cent Chromium-Molybdenum-Vanadium Steel Sheet as Affected by Heat-Treatment, Test Temperature and Thickness," *Preprint 72*, Am. Soc. Testing Mats., 1962.

(91) A. J. Repko, M. H. Jones, and W. F. Brown, Jr., "Influence of Sheet Thickness on Sharp-Edge-Notch Properties of a Titanium Alloy at Room and Low Temperatures," *ASTM STP No. 302*, Am. Soc. Testing Mats., 1962, p. 213.

(92) V. Weiss and J. G. Sessler, "Strain Controlled Fatigue in Pressure Vessel Materials," *Paper No. 63-WA-226*, Am. Soc. Mechanical Engrs., 1963.

(93) F. A. McClintock, "On the Plasticity of the Growth of Fatigue Cracks," in *Fracture in Solids*, Proceedings of AIME Metallurgical Society Conferences, Maple Valley, Washington, Interscience Publishers, New York and London, Vol. 20, 1962, pp. 66–102.

DISCUSSION

H. W. Liu[1]—Fracture mechanics encompasses an enormous body of knowledge, which includes fundamental theoies as well as practical experiments. It includes both the macroscopic phenomenological work as well as the microscopic mechanistic investigations. For their excellent appraisal, the authors should be complimented.

In this discussion, it is not intended to provide any new solution to fracture mechanics. It is rather intended to offer additional insight into the theoretical bases and the accepted practices in experimental investigations. With this understanding the direction of future research is clearly indicated.

The concept of fracture toughness, $\mathcal{G}_c$, can be derived from energy balance[2] as well as from the concept of stress and strain environments at the crack tip. The energy approach is well known and further elaboration is not necessary. An attempt will be made to bring forward the understanding of fracture mechanics from the concept of stress and strain environments. As noted in the appraisal, the stress-intensity factor, K, completely specifies the elastic stresses and strains in a region adjacent to the crack tip. It is well known that a plastic zone exists near the crack tip. It is not the elastic stresses and the elastic strains outside the plastic region that cause fracture. Rather, fracture results from the stresses and strains within the plastic zone. The elastic stresses are only a measure or an indicator of the stresses and strains within the plastic zone. The elastic stresses given by Eq 3 are approximate solutions, which are valid only in a region near the crack tip. The solid lines in Fig. 11 show the exact σ_x and σ_y in a cracked infinite plate along x-axis given by Inglis.[3] The dashed line is the approximate solution given by Eq 3. As the distance from the crack tip approaches zero, the approximate solution approaches the exact solution.

If the applied stresses in two specimens are $\bar{\sigma}_1$ and $\bar{\sigma}_2$ and the crack lengths are b_1 and b_2, respectively, and furthermore, for these two specimens, $K_1 = K_2$, according to Eq 3, the elastic stresses in these two specimens are identical. Figure 12 shows the ratio of σ_{y1} to σ_{y2} along the x-axis for different ratios of b_1/b_2. These curves were calculated from Inglis's exact solution. The figure indicates that near the crack tip the stresses are nearly equal to each other for various crack lengths. However, away from the crack tip, the stresses differ considerably even if K's are all the same. Therefore, it can be concluded that regions exist within which the stresses are approximately the same, if K's are the same. Let this region be prescribed by r' as shown in Fig. 13. If the plastic zone, r_p, is very

[1] Associate professor of metallurgy, Syracuse University, Syracuse. N. Y.

[2] A. A. Griffith, "The Phenomena of Rupture and Flow in Solids," *Philosophical Transactions*, Royal Society (London), Series A, Vol. 221, 1921.

G. R. Irwin, "Fracture Mechanics, Structural Mechanics," *Proceedings*, First Symposium on Naval Structural Mechanics, Pergamon Press, 1960.

H. W. Liu, "Fracture Criterion of Cracked Metallic Plate," *GALCIT SM 6329*, Graduate Aeronautical Labs, California Institute of Technology. July, 1963.

[3] E. E. Inglis, "Stresses in a Plate Due to the Presence of Cracks and Sharp Corners," *Transactions*, Institution of Naval Architects (London), Vol. 60, 1913, p. 219.

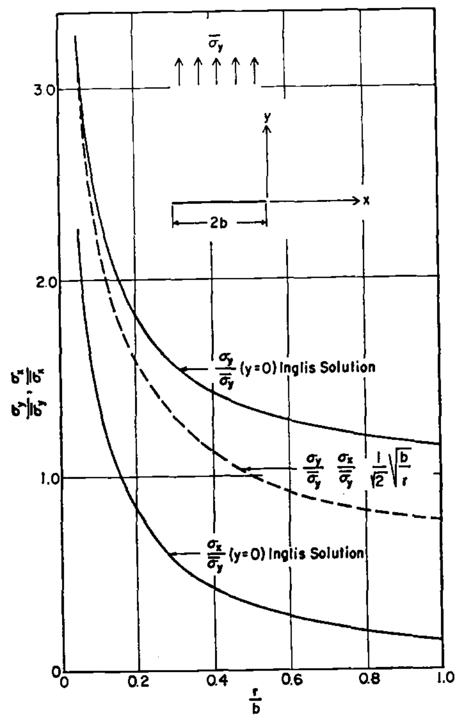

Fig. 11

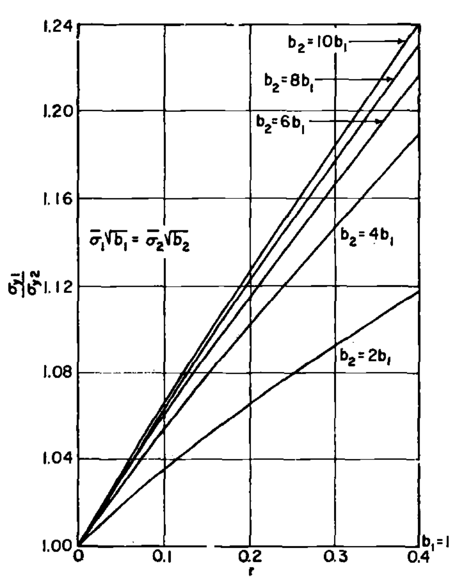

Fig. 12

small, that is, $r_p \ll r'$, the relaxation of stresses within the plastic region from that given by elastic solution will not change the stresses on r' significantly. Look at two regions bounded by r_1' and r_2' in two specimens. For these two specimens, $r_1' = r_2'$ and $K_1 = K_2$. Therefore, if the plastic zones are very small, the stresses on r_1' and r_2' are approximately the same. These two regions, bounded by r_1' and r_2', are geometrically identical and the applied stresses on the boundary are the same. Therefore, the stresses and strains at geometrically similar points, even within the plastic zone, are identical. Consequently, if one specimen fails at a stress and strain environment, so will the other at the same stress and strain environment. Therefore, it can be concluded that K_c for fracture is a constant; and $r_p \ll r'$ is a sufficient condition for a constant K_c. Small r_p implies low fracture stress and brittle mode of fracture.

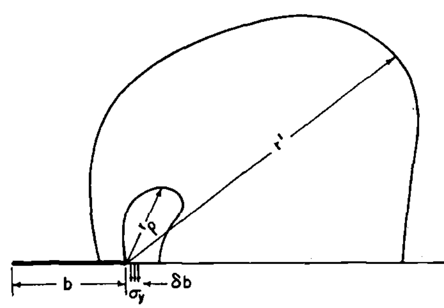

Fig. 13

If r_p is not small in comparison with r', the relaxation of the stresses in the plastic zone will change the stresses on r' significantly, so that the stress field of one crack tip interacts with the stress field of the other crack tip. For different crack lengths, the interaction is different. Therefore, the stresses on r' are no longer characterized by K. Hence K_c is no longer constant.

For a large plastic zone, in order to keep the condition of $r_p \ll r'$, the size of r' has to be enlarged. If r' is enlarged, Eq 3 will no longer give the correct stresses on r'. Figure 12 indicates that, in this case, σ_{y1} along the x-axis within the region r_1' is higher than σ_{y2} within the region r_2'. In order to give the same stress environment within r_1' and r_2', the applied stress on Specimen 2 has to be raised, or vice versa. Consequently, $K_{c1} < K_{c2}$, that is, K_c decreases with crack length. In this case, in order to maintain a constant K_c, an empirical correction factor is needed. This correction factor must be characterized by a small K_c increase for a long crack, and a considerable K_c increase for a short crack. Irwin's plastic-zone correction factor satisfies these requirements. The effective crack length, which is used to calculate K_{c1}, is the sum of the actual crack length plus the plastic-zone size, r_p. The correction factor, r_p, is more or less a constant. Therefore, for long cracks, that is, $2b \gg r_p$, the effect of the correction factor, r_p, is insignificant. On the other hand, for short cracks, the size of r_p relative to b increases; therefore, it increases the value of K_c considerably.

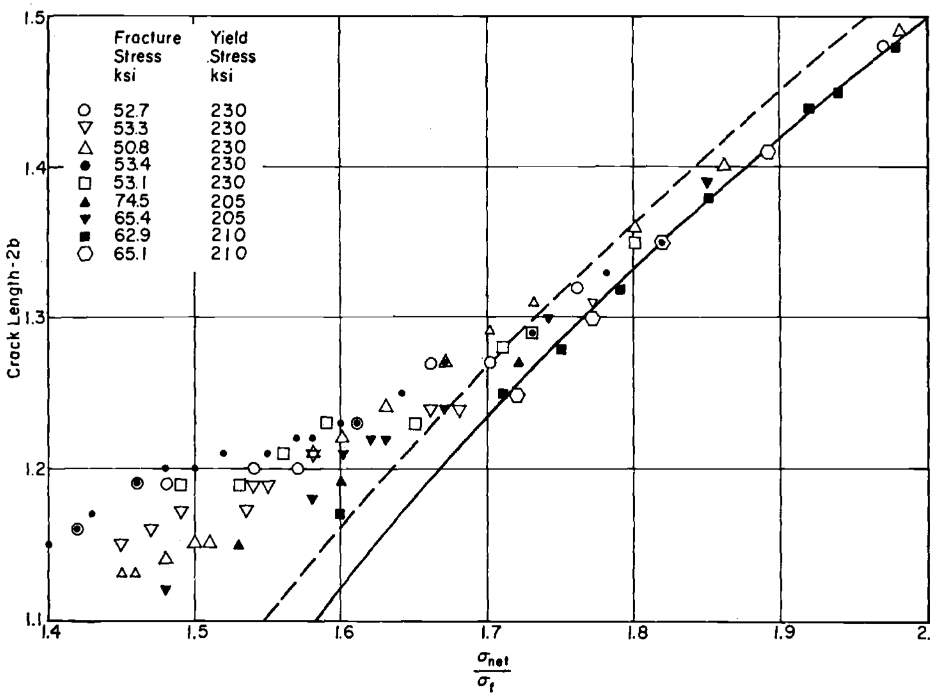

Fig. 14

The crack length is usually determined by either ink stain or visual observation of the "last unstable crack." This peculiar way of determining the crack length is another empirical correction factor. Figure 14 shows slow crack growth of centrally cracked 3-in. wide plates. The original fatigue cracks in the plate are 1 in. long. σ_f is the gross sectional fracture stress. As the load increases, the crack grows slowly. The solid line is the crack-growth line under the constant fracture load. The dashed line is the crack-growth line at 98 per cent of the fracture load. It is obvious that the crack growth at late stage is very unstable. The cracks grow with very little increase in load. For all practical purposes, the crack becomes very unstable at the length of 1.3 in., but the values used in calculating K_c are often 1.5 in or longer, if the last unstable crack length is used.

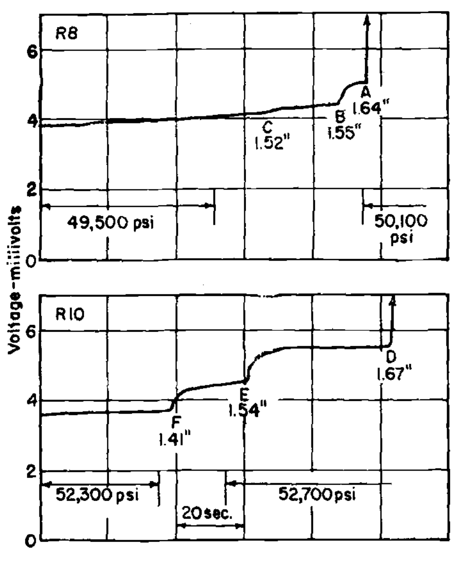

Fig. 15

Figure 15 shows the slow crack growth of the same type of specimens of Fig. 14, as measured by voltage output.[4] Figure 15 also indicates the instability of the crack growth at late stage. The "last unstable crack" is 1.64 and 1.67 in. long in comparison with the original 1-in. fatigue crack. The extra "added length" serves as another correction factor, with the similar characteristics of r_p, in order to give constant K_c.

These corrective measures are needed if the size of the plastic zone is large, that is, for ductile fractures. They are needed because of our meager knowledge with respect to stresses and strains within the plastic zone. It has been noted that the stresses and strains within plastic zones depend upon the plastic behaviors of the materials such as strain-hardening exponent, etc.[5] Therefore it is uncertain that these two corrective measures can take care of both the plastic-zone size effect and the material effect. Consequently, this leads to the conclusion that an understanding of stresses and strains within plastic zones is the next logical step for further advances in fracture mechanics.

This discussion is a portion of Ref (3) and (7), which were written while the author was at the Graduate Aeronautical Laboratories of the California Institute of Technology. The experimental work was conducted at the H. F. Moore Fracture Research Laboratory at the University of Illinois. The assistance extended to the author by these two institutions is gratefully acknowledged.

A. KENT SHOEMAKER.[6]—One of the questions frequently raised in this paper was the effect of the notch-root radius on the crack toughness of a laboratory specimen. Although some work has been reported for high-strength steels

[4] H. W. Liu, "Effect of Water on the Fracture Strength of Specimens with a Central Notch," NRL Project 62R19-05, *Technical Memorandum No. 123*, U. S. Naval Research Labs., August, 1960.

[5] William W. Gerberich, "Plastic Strains and Energy Density in Cracked Plates. I. Experimental Techniques and Results," *GALCIT SM 63-23*, Graduate Aeronautical Labs., California Institute of Technology, June, 1963.

H. W. Liu, "Qualitative Discussion on the Effects of Strains Within Plastic Enclave on Fracture Criterion," *GALCIT SM 63-32*, Graduate Aeronautical Labs., California Institute of Technology, September, 1963.

[6] Department of Theoretical and Applied Mechanics, University of Illinois, Urbana, Ill.

by the ASTM committee reports,[7] there are very few data available for mild or "low-strength" steels which are temperature- and rate-sensitive.[8] The purpose of this discussion is to present some of these data for mild steel.

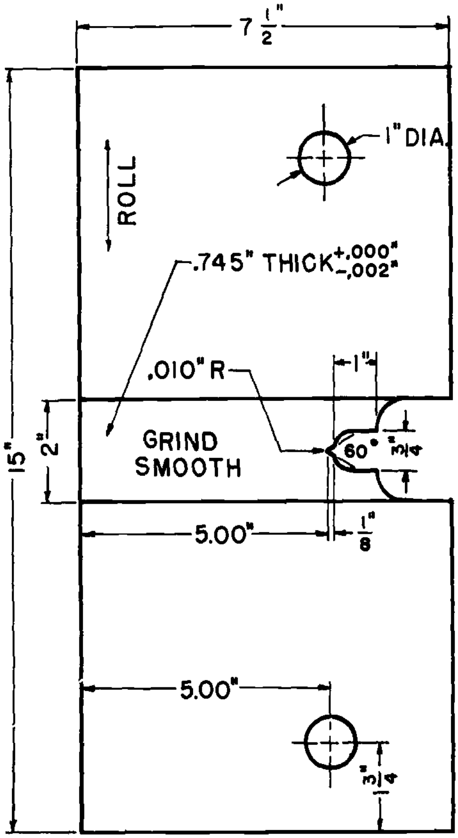

Fig. 16

In previous work, initial crack-extension (K^*_{Ic}) values were measured as a function of straining rate and temperature for $\frac{3}{4}$-in. thick A-201 mild steel[9] using a single-edge-notched specimen shown in Fig. 16. It was thought that the notch radius may have been too large to obtain minimum values of K^*_{Ic}. Subsequent experiments were made on specimens with notch radii varying from 0.0005 to 0.010 in. with essentially constant initial crack lengths and specimen geometry. Since no slow crack growth was observed in mild steel, the maximum load coincided with fracture initiation. These results for three different combinations of temperature and loading rate are shown in Fig. 17 in terms of the fracture load and the square root of the notch radii.

The notch radii of 0.0005, 0.001, 0.002, and 0.003 in. were fabricated by the use of a "string saw." A diamond abrasive compound was spread along the notch base and tungsten wires of the dimensions mentioned above were pulled back and forth across the notch base to make the desired radius. This sawing increased the crack length by an amount equivalent to three to four notch radii. The notch radii are quoted according to the radius of the wire used to cut them. The 0.005 and 0.010-in. radii were machined with a preshaped lathe tool mounted in a horizontal milling machine used in a fly-cutting manner.

The results, as shown in Fig. 17, indicated that at the low temperature, −270 F, the fracture load was approximately independent of the notch radius, while at −175 F the fracture load increased with increasing notch radius. There is enough scatter in the data, however, particularly at the lowest temperature and smallest notch radii,

[7] Fifth Report of the Special ASTM Committee, "Progress in Measuring Fracture Toughness and Using Fracture Mechanics," *Materials Research & Standards*, Vol. 4, No. 3, March, 1964, pp. 107–119.

[8] M. J. Manjoine, "Biaxial Brittle Fracture Tests," ASME *Paper No. 64-Met-3*, Am. Soc. Mechanical Engrs., 1964.

[9] A. K. Shoemaker, "The Influence of Temperature and Strain Rate on Crack Toughness of Mild Steel," *T&AM Report No. 235*, University of Illinois, Urbana, Ill., November, 1962.

to suggest a possible deviation from a straight-line relationship.

The trends can perhaps be explained by previous work[10] where it was found that for temperatures just below the transition range, equivalent to the −175 F data, fracture occurred after large numbers of microcracks had formed in the yielded zone at the crack tip. However, at still lower temperatures, equivalent to the −270 F data, few microcracks were found near the fracture initiation, thus indicating that cleavage fracture occurred from the first microcracks formed. Thus the independence of the fracture load with notch radius at −270 F is perhaps dependent upon a constant plastic-zone size necessary to form a microcrack. This very low-temperature cleavage fracture which initiated from the first formed microcracks would also indicate the possibility of greater data scatter at these temperatures; since the plastically deformed zone of material is very small, there is less probability of a random microcrack starting and growing in this smaller zone compared with a larger zone which occurs at a higher temperature. This is further exemplified by the two specimens which did not fracture at the very low temperature.

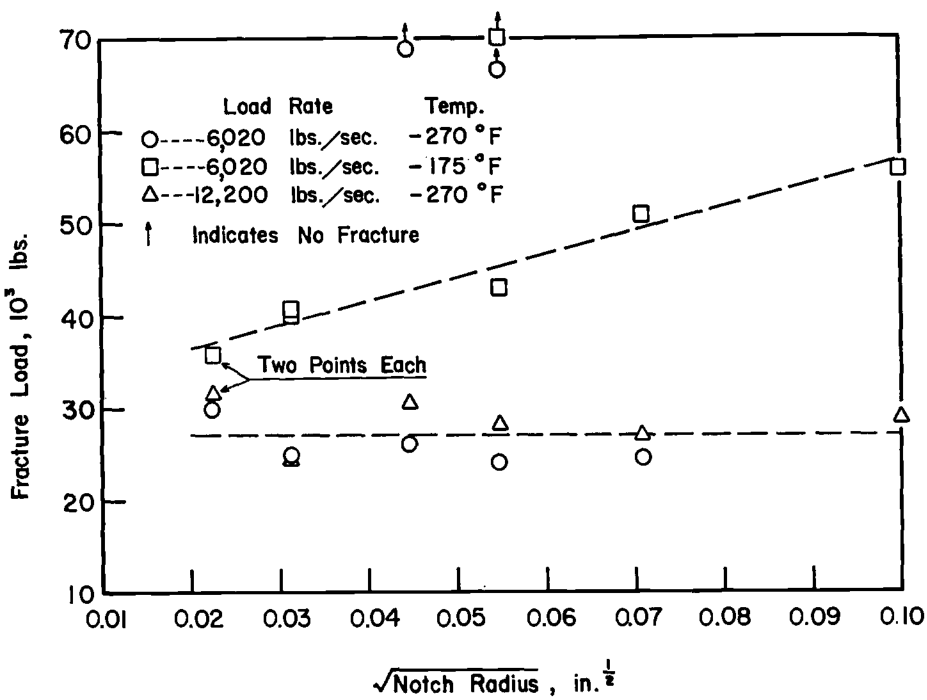

Fig. 17

The specimen which did not fracture at −175 F had not been cut by the string saw in the central section of the notch base. Thus the notch radius at the center section was somewhat in excess of 0.020 in.

[10] G. T. Hahn, W. S. Owen, B. L. Averbach, and M. Cohen, "Micromechanism of Brittle Fracture in a Low-Carbon Steel," *Welding Journal* (Research Supplement), Vol XXIV, No. 9, September, 1959, p. 367-s.

The data presented above are offered only as a preliminary study of the notch-sharpness effect on initial crack extension values for mild steel. The specimen configuration used did not lend itself to the fabrication of a natural crack so these data do not appear in Fig. 17. At the very low temperature, the possibility of a slight increase in fracture load as a natural crack tip is approached could be construed from the data. However, these data as well as the mechanism of fracture which cause them are far from conclusive and warrant further attention. It does appear that even though crack blunting occurs at the higher test temperature, a notch radius of not more than 0.0005 to 0.001 in. is necessary to approach minimum initial crack extension values for mild steel.

V. WEISS AND S. YUKAWA (*authors*).—The authors are grateful for the contributions of Prof. Liu and Mr. Shoemaker which serve to emphasize the importance of a better understanding of plasticity phenomena in the immediate vicinity of a stress raiser such as a notch or a crack. The data of Fig. 14, which show stable slow crack growth with increasing gross-section stress (load) clearly indicate the importance of a better understanding of the crack length–plastic zone size relationship for finite thickness and finite width specimens, and the complexity of the onset of crack instability in semi-brittle materials.

The microcrack explanation of the data in Fig. 17, as well as stress-state considerations, are probably applicable. The latter would suggest a varying stress biaxiality with varying root radius corresponding to the ratio of thickness to root radius. The plastic-zone size ahead of the notch is then determined not only by the value of the root radius but also by the corresponding stress state, that is, it would decrease on going from plane stress to plane strain.

STP381-EB/Apr. 1965

STRESS ANALYSIS OF CRACKS

BY PAUL C. PARIS[1] AND GEORGE C. SIH[1]

SYNOPSIS

A general survey of the results of elastic stress analyses of cracked bodie is the basic objective of this work. The stress-intensity-factor method ofs representing results is stressed and compared with other similar methods. All three modes of crack-surface displacements are considered, as well as specialized results applicable to plate and shell bending. Results for various media (for example, anisotropic, viscoelastic, or nonhomogeneous) are contrasted with the analysis of homogeneous isotropic media. The accuracy of the representation of the crack-tip stress fields by stress-intensity factor methods is discussed, pointing out some limitations of applicability. Methods of estimating and approximate analysis for stress-intensity factors in complicated practical circumstances are also discussed.

The redistribution of stresses in bodies caused by the introduction of a crack is one of the essential features which should be incorporated into an analysis of strength of structures with flaws. Moreover, the high elevation of stresses near the tip of a crack should receive the utmost attention, since it is at that point that additional growth of the crack takes place. As a consequence, it is the purpose of this paper to present a summary of current knowledge of crack-tip stress fields and of the means of determination of the intensity of those fields.

Small amounts of plasticity and other nonlinear effects may be viewed as taking place well within the crack-tip stress field and hence may be neglected in this presentation of the gross features of those fields. It is the subject of other discussions to assess the effects caused by the fields, for example, the plasticity within them and other requirements of formulation of a complete theory of fracture behavior.

In his now famous paper, Griffith (1)[2] made use of the stress solution provided by Inglis (2) for a flat plate under uniform tension with an elliptical hole which could be degenerated into a crack. However, neither Griffith nor his predecessors had the knowledge of stress fields near cracks which is now available, so as a consequence, he devised an energy-rate analysis of equilibrium of cracks in brittle materials. Sneddon (3) was the first to give stress-field expansions for crack tips for two individual examples; however, it was only later that Irwin (4,5) and Williams (6) recognized the general applicability of these field equations and extended them to the most general case for an isotropic elastic body (5). It is this analysis to which initial attention shall be given.

[1] Associate professor of mechanics, Lehigh University, Bethlehem, Pa.

[2] The boldface numbers in parentheses refer to the list of references appended to this paper.

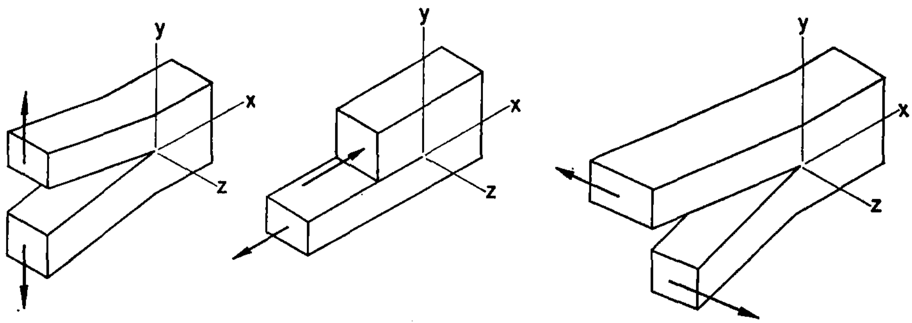

FIG. 1—The Basic Modes of Crack Surface Displacements.

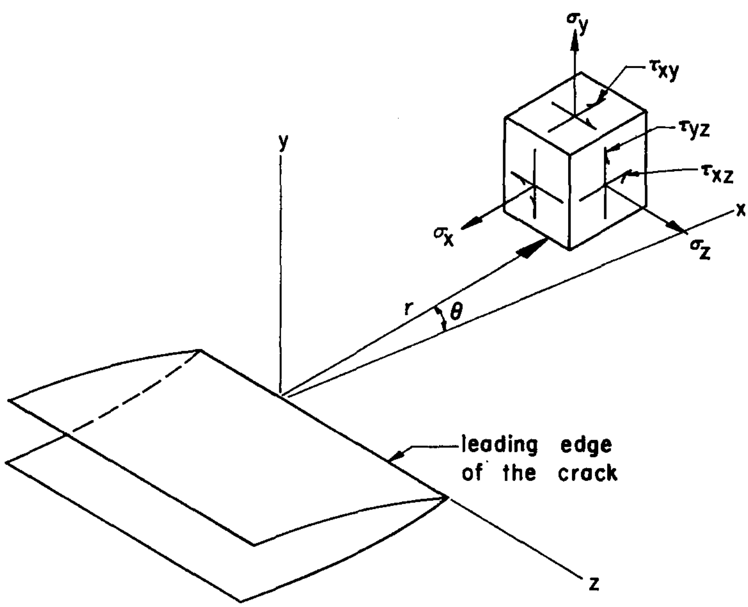

FIG. 2—Coordinates Measured from the Leading Edge of a Crack and the Stress Components in the Crack Tip Stress Field.

CRACK-TIP STRESS FIELDS FOR ISOTROPIC ELASTIC BODIES

The surfaces of a crack, since they are stress-free boundaries of the body near the crack tip, are the dominating influence on the distributions of stresses in that vicinity. Other remote boundaries and loading forces affect only the intensity of the local stress field.

The stress fields near crack tips can be divided into three basic types, each associated with a local mode of deformation as illustrated in Fig. 1. The opening mode, I, is associated with local displacement in which the crack surfaces move directly apart (symmetric with respect to the x-y and x-z planes). The edge-sliding mode, II, is characterized by displacements in which the crack surfaces slide over one another perpendicular to the leading edge of the crack (symmetric with respect to the x-y plane and skew-symmetric with respect to the

x-z plane). Mode III, tearing, finds the crack surfaces sliding with respect to one another parallel to the leading edge (skew-symmetric with respect to the x-y and x-z planes). The superposition of these three modes is sufficient to describe the most general case of crack-tip deformation and stress fields.

The most direct approach to determination of the stress and displacement fields associated with each mode follows in the manner of Irwin (4,7), based on the method of Westergaard (8). Modes I and II can be analyzed as plane-extensional problems of the theory of elasticity which are subdivided as symmetric and skew-symmetric, respectively, with respect to the crack plane. Mode III can be regarded as the pure shear (or torsion) problem. Referring to Fig. 2 for notation, the resulting stress and displacement fields are given below (a full derivation is found in Appendix I).

Mode I:[3]

$$\left.\begin{aligned}
\sigma_x &= \frac{K_{\mathrm{I}}}{(2\pi r)^{1/2}} \cos\frac{\theta}{2}\left[1 - \sin\frac{\theta}{2}\sin\frac{3\theta}{2}\right]\\
\sigma_y &= \frac{K_{\mathrm{I}}}{(2\pi r)^{1/2}} \cos\frac{\theta}{2}\left[1 + \sin\frac{\theta}{2}\sin\frac{3\theta}{2}\right]\\
\tau_{xy} &= \frac{K_{\mathrm{I}}}{(2\pi r)^{1/2}} \sin\frac{\theta}{2}\cos\frac{\theta}{2}\cos\frac{3\theta}{2}\\
\sigma_z &= \nu(\sigma_x + \sigma_y), \qquad \tau_{xz} = \tau_{yz} = 0\\
u &= \frac{K_{\mathrm{I}}}{G}[r/(2\pi)]^{1/2}\cos\frac{\theta}{2}\\
&\qquad\cdot\left[1 - 2\nu + \sin^2\frac{\theta}{2}\right]\\
v &= \frac{K_{\mathrm{I}}}{G}[r/(2\pi)]^{1/2}\sin\frac{\theta}{2}\\
&\qquad\cdot\left[2 - 2\nu - \cos^2\frac{\theta}{2}\right]\\
w &= 0
\end{aligned}\right\}\ldots(1)$$

Mode II:

$$\left.\begin{aligned}
\sigma_x &= -\frac{K_{\mathrm{II}}}{(2\pi r)^{1/2}} \sin\frac{\theta}{2}\left[2 + \cos\frac{\theta}{2}\cos\frac{3\theta}{2}\right]\\
\sigma_y &= \frac{K_{\mathrm{II}}}{(2\pi r)^{1/2}} \sin\frac{\theta}{2}\cos\frac{\theta}{2}\cos\frac{3\theta}{2}\\
\tau_{xy} &= \frac{K_{\mathrm{II}}}{(2\pi r)^{1/2}} \cos\frac{\theta}{2}\left[1 - \sin\frac{\theta}{2}\sin\frac{3\theta}{2}\right]\\
\sigma_z &= \nu(\sigma_x + \sigma_y), \qquad \tau_{xz} = \tau_{yz} = 0\\
u &= \frac{K_{\mathrm{II}}}{G}[r/(2\pi)]^{1/2}\sin\frac{\theta}{2}\\
&\qquad\cdot\left[2 - 2\nu + \cos^2\frac{\theta}{2}\right]\\
v &= \frac{K_{\mathrm{II}}}{G}[r/(2\pi)]^{1/2}\cos\frac{\theta}{2}\\
&\qquad\cdot\left[-1 + 2\nu + \sin^2\frac{\theta}{2}\right]\\
w &= 0
\end{aligned}\right\}\ldots(2$$

Mode III:

$$\left.\begin{aligned}
\tau_{xz} &= -\frac{K_{\mathrm{III}}}{(2\pi r)^{1/2}} \sin\frac{\theta}{2}\\
\tau_{yz} &= \frac{K_{\mathrm{III}}}{(2\pi r)^{1/2}} \cos\frac{\theta}{2}\\
\sigma_x &= \sigma_y = \sigma_z = \tau_{xy} = 0\\
w &= \frac{K_{\mathrm{III}}}{G}[(2r)/\pi]^{1/2}\sin\frac{\theta}{2}\\
u &= v = 0
\end{aligned}\right\}\ldots(3)$$

Equations 1 and 2 have been written for the case of plane strain (that is, $w = 0$) but can be changed to plane stress easily by taking $\sigma_z = 0$ and replacing Poisson's ratio, ν, in the displacements with an appropriate value. Equations 1, 2, and 3 have been obtained by neglecting higher-order terms in r. Hence, they can be regarded as a good approximation in the region where r is small compared to other planar (x-y plane) dimensions of a body such as crack length and exact in the limit as r approaches zero.

[3] See Appendix III for explanation of mathematical symbols.

The parameters, K_I, K_{II}, and K_{III} in the equations are stress-intensity factors[4] for the corresponding three types of stress and displacement fields. It is important to notice that the stress-intensity factors are not dependent on the coordinates, r and θ; hence they control the intensity of the stress fields but not the distribution for each mode. From dimensional considerations of Eqs 1, 2, and 3, it can be observed that

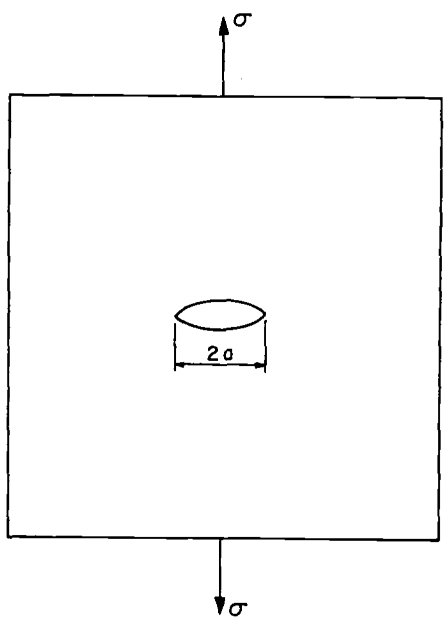

FIG. 3—An Infinite Cracked Sheet with Uniform Normal Stress at Infinity.

the stress-intensity factors must contain the magnitude of loading forces linearly for linear elastic bodies and must also depend upon the configuration of the body including the crack size. Consequently, stress-intensity factors may be physically interpreted as parameters which reflect the redistribution of stress in a body due to the introduction of a crack, and in particular they indicate the type (mode) and magnitude of force transmission through the crack tip region.

[4] These stress-intensity factors differ by a factor of $\pi^{1/2}$ with earlier definitions of them.

ELEMENTARY DIMENSIONAL CONSIDERATIONS FOR DETERMINATION OF STRESS-INTENSITY FACTORS

An infinite plate subjected to uniform tensile stress, σ, into which a transverse crack of length, $2a$, has been introduced, is shown in Fig. 3. As a two-dimensional problem of theory of elasticity, only two characteristic dimensions are present, σ and a. Moreover, this configura-

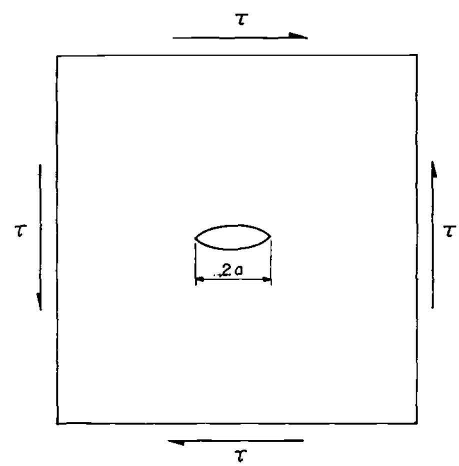

FIG. 4—An Infinite Cracked Sheet with Uniform In-Plane Shear at Infinity.

tion is symmetric with respect to the crack plane; therefore, only the first-mode fields are present. Then, simply from dimensional consideration (9) with Eqs 1, the only possibility is:

$$\left.\begin{aligned} K_I &= C_1\sigma a^{1/2} \\ K_{II} &= K_{III} = 0 \end{aligned}\right\} \qquad (4)$$

Hence, observations of symmetry and dimensional analysis can aid in the determination of stress-intensity factors. Though C_1 is undetermined by such considerations, later results will show it to be $\pi^{1/2}$, (see Eq 17). However, even if C_1 is left undetermined, the fracture-size effect can be predicted for this configuration, since[6] as $K_I \rightarrow K_{Ic}$, then

$$\sigma a^{1/2} = \text{constant} \quad (5)$$

By similar considerations of the plane-extensional problem of a plate under shear, as shown in Fig. 4, the stress-intensity factors are

$$\left.\begin{aligned} K_{II} &= \tau(\pi a)^{1/2} \\ K_I &= K_{III} = 0 \end{aligned}\right\} \quad (6)$$

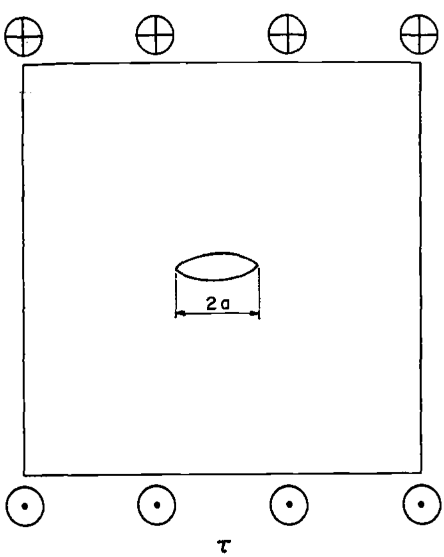

FIG. 5—An Infinite Body with a "Tunnel Crack" Subjected to Out-of-Plane Shear at Infinity.

Moreover, analogous results may be obtained for the problem shown in Fig. 5, that is, an infinity body with shear applied parallel to a tunnel crack of width, $2a$. They are:

$$\left.\begin{aligned} K_{III} &= \tau(\pi a)^{1/2} \\ K_I &= K_{II} = 0 \end{aligned}\right\} \quad (7)$$

Though these are relatively interesting examples, more complicated configurations are of practical importance; consequently, more powerful methods of analysis will be cited.

[6] $K_I \rightarrow K_{Ic}$, as a fracture criterion, is discussed in many other papers in this symposium.

Stress-intensity factors can be determined from the limiting values of elastic stress-concentration factors (7) as the root radius, p, of the notch approaches zero. Consider a symmetrically loaded notch whereupon the tip will be embedded within a mode I stress field. The maximum stress, σ_o will occur directly ahead of the notch. Again, dimensional considerations of Eqs 1 lead to

$$K_I = C_2\sigma_o(p)^{1/2} \quad (8)$$

In the limiting case, the notch approaches a crack, as $p \rightarrow 0$, or

$$K_I = \lim_{p \to 0} \frac{\pi^{1/2}}{2} \sigma_o p^{1/2} \quad (9)$$

The constant has been evaluated from Eq 4 and the stress-concentration solution for an elliptical hole in the configuration shown in Fig. 3, which is:

$$\sigma_o = \sigma[1 + 2(a/p)^{1/2}] \quad (10)$$

A multitude of stress-concentration solutions available in the works of Neuber (10), Peterson (11), Savin (12), Isida (13) and others can be used to determine stress-intensity factors for many configurations. Formulas corresponding to Eq 9 can be as easily derived for modes II and III. They appear in Appendix II.

From the above dimensional considerations, it is evident that the appearance of the $1/r^{1/2}$ type of singularity in the stress-field equations (Eqs 1, 2 and 3) is a controlling feature in fracture-size effects, the relationship of stress concentrations to stress intensity factors, and, as will be noted later, extension of fracture mechanics concepts to other than isotropic, elastic media.

STRESS-INTENSITY FACTORS FROM WESTERGAARD STRESS FUNCTIONS

Several sources (4,5,7,8) give Westergaard stress functions, Z, for crack problems. A discussion of the analysis of plane problems with this type of stress function is given in Appendix I.

For each of the three modes of crack-tip stress fields the Westergaard stress function in the neighborhood of the crack tip takes the form

$$Z = \frac{f(\zeta)}{\zeta^{1/2}}, \qquad \zeta = re^{i\theta} \quad \ldots\ldots\ldots(11)$$

where $f(\zeta)$ must be well behaved in that vicinity in order to ensure stress-free crack surfaces.[6] Hence in the region close to the crack tip, that is, $|\zeta| \to 0$, it is permissible to represent the stress function as (5):

$$Z\big|_{|\zeta|\to 0} = \frac{f(0)}{\zeta^{1/2}} \quad \ldots\ldots\ldots(12)$$

for mode I stress fields (see Appendix I). Comparing σ_y along the x-axis as computed from Eq 12 and as given in Eq 1 leads to:

$$K_{\mathrm{I}} = \lim_{|\zeta|\to 0} (2\pi\zeta)^{1/2} Z_{\mathrm{I}} \quad \ldots\ldots\ldots(13)$$

In a similar fashion for the other modes:

$$K_{\mathrm{II}} = \lim_{|\zeta|\to 0} (2\pi\zeta)^{1/2} Z_{\mathrm{II}} \quad \ldots\ldots\ldots(14)$$

$$K_{\mathrm{III}} = \lim_{|\zeta|\to 0} (2\pi\zeta)^{1/2} Z_{\mathrm{III}} \quad \ldots\ldots\ldots(15)$$

[6] Simple poles away from the crack tip will appear at locations of concentrated forces.

As an example, consider a plate with an infinite periodic array of cracks along a line with uniform tension, σ; the half period is b and the half-crack length, a, as shown in Fig. 6. The stress function for this configuration is (4):

$$Z_{\mathrm{I}} = \frac{\sigma \sin \frac{\pi z}{2b}}{\left[\left(\sin \frac{\pi z}{2b}\right)^2 - \left(\sin \frac{\pi a}{2b}\right)^2\right]^{1/2}} \quad \ldots(16)$$

In order to move the crack tip to the origin, substitute $z = x + iy = a + \zeta$ and trigonometric identities. Eliminating terms of the order of ζ compared to terms of the order of a, the limiting process in Eq 13 leads to:

$$\left.\begin{aligned} K_{\mathrm{I}} &= \sigma(\pi a)^{1/2}\left(\frac{2b}{\pi a} \tan \frac{\pi a}{2b}\right)^{1/2} \\ K_{\mathrm{II}} &= K_{\mathrm{III}} = 0 \end{aligned}\right\} \quad \ldots(17)$$

Referring to Fig. 6, the indicated axes of symmetry are lines devoid of shear stress. Subtracting a uniform normal stress, σ, in the horizontal direction leads to no change in K_{I} and leaves only small self-equilibrating normal stresses, σ_x, along these lines provided a is small compared to b. Consequently, it is regarded as permissible to cut the sheet along these lines and to use Eq 17 as an approximate solution for finite width strips with central cracks pro-

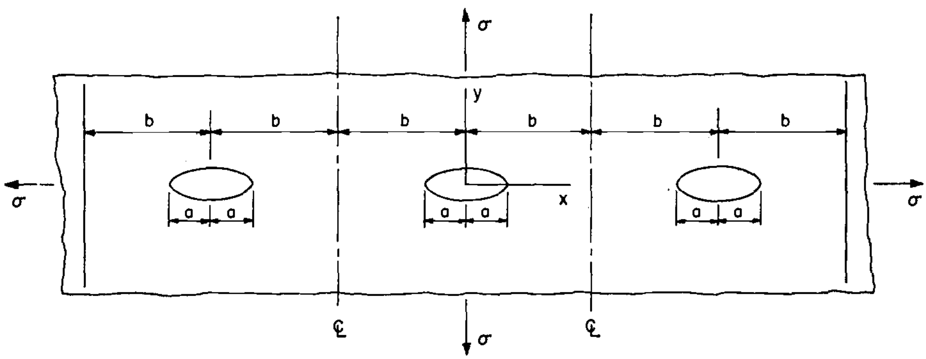

FIG. 6—A Periodic Array of Cracks Along a Line in a Sheet with Uniform Stress at Infinity.

vided a is less than $b/2$. Results computed for strips by Isida (13) and Kobayashi (14,15), which are accurate to much larger relative values of a, indicate that this practice is sound (within 7 per cent) (see Table 1).

Similarly, cutting the problem in Fig. 6 along the y-axis and similar lines leads to an approximate solution, Eq 17, for double-edge-notched strips which is acceptably accurate if a is greater than $b/2$ (within 2 per cent) (see Table 3). Bowie (16) has calculated results for edge-notched strips which verify this accuracy.

The configuration shown in Fig. 6 with the applied stress, σ, replaced by in plane-shear stress, τ, leads to:

$$Z_{II} = \frac{\tau \sin \dfrac{\pi z}{2b}}{\left[\left(\sin \dfrac{\pi z}{2b}\right)^2 - \left(\sin \dfrac{\pi a}{2b}\right)^2\right]^{1/2}} \quad \text{(18)}$$

Making use of Eq 14 results in:

$$\left.\begin{aligned} K_{II} &= \tau(\pi a)^{1/2}\left(\frac{2b}{\pi a}\tan\frac{\pi a}{2b}\right)^{1/2} \\ (K_I &= K_{III} = 0) \end{aligned}\right\} \quad \text{(19)}$$

In a like fashion, all results such as Eqs 16 and 17 for symmetric problems, mode I, are analogous to the corresponding mode II problem Eqs 18 and 19, obtained by rotation of boundary forces or stresses through 90 deg in plane, or both, when treating extension of infinite plates and certain other cases.

Moreover, for the corresponding mode III problem, with the stress, σ, replaced by out-of-plane shear, τ, for a body of infinite extent in all directions, the stress function is identical to Eq 18 and the stress-intensity factor is:

$$\left.\begin{aligned} K_{III} &= \tau(\pi a)^{1/2}\left(\frac{2b}{\pi a}\tan\frac{\pi a}{2b}\right)^{1/2} \\ (K_I &= K_{II} = 0) \end{aligned}\right\} \quad \text{(20)}$$

It can be noted that the above examples of stress-intensity factors from Westergaard stress functions, Eqs 17, 19 and 20, lead to the results in earlier examples, Eqs 4, 6, and 7, if b becomes very large compared to a.

Westergaard stress functions are available for many problems and with some experience it is easy to add solutions, but there are limitations to the scope of the method. The most serious drawback is that the method is normally restricted to infinite plane (two-dimensional) bodies with cracks along a single straight line. Another more versatile approach to plane problems is available.

STRESS-INTENSITY FACTORS FROM GENERAL COMPLEX STRESS FUNCTIONS

A complex stress-function approach developed by Muskhelishvili (17) and others has some advantages over the Westergaard method by treating a broader class of plane extensional problems.

An Airy stress function, Φ, must satisfy the boundary conditions of a problem and the biharmonic equation, that is (see Appendix I),

$$\nabla^4\Phi = 0 \quad \text{(21)}$$

The general solution to Eq 21 may be expressed as (17)

$$\Phi = \operatorname{Re}\left[\bar{z}\phi(z) + \chi(z)\right] \quad \text{(22)}$$

From this form for Φ, the sum of the normal stresses becomes

$$\sigma_x + \sigma_y = 4 \operatorname{Re}\left[\phi'(z)\right] \quad \text{(23)}$$

Defining a complex stress-intensity factor (18) by

$$K = K_I - iK_{II} \quad \text{(24)}$$

Eqs 1, 2, and 24 may be combined to give the same stress combination in the vicinity of a crack tip. The result is

$$\sigma_x + \sigma_y = \operatorname{Re}\left[\frac{\sqrt{2}}{(\pi\zeta)^{1/2}} K\right] \quad \text{(25)}$$

for a crack tip at z_1 and for corresponding coordinate directions, that is,

$$\zeta = z - z_1 \qquad (26)$$

Substitution of Eq 26 into Eq 25 and comparison of the result with Eq 23 lead to

$$K = K_{\mathrm{I}} - iK_{\mathrm{II}} = 2(2\pi)^{1/2} \lim_{z \to z_1} \cdot (z - z_1)^{1/2} \phi'(z) \qquad (27)$$

The function, $\phi(z)$, has been determined for a large number of crack problems (12,17–20), since with this technique conformal mapping of holes into cracks is permitted.

For a mapping function, $z = w(\eta)$, Eq 27 becomes

$$K = 2\sqrt{2\pi} \lim_{\eta \to \eta_1} (w(\eta) - w(\eta_1))^{1/2} \frac{\phi'(\eta)}{w'(\eta)} \qquad (28)$$

The mapping of a crack of length, $2a$, into a circular hole of unit radius is given by

$$z = w(\eta) = \frac{a}{2}\left(\eta + \frac{1}{\eta}\right) \qquad (29)$$

For this mapping, Eq 28 simplifies to

$$K = 2(\pi/a)^{1/2}\phi'(1) \qquad (30)$$

The example of a single concentrated force, F (per unit thickness), on a crack surface with arbitrary inclination, as shown in Fig. 7, is solved by (17,18):

$$\phi(\eta) = \frac{Fa}{4\pi(a^2 - b^2)^{1/2}} \left\{ -\frac{1}{\eta} + \left(\frac{\eta_o}{\eta_o - \eta}\right) \cdot \left[\left(\eta + \frac{1}{\eta}\right) - \left(\eta_o + \frac{1}{\eta_o}\right)\right] + \left(\eta_o - \frac{1}{\eta_o}\right) \cdot \left[\frac{\kappa}{1+\kappa} \log \eta - \log(\eta_o - \eta)\right] \right\} \qquad (31)$$

where η_o corresponds to $z = b$, $F = P - iQ$, and κ is an elastic constant, which for plane strain is $\kappa = 3.4\nu$.

Using Eq 30 with Eq 31, the stress-intensity factors are:

$$\left.\begin{aligned} K_{\mathrm{I}} &= \frac{P}{2(\pi a)^{1/2}}\left(\frac{a+b}{a-b}\right)^{1/2} + \frac{Q}{2(\pi a)^{1/2}}\left(\frac{\kappa - 1}{\kappa + 1}\right) \\ K_{\mathrm{II}} &= \frac{-P}{2(\pi a)^{1/2}}\left(\frac{\kappa - 1}{\kappa + 1}\right) + \frac{Q}{2(\pi a)^{1/2}}\left(\frac{a+b}{a-b}\right)^{1/2} \end{aligned}\right\} \qquad (32)$$

The concentrated force results, Eqs 32, provide the Green's functions to

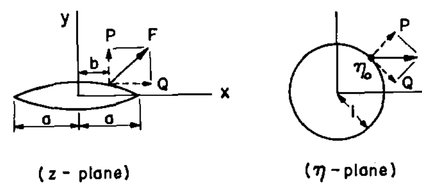

FIG. 7—A Concentrated Force (Per Unit Thickness) on the Surface of a Crack in an Infinite Sheet.

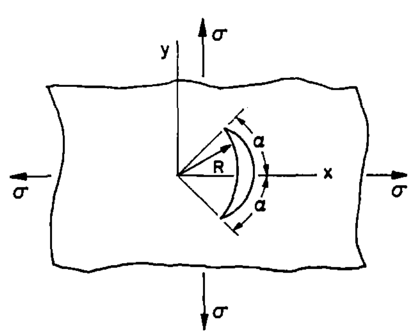

FIG. 8—A Curved Crack in an Infinite Sheet Subjected to Uniform Biaxial Tension.

solve any single straight-crack problem in an infinite plane from a knowledge of the stresses on the prospective crack surface with the crack absent, that is, $\sigma_y(x,0)$ and $\tau_{xy}(x,0)$. The solution is

$$\left.\begin{aligned} K_{\mathrm{I}} &= \frac{1}{(\pi a)^{1/2}} \int_{-a}^{a} \sigma_y(x,0)\left(\frac{a+x}{a-x}\right)^{1/2} dx \\ K_{\mathrm{II}} &= \frac{1}{(\pi a)^{1/2}} \int_{-a}^{a} \tau_{xy}(x,0)\left(\frac{a+x}{a-x}\right)^{1/2} dx \end{aligned}\right\} \qquad (33)$$

In order further to illustrate the versatility of the complex stress-function method, the problem of a crack of radius R, subtending an arc of angle, 2α, symmetrically with respect to the x-axis in an infinite sheet subjected to uniform biaxial tension may be treated, see Fig. 8. For this case, Muskhelishvili (17) gives

$$\phi'(z) = \frac{\sigma(R)^{1/2}}{2\left(1+\sin^2\frac{\alpha}{2}\right)} \cdot \left\{\frac{\frac{z}{R}-\cos\alpha}{\left[1-2\frac{z}{R}\cos\alpha+\frac{z^2}{R^2}\right]^{1/2}}+\sin^2\frac{\alpha}{2}\right\} \quad ..(34)$$

Relocation of a crack tip on the x-axis, as required by Eq 27, may be accomplished by the substitution:

$$\frac{\hat{z}}{R} = ie^{i\alpha}\left(\frac{z}{R}-i-\sin\alpha\cos\alpha\right) \quad ..(35)$$

whereupon Eqs 27, 34, and 35 give

$$\left.\begin{aligned} K_{\mathrm{I}} &= \frac{\sigma(\pi R)^{1/2}}{\left(1+\sin^2\frac{\alpha}{2}\right)} \cdot \left(\frac{\sin\alpha\,(1+\cos\alpha)}{2}\right)^{1/2} \\ K_{\mathrm{II}} &= \frac{\sigma(\pi R)^{1/2}}{\left(1+\sin^2\frac{\alpha}{2}\right)} \cdot \left(\frac{\sin\alpha\,(1-\cos\alpha)}{2}\right)^{1/2} \end{aligned}\right\} \quad ..(36)$$

Other notable examples of stress-intensity factors for rather complicated cases of plane extension have been provided (18,21–23), using this and similar methods. The power of this method for plane extension has been sufficiently illustrated, consequently, additional examples will be removed to Appendix II.

A similar complex-variable approach has been developed to determine stress-intensity factors in prismatic bars (with prismatic cracks) subjected to torsion and flexure (24–26). This type of configuration leads to mode III stress-intensity factors, some of which will also be tabulated in Appendix II.

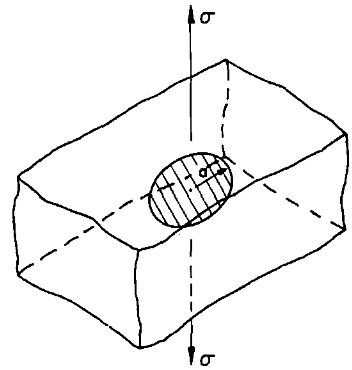

FIG. 9—A "Penny-Shaped" (Circular Disk) Crack in an Infinite Body Subjected to Uniform Tension.

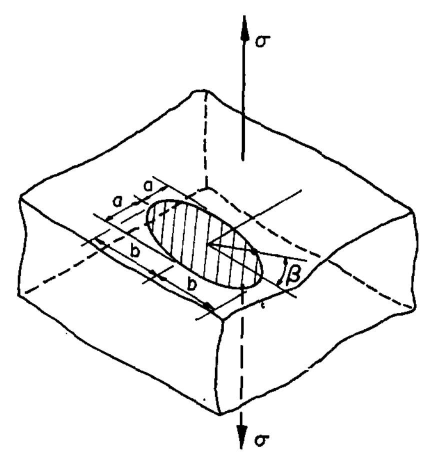

FIG. 10—An Elliptical Crack in an Infinite Body Subjected to Uniform Tension.

STRESS-INTENSITY FACTORS FOR SOME THREE-DIMENSIONAL CASES

Using a method employing Fourier transforms, Sneddon (3) treated the case of a circular disk crack of radius, a, in an infinite solid subjected to uniform tension, σ, normal to the crack plane, see Fig. 9. His results for crack-tip stress field expansions lead to:

$$K_{\mathrm{I}} = \frac{2}{(\pi)^{1/2}}\,\sigma(a)^{1/2} \quad \text{(37)}$$

(by symmetry $K_{\mathrm{II}} = K_{\mathrm{III}} = 0$)

The analysis of stresses near ellipsoidal cavities in infinite bodies subjected to tension has been discussed by Sadowsky (27) and Green (28). However, difficulties arise in the stresses computed from their results near the crack edge when the ellipsoid is degenerated into a crack, see Fig. 10. Subsequently, Irwin (29) calculated the stress-intensity factor at any location on the crack border, described by the angle, β, by comparing Green's results for displacements with Eq 1. The formulas obtained are:

$$K_{\mathrm{I}} = \frac{\sigma(\pi a)^{1/2}}{\Phi_o}\left(\sin^2\beta + \frac{a^2}{b^2}\cos^2\beta\right)^{1/4} \quad \text{(38)}$$

(by symmetry $K_{\mathrm{II}} = K_{\mathrm{III}} = 0$)

where Φ_o is the elliptic integral[7]

$$\Phi_o = \int_0^{\pi/2}\left[1 - \left(\frac{b^2 - a^2}{b^2}\right)\sin^2\theta\right]^{1/2} d\theta \quad \text{(39)}$$

Notice that for $b = \infty$, $\beta = \pi/2$, Eqs 38 and 39 reduce to Eq 4 or, for $b = a$, to Eq 37, with corresponding changes from Fig. 10 to Fig. 3 or Fig. 9.

Though the above results for three-dimensional problems are of extreme practical interest, the mathematical difficulty in attempting other such solutions is so great that a discussion of the possible methods would be of little interest. However, in practical application of results it must be kept in mind that all bodies are really three-dimensional and often the cracks which must be analyzed do not suit the idealized results exactly as presented here. Nevertheless, the results which are presented form the basis for sensible judgments from which three-dimensional effects may be assessed.

Moreover, as a prime example of the fact that three-dimensional effects are always present and yet may most often be justifiably neglected, consider sheet of finite thickness with a through-crack. If the sheet were infinitely thick, plane strain would apply; or, if infinitely thin, then plane stress would apply. But with finite thickness, a mixed situation of plane stress near the surfaces of the plate and plane strain in the interior occurs in the crack-tip stress field. Consequently, the stress-intensity factors computed for plane problems represent only their values averaged through the thickness. Therefore, considering that plane-stress versus plane-strain displacement fields differ by a factor of $(1 - \nu^2)$, the actual values of stress-intensity factors for a straight-through-crack can vary by $(1 - \nu^2)^{1/2}$ (or less) from the surface to the interior. The values at the surface are a maximum of 5 per cent less than computed values and, correspondingly, a maximum of 3 per cent more in the interior (for $\nu = 0.3$). Though crack-tip plasticity further complicates the situation, it is partially for this reason that the crack often begins to grow in the interior of a plate rather than at the surface to form a "tongue." Even though this effect is frequently observed, ignoring it leads to a desirable level of accuracy of computed values of stress-intensity factors in developing fracture criteria.[8]

EDGE CRACKS IN SEMI-INFINITE BODIES

The plane-extensional problem of an edge notch, a, into a semi-infinite plane subjected to tension, σ, has been discussed by several authors (30–32,16)

[7] Values of elliptic integrals are to be found in many mathematical tables.

[8] So-called pop-in tests actually make direct use of this effect.

(see Fig. 11). With dimensional analysis leading again to Eqs 4, with C_1 left unknown, the task is merely to evaluate that constant. However, formidable methods must be employed to obtain the effect of the free surface of the half-plane. These methods use series-type mapping functions with the complex variable stress-function method (16,30) and dual integral equations resulting from a Green's function approach (31,32) or both. The results may be

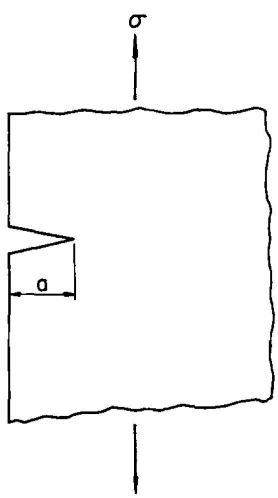

FIG. 11—An Edge Crack in a Semi-Infinite Sheet Subjected to Tension.

computed to any desired degree of accuracy and (within 1 per cent of each other) they are:

$$\left.\begin{aligned} K_{\mathrm{I}} &= 1.12\sigma(\pi a)^{1/2} \\ (K_{\mathrm{II}} &= K_{\mathrm{III}} = 0) \end{aligned}\right\} \quad (40)$$

Comparison of this result with either Eq 4 or Eq 17 leads to the conclusion that the free surface correction factor is 1.12 for edge notches perpendicular to uniform tension.

On the other hand, for the analogous mode III case, Eq 7 and Fig. 5 with the introduction of a free surface perpendicular to the crack plane along the center-line of the crack, no correction is required (26).[9] Therefore, corresponding to Fig. 12, the stress-intensity factor is:

$$\left.\begin{aligned} K_{\mathrm{III}} &= \tau(\pi a)^{1/2} \\ (K_{\mathrm{I}} &= K_{\mathrm{II}} = 0) \end{aligned}\right\} \quad (41)$$

There is no directly analogous mode II case corresponding to Figs. 11 and 12.

With these examples and their results, the methods of determination of "closed form" stress-intensity factors for some basic configurations have been

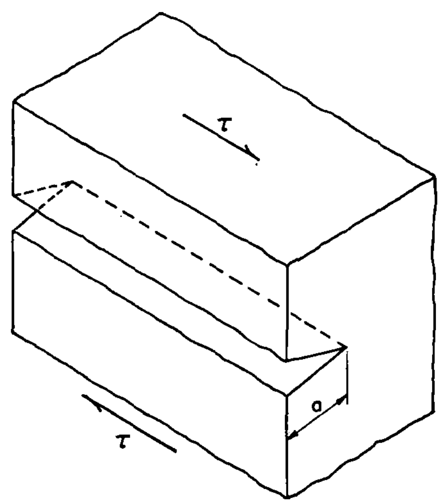

FIG. 12—An Edge Crack in a Semi-Infinite Body Subjected to Shear.

illustrated. Subsequently, some other types of problems which have not lent themselves to closed form solutions bear discussion.

Two-Dimensional Problems of Plate Strips with Transverse Cracks

The class of two-dimensional problems of plate strips with transverse internal, edge, and dual colinear edge cracks subjected to tension and in plane bending is of great practical interest for fracture testing procedures. However, closed-form solutions for such problems are not

[9] Unpublished results of G. Sih.

available and many of the approximate solutions in the literature are of doubtful accuracy. Therefore, it is important not only to cite these results but to give estimates of their accuracy.

The limitations on use of the so called "tangent" formula, Eq 17, for centrally cracked strips and double-edge-notched strips subjected to tension were already discussed. The work cited (13–16) which evaluated those limitations was from direct attacks on the strip problems.

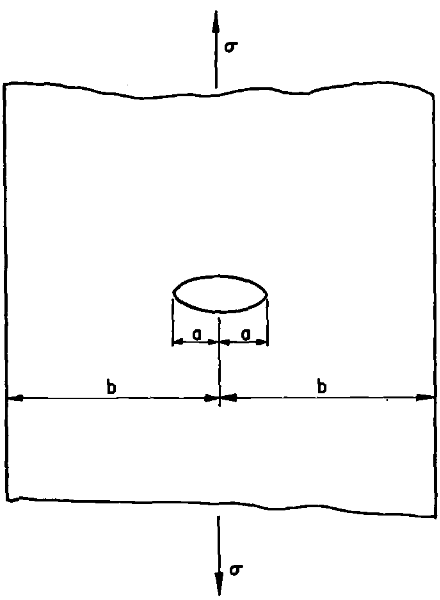

FIG. 13—A Central Crack in a Strip Subjected to Tension.

One of the most formidable approaches to this class of problems is found in the work of Isida (13,34–36). Isida has extensively developed mapping functions for strip problems for determination of stress concentrations at the tips of round-ended cracks of end radius, p. His results are presented in the form (13)

$$\sigma_o = \sigma_{max} = \frac{2\sigma a^{1/2}}{p^{1/2}} f(\lambda) \quad \ldots\ldots (42)$$

where λ is the ratio of crack length to strip width. The function $f(\lambda)$ is obtained as a power series as a result of using power-series mapping and stress functions. The form of Eq 42 lends itself to direct substitution into Eq 9 or alternately, to techniques developed by Kobayashi (14). The resulting stress-intensity factors can be computed to any degree of accuracy by Isida's methods, provided the power series employed in the analysis converge, which they do for relatively large variations in λ. Within this minor limitation, Isida's results lead to accuracies of within 1 or 2 per cent.

TABLE 1—CORRECTION FACTORS FOR A CENTRALLY CRACKED FINITE-WIDTH STRIP.

$\lambda = a/b$	$[2b/\pi a \tan \pi a/2b]^{1/2}$ [a]	$f(\lambda)$
0.074	1.00	1.00
0.207	1.02	1.03
0.275	1.03	1.05
0.337	1.05	1.09
0.410	1.08	1.13
0.466	1.11	1.18
0.535	1.15	1.25
0.592	1.20	1.33

[a] Eq 17.
[b] Isida (13).
Isida's values agree within 1 per cent of an approximation by Greenspan (100).

Isida has computed results in the form of Eq 42 for a variety of problems (13) of special interest in fracture testing such as the case of the centrally notched strip in tension, as shown in Fig. 13. Upon substitution of Eq 42 into Eq 9, it can be noted by comparing the result with Eq 17 that $f(\lambda)$ corresponds to the exact correction factor for the stress-intensity factor of a finite width strip whose approximate form is $[(2b/\pi a) \tan (\pi a/2b)]^{1/2}$. Table 1 compares the two to illustrate the accuracy of Eq 17.

Bueckner[10] (36) has developed integral equation procedures and solved many

[10] H. F. Bueckner in internal reports of the General Electric Co., Schenectady, N. Y.

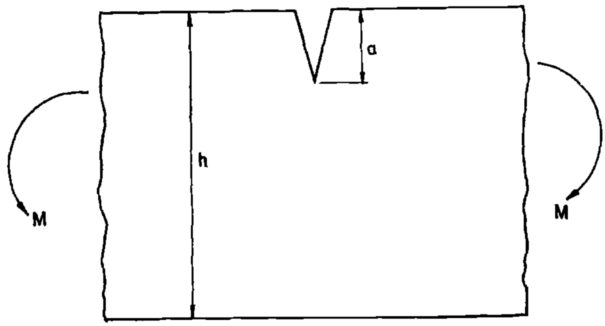

FIG. 14—An Edge Crack in a Strip Subjected to In-Plane Bending.

TABLE 2—STRESS-INTENSITY FACTOR COEFFICIENTS FOR NOTCHED BEAMS.

a/h.......	0.05	0.1	0.2	0.3	0.4	0.5	0.6 (and larger)
$g(a/h)$.....	0.36	0.49	0.60	0.66	0.69	0.72	0.73

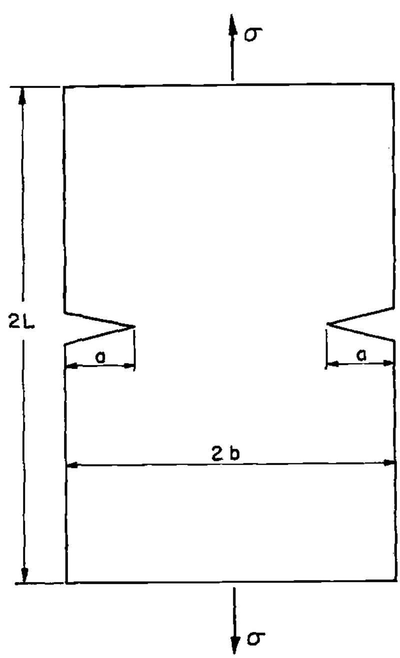

FIG. 15—Double-Symmetric Edge Cracks in Strip of Finite Length Subjected to Tension.

crack problems. He obtained (37) the solution to a strip with a single edge notch subjected to bending, see Fig. 14. The results so reported obviously lack the correction factor for a free surface, for small crack sizes discussed in conjunction with Eq 40, which is a 12 per cent error. However, as noted following Eq 17, the effect of the crack's emanation from a free edge disappears with deepening cracks; consequently, the error should diminish. The results are expressed as follows:

$$\left.\begin{aligned} K_{\rm I} &= \frac{6M}{(h-a)^{3/2}}\, g(a/h) \\ (K_{\rm II} &= K_{\rm III} = 0) \end{aligned}\right\} \quad \ldots\ldots (43)$$

where $g(a/h)$ is given in Table 2.

The values in Table 2 suit the limiting case of deep notches as determined from Neuber's results (10). Therefore, it might be presumed that Table 2 reports values with errors of far less than 12 per cent for a/h greater than 0.2. Several recent papers on notch-bending analysis agree with the values in Table 2 and these recent results also claim agreement with "compliance calibrations" for a/h in the normal testing range.

Bowie developed polynomial mapping functions for use with the complex stress function technique to solve plane problems, such as cracks emanating from circular holes (38) and the double-edge-notched strip in tension (16). The latter example, as illustrated in Fig. 15, provides an indication of the validity of

TABLE 3—CORRECTION FACTORS FOR A DOUBLE EDGE-NOTCHED STRIP.[a]

a/b	$h(a/b)$, $(L/b = 1.00)$	$h(a/b)$, $(L/b = 3.00)$	$[(2b/\pi a) \tan (\pi a/2b)]^{1/2} h(a/b)$ $(L/b \to \infty)$
0.1	1.13	1.12	1.12
0.2	1.13	1.11	1.12
0.3	1.14	1.09	1.13
0.4	1.16	1.06	1.14
0.5	1.14	1.02	1.15
0.6	1.10	1.01	1.22
0.7	1.02	1.00	1.34
0.8	1.01	1.00	1.57
0.9	1.00	1.00	2.09

[a] The last column agrees within 1 per cent with a similar formula proposed by G. R. Irwin on the basis of estimating the various effects. It is

$$K_I = \sigma (\pi a)^{1/2} \left[\frac{2b}{\pi a}\left(\tan \frac{\pi a}{2b} + 0.1 \sin \frac{\pi a}{b}\right)\right]^{1/2}$$

employing Eq 17 for this configuration. Comparing Bowie's results with Eq 17 is most lucidly accomplished using a correction factor, $h(a/b)$, on Eq 17, or

$$\left.\begin{aligned} K_{\mathrm{I}} &= \sigma(\pi a)^{1/2} \left(\frac{2b}{\pi a} \tan \frac{\pi a}{2b}\right)^{1/2} h(a/b) \\ (K_{\mathrm{II}} &= K_{\mathrm{III}} = 0) \end{aligned}\right\} \quad (44)$$

for which his computed values are given in Table 3.

From Table 3 it can be immediately observed that for low a/b values, the correction factor of 1.12 for a crack from a free surface, as illustrated by Eq 40, is present. As a/b increases, its effect disappears and Eq 17 applies as noted previously. The last column of Table 3 combines the two effects, that is, the free surface and the finite width strip, to give the complete correction factor (within 1 per cent) for all values of a/b. From this study it can be noticed that using Eq 40 for $a/b < 0.5$ and Eq 17 for $a/b > 0.5$ results in errors of less than 3 per cent for the configuration shown in Fig. 15, provided that $L/b > 3$. As a consequence, it has been illustrated that basic solutions such as Eqs 17 and 40 can often be used with proper judgment to provide approximate analyses of more difficult situations such as are shown in Fig. 15.

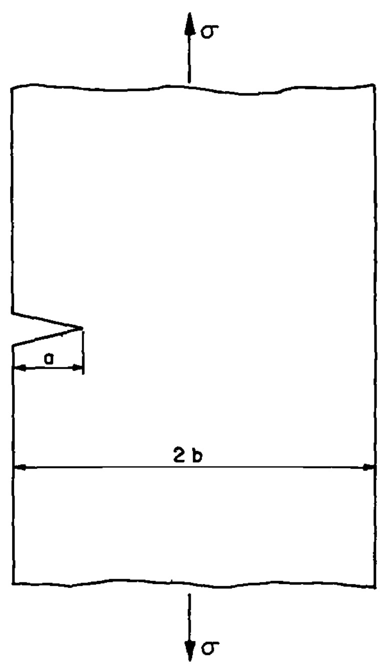

FIG. 16—A Single Edge-Cracked Strip Subjected to Tension.

Collocation procedures for strips of finite length have been developed by Kobayashi (15) and Gross.[11] As an ex-

[11] B. Gross, J. E. Srawley, and W. F. Brown, Jr., "Stress Intensity Factors for a Single Edge Notched Tension Specimen by Boundary Collocation of a Stress Function," unpublished report from NASA, Lewis Research Center.

ample of the method, Kobayashi treated the strip configuration in Fig. 13 using the general complex stress functions of Muskhelishvili (17), collocating equally space points on the sides and ends of the strip. He observed agreement within about 5 per cent of Isida's results as given in Table 1.

Gross treated the single-edge-notched strip using Williams' (6) eigenfunction representation of the Airy stress function. The configuration is shown in Fig. 16. He found that collocation at 20 or more boundary points was required to obtain convergence. His results can be stated in the form:

$$\left.\begin{array}{l} K_{\mathrm{I}} = \sigma(a\pi)^{1/2}k(a/b) \\ (K_{\mathrm{II}} = K_{\mathrm{III}} = 0) \end{array}\right\} \ldots\ldots (45)$$

where $k(a/b)$ is given as a correction factor for this strip problem in Table 4.

By comparison of Gross's results (Fig. 16) with Bowie's double-edge-notched specimen results (Fig. 15) (columns 2 and 3 of Table 4), the apparently large influence of bending due to the lack of symmetry in the single-edge-notch case is observed. Gross's results reportedly agree with experimentally measured values (that is, compliance measurements) within a few percentage points for $0.40 < a/b < 1.00$. Moreover, new results by Bowie (16) shown in column 4 of Table 4 assures the accuracy for this configuration.

Following the procedures of Kobayashi and Gross, it is a straightforward matter to solve additional problems. Moreover, similar numerical procedures based on collocation of boundary conditions in the mean, using other representations of the Airy stress function, or energy methods, or both, are available for development.

TABLE 4—CORRECTION FACTORS FOR A SINGLE EDGE-NOTCHED STRIP.

a/b	$k(a/b)^a$	$[(2b/\pi a)\tan(\pi a/2b)]\,k(a/b)^b$	$k(a/b)^c$
0.10	1.14	1.12	1.15
0.20	1.19	1.12	1.20
0.30	1.29	1.13	1.29
0.40	1.37	1.14	1.37
0.50	1.50	1.15	1.51
0.60	1.66	1.22	1.68
0.70	1.87	1.34	1.89
0.80	2.12	1.57	2.14
0.90	2.44	2.09	2.46
1.00	2.82	...	2.86

[a] Gross[11]
[b] Table 3 and Eq 44
[c] Bowie (16)

REINFORCED PLANE SHEETS

Many conventional structures are fabricated from plane sheets (plates) with reinforcing stiffeners or doubler plates attached by riveting, welding, and other means. Often the attachments are designed as crack-arrestors in order to provide so called "fail-safe" structures.

In order to analyze some of these configurations, it is appropriate to determine stress-intensity factors for cracks in sheets with stiffeners perpendicular to the cracks. Romualdi (39,40) and Paris (41,42) provided some early attempts to estimate the effect of rivet forces tending to hold a crack closed. Sanders (43) discussed the problem of action of an integral stiffener crossing the center of a crack. Isida (13,44) extended his methods to give results for centrally cracked strips with integrally reinforced edges and to infinite sheets with a periodic array of cracks along a line with interspersed integral stiffeners. Greif (45) has solved the problem of a single crack and an integral stiffener (passing outside the crack) in an infinite sheet, and in a continuation of that work the riveted stiffener has been treated.[12] Moreover, Terry (46) has analyzed some similar riveted and welded stiffener problems, as an extension of work by Erdogan (21). Cracks within one sheet of a riveted doubler-plated area of a structure were treated by Paris (41). Since

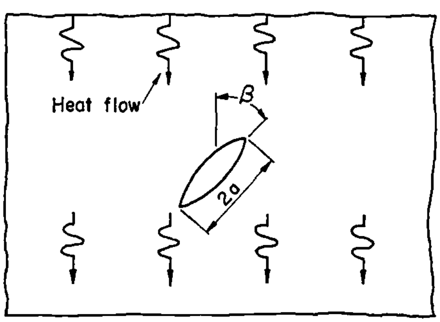

FIG. 17—An Insulated Crack Disturbing Uniform Heat Flow in a Sheet.

this class of problems is difficult to formulate, the methods employed are rather obtuse and specialized. Consequently, they will not be described here other than to remark that the most general approaches available are those of Isida (13), Greif (45) and Terry (46).

THERMAL STRESSES

It has been shown that the crack-tip stress field equations for isotropic bodies, Eqs 1, 2, and 3, also provide the proper field equations for thermal stress states (47) (with the unlikely exception of the crack tip as a point source of heat). Therefore, the concept of stress-intensity factors is in general applicable to thermal stress problems.

As an example, consider the case of uniform heat flow in a sheet, with an undisturbed temperature gradient, ∇T, at an angle, β, with respect to a crack of length, $2a$, acting as an insulator, as shown in Fig. 17. Florence and Goodier (48) have provided the complex stress function for this configuration. It is:

$$\phi(\eta) = \frac{iE\alpha a^2 \nabla T}{8} \sin\beta \log \eta \qquad (46)$$

as a consequence of similarity of the re-

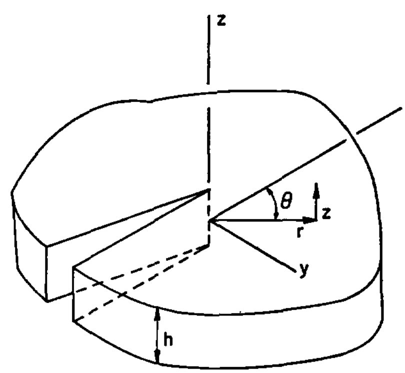

FIG. 18—Coordinates Used in a Cracked Plate Which Will Be Subjected to Transverse Bending.

sulting crack-tip stress field equation with ordinary (isothermal) plane extension, Eqs 29 and 30 may be applied to Eq 46 which results in:

$$\left.\begin{aligned} K_{\mathrm{II}} &= \frac{E\alpha a^{3/2}\nabla T}{4} \sin\beta \\ (K_{\mathrm{I}} &= K_{\mathrm{III}} = 0) \end{aligned}\right\} \qquad (47)$$

where α is the coefficient of thermal expansion and E is Young's modulus. Other examples (47), will be cited in Appendix II.

STRESS-INTENSITY FACTORS FOR THE BENDING OF PLATES AND SHELLS

The field equations for the stresses near a sharp notch in a plate subjected

[12] Private communication from J. L. Sanders, Jr.

to bending were first considered by Williams (49,50) who later applied like methods to a more detailed discussion of cracks (51). Using the classical Kirchhoff theory of plate bending, he obtained the following stress-field equations (see Fig. 18):

$$\left.\begin{aligned}
\sigma_r &= \frac{(7+\nu)}{2(3+\nu)}\frac{K_B}{(2\pi r)^{1/2}}\frac{z}{h}\cdot\left[\frac{(3+5\nu)}{(7+\nu)}\cos\frac{\theta}{2}-\cos\frac{3\theta}{2}\right] \\
&\quad+\frac{(5+3\nu)}{2(3+\nu)}\frac{K_S}{(2\pi r)^{1/2}}\frac{z}{h}\cdot\left[-\frac{(3+5\nu)}{(5+3\nu)}\sin\frac{\theta}{2}+\sin\frac{3\theta}{2}\right] \\
\sigma_\theta &= \frac{(7+\nu)}{2(3+\nu)}\frac{K_B}{(2\pi r)^{1/2}}\frac{z}{h}\cdot\left[\frac{(5+3\nu)}{(7+\nu)}\cos\frac{\theta}{2}+\cos\frac{3\theta}{2}\right] \\
&\quad-\frac{(5+3\nu)}{2(3+\nu)}\frac{K_S}{(2\pi r)^{1/2}}\frac{z}{h}\cdot\left[\sin\frac{\theta}{2}+\sin\frac{3\theta}{2}\right] \\
\tau_{r\theta} &= \frac{(7+\nu)}{2(3+\nu)}\frac{K_B}{(2\pi r)^{1/2}}\frac{z}{h}\cdot\left[-\frac{(1-\nu)}{(7+\nu)}\sin\frac{\theta}{2}+\sin\frac{3\theta}{2}\right] \\
&\quad+\frac{(5+3\nu)}{2(3+\nu)}\frac{K_S}{(2\pi r)^{1/2}}\frac{z}{h}\cdot\left[-\frac{(1-\nu)}{(5+3\nu)}\cos\frac{\theta}{2}+\cos\frac{3\theta}{2}\right]
\end{aligned}\right\}\quad\ldots(48)$$

where the constants in Williams' analysis (51) have been modified in order to define (18,52) the plate bending and plate shearing stress-intensity factors, K_B and K_S, in a manner consistent with (but not quite corresponding to) the first- and second-mode types, K_{I} and K_{II}, respectively, as defined by Eqs 1 and 2. Though polar instead of rectangular stress components are given for compactness in Eqs 48, the similarity of these results with Eqs 1 and 2 is immediately apparent. This similarity is further clarified upon computing K_B and K_S for some configurations and loadings of interest.

The governing equation for free bending of plates (no transverse loads) by the Kirchhoff theory is:

$$\nabla^4 w = 0 \quad\ldots\ldots\ldots\ldots\ldots(49)$$

where w is the transverse displacement. Consequently, an analysis (18) ensues of

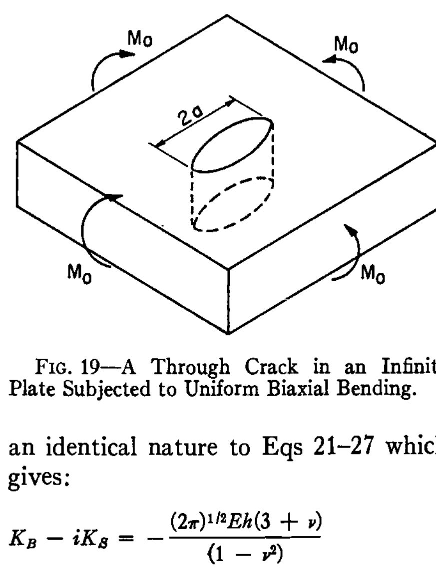

FIG. 19—A Through Crack in an Infinite Plate Subjected to Uniform Biaxial Bending.

an identical nature to Eqs 21–27 which gives:

$$K_B - iK_S = -\frac{(2\pi)^{1/2}Eh(3+\nu)}{(1-\nu^2)}\cdot\lim_{z\to z_1}(z-z_1)^{1/2}\phi_B'(z)\ldots(50)$$

where $\phi_B(z)$ is the plate bending stress function discussed extensively by Savin (12).

Furthermore, mapping is again permitted; or, as Eq 30 followed from Eq 27, for the mapping function given by Eq 29, Eq 50 becomes

$$K_B - iK_S = -(\pi/a)^{1/2}\frac{Eh(3+\nu)}{(1-\nu^2)}\phi_B'(1)\ldots(51)$$

For the example of an infinite plate subjected to uniform moment, M_o, all around the boundary, and with a crack of length, $2a$, as in Fig. 19, Savin (12) gives the stress function,

$$\phi_B(\eta) = -\frac{3M_o a(1-\nu)}{Eh^3} \cdot \left[\eta + \frac{(1-\nu)}{(3+\nu)}\frac{1}{\eta}\right] \quad \text{....(52)}$$

Using Eqs 51 and 52, the result is:

$$\left.\begin{aligned} K_B &= \frac{6M_o}{h^2}(\pi a)^{1/2} \\ (K_S &= 0) \end{aligned}\right\} \quad \text{.......(53)}$$

Since the stress in the surface layer of the plate, σ_o, away from the crack is

$$\sigma_o = \frac{6M_o}{h^2} \quad \text{.............(54)}$$

the analogy between Eqs 53 and 4 is evident.

Moreover, Erdogan (52) has shown experimentally that in brittle materials (like Plexiglas) the fracture mechanics concept of K_B reaching a critical value, K_{BC}, is appropriate and analogous to the extensional first-mode case, that is, K_{Ic}. Incidentally, Erdogan (53) also shows that the critical value of stress-intensity factors applies to the extension second mode, that is, K_{IIc}, which again is shown to be analogous to the shear case of bending, that is, K_{Sc}. Consequently, the plate bending and shearing stress-intensity factors as defined in Eqs 48 are of some immediate practical interest.

However, Eqs 1, 2, and 3 were purported to give *all* tip-stress fields for elastic bodies; yet the field for plate bending as predicted by Eqs 48 is not identical to them. This is because the classical Kirchhoff theory of bending is an approximate theory which does not take into account the details of the stress distribution near boundaries nor discontinuities in the plate. The crack-tip and crack-surface boundaries are locations where details are not clear.

Subsequently, Knowles (54) pointed out that using Reissner's (55) more accurate plate theory leads to a correction of Eqs 48 which on the surface of the plate makes them identical to Eqs 1 and 2, except for a constant factor. Moreover, the character and role of K_B and K_S are preserved through this correction. Hence, it is concluded that they are directly proportional to (completely analogous to) their counterparts, K_I and K_{II}, where elastic action is concerned. Williams (56) pointed this out in reference to the experiments by Erdogan (52). This correspondence has also been observed for fatigue crack growth.[13]

Therefore, both theoretical and experimental results for fracture tests have led to:

$$K_B = \frac{(3+\nu)}{(1+\nu)} K_I \quad \text{.........(55)}$$

on the surface of the plate. The sensibility of using the Kirchhoff theory to compute K_B values is also clear when it is reasoned that the values of stress-intensity factors reflect the intensity of general transmission of applied loads into the crack-tip region. The general properties of gross-load transmission are unaffected by the boundary layer of about one plate thickness, h, in which the Reissner theory applies. Consequently, Eq 55 is always correct for converting Kirchhoff theory stress-intensity factors, K_B, to the Reissner theory result, K_I, for a given configuration.

Several solutions for K_B and K_S are now available (18) and others can be obtained in a direct fashion using Eqs 50 or their equivalents for other types

---

[13] R. Roberts, Ph.D. dissertation, Lehigh University, 1964.

of stress functions. Some of the available results are tabulated in Appendix II.

The case of general bending and extension of thin shells with cracks has been shown by Sih (57) to give crack-tip stress fields equivalent to combining modes I and II with the bending fields, that is, Eqs 1 and 2, and Eq 48. Modes I and II result from extension of the middle surface of the shell, and the bending fields result from changes in the curvature of the middle surface. Consequently, the stress-intensity factor concept is also of general applicability to shells.

However, computing the values of the stress-intensity factors for particular configurations in shells is very difficult.

Moreover, it may be observed (57) that the extension and bending effects in shells will be coupled, so that the stress-intensity factors resulting from solutions must reflect this coupling. As a consequence of the coupling, formulas for stress-intensity factors will involve many parameters (coupling terms) so that they will, to say the least, be complicated.

Folias (58,59) and Ang (60), noting the similarity of equations for plates on elastic foundations and shallow spherical shells (61), have attempted some problems in these areas. However, no other attempts at the complete solutions to shell problems are known.

On the other hand, some parametric studies of possible shell effects on cracks in cylinders have been attempted in several articles (62–65). The results indicate that the experimental data on failure of cracked shells can in fact be correlated in terms of elastic shell parameters. Hence, it is hopeful that further progress can be made soon toward quantitative prediction of shell effects on an analytical basis.

The problem of crack-arrestor rings on shells is at least another degree more difficult. Nevertheless, since this problem is of prime interest in tear-resistant design, efforts are being made toward empirical methods of design (64,66). The complete analytical solution to such a problem is as yet improbable.

COUPLE-STRESS PROBLEMS WITH CRACKS

Another area analogous to shell problems through having similar governing equations is that of couple stresses (67,68). The formulation of couple-stress problems takes into account the gradients of stresses in terms of couples on infinitesimal elements in order to account for the effects of lattice curvature in crystals, and so forth. Setzer (69) has shown that for extension of cracked plates due to uniform applied stress away from the crack, no modification in the field equations (Eqs 1), nor the stress-intensity factors (for example, Eq 4), is required. However, where the applied stresses away from the crack possess gradients, the values of stress-intensity factors will be modified by factors of the form

$$\left[1 + A_1\left(\frac{l}{a}\right) + A_2\left(\frac{l}{a}\right)^2 + A_3\left(\frac{l}{a}\right)^3 + \cdots\right] \quad (56)$$

where l is a couple-stress (lattice) parameter or characteristic length of the material. The A_i are of the order of unity or smaller, and l is of the order of lattice dimensions; consequently, these results would be of a greatest interest in analyzing fine cracks in crystals, except for the fact that the methods involved are similar to and may be carried over to the analysis of shells.

ESTIMATION OF STRESS-INTENSITY FACTORS FOR SOME CASES OF PRACTICAL INTEREST

Armed with the principles of linear elastic theory, such as "the principle of superposition," and with an intuitive grasp of a strength-of-materials approach, it is possible to form estimates of stress-intensity factors. This was made partially evident in the case of an embedded elliptical crack in the discussion

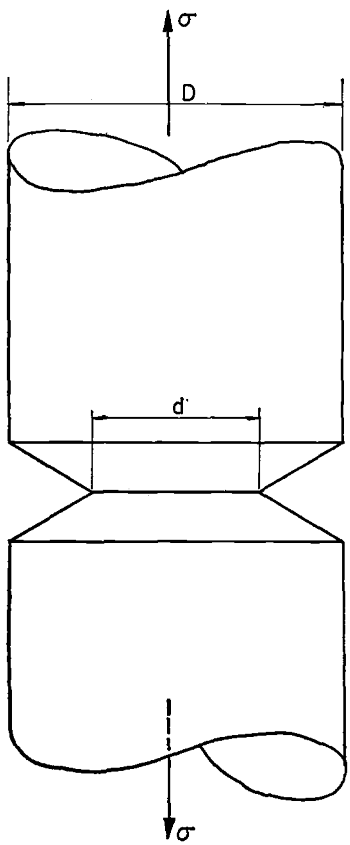

FIG. 20—A Circumferentially Cracked Round Bar Subjected to Tension.

of limiting cases following Eqs 38 and 39. Other situations where limiting cases of different problems are comparable were illustrated in Tables 1, 3, and 4 and examples in the text. Notice especially, as in these tables, that one problem solution often forms an upper or lower bound on the solution of others. These concepts will be employed in examples of estimating to follow.

Consider the configuration of a notched round bar with an outside diameter, D, and notched-section diameter, d, and subjected to extension causing a net-section stress, σ_{net} (see Fig. 20). From dimensional considerations and symmetry, it is noted that the stress-intensity factor may be stated in the form,

$$\left.\begin{aligned} K_{\mathrm{I}} &= \sigma_{\text{net}}(\pi D)^{1/2}F(d/D) \\ K_{\mathrm{II}} &= K_{\mathrm{III}} = 0 \end{aligned}\right\} \quad \ldots\ldots(57)$$

where $F(d/D)$ is an unknown dimensionless function of the diameter ratio. The end values (that is, $d/D \rightarrow 0$ or 1.0) of the function can be established by examining limiting cases.

As $D \rightarrow \infty$, dimensional analysis leads to

$$K_{\mathrm{I}} = C_3\sigma_{\text{net}}(\pi d)^{1/2} \quad \ldots\ldots\ldots(58)$$

thus, for small values of d/D,

$$F_u(d/D) = C_3(d/D)^{1/2} \quad \ldots\ldots\ldots(59)$$

the value of C_3 is found to be $[1/(2\sqrt{2})]$ using Eq 9 and the stress-concentration solution for the problem given by Neuber (10) and Peterson (11). Since the free surface introduced by the finite diameter of the bar lowers the stress-intensity factor, $F_u(d/D)$ is an upper bound on $F(d/D)$ for all values of d/D.

On the other hand, for $d/D \rightarrow 1$, Bowie's solution for the double-edge-notched sheet, Eq 44, simulates the problem upon substituting

$$\left.\begin{aligned} a &= \frac{D}{2}\left(1 - \frac{d}{D}\right) \\ \frac{a}{b} &= 1 - \frac{d}{D} \\ \sigma &= \sigma_{\text{net}}\left(\frac{d}{D}\right)^2 \end{aligned}\right\} \quad \ldots\ldots(60)$$

The result conforms with Eq. 57, that is,

$$K_{\mathrm{I}} = \sigma_{\mathrm{net}}(\pi D)^{1/2}\left[\left(\frac{d}{D}\right)^2 \cdot \left(\frac{1}{\pi}\tan\frac{\pi}{2}\left(1-\frac{d}{D}\right)\right)^{1/2} h\left(1-\frac{d}{D}\right)\right] \quad (61)$$

TABLE 5—STRESS-INTENSITY FACTOR COEFFICIENTS FOR NOTCHED ROUND BARS.

d/D	$F_L(d/D)$	$F_u(d/D)$	$F(d/D)$
0	0	0	0
0.1	...	0.111	0.111
0.2	0.046	0.158	0.155
0.3	...	0.194	0.185
0.4	0.118	0.223	0.209
0.5	...	0.250	0.227
0.6	0.185	0.274	0.238
0.65	0.203	...	0.240
0.70	0.217	0.296	0.240
0.75	0.226	...	0.237
0.80	0.230	0.317	0.233
0.85	0.224	...	0.225
0.90	0.205	0.336	0.205
0.95	0.162	...	0.162
0.97	0.130	...	0.130
1.00	0	0.353	0

Consequently,

$$F_L\left(\frac{d}{D}\right) = \left(\frac{d}{D}\right)^2 \cdot \left(\frac{1}{\pi}\tan\frac{\pi}{2}\left(1-\frac{d}{D}\right)\right)^{1/2} h\left(1-\frac{d}{D}\right) \quad (62)$$

where $h(\ )$ is as tabulated in Table 3. This function, $F_L(d/D)$ is a lower bound on $F(d/D)$ for all values of d/D, since the curvature of the bar causes increased crack-tip stress over the flat plate solution as d/D recedes from the value 1.

Finally, from Peterson's (11) stress-concentration values and Eq 9, and other considerations, the maximum value of $F(d/D)$ is estimated to be 0.240. Interpolating between these solutions results in the estimated values in Table 5.

By making use of careful judgment of the limits of applicability of the limiting cases, Eqs 59 and 62 and the analysis of stress concentration (11), the accuracy of $F(d/D)$ in Table 5 can be stated with

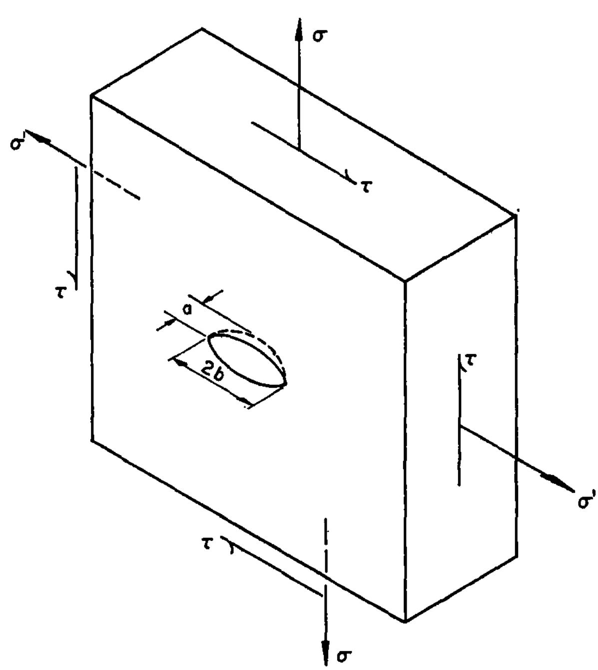

FIG. 21—A Semi-Elliptical Surface Crack in a Plate Subjected to General Extension.

confidence. With a d/D of 0 to 0.4, it is ± 3 per cent; with a d/D of 0.4 to 0.85, it is ± 5 per cent; and with a d/D of 0.85 to 1.0, it is ± 2 per cent. Therefore, a solution with sufficient precision for practical applications has been constructed.

This configuration is often used for fracture testing and a simplified formula is employed, that is (70),

$$K_I = 0.233\, \sigma_{net}(\pi D)^{1/2} \quad (63)$$

This formula seems most reasonable since 0.233 agrees with the values of $F(d/D)$ in Table 5 within 5 per cent over the range of d/D from 0.48 to 0.86. Further improvements in the accuracy of the values given would require a full analysis of the problem, such as suggested by Sneddon (71) or Bueckner.[14]

Another configuration, which has been discussed by Irwin (29), is that of a semi-elliptical surface crack in a plate (see Fig. 21). This configuration is both typical of flaws and is used in fracture testing (simulating this type of flaw). If the plate is subjected to general uniform extension by stresses, σ, σ' and τ, the stress, σ', parallel to the crack causes no singularity or no contribution to stress-intensity factors. Consequently σ' will be ignored.

If b/a is large and a/t small compared to 1, the stress-intensity factors at the end of the semi-minor axis, a, can be estimated from Eqs 17 and 20, making use of free-edge corrections as in Eqs 40 and 41. Then, the correction, Φ_o, in Eqs 38 and 39 should be applied as b/a values are reduced toward 1. However, the free-edge correction probably diminishes as b/a approaches 1, and the tangent correction in Eqs 17 and 20 is also an overcorrection in that limit. On the other hand, Eqs 44 and 45 and Table 4 show that single-edge notches induce bending which increases the stress-intensity factor, but less so in this case since the uncracked portion of the plate would inhibit bending. Finally, Table 1 shows the underestimation of the tangent correction as a/t becomes larger. Taking all these factors into account, Eqs 17, 20, 38–42, 44, and 45, and their considerations lead to the approximations:

$$\left.\begin{aligned} K_I &= \left[1 + 0.12\left(1 - \frac{a}{b}\right)\right] \cdot \frac{\sigma(\pi a)^{1/2}}{\Phi_o}\left(\frac{2t}{\pi a}\tan\frac{\pi a}{2t}\right)^{1/2} \\ K_{II} &= 0 \\ K_{III} &= \frac{\tau(\pi a)^{1/2}}{\Phi_o}\left(\frac{2t}{\pi a}\tan\frac{\pi a}{2t}\right)^{1/2} \end{aligned}\right\} \quad (64)$$

for the stress-intensity factors at the end of the semi-minor axis, a. For the ranges of b/a from 1 to 10 or more, and of a/t from zero to one half the accuracy is within about ± 5 per cent. Moreover, for b/a up to about 5 and a/t up to three fourths the accuracy is still probably better than ± 10 per cent, considering all the compensating errors. This case has at least provided a classic example of estimating methods using many other solutions for stress-intensity factors to treat an important problem which is all but impossible to solve directly.

A word of warning with complicated cases such as Eqs 64 is in order. If the crack-tip plasticity subtends a major portion (say one half) of the distance between the crack front and the back side of the plate, use of these equations would become indeed doubtful. Moreover, estimation of the amount of plasticity is clearly more complicated here than in other situations, but surely possible. Such estimates are beyond the scope of this discussion and the reader is referred to Ref (72). Moreover, in passing, it is noteworthy that restrictions on crack-tip plastic-zone sizes are always present in making direct

[14] Private communication from H. Bueckner.

applications of the elastic analyses (70). For certain situations estimated corrections to the analysis for crack tip plasticity effects have been proposed (41,70,72).

Estimates can be made for stress-intensity factors for quite arbitrary crack-front contours in three-dimensional bodies subjected to uniform tension, σ, perpendicular to the crack plane in the region including the whole crack. Consider the embedded crack whose plan view is shown in Fig. 22. Using the previous results for circular disk cracks, Eq 37, and for tunnel cracks, Eq 4, bounds on the values of stress-intensity factors can be established on the crack

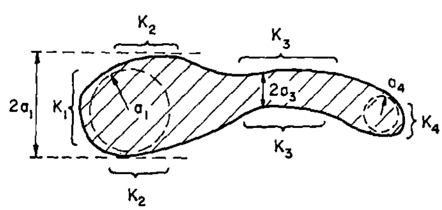

FIG. 22—The Plan View of an Irregular Crack in an Infinite Body.

front for various portions of the contour, where

$$\left.\begin{aligned} K_{\text{I}} &= K_1 \text{ or } K_2 \text{ or } K_3 \text{ or } K_4 \\ K_{\text{II}} &= 0 \\ K_{\text{III}} &= 0 \end{aligned}\right\} \quad \ldots\ldots (65)$$

the value of K_1 will be slightly greater than that for a disk crack of radius, a_1, but far less than a tunnel crack of width, $2a_1$. Therefore, from Eqs 4 and 37,

$$\frac{2}{\pi}\,\sigma(\pi a_1)^{1/2} < K_1 \ll \sigma(\pi a_1)^{1/2} \quad \ldots\ldots (66)$$

Since $2/\pi$ is about 0.64, if K_1 is guessed to be

$$K_1 \cong 0.75\,\sigma(\pi a_1)^{1/2} \quad \ldots\ldots (67)$$

the result is surely within ± 10 per cent along the whole portion of the contour marked, K_1, in Fig. 22. Now, K_2 is closer to the tunnel-crack case or, a guess is

$$K_2 \cong 0.85\,\sigma(\pi a_1)^{1/2} \quad \ldots\ldots (68)$$

The neck of width, $2a_3$, makes K_3 slightly higher than the comparable tunnel crack, or

$$K_3 \cong 1.05\,\sigma(\pi a_3)^{1/2} \quad \ldots\ldots (69)$$

Similar to K_1, the guess for K_4 is

$$K_4 \cong 0.75\,\sigma(\pi a_4)^{1/2} \quad \ldots\ldots (70)$$

These estimates are surely all correct within ± 10 per cent (and probably ± 5 per cent). Moreover, additional refinements are possible, such as noting that K_3 on the upper part of the contour is likely to be about 5 per cent less than on the lower contour in Fig. 22, due to the curvature of the centerline of the neck, $2a_3$.

Corrections can also be added for the proximity to a free surface, such as the tangent correction in Eq 17, or for the emanation of the crack from a free surface, such as Eq 40. The method of estimating has now been sufficiently illustrated to allow direct application to a multitude of examples. In order to develop confidence in estimating procedures, it is suggested that one may, for example, estimate the stress-intensity factor values for an elliptical crack using the above procedure, Eqs 66–70, and compare the results with the exact values, Eq 38.

STRESS FIELDS AND INTENSITY FACTORS FOR HOMOGENEOUS ANISOTROPIC MEDIA

An interest in stress analysis of cracks for various media, such as anisotropic, viscoelastic, or non-homogeneous materials, stems from two motivations. First, the effects of slight amounts of directionality, creep, and inhomogeneity on the stress distribution and intensity are useful in assessing the limits of applicability of the conceptual model of fracture mechanics based on linear elastic theory. In addition, studies of the stress analysis of these various types of media will provide the basis of extension of fracture mechanics to such materials.

Several authors have treated special cases of crack problems in anisotropic media, such as orthotropy (32,73,74) or particular configurations (75,76). However, the general anisotropic case can be treated in order to determine crack-tip stress fields and to define intensity factors in a manner completely analogous to Eqs 1, 2, and 3. The methods discussed extensively by Lekhnitzki (77) will be employed here.[15]

Hooke's law for a homogeneous (rectilinearly) anisotropic material is:

$$\left.\begin{aligned} \epsilon_x &= a_{11}\sigma_x + a_{12}\sigma_y + a_{13}\sigma_z \\ &\quad + a_{14}\tau_{yz} + a_{15}\tau_{xz} + a_{16}\tau_{xy} \\ \epsilon_y &= a_{21}\sigma_x + \cdots \\ \epsilon_z &= a_{31}\sigma_x + \cdots \\ \gamma_{yz} &= a_{41}\sigma_x + \cdots \\ \gamma_{xz} &= a_{51}\sigma_x + \cdots \\ \gamma_{xy} &= a_{61}\sigma_x + a_{62}\sigma_y + a_{63}\sigma_z \\ &\quad + a_{64}\tau_{yz} + a_{65}\tau_{xz} + a_{66}\tau_{xy} \end{aligned}\right\}\ldots(71)$$

where, from reciprocity

$$a_{ij} = a_{ji}$$

Referring to Fig. 2 for the coordinates and notation with respect to a crack front, the crack-tip stress fields may be resolved from two cases of plane problems which are defined as:

(1) Plane strain, that is, $(\partial u/\partial z) = (\partial v/\partial z) = w = 0$ or $\epsilon_z = \gamma_{yz} = \gamma_{xz} = 0$

(2) Pure shear, that is, $u = v = (\partial w/\partial z) = 0$ or $\epsilon_z = \epsilon_x = \epsilon_y = \tau_{xy} = 0$

The superposition of results from these plane problems will allow treatment of the general case of crack-tip stress fields similar to Eqs 1, 2, and 3.

Plane Strain:

For this case, Hooke's law may be reduced, using the restrictions on strain to eliminate the appearance of z-components of stress, to give:

$$\left.\begin{aligned} \epsilon_x &= A_{11}\sigma_x + A_{12}\sigma_y + A_{16}\tau_{xy} \\ \epsilon_y &= A_{21}\sigma_x + A_{22}\sigma_y + A_{26}\tau_{xy} \\ \gamma_{xy} &= A_{61}\sigma_x + A_{62}\sigma_y + A_{66}\tau_{xy} \end{aligned}\right\}\ldots(72)$$

where again, $A_{ij} = A_{ji}$ and the A_{ij} can be expressed in terms of a_{ij} directly if desired. Using an Airy stress function, U, with stress components defined as the usual second derivatives, equilibrium is automatically satisfied and the compatability equations lead to:

$$D_1 D_2 D_3 D_4 U = 0 \ldots\ldots\ldots(73)$$

where $D_k = (\partial/\partial_y) - \mu_k(\partial/\partial_x)$ and μ_k are the roots of

$$A_{11}\mu^4 - 2A_{16}\mu^3 + (2A_{12} + A_{66})\mu^2 - 2A_{26}\mu + A_{22} = 0 \ldots(74)$$

These elastic constants, μ_k, are complex or pure imaginary and occur in conjugate pairs (77), that is, $\mu_3 = \bar{\mu}_1$ and $\mu_4 = \bar{\mu}_2$. Defining the complex variables, z_1 and z_2, by

$$\left.\begin{aligned} z_1 &= x + \mu_1 y \\ z_2 &= x + \mu_2 y \end{aligned}\right\}\ldots\ldots\ldots(75)$$

the general solution to Eq 73 can be written, if $\mu_1 = \mu_2$,

$$U = U_1(z_1) + \bar{z}_1 U_2(z_1) + U_3(\bar{z}_1) + z_1 U_3(\bar{z}_1)$$

or, if $\mu_1 \neq \mu_2$,

$$U = U_1(z) + U_2(z_2) + U_3(\bar{z}_1) + U_4(\bar{z}_2) \ldots(76)$$

and with the further restriction that U must be real, they become

$$\left.\begin{aligned} U &= 2\,\mathrm{Re}[U_1(z_1) + \bar{z}_1 U_2(z_1)] \\ U &= 2\,\mathrm{Re}[U_1(z_1) + U_2(z_2)] \end{aligned}\right\}\ldots(77)$$

[15] The mathematical derivation of stress fields leading to Eqs 81–85 are not a requirement of useful interpretation of those results.

The similarity of the first case of Eq 77 with Eq 22 is appropriate since for isotropic media, $\mu_1 = \mu_2 = i$. Therefore, the orthotropic case with the crack on a principal plane which leads to $\mu_1 = \mu_2$ has been reduced to the same case as isotropic elasticity with the simple change of variable $z_1 = x + \mu_1 y$. The more general case of anisotropy, the second of Eq 77, or $\mu_1 \neq \mu_2$, will follow in the remaining discussion.

The stress and displacement components are found from the Airy stress function, U, by the usual combination of derivatives which give:

$$\left.\begin{aligned}
\sigma_x &= 2\,\mathrm{Re}[\mu_1^2 U_1''(z_1) + \mu_2^2 U_2''(z_2)] \\
\sigma_y &= 2\,\mathrm{Re}[U_1''(z_1) + U_2''(z_2)] \\
\tau_{xy} &= -2\,\mathrm{Re}[\mu_1 U_1''(z_1) + \mu_2 U_2''(z_2)] \\
&\text{and} \\
u &= 2\,\mathrm{Re}[p_1 U_1'(z_1) + p_2 U_2'(z_2)] \\
v &= 2\,\mathrm{Re}[q_1 U_1'(z_1) + q_2 U_2'(z_2)] \\
&\text{where:} \\
p_i &= A_{11}\mu_i^2 + A_{12} - A_{16}\mu_i \\
q_i &= A_{12}\mu_i + (A_{22}/\mu_i) - A_{26}\,.
\end{aligned}\right\} \quad \ldots(78)$$

Therefore, solution to any specific problem is reduced to finding the U_1 and U_2 which satisfy the boundary conditions.

Referring again to Fig. 2 and Eq 75, in the neighborhood of a crack tip, $|z_1|$ and $|z_2|$ are small compared to other planar dimension of problems. Consequently, the stress functions for cracks given by Lekhnitzki (77) may be reduced to the form,

$$\left.\begin{aligned}
U_1''(z_1) &= \frac{f_1(\mu_1, \mu_2, z_1)}{z_1^{1/2}} \\
U_2''(z_2) &= \frac{f_2(\mu_1, \mu_2, z_2)}{z_2^{1/2}}
\end{aligned}\right\} \quad \ldots\ldots(79)$$

where f_1 and f_2 are well-behaved in that neighborhood and some restrictions on their form are imposed by the stress-free crack surface boundary conditions. Imposing these conditions, as well as those mentioned earlier and then substituting the variable,

$$z = x + iy = re^{i\theta} \quad \ldots\ldots\ldots(80)$$

the crack-tip stress fields are found from Eqs 78 – 80 and can be stated in the form

$$\left.\begin{aligned}
\sigma_x &= \frac{K_{\mathrm{I}a}}{(2\pi r)^{1/2}}\,\mathrm{Re}\left[\frac{\mu_1\mu_2}{\mu_1 - \mu_2}\cdot\left\{\frac{\mu_2}{(\cos\theta + \mu_2\sin\theta)^{1/2}} - \frac{\mu_1}{(\cos\theta + \mu_1\sin\theta)^{1/2}}\right\}\right] \\
&\quad + \frac{K_{\mathrm{II}a}}{(2\pi r)^{1/2}}\,\mathrm{Re}\left[\frac{1}{\mu_1 - \mu_2}\cdot\left\{\frac{\mu_2^2}{(\cos\theta + \mu_2\sin\theta)^{1/2}} - \frac{\mu_1^2}{(\cos\theta + \mu_1\sin\theta)^{1/2}}\right\}\right] \\
\sigma_y &= \frac{K_{\mathrm{I}a}}{(2\pi r)^{1/2}}\,\mathrm{Re}\left[\frac{1}{\mu_1 - \mu_2}\cdot\left\{\frac{\mu_1}{(\cos\theta + \mu_2\sin\theta)^{1/2}} - \frac{\mu_2}{(\cos\theta + \mu_1\sin\theta)^{1/2}}\right\}\right] \\
&\quad + \frac{K_{\mathrm{II}a}}{(2\pi r)^{1/2}}\,\mathrm{Re}\left[\frac{1}{\mu_1 - \mu_2}\cdot\left\{\frac{1}{(\cos\theta + \mu_2\sin\theta)^{1/2}} - \frac{1}{(\cos\theta + \mu_1\sin\theta)^{1/2}}\right\}\right] \\
\tau_{xy} &= \frac{K_{\mathrm{I}a}}{(2\pi r)^{1/2}}\,\mathrm{Re}\left[\frac{\mu_1\mu_2}{\mu_1 - \mu_2}\cdot\left\{\frac{1}{(\cos\theta + \mu_1\sin\theta)^{1/2}} - \frac{1}{(\cos\theta + \mu_2\sin\theta)^{1/2}}\right\}\right]
\end{aligned}\right\} \quad \ldots(81)$$

$$+ \frac{K_{IIa}}{(2\pi r)^{1/2}} \operatorname{Re}\left[\frac{1}{\mu_1 - \mu_2} \cdot \left\{\frac{\mu_1}{(\cos\theta + \mu_1 \sin\theta)^{1/2}} - \frac{\mu_2}{(\cos\theta + \mu_2 \sin\theta)^{1/2}}\right\}\right] \quad \ldots (81)$$

where higher-order terms in r have been neglected. Reiterating, μ_1 and μ_2 are dimensionless elastic constants. Notice the striking similarity of Eqs 81 with

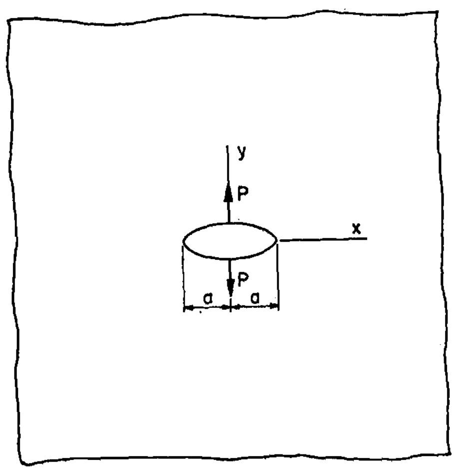

FIG. 23—A Crack in an Infinite Sheet Subjected to Centrally Applied Wedge Forces.

Eqs 1 and 2. The definitions of K_{Ia} and K_{IIa} have been chosen to be identical to K_I and K_{II} for the cases of symmetrical configurations with symmetric or skew-symmetric loadings, respectively.

Consequently, it can be shown that for the general anisotropic problem of the configuration illustrated in Fig. 1:

$$\left.\begin{aligned} K_{Ia} &= \sigma\,(\pi a)^{1/2} \\ K_{IIa} &= 0 \end{aligned}\right\} \ldots\ldots\ldots\ldots (82)$$

and for the problem in Fig. 2,

$$\left.\begin{aligned} K_{IIa} &= \tau\,(\pi a)^{1/2} \\ K_{Ia} &= 0 \end{aligned}\right\} \ldots\ldots\ldots\ldots (83)$$

Moreover, for the symmetrical wedge-force problem, as shown in Fig. 23, the stress functions are:

$$\left.\begin{aligned} U_1'(\zeta_1) &= \frac{iP\mu_2}{2\pi(\mu_1 - \mu_2)} \cdot \log\left[\frac{\zeta_1 + (\zeta_1^2 - a^2)^{1/2} - ia}{\zeta_1 + (\zeta_1^2 - a^2)^{1/2} + ia}\right] \\ U_2'(\zeta_2) &= \frac{-iP\mu_1}{2\pi(\mu_1 - \mu_2)} \cdot \log\left[\frac{\zeta_2 + (\zeta_2^2 - a^2)^{1/2} - ia}{\zeta_2 + (\zeta_2^2 - a^2)^{1/2} + ia}\right] \\ (\zeta_k &= +a + z_k) \end{aligned}\right\} \ldots (84)$$

Using Eqs 78 – 80 with Eqs 84 and comparing results with Eqs 81, it is found that

$$\left.\begin{aligned} K_{Ia} &= \frac{P}{(\pi a)^{1/2}} \\ K_{IIa} &= 0 \end{aligned}\right\} \ldots\ldots\ldots\ldots (85)$$

Equations 85 can also be obtained from the isotropic case, Eqs 32 or 33, directly. It is therefore easy to add a multitude of examples by simply constructing stress-intensity factors from symmetric and skew-symmetric isotropic counterparts. Attention shall now be turned to the condition of pure shear.

Pure Shear:

For this case the generalized Hooke's law, Eqs 71, may be reduced by the definition of pure shear to:

$$\left.\begin{aligned} \gamma_{yz} &= \frac{\partial w}{\partial y} = A_{44}\tau_{yz} + A_{45}\tau_{xz} \\ \gamma_{xz} &= \frac{\partial w}{\partial x} = A_{54}\tau_{yz} + A_{55}\tau_{xz} \end{aligned}\right\} \ldots (86)$$

where $A_{54} = A_{45}$. Substituting these expressions into the equilibrium equations, the result is

$$A_{44}\frac{\partial^2 w}{\partial x^2} - 2A_{45}\frac{\partial^2 w}{\partial x \partial y} + A_{55}\frac{\partial^2 w}{\partial y^2} = 0 \ldots (87)$$

which can be written

$$D_5 D_6 w = 0 \quad \text{(88)}$$

where, as previously defined,

$$D_k = \frac{\partial}{\partial y} - \mu_k \frac{\partial}{\partial x}$$

Comparing Eqs 87 and 88, μ_5 and μ_6 are the roots of

$$A_{55}\mu^2 - 2A_{45}\mu + A_{44} = 0 \quad \text{(89)}$$

It is observed that these roots are a conjugate pair, that is, $\mu_6 = \bar{\mu}_5$. Defining a complex variable, z_5, by

$$z_5 = x + \mu_5 y \quad \text{(90)}$$

the general solution to Eq 88 may be expressed as

$$w = W_1(z_5) + W_2(\bar{z}_5) \quad \text{(91)}$$

Since w must be real, for convenience W_2 can be taken as the negative of W_1 or

$$w = 2\,\mathrm{Im}\,[W_1(z_5)] \quad \text{(92)}$$

Referring to Fig. 2 for a description of the coordinates, in order to satisfy the stress-free crack surface conditions, W takes the form,

$$W_1 = A\,(z_5)^{1/2} \quad \text{(93)}$$

where A is a real constant in the vicinity of the crack tip. Making use of Eqs 80, 86, 90, 92, and 93, the stress may be written in the form:

$$\left.\begin{aligned} \tau_{yz} &= \frac{K_{IIIa}}{(2\pi r)^{1/2}}\,\mathrm{Re}\left[\frac{1}{(\cos\theta + \mu_5 \sin\theta)^{1/2}}\right] \\ \tau_{xz} &= \frac{K_{IIIa}}{(2\pi r)^{1/2}}\,\mathrm{Re}\left[\frac{\mu_5}{(\cos\theta + \mu_5 \sin\theta)^{1/2}}\right] \end{aligned}\right\} \quad \text{(94)}$$

where it is necessarily implied that near the crack tip

$$A = \frac{K_{IIIa}\,(A_{44}A_{55} - A_{45}^2)^{1/2}}{(2\pi)^{1/2}} \quad \text{(95)}$$

The anisotropic stress-intensity factor, K_{IIIa}, is defined so that it is also identical to its isotropic counterpart, K_{III}, for all boundary-value problems of pure shear. For example, for the configuration in Fig. 5 the result is

$$K_{IIIa} = K_{III} = \tau\,(\pi a)^{1/2} \quad \text{(96)}$$

upon constructing the solution and comparing the result with Eq 7.

Consequently, it has been shown that, for the general homogeneous anisotropic case, the crack-tip stress fields and their intensity factors, the complete analogy with the isotropic case is preserved. By judicious definition of the anisotropic stress-intensity factors, they are identical to those for the isotropic case. The resulting stress field equations (Eqs 81 and 94), when superimposed[16] give the most general state of stress in the neighborhood of a crack tip in an anisotropic body with any configuration or loading.

Perhaps most important of all is the fact that like the isotropic case, the $1/r^{1/2}$ singularity appears in the stress field equations (Eqs 81 and 94). This fact implies that fracture size effects for homogeneous anisotropic media will be identical to the isotropic case.

However, for nonhomogeneous anisotropy, such as polar orthotropy, discussed by Williams (73), singularities other than the $1/r^{1/2}$ type may appear, causing different size effects than the isotropic case.

CRACKS IN LINEAR VISCOELASTIC MEDIA

The deformation of cracks in plane viscous extension has been studied by Berg (78,79). He has shown that in a linear viscous sheet, elliptical holes (including the limiting cases of cracks and circles) always deform into other ellipses for the cases where additional separation is not taking place. The exclusion of separation means that adjacent

[16] Components of stress eliminated from the stress-strain laws should be re-introduced. They are derivable directly from the listed components in Eqs 81, 94, and 71.

points on the contour of the hole are remaining adjacent. This assumption may be somewhat restrictive, but it permits the important conclusion of ellipses deforming into ellipses, which in turn allows the use of increments of infinitesimal deformation analysis to provide a stress analysis of this class of problems.

Therefore, for stationary cracks Berg has shown that the treatment by Sih (80) of stress fields near sharp crack tips for arbitrary linear viscoelasticity is in fact pertinent even though "blunting" of the crack tip takes place. Sih has shown that the crack-tip stress fields are as given in Eqs 1, 2, and 3, where the stress-intensity factors are functions of time, that is,

$$\left.\begin{aligned} K_{\mathrm{I}} &= K_{\mathrm{I}}(t) \\ K_{\mathrm{II}} &= K_{\mathrm{II}}(t) \\ K_{\mathrm{III}} &= K_{\mathrm{III}}(t) \end{aligned}\right\} \qquad (97)$$

These stress-intensity factors may be regarded as representing the time history of intensity of a crack-tip stress field of constant spatial distribution.

Treatment of problems of moving (extending) cracks in viscoelastic media is currently unknown. However, they are obviously pertinent to formulating the condition instability of cracks in viscoelastic media where slow growth precedes sudden failure.

On the other hand, the fact that Eqs 1, 2, and 3 have been shown to apply to any crack in a linear viscoelastic body, leads to the conclusion that slight amounts of viscous action may cause time effects but size effect will be identical to the elastic case. Consequently viscous "strain-rate effects" in studies of fracture, see for example Refs (81–83), may be based on the usual elastic stress analysis, that is, Eqs 1, 2, and 3.

SOME SPECIAL CASES ON NONHOMOGENEOUS MEDIA WITH CRACKS

The general problem of nonhomogeneous media with cracks has as yet not been attacked. However, some special cases of practical interest have been treated.

The problem of two semi-infinite half-planes of different material bonded (or welded) together along a line (or plane) containing a crack has received the most attention (84–87). The applications of these analyses include faults in laminations in rock or other materials, cracks formed at steps in the thickness of plates in extension or bending, or both; stresses in glued joints and bond cracks in composite materials.

The stress fields (84,85) for crack tips along such bond lines take the form:

$$\sigma_{ij} = \frac{K}{(2\pi r)^{1/2}} f_{ij}(\epsilon, \theta, \log r) \quad \ldots\ldots (98)$$

where the terms of the type "log r" are shown (85) to be of little influence on the stress fields. Consequently, the $1/r^{1/2}$ type of singularity is the controlling factor in the stress field. Therefore, again the dimensional character of K is essentially preserved and fracture size effects will be identical to the homogeneous case.

However, Zak (88) observed that for a crack perpendicular to and reaching an interface between two materials, the coefficient, n, of the stress singularity, r^{-n}, will be other than $\frac{1}{2}$. If the new material being entered by the crack has a lower modulus of elasticity, then n will be greater than $\frac{1}{2}$ and vice versa. This seems to indicate a tendency to promote the entering of cracks in hard materials into softer ones due to the increased severity of the type of singularity.

Another implication here is that size effects in transmitting fracture from the harder phases of composite materials to a softer matrix will be different than the case of cracks in homogeneous materials. (More specifically, the stress required for failure should depend inversely upon the size of the hard phase grains to the nth power.)

INERTIAL EFFECTS ON THE STRESS FIELD OF A MOVING CRACK

Long before many solutions to elastostatic crack problems were available, Yoffe (89) presented the steady-state solution to a crack of constant length, $2a$, moving through plate subjected to uniform tension, σ. Moreover, she noted that the extending crack tip possessed a stress field of the form,

$$\sigma_{ij} = \frac{\sigma(\pi a)^{1/2}}{(2\pi r)^{1/2}} g_{ij}(\theta,C,E,\nu,\gamma) \quad \ldots\ldots(99)$$

where $\sigma(\pi a)^{\frac{1}{2}}$ can be recognized as the stress-intensity factor, C is the crack velocity, and γ is the mass density of the material. Notice that for all values of the crack velocity the $1/r^{1/2}$ singularity is preserved. McClintock (90) obtained similar results for steady-state problems of the mode III variety, pure shear. Both note that g_{ij} is virtually the same as the static case, Eq 1, up to crack speeds, C, of over 0.4 of the shear wave velocity, C_2, where

$$C_2 = \left(\frac{E}{2(1+\nu)\gamma}\right)^{1/2} \quad \ldots\ldots(100)$$

However, at some velocity, C, in the neighborhood of 0.5 C_2, the location of the maximum in the θ-direction stresses changes from $\theta = 0$ deg to an angle of about $\theta = 60$ deg to the crack tip and the distribution of stresses, g_{ij} in general becomes quite different from the static case. The highest triaxiality of stresses near the crack tip shifts from directly ahead of the crack to about $\theta = 60$ deg which is most easily observed from the calculations of Baker (91). Other authors (92–94) have re-emphasized these observations, including the transient states (91).

Experimental photoelastic studies (95) confirm these results and observations of crack branching at velocities near 0.5 C_2 add further evidence.

In addition, Mott (96) and Roberts (97) studied the acceleration of a crack through dimensional considerations and obtained results tentatively in agreement with those above.

Most important in this discussion of dynamic effects is that the stress fields, Eq 99, are preserved in a form nearly identical to the elastic stress up to very high velocities, that is, $C \rightarrow 0.5\ C_2$. Moreover, the $1/r^{1/2}$ singularity appears for all velocities so that fracture size effects are virtually unchanged.

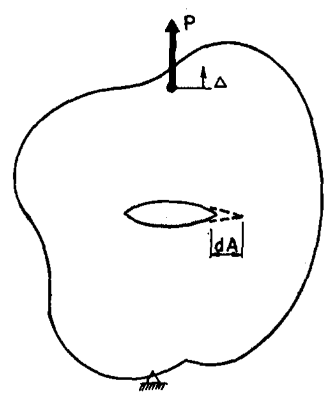

FIG. 24—A Crack in a Body of Arbitrary Shape Subjected to a Load.

ENERGY-RATE ANALYSIS OF CRACK EXTENSION

Griffith (1) in his original analysis of fracture and later Irwin (98) and Orowan (99) discussed the equilibrium and stability of cracks from an energy-rate viewpoint. Subsequently, Irwin (100,4,5) provided a more detailed study of the energy-rate analysis and its relationship to the crack-tip stress field approach. The details were further generalized and clarified by other authors (20,41,101). The results of these works prove the equivalence of the energy-rate and stress-intensity factor approaches. Application to "compliance calibration" (that is, experimental determination of energy rates) of test configurations is an additional benefit. This discussion will proceed to cover the essential features of energy considerations.

An elastic body subjected to loads and containing an extending crack provides an energy rate (that is, energy per unit of new crack area generated), $\mathcal{G}$, available for the crack-extension process. Referring to Fig. 24, the available energy for an increment of crack extension, dA, is provided from work done by the force, $Pd\Delta$, and the release, $-dV$, in the total strain energy, V, stored in the body (100). Consequently,

$$\mathcal{G} = P\frac{d\Delta}{dA} - \frac{dV}{dA} \quad \text{.......(101)}$$

the displacements of a linear elastic body are related to the load by

$$\Delta = \lambda P \quad \text{............(102)}$$

where λ is the compliance (that is, inverse spring constant), which depends upon the configuration, including the crack size, A.

The strain energy in the body is work done in loading, that is,

$$V = \frac{P\Delta}{2} = \frac{\lambda P^2}{2} \quad \text{.........(103)}$$

From Eqs 102 and 103 and, using the rule of differentiation,

$$\frac{d}{dA} = \frac{\partial}{\partial A} + \frac{dP}{dA}\cdot\frac{\partial}{\partial P} \quad \text{......(104)}$$

Eq 101 becomes

$$\mathcal{G} = \frac{P^2}{2}\frac{\partial\lambda}{\partial A} \quad \text{..........(105)}$$

Terms involving dP cancel in Eq 105. Therefore, the available energy rate, $\mathcal{G}$, for infinitesimal crack extension is independent of the type of load application, for example, fixed grips, constant forces, or intermediate cases. This result applies for an unlimited number of forces on the body (41) and for mixed types of load application (101).

Equation 105 is useful for the experimental determination of energy rates of test configurations. This is accomplished through measurement of the compliance, λ, as a function of crack size, A, in order to compute the derivative in Eq 105. Though this so-called "compliance calibration" method is straightforward in principal, the derivative depends on small changes in λ, which in practice require very accurate measurement techniques.

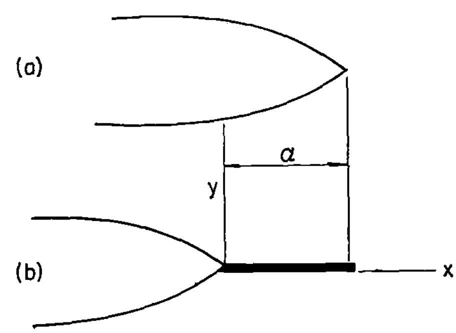

FIG. 25—The Tip of a Crack (*a*) Which Has Been Pulled Closed (*b*) Along a Segment Adjacent to the Tip.

THE EQUIVALENCE OF ENERGY-RATE AND STRESS-INTENSITY FACTOR APPROACHES

In the previous section it was noticed that the energy rate, $\mathcal{G}$, is independent of the type of load application. Hence, for convenience in the discussion to follow, the fixed-grip situation may be employed with no loss in generality of results.

If an elastic body is loaded and the grips (load-point displacements) are then fixed, the strain-energy change, dV/dA, is the only contribution to $\mathcal{G}$ (see Eq 101). Under this condition, the work required to close a small segment of the crack, α, as shown in Fig. 25, from the opened position, (a), to the closed position, (b), is identical to the change in the strain energy. The work can be computed as the crack-surface tractions required to close the crack times their closing displacements times one half (since the displacements will be proportional to the tractions). The tractions required are the stresses on the prospective crack surface with the tip at $x = 0$ as in Fig. 25(b). The displacements are the crack-surface displacements of corresponding points in Fig. 25(a).

Therefore, as originally proposed by Irwin (**4,5,7**), the energy rate, $\mathcal{G}$, can be obtained from these considerations in the form

$$\mathcal{G} = \frac{dV}{dA}\bigg|_{\text{fixed grips}} = \lim_{\alpha \to 0} \frac{2}{\alpha} \cdot \int_0^\alpha \left(\frac{\sigma_y v}{2} + \frac{\tau_{yx} u}{2} + \frac{\tau_{yz} w}{2} \right) dx \quad \text{..(106)}$$

The stresses, σ_y, τ_{yx} and τ_{yz}, may be obtained from the crack-tip stress field equations, such as Eqs 1, 2, and 3, with $r = x$ and $\theta = 0$. The corresponding displacements are also those of the crack-tip field equations, but with $r = \alpha - x$ and $\theta = \pi$.

For the isotropic case, the result of these substitutions and performance of the integration in Eq 106 leads to (for plane strain):

$$\mathcal{G} = \frac{1 - \nu}{2G} K_I^2 + \frac{1 - \nu}{2G} K_{II}^2 + \frac{1}{2G} K_{III}^2 \quad \text{..(107)}$$

The terms on the right-hand side of Eq 107 indicate that the energy-rate contribution of each mode of crack-tip stress field may be considered separately Since $E = 2(1 + \nu)G$, the separate contributions are (for plane strain):

$$\left.\begin{aligned} \mathcal{G}_I &= \frac{(1 - \nu^2)}{E} K_I^2 \\ \mathcal{G}_{II} &= \frac{(1 - \nu^2)}{E} K_I^2 \\ \mathcal{G}_{III} &= \frac{1 + \nu}{E} K_{III}^2 \end{aligned}\right\} \quad \text{.......(108)}$$

where

$$\mathcal{G} = \mathcal{G}_I + \mathcal{G}_{II} + \mathcal{G}_{III} \quad \text{......(109)}$$

Equations 108 and 109 also may be adopted to the case of plane stress by appropriately discarding $(1 - \nu^2)$ in the first two of Eqs 108.

TABLE 6—ELASTIC COEFFICIENTS RELATING ENERGY RATES TO STRESS-INTENSITY FACTORS.

$(\mathcal{G}_i = cK_i^2)$

(Values of c given below for the case of plane strain)

Mode	Isotropic (**5**)	Orthotropic (**32**) $A_{16} = A_{26} = A_{45} = 0$	Anisotropic
I......	$\frac{(1 - \nu^2)}{E}$	$\left(\frac{A_{11}A_{22}}{2}\right)^{1/2}\left[\frac{A_{22}}{A_{11}} + \frac{2A_{12} + A_{66}}{2A_{11}}\right]^{1/2}$	$\frac{1}{2}\,\mathrm{Im}\left[-A_{22}\frac{(\mu_1 + \mu_2)}{\mu_1\mu_2}\right]$
II......	$\frac{(1 - \nu^2)}{E}$	$\frac{A_{11}}{2}\left[\frac{A_{22}}{A_{11}} + \frac{2A_{12} + A_{66}}{2A_{11}}\right]^{1/2}$	$\frac{1}{2}\,\mathrm{Im}\,[A_{11}(\mu_1 + \mu_2)]$
III......	$\frac{(1 + \nu)}{E}$	$\frac{1}{2(A_{44}A_{55})^{1/2}}$	$\frac{1}{2}\frac{(A_{44}A_{55} - A_{45}^2)^{1/2}}{A_{44}A_{55}}$

As a consequence of Eqs 108 and 109, the direct relationship between energy rates and stress-intensity factors has been illustrated.

Equation 106 can also be used to determine the relationships between energy rates and stress-intensity factors for other elastic media. For example, the relationships for anisotropic media can be obtained by using the appropriate stress fields, Eqs 81 and 94, and corresponding displacements in Eq 106. Table 6 provides the modified elastic coefficients for the equivalent of Eqs 108 for orthotropic (32) and general anisotropic[9] media. Equation 109 applies to orthotropic media, but in its present form not to the general anisotropic case.

However, since cracks normally do not extend in a planar fashion (53) with K_{II} and K_{III} present, or even with K_I present in generally anisotropic media, these relationships are somewhat of academic interest. It is sufficient to have shown the equivalence of the energy-rate and stress-intensity factor approaches, in order that the direct relationship between the Griffith theory and current theories of fracture mechanics be fully understood.

OTHER EQUIVALENT METHODS OF STRESS ANALYSIS OF CRACKS AND NOTCHES

Several other methods of stress analysis of cracks and notches for incorporation into failure criteria have been proposed. The most notable in the recent literature are those developed by Neuber (10,102), Kuhn (66,103), and Barenblatt (23). Identical to the elastic field approach, each of these methods uses an elastic stress analysis to determine the general character of redistribution of force transmission around cracks. In addition, it is important to note that each of these analyses draws attention to a phenomenon at the crack tip which is regarded as that which precipitates failure.

More specifically, these phenomena are: developing a plastic particle of critical size, developing the ultimate stress at a specific radius from the crack tip, and developing stresses approaching the cohesive bond forces ahead of a crack, respectively. Now, since each of these phenomena occurs imbedded within the elastic crack-tip stress field, their occurrence will always correspond to having that stress field reach a critical value. As a consequence, these and any other methods which draw attention to specific critical phenomena at a crack tip, which proceed to use an essentially elastic stress analysis, will lead to a failure theory equivalent to the current fracture mechanics concept of critical values of stress-intensity factors.

Even though these alternative methods may be regarded as just as true, correct and, useful in a practical sense, the attention that each draws to a specific phenomenon within the crack-tip stress field embodies an assumption which is unnecessarily restrictive in formulating a failure criterion. The strength and generality of fracture mechanics as based on the stress-field approach is in part due to the absence of such an assumption.

On the other hand, this does not mean that the phenomena which do in fact occur within the stress fields near crack tips should be disregarded. Attention to the details of the processes by which materials resist cracking will undoubtedly lead to development of superior materials. Each of the alternative theories of fracture mentioned above (and others) does in fact draw attention to a phenomenon which may be a key feature in the fracture process. Therefore, their high worth in con'unction with and complimentary to the methods of fracture mechanics is clear.

LIMITATIONS OF THE CRACK-TIP STRESS FIELD ANALYSES

In this paper results of linear elastic stress analyses of cracked bodies have been presented for a typical variety of problems which have already been treated. The determination of stress-intensity factors for any particular problem can with time be accomplished. Therefore, the elastic stress analysis is not in itself a real limitation on fracture mechanics.

However, the accomplishment of a stress analysis does represent a delay in the application of fracture mechanics to configurations with cracks which have not yet been treated. Moreover, the accuracy of known solutions for stress-intensity factors represents a temporary limitation on the accuracy of immediate applications. Usually, this limitation is far less severe than others, such as variability of materials, in practical applications. Consequently, the elastic stress analysis itself may be regarded as "exact" and the real limitations of fracture mechanics come only in its application to situations where nonlinearity of material behavior at the crack tip (or elsewhere) disrupts the gross features of the stress distribution.

A certain amount of nonlinear behavior such as plasticity can be tolerated within the crack-tip stress field without grossly affecting the field outside the nonlinear region. Moreover, the disturbances, if embedded within identical fields, will themselves be identical and hence self-compensating in comparisons of fracture strengths. Therefore, it is important to resolve the relative sizes of zones of nonlinearity which can be tolerated within the crack-tip stress fields. This size is of course related to the relative size in which the field equations, such as Eqs 1, apply.

For the configuration shown in Fig. 3, the approximate stress, σ_y, ahead of the crack, obtained by substituting Eq 4 into Eq 1 and setting $\theta = 0$, is:

$$\sigma_{y\,\mathrm{approx}} = \frac{\sigma a^{1/2}}{(2r)^{1/2}} \quad \text{.......(109)}$$

The exact stress can be most easily determined by the Westergaard stress function technique, see Appendix I, and is:

$$\sigma_{y\,\mathrm{exact}} = \frac{\sigma(a + r)}{(2ar + r^2)^{1/2}} \quad \text{.....(110)}$$

where, in Eqs 109 and 110, r is the distance ahead of the crack tip along the crack line.

Now, taking the ratio of the exact to the approximate stresses gives:

$$\frac{\sigma_{y\,\mathrm{approx}}}{\sigma_{y\,\mathrm{exact}}} = \frac{\left(1 + \frac{r}{2a}\right)^{1/2}}{\left(1 + \frac{r}{a}\right)} \quad \text{.....(111)}$$

In a similar fashion, this ratio may also be computed for the configuration shown in Fig. 23 and is:

$$\frac{\sigma_{y\,\mathrm{approx}}}{\sigma_{y\,\mathrm{exact}}} = \left(1 + \frac{r}{a}\right)\left(1 + \frac{r}{2a}\right)^{1/2} \quad \text{..(112)}$$

The types of loading in these two configurations, Figs. 3 and 23, are opposite extremes, yet Eqs 111 and 112 show similar deviations of the approximate stresses from the exact, at like values of r/a. Therefore, if the relative tolerable size (compared to crack size, a) of zone of nonlinearity can be established for one configuration it is bound to be applicable to others.

Recent experimental evidence (70) indicates the validity of the elastic stress field approach up to stress levels, σ, of 0.8 of the yield strength, σ_{yp}, for the configuration shown in Fig. 3. For this configuration, the width, ω, of the zone of plasticity is predicted to be (72):

$$\omega = \frac{1}{2}\left(\frac{\sigma}{\sigma_{YP}}\right)^2 a \quad \text{.........(113)}$$

Substituting the upper limit of stress, $\sigma = 0.8\ \sigma_{YP}$, mentioned above, the relative size, w/a or r/a, for reasonable accuracy is about 0.3 from Eq 113. For this value of r/a, Eq 111 predicts a deviation of actual stresses from the field equations of about 20 per cent. Thus it appears that the zone of nonlinearity at a crack tip may be fairly sizable, that is, of the order of 0.3 of the crack length (and other planar dimensions such as net-section width), without grossly disturbing the usefulness of the elastic stress field approach. However, a more extensive evaluation of this limitation should be the subject of further research.

In addition to nonlinearity in the region of the crack tip, consideration of other conditions (such as anisotropic and viscous effects having cracks in the bond line between dissimilar materials, thermal stresses, couple stresses, inertial effects of moving cracks) and of all three modes of crack-tip stress fields, has led to positive results. The conclusion is that the current techniques of fracture mechanics may be extended to all of these areas, since similar types of crack-tip stress fields exist for them and the stress-intensity factor methods of assessing failure should apply equally well. At any rate, this conclusion should give full confidence that slight amounts of these effects do not invalidate the useful application of the concepts of fracture mechanics.

As a consequence of the above remarks, it is observed that the only real limitation of elastic stress analysis commences with the advent of sizable zones of nonlinearity that is, plasticity, at the crack tip. The current hope for extension of the applicability of fracture mechanics to such situations lies in developing a full analysis based on the theory of plasticity. This topic is a subject left for other discussions.

Acknowledgment:

The authors gratefully acknowledge the support of this work under the NASA Grant NsG 410 to the Lehigh University Institute of Research. Portions of the analysis were based on previous work supported under grants from the National Science Foundation, G24145, and the Boeing Co.

The many suggestions and data provided by W. F. Brown, O. L. Bowie, and G. R. Irwin were most helpful in preparation of this paper. Appreciation is also expressed for aid in collecting information for Appendix II given by M. Kassir of the Department of Mechanics of Lehigh Univerisity.

APPENDIX I

THE WESTERGAARD METHOD OF STRESS ANALYSIS OF CRACKS

Any elementary text on the theory of elasticity gives a full development of the equations for plane extension. The equilibrium equations are:

$$\left.\begin{aligned} &\frac{\partial \sigma_x}{\partial x} + \frac{\partial \tau_{xy}}{\partial y} = 0 \\ &\frac{\partial \tau_{xy}}{\partial x} + \frac{\partial \sigma_y}{\partial y} = 0 \\ &\tau_{xy} = \tau_{yx} \end{aligned}\right\} \quad \text{........(114)}$$

The strain-displacement relationships and Hooke's law lead to the compatability equation:

$$\nabla^2(\sigma_x + \sigma_y) = \left(\frac{\partial^2}{\partial x^2} + \frac{\partial^2}{\partial y^2}\right)(\sigma_x + \sigma_y) = 0 \quad \text{..(115)}$$

The equilibrium equations (114) are automatically satisfied by defining an Airy stress function, Φ, in terms of its relationship to the stresses, that is,

$$\left.\begin{aligned}\sigma_x &= \frac{\partial^2\Phi}{\partial y^2}\\ \sigma_y &= \frac{\partial^2\Phi}{\partial x^2}\\ \tau_{xy} &= \frac{-\partial^2\Phi}{\partial x\partial y}\end{aligned}\right\}\quad\text{(116)}$$

Substituting Eq 116 into Eq 115 leads to:

$$\nabla^4\Phi = \nabla^2(\nabla^2\Phi) = 0 \quad\text{(117)}$$

In order to solve a problem, the stress function, Φ, must satisfy Eq 117 and the boundary conditions of that problem.

Choosing the stress function, Φ, to be:

$$\Phi = \psi_1 + x\psi_2 + y\psi_3 \quad\text{(118)}$$

it will automatically satisfy Eq 117 if the ψ_i are each harmonic, that is,

$$\nabla^2\psi_i = 0 \quad\text{(119)}$$

Define a complex variable, z, by

$$z = x + iy \quad\text{(120)}$$

Functions of that complex variable, $\bar{\bar{Z}}(z)$, and its derivatives,

$$\bar{Z} = \frac{d\bar{\bar{Z}}}{dz}, \qquad Z = \frac{d\bar{Z}}{dz}, \qquad Z' = \frac{dZ}{dz} \quad\text{(121)}$$

have harmonic real and imaginary parts, if the function is analytic, for example, if $\bar{Z} = \text{Re}\,\bar{Z} + i\,\text{Im}\,\bar{Z}$, then

$$\nabla^2(\text{Re}\,\bar{Z}) = \nabla^2(\text{Im}\,\bar{Z}) = 0 \quad\text{(122)}$$

This is a result of the Cauchy-Riemann conditions, that is,

$$\left.\begin{aligned}\frac{\partial\text{Re}\,\bar{Z}}{\partial x} &= \frac{\partial\text{Im}\,\bar{Z}}{\partial y} = \text{Re}\,Z\\ \frac{\partial\text{Im}\,\bar{Z}}{\partial x} &= -\frac{\partial\text{Re}\,\bar{Z}}{\partial y} = \text{Im}\,Z\end{aligned}\right\}\quad\text{(123)}$$

Equations 123 may be used to differentiate these functions $\bar{\bar{Z}}$ through Z.

First Mode:

In conformity with Eqs 118–123, Westergaard (8) defined an Airy stress function, Φ, by

$$\Phi_{\text{I}} = \text{Re}\,\bar{\bar{Z}}_{\text{I}} + y\,\text{Im}\,\bar{Z}_{\text{I}} \quad\text{(124)}$$

which as a consequence automatically satisfies equilibrium and compatability, Eqs 114 and 117.

Using Eqs 116 and 123, the stresses resulting from Φ, as defined in Eq 124, are

$$\left.\begin{aligned}\sigma_x &= \text{Re}\,Z_{\text{I}} - y\,\text{Im}\,Z_{\text{I}}'\\ \sigma_y &= \text{Re}\,Z_{\text{I}} + y\,\text{Im}\,Z_{\text{I}}'\\ \tau_{xy} &= -y\,\text{Re}\,Z_{\text{I}}'\end{aligned}\right\}\quad\text{(125)}$$

Now any function, Z_{I}, which is analytic in the region except for a particular branch cut along a portion of the x-axis will have the form

$$Z_{\text{I}} = \frac{g(z)}{[(z+b)(z-a)]^{1/2}} \quad\text{(126)}$$

This will solve crack problems for a crack along the x-axis from $x = -b$ to $x = a$, ($y = 0$), if $g(z)$ is well behaved, since the stresses, σ_y and τ_{xy}, along that interval are zero, provided that

$$\text{Im}\,g(x) = 0 \text{ (for } -b < x < a) \quad\text{(127)}$$

For example, if the function

$$Z_{\text{I}} = \frac{\sigma z}{(z^2 - a^2)^{1/2}} \quad\text{(128)}$$

is examined, it solves the problem of a stress-free crack at $-a < x < a$, $y = 0$, and leads to boundary conditions of uniform biaxial stress, σ, at infinity (see Fig. 3).

Now, reverting to the more general case, Eq 126, a substitution of variable

$$\zeta = z - a \quad\text{(129)}$$

leads to

$$Z_{\text{I}} = \frac{f(\zeta)}{\zeta^{1/2}} \quad\text{(130)}$$

where, from Eqs 126 and 127, $f(\zeta)$ is well behaved for small $|\zeta|$ (that is, near the crack tip at $x = a$). Moreover, in that region, as $|\zeta| \to 0$, f may be replaced by a real constant, or Eq 130 may be written

$$Z_{\text{I}}\,\Big|_{|\zeta|\to 0} = \frac{K_{\text{I}}}{(2\pi\zeta)^{1/2}} \quad\text{(131)}$$

Other stress functions, Z_{I}, for crack problems, such as Eq 16, will also always lead to this form. Noting that Eq 131 may be substituted into Eqs 125, and using polar coordinates, that is,

$$\zeta = re^{i\theta} \quad \text{(132)}$$

the crack-tip stress field is:

$$\left.\begin{aligned}\sigma_x &= \frac{K_{\mathrm{I}}}{(2\pi r)^{1/2}}\cos\frac{\theta}{2}\left[1-\sin\frac{\theta}{2}\sin\frac{3\theta}{2}\right]\\ \sigma_y &= \frac{K_{\mathrm{I}}}{(2\pi r)^{1/2}}\cos\frac{\theta}{2}\left[1+\sin\frac{\theta}{2}\sin\frac{3\theta}{2}\right]\\ \tau_{xy} &= \frac{K_{\mathrm{I}}}{(2\pi r)^{1/2}}\sin\frac{\theta}{2}\cos\frac{\theta}{2}\cos\frac{3\theta}{2}\end{aligned}\right\} \quad \text{(133)}$$

where, from Eq 131,

$$K_{\mathrm{I}} = \lim_{|\zeta|\to 0} (2\pi\zeta)^{1/2} Z_{\mathrm{I}} \quad \text{(134)}$$

The strain in the y-direction can be written in terms of displacements and stresses by Hooke's law, or

$$\epsilon_y = \frac{\partial v}{\partial y} = \frac{\sigma_y}{E} - \frac{\nu}{E}(\sigma_x + \sigma_z) \quad \text{(135)}$$

For plane strain, Hooke's law ($\epsilon_z = 0$) also leads to

$$\sigma_z = \nu(\sigma_x + \sigma_y) \quad \text{(136)}$$

Substituting Eqs 125 and 136 into Eq 135 and integrating lead to

$$v = \frac{1+\nu}{E}[2(1-\nu)\,\mathrm{Im}\,\bar{Z}_{\mathrm{I}} - y\,\mathrm{Re}\,Z_{\mathrm{I}}] \quad \text{(137)}$$

Similarly, consideration for ϵ_x gives

$$u = \frac{1+\nu}{E}[(1-2\nu)\,\mathrm{Re}\,\bar{Z}_{\mathrm{I}} - y\,\mathrm{Im}\,Z_{\mathrm{I}}] \quad \text{(138)}$$

Substituting Eqs 131 and 132 into Eqs 137 and 138 and noting $E = 2G(1+\nu)$ lead to

$$\left.\begin{aligned}u &= \frac{K_{\mathrm{I}}}{G}(r/2\pi)^{1/2}\cos\frac{\theta}{2}\cdot\left[1-2\nu+\sin^2\frac{\theta}{2}\right]\\ v &= \frac{K_{\mathrm{I}}}{G}(r/2\pi)^{1/2}\sin\frac{\theta}{2}\cdot\left[2-2\nu-\cos^2\frac{\theta}{2}\right]\\ &\text{(for plane strain, } w = 0)\end{aligned}\right\} \quad \text{(139)}$$

Equations 133, 134, 136, and 139 are the resulting crack-tip stress and displacement field, that is, Eqs 1 and 13, for the first mode.

Second Mode:

Instead of choosing the Airy stress function as in Eq 124, it is equally permissible to choose the form,

$$\Phi_{\mathrm{II}} = -y\,\mathrm{Re}\,\bar{Z}_{\mathrm{II}} \quad \text{(140)}$$

Repeating all of the operations from Eqs 124–139 and again making use of Eqs 114–123 lead to:

$$\left.\begin{aligned}\sigma_x &= 2\,\mathrm{Im}\,Z_{\mathrm{II}} + y\,\mathrm{Re}\,Z_{\mathrm{II}}'\\ \sigma_y &= -y\,\mathrm{Re}\,Z_{\mathrm{II}}'\\ \tau_{xy} &= \mathrm{Re}\,Z_{\mathrm{II}} - y\,\mathrm{Im}\,Z_{\mathrm{II}}'\end{aligned}\right\} \quad \text{(141)}$$

and

$$\left.\begin{aligned}u &= \frac{1+\nu}{E}\cdot[2(1-\nu)\,\mathrm{Im}\,\bar{Z}_{\mathrm{II}} + y\,\mathrm{Re}\,Z_{\mathrm{II}}]\\ v &= \frac{1+\nu}{E}\cdot[-(1-2\nu)\,\mathrm{Re}\,\bar{Z}_{\mathrm{II}} - y\,\mathrm{Im}\,Z_{\mathrm{II}}]\end{aligned}\right\} \quad \text{(142)}$$

and in the neighborhood of a crack tip, that is, $|\zeta| \to 0$,

$$Z_{\mathrm{II}}\Big|_{|\zeta|\to 0} = \frac{K_{\mathrm{II}}}{(2\pi\zeta)^{1/2}} \quad \text{(143)}$$

or

$$K_{\mathrm{II}} = \lim_{|\zeta|\to 0}(2\pi\zeta)^{1/2}Z_{\mathrm{II}} \quad \text{(144)}$$

In addition, near the crack tip, substitution of Eq 143 into Eqs 141 and 142 leads to:

$$\left.\begin{aligned}\sigma_x &= \frac{-K_{\mathrm{II}}}{(2\pi r)^{1/2}}\sin\frac{\theta}{2}\cdot\left[2+\cos\frac{\theta}{2}\cos\frac{3\theta}{2}\right]\\ \sigma_y &= \frac{K_{\mathrm{II}}}{(2\pi r)^{1/2}}\cos\frac{\theta}{2}\sin\frac{\theta}{2}\cos\frac{3\theta}{2}\\ \tau_{xy} &= \frac{K_{\mathrm{II}}}{(2\pi r)^{1/2}}\cos\frac{\theta}{2}\cdot\left[1-\sin\frac{\theta}{2}\sin\frac{3\theta}{2}\right]\end{aligned}\right\} \quad \text{(145)}$$

and, for plane strain,

$$\left.\begin{aligned} u &= \frac{K_{II}}{G}(r/2\pi)^{1/2}\sin\frac{\theta}{2} \cdot \left[2 - 2\nu + \cos^2\frac{\theta}{2}\right] \\ v &= \frac{K_{II}}{G}(r/2\pi)^{1/2}\cos\frac{\theta}{2} \cdot \left[1 - 2\nu + \sin^2\frac{\theta}{2}\right] \end{aligned}\right\} \quad (146)$$

These results are reflected in Eqs 2 and 14, for the second mode.

The first and second modes may be superimposed, since

$$\Phi = \Phi_I + \Phi_{II} \quad (147)$$

is a perfectly permissible Airy stress function, in which case stress and displacement components should simply be added to each other.

Third Mode:

The plane (two-dimensional) problem of pure shear may be specified by:

$$u = 0, \quad v = 0, \quad w = w(x,y) \quad (148)$$

The strain-displacement equations and Hooke's law give (105)

$$\left.\begin{aligned} \gamma_{xz} &= \frac{\partial w}{\partial x} = \frac{\tau_{xz}}{G} \\ \gamma_{yz} &= \frac{\partial w}{\partial y} = \frac{\tau_{yz}}{G} \end{aligned}\right\} \quad (149)$$

The stress components, σ_x, σ_y, σ_z, and τ_{xy}, all vanish so the equilibrium equations become

$$\frac{\partial \tau_{xz}}{\partial x} + \frac{\partial \tau_{yz}}{\partial y} = 0 \quad (150)$$

which, when combined with Eqs 149, gives

$$\nabla^2 w = 0 \quad (151)$$

Choosing

$$w = \frac{1}{G}\,\mathrm{Im}\, Z_{III} \quad (152)$$

leads to

$$\left.\begin{aligned} \tau_{xz} &= \mathrm{Im}\, Z_{III}' \\ \tau_{yz} &= \mathrm{Re}\, Z_{III}' \end{aligned}\right\} \quad (153)$$

The stress function, Z_{III}, for a crack along the negative y-axis to the origin, takes the form near the crack tip

$$Z_{III}\Big|_{|\zeta|\to 0} = \frac{K_{III}}{(2\pi\zeta)^{1/2}} \quad (154)$$

Consequently,

$$K_{III} = \lim_{|\zeta|\to 0} (2\pi\zeta)^{1/2} Z_{III} \quad (155)$$

Moreover, substituting Eq 154 into Eqs 152 and 153 and using Eq 132 lead to

$$\left.\begin{aligned} \tau_{xz} &= -\frac{K_{III}}{(2\pi r)^{1/2}}\sin\frac{\theta}{2} \\ \tau_{yz} &= \frac{K_{III}}{(2\pi r)^{1/2}}\cos\frac{\theta}{2} \end{aligned}\right\} \quad (156)$$

and

$$w = \frac{K_{III}}{G}(2r/\pi)^{1/2}\sin\frac{\theta}{2} \quad (157)$$

These results are reflected in Eqs 3 and 15 for the third mode.

APPENDIX II

A HANDBOOK OF BASIC SOLUTIONS FOR STRESS-INTENSITY FACTORS AND OTHER FORMULAS

The results to be presented for stress-intensity factors will conform with their definition as implied by Eqs 1–3, 48, 81, and 94. References which contain further results and details will be listed for the readers convenience.

A selection of solutions for stress-intensity factors, in addition to those already listed, will be chosen on the basis of their generality. Since superposition may be used, that is, addition of the stress-intensity factors for each mode, the results which lend themselves to generation of other solutions will be emphasized.

Formulas for Determination of Stress-Intensity Factors from Stress Concentrations:[9]

Mode I:

$$K_{\text{I}} = \lim_{p\to 0} \frac{\pi^{1/2}}{2} \sigma_{\max} p^{1/2} \quad \ldots\ldots(158)$$

provided $K_{\text{II}} = K_{\text{III}} = 0$, and where p is the tip radius of the notch and $\sigma_{\max}$ is the maximum normal stress adjacent to the tip (see Eq 9).

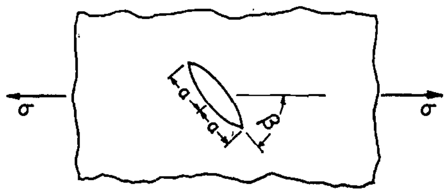

FIG. 26—A Crack in an Infinite Sheet Subjected to Uniform Tension at an Arbitrary Inclination.

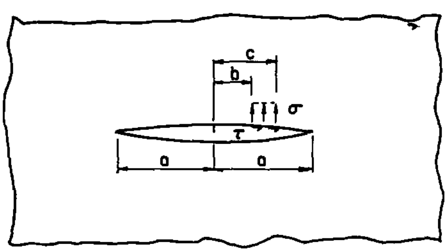

FIG. 27—A Crack in an Infinite Sheet with Uniform Loads on Part of the Crack Surface.

Mode II:

$$K_{\text{II}} = \lim_{p\to 0} \pi^{1/2} \sigma_{\max} p^{1/2} \quad \ldots\ldots(159)$$

provided $K_{\text{I}} = K_{\text{III}} = 0$ etc.

Mode III:

$$K_{\text{III}} = \lim_{p\to 0} \pi^{1/2} \tau_{\max} p^{1/2} \quad \ldots\ldots(160)$$

provided $K_{\text{I}} = K_{\text{II}} = 0$, and where $\tau_{\max}$ is the maximum shear stress adjacent to the tip of the notch.

Infinite Sheets Subjected to in-Plane Loads: (See Fig. 26).

$$\left.\begin{aligned} K_{\text{I}} &= \sigma \sin^2 \beta (\pi a)^{1/2} \\ K_{\text{II}} &= \sigma \sin \beta \cos \beta (\pi a)^{1/2} \\ \phi(\eta) &= -\frac{\sigma(1 - e^{2i\beta})a}{4\eta} \end{aligned}\right\} \quad \ldots(161)$$

These cases may be found by the method of Ref (**18**) or via Eqs 33 or by superimposing results of Eqs 4 and 6. (Note that all other cases of uniform loading at infinity or on the crack surface may be derived from this case by superposition.)

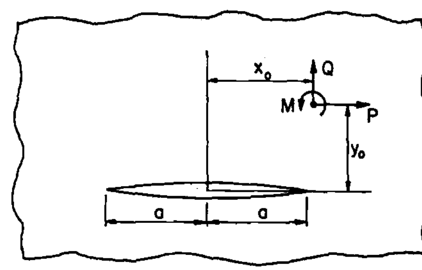

FIG. 28—A Crack in an Infinite Sheet Subjected to an Arbitrary Force and Couple at a Remote Point.

For the right end of the crack in Fig. 27,

$$\left.\begin{aligned} K_{\text{I}} &= \frac{\sigma a^{1/2}}{2\pi^{1/2}} \left\{ \sin^{-1}\frac{c}{a} - \sin^{-1}\frac{b}{a} - \left(1 - \frac{c^2}{a^2}\right)^{1/2} + \left(1 - \frac{b^2}{a^2}\right)^{1/2} \right\} \\ &\quad + \frac{\tau(c-b)}{2(\pi a)^{1/2}} \left(\frac{\kappa - 1}{\kappa + 1}\right) \\ K_{\text{II}} &= \frac{\sigma(c-b)}{2(\pi a)^{1/2}} \left(\frac{\kappa - 1}{\kappa + 1}\right) + \frac{\tau a^{1/2}}{2\pi^{1/2}} \\ &\quad \cdot \left\{ \sin^{-1}\frac{c}{a} - \sin^{-1}\frac{b}{a} - \left(1 - \frac{c^2}{a^2}\right)^{1/2} + \left(1 - \frac{b^2}{a^2}\right)^{1/2} \right\} \end{aligned}\right\} \quad \ldots(162)$$

where

$\kappa = 3 - 4\nu$ (plane strain)

$\kappa = (3 - \nu)/(1 + \nu)$ (plane stress)

See also Eqs 32.

For the right end of the crack in Fig. 28,

$$K = K_{\mathrm{I}} - iK_{\mathrm{II}} = \frac{1}{2(\pi a)^{1/2}(1+\kappa)}$$

$$\Bigg\{(P + i\;\,)\left[\frac{a + z_0}{(z_0{}^2 - a^2)^{1/2}} - \frac{\kappa(a + \;_0)}{(z_0{}^2 - a^2)^{1/2}} - 1 + \kappa\right]$$

$$+ \frac{a(P - iQ)(\bar{z}_0 - z_0) + ai(1+\kappa)M}{(\bar{z}_0 - a)(\bar{z}_0{}^2 - a^2)^{1/2}}\Bigg\} \quad \ldots (163)$$

where

$z_0 = x_0 + iy_0$

$\bar{z}_0 = x_0 - iy_0$

See Refs (**21**–**23**) or Eqs 33.

At the near ends of two equal colinear cracks (see Fig. 29),

$$\left.\begin{aligned} K_{\mathrm{I}} &= \sigma(\pi/a)^{1/2}\,\frac{b^2\dfrac{E(k)}{K(k)} - a^2}{(b^2 - a^2)^{1/2}} \\ K_{\mathrm{II}} &= \tau(\pi/a)^{1/2}\,\frac{b^2\dfrac{E(k)}{K(k)} - a^2}{(b^2 - a^2)^{1/2}} \end{aligned}\right\} \quad \ldots (164)$$

At the far ends (see Fig. 29),

$$\left.\begin{aligned} K_{\mathrm{I}} &= \sigma\,(\pi b)^{1/2}\left(\frac{1}{k} - \frac{E(k)}{kK(k)}\right) \\ K_{\mathrm{II}} &= \tau\,(\pi b)^{1/2}\left(\frac{1}{k} - \frac{E(k)}{kK(k)}\right) \end{aligned}\right\} \quad \ldots (165)$$

where $k = [1 - (a^2/b^2)]^{1/2}$ is the modulus of the complete elliptic integrals $E(k)$ and $K(k)$ of the first and second kind, respectively. See Refs (**38**,**23**); and for concentrated forces on the crack surface, see Ref (**21**).

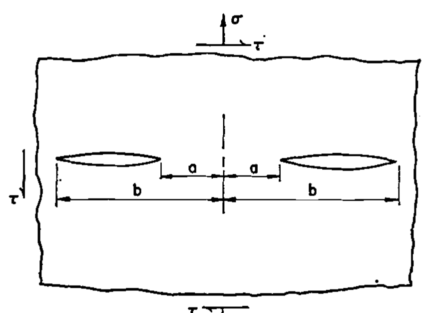

FIG. 29—Two Equal Colinear Cracks in an Infinite Sheet Subjected to Uniform Extension.

For an infinite array of cracks at the ends, denoted by e in Fig. 30,

$$\left.\begin{aligned} K_{\mathrm{I}} = {} & \frac{\sigma\,(4b)^{1/2}\sin\dfrac{\pi c}{2b}}{\left(\cos\dfrac{\pi e}{2b}\left(\sin\dfrac{\pi e}{2b} + \sin\dfrac{\pi c}{2b}\right)\right)^{1/2}} \\ & + \frac{P\left(\sin\dfrac{\pi c}{2b}\right)^{1/2}}{\left(b\sin\dfrac{\pi e}{2b}\cos\dfrac{\pi e}{2b}\cdot\left(\sin\dfrac{\pi e}{2b} + \sin\dfrac{\pi c}{2b}\right)\right)^{1/2}} \\ K_{\mathrm{II}} = {} & 0 \end{aligned}\right\} \quad \ldots (166)$$

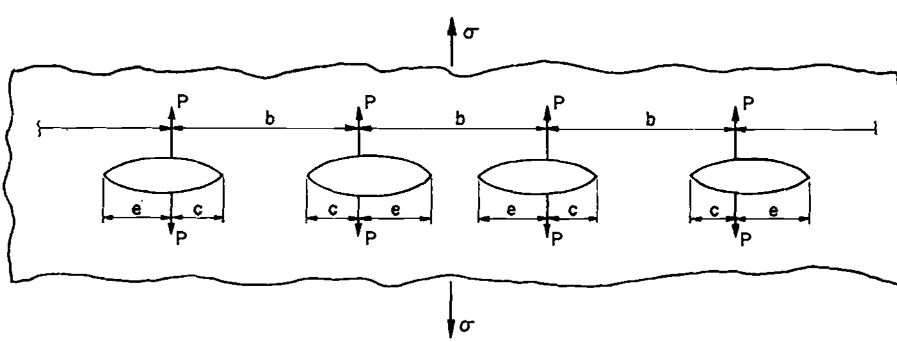

FIG. 30—An Infinite Array of Colinear Cracks in an Infinite Sheet.

For further information see Refs (**4,5**). Note that this result may be used to evaluate eccentrically located cracks in panels.

For the semi-infinite crack in Fig. 31,

$$\left.\begin{aligned} K_{\mathrm{I}} &= \frac{P}{(2\pi c)^{1/2}} \\ K_{\mathrm{II}} &= \frac{Q}{(2\pi c)^{1/2}} \end{aligned}\right\} \quad \ldots (167)$$

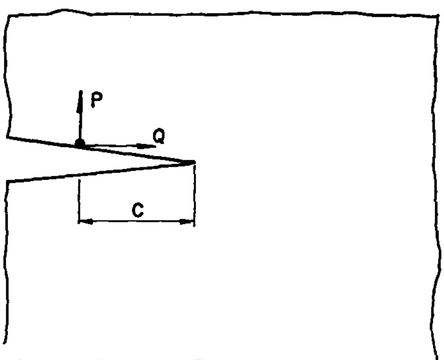

FIG. 31—An Infinite Sheet with a Semi-infinite Crack.

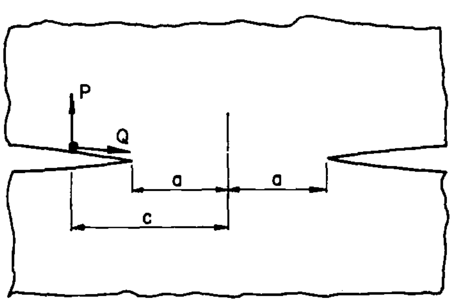

FIG. 32—An Infinite Sheet with Colinear Semi-infinite Cracks with a Concentrated Force.

For further information, see Eqs 32 or Ref (**21**).

For the two semi-infinite cracks in Fig. 32: At the left crack tip,

$$K_{\mathrm{I}} = \frac{P(c^2 - a^2)^{1/2}}{2(\pi a)^{1/2}\,(c - a)}$$

$$K_{\mathrm{II}} = \frac{Q(c^2 - a^2)^{1/2}}{2(\pi a)^{1/2}\,(c - a)}$$

At the right crack tip,

$$\left.\begin{aligned} K_{\mathrm{I}} &= \frac{P(c^2 - a^2)^{1/2}}{2(\pi a)^{1/2}\,(c + a)} \\ K_{\mathrm{II}} &= \frac{Q(c^2 - a^2)^{1/2}}{2(\pi a)^{1/2}\,(c + a)} \end{aligned}\right\} \quad \ldots (168)$$

For further information, see Ref (**21**).

Stress concentrations for deep hyperbolic notches (see Fig. 33 and Ref (**10**)) are as follows.

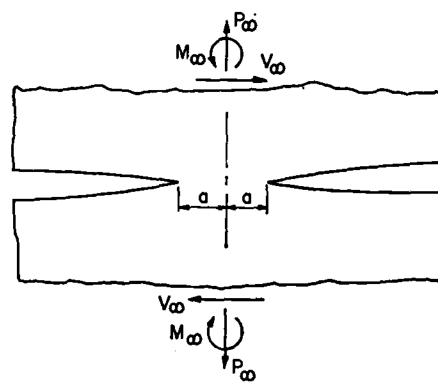

FIG. 33—An Infinite Sheet with Load Transmitted across a Neck Between Hyperbolic Notches (Cracks).

For P_∞ (force per unit thickness) alone:

$$\left.\begin{aligned} \frac{\sigma_{\max}}{\sigma_{\mathrm{net}}} &= \frac{2\left(\dfrac{a}{p}\right)^{1/2}\left(1 + \dfrac{p}{a}\right)}{\left(1 + \dfrac{p}{a}\right)\tan^{-1}\left(\dfrac{a}{p}\right)^{1/2} + \left(\dfrac{p}{a}\right)^{1/2}} \\ \sigma_{\mathrm{net}} &= \frac{P_\infty}{2a} \end{aligned}\right\} \quad \ldots (169)$$

For V_∞ alone:

$$\left.\begin{aligned} \frac{\sigma_{\max}}{\tau_{\mathrm{net}}} &= \frac{\left(\dfrac{a}{p} + 1\right)^{1/2}}{\left(1 + \dfrac{p}{a}\right)\tan^{-1}\left(\dfrac{a}{p}\right)^{1/2} - \left(\dfrac{p}{a}\right)^{1/2}} \\ \tau_{\mathrm{net}} &= \frac{V_\infty}{2a} \end{aligned}\right\} \quad \ldots (170)$$

For M_∞ alone:

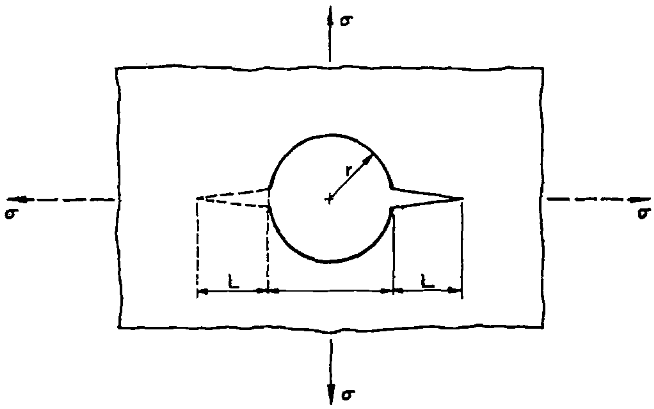

FIG. 34—A Crack (or Cracks) Emanating from a Circular Hole in a Sheet.

TABLE 7—STRESS-INTENSITY FACTOR COEFFICIENTS FOR CRACKS EMANATING FROM A CIRCULAR HOLE.

L/r	$F(L/r)$, One Crack		$F(L/r)$, Two Cracks	
	(uniaxial stress)	(biaxial stress)	(uniaxial stress)	(biaxial stress)
0.00	3.39	2.26	3.39	2.26
0.10	2.73	1.98	2.73	1.98
0.20	2.30	1.82	2.41	1.83
0.30	2.04	1.67	2.15	1.70
0.40	1.86	1.58	1.96	1.61
0.50	1.73	1.49	1.83	1.57
0.60	1.64	1.42	1.71	1.52
0.80	1.47	1.32	1.58	1.43
1.0	1.37	1.22	1.45	1.38
1.5	1.18	1.06	1.29	1.26
2.0	1.06	1.01	1.21	1.20
3.0	0.94	0.93	1.14	1.13
5.0	0.81	0.81	1.07	1.06
10.0	0.75	0.75	1.03	1.03
∞	0.707	0.707	1.00	1.00

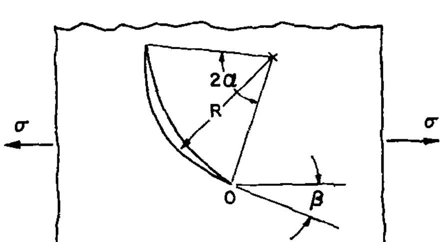

FIG. 35—A Circular-Arc Crack in an Infinite Sheet Subjected to Uniform Tension in an Arbitrary Direction.

$$\left.\begin{aligned} \frac{\sigma_{max}}{\sigma_{net}} &= \frac{4\left(\dfrac{a}{p}\right)^{1/2}}{3\left[\left(\dfrac{p}{a}\right)^{1/2} + \left(1-\dfrac{p}{a}\right)\tan^{-1}\left(\dfrac{a}{p}\right)^{1/2}\right]} \\ \sigma_{net} &= \frac{3M_\infty}{2a^2} \end{aligned}\right\} \quad (171)$$

Using Eqs 158 and 159, for the right crack crack tip,

$$\left.\begin{aligned} K_{I} &= \frac{P_\infty}{(\pi a)^{1/2}} + \frac{2M_\infty}{\pi^{1/2}a^{3/2}} \\ K_{II} &= \frac{V_\infty}{(\pi a)^{1/2}} \end{aligned}\right\} \quad (172)$$

For further information, see Refs (**10,42**).

For cracks emanating from a circular hole (see Fig. 34 and Table 7),

$$\left.\begin{aligned} K_{I} &= \sigma\sqrt{L\pi}\,F\left(\frac{L}{r}\right) \\ K_{II} &= 0 \end{aligned}\right\} \quad (173)$$

For further information, see Ref (**38**).

For a circular crack (see Fig. 35): for the crack tip at 0,

$$
\left.
\begin{aligned}
K_{\mathrm{I}} = {} & \frac{\sigma(\pi R \sin \alpha)^{1/2}}{2\left(1 + \sin^2 \frac{\alpha}{2}\right)} \left\{ \cos \frac{\alpha}{2} \right. \\
& + \cos\left(2\beta + \frac{5}{2}\alpha\right)\left[\sin^2 \frac{\alpha}{2}\right] \\
& - \cos\left(2\beta + \frac{3}{2}\alpha\right)\left[\cos^2 \frac{\alpha}{2} \right. \\
& \left. - \sin^4 \frac{\alpha}{2}\right] - \sin\left(2\beta + \frac{3}{2}\alpha\right) \\
& \left. \cdot \left[\sin \alpha \sin^2 \frac{\alpha}{2}\right] \right\} \\
K_{\mathrm{II}} = {} & \frac{\sigma(\pi R \sin \alpha)^{1/2}}{2\left(1 + \sin^2 \frac{\alpha}{2}\right)} \left\{ \sin \frac{\alpha}{2} \right. \\
& + \sin\left(2\beta + \frac{5}{2}\alpha\right)\left[\sin^2 \frac{\alpha}{2}\right] \\
& + \sin\left(2\beta + \frac{3}{2}\alpha\right)\left[\cos^2 \frac{\alpha}{2} \right. \\
& \left. - \sin \frac{\alpha}{2}\right] - \cos\left(2\beta + \frac{3}{2}\alpha\right) \\
& \left. \cdot \left[\sin \alpha \sin^2 \frac{\alpha}{2}\right] \right\}
\end{aligned}
\right\} \quad \ldots (174)
$$

For further information, see Ref (**18**).

Some Cases of Specified Displacements in Infinite Planes:

For an infinite rigid wedge of constant thickness (see Fig. 36),

$$
\left.
\begin{aligned}
K_{\mathrm{I}} &= \frac{Eh}{(2\pi a)^{1/2}} \quad \text{(for plane stress)} \\
K_{\mathrm{II}} &= 0
\end{aligned}
\right\} \quad \ldots (177)
$$

For further information, see Ref (**23**), which also has a discussion of other examples of wedging.

When stress is applied first, then the boundaries are clamped, and then a crack is introduced, this sequence (see Fig. 37) results in constant energy release rate, $\mathcal{G}_{\mathrm{I}}$, or

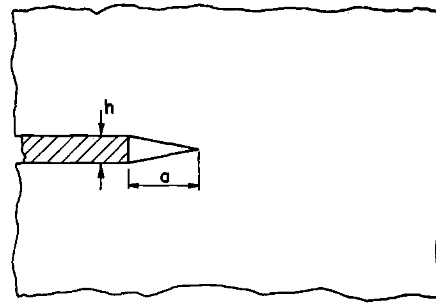

FIG. 36—A Semi-infinite Crack Propped open by a Wedge of Constant Thickness.

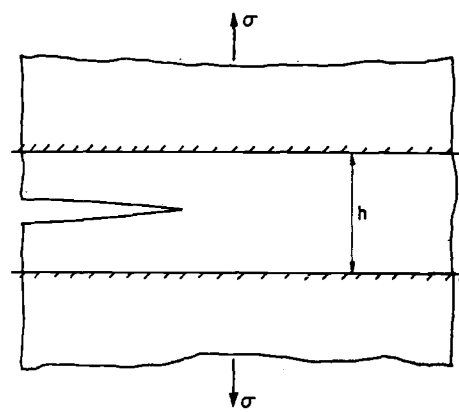

FIG. 37—A Sheet Which is Loaded and Clamped Prior to Introduction of a Crack.

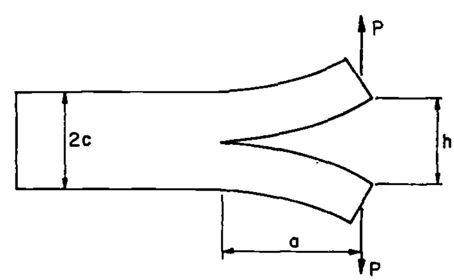

FIG. 38—The Splitting of a Rod of Rectangular Section.

$$
\left.
\begin{aligned}
K_{\mathrm{I}} &= \frac{\sigma h^{1/2}}{2^{1/2}} \\
K_{\mathrm{II}} &= 0
\end{aligned}
\right\} \quad \ldots\ldots\ldots\ldots (178)
$$

For further information, see Ref (**42**).

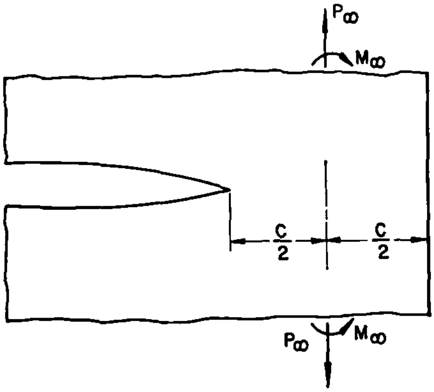

FIG. 39—Semi-finite Notch Approaching the Free Edge of a Half-Plane.

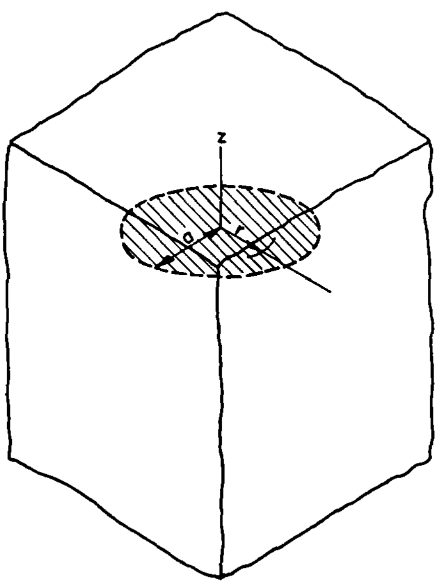

FIG. 40—Axisymmetrical Loading of a Body with a Circular Disk Crack.

A Case of the Splitting of Rods, that is, slender rectangular members ($a \gg 2c$) (see Fig. 38):

Under wedging:

$$\left.\begin{aligned} K_{\mathrm{I}} &= \frac{3^{1/2}\,Ehc^{3/2}}{4a^2} \\ K_{\mathrm{II}} &= 0 \end{aligned}\right\} \qquad (179)$$

Under forces:

$$\left.\begin{aligned} K_{\mathrm{I}} &= \frac{2(3)^{1/2}\,Pa}{c^{3/2}} \\ K_{\mathrm{II}} &= 0 \end{aligned}\right\} \qquad (180)$$

For further information, see either Ref (**23**) or (**105**).

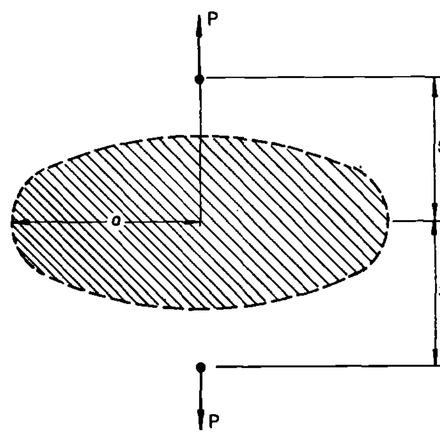

FIG. 41—Concentrated Forces Applied to the Axis of a Circular Disk Crack in an Infinite Body.

A Semi-Infinite Notch Approaching the Free Edge of a Half-Plane (see Fig. 39):

$$\left.\begin{aligned} K_{\mathrm{I}} &= \pi^{1/2}\left(\frac{4\pi - 12}{\pi^2 - 8}\right)\frac{P_\infty}{c^{1/2}} \\ &\quad + \pi^{1/2}\left(\frac{4\pi - 8}{\pi^2 - 8}\right)\frac{M_\infty}{c^{3/2}} \\ K_{\mathrm{II}} &= 0 \end{aligned}\right\} \qquad (181)$$

For further information, see Refs (**10,37**).

Axisymmetrical Loading of a Body with a Circular Disk Crack:

For an axisymmetrical normal pressure distribution, $p(r)$, on both crack surfaces (see Fig. 40),

$$\left.\begin{aligned} K_{\mathrm{I}} &= \frac{2}{(\pi a)^{1/2}}\int_0^a \frac{rp(r)}{(a^2 - r^2)^{1/2}}\,dr \\ K_{\mathrm{II}} &= 0 \end{aligned}\right\} \qquad (182)$$

For further information, see Ref. (**23**)

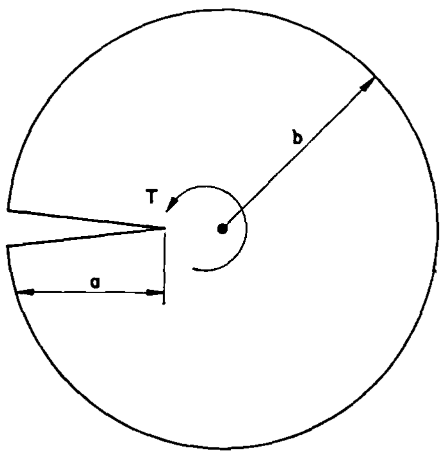

FIG. 42—Torison of a Cylindrical Bar with a Partial Radial Crack.

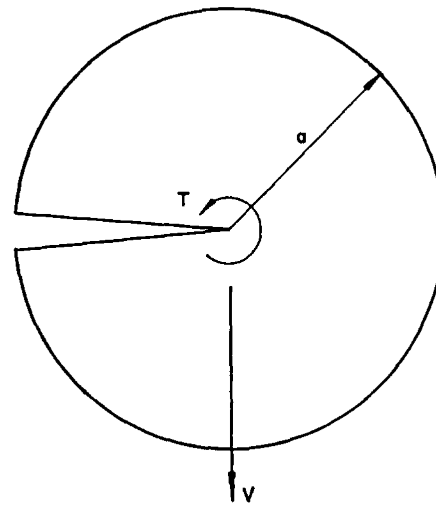

FIG. 43—Torsion and Beam Shear of a Cylindrical Bar with a Radial Crack.

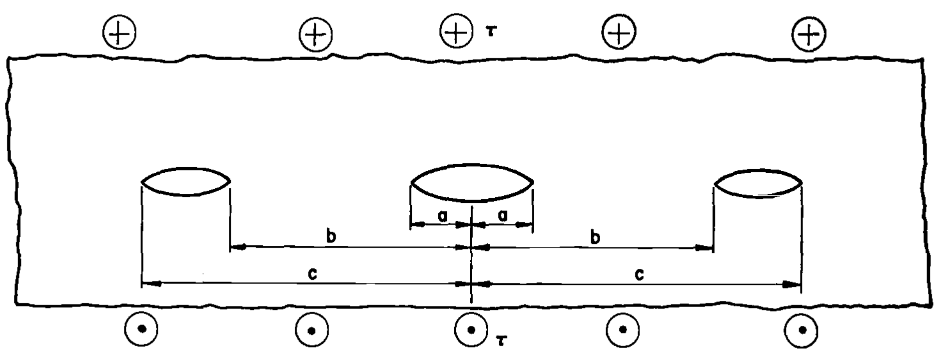

FIG. 44—An Infinite Body with "Tunnel" Cracks Under Longitudinal (Pure) Shear.

Note that with superposition, this enables treatment of all cases of axisymmetrical loading.

For the type of circular disk crack shown in Fig. 41, the K-values are:

$$\left.\begin{aligned} K_{\mathrm{I}} &= \frac{P}{(\pi a)^{3/2}} \frac{\left[1 + \left(\dfrac{2-\nu}{1-\nu}\right)\dfrac{s^2}{a^2}\right]}{\left[1 + \dfrac{s^2}{a^2}\right]^2} \\ K_{\mathrm{II}} &= 0 \end{aligned}\right\} \quad \ldots\ldots(183)$$

Equations 182 may also be used. For further information, see Ref (**23**).

Torsion and Beam Shear of Prismatic Bars with Cracks:

The K-values in prismatic bars under torsion for the type of crack shown in Fig. 42 are:

$$\left.\begin{aligned} K_{\mathrm{I}} &= K_{\mathrm{II}} = 0 \\ K_{\mathrm{III}} &= \frac{(1+\alpha)^{3/2}(1-\alpha)^3\,[2(1-\alpha) + \alpha^{1/2}(mJ_0 + J_1)]\pi^{1/2}\,T}{\alpha^2\{2\pi^2 - [2(1-\alpha)^2 A^2 + \alpha(A+B)^2]\}\,a^{5/2}} \end{aligned}\right\} \quad \ldots(184)$$

where

$\alpha = (b - a)/b$

$$m = \tfrac{1}{2}[\alpha + 1/\alpha]$$

$$J_0 = 4 \arctan (\alpha)^{1/2}$$

$$J_1 = [-(1 - \alpha)/4\alpha]\,[4(\alpha)^{1/2} - (1 - \alpha)J_0]$$

$$A = 1/\alpha\,[(1 + \alpha)^2 (\arctan (\alpha)^{1/2})/(\alpha)^{1/2} - (1 - \alpha)]$$

$$B = [(1 - \alpha)/\alpha]\,[2 - \tfrac{3}{4}(1 - \alpha)\,A]$$

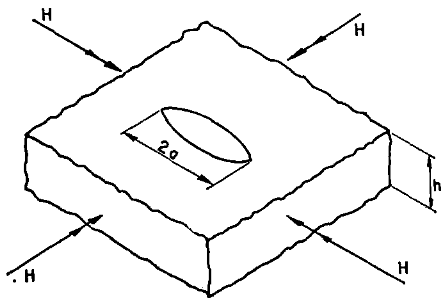

FIG. 45—A Plate Subjected to Uniform Twisting Moments at Infinity

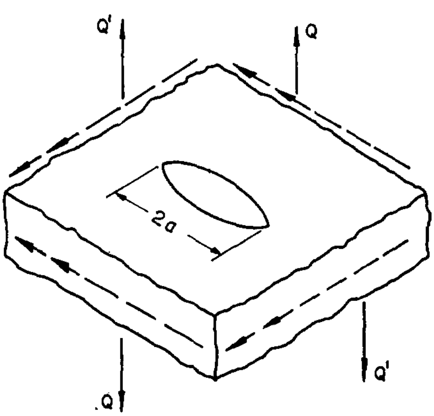

FIG. 46—A Plate with Uniform Shear at Infinity.

For further information, see Ref (**26**). Several other configurations are treated in Refs (**24,25**).

For torsion and beam shear (Fig. 43) the K-values are:

$$\left.\begin{aligned} K_{I} &= K_{II} = 0 \\ K_{III} &= 0.969\,\frac{T}{a^{5/2}} - \left(\frac{6.95 + 6.47\nu}{1 + \nu}\right)\frac{V}{a^{3/2}} \end{aligned}\right\} \ldots (185)$$

For further information, see Refs (**26,24**).

Cracks under Longitudinal (Pure) Shear:

The K_{I} and K_{II} values for the three cracks shown in Fig. 44 are all zero; the K_{III} values vary with the location of the crack tips as follows:

For the crack tips at a:

$$K_{III} = \pm \left(\frac{(c^2 - a^2)}{(b^2 - a^2)}\right)^{1/2} \frac{E(k)}{K(k)} \cdot \tau(\pi a)^{1/2}$$

For the crack tips at b:

$$K_{III} = \pm \left(\frac{(b^2 - a^2)}{(c^2 - b^2)}\right)^{1/2} \cdot \left[1 - \left(\frac{c^2 - a^2}{b^2 - a^2}\right)\frac{E(k)}{K(k)}\right] \tau(\pi b)^{1/2}$$

For the crack tips at c:

$$K_{III} = \pm \left(\frac{(c^2 - a^2)}{(c^2 - b^2)}\right)^{1/2} \cdot \left[1 - \frac{(Ek)}{K(k)}\right] \tau(\pi c)^{1/2} \quad \ldots (186)$$

where

$$k = \left(\frac{(c^2 - a^2)}{(c^2 - b^2)}\right)^{1/2}$$

is the modulus of the complete elliptic integrals, $E(k)$ and $K(k)$ of the first and second kind, respectively.

For further information, see Ref (**106**).

The Flexure of Infinite Plates:

A plate subjected to pure twisting moment (per unit length), H, at infinity (see Fig. 45) gives:

$$\phi_B(\eta) = -\frac{iHa}{2D(3 + \nu)\eta}$$

or

$$\left.\begin{aligned} K_B &= 0 \\ K_S &= \frac{6H}{h^2}\,(\pi a)^{1/2} \end{aligned}\right\} \ldots\ldots\ldots (187)$$

For further information, see Ref (**18**).

Uniform shear (per unit length), Q, at

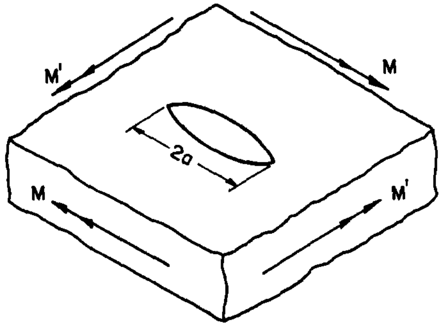

FIG. 47—A Plate with Uniform Bending Moments at Infinity.

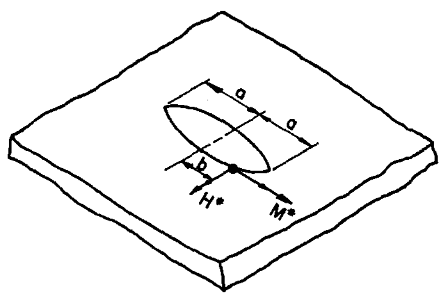

FIG. 48—A Concentrated Couple of Arbitrary Direction on a Crack Surface in an Infinite Plate.

infinity (moments required for equilibrium shown dotted in Fig. 46), gives:

$$\phi_B(\eta) = \frac{Qa^2}{12D}\left[\eta^2 + \left(\frac{1-\nu}{3+\nu}\right)\frac{3}{\eta^2}\right]$$

or

$$\left.\begin{aligned} K_B &= 0 \\ K_S &= \frac{8\pi^{1/2}Qa^{3/2}}{h^2} \end{aligned}\right\}\cdots\cdots\cdots(188)$$

The results are independent of Q'.

For further information, see Ref (18).

For uniform moments at infinity (see Fig. 47),

$$\left.\begin{aligned} K_B &= \frac{6M}{h^2}(\pi a)^{1/2} \\ K_S &= 0 \end{aligned}\right\}\cdots\cdots\cdots(189)$$

The results are independent of M'.

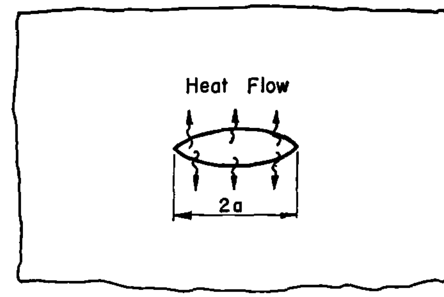

FIG. 49—A Sheet with Uniform Temperature Imposed on the Crack Surface.

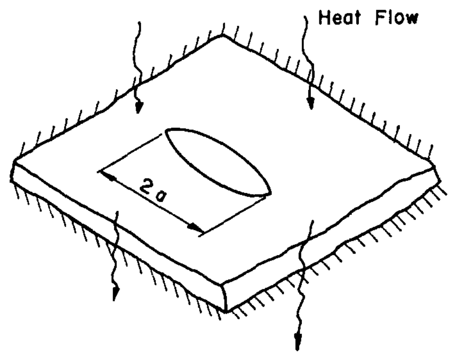

FIG. 50—A Clamped Plate with a Uniform Thermal Gradient Through the Thickness.

For further information, see Ref (18).

For a concentrated couple on the crack surface (see Fig. 48),

$$\left.\begin{aligned} K_B &= \frac{3M^*}{h^2(\pi a)^{1/2}}\left(\frac{a+b}{a-b}\right)^{1/2} + \frac{3H^*}{2h^2(\pi a)^{1/2}}(1+\nu) \\ K_S &= \frac{3M^*}{2h^2(\pi a)^{1/2}}(1+\nu) - \frac{3H^*}{h^2(\pi a)^{1/2}}\left(\frac{a+b}{a-b}\right)^{1/2} \end{aligned}\right\}\cdots(190)$$

Thermal Stress Problems:

A plate with uniform temperature supplied on the crack surface (see Fig. 49) gives:

$$\left.\begin{aligned} K_{\text{I}} &= -\frac{E\alpha\, a^{1/2}\, q}{\pi^{1/2}(1+\kappa)\mu} \\ K_{\text{II}} &= 0 \end{aligned}\right\}\cdots\cdots\cdots(191)$$

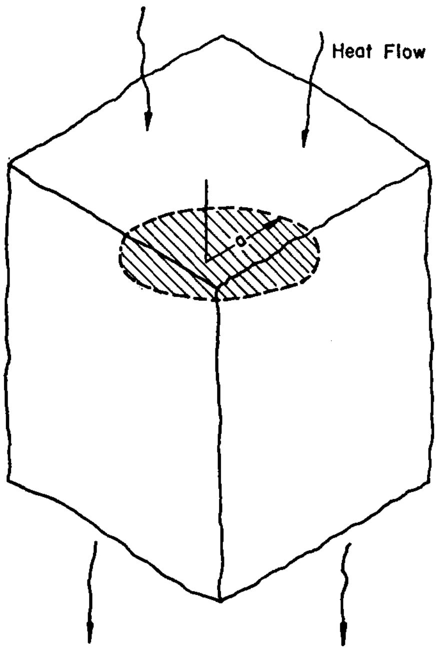

FIG. 51—An Infinite Body with a Uniform Thermal Gradient Normal to an Insulated Circular Disk Crack.

where

μ = thermal conductivity
q = rate of total heat per unit thickness supplied to the plate

For further information, see Ref (47). Note that this case has significance for high pressure gas escaping through a crack.

A clamped plate with a thermal gradient through the thickness (see Fig. 50) gives:

$$\left.\begin{aligned} K_B &= \frac{\alpha E h \nabla T (\pi a)^{1/2}}{2(1-\nu)} \\ K_S &= 0 \end{aligned}\right\} \text{.......} (192)$$

For further information, see Ref (47).

An infinite body with a circular disk crack perpendicular to a thermal gradient (see Fig. 51) gives:

$$\left.\begin{aligned} K_{\mathrm{II}} &= \frac{E\alpha \nabla T a^{3/2}}{3\pi(1-\nu)} \\ K_{\mathrm{I}} &= K_{\mathrm{III}} = 0 \end{aligned}\right\} \text{........} (193)$$

For further information, see Ref (107).

APPENDIX III

NOTATION

A = Crack-surface area
a = Half-crack length of internal crack or crack depth of surface crack
A_{ij} = Elastic compliance coefficients for Hooke's law of plane problems of anisotropic media
$\bar{a}_{ij}$ = Elastic compliance coefficients for the general Hooke's law of anisotropic media
b = Half-width of a strip
C_1, C_2 = Constants
C = Crack velocity
D_k = Complex differential operators ($K = 1, \cdots, 6$)
D = Round bar diameter
d = Notch diameter
E = Modulus of elasticity
F = $P - iQ$, force with complex representation (per unit thickness)
G = Shear modulus of elasticity
$\mathcal{G}_{\mathrm{I}}$, $\mathcal{G}_{\mathrm{II}}$, $\mathcal{G}_{\mathrm{III}}$ = Energy rates associated with each mode of cracking
h = Depth of a beam or plate
i = $(-1)^{1/2}$
$K = K_{\mathrm{I}} - iK_{\mathrm{II}}$ = Stress-intensity factor with complex representation
K_{I}, K_{II}, K_{III} = Stress-intensity factors for each mode (subscript "a" indicates anisotropic type)
K_1, K_2, K_3, K_4 = Stress intensity at various points on a crack contour
K_B, K_S = Plate and shell bending and shearing stress-intensity factors
L = Half-length of a strip
l = A couple-stress elastic constant
M = Applied bending moment (per unit thickness)
P = Force (per unit thickness)
p = Crack-tip radius
p_i, q_i = Anisotropic elastic constants

R = Radius of a curved crack
r = Radial coordinate from a crack tip
T = Temperature or torque
t = Sheet thickness (or time)
U, U_1, U_2 = Stress functions for anisotropic media
u, v, w = Displacement components
V = Strain energy
Z, Z_I, Z_{II}, Z_{III} = Westergaard stress functions
$\bar{\bar{Z}}, \bar{Z}, Z, Z'$ = Successive derivatives of a Westergaard stress function
z = Complex variable
z_1, z_2, z_3 = Modified complex variables for anisotropic analysis
α = An angle (or closing segment of a crack)
β = An angle
γ = Mass density
$\gamma_{xy}, \gamma_{yz}, \gamma_{xz}$ = Shear strain components
Δ = Displacement
∇ = Gradient $[(\partial/\partial x) + (\partial/\partial y)]$
∇^2, ∇^4 = Harmonic and biharmonic operators
ϵ = The bi-elastic constant of joined halfplanes
$\epsilon_x, \epsilon_y, \epsilon_z$ = Normal strain components
ζ = A complex variable (origin at the crack tip)
ζ_1, ζ_2 = Modified complex variables for anisotropic media
η = Complex variable in the mapped plane
θ = Angular coordinate measured from the crack plane
κ = An elastic constant for plane stress or strain (see Eqs 162)
λ = Compliance of a linear-elastic body
μ, μ_k = Elastic constants for anisotropic media ($k = 1, \cdots, 6$)
ν = Poisson's ratio
σ, τ = Normal and shear stress (applied at infinity)
σ_o = Maximum stress at a notch
σ_{net} = Net-section stress (average)
$\left.\begin{matrix}\sigma_{ij} - \sigma_x, \sigma_y, \sigma_z \\ \tau_{xy}, \tau_{yz}, \tau_{xz}\end{matrix}\right\}$ Rectangular components of stress
$\sigma_r, \sigma_\theta, \tau_{r\theta}$ = Polar components of stress
Φ = Airy stress function
ϕ = A complex stress function for plane stress or strain
Φ_o = An elliptic integral
ϕ_B = A complex stress function for plate bending
χ = A complex stress function for plane stress or strain
ψ_i = Harmonic functions
$\left.\begin{matrix}F(\ ), g(\ ), \\ h(\ ), k(\ )\end{matrix}\right\}$ = A function of
Re, Im = Real and imaginary parts of complex functions

REFERENCES

(1) A. A. Griffith, "The Phenomena of Rupture and Flow in Solids," *Transactions*, Royal Soc. London, Vol. 221, 1920.
(2) C. E. Inglis, "Stresses in a Plate Due to the Presence of Cracks and Sharp Corners," *Proceedings*, Inst. Naval Architects, Vol. 60, 1913.
(3) I. N. Sneddon, "The Distribution of Stress in the Neighborhood of a Crack in an Elastic Solid," *Proceedings*, Royal Soc. London, Vol. A-187, 1946.
(4) G. R. Irwin, "Analysis of Stresses and Strains Near the End of a Crack Traversing a Plate," *Transactions*, Am. Soc. Mechanical Engrs., *Journal of Applied Mechanics*, 1957.
(5) G. R. Irwin, "Fracture," *Handbuch der Physik*, Vol. VI, Springer, Berlin, 1958.
(6) M. L. Williams, "On the Stress Distribution at the Base of a Stationary Crack," *Transactions*, Am. Soc. Mechanical Engrs., *Journal of Applied Mechanics*, 1957.
(7) G. R. Irwin, "Fracture Mechanics," *Structural Mechanics*, Pergamon Press, New York, N. Y., 1960.
(8) H. M. Westergaard, "Bearing Pressures and Cracks," *Transactions*, Am. Soc. Mechanical Engrs., *Journal of Applied* Mechanics, 1939.
(9) P. C. Paris, "Stress-Intensity-Factors by Dimensional Analysis," Lehigh University, Inst. of Research Report, 1961.
(10) H. Neuber, *Kerbspannungslehre*, Springer, Berlin, 1937 and 1958; English translation available from Edwards Bros., Ann Arbor, Mich.
(11) R. E. Peterson, *Stress Concentration Design Factors*, John Wiley & Sons, Inc., New York, N. Y., 1953.
(12) G. Savin, *Stress Concentration Around*

Holes, Pergamon Press, New York, N. Y., 1961.

(13) M. Isida, "The Effect of Longitudinal Stiffeners in a Cracked Plate Under Tension," *Proceedings*, Fourth U.S. Congress of Applied Mechanics, 1962.

(14) A. S. Kobayashi and R. G. Forman, "On the Axial Rigidity of a Perforated Strip and the Strain Energy Release Rate in a Centrally Notched Strip Subjected to Uniaxial Tension," *Preprint No. 63-WA-29*, Am. Soc. Mechanical Engrs., 1963.

(15) A. S. Kobayashi, R. B. Cherepy, and W. C. Kinsel, "A Numerical Procedure for Estimating the Stress Intensity Factor of a Crack in a Finite Plate," *Preprint No. 63-WA-24*, Am. Soc. Mechanical Engrs., 1963.

(16) O. L. Bowie, "Rectangular Tensile Sheet with Symmetric Edge Cracks," *Transactions*, Am. Soc. Mechanical Engrs., *Journal of Applied Mechanics*, Vol. 31, Ser. E, No. 2, June, 1964, pp. 208–212.

(17) N. I. Muskhelishvili, *Some Basic Problems of Mathematical Theory of Elasticity* (published in Russian in 1933); English translation, P. Noordhoff and Co., 1953.

(18) G. Sih, P. Paris, and F. Erdogan, "Crack Tip Stress Intensity Fractors for Plane Extension and Plate Bending Problems," *Transactions*, Am. Soc. Mechanical Engrs., *Journal of Applied Mechanics*, 1962.

(19) I. S. Sokolnikoff, *Mathematical Theory of Elasticity*, McGraw-Hill Book Co., Inc., New York, N. Y., 1956.

(20) J. L. Sanders, Jr. "On the Griffith-Irwin Fracture Theory," *Transactions*, Am. Soc. Mechanical Engrs., *Journal of Applied Mechanics*, 1960.

(21) F. E. Erdogan, "On the Stress Distribution in Plates with Colinear Cuts Under Arbitrary Loads," *Proceedings*, Fourth U. S. National Congress of Applied Mechanics, 1962.

(22) G. Sih, "Application of Muskhelishvili's Method to Fracture Mechanics," *Transactions*, The Chinese Assn. for Advanced Studies, November, 1962.

(23) G. I. Barenblatt, "Mathematical Theory of Equilibrium Cracks in Brittle Fracture," *Advances in Applied Mechanics*, Vol. VII, Academic Press, New York, 1962.

(24) G. Sih, "On Crack Tip Stress-Intensity-Factors for Cylindrical Bars under Torsion," *Journal of the Aerospaces Sciences*, 1962.

(25) G. Sih, "The Flexural Stress Distribution Near a Sharp Crack," *Journal*, Am. Inst. Aeronautics and Astronautics, 1963.

(26) G. Sih, "Strength of Stress Singularities at Crack Tips for Flexural and Torsional Problems," *Transactions*, Am. Soc. Mechanical Engrs., *Journal of Applied Mechanics*, 1963.

(27) M. A. Sadowsky and E. G. Sternberg, "Stress Concentration Around a Triaxial Ellipsoidal Cavity," *Transactions*, Am. Soc. Mechanical Engrs., *Journal of Applied Mechanics*, 1949.

(28) A. E. Green and I. N. Sneddon, "The Stress Distribution in the Neighborhood of a Flat Elliptical Crack in an Elastic Solid," *Proceedings*, Cambridge Philosophical Soc., Vol. 46, 1950.

(29) G. R. Irwin, "The Crack Extension Force for a Part Through Crack in a Plate," *Transactions*, Am. Soc. Mechanical Engrs., *Journal of Applied Mechanics* 1962.

(30) L. A. Wigglesworth, "Stress Distribution in a Notched Plate," *Mathematika*, Vol. 4, 1957.

(31) G. R. Irwin, "The Crack Extension Force for a Crack at a Free Surface Boundary," *Report No. 5120*, Naval Research Lab., 1958.

(32) G. R. Irwin, "Analytical Aspects of Crack Stress Field Problems," *T&AM Report No. 213*, University of Illinois, March, 1962.

(33) M. Isida, "On the Tension of a Strip with a Central Elliptical Hole," *Transactions*, Japan Soc. Mechanical Engrs., Vol. 21, 1955.

(34) M. Isida, "On the In-Plane Bending of a Strip with a Central Elliptical Hole," *Transactions*, Japan Soc. Mechanical Engrs., Vol. 22, 1956.

(35) M. Isida, "On the Tension of a Semi-Infinite Plate with an Elliptical Hole," *Transactions*, Japan Soc. Mechanical Engrs., Vol. 22, 1956.

(36) H. F. Bueckner, "Some Stress Singularities and Their Computation by Means of Integral Equations," *Boundary Value Problems in Differential Equations*, edited by R. E. Langer, University of Wisconsin Press, Madison, Wis., 1960.

(37) D. H. Winne and B. M. Wundt, "Application of the Griffith-Irwin Theory of Crack Propagation to Bursting Behavior of Disks," *Transactions*, Am. Soc. Mechanical Engrs., Vol. 80, 1958.

(38) O. L. Bowie, "Analysis of an Infinite Plate Containing Radial Cracks Originating from the Boundary of an Internal

Circular Hole," *Journal of Mathematics and Physics*, Vol. 35, 1956.

(39) J. P. Romualdi, J. T. Frasier, and G. R. Irwin, "Crack Extension Force near a Riveted Stringer," *Report No. 4956*, Naval Research Lab., May, 1957.

(40) J. P. Romualdi and P. H. Sanders, "Fracture Arrest by Riveted Stiffeners," *Proceedings*, Fourth Midwest Conference on Solid Mechanics, University of Texas Press, 1959/1960.

(41) P. C. Paris, "The Mechanics of Fracture Propagation and Solutions to Fracture Arrestor Problems," *Document No. D2-2195*, Boeing Co., 1957.

(42) P. C. Paris, *A Short Course in Fracture Mechanics*, University of Washington Press, 1960.

(43) J. L. Sanders, Jr., "Effect of a Stringer on the Stress Concentration Factor Due to a Crack in a Thin Sheet," *NASA Tech. Rep. R-13*, Nat. Aeronautics and Space Administration, 1959.

(44) M. Isida, "Stress Concentration Due to a Central Transverse Crack in a Strip Reinforced on Either Side," *Journal*, Japan Soc. Aero-Space Sciences, Vol. 10, 1962.

(45) R. Greif and J. L. Sanders, Jr., "The Effect of a Stringer on the Stress in a Cracked Sheet," Harvard University, Cambridge, Mass., June, 1963; also ASME *Preprint No. 64WA/APM*, to be published in *Journal of Applied Mechanics*.

(46) T. Terry, "Analysis of a Reinforced Infinite Plate Containing a Single Crack," Ph.D. dissertation, Lehigh University, September, 1963.

(47) G. Sih, "On the Singular Character of Thermal-Stresses Near a Crack Tip," *Transactions*, Am. Soc. Mechanical Engrs., *Journal of Applied Mechanics*, Vol. 29, 1962.

(48) A. L. Florence and J. N. Goodier, "Thermal Stress Due to Disturbance of Uniform Heat Flow by an Ovaloid Hole," *Transactions*, Am. Soc. Mechanical Engrs., *Journal of Applied Mechanics*, Vol. 27, 1960.

(49) M. L. Williams, "Surface Stress Singularities Resulting from Various Boundary Conditions in Angular Corners of Plates under Bending," *Proceedings*, First U. S. National Congress of Applied Mechanics, June, 1951.

(50) M. L. Williams and R. H. Owens, "Stress Singularities in Angular Corners of Plates Having Linear Flexural Rigidities for Various Boundary Conditions," *Proceedings* Second, U. S. National Congress of Applied Mechanics, June, 1954.

(51) M. L. Williams, "The Bending Stress Distribution at the Base of a Stationary Crack," *Transactions*, Am. Soc. Mechanical Engrs., *Journal of Applied Mechanics*, 1961.

(52) F. Erdogan, O. Tuncel, and P. Paris, "An Experimental Investigation of the Crack Tip Stress Intensity Factors in Plates under Cylindrical Bending," *Transactions*, Am. Soc. Mechanical Engrs., *Journal of Basic Engineering*, 1962.

(53) F. Erdogan and G. Sih, "On Crack Extension in Plates under Plane Loading and Transverse Shear," *Transactions*, Am. Soc. Mechanical Engrs., *Journal of Basic Engineering*, 1963.

(54) J. K. Knowles and N. M. Wang, "On the Bending of an Elastic Plate Containing a Crack," *GALCIT SM 60-11*, California Inst. of Technology, July, 1960.

(55) E. Reissner, "The Effect of Transverse Shear Deformation on the Bending of Elastic Plates," *Transactions*, Am. Soc. Mechanical Engrs., *Journal of Applied Mechanics*, Vol. 12, 1945.

(56) M. L. Williams, published discussion of Ref (52). See also Ref (74).

(57) G. Sih and D. Setzer, published discussion of Ref (58), *Transactions*, Am. Soc. Mechanical Engrs., *Journal of Applied Mechanics*, 1964.

(58) E. S. Folias and M. L. Williams, "The Bending Stress in a Cracked Plate on an Elastic Foundation," *Journal of Applied Mechanics*, 1963.

(59) E. S. Folias, Ph.D. dissertation, California Inst. of Technology, 1963.

(60) D. D. Ang, E. S. Folias, and M. L. Williams, "The Effect of Initial Spherical Curvature on the Stresses near a Crack Point," *GALCIT SM 62-4*, California Inst. of Technology, May, 1962.

(61) E. Reissner, "Stress and Displacements of Shallow Spherical Shells," *Journal of Mathematics and Physics*, Vol. 25, 1964.

(62) E. E. Sechler and M. L. Williams, "The Critical Crack Length in Pressurized Cylinders," *GALCIT 96*, California Inst. of Technology, Final Report, September, 1959.

(63) M. L. Williams, "Some Observations Regarding the Stress Field near the Point of a Crack," *Proceedings*, Crack Propagation Conference (Cranfield, England), September, 1961.

(64) J. I. Bluhm and M. M. Mardirosian, "Fracture Arrest Capabilities of An-

nularly Reinforced Cylindrical Pressure Vessels," *Experimental Mechanics*, Vol. 3, 1963.

(65) R. W. Peters and P. Kuhn, "Bursting Strength of Unstiffened Pressure Cylinders with Slits," *NASA TN 3993*, Nat. Aeronautics and Space Administration, April, 1956.

(66) P. Kuhn, "The Prediction of Notch and Crack Strength under Static and Fatigue Loading," presented at the SAE-ASME Meeting, New York, N. Y., April, 1964.

(67) Z. and F. Cosserat, *Théorie des Corps Déformables*, A. Hermann et Fils, Paris, 1909.

(68) R. D. Mindlin, "Influence of Couple Stresses on Stress Concentrations," *Experimental Mechanics*, Vol. 3, 163.

(69) D. Setzer, "An Elasto-Static Couple Stress Problem: Extension of an Elastic Body Containing a Finite Crack," Ph.D. dissertation, Lehigh University, December, 1963.

(70) Anon., "Screening Tests for High-Strength Alloys Using Sharply Notched Cylindrical Specimens," Fourth Report of Special ASTM Committee, *Materials Research & Standards*, Vol. 2, 1962.

(71) I. N. Sneddon, "Crack Problems in Mathematical Theory of Elasticity," *Report No. ERD-126/1*, North Carolina State College, May, 1961.

(72) G. R. Irwin and F. A. McClintock, "Plasticity Modifications to Crack Stress Analysis," see p. 84.

(73) R. L. Chapkis and M. L. Williams, "Stress Singularities for a Sharp-Notched Polarly Orthotropic Plate," *Proceedings*, Third U. S. Congress of Applied Mechanics, 1958.

(74) D. D. Ang and M. L. Williams, "Combined Stresses in an Orthotropic Plate Having a Finite Crack," *Journal of Applied Mechanics*, 1961.

(75) T. J. Willmore, "The Distribution of Stress in the Neighborhood of a Crack," *Quarterly Journal of Mechanics and Applied Mathematics*, Vol. II, Part I, 1949.

(76) G. C. Sih and P. C. Paris, "The Stress Distribution and Intensity Factors for a Crack Tip in an Anisotropic Plate Subjected to Extension," Lehigh University, Inst. of Research Report, October, 1961.

(77) S. G. Lekhnitzki, *Anisotropic Plates*, translated by E. Stowell, Am. Iron and Steel Inst., New York, N. Y., 1956. (See alternatively a newer translation available through Holden-Day Book Co., San Francisco, Calif.)

(78) C. A. Berg, "The Influence of Viscous Deformation on Brittle Fracture," D.Sc. dissertation, Massachusetts Inst. of Technology, June, 1962.

(79) C. A. Berg, "The Motion of Cracks in Plane Viscous Deformation," *Proceedings*, Fourth U.S. National Congress of Applied Mechanics, 1962.

(80) G. C. Sih, "Viscoelastic Stress Distribution near the End of a Stationary Crack," Lehigh University, Inst. of Research Report, July, 1962.

(81) J. Krafft and G. R. Irwin, "Crack Velocity Considerations," see p. 114.

(82) J. Krafft and A. M. Sullivan, "Effects of Speed and Temperature upon Crack Toughness and Yield Strength in Mild Steel," *Transactions*, Am. Soc. Metals, Vol. 56, 1963.

(83) G. R. Irwin, "Crack Toughness Testing of Strain Rate Sensitive Materials," *Transactions*, ASME, *Journal of Basic Engineering*, 1964.

(84) M. L. Williams, "The Stresses Around a Fault or Crack in Dissimilar Media," *Bulletin*, Seismological Soc. Am., Vol. 49, 1959.

(85) F. Erdogan, "Stress Distribution in a Non-Homogeneous Elastic Plane with Cracks," *Transactions*, ASME, *Journal of Applied Mechanics*, Vol. 30, 1963.

(86) G. Sih and J. Rice, "The Bending of Plates of Dissimilar Materials with Cracks," *Transactions*, ASME, *Journal of Applied Mechanics*, Vol. 31, 1964. See also: J. Rice and G. Sih, "Plane Problems of Cracks in Dissimilar Media," Lehigh University, Inst. of Research Report, April, 1964.

(87) F. Erdogan and L. Y. Bahar, "On the Stress Distribution in Bonded Dissimilar Materials with a Circular Cavity," to be published in *Journal of Applied Mechanics*, 1964–1965.

(88) A. R. Zak and M. L. Williams, "Crack Point Stress Singularities at a Bimaterial Interface," *GALCIT SM42-1*, California Inst. of Technolgoy, January, 1962.

(89) E. Yoffe, "The Moving Griffith Crack," *Philosophical Mag.*, Ser. 7, Vol. 42, 1951.

(90) F. McClintock and P. Sukhatme, "Traveling Cracks in Elastic Materials under Longitudinal Shear," *Journal of Mechanics and Physics of Solids*, Vol. 8, 1960.

(91) B. R. Baker, "Dynamic Stresses Created by a Moving Crack," *Journal of Applied Mechanics*, Vol. 29, 1962.

(92) J. W. Craggs, "On the Propagation of a Crack in an Elastic-Brittle Material," *Journal of Mechanics and Physics of Solids*, Vol. 8, 1960.
(93) D. D. Ang, "Some Radiation Problems in Elastodynamics," Ph.D. dissertation, California Inst. of Technology, 1958.
(94) B. Cotterell, "On the Nature of Moving Cracks," *Journal of Applied Mechanics*, 1964.
(95) A. A. Wells and D. Post, "The Dynamic Stress Distribution Surrounding a Running Crack—a Photoelastic Analysis," *NRL Report No. 4935*, Naval Research Lab., April, 1957.
(96) N. F. Mott, "Fracture of Metals: Theoretical Considerations," *Engineering*, Vol. 165, 1948.
(97) D. K. Roberts and A. A. Wells, "The Velocity of Brittle Fracture," *Engineering*, Vol. 178, 1954.
(98) G. R. Irwin and J. Kies, "Fracturing and Fracture Dynamics," *Welding Research Journal* (Research Supplement), 1952. See also references to earlier work in this paper.
(99) E. Orowan, "Fundamentals of Brittle Behavior of Metals," *Fatigue and Fracture of Metals*, John Wiley & Sons, Inc., New York, N. Y., 1952. See also earlier work referenced therein.
(100) G. R. Irwin, "A Critical Energy Rate Analysis of Fracture Strength," *Welding Journal* (Research Supplement), 1954.
(101) H. F. Bueckner, "The Propagation of Cracks and Energy of Elastic Deformation," *Transactions*, Am. Soc. Mechanical Engrs., *Journal of Applied Mechanics*, 1958.
(102) J. L. Sanders, "On the Griffith-Irwin Fracture Theory," *Transactions*, Am. Soc. Mechanical Engrs., *Journal of Applied Mechanics*, Ser. E, Vol. 82, 1960.
(103) H. Neuber, discussion in Ref (7), *Structural Mechanics*, Pergamon Press, New York, N. Y., 1960.
(104) P. Kuhn and I. E. Figge, "Unified Notch-Strength Analysis for Wrought Aluminum Alloys," *NASA TN D-1259*, Nat. Aeronautics and Space Administration, 1962.
(105) J. J. Gilman, *Fracture*, edited by Averbach et al, John Wiley & Sons, Inc., New York, N. Y., 1959.
(106) G. C. Sih, "Boundary Problems for Longitudinal Shear Cracks," *Proceedings*, Second Conference on Theoretical and Applied Mechanics, Pergamon Press, New York, N. Y., 1964.
(107) A. L. Florence and J. N. Goodier, "The Linear Thermoelastic Problem of Heat Flow Disturbed by a Penny-shaped Insulated Crack," *International Journal of Engineering Science*, Vol. 1, No. 4, 1963.

DISCUSSION

H. F. Bueckner[1]—It might be well to review briefly the stress-analysis situation regarding the notched round bar in tension, since this geometry appears to be important from the standpoint of fracture testing. Several treatments of this problem can be found in the literature and are compared in Table 8, which gives the coefficient, $F(d/D)$, of Eq 57 in the paper, as derived from various references. The values used by Lubahn[2] and by Wundt[3] represent my first and second estimates, respectively. The first estimate was based on extrapolation of Peterson's published stress-concentration factors[4] to a vanishingly small radius of curvature. These values agree well with those reported by Irwin[5] who used the same procedure. The results obtained by this extrapolation method are, of course, only at best as accurate as the stress-concentration factors from which they are derived. The second estimate was made using Neuber's formula for deep notches in combination with a computation for a notch in an elastic half plane.[6]

TABLE 8—COEFFICIENTS FOR COMPUTATION OF THE STRESS-INTENSITY FACTOR, K_I FOR A NOTCHED ROUND BAR.
$[K_I = F(d/D)\sigma_N (\pi D)^{1/2}]$

Notch Depth, d/D	$F(d/D)$ as given by:				
	Lubahn[a]	Irwin[b]	Wundt[c]	Paris[d]	Present Solution[e]
0.5	0.230	0.224	0.239	0.227	0.240
0.6	0.234	0.232	0.252	0.238	0.255
0.707	0.229	0.233	0.258	0.240	0.259
0.8	0.217	0.224	0.250	0.233	0.251
0.9	0.195	0.199	0.210	0.205	0.210

[a] See footnote 2.
[b] See footnote 5.
[c] See footnote 3.
[d] From Table 5 of the paper.
[e] To be published.

Recently I completed a more rigorous analysis[7] of the problem using a certain singular integral equation, the kernel of which is found by means of Fourier transforms. The coefficients derived from this solution are shown in the last column

[1] General Electric Co., Large Steam Turbine-Generator Dept., Schenectady, N. Y.

[2] J. D. Lubahn, "Experimental Determination of Energy Release Rate," *Proceedings*, Am. Soc. Testing Mats., Vol. 59, 1959, p. 885.

[3] B. M. Wundt, "A Unified Interpretation of Room Temperature Strength of Notch Specimens as Influenced by Size," *ASME Paper No. 59*, MET 9, 1959.

[4] R. E. Peterson, "*Stress Concentration Design Factors*," John Wiley & Sons, Inc., New York, N. Y., 1953.

[5] G. R. Irwin, "Supplement to: Notes for May, 1961 meeting of ASTM Committee for Fracture Testing of High-Strength Metallic Materials."

[6] H. F. Bueckner, "Some Stress Singularities and Their Computation by Means of Integral Equations," *Boundary Problems in Differential Equations*, edited by R. E. Langer, University of Wisconsin Press, Madison, Wisc., 1960, pp. 215–230.

[7] To be published.

of Table 8 and are considered to provide values of K_I having an accuracy within 1 per cent. It is interesting to note that the coefficients obtained by the present analysis agree well with those used by Wundt, but are higher than those given by Irwin or by Paris. Considering, for example, a notched round bar with $d/D = 0.707$, a geometry commonly used in fracture testing, the ASTM Special Committee[8] gives the following expression for the stress-intensity factor:

$$K_I = 0.414 \sigma_N (D)^{1/2}$$

The coefficient in this equation corresponds to the value 0.233 in Eq 57 of the paper. The present analysis yields a value of 0.259, about 10 per cent higher than that given by the above expression.

---

[8] "Screening Tests for High-Strength Alloys Using Sharply Notched Cylindrical Specimens," Fourth Report of a Special ASTM Committee, *Materials Research & Standards*, Vol. 2, March, 1962, pp. 196–203.

PLASTICITY ASPECTS OF FRACTURE MECHANICS

By F. A. McClintock[1] and G. R. Irwin[2]

Fracture mechanics, broadly speaking, represents knowledge of the influence of loading and geometry on fracture. Figure 1 shows the size range of significant events involved in the crack-extension process. Until the ion and electron cloud configuration shown schematically at the far left can be analyzed from wave mechanics, and the results integrated through ten orders of magnitude, it will be necessary to work with a series of different models, each appropriate to its own size range. Boundary conditions for each model are found from the next largest and next smallest scales. The smaller the size of the model from which we can integrate through larger sizes to obtain the fracture load for a given geometry, the broader the range of conditions which can be predicted or correlated from given experimental data. From whatever level we do start, it will be necessary to introduce test data to substitute for lack of knowledge (or cost of analysis) in the smaller regions.

From this point of view, it is present practice to correlate fracture on the basis of the leading term of the series expansion of the elastic stress distribution about the tip of the crack (**1–5**).[3] As discussed below, these terms represent mathematical infinities of stress and strain at the very tip of the crack. Although yielding prevents attaining these infinities, the leading terms still describe the stress distribution at intermediate distances. These will be called elastic singularities or intensities. The scale corresponds to the next to the largest configuration of the example of Fig. 1. It is the object of this paper to consider the next smaller scales of size, where the elastic singularity is distorted by the embedded plastic zone, and plastic strain is important, but the field may still be regarded as a homogeneous continuum. In certain "ideal" situations, an elastic singularity dominates and controls the enclosed plasticity. With higher stress levels or smaller specimens, there may be no region between the plastic zone and the boundaries of the specimen that can be characterized by an elastic stress singularity. In any event, the elastic and plastic relationships deserve careful study both as viewpoints for understanding phenomena at finer scale and for practical applications of this knowledge. By limiting our considerations to the macroscopic domain, certain relatively simple analytical models are available to serve as a basis for calculations and to furnish a quantitative basis for description. The discussion of such possibilities is one purpose of this paper and will be treated first. Comments will then be given relative to effects of plasticity in crack toughness testing. In contrast to linear elastic fracture mechanics, plastic fracture mechanics is still relatively incomplete and so it must be illustrated rather than treated compre hensively.

---

[1] Professor of mechanical engineering, Massachusetts Institute of Technology, Cambridge, Mass.

[2] Superintendent, Mechanics Division, U.S. Naval Research Laboratory, Washington, D. C.

[3] The boldface numbers in parentheses refer to the list of references appended to this paper.

SYMBOLS

- a = crack half-length
- A, B = parameters defined by Eqs 35 and 36
- $f, \bar{f}$ = parameters in Eqs 29 and 30 describing the shape of the plastic zone
- $\mathcal{G}$ = linear elastic strain energy release rate
- k = yield strength in shear
- K_{I} = stress-singularity or intensity factor for crack-opening mode
- θ = angular coordinate from the line directly ahead of the crack
- μ = shear modulus
- ρ_s = smallest homogenous region to which fracture criterion, Eq. 10, applies
- σ = normal tensile stress at infinity (gross-section stress)
- σ_N = mean normal tensile stress across net section
- σ_Y = yield strength under combined stress

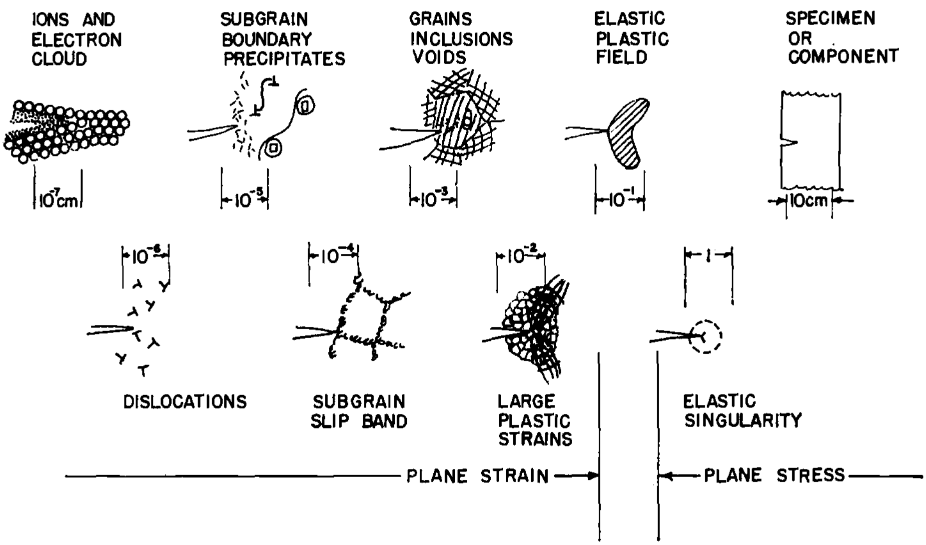

FIG. 1—Schematic Illustrations of Fracture Veiwed at Different Scales. For the Stress State it Is Assumed the Specimen or Component Thickness Is One Millimeter.

- K_{III} = stress-singularity factor for shear parallel to the leading edge of the crack
- r_Y = crack-size plasticity correction for the linear elastic model
- r = radial coordinate from the crack tip
- R = radial coordinate to boundary of plastic zone
- R_0 = radial coordinate to boundary of plastic zone directly ahead of the crack
- W = total width of symmetrical notched specimen
- γ = shear strain
- γ_Y, γ_F = shear strain at yielding and fracture, respectively
- σ_{YS} = yield strength in uniaxial tension
- τ = shear stress at infinity in Mode III (gross-section stress)
- τ_N = net-section shear stress in Mode III.

KINDS OF ELASTIC AND PLASTIC STRESS AND STRAIN FIELDS

For a material of finite yield strength, when the dimensions of the crack and of the component are sufficiently large and the applied stress is sufficiently small, the plastic zone may be regarded as negligibly small and the simplest analytical model is the one which centers attention on the elastic stress distribution at the crack border. As has been shown (1–5), this distribution can be regarded as the sum of the leading terms of the series expansion of each of three stress distributions, one for each of three modes of deformation shown in Fig. 2.

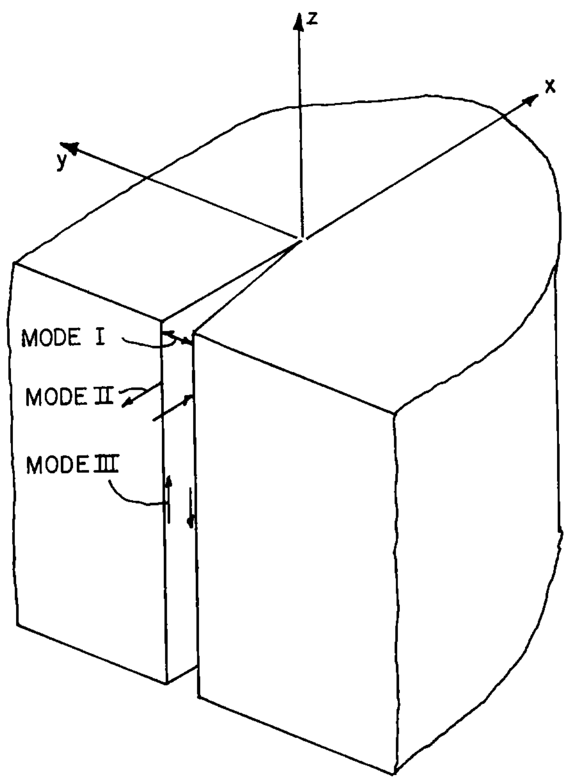

FIG. 2—Modes of Deformation of a Crack.

Mode I: Tension normal to the faces of the crack (either plane strain or plane stress),

Mode II: Shear normal to the leading edge of the crack (plane strain or plane stress),

Mode III: Shear parallel to the leading edge of the crack (anti-plane strain).

Aside from additive uniform stress fields, three scalar constants, or stress-singularity coefficients, K, are all that is needed to specify completely the stress distributions near the border of the crack. Consider, for example, the elastic stress singularity for Mode III, longitudinal (or parallel) shear. Assume the crack lies in the left half of the x,z-plane with the leading edge of the crack along the z-axis. Cylindrical polar coordinates around the z-axis are also used with θ measured from the right half of the x,z-plane. The shear stress components are:

$$\left.\begin{aligned} \tau_{\theta z} &= \left(\cos\frac{\theta}{2}\right)\frac{K_{\text{III}}}{(2\pi r)^{1/2}} \\ \tau_{rz} &= \left(\sin\frac{\theta}{2}\right)\frac{K_{\text{III}}}{(2\pi r)^{1/2}} \end{aligned}\right\} \qquad \ldots\ldots\ldots(1)$$

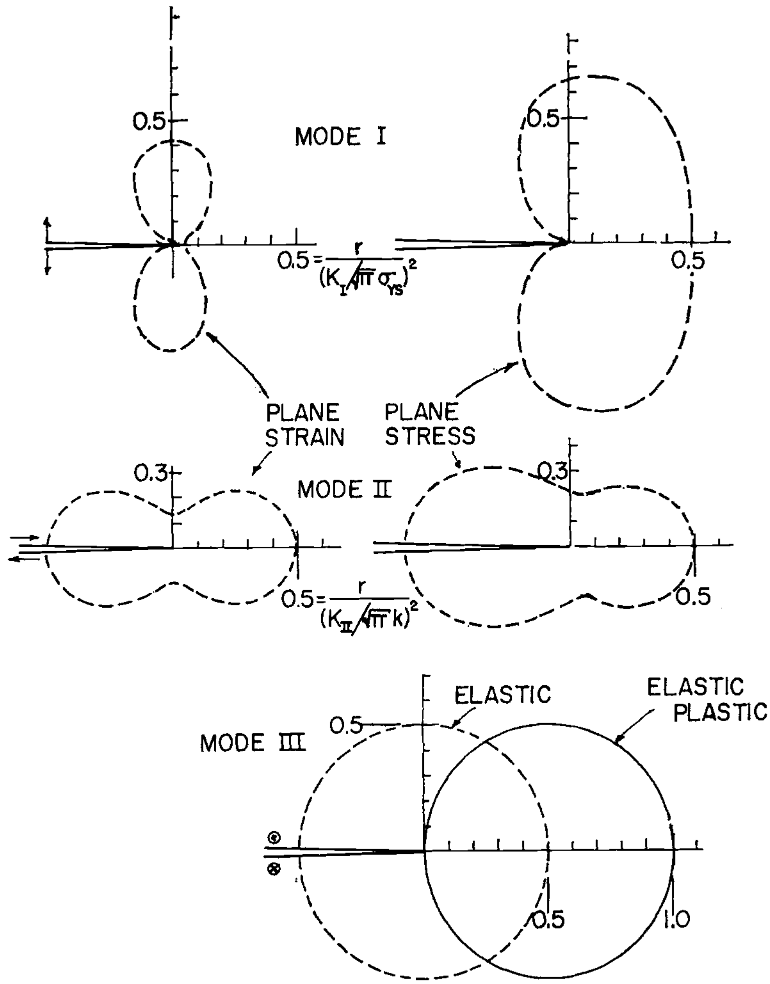

Fig. 3—Elastic Stress Singularities of the Different Crack Deformation Modes Viewed in Terms of Mises Yield-Limit Lines. Poisson's Ratio Is Assumed to Be 1/3.

The loci of fixed values of the maximum shear stress are simply concentric circles around the border or leading edge of the crack.

The constants, K, are determined by the size and shape of the part and the applied loads. For instance, for a crack of length $2a$ in an infinite body,

$$K_{\text{III}} = \tau(\pi a)^{1/2} \qquad (2)$$

where τ is the value of τ_{yz} remote from the crack (gross-section stress). Values of the K's for other shapes and configurations are available in the literature.

The three elastic stress singularities are illustrated in Fig. 3 by indicating the locus of points at which the Mises yield criterion would be exceeded if the elastic stress distribution were unaffected by yielding, assuming Poisson's ratio to be 1/3. The difference between the hypothetical plane-strain and plane-stress loci is not due to the stress components in the plane, which are identical, but to presence or absence of transverse constraint. Of course, yielding affects the stress distribution outside the plastic zone and thus modifies the shape of the plastic zone itself. Such a result from the analysis for longitudinal shear (5) (Mode III) is shown as a solid line in Fig. 3.

If the plastic zone is small enough relative to the length of the crack and to the distance to the next nearest boundary of the part, there will still be a region intermediate between the plastic-zone size and the crack-length or part size, in which the elastic stress singularity is a good approximation to the stress, as shown in Fig. 4.

When the elastic stress distribution sets the boundary conditions for the plastic region within it, since the tendency for unstable fracture in the presence of plastic flow turns out to be relatively independent of how a given state of applied stress and crack length was reached, the elastic stress singularities are expected to have unique values at the onset of unstable fracture. Thus, the intensity of the elastic stress singularity can be used to predict the fracture of the prototype from the fracture of a specimen.

When the crack or the notched specimen is sufficiently small, the plastic zone can be so large relative to the size of the part that there is no intermediate elastic

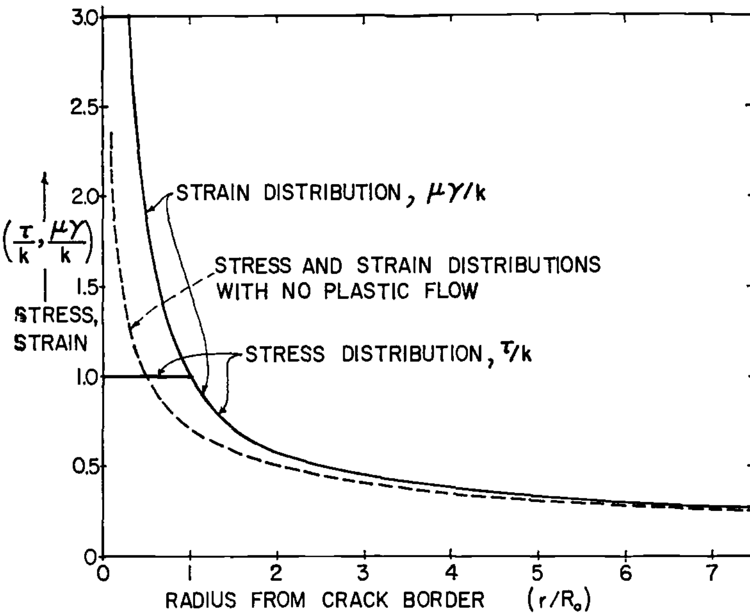

FIG. 4—Effect of Yielding upon Stress Near the Crack from Mode III Elastic-Plastic Analysis. Yielding at Stress k of a Material with Shear Modulus μ Translates the Stress Curve Away from the Crack by the Amount $R_0/2$, Half the Maximum Extent of the Plastic Zone.

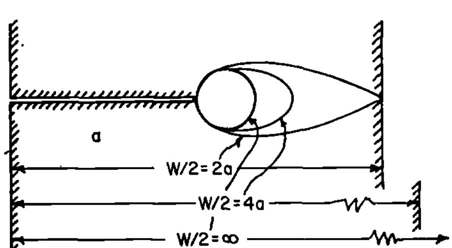

FIG. 5—Effect of Net Section Width on Plastic Zone Shape for a Mode III Elastic Singularity of Fixed Intensity.

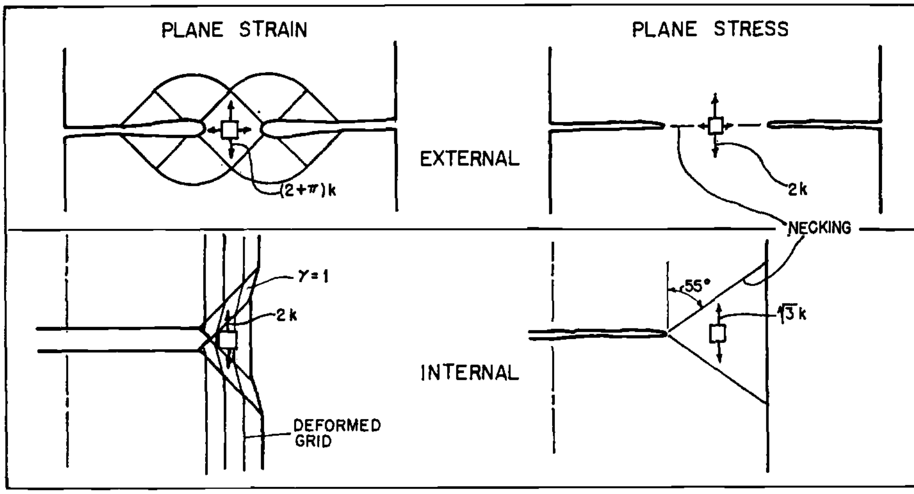

Fig. 6—Slip Line Fields for Fully Plastic Tension Modes.

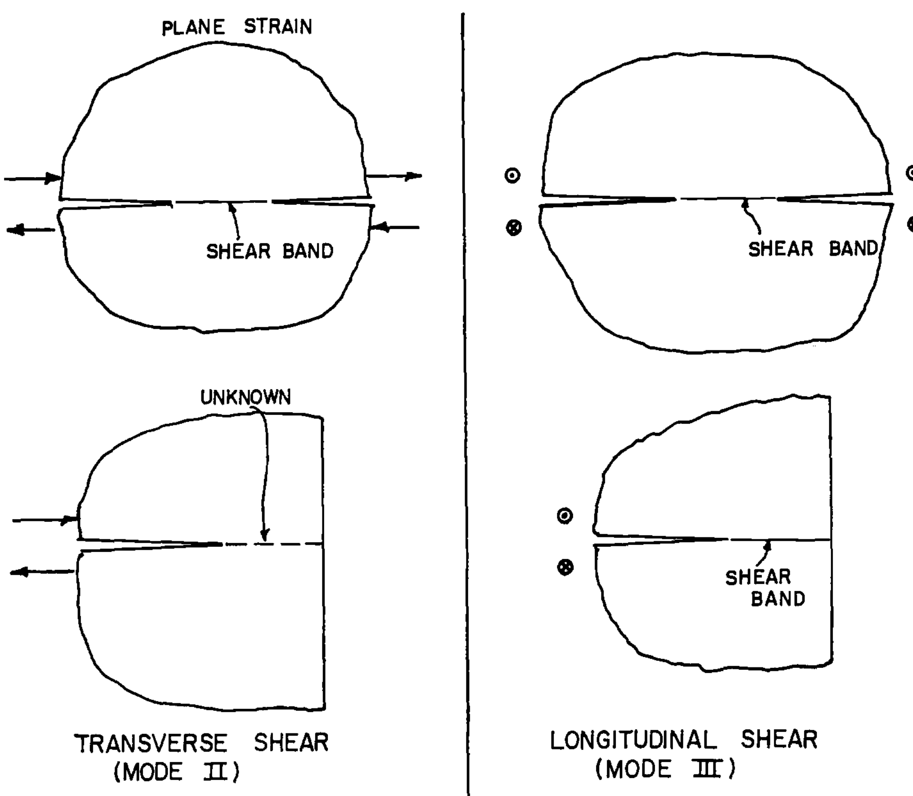

Fig. 7—Slip Line Fields for Fully Plastic Shear Modes.

region where the stress distribution closely resembles the stress singularity of Eq 1. This situation is illustrated by the noncircular Mode III plastic zones shown in Fig. 5, and is expected as the net-section stress for crack propagation approaches the yield strength. There is a significant interaction between the plastic zone and the boundary of the part, so no intermediate elastic region exists where the stress distribution can be adequately described by an elastic stress singularity. The question now arises as to whether there are relatively simple analytical models for fracture in terms of the next finer-scale point of view, namely, the plastic stress and strain fields. Such models, if available and appropriate, might permit prediction of large-scale fracture behavior from tests with much smaller specimens than are needed for tests of the present K_c and K_{Ic} type. Unfortunately, there are as yet no data or calculations available for the plastic strain distribution at the border of a sharp crack for the practically important situation of plane-strain tension, Mode I. In order to gain insight, we shall therefore turn directly to a number of fully plastic configurations, illustrated in Figs. 6 and 7.

The chief characteristic of fully plastic flow which distinguishes it from elastic deformation is the fact that a stress or strain field cannot gradually die out, but must extend all the way from one free boundary to another. In mathematical terms, this is a consequence of the fact that the governing equations are hyperbolic rather than elliptic. Roughly, the difference is analogous to the difference between supersonic and subsonic flow. The practical consequence of this difference is that in linear elasticity, the character of a crack border stress singularity is not influenced, except in magnitude, by the presence or shape of the nearest free boundary. However, as shown by the internally and externally notched plane-strain cases in Fig. 6, the plastic flow is fundamentally different as a result of the differences in the nearest free boundary. With the external notch there is localized strain directly ahead of the notch; with the internal notch there is not. Under plane strain, for the external notch there is an infinite strain singularity immediately above and below the tip of the notch and the equivalent strain in front of the notch is approximately $(2/\sqrt{3})$ (extension/ligament width) (6); whereas for the internal notch the only stain is a shear srtrain of value unity (equivalent strain $= 1/\sqrt{3}$) along the 45-deg bands running off to either side of the tip of the notch (McClintock, unpublished). Furthermore, the stress on the net section is different, the maximum stress being $(1 + \pi/2)$ times higher for the external notch than for the internal one. Finally, there is a marked difference between the stress distributions in plane stress (7) and plane strain, since under plane stress the maximum stress is only $2/\sqrt{3}$ times higher in the externally notched than in the internally notched specimen.

Under forward shear, only the plane-strain externally notched case has been solved (8). For the internally notched specimen some twelve different flow fields were considered and disproved by Walter (9). The result for longitudinal shear (Mode III) can be readily proven from the uniqueness and rigidity theorems of limit analysis, or can be taken as the limiting case of the elastic-plastic solution discussed above (5). The primary result from study of these shear fields, along with plane-stress tension, is that theoretically the plastic deformation is confined to thin bands, with a resulting intense strain concentration. In actual fact, a small amount of strain hardening will "wash out" this high strain concentration (10). Thus, in contrast to elastic problems, the material will markedly influence the shape of the strain singularity through its strain-hardening characteristics. This effect is least evident in the plane-strain tensile mode.

Despite the complexities indicated above, a certain degree of unification can be gained from a study of specimens which become fully plastic. In tensile fracture, the extremes of fully plastic behavior correspond to ultimate strength measurements under various degrees of biaxiality in plane stress or plane strain. With suitable allowance for strain hardening, the load necessary for fracture can be predicted as the load necessary for plastic instability.

The toughness of a service component which will fracture only after the development of fully plastic instability is substantial and probably adequate. However, fully plastic behavior in the laboratory specimen does not permit us to predict that fully plastic behavior will occur in a service component at much larger scale. Dimensional influences of various kinds are involved. The largest one is the size of the enclosed plastic zone. Others are related to the mechanisms at the tip of the crack which limit the size of the plastic zone. These may include the inhomogeneous nature of plastic flow (slip lines or subgrains) or statistical effects (flaw probability). There are still other dimensional factors at smaller scale. If the crack inserted in the test sample is comparable in size to the cracks of interest in the service component, then the influence upon crack extension of small dimensional factors, including flaws, is modeled in the test specimen closely enough for practical purposes. If the crack in the laboratory specimen propagates with an enclosed plastic zone, then a similar behavior can be predicted in the larger service component. However, when general yielding occurs across the net section of the laboratory specimen prior to fracture, the change in constraint may change the local fracture conditions quantitatively or even qualitatively. From such test results, determination of the size of the enclosed plastic zone which must, conceptually, develop in a large enough specimen is indirect and uncertain. This information is needed to predict fracture behavior for a wide range of crack sizes in a large service component.

As an escape from the disadvantage of small specimen, Wells has suggested using measurements of crack-opening displacement (11). The suggestion of Wells is essentially equivalent to assuming that an intensity of plastic strain, critical for fracture, exists adjacent to the crack border which can be predicted from measurements of the tensile direction movement of the crack surfaces. If deviations from the assumptions basic to this proposal were not serious (no differences in constraint between the enclosed and fully plastic cases and similar strain distributions), knowledge of the crack-opening displacement might be used with some confidence to predict the size of the enclosed plastic zone which would be expected in a large enough specimen. Wells's idea deserves further study and can be better explained at a later point in this paper.

LONGITUDINAL (OR PARALLEL) SHEAR, MODE III

As noted above, there is no analytical model of elastic-plastic deformation near a Mode I or Mode II crack. Turning to fully plastic situations is of limited help because the connection from these strain patterns to those in the enclosed plastic zone has not been developed. These facts greatly enhance the utility of elastic-plastic analysis for the third mode, in which all displacements are parallel to the crack border.

Thorough study of the Mode III elastic-plastic analytical model is supported by the following points:

1. Problems can be solved in relatively simple terms without loss of continuity between the small, enclosed plastic-zone situation and the point of development of fully plastic flow (4).
2. The mathematical analysis can be checked and supplemented by experimental observations (12).
3. Derivation of the plane-stress tensile-mode plastic-zone correction factor by assuming this factor analogous to the same factor for Mode III, shows agreement with observations (13).
4. With the aid of appropriate fracture criteria, the Mode III considerations permit descriptive representation of instability after varying amounts of stable crack growth (14).
5. Increasing use of the Mode III elastic-plastic solutions to assist representation and analysis of experimental results can be expected until equally convenient and versatile analysis models are developed which are specific to the opening mode.

The applicability of Mode III solutions to tensile fracture by analogy has been discussed by McClintock (13,15) for plane stress and for plane strain of an anisotropic material with no displacement in the x-direction. The analogies hold good only when the ratio of yield strength to modulus is low enough so that displacements are negligible compared with the size of the plastic zone. Furthermore, the transverse stress components are indeterminate in the model so that effects of triaxial tension on the local ductility of the material are not predicted. Within these limitations, the analogy suggests a number of phenomena easily recognized in the tensile problem, such as the occurrence of local yielding, the increased plastic strain concentration, and the change in stress direction as well as the incremental changes of plastic strain as the crack advances. Consideration of the model and of its limitations suggests the following procedure for obtaining the Mode I analog from the Mode III elastic-plastic solution:

Applied gross-section stress
$\tau \rightarrow \sigma$
Yield strength
$k \rightarrow \sigma_Y$
Modulus of elasticity
$\mu \rightarrow E$
Stress-singularity factor
$K_{\mathrm{III}} \rightarrow K_{\mathrm{I}}$
Strain-energy release rate
$2\mu \mathcal{G}_{\mathrm{III}} \rightarrow E\mathcal{G}_{\mathrm{I}}$ (plane stress)
$\rightarrow \dfrac{E}{1-\nu^2}\mathcal{G}_{\mathrm{I}}$ (plane strain)

We now turn to a summary of principal characteristics and results for the elastic-plastic crack under longitudinal shear.

Initial Strain Distribution:

For zero strain hardening, the strain at a point r is given in terms of the radius through that point from the crack tip to the elastic-plastic boundary R, the yield strength in shear k, and the shear modulus μ, by:

$$\gamma_{z\theta} = (k/\mu)R/r, \quad \gamma_{zr} = 0 \ldots\ldots (3)$$

Note the increased strain concentration in the plastic region. The strain varies inversely with the radius rather than as its square root as it does in the elastic case. When the plastic zone lies in a small enough region to be enclosed by an elastic stress singularity of the type of Eqs 1 and 2, the elastic-plastic boundary is circular and its radial coordinate from the crack tip is given in terms of the radius for $\theta = 0$ by:

$$R = R_0 \cos \theta \ldots\ldots\ldots\ldots (4)$$

It was noted by Irwin and Koskinen (16) that this result can be easily verified, since both stress components on the boundary of the plastic zone, required by equilibrium and the yield criterion within the plastic zone, exactly match the elastic stress components expected from a crack whose tip is at the center of the plastic zone rather than on its circumference (see Fig. 3). Furthermore, the displacements on the elastic-plastic boundary define the displacements throughout the plastic zone because there is no radial shear strain.

At higher stress levels, as the plastic-zone size, R_0, approaches the crack length or approaches a second free surface, the plastic zone elongates, as shown by the calculations of Koskinen cross-plotted in Fig. 5. Thus, for the same maximum extent of the plastic zone, the strain is more concentrated on the mid-plane when the net-section stress is large than when it is small. This aspect suggests that a one-parameter characterization of the plastic zone will lose accuracy as the net-section stress approaches the yield strength.

General Aspects of Stable and Unstable Crack Extension:

In the absence of any crack extension, the load must rise until fully plastic yielding develops. Thus the occurrence of a maximum load point prior to general yielding of the net section is due to actual crack extension. For the usual crack toughness specimens, assuming constant time rate of separation of the grips, a small crack speed of the order of specimen width divided by loading time is sufficient for the attainment of maximum load and the start of load relaxation (17). In fracture tests with essentially plane strain at the crack border, observations suggest a relatively abrupt onset of fast fracture from a stationary crack border (18,19). On the other hand, a substantial slow crack extension usually precedes instability in crack toughness tests of high-strength metals when the crack-border plastic zone is large relative to the plate thickness (17,18). At a later point it will be shown that a tendency to either condition can be represented by appropriate tensile analogs of Mode III problems.

Loading Without Crack Growth:

Let us first examine the relationship between the plastic-deformation work in the crack-border plastic zone and the strain energy release rate from the completely linear elastic field, $\mathcal{G}_{III}$, during the stage prior to movement of the crack. In a unit thickness volume element, $r\,dr\,d\theta$, within the plastic zone, the inelastic deformation work is given by:

$$d\Omega = \frac{k^2}{\mu}\left(\frac{R}{r} - 1\right) r\,dr\,d\theta \ldots\ldots (5)$$

The integral of $d\Omega$ over the plastic zone gives the result

$$\Omega = \frac{k^2}{\mu} A \ldots\ldots\ldots\ldots (6)$$

where A is the area of the zone. If the zone is relatively small so that the shape is circular, and we let $r_Y = R_0/2$ be the radius of this circle,

$$\Omega = \frac{k^2}{\mu} \pi r_Y^2 \ldots\ldots\ldots\ldots (7)$$

For a Mode III plastic zone of this kind, we know, from the elastic-plastic solution, that

$$r_Y = \frac{K_{III}^2}{2\pi k^2} = \frac{\mu \mathcal{G}_{III}}{\pi k^2} \ldots\ldots\ldots (8)$$

As the plastic zone grows to the size R_0, the position of the crack border for purposes of linear elastic analysis advances by the amount, r_Y.

In linear elastic fracture mechanics, an extension movement, α, of the crack border in the presence of a crack-extension force, $\mathcal{G}$, implies a stress field energy loss (per unit of thickness or crack-border length) equal to $\alpha\mathcal{G}$. The analysis provided in Irwin's definition of $\mathcal{G}$ (3) represented $\alpha\mathcal{G}$ in terms of the release movement of closure forces along the segment α. This analysis has been shown to be mathematically equivalent to representation of the stress field energy loss in terms of the load and load displacement for the entire specimen (34,35).

From Eqs 7 and 8, Ω equals $\mathcal{G}_{III} r_Y$, which suggests the movement, r_Y, of the force, $\mathcal{G}_{III}$, provides the stress field energy loss utilized in the plastic work. However, $\mathcal{G}_{III}$ is not constant during loading, but increases in proportion to r_Y. Thus, only $\frac{1}{2}\mathcal{G}_{III} r_Y$, or half the necessary supply of strain energy, can be found from study of the change in compliance of the specimen in terms of linear elastic analysis. That is, only half the necessary strain energy would go out of the linear elastic strain field at its singularity as the crack advanced by r_Y. (This energy flux represents the surface energy in a Griffith-theory treatment.) But the energy available for plastic work is that which flows across the elastic-plastic boundary in the actual material. This latter flux consists of not only the energy flux out through the singularity, but also the increase in the elastic energy in that region of the linear elastic strain field which is plastic in the actual case. The total flux across the elastic-plastic boundary must equal the plastic work plus the residual elastic energy of the region within the plastic zone. To verify this, the energy balance can be written as:

$$\frac{1}{2}\mathcal{G}_{III} r_Y + \int \frac{\tau_{rz}^2 + \tau_{\theta z}^2}{2\mu}\, dA = \int d\Omega + \int \frac{k^2}{2\mu}\, dA \quad \ldots\ldots (9)$$

Integration and rearrangement with the aid of Eqs 1, 7, and 8 confirm the identity.

The fact that energy is consumed in the nonlinear dissipation process at a rate which is twice the linear elastic $\mathcal{G}$ value was initially surprising to the authors. Although the result has been demonstrated only for the growth of the plastic zone prior to crack motion, it appears that in general the linear elastic analysis does not provide the total stress field energy loss. Thus, a degree of uncertainty relative to the energy balance local to the plastic zone is inherent in the linear elastic analysis. For this reason the physical interpretation of K is somewhat easier to discuss than that of $\mathcal{G}$. In terms of interests central to this paper, this result enhances the advantage of representing initiation, growth, and unstable acceleration of crack extension in terms of separation mechanisms occurring at a finer scale. This problem will be discussed next.

Fracture Criteria:

Within the plastic zone in Mode III, a fracture criterion cannot be based upon stress because increasing the load merely enlarges the plastic zone, within which the stress level stays at the constant value, k. (In other modes, of course, different states of stress would modify the fracture criterion.) A fracture criterion cannot be based upon strain alone because the analysis indicates an infinite plastic strain at the crack border, no matter how little the applied stress.

The limits of continuum analysis suggested by Fig. 1 may now be considered. Presumably the average strain, from the crack border across the small region containing the micro-separation processes, is finite, and strains larger than this in the analytical model do not possess physical significance. Furthermore, from physical considerations, fracture in this region will depend only on the stress and strain in this region. External actions will be felt only insofar as they affect the local stress and strain. The average strain in the plastic zone within a small distance, ρ_s, from the crack border might therefore be established as a fracture criterion. This is equivalent to considering a critical displacement across a small element of width, ρ_s, within the plastic zone. While such a criterion may appear similar to the displacement criterion suggested recently by a number of writers (20,21,22), the displacement alone is not sufficient for a fracture criterion without stating in how small a region the fracture displacements are concentrated. Alternatively, we could use the strain, γ_F, at a given point ($r = \rho_s$, $\theta = 0$) as a fracture criterion (14):

$$\text{Fracture when } \gamma = \gamma_F \text{ at } r = \rho_s \ldots (10)$$

This choice is analytically simpler and will be used in this discussion. Note that this criterion may be applied to cases where strain is uniform over a region large compared with the structural size, ρ_s, as in the ordinary torsion test, where γ_F can be observed directly. The structural size, ρ_s, is regarded here as the size set by grain size, inclusion spacing, or slip-line spacing at which one can no longer regard the material as a homogeneous plastic continuum but must turn to the next smaller scale model of Fig. 1.

To illustrate this fracture criterion, let us first apply it to the more familiar case of fracture in a brittle, linearly elastic material. Here the stress aspect is significant and the criterion could be based on either stress or strain. Practically, such Mode III fractures are not observed, but the tensile analogy may make such a treatment of interest. We assume fracture occurs when the strain at a certain small distance, ρ_s, from the crack border reaches the critical value, γ_F, which in a brittle elastic material is τ_F/μ. It is assumed the micro-separation process occurs on an atomic scale, so $\rho_s = b$, the lattice spacing in a crystal or the network spacing in glass. The fracture stress, τ_F, can be assumed to have an ideally high value, say equal to $\mu/2\pi$.

The critical stress singularity can now be estimated, since, from Eq. 1,

$$r = \frac{K_{\mathrm{III}}^2}{2\pi\tau^2}, \quad \text{or} \quad K_{\mathrm{III}c}^2 = 2\pi b(\mu/2\pi)^2 \ldots (11)$$

The surface energy, T, which is half the critical strain energy release rate, $\mathcal{G}_{\mathrm{III}c}$, may also be estimated:

$$T = \mathcal{G}_{\mathrm{III}c}/2 = K_{\mathrm{III}c}^2/4\mu = b\mu/8\pi \ldots (12)$$

For iron, taking $b = 3$ A and $\mu = 11 \times 10^6$ psi gives 900 ergs/cm^2, compared to the 2400 ergs/cm^2 for tension estimated by Gilman (23), a plausible outcome under the assumptions.

In this illustration, as in others where the plastic or nonlinear zone is comparable in size to the structural size, ρ_s, a fracture criterion such as Eq 10 is equivalent to the Griffith crack theory. However, with plastic flow, the fracture work rate may be much greater than theoretical estimates of surface energy for the solid state of the material. We therefore turn to the plastic case, considering first the initiation of cracking.

Initiation of Crack Extension:

Cracking should initiate when the strain distribution of Eq 3 is such as to satisfy the fracture criterion of Eq 10:

$$\gamma_F = \gamma_Y R_{0i}/\rho_s, \ldots \ldots \ldots (13)$$

where the yield strain, $\gamma_Y = k/\mu$, is introduced for convenience. For low stress levels, the extent of the plastic zone for initiation, R_{0i}, can be expressed in terms of the stress singularity from

Eq 8 and the critical value of the stress singularity for fracture can be found:

$$K_{IIIi} = k(\pi R_{0i})^{1/2} = (\pi\rho_s\gamma_F/\gamma_Y)^{1/2} \ldots (14)$$

At higher stress levels these expressions require modification. A first approximation can be obtained by assuming that the elastic stress field is that corresponding to the crack in a purely elastic solid whose extent is greater than the actual crack length, a, by the amount, r_Y. Combination of Eqs 2 and 8 then leads to

$$r_Y = \frac{(a + r_Y)\tau^2}{2k^2}, \text{ or } r_Y = \frac{a\tau^2/2k^2}{1 - \tau^2/2k^2} \ldots (15)$$

In order to allow for the increase of the elastic singularity due to finite plate width, the above equation can be modified (24) to:

$$\frac{2\pi r_Y}{W} = \left(\frac{\tau}{k}\right)^2 \tan\left(\frac{\pi a}{W} + \frac{\pi r_Y}{W}\right) \ldots (16)$$

Equations 15 and 16 tend to underestimate the plastic-zone size by increasing amounts as τ/k increases above 0.5, and Eq 16 is implicit. We present here an alternative representation, which is closer to theoretical solutions of the problem (4,5,22). This is found by multiplying the expression for low stress applied to an infinite plate by a series of factors, the first of which accounts for the increase in linear elastic stress singularity due to the finite width of a plate, while the second accounts for the increase in radius of plastic zone due to increased stress in a plate of infinite width. At the stress level, $\tau/k = W/(W - 2a)$, equilibrium requires that the plastic zone should extend all across the specimen so that:

$$R_0 = a\left(\frac{\tau}{k}\right)^2 F_W F_\tau \rightarrow \left(\frac{W}{2} - a\right) \ldots (17)$$

Since this is not predicted by the above factors, a final correction is introduced to make up the difference, giving:

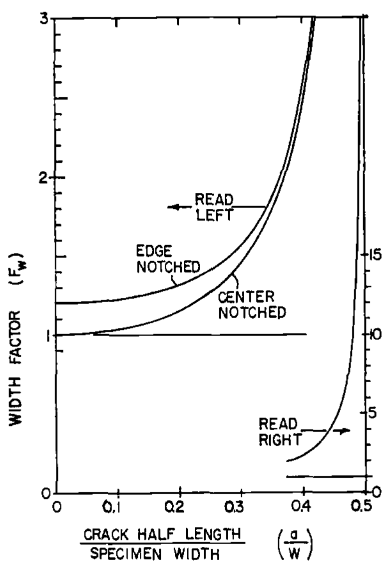

FIG. 8—Plastic Zone Correction Factor for Finite Specimen Width, F_W (Deduced from Ref. 24, and Eqs 4 and 11 or 19).

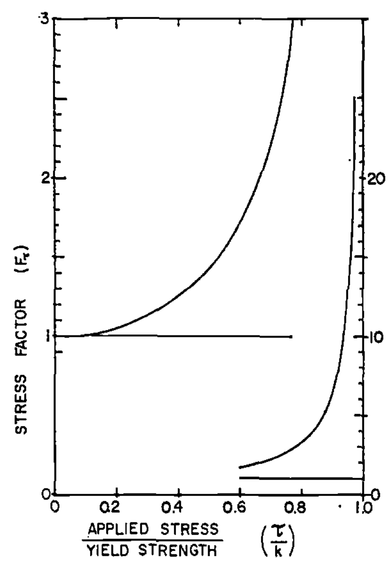

FIG. 9—Plastic Zone Correction Factor for High Stress Level in Infinite Solid, F_τ (Deduced from Refs. 4, 14, or 22).

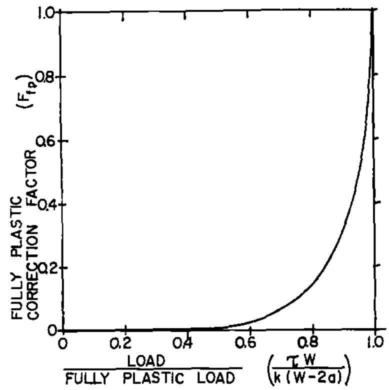

FIG. 10—Plastic Zone Correction Factor for Close Approach to Fully Plastic Yielding, $F_{fp} = 1 - \{1 - [(\tau/k)\cdot(W/W - 2a)]^6\}^{1/2}$.

When fracture data are represented in terms of K values, it seems inappropriate to employ a complex procedure to allow for the plastic zone because the linear elastic viewpoint tends to lose meaning in the approach toward conditions of general yielding. Correspondingly, the equation for K^2 from Ref (24) (shown here in the form of Eq 16) does not accurately predict the size of the plastic zone at high stress levels. Furthermore, effects due to alteration of the plastic zone, when growth of the plastic zone is accompanied by slow crack extension (discussed in the next section) have not been taken into account. However, one can note that modifications of the r_Y correction of Ref (24), for purposes of *empirical* extension of the K value representation into the high stress level range, are possible. For such purposes, the r_Y correction might be replaced by any allowance for plastic yielding that

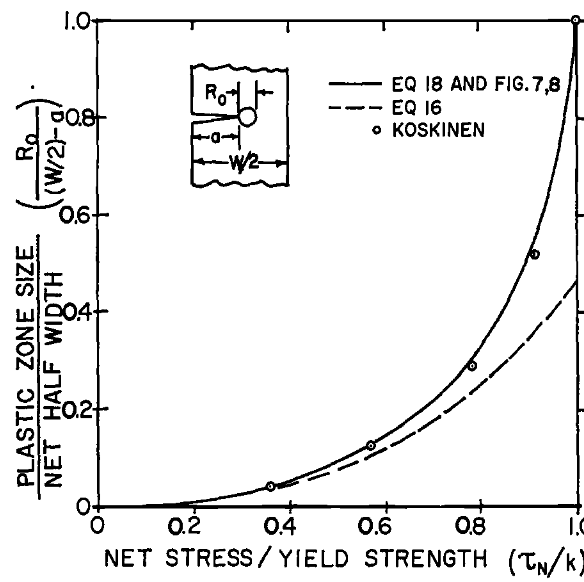

FIG. 11—Plastic Zone Size from Eq 18 in Comparison with Eq 16 for $W = 4a$. Points Are from Koskinen (5). For $W = 4a$, $\tau_N = 2\tau$.

$$R_0 = a\left(\frac{\tau}{k}\right)^2 F_W F_\tau \cdot\left\{1 + \left[\frac{(W/2) - a}{a(\tau/k)^2 F_W F_\tau} - 1\right] F_{fp}\right\} \quad (18)$$

The required factors are given in Figs. 8, 9, and 10. These two methods are compared with the numerical results for a crack half way through in Fig. 11.

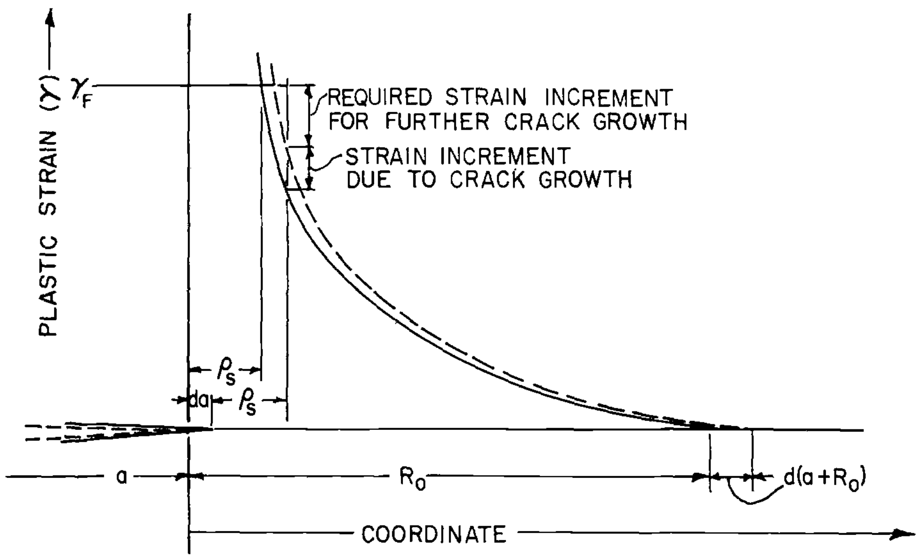

FIG. 12—Strain Increments Related to Crack Growth.

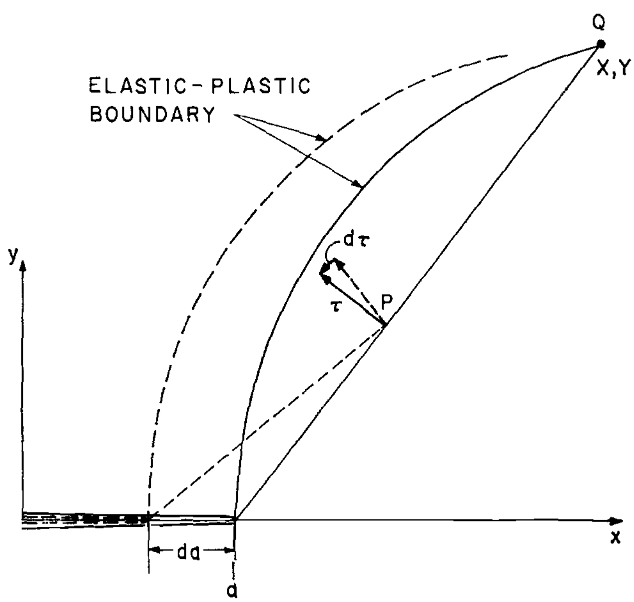

FIG. 13—Change in Stress Direction Related to Crack Growth.

seems more suitable. We will return to this topic later.

Crack Growth and Instability:

In studying crack growth, one might at first hope that an understanding could be obtained directly from energy considerations based on estimates of the work done in the plastic zone. If this work were calculated using the strain field of the static crack, there would be no account taken of the plastic strain due to crack growth itself. An examination of the energy balance, therefore, requires study of a moving crack to the point where the maximum load is reached, so that the energy required can be supplied solely from the surrounding field. The condition for a load maximum is governed in part by the conditions for local fracture. Thus it is necessary to treat the problem so that the relation of stress to crack growth is would be less than the fracture strain, no further cracking would occur.

Actually, however, there is a strain due to the advance of the crack. The solution to the mechanics problem of a crack growing in Mode III shear indicates that at a particular point in the plastic zone, the direction of the stress changes, as indicated in Fig. 13. This produces an elastic strain which, through the compatibility equations, enforces a plastic strain. From the mechanics of the problem, it turns out that, if the

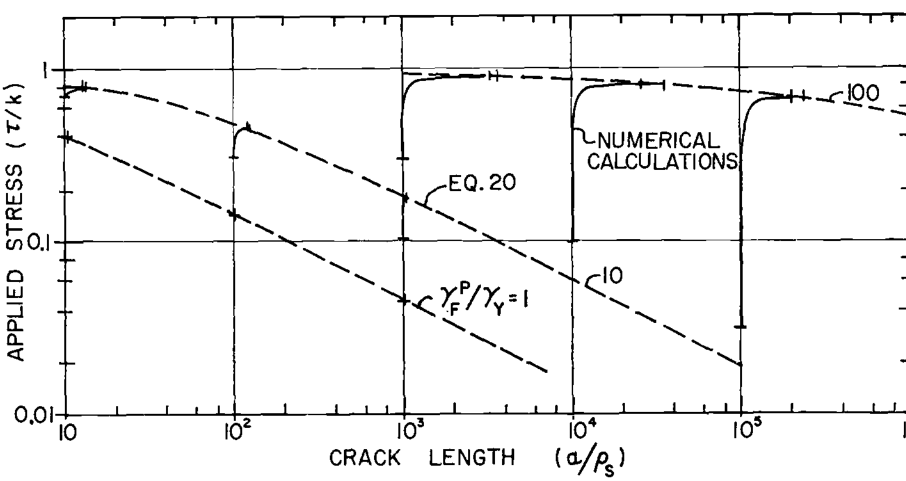

FIG. 14—Stress Level for Instability of Mode III Cracks after Increasing Loads and Crack Growth. Upper and Lower Bounds to the Unstable Crack Size Are Shown by Vertical Ticks.

controlled by a specific fracture condition such as Eq 10. The illustration which follows assumes a central crack in a specimen with the crack length negligible in comparison with specimen dimensions.

Consider first whether the fracture criterion of Eq 10 would be satisfied if the crack were to advance by an amount, da, without any plastic strain due to the advance of the crack. The strain at the point, ρ_s, ahead of the crack border would be that found from the strain distribution of Eq 3, indicated by the solid line in Fig. 12. Since this strain crack is currently at the point a, then the increment of plastic strain, $d\gamma^p$, at a point x ahead of the crack, due to an advance of the crack by da, is (13,14,25):

$$d\gamma^p = \frac{\gamma_Y}{x - a}\left\{1 + \frac{R_0}{a} + \ln\frac{R_0}{x - a}\right\} da \quad (19)$$

At first, as indicated by the dashed line in Fig. 12, this strain increment is not enough to offset a decrease in strain due to the fact that the crack is advancing into material with less prior strain. Therefore, an additional increase in applied stress is required. When this increase has been enough to satisfy the fracture criterion, an additional increment of fracture will occur, and so on. The resulting integral equations are involved and require precise numerical integration, carried out along the general lines of Ref. (14) but with the corrected form for the strain due to crack growth, Eq 19, from Ref. (13). Detail regarding the numerical techniques is given in Ref. (26). The results are presented in Fig. 14.

As noted in preliminary calculations, and as observed in foil testing (14), the stress level required to make a crack propagate at first increases rapidly, but then more slowly until eventually a maximum stress is reached. At this point, the crack becomes unstable. At low stress levels, the crack length at instability approaches an inverse square root dependence on the applied stress. This is expected since the plastic zone is then surrounded by a characteristic elastic stress field, described except near the plastic zone by Eq 1 as shown on Fig. 4. Both the crack length at instability and the amount of crack growth to instability depend markedly on the ductility of the material. At high stress levels, the applied stress is, of course, limited by the yield strength.

A careful examination of the curve for a given local ductility, $(\gamma_F{}^p/\gamma_Y)$, shows the amount of crack growth prior to instability to be higher at lower stress levels, although it may not at first appear this way from the logarithmic scale.

One would like to apply these results to tension fracture testing in which the fracture contains a central region of plane-strain separation. Investigations of K_c have naturally centered upon metals with the highest strength consistent with a moderate degree of toughness. As a result, a high proportion of the K_c testing experience is with tests in the fracture mode transition range, a region in which there is a gradual development of shear lips from the corners of the sharp starting notch. Typically, the crack-growth region in which the shear fracture obtains its characteristic running crack size is essentially the magnitude of slow or stable cracking. During the stable period, the degree of plane strain is decreasing and the corresponding increase of oblique shear separation must be regarded as contributing in a major way to the restraint against instability in the onset of fast fracture. For these reasons, a close quantitative comparison of the Mode III fracture with K_c tests in the transition range is not advisable. It is interesting to note, however, that the ink stain slow crack indications show a stable crack extension which is of the order of the formally estimated plastic-zone size at instability, R_{0c}, a result consistent with the lower ranges of ductility shown in Fig. 14. The corresponding value of 10 for $\gamma_F{}^p/\gamma_Y$ may seem low, but is consistent with the recently developed quantitative criterion for ductile fracture by the growth of holes when there is a high state of triaxial tension (as in Mode I plane strain) in front of a crack (27).

As a second illustration of these results, Krafft (28) has noted that the value of K_{Ic} for tests of a given material at different temperatures or strain rates appears to vary in proportion to the strain-hardening exponent, n. This might be expected for two reasons. First, for viscous materials, instability (crack growth with constant load) does not occur, since the strain distribution in a viscous material is identical to that in an elastic material and as a result there is no strain increment due to crack growth itself. Since a viscous material is in some ways analogous to a strongly strain-hardening material, from the mechanics alone one would expect a lower tendency to instability. Second, if fracture is associated with the growth of holes, then the fracture strain itself increases strongly with n (27). A quantitative development of these ideas is not possible at this stage due to the geometrical complications discussed above.

Because of the cost and inconvenience of numerical calculations, it would be desirable to have a closed-form solution for the crack growth plotted in Fig. 14. Fortunately, conditions for final instability are evaluated more easily than those for growth, since the condition of instability is that the rate of increase of stress becomes zero. It also turns out that one may assume that the size of the plastic zone is nearly constant as the highly strained plastic region just ahead of the crack sweeps over the point in question. The validity of this approximation is checked by a detailed study of the equations or by comparing the results of the analysis with Fig. 14. The resulting expression for the radius of the plastic zone at instability is given in terms of its ratio to the crack half-length, $P = R_c/a$, where P is a function of the stress level alone, in a plate of infinite width (13):

$$R_{0IIIc} = \rho_s \exp \{-(1 + P) + [(1 + P)^2 + 2(\gamma_F{}^p/\gamma_Y)]^{1/2}\} \quad (20)$$

For low stress levels, the ratio of the radius of the plastic zone to the crack length will be small compared with unity, and for ductile materials the plastic strain at fracture will be large compared with the yield strain, giving

$$R_{0IIIc} = a(\tau/k)^2 = \rho_s \exp [-1+(2\gamma_F{}^p/\gamma_Y)^{1/2}] \quad (21)$$

For completely brittle materials with $\gamma_F{}^p = 0$, $\rho_s = b$, Eq 20 becomes

$$R_{0IIIc} = b \quad (22)$$

which is identical to the condition for initiation, since there is no stable crack growth in completely brittle materials. For actual materials, it might be a better approximation to the nonlinear elastic force curves to assume a "plastic" strain equal in magnitude to the linear strain at the ideal strength of the material, $\tau_i/\mu = 1/2\pi$. For such small ductilities, the apparent surface energy, T, is almost identical to that obtained by applying the fracture criterion to a linear elastic solid, Eq 12:

$$T = \frac{b\mu}{16\pi} \exp [-1 + (1 + 2\gamma_F{}^p/\gamma_Y)^{1/2}] = \frac{2.08 b\mu}{16\pi} \quad (23)$$

From Eqs 21 and 8, for ductile materials at low stress levels,

$$\mathcal{G}_{IIIc} = \frac{\pi\rho_s k^2}{2\mu} \exp [-1 + (2\gamma_F{}^p/\gamma_Y)^{1/2}] \quad (24)$$

Note that again G_{IIIc} denotes not the actual strain energy release rate, but rather that from a linearly elastic one having the same stress distribution at large distances from the plastic zone.

Equation 21 shows that at low stress levels the condition for instability can be characterized in terms of the size of the plastic zone. R_{0IIIc} can, therefore, serve as an alternate to K_{IIIc} in describing the tendency to unstable cracking. At high stress levels, however, Eq 20 shows that R_0 depends not only on ρ_s and γ_F, but also on the stress ratio (through the plastic-zone ratio, P). Alternatively, rewriting Eq (20) in terms of critical crack length, the material characteristics, ρ_s and γ_F, cannot be separated from the test configuration in terms of a and P. There is no one parameter, corresponding to K_{IIIc} or R_{0IIIc} (in low stress applications), which can correlate behavior over a large variety of crack lengths at high stress level. Thus, to extend the analysis of fracture (following slow crack growth) beyond regions representable in terms of a linear elastic model, it is not only reasonable but necessary to base the fracture criterion upon characteristics of the small critical region of the plastic

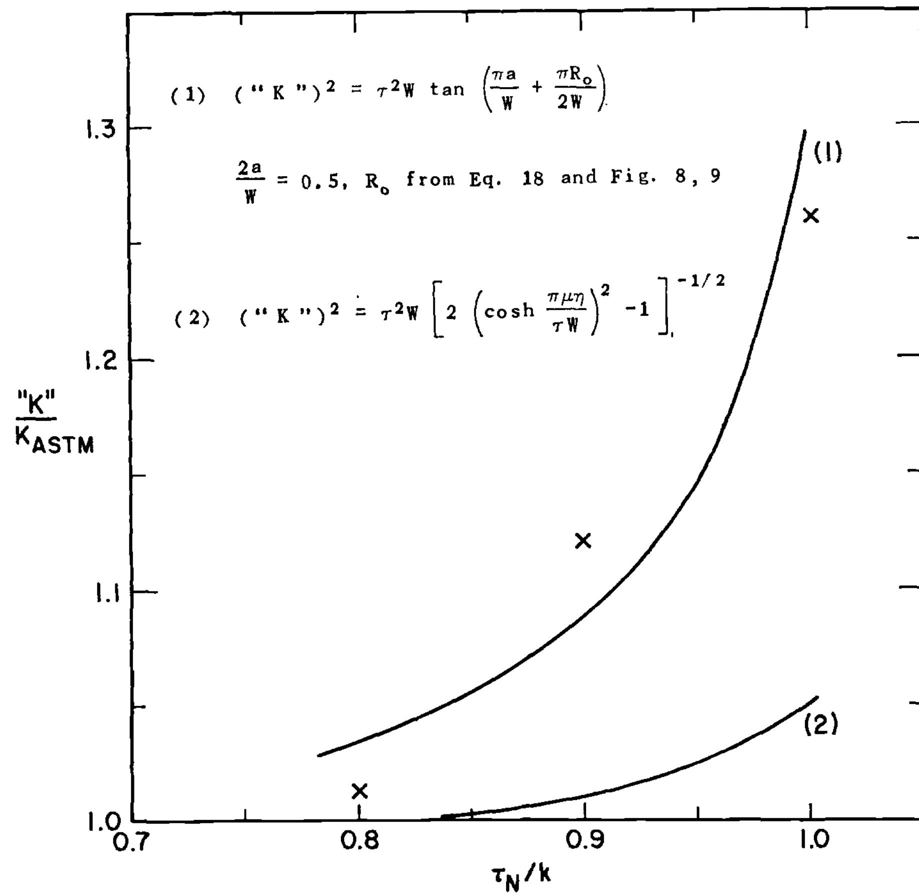

FIG. 15—Observations of High Stress Level Trend of K_c Values (x) Are Shown in Relation to a Prediction, Curve (*1*), from Mode III Analysis Using Equation (18). Also Shown, Curve (*2*), Is a Lower Bound on the Amount of the Trend Which Can Be Expected to Disappear When K_c Is Based upon Compliance Observations.

zone, in consistency with the local nature of the separation process.

Empirical Trend of High Stress Level K_c *Results:*

Under certain conditions (17), values of K_c measured as suggested in Ref. (24) are not constant when the net-section stress at the onset of unstable cracking, σ_N, exceeds 0.8 σ_{YS}. In Fig. 15, the points marked with an x represent the correction factors which would be necessary to eliminate the high stress level trend found in a study of the effect of specimen size with $2a_0/W$ held constant, using 0.05-in. thick 7075-T6 aluminum, shown in Fig. 2 of Ref (17). The values of $2a/W$ at the onset of instability were in the range of 0.4 to 0.5, and the latter figure was adopted in this comparison. Calculations were made using Figs. 8, 9, and 10 and Eq 18. The results, as shown by Curve 1 in Fig. 15, indicate corrections of the right order result if we simply expand the r_Y plastic-zone correction of Ref (24) in proportion to R_0 from the Mode III analysis.

In crack toughness testing of the K_c

and K_{Ic} type, measurements of displacements near the crack or near the loading points can be used along with a calibration to determine the effective crack size (31). This procedure contains an inherent adjustment for the plastic zone in that the "apparent compliance" (reciprocal of the secant modulus) is increased by stress relaxation in the plastic zone. This form of correcting for the plastic zone may differ appreciably from the r_Y correction procedure of Ref (24) at high stress levels. Rough estimates based upon

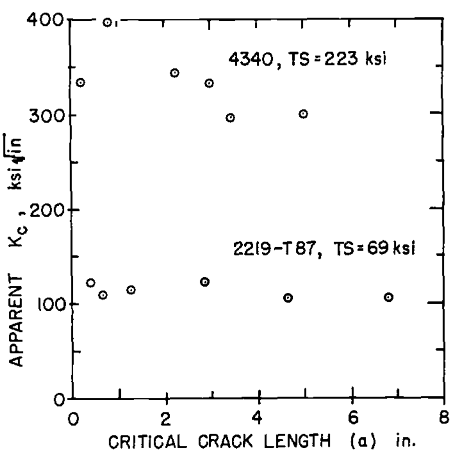

FIG. 16—Critical Stress Singularity from Data of Ref. (29) Calculated According to Figs. 7 and 8.

Mode III elastic-plastic analysis suggest that use of the "apparent compliance" method should reduce the magnitude of the high stress level trend in K_c measurements.

For Curve 2 of Fig. 15, values of K were estimated from the Mode III analysis crack-opening displacement, η. Curve 2 assumes the effective crack size would be estimated from observation of crack-opening displacement at the leading edge of the real crack. At this position the high stress level stretch of the plastic zone in the x-direction has a minimum influence upon displacements. Curve 1 overestimates the effect of the plastic zone upon displacements by placing the mathematical end of the linear elastic crack well beyond the center of gravity of the plastic-zone area. Both curves would be elevated somewhat if calculated for the value $2a = 0.4W$ of the data rather than for $2a = 0.5W$. Curves 1 and 2 furnish crude upper and lower bound estimates of the effect of using apparent compliance to provide the effective crack size for a linear elastic computation of K.

The correction factors of Figs. 8, 9, and 10 were also applied to the data given in Figs. 1 and 2 of Ref (29), as shown in Fig. 16. Apparently, for small cracks in large sheets ($2a/W < 0.25$) the fully plastic factors should not be applied. It must be borne in mind that these correction techniques, applied to Mode I, are empirical in nature. Nevertheless, so long as test results show constancy of the critical K values extending across from the low net section stress range, critical K values determined at high stress level retain a very real physical meaning.

Crack-Opening Considerations:

From the Mode III elastic-plastic solution, the crack opening, 2η, at $r = 0$ is:

$$2\eta = \int_{-\pi/2}^{\pi/2} \gamma_{z\theta}\, r d\theta = \frac{k}{\mu} \int_{-\pi/2}^{\pi/2} R d\theta \quad (25)$$

For the circular plastic zone, $R = R_0 \cos \theta$, and

$$2\eta = \frac{2kR_0}{\mu} \quad (26)$$

From Eq 8, the strain energy release, $\mathcal{G}_{III}$, is related to the crack opening by

$$\mathcal{G}_{III} = \frac{\pi}{4} k(2\eta) \quad (27)$$

The tensile analog is

$$\mathcal{G}_{I} = \frac{\pi}{4} \sigma_Y(2\eta) \quad (28)$$

Neglecting the difference between $\pi/4$ and unity, one can interpret this expression as indicating that 2η times the yield stress provides a measure of the work rate for crack extension. Wells pointed out this interpretation (11). Assuming the indicated proportionality might continue to hold when the plastic zone was comparatively large and even for general yielding, Wells suggested that measurements of the plastic crack-opening displacement should be studied as a possible means for permitting crack toughness determinations using specimens of relatively small size. This hypothesis would be necessarily valid if the stress and strain in front of the crack were always the same for the same crack opening.

Consider next the expression for the crack opening, 2η, in Mode III analysis when the plastic zone is no longer circular. If we write

$$R = R_0 f(\theta) \qquad (29)$$

then

$$2\eta = \frac{kR_0\pi\bar{f}}{\mu} \qquad (30)$$

where $\bar{f}$ is the average value of f in the range $-\pi/2$ to $\pi/2$. From Koskinen's graphs (5), $\bar{f}$ decreases as the plastic zone elongates, as may be seen from the strain distributions in Fig. 17.

If the average radius of the plastic zone were a constant fraction of R_0, then since R_0 determines the local strain according to Eq 3, the displacement fracture criterion would be equivalent to that based on the strain at a small distance, ρ_s, from the crack border. Since $\bar{f}$ is not constant, these two criteria are not equivalent at different stress levels. An enhancement of this difference would be expected when the fully plastic zone is not confined to a slit as in Mode III deformation, but tends to spread out laterally, as in plane-strain Mode I deformation. Experimental data permitting a comparison of these two criteria would be quite helpful. For the displacement criterion, the data would be the

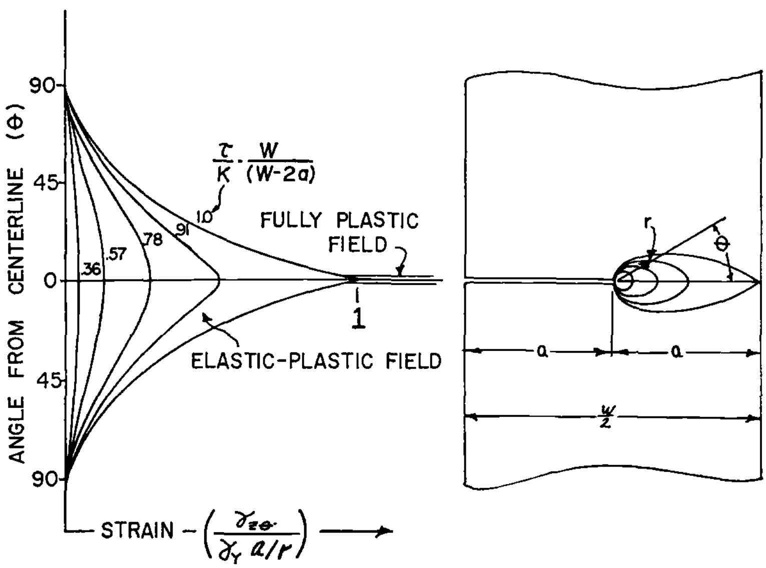

FIG. 17—Strain Localization at High Stress Levels from Ref. 5, Expressed in Generalized Form.

displacements at the crack border. For the fracture strain and structural size, the data would be the reduction of area of unnotched specimens, the effect of triaxial stress on fracture strain, and micrographs of the structure. In addition, it would be desirable to report yield strength, tensile strength, and uniform elongation so that a reasonable approximation to the stress-strain curve can be obtained.

$$2\eta = 2a\tau^2/k\mu \qquad (31)$$

For unloading from τ_{max},

$$2\eta = 2a\tau_{max}^2/k\mu + 2a(\tau_{max} - \tau)^2/(2k)\mu \qquad (32)$$

For reloading, from $\tau = 0$,

$$2\eta = a\tau_{max}^2/k\mu + 2a\tau/(2k)\mu \qquad (33)$$

At the face of the specimen, the elastic-plastic displacements are found from the elastic solution for a crack whose length is r_Y greater than the actual crack length,

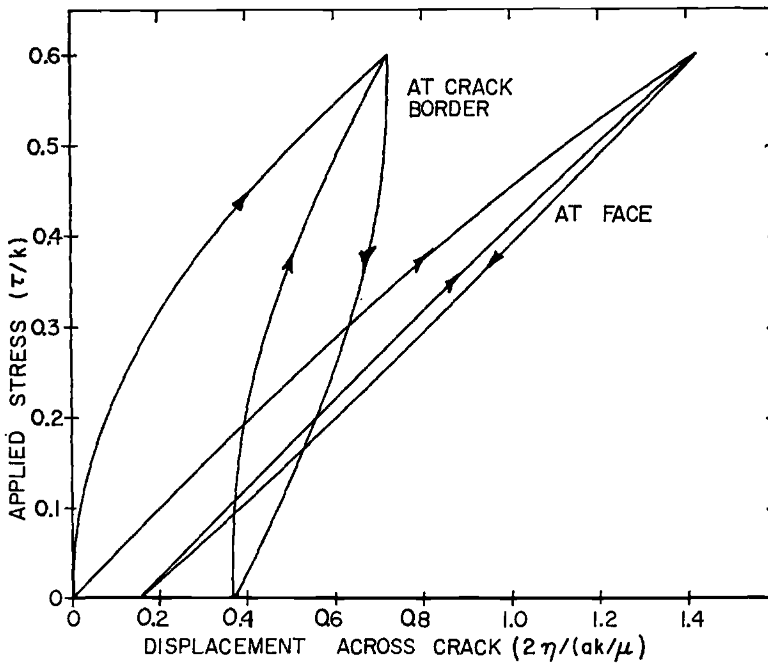

FIG. 18—Displacement Across Crack and Hysteresis Loops for Mode III.

One of the interesting by-products of Eq 26, coupled with the concept that unloading can be regarded as superimposing a reversed load with the yield strength equal to twice the initial yield strength in shear (4), is a prediction of the hysteresis loop on unloading and reloading without crack growth. If the plastic zone remains circular, the displacement hysteresis loop at the crack border can be found from Eqs 26, 8, and 2, in terms of the applied stress. For loading,

as noted above. The elastic solution corresponding to Fig. 2 (Mode III) can be found, for example, by a conformal mapping (30). For the elastic case, with the origin of coordinates at the crack face, and the x-axis parallel to the crack, the z-direction displacement, w, turns out to be given by:

$$w = (\tau/\mu)(\text{imaginary part of } [(x + iy)^2 - a^2]^{1/2}) \qquad (34)$$

where a must be replaced by $a + r_Y$ to allow for the shift of the stress field due to plastic strain. The horizontal displacement between points at $\pm y$ on the face of the elastic-plastic solid (Fig. 2) is then found from Eqs 2 and 8

$$2w = \left(\frac{2\tau}{\mu}\right)(y^2 + [a + a\tau^2/2k^2]^2)^{1/2}$$

$$\approx \frac{2\tau}{\mu}(y^2 + a^2)^{1/2}\left[1 + \frac{a^2}{2(y^2 + a^2)}\frac{\tau^2}{k^2}\right] \quad \text{..(35)}$$

which is of the form,

$$2w = (A\tau/\mu)(1 + B\tau^2/k^2) \quad \text{......(36)}$$

For unloading, from τ_{max},

$$2w_1 = (A\tau_{max}/\mu)(1 + B\tau_{max}^2/k^2) - [A(\tau_{max} - \tau)/\mu][1 + B(\tau_{max} - \tau)^2/(2k)^2] \quad \text{..(37)}$$

For reloading, from $\tau = 0$,

$$2w_2 = (3AB\tau_{max}^3/4\mu k^2) + (A\tau/\mu) \cdot [1 + B\tau^2/(2k)^2] \quad \text{..(38)}$$

The maximum width of the hysteresis loop on unloading and reloading occurs at $\tau = \tau_{max}/2$:

$$2(w_1 - w_2) = \frac{3AB\tau_{max}^3}{16\mu k^2}$$

$$= \frac{3}{16}\frac{a^2}{(y^2 + a^2)^{1/2}}\frac{\tau_{max}^3}{k^2\mu} \quad \text{..(39)}$$

The displacement hysteresis loops for both the face of the specimen and the crack border are shown in Fig. 18, calculated under the assumption that the plastic zone remains circular. At the stress levels shown, this assumption is of marginal validity for the initial loading phase of the cycle but is quite good for the unloading and reloading, since the yield strength in the reverse direction is double the original. Equation 39 for $\tau_{max}/k = 0.56$, $k/\mu = 0.007$, $a_0 = 0.40$ in., $y = 1$ in. indicates a hysteresis loop width of 34×10^{-6} in. for the specimens of Ref (31), whereas of the order of 300×10^{-6} in. was observed. Any Bauschinger effect and the finite width of the specimen would, of course, tend to increase the estimate of the width of the hysteresis loops. However, the major factor introducing the large difference may be the shape of the crack. A loop width as small as 30 microinches would not have been observable within the precision of Boyle's work. Prior to formation of the central tongue of plane-strain fracture, Boyle observed no significant hysteresis. At the comparison point where the factor of 10 difference is noted, a substantial central region of plane-strain fracture had formed. Observations with a thick plate specimen in cyclic loading to lower stress levels would provide a better comparison because the leading edge of the crack would be in plane strain and nearly straight through the thickness of the specimen.

An interesting result of the deflection analysis is that the crack does not close on unloading, but a slight compressive stress would close the crack, first at the face. Application of these results in their present form to fatigue cracking is of some interest. However, it should be noted that the residual stress and strain behind the growing crack may contribute a significant influence and this has not yet been taken into account.

EMPIRICAL REPRESENTATION OF CRACK-EXTENSION OBSERVATIONS

When the plastic zone is relatively small, the representation of the test observations in terms of K values has a good theoretical basis because in this case a variety of plausible fracture criteria predict that similar behavior will occur for similar values of K. The representation of fracture behavior in terms of K values becomes increasingly empirical as increases of plastic-zone size modify the shape of the plastic zone by significant amounts. Measurements indicate that values of K_c and K_{Ic} computed with the adjustment of a small plastic-zone type correction factor remain nearly constant over a large fraction of the range of σ_N below the yield level.

However, in the upper part of this region and certainly above it, the characterization of fracture behavior in terms of K values is largely an empirical data representation formality. This is indicated by the fact that when the unstable crack length, $2a$, in a sharp-notched sheet tension test is less than one quarter of the specimen width, the test result expressed in terms of K_c does not drop below the large specimen K_c value until σ_N exceeds σ_{YS} (17). In other words, the elementary plasticity correction factor derived from Eq 16 is much less successful when $2a/W$ is in the recommended range of 0.3 to 0.5 than when $2a/W$ is smaller. However, the shape changes of the plastic zone, indicated by Mode III analysis, are as extreme in the range $0.8 < \tau_N < k$ for small values of $2a/W$ as in the range used in the recommended K_c test specimens. Thus the observed success of the K_c computation in the range $0.8\ \sigma_{YS} < \sigma_N < \sigma_{YS}$, when $2a/W$ is small, is an empirical success not yet clearly understood.

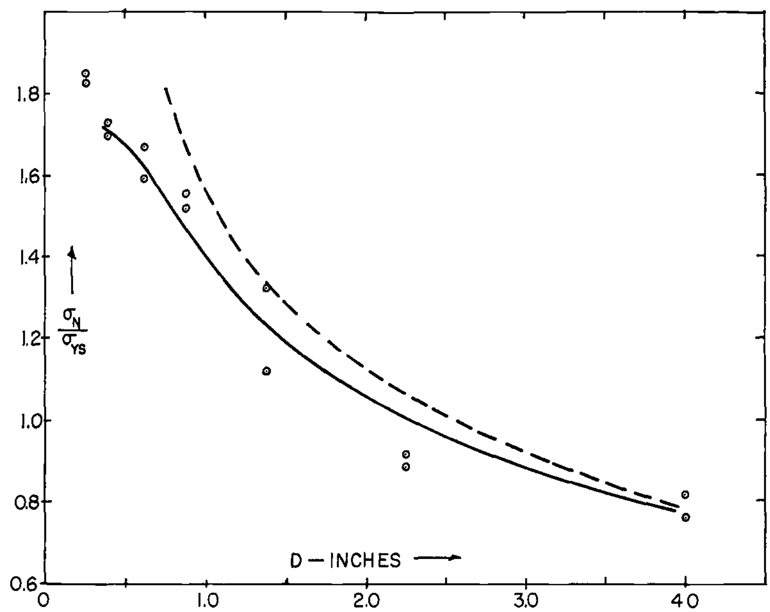

FIG. 19—Ratio of Net Stress to Yield Stress as a Function of Bar Diameter for Circumferentially Notched Round Bars of Medium-Strength Steel ($\sigma_{YS} \approx 85$ ksi). The Solid Curve is Fitted to the Data Using Adjustment of the Plastic Zone Factor. The Dashed Line Represents a Simple Inverse Square Root Relationship.

However, empirical representations of fracture data in the high stress level range are of value and various methods have been suggested. As will be shown, when the critical K values for large specimens are available, the task of devising a successful empirical representation of fracture test results is comparatively easy.

If values of the yield strength and ultimate tensile strength are known, then the stress limitations of a specimen of given geometry, as the size is reduced to a fully plastic situation, can be estimated with sufficient accuracy for most practical applications. In a graph of net-section stress versus specimen size the only remaining task is to fair a line from the curve representative of the constant K value range to the upper stress level limit across the small specimen range of the abscissa. Presumably this would be done by drawing a line through such experimental points as are available. Even in the absence of small specimen size experimental results, a curve could be drawn to the ultimate strength limit based upon general experience which would have as much accuracy as pertains to our understanding of how to use such data in practical applications.

The plane-strain plastic-zone correction factor suggested by Irwin (32) resulted from an attempt at empirical data representation and can be cited as an illustration of the above comments. Figure 19 shows σ_N/σ_{YS} as a function of specimen size for notched round bar tests of a rotor steel from work by Yukawa and Wundt (33). The notch root radius was about 0.003 in. and no slow crack growth from the notch was observed prior to fracture. Although a sharper notch might have resulted in lower values, the one used was believed to be closely similar in all the test bars. Thus the results are suitable for study of the plastic-zone influence under static crack border fracture conditions. The material had a yield strength of 83 ksi and in all specimens the net section at the notch was half the gross section.

If the plastic zone is ignored, the value of K can be computed from

$$K = 0.233\sigma_N(\pi D)^{1/2} \quad \ldots\ldots\ldots (40)$$

where D is the gross section diameter of the test specimen. Assuming K from Eq 40 to be constant results in a data-representation curve shown as a dashed line in Fig. 19. The slope of this line is too steep to fit the data in the approach to small specimen sizes.

The coefficient 0.233 in Eq 40 is a function of relative notch depth which has a maximum value when the net-section diameter, d, is nearly $D/\sqrt{2}$. Therefore, the coefficient can be regarded as invariant during small increases of notch depth. The elementary estimate of plastic-zone influence (Eq 16) consists in placing the crack border (for computational purposes) at a notch depth increased by an amount $(p/2\pi)(K_{Ic}/\sigma_{YS})^2$, where p is a proportionality factor. We can, therefore, consider representation of the data by the equation, replacing σ_N of Eq 40 by the net-section stress, $\sigma_N(d/d_{eff})^2$:

$$K_{Ic}\left(1 - p\frac{\sqrt{2}\,K_{Ic}^2}{\pi D\sigma_{YS}^2}\right)^2 = 0.233\sigma_N\,(\pi D)^{1/2} \quad \ldots (41)$$

If p is taken as unity, the assumed plastic-zone adjustment is the same as has been employed for application to plane-stress data.

From Eq 41, σ_N, as a function of D with K_{Ic} constant, has a maximum value (in the range of very small specimens) given by:

$$= \left(\frac{\sigma_N}{\sigma_{YS}}\right)_{\max} \frac{0.64}{0.233\sqrt{5}\,(p\sqrt{2})^{1/2}} \quad \ldots (42)$$

An empirical extension of the data representation in terms of K values can be obtained, using Eq 41, by adjusting the value of p so that the right side of Eq 42 is about 1.7. A value of p of about one third serves this purpose.

From general considerations, as shown in Fig. 3, the size of the plane-strain plastic zone should be smaller than that of the plane-stress plastic zone for equal values of (K/σ_{YS}). A size-reduction factor of one third is not unreasonable. At the present time basic considerations do not provide a definite value. Theoretically, for a deep enough notch, σ_N might be made as large as 2.7 σ_{YS}. However, among reported results of notched-bar tests, where the net-section area is half the gross-section area, the σ_N/σ_{YS} values shown in Fig. 19 are about as high as are normally found, probably due to yielding in the shoulders (19). We conclude from this that empirical considerations suggest use of a plane-strain plastic-zone correction factor which is smaller than r_Y for plane stress by about one third. For numerical simplicity in Eq 41, the value suggested by Irwin was $p = (2)^{-3/2}$. The solid curve on Fig. 19 shows the relationship of the data points to Eq 41, with this value of p. From the suggested p value the equation for the plane-strain plastic-zone correction factor becomes

$$r_Y = \frac{K_{Ic}^2}{4\sqrt{2}\,\pi\sigma_{YS}^2} \quad \text{........(43)}$$

This can be regarded as equivalent to Eq 11 with an upward adjustment of the yield stress by a factor of about 1.7.

Use of the plane-strain plastic-zone correction factor has been of minor importance in calculation of the crack toughness, K_{Ic}. The same degree of success in data fitting shown on Fig. 19 has not occurred with other sets of data. Tests of 7075-T6 aluminum and of high-strength steel notched tensile bars indicate $\sigma_N = 1.2\ \sigma_{YS}$ is about the limit of the range which can be characterized by a constant value of K_{Ic} even with the aid of the correction factor (17). Within this range, use of the correction factor scarcely has a significant effect on the resultant K_{Ic} values. Thus, from experimental studies of crack toughness currently available we really know very little about the Mode I plane-strain plastic zone beyond certain general aspects which might be derived from intuitive considerations.

On the other hand, knowledge of the nature and extent of the Mode I plastic zone is of basic importance if we are to advance our understanding of crack toughness beyond the linear elastic viewpoint.

CONCLUSIONS

Because of its comparative simplicity, the Mode III elastic-plastic analysis has been used to study a number of the effects of plasticity on crack extension. The following conclusions are important for a general understanding of elastic-plastic fracture:

1. Only one half the strain energy required for plastic flow on increase in load can be found from study of the change in compliance of the specimen and the corresponding $\mathcal{G}$ value using linear elastic analysis.
2. A re-examination of Eqs 20 and 21 for instability in ductile fracture shows that at high stress levels no one parameter, corresponding to $\mathcal{G}$ for a linear elastic model, will characterize unstable crack growth at the scale of the model of homogeneous plasticity. It rather appears that it will be necessary to base a fracture criterion on the local stress and strain in a small region just ahead of the crack and to predict fracture from this, coupled with the mechanics in each case.
3. The idea of basing the fracture criterion on the displacement across the leading edge of the crack is not consistent with basing the fracture criterion on the local stress and strain just ahead of the crack. Although predictions from the two criteria are equivalent at low stress levels, different results would be predicted for experiments at stress levels near those required for general yielding.
4. The hysteresis in the displacements across the crack for loading and unloading have been evaluated at low stress levels. For a stress-zero-stress cycle, the width of the hysteresis loop is proportional to the cube of the stress.

With specific reference to tension fracture testing:

5. A more complete study of the stress and strain distribution for cracks under tension is needed, not only under in-

creasing load, but also for increasing length.

6. To assist in further basic understanding of the problem, work intended for research rather than for acceptance testing should not only include data recommended in Ref. (29), but also metallographic and micrographic observations to indicate the mechanisms of fracture and the structural size, ρ_s, below which the homogeneous theory cannot be applied. In addition, for more information on the strain hardening, the uniform elongation of unnotched specimens should be reported, even if only that obtained by measuring the reduction of area away from the neck in an ordinary tension test.

7. Pending more exact solutions, the tendency of K_c measurements to fall below the characteristic large specimen value when σ_N exceeds 0.8 σ_{YS} might be removed by the adoption of a plastic-zone correction factor based in an empirical way upon Koskinen's calculations of the high stress level shape of the Mode III plastic zone (Figs. 8, 9, and 10 and Eq 18). Alternatively, a substantial part of the high stress level K_c trend may disappear if effective crack length is based upon the apparent compliance of the specimen at fracture.

Acknowledgment:

The support of part of this work by the National Science Foundation through Grant G-14995 is deeply appreciated. The work of J. Mahoney on digital computations for the Mode III instability was invaluable. These were carried out through the courtesy of the Computation Center, Massachusetts Institute of Technology. The experience and background obtained from fracture studies at the U.S. Navel Research Laboratory were equally helpful.

APPENDIX

SUMMARY OF RELATIONSHIPS BETWEEN LINEAR-ELASTIC AND PLASTICITY VIEWPOINTS

The first report of the ASTM Special Committee on Fracture Testing of High-Strength Metallic Materials (24) suggested allowance for the plastic zone at the crack border could be made by adding to the half-length, a, of the crack, an adjustment, r_Y, given by:

$$r_Y = \frac{1}{2\pi}\left(\frac{K}{\sigma_Y}\right)^2 \quad \text{(A1)}$$

This adjustment was intended to assist accuracy of the stress-field representation in a region where the plastic zone, although enclosed by a surrounding elastic stress field, was not small enough to be ignored in the test analysis.

For conditions of this nature no direct elastic plastic treatment of opening mode cracks is available at the present time. We can, however, utilize the tensile analog of a Mode III elastic-plastic solution as indicative of the major influences of local plastic deformation. Specifically, the Mode III elastic-plastic treatment states that, when the plastic zone is small relative to crack size and net section, the plastic-zone boundary is circular (as shown in Fig. 5) and the radius of this circle, r_Y, is given by:

$$r_Y = \frac{1}{2\pi}\left(\frac{K_{III}}{k}\right)^2 \quad \text{(A2)}$$

This treatment assumes a perfectly plastic material (zero strain hardening). The resistance to plastic shear is k. At and outside the boundary of the plastic zone, the elastic stresses and strains are identical to those given by a linear elastic Mode III solution in which the leading edge of the crack is placed, for analysis purposes, at the center of the circular plastic zone.

Clearly Eq A1 is the tensile analog of Eq A2. Thus the plastic-zone correction factor.

r_Y, suggested in Ref (24), is identical to the first-order correction one finds by taking the tensile analog of the Mode III elastic-plastic treatment. A simple account of the actual ideas initially employed in "correcting" for the plastic zone is given in Ref (32) of the paper.

The Mode III plastic zone is only circular in the limit as its dimensions approach negligible size in comparison with the crack length and the net section. Numerical calculations of the size and shape of the plastic zone at high values of net-section stress, where the shape is no longer circular, have been made by Koskinen (5) as discussed in the paper. Simple inspection of these results suggests that, when the net-section stress, τ_N, is less than 0.8 k, the plastic zone is sufficiently enclosed and nearly enough like a circle in shape so that a close fit of the adjusted linear elastic treatment to experimental results would be expected. Correspondingly, K_c testing experience with $2a/W$ in the range of 0.3 to 0.5 suggests that K_c values remain constant with decrease of specimen dimensions until the net-section stress, σ_N, becomes greater than 0.8 σ_{YS} (17,29). For $2a/W < 0.25$, the test data show no high stress level trend in the values of K_c until $\sigma_N > \sigma_{YS}$ (17).

When the plastic-zone size is a large fraction of the net section or of the crack size, the adjusted linear elastic analysis does not represent the stress field near the crack with realistic accuracy. Use of this viewpoint in such regions is semi-empirical rather than empirical. So long as testing experience shows negligible difference between a critical K value measured at low stress level with a large specimen and a critical K value measured for the same material at high stress level with a small specimen, then the K_c or K_{Ic} parameter has a useful significance over the entire size and stress range investigated. Some indication of the accuracy limits of the linear elastic treatment, adjusted for plasticity using Eq A1, can be obtained by elastic-plastic analysis. However, the practical usefulness of the adjusted linear elastic model, when applied semi-empirically to fracture tests in the high stress level range, must be determined from testing experience.

The tensile analog of k in Eq A2 is σ_Y in Eq A1. In plane-stress K_c testing, σ_Y has been commonly given the value of the 0.2 per cent offset uniaxial tensile yield strength, σ_{YS}. For plane-strain K_{Ic} tests, the r_Y adjustment tends to be less important. Section III of this paper discussed a plane strain, r_Y, which was equivalent to taking $\sigma_Y = (8)^{1/4}\sigma_{YS}$. These particular values of σ_Y for plane stress and plane strain are arbitrary. Plasticity considerations indicate these choices are plausible but do not indicate how to modify or improve them. For this reason the employment of moderate alterations of r_Y in order to obtain a better fit of fracture data to a constant critical K value can be justified. A recent paper by Getz, Pierce, and Calvert (36) provides an example. On the other hand, in K_c and K_{Ic} testing using the customary specimens, use of the r_Y values noted above seems desirable for consistency in reporting of test results.

From the linear elastic viewpoint, the K factor characterizes the level of tensile stress acting near the crack to cause separation, and critical values of K provide a basis for predicting unstable fracturing in a service component as a function of stress level and crack size. From a plasticity viewpoint, the counterpart of the K factor consists in a representation of the critical condition of plastic strain in a small portion of the plastic zone adjacent to the leading edge of the crack. The paper provides specific illustration of this idea by stating the critical condition in terms of a strain, γ_F, at a fixed small distance, ρ_s, from the leading edge of the crack. Calculations have been made of the consequences of this assumption using the Mode III elastic-plastic analysis.

Application of this type of analysis can be made to fracture experiments either assuming unstable crack extension starts immediately, as if from a stationary crack border, or that unstable crack extension develops only after a significant amount of stable crack growth. Results corresponding to the latter have been obtained by McClintock using a step-wise or incremental calculation plan and are summarized in Fig. 14. The amount of stable crack growth before instability is an increasing function of the ratio, R_0/ρ_s, where R_0 is the straight-ahead size of the plastic zone. As R_0/ρ_s drops below 10, the stable growth approaches a negligible amount.

The implications of these results depend upon how one interprets the structural length factor, ρ_s. Previously in this paper grain size or inclusion spacings were suggested as indicative of the magnitude of ρ_s. Larger estimates are possible. For example, microscopic examination of the leading portion of a segment of plane-strain extension, marked by heat tinting, permits examination of the sizes of the crack front irregularities. If the major irregularities are accepted as giving the magnitude of ρ_s, then ρ_s must be comparable in size to plastic zone for plane-strain conditions. This would support the idea of regarding abrupt crack extension instability from a stationary crack border as normal behavior for plane-strain conditions. When shear lips are present, the central tongue of plane-strain fracture tends to grow in steps of varying size, and choice of a particular value for ρ_s is rather difficult. Although uncertainties of interpretation remain which deserve additional study, the results of calculations can be regarded as in agreement with experimental observations.

The simplification of neglecting the influence on the plastic zone of stable crack extension was implicit in the analysis of the r_Y crack-length adjustment given previously. Under similar terms, the Mode III elastic-plastic analysis provides a simple analytical basis for definition of length factors which can be regarded as characterizing crack-extension behavior. The crack-opening displacement, η, is an example of such a length factor. The use of this length factor as a fracture criterion in a proposal by Wells (11) was discussed in the paper.

Plasticity aspects of fracture necessarily connect with linear elastic fracture mechanics in a smooth way. When the conditions for unstable fracture are stated in terms of a critical strain, γ_F (at $r = \rho_s$), or in terms of a critical opening displacement, η_F (at the crack border), it is desirable to bear in mind that these are simply and directly related to critical values of K and $\mathcal{G}$ when the plastic zone is relatively small. These connections are of practical importance. In investigations of the service fractures of primary interest, those which occur prior to general yielding, an adjusted linear elastic analysis is still the most convenient method for connecting any specific fracture criterion with the stress level and crack size

REFERENCES

(1) M. L. Williams, "Stress Distributions at the Base of a Stationary Crack," *Journal of Applied Mechanics*, Vol. 24, 1957, p. 104.

(2) G. R. Irwin, "Relation of Stresses Near a Crack to the Crack Extension Force," *IXth International Congress of Applied Mechanics*, Vol. VIII, Paper No. 101(II), Univ. of Brussels, 1957, pp. 245–251.

(3) G. R. Irwin, "Fracture," *Springer Encyclopedia of Physics*, Vol. VI, 1958, p. 551.

(4) J. A. H. Hult and F. A. McClintock, "Elastic-Plastic Stress and Strain Distribution Around Sharp Notches Under Repeated Shear," *IXth International Congress of Applied Mechanics*, Vol. 8, Univ. of Brussels, 1957, p. 51.

(5) M. F. Koskinen, "Elastic-Plastic Deformation of a Single Grooved Flat Plate Under Longitudinal Shear," *Transactions*, Am. Soc. Mechanical Engrs, Vol. 85, D, 1963, p. 585.

(6) J. E. Neimark, "The Initiation of Ductile Fracture in Tension," ScD Thesis, Dept. of Mechanical Engrg, *Mass. Institute of Tech.*, 1959.

(7) R. Hill, "On Discontinuous Stress States with Special Reference to Necking in Thin Sheets," *Journal of Mechanics and Physics of Solids*, Vol. 1, 1952, p. 19.

(8) A. P. Green, "The Plastic Yielding of Metal Junctions Due to Combined Shear and Pressure," *Journal of Mechanics and Physics of Solids*, Vol. 2, 1955, p. 197.

(9) J. C. Walter, "Cracking from Notches under Transverse Shear," M.Sc. Thesis, Dept. Mechanical Engrg, *Mass. Institute of Tech.*, 1959.

(10) S. S. Rhee and F. A. McClintock, "On the Effects of Strain Hardening on Strain Concentrations," *Proceedings*, 4th U.S. Nat. Congress of Applied Mechanics, 1962, p. 1007.

(11) A. A. Wells, "Application of Fracture Mechanics at and Beyond General Yield-

ing," *British Welding Research Assoc. Report M13/63*, British Welding Journal, Nov. 1963, pp. 563–570.

(12) J. B. Walsh and A. C. Mackenzie, "Elastic Plastic Torsion of a Circumferentially Notched Bar," *Journal of Mechanics and Physics of Solids*, Vol. 7, 1959, p. 247.

(13) F. A. McClintock, "On the Plasticity of the Growth of Fatigue Cracks," *Fracture of Solids*, John Wiley and Sons, Inc., New York, N. Y., 1963, p. 65.

(14) F. A. McClintock, "Ductile Fracture Instability in Shear," *Journal of Applied Mechanics*, Vol. 25, 1958, p. 582.

(15) F. A. McClintock, Discussion of "Fracture Testing of High Strength Sheet Materials," *Materials Research & Standards*, Vol. 1, 1961, p. 277.

(16) G. R. Irwin, M. F. Koskinen, discussion and author's closure to Ref (5), *Transactions*, Am. Soc. Mechanical Engrs., Vol. 85, D, 1963, p. 590.

(17) G. R. Irwin, "Relation of Crack Toughness Measurements to Practical Applications," *Welding Journal Research Supplement*, Nov. 1962.

(18) G. R. Irwin, "Crack Toughness Testing of Strain Rate Sensitive Materials," *Transactions*, Am. Soc. Mechanical Engrs (to be published).

(19) F. A. McClintock, "On Notch Sensitivity," *Welding Journal Research Supplement*, Vol. 26, 1961, p. 202-s.

(20) D. S. Dugdale, "Yielding of Steel Sheets Containing Slits," *Journal of Mechanics and Physics of Solids*, Vol. 8, 1960, p. 10.

(21) F. A. Field, "Yielding in a Cracked Plate in Longitudinal Shear," *Transactions*, Am. Soc. Mechanical Engrs, Vol. 30, E, 1963, p. 622.

(22) B. A. Bilby, A. H. Cottrell, and K. H. Swinden, "The Spread of Plastic Yield from a Notch," *Proceedings Royal Society*, A, Vol. 272, 1963 p. 304.

(23) J. J. Gilman, "Cleavage and Ductility in Crystals," *Proceedings*, Int. Conference on Atomic Mechanisms of Fracture, Techn. Press, Mass. Inst. of Tech., Cambridge, Mass. and John Wiley and Sons, New York, N.Y., 1959, p. 193.

(24) "Fracture Testing of High Strength Sheet Materials," First Report of Special ASTM Committee, *ASTM Bulletin*, Jan. 1960.

(25) J. A. H. Hult, "Fatigue Crack Propagation in Torsion," *Journal of Mechanics and Physics of Solids*, Vol. 6, 1957, p. 47.

(26) F. A. McClintock, "Numerical Integration of Shear Cracking Equations, II" Res. Mem. No. 8, Fatigue and Plasticity Lab., Dept. Mech. Eng., Mass. Inst. of Techn., 1958.

(27) F. A. McClintock, "A Criterion for Ductile Fracture by Growth of Holes," submitted to *Journal of Applied Mechanics*, 1965.

(28) J. M. Krafft, "Correlation of Plane-Strain Crack Toughness with Strain Hardening Characteristics of a Low-, a Medium-, and a High-Strength Steel," *Applied Materials Research*, Dec. 1963.

(29) Fifth Report of Special ASTM Committee on Fracture Testing of High Strength Materials, *Materials Research & Standards*, Vol. 4, March 1964, p. 107.

(30) J. R. Lawson, "Crack Surface Displacements for an Elastic Material Under Longitudinal Shear," Res. Mem. No. 46, Fatigue and Plasticity Lab., Dept. of Mech. Eng., Mass. Inst. of Tech., 1963.

(31) R. W. Boyle, "A Method for Determining Crack Growth in Notched Sheet Specimens," *Materials Research & Standards*, Vol. 2, Feb., 1962 p. 646.

(32) G. R. Irwin, "Pla,stic Zone Near a Crack and Fracture Toughness," *Seventh Sagamore Ordnance Materials Research Conference*, Aug. 1960.

(33) B. M. Wundt, "Unified Interpretation of Room Temperature Strength of Notched Specimens as Influenced by Their Size," Am. Soc. Mech. Engrs paper *59-MET-59*, 1959.

(34) H. F. Bueckner, "The Propagation of Cracks and Energy of Elastic Deformation," *Transactions*, Am. Soc. Mech. Engrs., Vol. 80, 1958, p. 1225.

(35) J. L. Sanders, Jr., "On the Griffith-Irwin Fracture Theory," *Transactions*, Am. Soc. Mech. Engrs, Vol. 27, Series E, 1960, p. 352.

(36) D. L. Getz, W. S. Pierce, H. F. Calvert, "Correlation of Uniaxial Notch Tensile Data with Pressure-Vessel Fracture Characteristics," Am. Soc. Mech. Engrs Paper No. *63-WA-187*, Nov. 1963.

STP381-EB/Apr. 1965

CRACK-VELOCITY CONSIDERATIONS

BY J. M. KRAFFT[1] AND G. R. IRWIN[1]

SYNOPSIS

If resistance to crack growth always increased with crack velocity, then its measure at nil velocity, $\mathcal{G}_c$ or $\mathcal{G}_{Ic}$, would always represent minimum toughness and thus a safe criterion. The practical difficulty arises if an increased crack speed, or loading rate of a fixed crack, results first in a decrease in R, possibly to some minimum, prior to its increase for the "stable" propagation balance. Arrest of such a crack will require reduction of the crack driving force, $\mathcal{G}$, at least to minimum R. In strain-rate and temperature-sensitive materials this minimum can lie far below initiation levels. Even in relatively high-strength materials, speed-thermal effects can be large.

The onset and arrest of rapid fracture provide relatively abrupt measurement points suitable for crack toughness evaluation. An understanding of these behaviors can be sought through study of the influence of plastic flow properties. Use of strain-rate sensitive materials over a wide range of temperatures and strain rates permits study of the influences of flow properties without alteration of the inherent flaws. A correlation of rising-load K_{Ic} values with the strain-hardening exponent, n, suggests that the onset of fast fracture is controlled to a substantial degree by a tensile instability with a simple relationship to the strain-hardening exponent. The limited information available suggests that crack-arrest conditions can be predicted on the basis of adiabatic values of n at high strain rates.

Measurements of crack motion during brittle fracture of various metallic and glassy solids result in maximum speeds no greater than about half the elastic shear wave velocity (1)[2] and correspondingly $\frac{6}{10}$ of the Rayleigh wave limit (2) for propagation of the linear elastic crack stress field. Below this limiting velocity, the speed of a running crack appears to rise and fall in phase with the crack driving force, $\mathcal{G}$. Such behavior can be expected: (1) if the release of elastic strain energy with crack extension (the crack driving force, $\mathcal{G}$) is nearly balanced against the inelastic fracture work rate (the crack resistance, R) even during fast propagation; and (2) if R is a continuous and increasing function of crack velocity. Such rapid crack extension can be regarded as essentially stable in the sense that an increase of the crack-extension force, $\mathcal{G}$, is required to produce an increase of the speed.

In practical evaluation of material toughness, behavioral characteristics which lead into or from this stable range of crack speed are most important: measurements of the stress conditions

[1] Section head and superintendent, respectively, Mechanics Div., U. S. Naval Research Laboratory, Washington, D. C.

[2] The boldface numbers in parentheses refer to the list of references appended to this paper

for initiation or for arrest of the rapid crack-extension process. If resistance to crack growth always increased with crack velocity, then its measure at nil velocity, $\mathcal{G}_c$ or $\mathcal{G}_{Ic}$, would always represent minimum toughness and thus a safe criterion. The practical difficulty arises if an increased crack speed, or loading rate of a fixed crack, results first in a decrease in R, possibly to some minimum, prior to its increase for the "stable" propagation balance. Arrest of such a crack will require reduction of the crack driving force, $\mathcal{G}$, at least to minimum R. In strain-rate and temperature-sensitive materials, this minimum can lie far below initiation levels. Even in relatively high-strength materials, speed-thermal effects can be large. For these reasons, crack-velocity considerations are of practical as well as of basic importance in crack toughness measurements.

RUNNING CRACKS

In studies of fracture surfaces, observation of small cracks adjacent to the main fracture indicate that a locally discontinuous behavior is characteristic of crack extension, regardless of the crack speed (3). At any stage, the separation process is contingent upon a supply of crack driving force sufficient to overrun localized regions of greatest fracture strength. However, in the fast propagation range, such tough regions are quickly overrun so that the attachment of an average speed to forward movement of the separation process seems an appropriate simplification. Observations

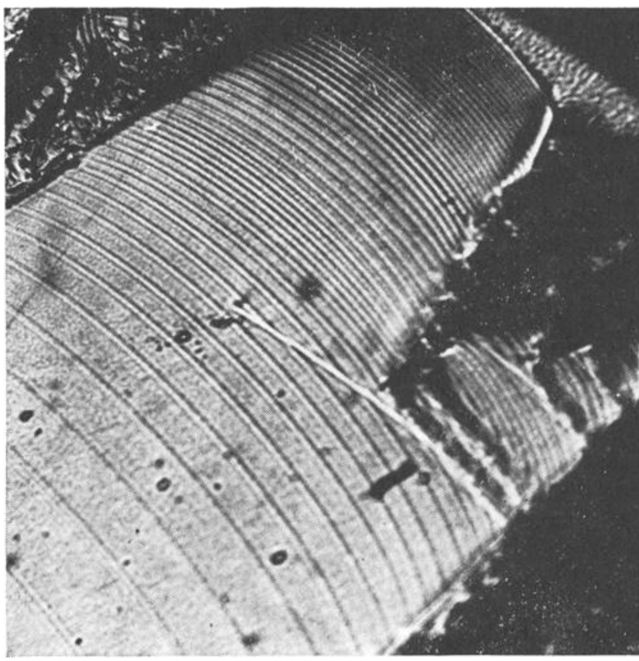

FIG. 1—Arrest of a Running Crack in Plexiglas Sheet Modulated by 80-kc Shear Wave, Typifies Finite Velocity up to Arrest Point for Rate-Sensitive Materials. (From Unpublished Results of A. B. J. Clark.)

of crack propagation with such an averaging scale, or as a continuous process, are illustrated first.

To observe a running crack in regions where its speed is changing rapidly, the ripple-marking method of Kerkhof (4) is a useful technique. A running brittle crack tends to remain normal to the direction of greatest tension. If a vibration is introduced with a shear component on the plane of the crack normal to the crack border, the fracture surface tilts in a periodic manner, producing shallow ripples easily visible with specular lighting. As an example of such an experiment, Fig. 1 shows the last 5 mm prior to arrest of a fracture segment 7 mm long produced in a plate of Plexiglas at the Naval Research Laboratory (NRL) by A. B. J. Clark. The superimposed wave frequency was 80 kc, traveling counter to the direction of crack propagation. In the region shown, the crack speed in the central smooth section decreases by a factor of 20 prior to crack arrest. The central region is bordered by regions of greater roughness, presumably related to plane-stress yielding at the plate surfaces. As the speed of crack extension in the central region decreases, these regions grow in size and accept larger fractions of the (decreasing) crack driving force until arrest occurs.

Plexiglas is composed of a linear polymer, polymethyl methacrylate, and the tendencies toward preferred orientation in regions of large strain make its behavior somewhat visco-elastic and strain-rate sensitive. It will be noted that its ripple markings (Fig. 1) do not approach zero spacing at the arrest line, but at a finite one suggestive of threshold velocity minimum for crack arrest. On the other hand, the less rate-sensitive epoxies (cross-linked polymers), particularly glass, tend to exhibit a terminal ripple spacing more nearly like

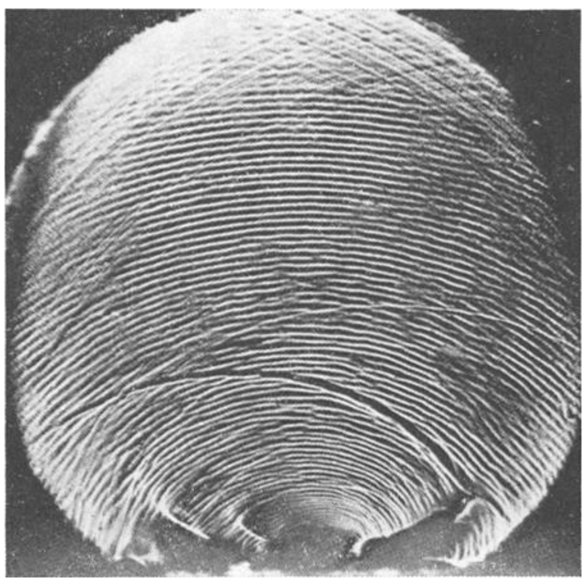

FIG. 2—Initiation of a Crack in a Glass Rod Modulated by 500-kc Shear Wave, Typifies Gradual Velocity Change for Materials of Low Rate-Sensitivity. Taken from Kerkhof (5).

that of a mathematical limit point of an infinite series.

A corresponding graduality is observed in the initiation of a crack in materials of low rate sensitivity. Figure 2, from a paper by Kerkhof (5), shows a tensile fracture through a glass rod. The successive crack-border positions are outlined here by ripple markings of 500 kc traveling perpendicular to the crack surface. The highest velocity reached was half the limiting crack speed. In the lower part of the figure, the fracture may be seen to exhibit markings which approach zero spacing toward the position of the initial crack. The latter was not sufficiently co-planar with the main fracture surface to be illuminated in the photograph.

One can see traces of Wallner-line ripples curving across the main pattern of ripple markings in Fig. 2. These originated from vibrations related to local irregularities of separation, particularly at the intersection of the crack border with the free surface of the rod. Indeed, it was the use of Wallner lines by Smekal (6) for measurements of crack speed which suggested the use of ultrasonic vibrations.

CRACK BORDER INSTABILITY IN K_c TESTING

In studies of the running crack, it seems natural to discuss behavior primarily in terms of the stable balance between the supply of stress field energy and the energy dissipated in the separation process. In contrast, when we discuss onset and arrest of crack propagation, it seems more appropriate to center attention upon factors which would introduce instability and would lead to rapid acceleration or deceleration of the crack movement.

When slow cracking is observed in a K_c test, the crack growth is accompanied by a steady increase of resistance which stabilizes the process. Unless abrupt acceleration occurs earlier, the maximum load point will be reached when the crack speed is about equal to W/t, where W is the specimen width and t is the time to reach maximum load at constant head speed (7). Concurrently with this, the increase of crack growth resistance, R, and of the crack driving force, $\mathcal{G}$, are just matched with the load constant. For example, in early crack toughness testing at NRL, examinations of 24 frame per second motion picture records of tests of 12-in. wide sheets of high-strength aluminum alloy (8) indicated that a crack speed of about W/t developed in coincidence with the maximum load point. The sheet thickness was 0.050 in. or less, and most of the slow growth was full oblique-shear separation. The majority of these tests showed complete separation in one frame of the film close to the maximum load point. Evidently the gradual development of the maximum load point was a marginal thing.

It is possible to use a gradually developed maximum load instability, of the above kind, to explain a tendency of K_c to decrease with decrease of specimen size and increase of net-section stress. If one assumes, somewhat inaccurately, that the rate of increase of resistance to crack extension with growth of the crack is not influenced by specimen width, then the match between the constant load increase of $\mathcal{G}$ with crack length and the increase of resistance can be expected to occur at lower values of resistance, the smaller the specimen (9). The pattern of resistance growth corresponds to the development of the shear lips with crack growth. Alternatively, this trend of K_c can be explained using the Mode III elastic-plastic analysis to provide an enhanced plastic-zone correction factor. Not only the magnitude of the trend, but also the observed disappearance of the trend when the net-section stress is less than 0.8 σ_{YS}, can be explained in this way (10). If the latter is accepted, then the former is unnecessary and this, in turn, leaves in doubt the crack speed at the point of rapid acceleration.

In terms of strain rates near the crack border (11,12), there is a quite large difference between assuming that acceleration is abrupt from a stationary crack border and assuming that the crack speed at instability is W/t. The W/t crack speed, although small for usual test conditions, increases the strain rate by an amount equivalent to several orders of magnitude of increase in the loading speed. Thus the questions discussed above on the nature of the K_c instability are of importance when the crack toughness of the material is known to be sensitive to strain rate.

Instability at a Plane-Strain Crack Border

Consider next the development of instability in a K_{Ic} test using either a notched round bar or a plate specimen thick enough so that the shear lips do not delay the initial unstable acceleration of the crack border. At one stage, such small separations as may have formed near the border of the initial crack are surrounded by areas of stronger material which accept the increase of tensile load. At a later stage, the spreading and joining of the initial separations surround and overload the local regions of highest strength so that these no longer block the forward movement of the separation process. At this point, the process is quite unstable and must accelerate rapidly. Even when the stabilizing influence of the shear lip is large enough so that substantial amounts of plane-strain separation precede the development of final rapid separation, the first plane-strain instability is often abrupt enough for a pop-in type of K_{Ic} determination (12).

Of course, slow stable plane-strain crack extension may occur in the presence of stress corrosion or with cyclic loading. Gross weakness of internal planes normal to the crack border may introduce small internal shear lips to postpone instability by providing a local region of plane stress. In the absence of such factors, however, it is difficult to understand how even small amounts of plane-strain crack-border motion can occur without immediate development of rapid, progressive fracture. Thus one can assume that, in normal behavior, onset of fast separation at a plane-strain crack border results from a development of critical conditions in advance of the border during a final loading period in which the crack border is essentially stationary. The assumption of a stationary crack border simplifies the task of studying the relationship of plastic flow properties upon K_{Ic} over a range of temperatures and strain rates. The success of correlations resulting from these studies, in turn, tends to justify the assumption of a stationary crack border prior to initiation.

General Strain-Rate Influences

The Fifth Report of the ASTM Special Committee states that slow testing speed crack-toughness evaluations are adequate for most applications when the strain-rate sensitivity of the material does not exceed that found in martensitic steels heat-treated to a yield strength, σ_{YS}, of 200 ksi or more (13). Measurements of the plastic yield properties of various steels provide a reasonable basis for this attitude. There is a tendency for the absolute sensitivity of yield strength to strain rate to remain at about the same value independent of large changes in σ_{YS}. For example, the 3 per cent (strain) flow stress of both low- and high-strength steels typically exhibit an increase of about 6 ksi for a tenfold increase in strain rate. Thus a factor of 10^5 in strain rate, corresponding to a change from static testing to impact speeds, causes about a 30-ksi increase of the flow stress. This is a change of nearly 100 per cent for a plain carbon steel. The corresponding decrease of crack toughness is quite large. On the other hand, for the class of steels defined above as relatively insensitive to strain rate, a 30-ksi elevation of the flow stress is no more than a 15 per cent effect.

INFLUENCES OF TEMPERATURE AND LOADING RATE UPON K_{Ic} VALUES

Information currently emerging from studies of effects of temperature and loading rate upon K_{Ic} values suggests that it may be possible to understand onset of fast fracture and crack arrest on similar terms. These terms center attention upon plastic flow properties of the material and their influence upon resistance to plane-strain extension of a crack (14). From the point of view adopted, K_{Ic} is jointly determined by inherent flaws, such as poorly bonded inclusions or grain-boundary impurities, and by plastic flow properties. Although the inherent flaws in various plates of metal may differ depending upon fabrication and other factors, tests using specimens from a single plate over a wide range of temperature and strain rate, which alter the plastic flow properties, permit a study of the influence of these properties upon the crack toughness.

It is desirable to restrict these investigations, initially, to plane strain for various reasons, one of which is analytical. The analysis requires association of results from plastic deformation tests (performed with tension or compression specimens) with plastic strains and strain rates adjacent to the crack border. To do this in a consistent and appropriate way, one must assume either that the crack border is stationary prior to instability or that the crack motion has a known value. The complexities associated with the latter choice are quite formidable. Furthermore, the simpler, stationary crack-border assumption seems justified by factors previously discussed.

An additional assumption is necessary which is equivalent to stating the dependency of plastic strain upon distance from the crack border. One can make this choice without actual knowledge of the exact dependency because the effects of different reasonable hypotheses on the calculated strain rate are scarcely significant in their influence upon plastic flow properties. For example, if we assume that the strain, ϵ, at distance, d, ahead of the crack border has the inverse first-power dependency suggested by the Mode III elastic-plastic solution (15), then

$$\epsilon = \epsilon_Y \left(\frac{2r_Y}{d}\right) \qquad (1)$$

where $2r_Y$ is the formal calculation of plastic-zone size from

$$2r_Y = \frac{1}{\pi}\left(\frac{K_{Ic}}{\sigma_Y}\right)^2 \qquad (2)$$

In a rising load test such that K is proportional to the loading time, t,

$$\dot{\epsilon} = 2\epsilon/t \qquad (3)$$

Equation 3 neglects the variation of σ_Y with time rates, this factor being of minor importance.

If we assume, in place of Eq 1, that

$$\epsilon = \epsilon_Y \left(\frac{r_Y}{d}\right)^{1/2} \qquad (4)$$

this assumption is equivalent to an elastic strain dependency. Using $K \propto t$ and Eq 4, one finds

$$\dot{\epsilon} = \epsilon/t \qquad (5)$$

which differs from Eq 3 by a factor of 2.

Equation 5 is preferred here for the following reasons: (1) rounding of the crack tip by plastic strain as well as work hardening would tend to reduce the strain gradient of Eq 1; and (2) as noted later, Eqs 4 and 5 permit definition of a process zone-length factor which is invariant with temperature and strain rate.

Nevertheless, when we center attention on a particular strain, ϵ_1, at a distance, d_1, we can bear in mind that Eqs 4 and 5 are, to some degree, schematic. The length, d_1, may require a proportionality factor or a special starting point for measurement. In any case, to examine whether values of K_{Ic} correlate with values of flow stress, σ_f, or strain-hardening exponent, n (corresponding to a strain, ϵ_1), the appropriate values of σ_f and n can be obtained from plastic flow studies, assuming the strain rate applicable to the K_{Ic} test is (ϵ_1/t). Examinations of this type show a strong correlation tendency indicative of a direct proportionality between K_{Ic} and n over a wide range of temperatures and strain rates (13). Two examples will be shown.

INITIATION $K_{Ic(T)}$ IN A MILD STEEL

Consider first the data on a mild steel plate, a part of Specimen No. 39 of the University of Illinois wide-plate series, as shown in Fig. 3. Here one may compare the critical stress-intensity factor, K_{Ic}, with the time rate of increase in this factor, $\dot{K}$, computed as K_{Ic}/t. In this graph, both coordinates are divided by Young's modulus for comparison with plastic strain measurements.

Now it is evident that the range of validity for linear elastic analysis of the tests is limited to rather low temperatures with this mild steel. One can, in principal, raise this restriction by testing suitably large specimens, as for example the large beams and spin disks tested in the rotor steel investigations (11). However, there are situations where this would be impossible and, in any case, large specimens are inconvenient, expensive, and even more difficult to load rapidly. This difficulty augments interest in finding correlations between plastic flow properties and crack toughness, since such correlations might be used to extend the crack toughness data into a range otherwise impractical because of the required specimen size. The correlation of plane-strain crack toughness, K_{Ic}, with the strain-hardening exponent, n, appears to be suitable for such purposes, and is shown in Fig. 3 for

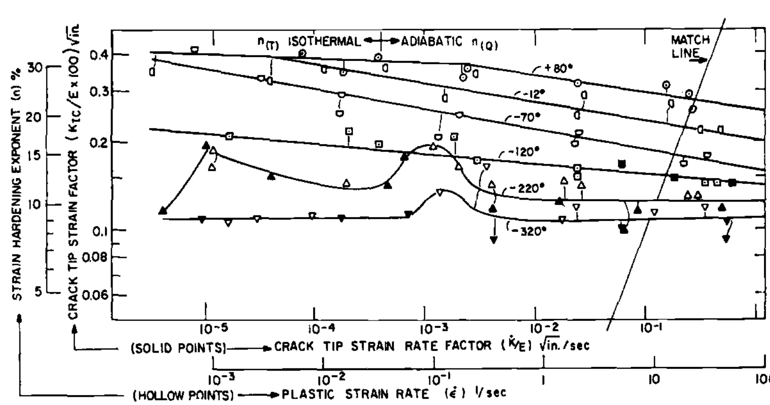

FIG. 3—Correlation for Setting Proportionality Between Isothermal Fracture Toughness, $K_{Ic(T)}$ and Isothermal Strain-Hardening Exponent, $n_{(T)}$, the Crack Re-initiation Values for University of Illinois Mild Steel Plate.

the mild steel plate material (17). Here the strain-hardening exponent was measured with small compression specimens $\frac{1}{4}$ in. in outside diameter and $\frac{3}{8}$ in. long, the K_{Ic} with single-edge notch specimens as reported in Ref (18).

MODEL FOR BRITTLE FRACTURE BY TENSILE INSTABILITY

Now the observation of a similarity between K_{Ic} and n in their dependency upon temperature and strain rate merits some sort of rationale. The basis used in Ref (14) was perhaps oversimplified, but it still appears to suffice for all data available at this writing:

The model requires two assumptions. First, the process of tensile instability and rupture actually occurs in a small element adjacent to the crack border. This can be regarded schematically as composed of minute short, uniaxial tensile ligaments, freed from the surrounding triaxial state of stress by the free surface of the crack tip and by other holes growing under the influence of the dominating crack border tensile stress field. The dimples seen in electron fractographs are thought, as suggested by Beachem (11), to represent the broken ends of these ligaments. Second, it is assumed that the tensile plastic strain distribution approaching the real crack tip can be regarded as increasing continuously up to the elemental cell in accordance with the inverse square root of d.

With these assumptions, it is seen that a constant proportionality between K_{Ic} and n suggests that the instability is closely related to a length factor at the crack border given by:

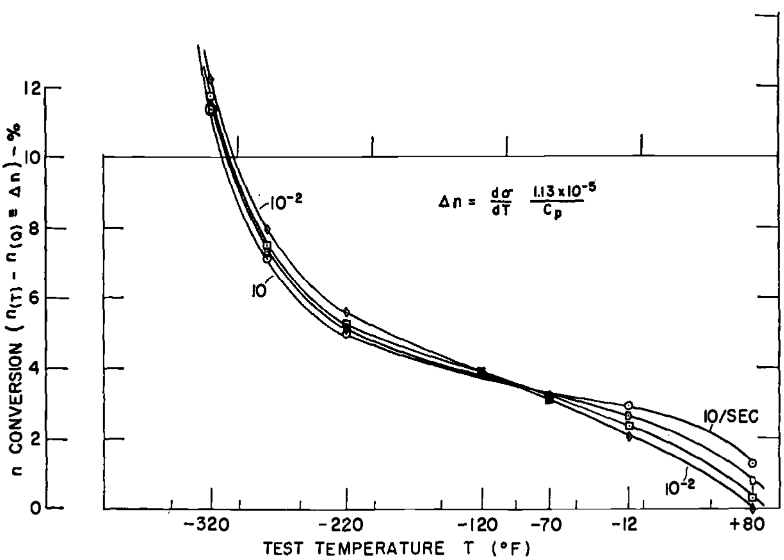

FIG. 4—Thermal Correction of Strain-Hardening Exponent, Δn, *Versus* Test Temperature, T_o, for University of Illinois Plate of Fig. 3.

$$d_T = \frac{1}{2\pi}\left(\frac{K_{Ic}}{nE}\right)^2\left(\frac{n}{\epsilon_1}\right)^2 \quad \text{........(6)}$$

where ϵ_1 is regarded as the critical strain. The length factor is constant if n/ϵ_1 is constant. From the fact that instability of a tension bar occurs when $\epsilon_1 = n$, it is natural to try this assumption with the data. In this event, the strain rates for the K_{Ic} and n determinations should be properly matched when

$$\frac{\dot{K}}{K_{Ic}} = \frac{\dot{\epsilon}}{n} \quad (7)$$

That the data can indeed be matched while this constraint is imposed may be seen in Fig. 3 for the University of Illinois plate (17), as in other data previously reported (14).

petition between the thermal softening and the normal strengthening of isothermal work hardening. The effect is greater at very low temperatures. Because of the vanishing specific heat near absolute zero, the temperature rise for a given plastic deformation energy is higher. The extent of the effect on the

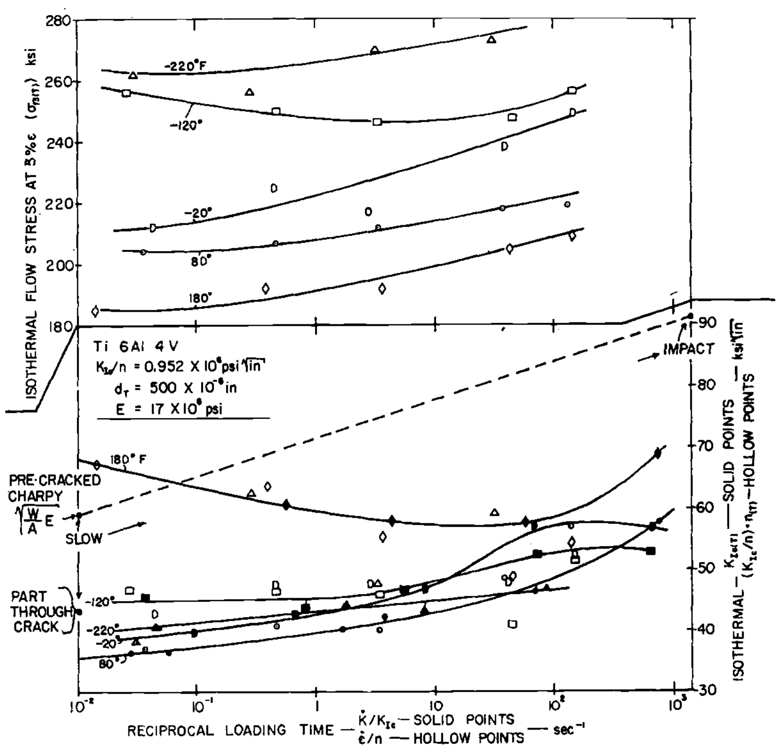

FIG. 5—For a High-Strength Titanium Alloy, Flow Strength, $\sigma_{fs(T)}$, Increases with Speed *Versus* Temperature but so Does Initiation Crack Toughness, $K_{Ic(T)}$, unlike BCC steel shown in Fig. 3. Precracked Charpy W/A, after Hartbower (22,23), shows the same trend.

ADIABATIC HEATING

It was pointed out by Zener and Hollomon (20,21) that adiabatic heating could greatly augment the tendency for local shear instability by diminishing the strain-hardening tendency. This effect is relevant to the tensile instability, regarded here as the governing process for onset of rapid Mode I plane-strain separation. The process is one of competition between the thermal softening and the normal strengthening of isothermal work hardening.

strain-hardening exponent, n, is typified by the correction curves for the University of Illinois plate which are shown in Fig. 4, taken from Ref (17).

In general, the time of straining, which will become too short for conduction of the generated heat to the surrounding metal, will increase as the square of the linear dimension of the deformed enclave, d, and decrease as the coefficient of thermal diffusivity, α,

$$t \cong d^2/\alpha \quad (8)$$

For an enclave as small as the plastic zone, $2r_Y$, or the still smaller process zone, d_T, the crack-initiation process in the K_{Ic} test is seen to be fully isothermal throughout the available loading-speed range. Thus it is proper to compare isothermal strain-hardening values, $n_{(T)}$, with the $K_{Ic(T)}$. This has been done in the n data shown in Fig. 3 by correcting n values obtained at strain rates greater than isothermal, using Fig. 4.

INITIATION $K_{Ic(T)}$ IN 6Al-4V TITANIUM ALLOY

For mild steel, a decreasing trend of crack toughness with increasing loading speed (Fig. 3) is quite typical. However, this behavior is not observed in all types of metals. For example, hard titanium (6Al-4V) shows just the opposite trend as may be seen in Fig. 5. Here isothermal values, $K_{Ic(T)}$ and $n_{(T)} \times (K_{Ic}/n)$ are displayed on a linear scale against log $1/t$, where the ratio of K_{Ic}/n was previously determined from a logarithmic matching plot similar to that of Fig. 3. In testing the titanium alloy, a procedure of step-wise straining-quenching cycles provided a direct measure of isothermal flow properties even at high strain rates, as described in Ref (17).

At room temperature, K_{Ic} was also evaluated with a part-through crack specimen by Hartbower (22) and an agreement may be seen in Fig. 5.

COMPARISON WITH PRECRACKED CHARPY

It would be expected from the n-value trends shown at room temperature and below for this titanium alloy, that initiation of crack propagation would be easier for static than for dynamic loading. Indeed, the authors' study of this material was an investigation of just such a finding by Hartbower, whose W/A values from precracked Charpy tests were larger for impact than for static loading. These are superimposed on the K_{Ic} plot of Fig. 5, reduced to K coordinates as $[E(W/A)]^{1/2}$, with the Charpy blow put in at $1/t \cong 1.5 \times 10^3$ as estimated elsewhere (11). A 50 per cent increase is reflected in both $[E(W/A)]^{1/2}$ and $K_{Ic(T)}$ measurements with the 10^5 increase in loading speed. The Charpy energy result might be expected to be somewhat higher than K_{Ic}, as it includes some contribution from surface shear lip energy which is not included in the plane-strain process.

INFLUENCE OF FLOW STRENGTH SPEED VERSUS TEMPERATURE SENSITIVITY

The isothermal flow stress at 3 per cent strain $\sigma_{f3(T)}$ is also plotted in Fig. 5 and a strengthening with speed increase and temperature decrease is observed, except at -120 F. This behavior is also found in mild steel as may be seen by looking forward to Fig. 6; yet the fracture toughness versus speed tendencies in the two materials are directly opposite. It seems pertinent to note an observation of Beeuwkas (23), who pointed out that the absolute slope of the stress-strain curve, θ, for body-centered cubic (BCC) metals tends to remain constant with changing temperature and speed. For mild steel of this class, n (and thus K_{Ic}) would vary inversely as the flow stress, σ_f, since $(n \sim \theta/\sigma_f)$. For face-centered cubic (FCC) metals, Beeuwkas observed θ increasing with speed/temperature which, if a stronger effect than the increasing σ_f, would necessitate a rising n or K_{Ic}. Since the titanium alloy is partially β-phase and thus non-BCC, it might well possess characteristics similar to the FCC metals consistent with the result shown in Fig. 5.

EQUIVALENCE OF LOADING RATE TO CRACK SPEED

Crack-arrest K-value measurements require relatively large specimens and are generally more complex than rising load tests based upon onset of crack propagation. Correspondingly there has been less experimental work. No more than a brief summary will be attempted here.

A series of possible length factors can be derived from analysis of the crack-border plastic zone. These are, in addition to the length factor, d_T, already discussed:

(1) The opening displacement, 2η, at the crack border, based upon analogy with the Mode III elastic-plastic analysis:

$$\eta = \frac{4(\epsilon_1)^2}{\epsilon_Y} d_T \quad \text{(9)}$$

(2) The distance, d_N, from the crack border to the point where $\epsilon = \epsilon_1$, based upon Eq 1:

$$d_N = [(2d_T)(2r_Y)]^{1/2} \quad \text{(10)}$$

(3) The plastic zone size, $2r_Y$, as given by Eq 2.

Discussion will be based upon use of the length factor, d_T. However, since d_T is the smallest of the four length factors and the analysis is schematic only, we will refer to the length factor as qd_T, where q might be an order of magnitude larger than unity, or smaller, d_F/d_T, as in Ref (14).

The strain rate of interest in advance of a moving crack approaching arrest is presumably the strain rate, where ϵ has the critical value, ϵ_1. This, in turn, we would tend to associate with the strain-hardening exponent, n, under ambient conditions of temperature and time rate. From Eq 4, this strain rate is given by:

$$\dot{\epsilon} = \epsilon_1 \frac{\dot{a}}{2qd_T} \quad \text{(11)}$$

where $\dot{a}$ is the crack speed.

An approximate estimate of the crack speed necessary for an adiabatic fracture process zone may be obtained by dividing the length factor, qd_T, by the time, $(qd_T)^2/\alpha$, where α is the thermal-diffusion coefficient. Thus,

$$\dot{a}_{crit} = \frac{\alpha}{qd_T} \quad \text{(12)}$$

Inserting this value into Eq 11 gives a result consistent with Eq 8, within a factor of 2. Thus, with a sufficient increase of loading speed, one might expect a continuous trend of strain rate and thermal conditions from high-speed rising load tests into the moving crack range. From this one might conclude no difference will be found between values of K_I at crack arrest and values of K_{Ic} in a rising load test, fast enough to match the velocity of the crack just prior to arrest (7). However, reservations must be made to allow for the fact that the temperature distribution around the moving crack border differs substantially from that near the stationary crack border prior to instability. From the general nature of the difference, it can be argued that crack-arrest values of K_I might correspond to a larger adiabatic effect and a lower toughness than the K_{Ic} values which would be found even in the most rapid types of rising load testing.

This discussion cannot resolve uncertainties thus introduced. However, it is clear that, for a typical strain-rate sensitive steel, an abrupt arrest should occur when the crack speed drops below the value given by Eq 12. The process zone at crack arrest is therefore adiabatic. Furthermore, unless ways can be found to shorten greatly the load rise time in K_{Ic} evaluations, these will generally correspond to isothermal conditions in the process zone and thus to higher values of K_{Ic} and n than for crack arrest.

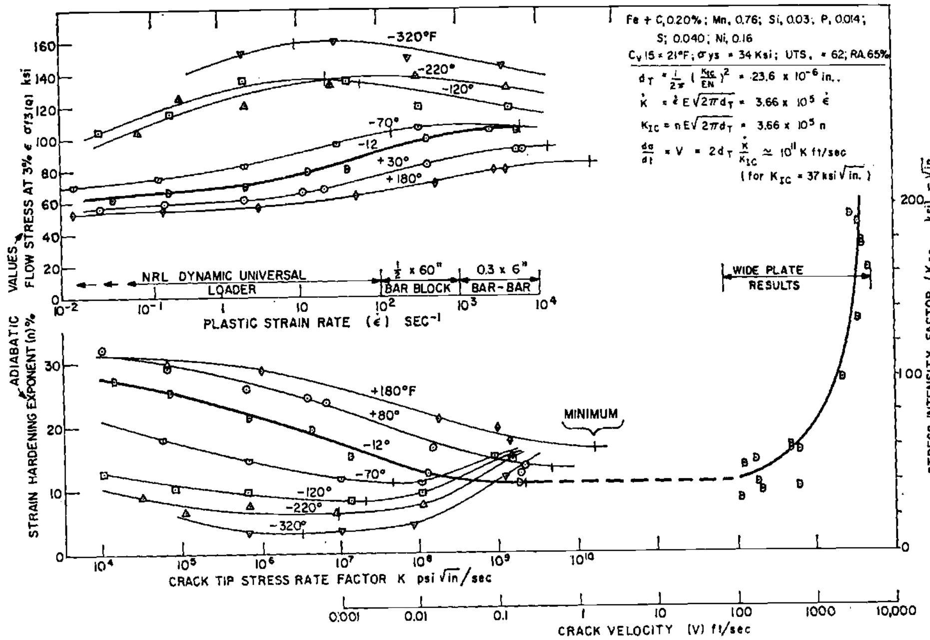

FIG. 6—For the Freely Propagating Crack or Its Arrest, Adiabatic $n_{(Q)}$ and Thus $K_{Ic(Q)}$ Values from Compression Tests Are Compared with K Calculated for Propagating Cracks in the Wide Plates. Adiabatic 3 per cent Flow Stress, $\sigma_{f3(Q)}$, Is Shown on Upper Plot.

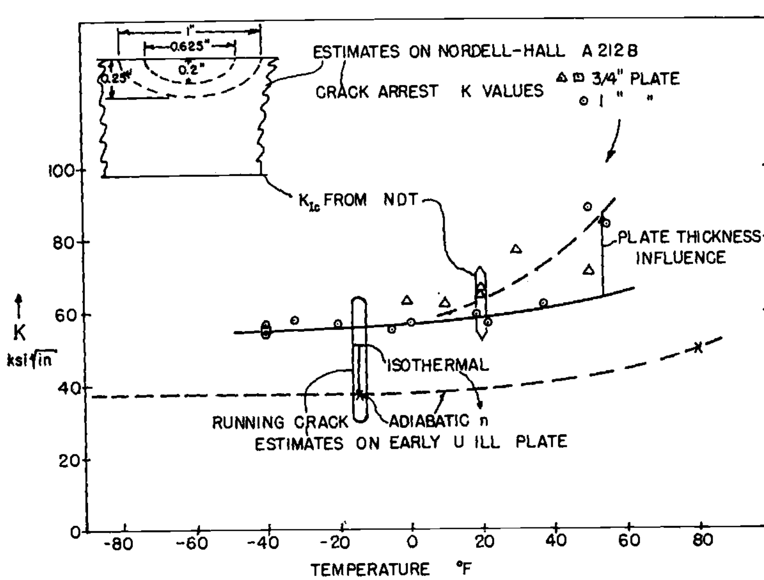

FIG. 7—Comparison of Various Estimates of K for Crack Arrest for Two Mild Steels.

VELOCITY PRIOR TO CRACK ARREST

From the preceding discussion, it is of interest to compare K_{Ic} estimates from adiabatic n determinations with values of K approached by a decelerating crack. This can be done using values of K for low crack speeds derived from University of Illinois strain-gage data for the mild steel of Fig. 3.

An attempt of this sort for the University of Illinois plate material is reproduced from Ref (17) in Fig. 6. Added to flow data from Fig. 3 (fast enough to be adiabatic) are points some 10 and 100 times higher in strain rate obtained with Hopkinson-Kolsky type bar loaders. The K value scales are based upon the correlation between K_{Ic} and n, established in Fig. 3.

A consistent pattern of speedwise behavior is evident. Regions of minimum K_{Ic} may be seen to occur at very low speeds for temperatures of -70 F and down; then, at much greater speeds, for -12 F and up. A corroborative pattern for 301 stainless steel crack-propagation results (that is, K_c tests, of Witzel) is reported by Christian and Hurlick (24).

At the right side of Fig. 6 are shown the K values estimated from strain-gage observations at various crack speeds. The trend of the data indicates a K-value range for crack arrest which is consistent with the minimum toughness level for -12 F.

CRACK-ARREST MEASUREMENTS

Figure 7 shows estimates of K at crack arrest from wide-plate tests at the University of Illinois (25). In these tests, the crack ran outward from a vertical weld residual stress zone of high tension. From the value of the moderate tensile stress applied to the plate, the crack length, and an assumed distribution of residual stress, it was possible to estimate values of K for the observed arrests. It was necessary to assume the residual stress distribution from separate studies of residual stress in similarly welded specimens. The results show very little temperature sensitivity in the range from -50 to $+20$ F. Above this temperature, estimates of the relative size of the plastic zone predict a significant plane-stress influence upon the results and a major portion of the upward trend of the K values above 20 F must be due to this influence.

The nil-ductility temperature (NDT) values from tests of the Pellini-Puzak drop-weight type were reported as in the range of 20 to 30 F for the test plates. Estimates of K_I can be derived for comparison from the nature of the small-flaw drop-weight test as suggested in Ref (7). The results of this comparison shown in Fig. 7 indicate that the drop-weight NDT test can be regarded as controlled by the same toughness as pertained to the crack arrests. The degree of numerical agreement is encouraging but not definitive. The numerical work contains a number of uncertainties which were resolved by arbitrary rough estimates. In addition, some ambiguity exists as to whether the small-flaw drop-weight test should be regarded as controlled by crack arrest or by onset of plane-strain fracture.

SUMMARY

1. The onset of rapid fracture and crack arrest provide relatively abrupt measurement points suitable for crack-toughness evaluation.

2. An understanding of these behaviors can be sought through study of the influence of plastic flow properties.

3. Use of strain-rate sensitive materials over a wide range of temperatures and strain rates permits study of the influences of flow properties without alteration of the inherent flaws.

4. A correlation of rising-load K_{Ic} values with the strain-hardening exponent, n, is found which suggests the

onset of fast fracture is controlled to a substantial degree by a tensile instability with a simple relationship to the strain-hardening exponent.

5. The limited information available suggests that crack-arrest conditions can be predicted on the basis of adiabatic values of n at high strain rates.

REFERENCES

(1) G. R. Irwin, "Fracture," *Encyclopedia of Physics*, Springer, Berlin, Vol. VI, 1958, pp. 551–590.

(2) E. H. Yoffe, "The Moving Griffith Crack," *Philosophical Magazine*, Vol. 42, 1951, p. 739.

(3) J. A. Kies, A. M. Sullivan, and G. R. Irwin, "Interpretation of Fracture Markings," *Journal of Applied Physics*, Vol. 21, 1950, p. 716.

(4) F. Kerkhof, "Analyse des Spröden Zugbruches von Gläsern mittels ultraschall," *Naturwiss*, Vol. 40, 1953, p. 478.

(5) F. Kerkhof, "Über den Bruchvorgang beim Manteldruckversuch," *Glastechnische Berichte*, Vol. 33, H.12, 1960, S. 456–459

(6) A. Smekal, "Verfahren zur Messungvon Bruchfortpflanzungs geschwondigkeitan an Bruchflaschen," *Glastechnische Berichte*, Vol. 23, 1950, p. 57.

(7) G. R. Irwin, "Crack Toughness Testing of Strain Rate Sensitive Materials," *ASME Paper 63-WA-217*, Am. Soc. Mechanical Engrs., November, 1963.

(8) H. L. Smith, J. A. Kies, and G. R. Irwin, "Fracture Toughness of Materials for Aircraft and Missiles," *Proceedings*, 3rd Navy Science Symposium on Materials Research in The Navy, Office of Naval Research, Washington, *ASTIA Report 217823*. Philadelphia, March, 1959.

(9) J. M. Krafft, A. M. Sullivan, and R. W. Boyle, "Effect of Dimensions on Fast Fracture Instability of Notched Sheets," Crack Propagation Symposium, Cranfield, 1961.

(10) G. R. Irwin, Discussion of paper by M. F. Koskinen, *Transactions*, Am. Soc. Mechanical Engrs., Vol. 85, Series D, 1963, p. 591.

(11) J. M. Krafft and A. M. Sullivan, "Effects of Speed and Temperature on Crack Toughness and Yield Strength in Mild Steel," *Transactions Quarterly*, Am. Soc. Metals, Vol. 56, No. 1, March, 1963, p. 160.

(12) R. W. Boyle, A. M. Sullivan, and J. M. Krafft, "Determination of Plane Strain Fracture Toughness with Sharply Notched Sheets," *Welding Journal* (Research Supplement), Vol. 27, No. 9, September, 1962, p. 428.

(13) "Progress in Measuring Fracture Toughness and Using Fracture Mechanics," *Materials Research & Standards*, Vol. V, No. 3, March, 1964, p. 107.

(14) J. M. Krafft, "Correlation of Plane Strain Crack Toughness with Strain Hardening Characteristics of a Low, a Medium and a High Strength Steel," *Applied Materials Research*, Vol. 3, April, 1963, p. 88.

(15) F. A. McClintock and J. A. H. Hult, "Elastic-Plastic Stress and Strain Distributions around Sharp Notches in Repeated Shear," Ninth International Congress on Appl. Mech., Brussels, 1956.

(16) D. H. Winne and B. M. Wundt, "Application of the Griffith-Irwin Theory of Crack Propagation to the Bursting Behavior of Disks," *Transactions*, Am. Soc. Mechanical Engrs., Vol. 80, 1958, p. 1643.

(17) J. Eftis and J. M. Krafft, "A Comparison of the Initiation with the Rapid Propagation of a Crack in a Mild Steel Plate," *Paper 64 MET 16*, Am. Soc. Mechanical Engrs., May, 1964.

(18) A. M. Sullivan, "New Specimen Design for Plane Strain Fracture Toughness Tests," *Materials Research & Standards*, Vol. 4, January, 1964, p. 20.

(19) C. D. Beachem, "An Electron Fractographic Study on the Influence of Plastic Strain Conditions upon Ductile Rupture Processes in Metals," *Transactions*, Am. Soc. Metals, Vol. 56, September, 1963, p. 318.

(20) C. Zener and J. H. Hollomon, "Effect of Strain Rate upon Plastic Flow of Steel," *Journal of Applied Physics*, Vol. 15, January, 1944, p. 22.

(21) T. A. Read, H. Marcus, and J. McCaughey, "Plastic Flow and Rupture of Steel at High Hardness Levels," *Fracturing of Metals*, Am. Soc. Metals, Cleveland, Ohio, 1948.

(22) G. M. Orner and C. E. Hartbower, "Sheet Fracture Toughness Evaluations by Charpy Impact and Slow Bend," *Welding Journal*, Vol. 40, 1961, p. 405s.

(23) R. Beeuwkas, Jr., "Plasticity and Fracture," *Proceedings*, Third Sagamore Ordnance Materials Research Conference, Duke University, Durham, N. C., December, 1956, p. 89.

(24) J. L. Christian and A. Hurlick, "Physical and Mechanical Properties of Pressure Vessel Materials for Application in a Cryogenic Environment," *ASD TDR 63-258, Pt. II*, February, 1963.

(25) W. J. Nordell and W. J. Hall, "Two Stage Fracturing in Welded Mild Steel Plates," University of Illinois Report, October 1963, to be published in *Welding Journal*.

DISCUSSION

CARL E. HARTBOWER[1]—One observation that may be overlooked in reading this excellent paper is the quantitative correlation found between the part-through crack (PTC) and the single-edge notched (SEN) tension specimens in 0.1-in. thick 6Al-4V titanium alloy. The fracture toughness values obtained from the two test specimens were, for all practical purposes, the same: the stress-intensity factor, K_{Ic} (ksi $\sqrt{\text{in.}}$), was 36.4 for the SEN specimen, and 41.0 for the PTC specimen. The 6Al-4V titanium was ring-rolled to a section thickness of ½ in., solution-treated and machined to 0.1-in. wall thickness. Aging resulted in a 0.2 per cent offset yield strength of 156.5 ksi. The individual test results from five PTC tension specimens are presented in Table 1. The PTC tension specimen was 8 in. long and 1 in. wide in the gage section. Note that in spite of an appreciable (deliberate) variation in crack length and shape, the computed values of fracture toughness were essentially constant.

TABLE 1—PART-THROUGH-CRACK (PTC) TENSION DATA.
(6Al-4V Titanium Alloy at 156.5 ksi Yield Strength)

Specimen No.	Surface Crack, in.		$a/2c$	Gross Specimen		Fracture		F/Fy	Shape, Q	Fracture Toughness	
	Depth	Length		Width, in.	Area, in.^{2}	Load, lb	Stress, ksi			K_{Ic}	G_{Ic}
1	0.030	0.110	0.273	0.998	0.100	14 375	143.8	0.92	1.36	41.3	93.0
2	0.040	0.100	0.400	0.996	0.100	14 150	141.5	0.90	1.82	40.7	90.2
3	0.040	0.140	0.286	1.000	0.100	12 500	125.0	0.80	1.44	40.4	88.5
4	0.060	0.220	0.263	0.998	0.100	9 850	98.5	0.63	1.42	39.3	83.6
5	0.060	0.220	0.273	1.002	0.100	10 875	108.8	0.70	1.43	43.2	101.2

TABLE 2—VARIATION IN STRESS-INTENSITY FACTOR WITH STRAIN RATE, K_{Ic} (ksi $\sqrt{\text{in.}}$)

SEN Test		Charpy $[(W/A)E]^{1/2}$	
45/sec	10^{-3}/sec	Impact	0.02 in./sec
60	38	106	55

The authors have observed that both the stress-intensity factor and the strain-hardening exponent increased with increased loading rate. Increasing fracture toughness with increasing rate of loading has been observed in several metals using the precracked Charpy test (see Figs. 16 and 17 in Orner and Hartbower[2]

[1] Research engineering specialist, Aerojet-General Corp., Solid Operations, Sacramento, Calif.

[2] G. M. Orner and C. E. Hartbower, "Sheet Fracture Toughness Evaluated by Charpy Impact and Slow Bend," *Welding Journal*, Vol. 40, No. 9, September, 1961, p. 405-s.

and Table 4 in Hartbower and Orner.[3] The data obtained by Irwin and Krafft show the upward trend of K_{Ic} and n with speed to be quantitatively of the same degree as shown by the precracked Charpy. However, the values obtained from the precracked Charpy tests in slow bend and impact (Table 2) are higher than those obtained from the SEN tension specimen. This effect would be expected considering that the precracked Charpy involves both plane-strain and plane-stress fracture.

[3] C. E. Hartbower and G. M. Orner, "Metallurgical Variables Affecting Fracture Toughness in High Strength Sheet Alloys," Air Force Technical Documentary Report No. *ASD-TDR-62-868*, October, 1962.

Test Methods

STP381-EB/Apr. 1965

FRACTURE TOUGHNESS TESTING METHODS

By John E. Srawley[1] and William F. Brown, Jr.[1]

Synopsis

A comprehensive survey is presented of current methods of fracture toughness testing that are based on linear elastic fracture mechanics. General principles are discussed in relation to the basic two-dimensional crack-stress field model, and in relation to real, three-dimensional specimens. The designs and necessary dimensions of specimens for mixed mode and opening mode (plane-strain) crack toughness measurements are considered in detail. Methods of test instrumentation and procedure are described. Expressions for calculation of crack toughness values are given for the common types of specimens.

In keeping with the purpose of the symposium of which it is a part, this survey of fracture toughness test methods will be restricted to those methods that have their basis in linear elastic fracture mechanics, or that can be treated satisfactorily by the methods of linear elastic fracture mechanics at the present time. This restriction of scope carries with it no implication that there are not other methods worthy of consideration. In the opinion of the authors, some of the arbitrary empirical procedures for evaluating fracture toughness are, and will continue to be, of great value, having been proved by correlation with service-failure studies. In this connection reference can be made to the reviews by Tipper (**1,2**),[2] and in particular to the work of Pellini and his colleagues at the U.S. Naval Research Laboratory (**3,4**). The prime purpose of the symposium, however, is to clarify the concepts and methods of linear elastic fracture mechanics and to evaluate objectively the usefulness of these concepts and methods for rational engineering analysis of fracture problems. From a practical point of view, the arbitrary empirical procedures (the most familiar being notched-bar transition temperature testing) are most useful for evaluating structural steels in the lower range of yield strengths. The application of steels in the higher range of yield strengths and of titanium and aluminum alloys calls for much more discriminating evaluation to the point of being able to estimate the strength of structural elements containing cracks. Thus, it is desirable that fracture toughness testing of such materials shall be based on the principles of mechanics as applied to cracked bodies.

Because of its rapid development over the last decade or so, fracture mechanics has seemed confusing to many interested parties (and we do not exclude ourselves). It is, therefore, useful to keep in mind the simple essentials of the discipline as we proceed to develop the subject

[1] Head, Fracture Section, and chief, Strength of Materials Branch, Lewis Research Center, National Aeronautics and Space Administration, Cleveland, Ohio.

[2] The boldface numbers in parentheses refer to the list of references appended to this paper.

in the later sections. In the simplest terms, the fracture toughness of a material determines how big a crack the material is able to tolerate without fracture when loaded to a level approaching that at which it would fail by excessive plastic deformation. For example, how big a crack could be tolerated in the wall of a pressure vessel manufactured from Brand X steel when the nominal hoop stress is raised to 90 per cent of the yield strength?

Naturally, every reasonable effort would be made to avoid having any cracks or like defects in the structure. But grievous experience tells us unmistakably that it would be quite unrealistic to depend upon the total absence of crack-like defects, however good our intentions. If something fairly quantitative about the crack tolerance of materials were known, we could be more realistic and could take more effective measures with regard to inspection, quality control, proof testing, and avoidance of development of cracks in service. For one thing, that material having the greatest crack tolerance at the stress level contemplated could be selected out of those having adequate yield strength and that were satisfactory in other respects. Or we could decide, according to the application in mind, how far we could go in reducing weight and bulk by employing materials of greater yield strength at the expense of reduced crack tolerance. In this connection, the dimensions of cracks that have been discovered to be the origins of fracture failures of critical structures range from a few thousandths of an inch in the case of some steels with yield strengths approaching 250,000 psi up to more than a foot in diameter in the case of at least one low-strength steel casting.

The most direct way of evaluating the crack tolerance of a material apparently would be to test a series of specimens provided with cracks of graded sizes to determine an empirical relation between strength and crack size. But the problem is not simply a matter of crack size. In addition, crack shape, bulk of the member (that is, thickness of a plate), orientation of the crack in relation to the fibering of the material, temperature, and rate of loading all may affect the fracture strength of a structural member of a given material. To take into account all these factors in a purely empirical test program would require very large numbers of specimens for each material evaluated. The burden of testing can be considerably reduced, however, by applying knowledge of the mechanics of fracturing, which is best represented at the present time by linear elastic fracture mechanics.

We shall assume familiarity with the concepts, assumptions, and stress-analysis aspects of current linear elastic fracture mechanics, since these are reviewed in considerable detail in other contributions to the symposium. For additional information, reference can be made to the reports of the ASTM Special Committee on Fracture Testing of High-Strength Metallic Materials (5–9), hereinafter referred to as the ASTM Special Committee on Fracture Testing. In these references, the discussion is often in terms of K, the stress-intensity factor of the elastic stress field local to the crack, rather than in terms of $\mathcal{G}$, the crack-extension force, or strain-energy release rate with respect to crack extension. For reasons that will become apparent, it is more convenient in this dissertation to develop our subject primarily in terms of $\mathcal{G}$ rather than K. This should cause no difficulty if the simple relations between these two quantities are kept in mind: $K^2 = E\mathcal{G}$ for plane stress, and $K^2 = E\mathcal{G}/(1 - \nu^2)$ for plane strain, where E is Young's modulus and ν is Poisson's ratio.

A satisfactory fracture toughness test, in the present context, is simply a model fracture experiment designed to satisfy two essential requirements, namely: (1) the specimen dimensions and loading arrangement must be such that the value of the crack-extension force, $\mathcal{G}$, can be calculated with sufficient accuracy at any stage of the test at which the values of the load and the crack dimensions are known; and (2) the values of the load and the crack dimensions at the point of instability of crack extension can be measured with sufficient accuracy. As will be shown later, it follows from the first of these requirements that the crack dimensions, and therefore the dimensions of the specimen in which the crack is contained, must exceed certain minimum values that increase as the ratio of $E\mathcal{G}_c$ to the square of the yield strength of the material. Since there is a general tendency for $\mathcal{G}_c$ to increase as the level of yield strength of structural materials is decreased, it follows further that the minimum necessary dimensions of a specimen of a given type increase very rapidly as the yield-strength level of the materials to be tested decreases. To illustrate this point, whereas the over-all diameter of the smallest circumferentially crack-notched round bar necessary to measure the plane-strain crack toughness, $\mathcal{G}_{Ic}$, of a steel having a yield strength of 300,000 psi would probably be less than 0.2 in., the smallest diameter necessary for a steel having a yield strength of 150,000 psi might exceed 5 in.

In order to minimize specimen dimensions as much as possible, thereby making most effective use of available test material and testing machine loading capacity, types of specimens have been developed in which the dimensions of the simulated crack are appreciable fractions of the over-all specimen dimensions. The expressions for $\mathcal{G}$ for such specimens are necessarily more complicated than the simple expression $E\mathcal{G} = \pi\sigma^2 a$, which applies to a straight, through-thickness crack of length, $2a$, in a flat plate of width, W, greater than $20a$, under uniform tensile stress, σ. Sufficiently accurate expressions have been obtained by mathematical or experimental methods for a number of useful types of specimens, which are discussed later. These include specimens that are loaded in bending as well as tension.

While linear elastic fracture mechanics is probably about the simplest form of strength of materials approach that could be taken in the study of fracturing phenomena, it is nevertheless quite a complex subject. This results from the inherent complexity of the fracture behavior of actual materials. Consequently, the subject of fracture toughness testing will be developed in stages, starting with a simple, idealized model of a fracture toughness test specimen that is referred to as the quasi-two-dimensional prototype specimen. This is an abstraction of the wide-plate specimen referred to in the preceding paragraph in which the thickness of the plate is ignored. This will allow development of the important concepts of crack-extension resistance and fracture instability in essentially two-dimensional terms. Next we consider the complications associated with finite thickness and the change in fracturing behavior and apparent toughness as the thickness is varied through the transition from slant, or plane-stress, fracture mode to square, or plane-strain fracture mode. This leads to consideration of the measurement of plane-strain crack toughness, $\mathcal{G}_{Ic}$, which is of particular importance in that it represents a practical lower limit to the fracture toughness of a material under given conditions. At this point we are in a position to consider practical specimen types that require reasonable amounts of material and loading capacity. The narrow symmetrical plate types of specimen for general $\mathcal{G}_c$ testing are discussed first, and then several types of specimens suitable only for $\mathcal{G}_{Ic}$ testing are discussed in sequence. In these sections, the question of $\mathcal{G}_c$ measurement capacity in relation to specimen size is discussed for each type of specimen. A summary table is provided for comparison of the various types of $\mathcal{G}_{Ic}$ measurement specimens. In the remaining sections the topics of test instrumentation and procedure and certain aspects of specimen design and preparation are taken up. An appendix provides ready reference information on the various types of specimens, giving proportioned sketches and appropriate expressions for $\mathcal{G}$ in compact form in each case.

We have one final comment before proceeding to the body of the dissertation. Some readers may tend to become impatient with the complexity of the subject and its incomplete status as they proceed through the text. We would remind them that other branches of applied mechanics of structural materials are no less complex nor more complete (for example, inelastic distortion of structures). In his classic treatise (10), Love says "The conditions of rupture are but vaguely understood, and may depend largely upon these and other accidental circumstances. At the same time, the question is very important, and a satisfactory answer to it may suggest in many cases causes of weakness previously unsuspected, and, in others, methods of economizing material that would be consistent with safety." The problems that fracture mechanics sets out to solve are still somewhat vaguely understood, yet the progress that has been made in recent years is most encouraging, and surely justifies what further effort is required to provide us with a sound engineering method for dealing with the risk of fracture.

SYMBOLS

a, a_0, a_m = length, half-length, or depth of crack according to type of specimen, Figs. 29–30; subscript 0 refers to initial value; m refers to measured value at instability

A = net cross-sectional area of cracked Charpy specimen

B = thickness of plate or bend specimen

c = half-length of surface crack, Fig. 30(d)

C, C_0 = compliance of selected gage length of specimen, that is, reversible change in gage length per unit load; subscript 0 refers to initial value of C for specimen without crack

C_g, C_{Ig} = $\mathcal{G}_c$ or $\mathcal{G}_{Ic}$ measurement capacity of specimen, that is, estimated maximum value of $\mathcal{G}_c$ or $\mathcal{G}_{Ic}$ that could be measured with acceptable accuracy for specimen of given dimensions made of material of given yield strength and elastic modulus

d, d_0 = average diameter of crack-notched section of round notched bar, Fig. 30(e); subscript 0 refers to value without plastic-zone correction

D = major diameter of round notched bar, Fig. 30(e); *also*, distance of axis of loading from cracked edge of single edge-notched tension specimen

e = displacement, that is, change in selected gage length of specimen

E = Young's modulus; *also*, electrical potential difference between two selected positions on specimen; E_0 refers to value of the electrical potential difference for specimen without crack

$\mathcal{G}, \mathcal{G}_I$ = strain-energy release rate with crack extension per unit length of crack border, or, crack-extension force; subscript I refers to opening mode of crack extension; without subscript, mode is unspecified

$\mathcal{G}_c$, $\mathcal{G}_{Ic}$ = critical value of $\mathcal{G}$ or $\mathcal{G}_I$ at point of instability of crack extension, taken to be measure of fracture toughness of material

K, K_I = stress-intensity factor of elastic stress field in vicinity of crack front; subscript I refers to opening mode of crack extension; without subscript, mode is unspecified

K_c, K_{Ic} = critical value of K or K_I at point of instability of crack extension, taken to be an alternative measure of crack toughness of material

L = effective length of fracture toughness specimen; *also*, moment arm length of bend specimen, that is, half the difference between major and minor spans

M = dimensionless coefficient in expression for $\mathcal{G}$ for round notched bar

P = load applied to specimen

r_Y, r_{IY} = plastic-zone correction term added to measured crack length; subscript I applies to plane-strain conditions and r_{IY} is taken to be $r_Y/3$

R = crack-extension resistance of material at crack tip that opposes $\mathcal{G}$

U = loss of pendulum energy in impact test, or, area under load-deflection curve of test of cracked Charpy specimen

W = width of plate specimen or depth of rectangular section beam specimen

ν = Poisson's ratio

σ, σ_c = gross stress applied to specimen in tension, that is, applied load divided by WB in case of plate specimen, or $\pi D^2/4$ in case of notched round bar; subscript c refers to the point of instability of crack extension

σ_{net} = average net-section stress for a symmetrical plate specimen in tension

σ_{nom} = nominal stress at position of crack tip for a single edge-notched tension specimen or bend specimen

σ_N = net-section stress for round notched bar

σ_{YS} = uniaxial tensile yield strength (0.2 per cent offset)

GENERAL CONSIDERATIONS

The Quasi-Two-Dimensional Prototype Specimen:

It is desirable to discuss the general concepts that apply to all fracture mechanics type toughness tests before considering in detail the various types of fracture toughness test specimens that are in common use. To do this we shall start with a simple, idealized model and then introduce systematically the various complications encountered with real specimens. We refer to this model as a quasi-two-dimensional prototype specimen, and it may be visualized as a flat sheet of width W, under uniform uniaxial tension σ, and containing a straight, ideal crack of length $2a$, less than $W/10$, in the center and normal to the direction of the applied stress. The thickness is regarded as vanishingly small and the length sufficient so that the stress-field disturbance due to the crack is insignificant at the ends.

This model is an idealization of an otherwise similar plate specimen of finite thickness, B. For such a real specimen, as we shall discuss later, the crack-front configuration may be quite complex, and $\mathcal{G}$ (the crack-extension force per unit length of crack border, or strain-energy release rate with crack extension per unit length of crack border) has, in general, a different value at each position along the crack border. With the quasi-two-dimensional model we need consider only a single value of $\mathcal{G}$, which we may regard as a sort of average value for the real crack in the plate of finite thickness. The state of the stress field is assumed to be one of generalized plane stress, and the appropriate expression for $\mathcal{G}$ is $E\mathcal{G} = \pi\sigma^2 a$ (11).

Criterion of Fracture Instability—In a typical fracture toughness test, the load on the specimen is raised continuously until a point is reached at which unstable crack extension occurs. In order to define this more precisely, it has to be appreciated that the load is not the independent variable in the test. The variable that is actually most nearly under the control of the operator is the separation of the heads of the testing machine. For our purposes, this can be regarded as equivalent to the over-all extension of the specimen, e, which will be taken as the independent test variable. (In the case of a bend specimen, e would be the specimen deflection.) The criterion for the point of instability of crack extension in the test is, then, that the load, P, as a function of e, reaches a stationary value, that is, either a maximum or a point of inflection of zero slope. In mathematical terms, $dP/de = 0$. At this point, the ability to control the load is lost, at least temporarily, and that is why the load cannot be regarded as the independent variable.

The value of $\mathcal{G}$ at the point of instability can be calculated from measurements of the load and the instantaneous crack length at that point and is designated $\mathcal{G}_c$. Either $\mathcal{G}_c$ or K_c (equal to the square root of $E\mathcal{G}_c$ for plane-stress conditions) is taken as a measure of fracture toughness of the material.

This operational definition of the point of instability of crack extension, and the corresponding definitions of $\mathcal{G}_c$ and K_c, correspond to those adopted by the ASTM Special Committee on Fracture Testing (5). To correct a common misapprehension, $\mathcal{G}_c$ and K_c are not necessarily independent of specimen dimensions other than thickness, as will be shown in the next section. Nevertheless, they do have useful quantitative significance as measures of fracture toughness.

In some of the literature on fracture mechanics, $\mathcal{G}_c$ is defined in different terms, for instance, as the value of the crack-extension force at onset of rapid crack propagation. Such a definition is too vague as an operational definition for testing purposes, and may be even somewhat misleading in seeming to imply that continuing slow crack extension is to be expected at constant levels of $\mathcal{G}$ less than $\mathcal{G}_c$. Such behavior, fortunately, is unusual and, when observed, indicates a need for careful investigation of the material and the environment in which the test is conducted. To avoid ambiguity in conducting and interpreting fracture toughness tests, the precise operational definition of $\mathcal{G}_c$ is to be preferred.

Crack-Extension Resistance and Occurrence of Instability—To appreciate the conditions that must be satisfied in valid fracture toughness tests, and to understand properly the results that are obtained, it is necessary to be familiar with the current concept of the growth of resistance to crack extension during a test. This concept was originated by Irwin (12), and is mentioned in the first report of the ASTM Special Committee on Fracture Testing, but has not been given much emphasis heretofore. The most extensive previous discussion is probably that given by Krafft et al (13).

The essence of this concept is that, as the crack-extension force, $\mathcal{G}$, is increased during a test, it is opposed by an increasing resistance to crack extension, R, of the material at the crack tip, so that equilibrium between $\mathcal{G}$ and R is maintained up to the point of instability. The crack-extension resistance, R, may be thought of as analogous to the increasing resistance to plastic deformation due to work hardening, which opposes the applied stress in an ordinary tension test. In this case also, there is a point of instability at which $dP/de = 0$.

By definition, $\mathcal{G}_c$ is equal to the value of R at instability and beyond this point $\mathcal{G}$ increases more rapidly with e than does R. Now, although the values of $\mathcal{G}$ and R are equal up to the point of instability, these quantities represent distinctly different physical entities and have different functional relations to the subsidiary test variables, σ and a. For the prototype specimen, as noted earlier, $\mathcal{G} = \pi\sigma^2 a/E$, but the dependence of R on these variables has yet to be discussed. Before doing this, it should be noted that there is a condition which must be satisfied at the point of instability that may be derived as follows.

Since $(\mathcal{G} - R)$ is equal to zero up to the point of instability, $d(\mathcal{G} - R)$ is also equal to zero up to this point. Expressing this in terms of the subsidiary variables, σ and a, yields:

$$d(\mathcal{G} - R)/de = 0 = (\partial\mathcal{G}/\partial\sigma)(d\sigma/de) + (\partial\mathcal{G}/\partial a)(da/de) - (\partial R/\partial\sigma)(d\sigma/de) - (\partial R/\partial a)(da/de) \quad (1)$$

At instability, $d\sigma/de = 0$ by definition, and Eq 1 reduces to

$$(\partial\mathcal{G}/\partial a)_{\sigma=\sigma_c} = (\partial R/\partial a)_{\sigma=\sigma_c} \ldots\ldots (2)$$

where σ_c is the stationary value of σ at instability.

The significance of this is illustrated in Fig. 1, which shows a plane section through the surface representing $\mathcal{G}$ as a function of σ and a for the constant value of σ equal to σ_c. In the simple case of the prototype specimen, the trace of the $\mathcal{G}$ surface is the straight line, $\mathcal{G} = \pi\sigma_c^2 a/E$, as shown. In general, it would be an upward-sweeping curve. The curve representing R in the figure is a projection onto the plane section of a three-dimensional curve representing a relation, as yet unspecified, among R, σ, and a. This three-dimensional curve must lie in the $\mathcal{G}$-surface up to the point of instability if R is equal to $\mathcal{G}$ up to this point. Equation 2 expresses the condition that the trace of the $\mathcal{G}$-surface in Fig. 1 must be tangent to the projection of the R-curve at the point of instability. A similar figure for a constant value of σ less than σ_c would show the $\mathcal{G}$-surface

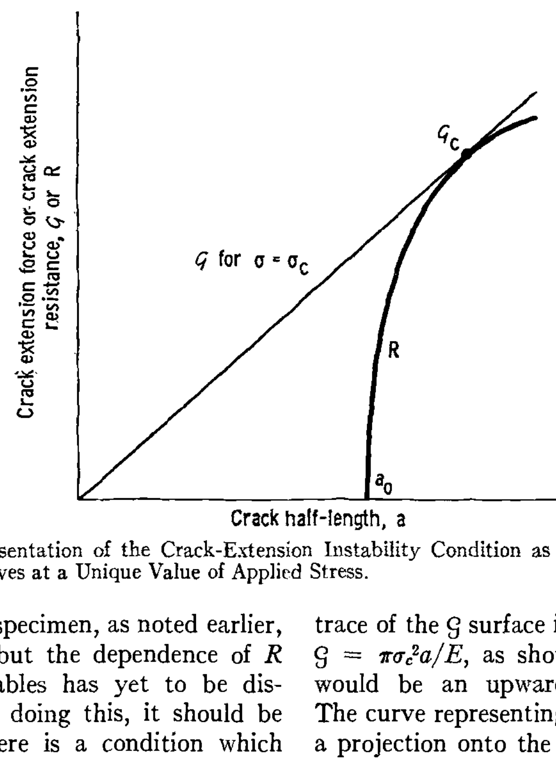

FIG. 1—Representation of the Crack-Extension Instability Condition as a Tangency Between the $\mathcal{G}$- and R-Curves at a Unique Value of Applied Stress.

trace intersecting the projection of the R-curve.

In a fracture toughness test, as normally conducted, the value of only one point on the crack-extension resistance curve is determined, namely, the instability point for the particular specimen used, which is called $\mathcal{G}_c$. This

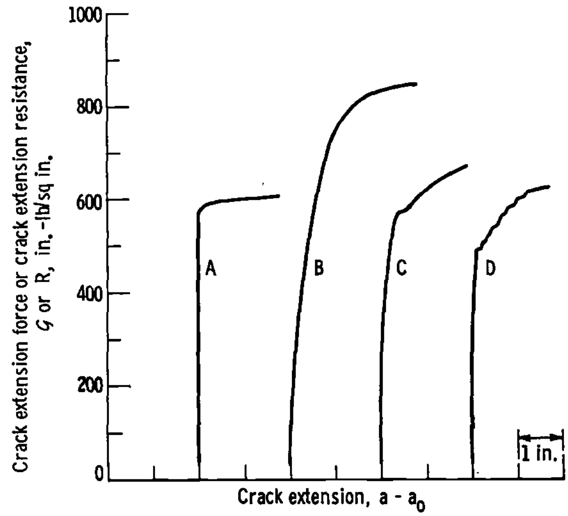

A Sharply defined instability.
B Representative of actual behavior of Al 7075-T6, according to Krafft (**13**).
C Transient instability due to sudden extension in opening mode (pop-in) followed by further, mixed-mode, stable crack extension.
D Discontinuous growth of crack-extension resistance characteristic of real materials to some degree. Other examples are actually smoothed versions of this sort of behavior.

FIG. 2—Some Conceivable Types of Crack-Extension Resistance Curves.

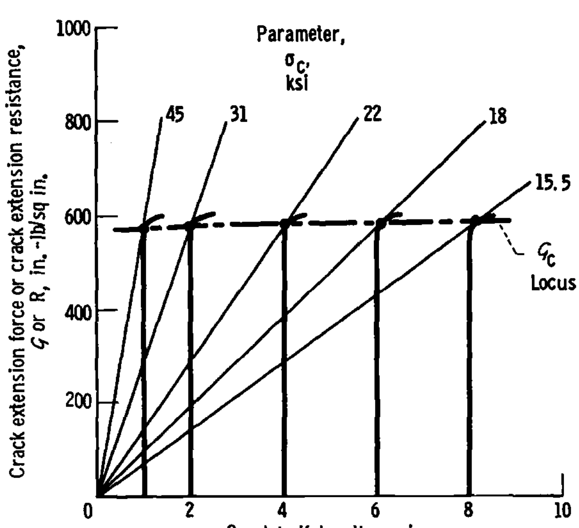

FIG. 3—Crack-Extension Instability Condition for Various Crack Lengths in a Brittle Material.

is something like determining only the ultimate tensile strength in an ordinary tension test. How nearly independent of crack length $\mathcal{G}_c$ will be for a group of tests on the same material, but using specimens with different initial crack lengths, will depend upon the form of the R-curve for the material. To characterize the fracture toughness of a material thoroughly, it would be necessary to determine the entire R-curve. Fortunately, experience suggests that $\mathcal{G}_c$ is sufficiently independent of crack length to provide a single-valued representation of the fracture toughness of most materials for most practical purposes. Where this is not the case, the R-curve can be determined by using a sufficiently large specimen, and then used for a more detailed study of a potential fracturing situation than would be possible from a knowledge only of a single $\mathcal{G}_c$ value.

The only published data on R-curves seem to be those given in Ref. (13) for 7075-T6 aluminum. Consequently, very little is known, in general, about the forms of R-curves and the factors upon which they depend. Krafft and coworkers, however, have proposed a very plausible working hypothesis that is consistent with their observations (13) and which will be utilized here. The hypothesis can be stated as follows: for a given material in an inert environment under given conditions of testing speed and temperature, the resistance to crack extension, R, is primarily a function of the magnitude of crack extension, $(a - a_0)$, and is independent of the initial crack length, $2a_0$. This implies also that R is not directly a function of σ, only indirectly in that both R and σ are related to $(a - a_0)$. This hypothesis refers to an ideally sharp starting crack and, in effect, assumes that an invariant sequence of development of crack-front configuration and associated plastic zone occurs as $(a - a_0)$ increases, whatever the value of $2a_0$. Study of the fracture surfaces of specimens having different initial crack lengths lends considerable support to this concept of an

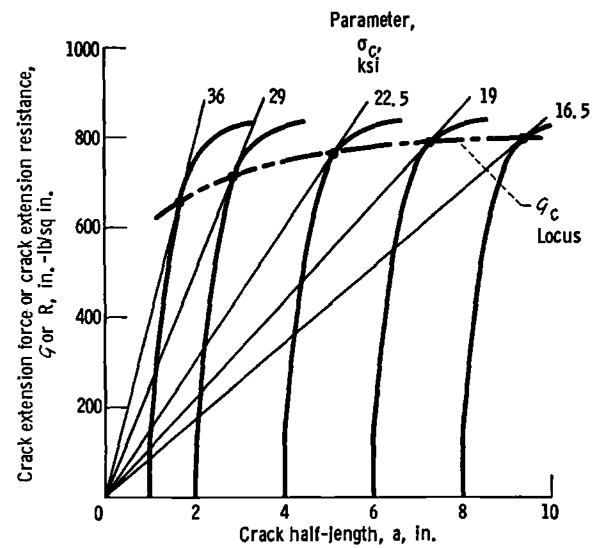

FIG. 4—Dependence of $\mathcal{G}_c$ on Initial Crack Length for Material Having Crack-Extension Resistance Curve of Type B, Fig. 2 (Al 7075-T6).

invariant pattern of development for specimens of the same thickness. At this point, the question of thickness is still neglected, but will be dealt with in a later section.

If this is accepted as a working hypothesis, the approximate form of the R-curves for a variety of materials can be inferred from unpublished data obtained by the present authors. Figure 2 shows some examples, Curves A, B, and C, representing smoothed versions of actual behavior. The curves for real materials are always more or less erratic on a fine scale, as indicated by Curve D. Curve A represents a case approaching ideal brittle behavior, in which case $\mathcal{G}_c$ would be virtually invariant. This point is illustrated in Fig. 3 which shows the points of tangency of $\mathcal{G}$-traces to R-curves of type A for several different initial crack lengths. This figure and others that follow are representations of the same kind as Fig. 1. In Fig. 3, the R-curves are identical except for lateral displacements of the origins to different values of the initial crack half-length. For this type of R-curve, $\mathcal{G}_c$ is almost constant, the locus tending to slightly lower values for shorter initial crack lengths. In practice, behavior of this sort is to be expected when the specimen breaks with a square, brittle-appearing fracture.

Figure 4 is a plot similar to Fig. 3 except that the R-curve is that shown as type B in Fig. 2. This curve is a good fit to the data for 7075-T6 aluminum reported in Ref (13). The dependence of $\mathcal{G}_c$ on initial crack length is quite considerable in this case, compared with that shown in Fig. 3. When specimens are used for which $2a_0$ is about $0.3W$ or greater, the situation is further complicated and $\mathcal{G}_c$ may have a maximum value at some value of $2a_0$, as will be shown later.

To summarize thus far, some of the general aspects of fracture mechanics toughness testing have been considered by referring to a quasi-two-dimensional prototype model specimen that has enabled us to defer consideration of some of the complexities involved when real specimens are considered. An operational definition has been given of the point of instability of crack extension in a test, and $\mathcal{G}_c$ has been defined as the value of the crack-extension force at that point; K_c is defined similarly. The concept of crack-extension resistance, R, has been discussed, and the working hypothesis that R is primarily a function of the magnitude of crack extension, $(a - a_0)$, independent of initial crack length, has been assumed. On this basis, it has been shown that $\mathcal{G}_c$ may depend to some extent on the initial crack length, the extent of the dependence varying according to the form of the R-curve for the material. Thus, $\mathcal{G}_c$ is not to be regarded as an invariant property of the material,

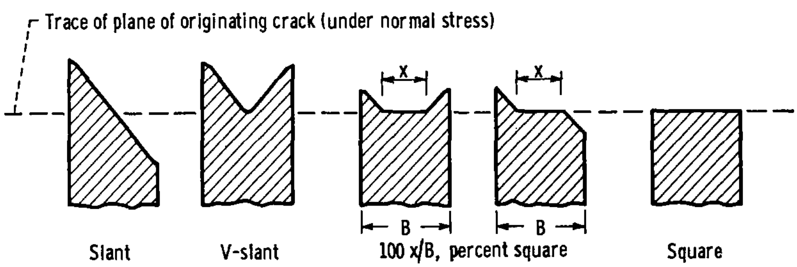

FIG. 5—Recommended Descriptive Terms for Types of Fracture Surfaces Observed in Plate Specimens Illustrated by Section Views Taken Normal to Direction of Propagation.

but rather as a somewhat arbitrary underestimate of the limiting value of R for a long crack in a wide plate of the material.

Actual Cracks in Specimens of Finite Thickness:

We are now in a position to consider real, wide-plate specimens of finite thickness, B, in other respects similar to the quasi-two-dimensional prototype. Anyone familiar with fractures of plate specimens knows the common forms that they might take, as illustrated by schematic section views in Fig. 5. The two extreme types of fracture are here referred to by the terms "slant" and "square" in preference to the more usual terms "shear" and "flat." The term "shear" is misleading because this type of fracture does not necessarily occur by relative displacement of the two surfaces in their common plane, and the term "flat" is ambiguous because a slant fracture can be as flat as a square fracture.

Since only the extreme slant and square types of fracture surface are roughly flat, it is clear that the front of an extending crack in a real plate is not even roughly represented by a straight line, except possibly in the extreme cases. Actually, as is well known, the front of a square fracture is roughly parabolic with the most advanced point at mid-thickness. For a fully developed slant fracture, the front is almost straight, as shown in Fig. 6(a). This has been established by terminating tests of steel specimens at a point short of instability. In each case, the specimen was removed from the testing machine, heat-tinted to mark the crack boundary (the use of a liquid staining medium for this purpose is not reliable), then loaded again to complete the fracture. In the general case of a mixed fracture consisting of a central square strip with slant borders, the crack front must be a nonplanar curve. A good example of this case, obtained by the heat-tinting procedure, is illustrated in Ref (14).

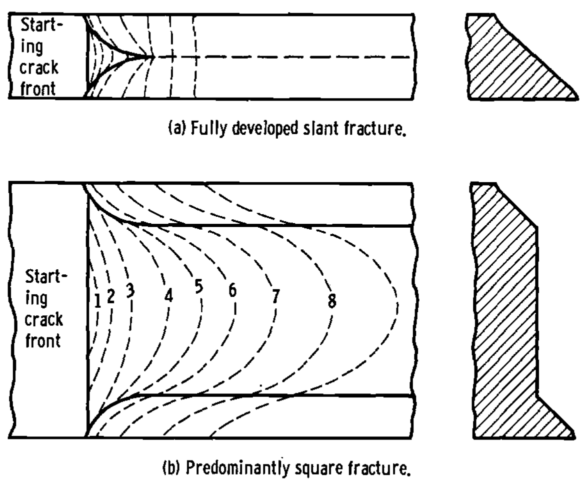

FIG. 6—Schematic Drawing of Various Successive Positions of Crack Fronts, Shown as Dashed Lines, in Specimens Having (a) Fully Developed Slant Fracture or (b) Predominantly Square Fracture (about 70 per cent Square).

The value of $\mathcal{G}$ for a given load varies with position along the crack front according to the curvature at that position. Unfortunately, no detailed analysis has been made for a curved front of a through-thickness crack in a plate, though some insight can be gained by reference to Irwin's discussion of the case of a semi-elliptical part-through crack (15). Consequently, it has to be assumed that a single average value of $\mathcal{G}$ can be taken to apply to the whole crack front with sufficient accuracy for practical purposes. Essentially, the finite thickness plate is treated in the same way as the quasi-two-dimensional prototype specimen, and it is important to realize this because the generalized plane-stress model is only an approximation to the real specimen, even in the case of a thin sheet specimen fracturing with a fully developed slant fracture. Where apparent inconsistencies in test results occur, the adequacy of this model to represent the actual test specimen should be carefully reconsidered.

The assumption of an average value of $\mathcal{G}$ involves some assumption about the value of the effective crack length, $2a$, to be used in calculating $\mathcal{G}$. This will depend on the method of measurement and will be discussed in a later section. It also involves the use of a plastic-zone correction term, also discussed later. At this point it is sufficient to note that uncertainty about the value of $2a$ at instability is the largest source of error in $\mathcal{G}_c$ measurements.

Dependence of $\mathcal{G}_c$ and Fracture Appearance on Thickness—For a given material at a given temperature and testing speed, both the appearance of the fracture of a plate specimen and the $\mathcal{G}_c$ value will depend upon the thickness. This dependence is not the result of the metallurgical processing involved in reducing the plate to various thicknesses, because the effect can be demonstrated by testing specimens of different thicknesses obtained by machining from plate stock of the same initial thickness. Metallurgical processing effects may also occur, but these should not be confused with the intrinsic effect of thickness.

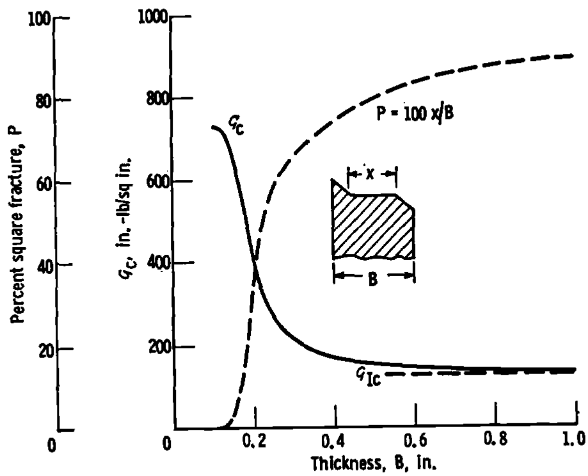

FIG. 7—Dependence of $\mathcal{G}_c$ and Fracture Appearance (in Terms of Percentage of Square Fracture) on Thickness of Plate Specimens. Schematic, but Based on Data for Aluminum 7075-T6.

The intrinsic effect of thickness is illustrated in Fig. 7, which is based on data for 7075-T6 aluminum from Ref (16). The curve is qualitatively typical of many high-strength metallic materials. The quantitative aspects, such as the peak value of $\mathcal{G}_c$, the lower limiting value for large thickness $\mathcal{G}_{Ic}$, the thickness at which $\mathcal{G}_c$ is greatest, and the range of thickness over which the major part of the fracture mode transition occurs, are all dependent upon the material and the testing temperature (and, in some cases, on the speed of testing). For a particular material at a particular temperature, these aspects depend upon the yield-strength level when this is varied by thermal or mechanical treatment.

The initial, ascending portion of the curve of $\mathcal{G}_c$ versus thickness is associated with fractures that are fully slant or V-slant, and is commonly explained by assuming that the volume of associated plastically deformed material per unit length of fracture is proportional to the square of the thickness. This follows from the assumption that the patterns of plastic deformation for different thicknesses in this range are geometrically similar, which agrees with observation. If it is further assumed that the density of plastic-deformation energy is constant throughout the plastically deformed volume, the plastic work per unit thickness per unit crack extension, which is equated with $\mathcal{G}_c$, is directly proportional to the thickness. Actually, the available data are only sufficient to confirm that $\mathcal{G}_c$ does increase with thickness in this range, not to confirm any particular form of the relation. It seems unlikely that there should be a simple linear dependence.

The descending portion of the curve of $\mathcal{G}_c$ versus thickness is associated with the occurrence and progressive dominance of square-fracture surface in the center of the plate thickness. At sufficiently large thicknesses, the slant fracture borders occupy a negligible proportion of the total fracture surface, and $\mathcal{G}_c$ approaches a lower limiting value, $\mathcal{G}_{Ic}$, referred to as the plane-strain fracture toughness, or the opening-mode fracture toughness. In the case of square fracture, it is usually assumed that the layer of associated plastically deformed material extends for a constant distance from the fracture surface, independent of the plate thickness. On the assumption that the density of plastic-deformation energy depends only upon the distance from the fracture surface, then the plastic work per unit thickness per unit crack extension, $\mathcal{G}_{Ic}$ will be independent of thickness for a completely square fracture (13,17).

The subscript I refers to the first of three component modes of crack extension distinguished by Irwin (18–20). In this mode, the mating crack surfaces separate as the crack extends so that their relative displacement is normal to the fracture plane; hence, it is called the opening mode. It corresponds to the intuitive concept of cleavage separation (but should not be confused with cleavage in a microcrystalline sense). Modes II and III are referred to as the edge-sliding mode and the screw-sliding mode, respectively (analogous to the concepts of edge and screw dislocations in crystals). In the two sliding-component modes, there is no relative displacement of the mating crack surfaces in the direction of their normal, the surfaces are supposed to slide over one another either in the direction of crack extension or normal to it. Any arbitrary mode of crack extension can be represented as a linear combination of these three component modes, and the three quantities, $\mathcal{G}_I$, $\mathcal{G}_{II}$, and $\mathcal{G}_{III}$, are the corresponding rates of transfer with crack extension of energy from the surrounding elastic strain field to other forms (18).

From a macroscopic point of view, square fractures are usually considered to result from simple mode I crack extension in a gross sense. In microscopic detail, they are quite complex and may involve a variety of fracture modes, as discussed in another contribution to this symposium. In practice, $\mathcal{G}_{Ic}$ refers to the gross average toughness value for macroscopic opening-mode crack extension. Slant fractures that occur when specimens are loaded in tension (in contrast to torsion) are not the result of pure sliding-mode crack extension in a gross sense. As can be deduced by observing such specimens during tests, the component of relative displacement normal to the crack surfaces is considerable. Fractographic examination confirms that this must be so because the ductile dimples observed on slant-fracture surfaces of specimens broken in tension are not generally pronouncedly elongated in one particular direction (21).

The plane-strain, or opening-mode, crack toughness, $\mathcal{G}_{Ic}$, is of special importance in that it represents a practical lower limit to the fracture toughness of a material in a given condition and at a given temperature and rate of testing. The possibly lower values of $\mathcal{G}_c$ for very small thicknesses are only rarely of practical importance, and apparently no such values have yet been measured for any material. There are many practical applications where the fracture, if it occurred, would be virtually completely square, and the relation of load-bearing capability to crack dimensions would be governed by $\mathcal{G}_{Ic}$. Even when the section of the load-bearing member is thin enough so that the fracture would be partly or entirely slant, the load-bearing capability might be governed by $\mathcal{G}_{Ic}$ rather than by the value of $\mathcal{G}_c$ measured for the actual thickness, unless the ratio $\mathcal{G}_c/\mathcal{G}_{Ic}$ exceeded some value that would depend upon the shape and size of the initial crack. More detailed discussion of this point can be found in Refs (6) and (20). From the point of view of having a single value representing the

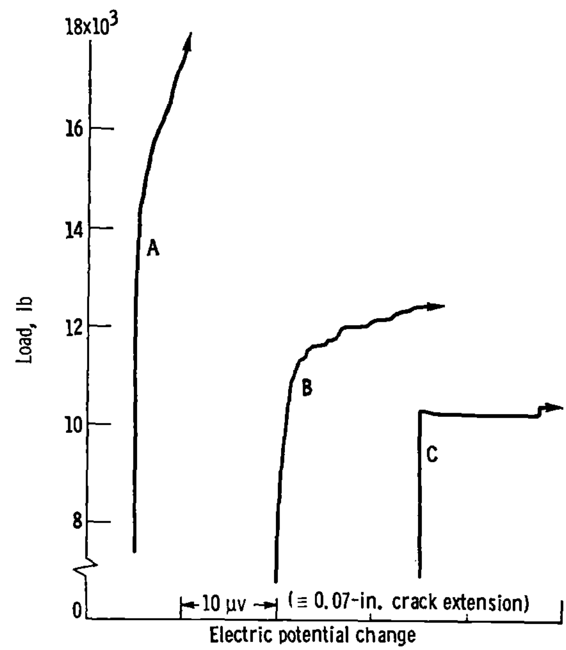

FIG. 8—Typical Examples of Load Versus Electric Potential Records for Single-Edge-Notched Specimens of a Maraging Steel Aged 3 Hr at 600 F, *A;* 1000 F, *B;* and 800 F, *C.*

fracture toughness of a material, $\mathcal{G}_{Ic}$ is independent of the dimensions of the specimen (provided that these are sufficiently large for a proper $\mathcal{G}_{Ic}$ measurement) in contrast to $\mathcal{G}_c$, which depends strongly on thickness and to some extent on crack length, as we have seen. Of course, materials exhibit nonuniformity and anisotropy with respect to $\mathcal{G}_{Ic}$, just as they do for other properties, and this has to be taken into consideration in evaluating a material. In general, in the absence of more specific information, it will always be a safe practice to use a properly determined value of $\mathcal{G}_{Ic}$ as the measure of the toughness of a material, except possibly in some cases of very thin sheet or foil.

$\mathcal{G}_{Ic}$ Measurement at Meta-instability or Pop-in—The most obvious way to measure $\mathcal{G}_{Ic}$ would be to test a sufficiently thick plate specimen of the material. This might not always be convenient, or even possible, and certainly would not be very economical of material. Because of the importance of $\mathcal{G}_{Ic}$, a number of different types of specimens have been developed for measuring it. At this point, it is convenient to discuss the concept of metainstability and the so-called pop-in method of measuring $\mathcal{G}_{Ic}$, which applies to several of these types of specimens and which makes it possible to use thinner specimens than would be required to obtain an almost entirely square fracture.

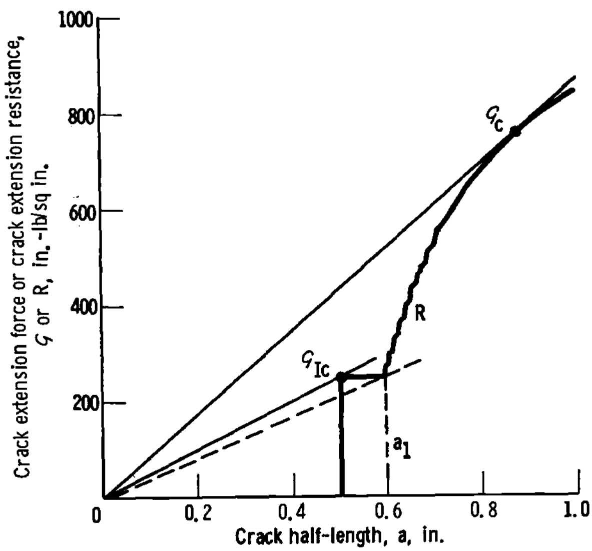

FIG. 9—Meta-instability ($\mathcal{G}_{Ic}$) and Ultimate Instability ($\mathcal{G}_c$) for Wide Plate Specimen Exhibiting Pronounced Pop-In Behavior.

The pop-in method of $\mathcal{G}_{Ic}$ determination was first proposed by Boyle et al (22) who observed in tests of sheet specimens of 7075-T6 aluminum that the first appreciable extension of the crack occurred as a distinct burst or pop-in that was then followed by a stage of gradual crack extension as the load was further increased. The same phenomenon had been observed by numerous other investigators in the form of an audible ping or click at the pop-in load, but its significance had apparently not been appreciated. Boyle and co-workers were able to show that the value of $\mathcal{G}$ at pop-in was essentially the same as the value of $\mathcal{G}_{Ic}$, which would be determined with a sufficiently thick plate specimen.

The term "pop-in" is descriptive of what actually occurs, namely, an abrupt extension of the crack front from its initial position to some position such as that labeled *5* in Fig. 6(*b*), while the load remains constant or even drops slightly. The crack movement can be followed during a test by using the output from either an electrical potential measuring device or a displacement gage to drive an *X*-*Y* recorder, as discussed in a later section. Figure 8 shows three contrasting examples of electric potential change (at constant current) versus load for specimens of maraging steel 0.2 in. thick. Example *A* represents material aged 3 hr at 600 F, *B* aged at 1000 F, and *C* aged at 800 F. The arrows indicate interruption of the tests for heat-tinting to mark the crack-front positions. Whereas example *C* exhibits very distinct pop-in behavior, example *B* is somewhat ambiguous, and example *A* is apparently not interpretable in terms of pop-in at all. In the case of example *C*, the heat-tinting procedure showed that the shape of the crack front after pop-in was approximately that shown as position *5* in Fig. 6(*b*), although the fracture in this case was less than 50 per cent square. These three examples serve to make the further point, to which we return later, that distinct pop-in behavior is not always observed and, therefore, cannot be depended upon for $\mathcal{G}_{Ic}$ measurement in all cases.

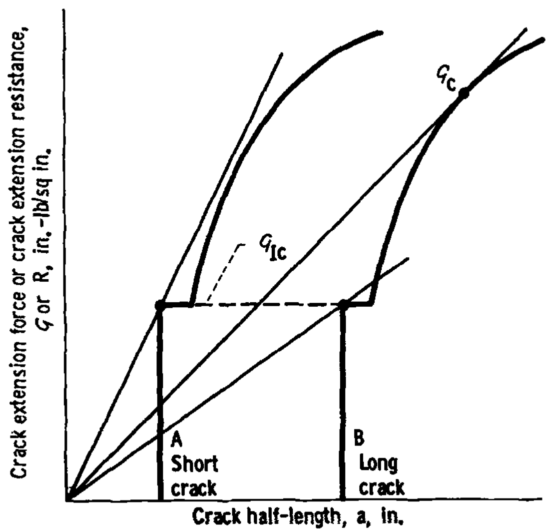

A Short crack, specimen breaks at load corresponding to $\mathcal{G}_{Ic}$.
B Long crack, ultimate load is considerably higher than that corresponding to $\mathcal{G}_{Ic}$. Significance discussed in text.

FIG. 10—Instability Behavior of Wide Plate Specimens Having Different Crack Lengths.

When pop-in does occur, it satisfies the instability condition $d\sigma/de = 0$, but the instability is only temporary, so that it is referred to as meta-instability. It will now be considered in terms of the crack-extension resistance curves that were discussed earlier. Figure 9 shows a projected curve of *R* versus *a* which is derived from the records of tests of the maraging steel aged 3 hr at 800 F, the records being similar to example *C* of

Fig. 8, but carried to more advanced stages. As the specimen is extended, the slope of the $\mathcal{G}$ versus a trace increases in proportion to σ^2. The $\mathcal{G}$-trace intercepts the R-curve so that equilibrium is maintained until the step in the R-curve is reached. At this point, the value of R over a certain interval of $(a - a_0)$ is less than the value of $\mathcal{G}$ corresponding to the stress at the point, $\mathcal{G}_{Ic}$. Thus, the balance between $\mathcal{G}$ and R is temporarily upset force of the excess elastic strain energy of the system. This may be referred to as the ultimate instability point of the test as distinguished from the meta-instability that occurs at $\mathcal{G}_{Ic}$.

One of the consequences of the hypothesis that the value of R is a function only of $(a - a_0)$ is illustrated in Fig. 10. This represents two wide-plate specimens, supposedly identical except that the initial crack lengths are different.

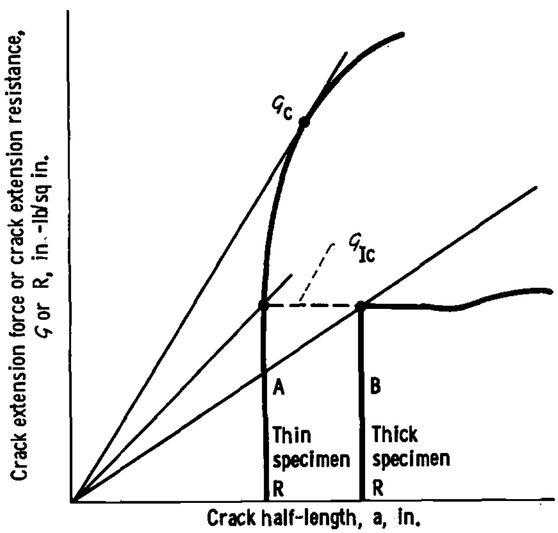

A Thin specimen, no well-defined pop-in.
B Thick specimen, pop-in occurs at maximum load.

FIG. 11—Extreme Cases of Pop-In Behavior.

until the crack has extended to the point a_1, or somewhat beyond. The extent to which the load drops in this interval is a function of several variables. However, $\mathcal{G}$ and R will again become balanced at some value of a slightly greater than a_1, and will remain so, on the average, until the point $\mathcal{G}_c$ is reached. Beyond this point, the load cannot increase further, and, even though extension of the specimen is halted at this point, the excess of $\mathcal{G}$ over R will continue to increase with increasing a, so that crack extension accelerates under the driving The R-curves are, therefore, identical but originate at different values of a_0. The behavior of the specimen with the longer crack, case B, is the same as that described in connection with Fig. 9. The behavior of the specimen with the shorter crack, case A, will be different in that ultimate instability will be reached at $\mathcal{G}_{Ic}$, that is, the load cannot increase beyond the value reached at pop-in. If extension of the specimen is maintained at a steady rate, the load will drop at pop-in, then may increase again slightly, but the load at which

$\mathcal{G}$ and R are equal at any subsequent stage of crack extension will always be less than the pop-in load. Thus, the load-bearing capability of the specimen is controlled by $\mathcal{G}_{Ic}$ and not by some higher value of $\mathcal{G}_c$, even though a higher value could be measured by using a specimen with a longer crack, as in case B. This comparison emphasizes the point that was made earlier about the controlling significance of $\mathcal{G}_{Ic}$ in some cases, bearing in mind that test specimens are nothing more than simple examples of structural members.

Two contrasting examples of schematic R-curves are shown in Fig. 11. Example A represents a relatively thin specimen in which the developed fracture is fully slant and the initial, triangular region of square fracture (see Fig. 6(a)) is quite small. The magnitude of the pop-in is reduced to the point where it cannot be detected with confidence, and $\mathcal{G}_{Ic}$ cannot be measured with any confidence of accuracy. In a case like this, it may be possible to obtain a well-defined pop-in measurement of $\mathcal{G}_{Ic}$ if a specimen of sufficiently greater thickness can be tested. But it should not be assumed that this will always be the case. The authors have found, by using SAE 4340 steel specimens, for instance, that well-defined pop-ins do not always occur even when specimens are used that are sufficiently thick for the developed fractures to be more than 50 per cent square. This raises the question of how $\mathcal{G}_{Ic}$ might be measured for such materials, but there is no satisfactory answer to this question yet. It is hoped that research currently in progress may resolve the matter. While it is sometimes assumed that $\mathcal{G}_{Ic}$ measurements can always be satisfactorily made by testing round notched bars of sufficient size (which are discussed later), there is really no conclusive evidence at the present time that this assumption is warranted.

Example B in Fig. 11 represents the other extreme, in which the developed fracture of a plate specimen is almost entirely square, the pop-in is very pronounced, and the subsequent increase in R is very gradual because there is very little development of slant-fracture borders. For any practical initial crack length, the load cannot increase beyond the value at pop-in, so that $\mathcal{G}_{Ic}$ is well defined by the maximum load value and the initial crack length. The record of load versus crack length in this case will show a sharp peak at the load corresponding to $\mathcal{G}_{Ic}$, followed by a rapid decrease of the load.

In this section an attempt has been made to describe and explain the pop-in phenomenon and its use for $\mathcal{G}_{Ic}$ measurement by reference to the Krafft hypothesis of an invariant curve of R versus $(a - a_0)$. It is worth repeating that this hypothesis, while probably a good first approximation, may require some modification in the light of future experimental information. In fact, it will be an important aspect of fracture mechanics research in the immediate future to conduct experiments designed to test and extend this hypothesis. It seems likely that, while the dominating factor upon which R depends for a given material, thickness and testing conditions, is indeed $(a - a_0)$, there may well be a secondary influence of initial crack length. This might be quite significant when the initial crack length is sufficiently short so that the net section stress at $\mathcal{G}_c$ approaches the yield strength of the material. This is a situation that might be avoided in fracture mechanics testing but that is not always avoidable in practical fracture problems.

PRACTICAL SPECIMEN TYPES

The discussion has so far centered around flat tension specimens having transverse cracks of length less than one tenth the specimen width. These are conveniently simple for the purpose of discussing general concepts. In subsequent sections, various types of specimens will be considered that are more suitable for practical testing purposes, either because they require less material and lower testing load capacity, or because they provide conditions of greater elastic constraint. First, two types of specimen will be considered that are primarily intended for general $\mathcal{G}_c$ (mixed mode) toughness testing but that may sometimes be used for $\mathcal{G}_{Ic}$ measurement by the pop-in method. Then those specimen types that are regarded as suitable only for $\mathcal{G}_{Ic}$ measurement will be considered. While the specimen types discussed here are those having the most general application, there are numerous other types that have been, or could be, devised for special purposes, the only qualification being that a satisfactory specimen design must be amenable to a sufficiently accurate stress analysis to obtain an accurate expression for $\mathcal{G}$. This could be obtained either mathematically or experimentally, as illustrated by Refs (23) and (24), respectively. In particular, Winne and Wundt (25) have discussed the use of notched rotating disks, and Ripling et al (26) have discussed specimens for measurement of fracture toughness of adhesive joints.

In connection with each of the practical specimen types we shall discuss the appropriate expression for $\mathcal{G}$ and the value of the effective crack length to be used in calculating $\mathcal{G}$, including the plastic-zone correction term that is added to the observed value of the actual crack length. We shall also discuss the capacities of the various types of specimens for measurement of $\mathcal{G}_c$ or $\mathcal{G}_{Ic}$ in relation to specimen size. For this purpose, an unfamiliar symbol representing the $\mathcal{G}_c$ measurement capacity, namely C_g, is introduced to represent the maximum value of $\mathcal{G}_c$ that could be measured with acceptable accuracy with a specimen of given dimensions made of a material of given yield strength and elastic modulus. This will allow a summary comparison to be made of the different types of specimens for $\mathcal{G}_{Ic}$ testing, which indicates the merits and limitations of each type.

Symmetrical Plate Specimens for General $\mathcal{G}_c$ Measurement:

These two types of specimens are illustrated in Fig. 29 (see the Appendix). The center-cracked type (*a*) is provided with a simulated central transverse crack of initial length, $2a_0$, equal to about $0.3W$, where W is the width; it is obviously a modification of the wide-plate specimen having a longer crack for a given width. The symmetrically edge-cracked type (*b*) is provided with equal transverse edge cracks of initial length, a_0, equal to about $0.15W$. These two specimens are essentially equivalent except for a slight difference in the expressions for $\mathcal{G}$, and the choice between them is mainly a matter of convenience in preparation. The discussion will, therefore, be confined largely to the center-cracked specimen with the understanding that it applies in general equally to the symmetrically edge-cracked specimen.

The elastic strain energy field in the vicinity of the ends of the crack is appreciably influenced by the proximity to the free edges of the specimen when $2a/W$ exceeds about 0.1. Consequently, $\mathcal{G}$ is then no longer given with sufficient accuracy by the equation, $E\mathcal{G} = \pi\sigma^2 a$. The appropriate expression recommended by the ASTM Special Committee on Fracture Testing (5) is the tangent form derived by Irwin (12,18) from an analysis by Westergaard (27): $E\mathcal{G} = \sigma^2 W \tan (\pi a/W)$. An earlier expression was derived by Kies (28) from the work of Greenspan (29), and is known as the Greenspan or polynomial form. While this form is occasionally still used, it is preferable to use the tangent form in the interests of consistency with the majority of investigators. To show that the difference between these expressions is not inconsequential, they are compared in Fig. 12 on a dimensionless basis, $E\mathcal{G}/\pi\sigma^2a$, which is equal to the configurational or geometric factor in each case, being plotted versus $2a/W$.

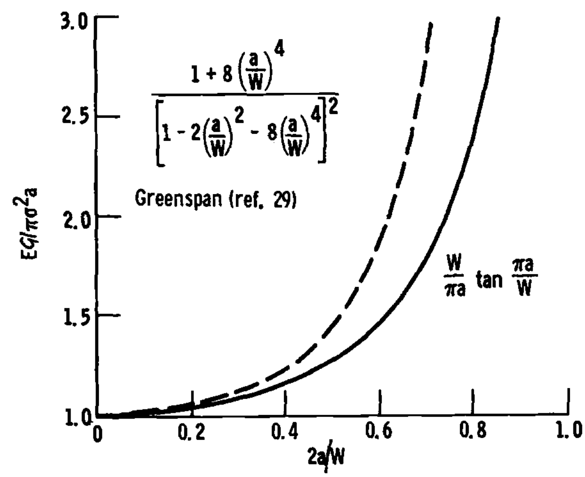

FIG. 12—Comparison of the Irwin Tangent Expression and the Greenspan Equation for Symmetrically Center-Cracked Plate Specimens.

Effective Crack Length and Plastic-Zone Correction Term—The value of the effective crack length, $2a$, which should be used in calculating $\mathcal{G}$ from the tangent equation given above, is not simply the estimated average length of the actual crack at instability, $2a_m$, but also includes a term, $2r_Y$, to correct for the stress-relaxing effect of the plastically deformed zones at each end of the crack; that is, $a = a_m + r_Y$. When a state of generalized plane stress is assumed, as in the case of a $\mathcal{G}_c$ measurement at ultimate instability, r_Y is taken to be equal to $E\mathcal{G}/2\pi\sigma_{YS}^2$, where σ_{YS} is the 0.2 per cent offset tensile yield strength. For a state of plane strain, usually assumed for $\mathcal{G}_{Ic}$ measurements, r_{IY} may be taken as one third of the plane-stress value, that is, $E\mathcal{G}/6\pi\sigma_{YS}^2$. The basis for these correction terms has been thoroughly discussed in the literature (5,12,30) and is also discussed in other papers in this symposium, so that no extensive discussion is needed here. It is important for our purpose, however, to emphasize the point that this method of correcting an assumed elastic stress analysis to take account of inelastic strain in a limited region is somewhat arbitrary and approximate. For this reason, calculated values of $\mathcal{G}$ should be regarded as increasingly inaccurate, the greater the ratio r_Y/a. This is one factor that should be considered in deciding how large a specimen is needed for an accurate measurement of $\mathcal{G}_c$, but the basis of the current recommendation of the ASTM Special Committee on Fracture Testing on this point is somewhat different, as is discussed later.

The calculation of $\mathcal{G}$ is complicated by the inclusion of the plastic-zone correction term, which itself is a function of

$\mathcal{G}$. Except in the simplest case of the wide-plate specimen, $\mathcal{G}$ cannot be expressed as an explicit function of the load and the specimen dimensions, and must be calculated from the implicit equation by either a graphical or an iteration procedure. The graphical procedure for the symmetrically cracked plate specimens is described in Ref (5). The iteration procedure is simply a matter of first calculating a first approximation to $\mathcal{G}$ by neglecting r_Y, next a second approximation to $\mathcal{G}$ entailing a value of r_Y based on the first approximation to $\mathcal{G}$, and so on. Convergence will normally be very rapid, and the iteration procedure is the natural one to use for a digital computer calculation program.

$\mathcal{G}_c$ *Measurement Capacity in Relation to Specimen Size*—If the width of a center-cracked plate specimen is less than some value that is directly proportional to the value of $\mathcal{G}_c$ to be measured, the average net-section stress at instability will exceed the uniaxial tensile yield strength of the material. A test of this sort is not represented even approximately by a linear elastic stress field model, and therefore does not provide a useful measurement of $\mathcal{G}_c$. Even when instability occurs at an average net-section stress less than the yield strength, the accuracy of $\mathcal{G}_c$ measurement is lower, the greater the value of r_Y/a, as mentioned above. The ratio r_Y/a increases in proportion to the square of the ratio of the average net-section stress to the yield strength for a given value of $2a/W$. It follows that the larger the specimen that is tested, the more accurate the measurement of $\mathcal{G}_c$ is likely to be. Similar considerations apply to the specimens for $\mathcal{G}_{Ic}$ testing, which will be discussed later.

It is of considerable practical importance to be able to estimate how large a value of $\mathcal{G}_c$ could be measured with acceptable accuracy by using a center-cracked specimen of a given width, W. For this purpose the ASTM Special Committee on Fracture Testing has suggested the criterion that the $\mathcal{G}_c$ measurement will be sufficiently accurate if the average net-section stress at instability does not exceed 80 per cent of the 0.2 per cent offset tensile yield strength, σ_{YS} (9). This is a tentative recommendation, based upon a limited number of tests of specimens having different widths and crack lengths which indicated that $\mathcal{G}_c$ was independent of width and crack length when this condition was satisfied. It would appear that the materials used for these tests must have R-curves of a type that would result in $\mathcal{G}_c$ being insensitive to crack length, that is, like type A in Fig. 2 rather than like types B or C. It should be noted that there is a distinction to be made here between an intrinsic dependence of $\mathcal{G}_c$ on crack length due to the shape of the R-curve, which exists even when the test is well represented by the linear elastic stress field model, and an apparent dependence of $\mathcal{G}_c$ on crack length that occurs when the average stress is too close to yield to be properly represented by the linear elastic model.

Substituting the condition, $\sigma_{net} = 0.8\sigma_{YS}$, in the tangent equation yields, for C_g, the maximum value of $\mathcal{G}_c$ that could be measured with acceptable accuracy for a given yield strength, elastic modulus, and specimen dimensions:

$$C_g = 0.64(\sigma_{YS}^2/E) \cdot W[1 - (2a_m/W)]^2 \tan(\pi a/W)$$

where a_m is the estimated average half-length of the actual crack at instability, and $a = a_m + r_Y$.

This expression for C_g can be regarded as the product of four distinct factors, each having a particular significance: (*1*) the numerical constant 0.64 represents a factor of utilization based upon experimental results; (*2*) σ_{YS}^2/E represents the dependence of C_g on the properties of the material under test; (*3*) the width, W, is the characteristic dimension representing specimen size; and (*4*) $[1 - (2a_m/W)]^2 \tan (\pi a/W)$ is a dimensionless factor representing the effect of ratio of crack length to width.

The length of the specimen should be proportional to W, and chosen to be varied over a considerable range for a given value of W, as indicated in Fig. 29, and will be discussed later.

From the expression for C_g given above, it follows that the most efficient value of $2a_m/W$ will be that for which the quantity $0.64[1 - (2a_m/W)]^2 \tan (\pi a/W)$, which is equal to EC_g/σ_{YS}^2W, is greatest. This is plotted versus $2a_m/W$ in Fig. 13, showing that the maximum occurs in the range of $2a_m/W$ between

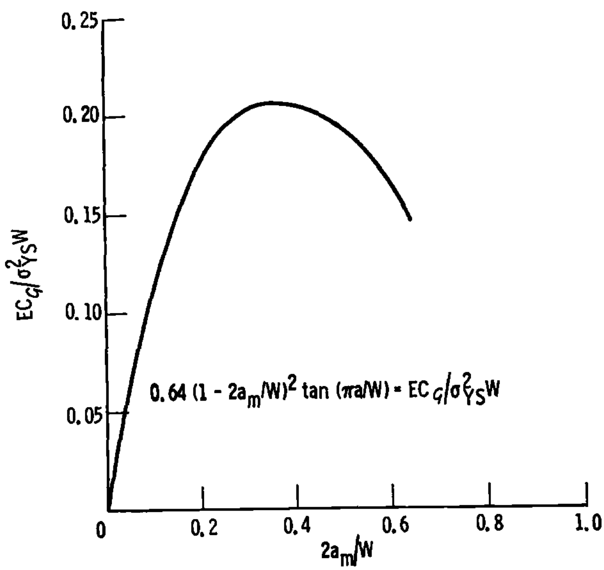

FIG. 13—Measurement Capacity of Symmetrically Center-Cracked Specimens as a Function of Relative Crack Depth.

sufficient so that there is a region of uniform stress distribution between the crack and each of the end regions of the specimen through which the load is applied. Photoelastic studies have confirmed that the proportions of the specimens shown in Fig. 29 of the appendix are just about sufficient for the pin-loading method shown. With proportionately shorter specimens, the interference between the stress field of the crack and that of each of the loading pinholes would be appreciable. Specimen thickness for $\mathcal{G}_c$ measurement may be 0.3 and 0.4. This is the basis for the recommendation that $2a_0$ should be about $0.3W$ for the center-cracked specimen. The useful range of $2a_m/W$ extends up to about 0.6; beyond this point, the accuracy of the expression for $\mathcal{G}$ becomes increasingly dubious (*12*). Furthermore, the accuracy of the estimate of $\mathcal{G}$ becomes increasingly dependent on the accuracy of the value of a that is used, and this is the least accurate of the several measurements from which $\mathcal{G}$ is calculated. Thus, if $2a_m/W$ exceeds 0.6 in any test, the result should not be used for anything more than a rough estimate of $\mathcal{G}_c$. Additional tests of wider specimens are necessary for accurate $\mathcal{G}_c$ measurement in such cases.

For values of $2a_m/W$ much less than 0.3, limitation of the average net-section stress to 80 per cent of the yield strength may not be a sufficient indication that an acceptably accurate determination of $\mathcal{G}_c$ will result. The reason for this is that, for $\sigma_{net} = 0.8\sigma_{YS}$, the ratio r_Y/a increases as $2a_m/W$ decreases, as shown in Fig. 14. To a first approximation, if the estimate of r_Y as $E\mathcal{G}/2\pi\sigma_{YS}^2$ is in error, the consequent error in the calculated value of $\mathcal{G}$ will be proportional to r_Y/a multiplied by the error in r_Y. In Ref (30), it is suggested that the value of r_Y is unlikely to differ from the estimate $E\mathcal{G}/2\pi\sigma_{YS}^2$ by more than about ± 25 per cent, so that the consequent error in the calculated value of $\mathcal{G}$ would be expected to be no greater than $25r_Y/a$ per cent. The value of this limit increases from 4.4 per cent at $2a_m/W$ equal to 0.3, to 8 per cent as $2a_m/W$ approaches zero (from Fig. 14). In general, it would seem desirable that r_Y/a should not exceed about 0.2, so that any associated error in $\mathcal{G}$ would be likely to be less than 5 per cent.

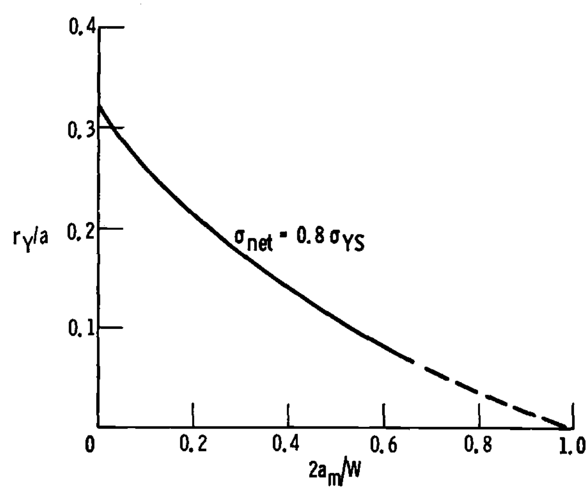

FIG. 14—Ratio of Plastic-Zone Correction to Effective Crack Half-Length as Function of r_Y/a for $\sigma_{net} = 0.8\,\sigma_{YS}$.

Bearing in mind these considerations regarding accuracy, we may estimate the $\mathcal{G}_c$ measurement capacity of a center-cracked specimen, C_g, by referring to Fig. 13. The value of the ordinate for a given value of $2a_m/W$ is equal to the value of EC_g/σ_{YS}^2W. When $2a_m/W$ is between 0.3 and 0.45, C_g is slightly greater than $0.2W\sigma_{YS}^2/E$, and this value may be regarded as the maximum $\mathcal{G}_c$ measurement capacity of the center-cracked type of specimen. The maximum K_c measurement capacity is, therefore, about $0.45\sigma_{YS}W^{1/2}$. The same figures can be used in estimating the toughness measurement capacities of symmetrically edge-cracked specimens.

Variation of $\mathcal{G}_c$ with Crack Length and Specimen Width—The preceding discussion of $\mathcal{G}_c$ measurement capacity involved the implicit assumption that $\mathcal{G}_c$ would be independent of initial crack length, as would be the case for a material with an R-curve similar to type A in Fig. 2. Assuming $\mathcal{G}_c$ to be independent of initial crack length enabled us to avoid an unduly complicated discussion of $\mathcal{G}_c$ measurement capacity, and the conclusions reached are not substantially different from those that would have followed from a more general discussion.

Having dealt with the question of $\mathcal{G}_c$ measurement capacity in this manner, it is now necessary to return to the question of how $\mathcal{G}_c$ might depend upon crack length and specimen width in the case of a material having a different kind of R-curve, for instance, type B of Fig. 2. This question was discussed earlier with reference to center-cracked plate specimens for which $2a/W$ was less than 0.1 (Fig. 4); we now extend the discussion to consider specimens for which $2a/W$ is greater than 0.1.

Figure 15 shows an R-curve that is identical with those in Fig. 4 apart from scale. The particular $\mathcal{G}$-traces that are tangent to the R-curve for specimens of widths 2, 3, 6, and 12 in. are also shown, the initial crack length being 1 in. in each case. These $\mathcal{G}$-traces are no longer straight lines, as in Fig. 4, but are constructed from the equation, $E\mathcal{G} = \sigma^2 W \tan(\pi a/W)$, the appropriate values of σ required to satisfy the tangency condition being obtained by graphical interpolation. As discussed earlier, the points of tangency represent the values of $\mathcal{G}_c$ that would be measured according to our criterion of instability. The main point of Fig. 15 is that, for a given initial crack length and an R-curve of this type, the measured value of $\mathcal{G}_c$ decreases as the specimen width is decreased. Furthermore, the dependence of $\mathcal{G}_c$ on W is stronger, the larger the value of $2a_0/W$. These conclusions are, of course, drawn from a construction on the basis of the hypothesis that R is a function of $(a - a_0)$ only (13). The results given in Ref. (13) for 7075-T6 aluminum are generally consistent with Fig. 15, the R-curve in that figure having been obtained from those results, but the agreement between measured and predicted

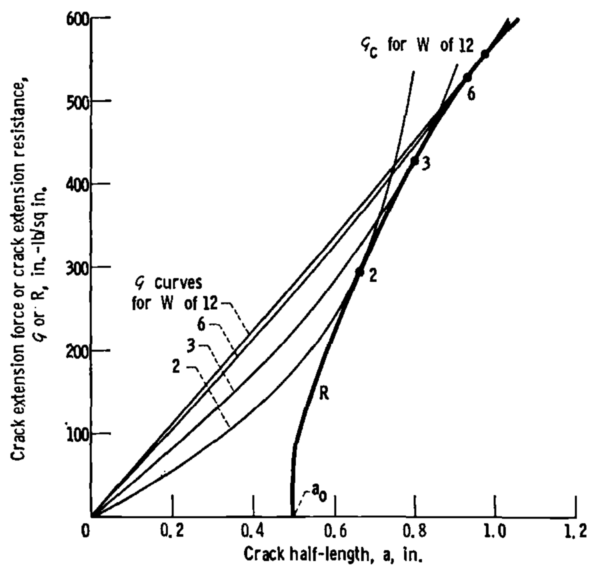

FIG. 15—Dependence of $\mathcal{G}_c$ on Specimen Width, W, for Center-Cracked Plate Specimens Having the Same Initial Half-Crack Length.

values of $\mathcal{G}_c$ is no more than fair. This simply means that more extensive experimental investigation of the hypothesis is needed; the fact that $\mathcal{G}_c$ may depend upon specimen width in the manner shown by Fig. 15 is not in question. However, the degree of the dependence will depend upon the material, its thickness, and upon testing speed and temperature, and may be imperceptible in some cases.

two effects oppose one another when the specimen width is kept constant and the crack length varied, as in Fig. 16. The crack-length effect dominates for the smaller values of $2a_c/W$, resulting in an initial increasing trend of $\mathcal{G}_c$ with $2a_0/W$. For values of $2a_0/W$ greater than about 0.35, however, the effect of the restricted specimen width dominates and the trend is reversed. Of course, this is just one example, and it is to be

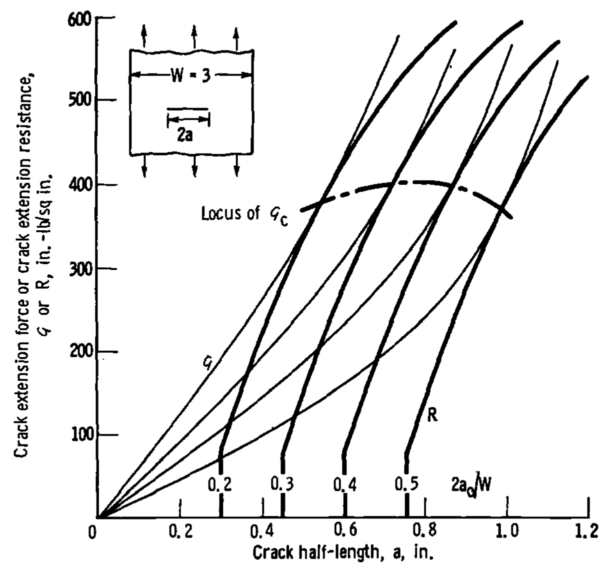

FIG. 16—Dependence of $\mathcal{G}_c$ on Relative Initial Crack Length for a Finite Width Specimen Having an R-Curve Identical to That of Figs. 4 and 15.

Figure 16 shows the predicted dependence of $\mathcal{G}_c$ on $2a_0/W$ for a fixed specimen width of 3 in. when the R-curve is identical with that of Fig. 15. The value of $\mathcal{G}_c$ does not vary greatly over the range of $2a_0/W$ between 0.2 and 0.5, and the locus has a maximum at $2a_0/W$ equal to about 0.35. The contrast between this figure and Figs. 4 and 15 is rather surprising. The explanation is that $\mathcal{G}_c$ increases with increasing crack length, as in Fig. 4, but decreases as $2a_0/W$ increases for a given value of the initial crack length, as in Fig. 15. These expected that the form of the $\mathcal{G}$-locus will vary with the form of the R-curve, but the opposing effects will exist to some degree in any case. Perhaps the most important point to make about this is that it is possible to obtain a false impression of the degree of independence of $\mathcal{G}_c$ from a series of tests in which the specimen width is kept constant and the initial crack length is varied.

Since the measured value of $\mathcal{G}_c$ will depend upon both initial crack length and specimen width to a greater or lesser degree, depending upon the form of the R-curve for the material and thickness under investigation, there is some question as to how to make use of particular $\mathcal{G}_c$ measurements. This question cannot be satisfactorily answered until the R-curves of a sufficient variety of materials have been determined and evaluated in sufficient detail. At the present time it would seem only prudent to evaluate $\mathcal{G}_c$ for several crack lengths in the case of any material and thickness that is intended to be used in a particular application.

As far as evaluating the fracture toughness of materials in general is concerned, $\mathcal{G}_{Ic}$ is apparently independent of any specimen dimension and thus provides an invariant fracture characteristic for many of the materials of engineering interest. This is the main reason why effort on $\mathcal{G}_{Ic}$ testing has increased in recent years at the expense of effort on $\mathcal{G}_c$ testing.

We do not wish to leave the impression, however, that $\mathcal{G}_c$ testing should be abandoned in favor of $\mathcal{G}_{Ic}$ testing exclusively. Rather, we would suggest that $\mathcal{G}_c$ tests should be conducted primarily in relation to specific structural components and should be conducted in sufficient detail that the $\mathcal{G}_c$ values determined are relevant to circumstances of failure that are pertinent to the component in question. For example, in an airplane skin, tolerance for a crack several inches long is desirable, if not mandatory, but in a rocket casing it may be necessary to use materials that cannot tolerate cracks that are only a fraction of an inch long. These different cases call for different approaches to $\mathcal{G}_c$ testing. Material selection in relation to risk of fracture should entail at least two stages. The first, screening stage would utilize a standardized specimen appropriate to the application and would serve to reduce the number of candidate materials to a preferred few. These would then be subjected to more extensive testing involving a range of crack sizes, perhaps even to determination of the entire R-curve for the thickness of interest. What is most important is that it should be appreciated that neither the planning nor the interpretation of $\mathcal{G}_c$ tests is a routine matter.

Before leaving the subject of $\mathcal{G}_c$ testing to take up $\mathcal{G}_{Ic}$ testing, we need to discuss the question of specimen thickness. This will lead naturally into a general discussion of $\mathcal{G}_{Ic}$ measurement and then to consideration of other types of specimen for this purpose.

Thickness of Symmetrical Plate Specimens—The ASTM Special Committee on Fracture Testing has recommended that the specimen thickness, B, for mixed mode or slant mode $\mathcal{G}_c$ measurement should be between $W/45$ and $W/16$, except that the lower limit need not apply if proper measures are taken to prevent buckling around the crack when B is less than $W/45$ (5). In the experience of one of the authors, buckling of symmetrically edge-cracked specimens is less apt to occur than is the case with center-cracked specimens. In any case, supporting the specimen between lubricated face plates is an effective method of preventing buckling of thin specimens and ensuring that accuracy of $\mathcal{G}_c$ measurement is not impaired thereby.

The restriction that B should not exceed $W/16$ applies only when it is desired to measure $\mathcal{G}_c$, as distinct from $\mathcal{G}_{Ic}$, by the pop-in method. It has to do with the change in crack-front configuration as the crack extends from the initial fatigue crack front, which is nearly square and straight, in the stable range preceding instability. It is useful at this point to refer to Fig. 6. With the assumption that the crack will eventually develop into the slant type (the most extreme case), the distance over which the development takes place will be roughly proportional to B, and of about equal magnitude (Fig. 6(a)). For $2a_0/W$ equal to about 0.3 and B not greater than $W/16$, development of full slant fracture should be completed at some value of $2a_m/W$ less than 0.6. For greater thicknesses, there is a possibility that development of full slant fracture may not be complete when $2a_m/W$ equals 0.6 and instability might occur at some value of $\mathcal{G}$ lower than that appropriate to the thickness and width. While no specific data are available on this point, general experience indicates that there is good reason to respect this restriction.

For materials of such thickness that the specimen will exhibit a predominantly square fracture, the restriction could be less severe, as implied in Ref. (5). For $\mathcal{G}_{Ic}$ measurements, there appears to be no basic reason to impose any upper limit on the thickness, but there is an optimum value of the ratio B/W, as we shall now discuss.

In their original study of the pop-in method of $\mathcal{G}_{Ic}$ measurement, Boyle et al (22) observed distinct pop-in indications with 7075-T6 aluminum specimens that had thicknesses no less than $2E\mathcal{G}_{Ic}/\pi\sigma_{YS}^2$, that is, not less than four times the value of r_Y corresponding to $\mathcal{G}_{Ic}$. Distinct pop-in indications were not observed with specimens that were thinner than this. The qualitative explanation of these observations is that, when the plane-stress plastic-zone size approaches one half the specimen thickness, the component of stress in the thickness direction will be relaxed along the major part of the crack front so that a state of plane strain no longer prevails. It is to be expected that the limiting value of the ratio r_Y/B for distinct pop-in detection would differ somewhat from one material to another, but in the absence of any additional information, we shall make use of the conclusion from Ref (22) that B should not be less than $2E\mathcal{G}_{Ic}/\pi\sigma_{YS}^2$, as a necessary condition for a satisfactory pop-in $\mathcal{G}_{Ic}$ measurement. It should be appreciated, however, that it is not necessarily also a sufficient condition in all cases. As mentioned earlier, it appears that some materials may not exhibit any distinct $\mathcal{G}_{Ic}$ meta-instability.

In Ref (22) it is also suggested that the specimen width for $\mathcal{G}_{Ic}$ measurements can be as small as $10E\mathcal{G}_{Ic}/\pi\sigma_{YS}^2$. This corresponds to a restriction of the average net-section stress to be less than the yield strength, rather than less than 80 per cent of the yield strength as recommended by the ASTM Special Committee on Fracture Testing for $\mathcal{G}_c$ measurements. Until more data become available to support the less restrictive estimate of Ref (22), it appears advisable to adhere to the ASTM committee's recommendation for $\mathcal{G}_{Ic}$ pop-in measurement as well as for $\mathcal{G}_c$ testing, and we shall do so here.

From these considerations, we are led to suggest that the optimum range of B/W for symmetrically cracked plate specimens used for pop-in $\mathcal{G}_{Ic}$ measurement is between $\frac{1}{5}$ and $\frac{1}{10}$. This does not mean that specimens of width greater than $10B$ should not be used when it is convenient to do so, only that the $\mathcal{G}_{Ic}$ measurement capacity in that case will be limited by the thickness, not by the width. Also, specimens having W less than $5B$ could be used, but when the available form of the material to be tested makes this desirable, it is both more convenient and more efficient to use single-edge-notched specimens, loaded either in tension or bending, as will be discussed in subsequent sections. With one exception, it will be assumed that the $\mathcal{G}_{Ic}$ measurement capacities of all types of plate specimens are limited to the same extent by thickness, namely,

$C_{1g} = \pi\sigma_{YS}^2 B/2E$, according to the preceding discussion. The exception is the surface-cracked type of plate specimen in which the crack propagates initially in the thickness direction of the specimen, not in the width direction as in the other types.

Plane-Strain Plastic-Zone Correction Term—$\mathcal{G}_{Ic}$ and K_{Ic} Calculations—Before considering the other types of specimens that are intended for plane-strain crack toughness testing, there are two general points that are relevant to all such tests. First, in calculating values of $\mathcal{G}_{Ic}$, a plastic-zone correction term may be added to the estimated average value of the actual crack length, just as in the case of $\mathcal{G}_c$ calculations. There are two differences, however: (*1*) it is assumed that no stable crack extension occurs, and the initial crack length is used in the calculation; and (*2*) the plane-strain plastic-zone correction term is taken to be one third of the plane-stress term, that is, $r_{IY} = r_Y/3 = E\mathcal{G}_{Ic}/6\pi\sigma_{YS}^2$ (22,30). This term can often be neglected entirely without significantly affecting the accuracy of the $\mathcal{G}_{Ic}$ measurement. When it is taken into account, the $\mathcal{G}_{Ic}$ calculation is most readily carried out by the aforementioned iteration procedure. Usually, only one iteration is necessary.

The other point concerns the relation between K_{Ic} and $\mathcal{G}_{Ic}$. As mentioned earlier, for plane-strain conditions: $K_I^2 = E\mathcal{G}_I(1 - \nu^2)$. However, for pop-in $\mathcal{G}_{Ic}$ tests, there is an unresolved question as to the degree to which the stress field in the vicinity of the middle of the crack front approaches a state of plane strain (24). As in Ref (22), it is usual to calculate K_{Ic} from the plane-strain relation given above simply because there is no basis at present for estimating the degree to which the stress state deviates from one of plane strain. The possible error in the calculated value of K_{Ic} resulting from this assumption could not exceed about 5 per cent and is probably much less.

Specimen Types Suitable for $\mathcal{G}_{Ic}$ Measurement Only:

The types of specimens in this category that will be discussed are illustrated in Fig. 30(*a–e*) (see the Appendix) as follows:

(*a*) single-edge-notched plate specimen loaded in tension
(*b*) notched rectangular section bend specimen, three-point loading
(*c*) notched rectangular section bend specimen, four-point loading
(*d*) surface-cracked (or part-through cracked) plate specimen
(*e*) circumferentially notched round bar specimen

While these specimens are referred to for brevity as notched specimens, it is to be understood that the notches should always terminate in sharp cracks, usually provided by fatigue stressing.

Single-Edge-Notched Tension Specimens—This type of specimen was first introduced for the purpose of plane strain crack toughness measurement by G. R. Irwin, J. M. Krafft, and A. M. Sullivan in an unpublished memorandum to the ASTM Special Committee on Fracture Testing in August, 1962. Subsequently, Sullivan published a discussion of the particular design of the single-edge-notched specimen used by these investigators (31).

A single-edge-notched tension specimen can be regarded as derived from either type of symmetrically cracked plate specimen by bisecting along the longitudinal centerline and shortening accordingly. Since this operation affects neither the thickness nor the simulated crack size (a_0 remains the same), it might be expected that the $\mathcal{G}_{Ic}$ measurement capacity of each half would be about the same as that of the symmetrical specimen from which it was derived. If this were the case, the amount of material required for a single-edge-notched specimen of given $\mathcal{G}_{Ic}$ measurement capacity would be only one fourth the amount required for a symmetrically cracked specimen of equal capacity, with the assumption of the same ratio of length to width for the two types of specimens. Actually, the size advantage of the single-edge-notched specimen is probably not nearly this great, but it does have another advantage in requiring considerably less load to determine a given $\mathcal{G}_{Ic}$ value than does a symmetrically cracked specimen. This could be a determining factor in the choice of specimen type when it is necessary to test very large specimens of materials having high ratios of toughness to yield strength.

Up to the present time, no expression for $\mathcal{G}$ in closed form has been derived for single-edge-notched tension specimens. Approximate expressions of very good accuracy have been obtained, however, by a mathematical procedure of boundary collocation applied to a suitable stress function (23) and by the experimental compliance measurement procedure (24). The experimental method was originally suggested by Irwin and Kies (32), and, in principle, is of general utility. The expression for $\mathcal{G}_{Ic}$ given in Fig. 30(*a*) is taken from Ref (24) and applies strictly only for the given values of D/W and L/W, where D is the distance of the axis of loading from the cracked edge of the specimen and L is the distance between loading pinholes. In Fig. 30(*a*), D/W is $\frac{1}{2}$, and L/W is $\frac{8}{3}$.

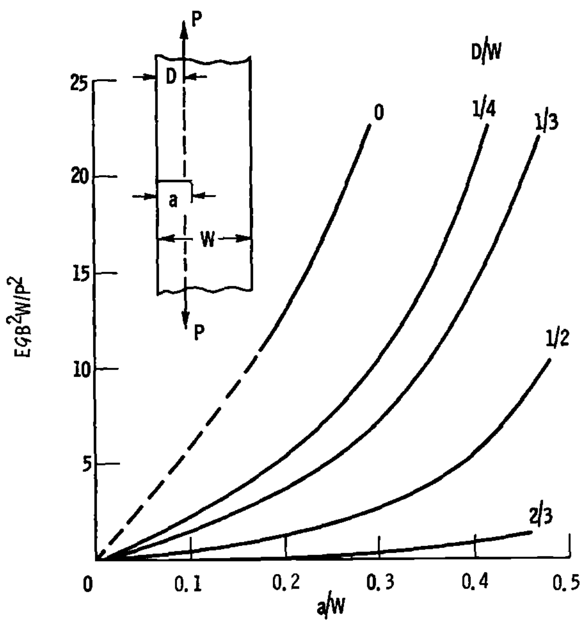

FIG. 17—Relation Between the Calibration Factor and a/W for Single-Edge-Notched Tension Specimens for Several Locations of the Load Axis.

It is convenient to express the results of collocation computations or of experimental compliance measurements in the form of dimensionless factors that are functions of $\mathcal{G}$, the applied load, P, and the pertinent specimen dimensions. In the case of single-edge-notched tension specimens for given values of D/W and L/W, the appropriate dimensionless factor is $E\mathcal{G}B^2W/P^2$, which depends only upon a/W. That is to say, if the proportions of the specimen dimensions other than thickness are kept constant, the value of $E\mathcal{G}B^2W/P^2$ for a given value of a/W will be the same regardless of the size of the specimen, its thickness, or the material from which it is made. This factor can therefore be expressed universally as a function of a/W in the form of a table, a curve, or a suitable polynomial in a/W obtained by least-squares best-fit procedures applied to the tabulated results. The polynomial form is a convenient way to express the relation between $E\mathcal{G}B^2W/P^2$ and a/W compactly, as in the Appendix. Experience has shown that a third-degree polynomial is sufficient to provide an adequate fit, as discussed in more detail in Ref. (24).

The ratios L/W and D/W are additional parameters that cannot be combined with $E\mathcal{G}B^2W/P^2$ into a more general dimensionless factor in any simple way for the single-edge-notched tension specimen. (It will be shown later, however, that a rather more general dimensionless factor can be devised for bend specimens.) Providing L/W is sufficiently large, the effect of small variations of L/W on $E\mathcal{G}B^2W/P^2$ is negligible, and the expression for $E\mathcal{G}_{Ic}B^2W/P^2$ given in Fig. 30(a) can be used with confidence provided that L/W is held to $\frac{8}{3}$ within 5 per cent. If circumstances make it necessary to use a shorter specimen, such as that described in Ref (31), an experimental calibration should be conducted for the specific specimen proportions to be used. In this case it would be advisable to read the discussions relating to specimen length that are to be found in Refs (23) and (24).

The value of $E\mathcal{G}B^2W/P^2$ for a given value of a/W depends very strongly on D/W, as shown in Fig. 17. The curves shown in this figure for various values of D/W are derived from unpublished work by B. Gross of NASA, who used the boundary-collocation procedure mentioned earlier. The figure is intended to be illustrative only, not for calculation purposes. The main point to be made from it is that once a value of D/W has been decided upon and an accurate expression for $E\mathcal{G}B^2W/P^2$ versus a/W obtained for that value of D/W, it should be held within close tolerances in order to avoid errors that would result from deviations from the nominal value.

There is actually no good reason to choose a value of D/W different from $\frac{1}{2}$, for which an expression for $E\mathcal{G}B^2W/P^2$ of adequate accuracy already exists (Fig. 30(a) and Refs (23) and (24)). It is true that the load required to measure a given value of $\mathcal{G}_{Ic}$ will be lower the smaller is D/W, but this load could be reduced even more by using a bend specimen instead of loading in tension. On the other hand, the sensitivity of $\mathcal{G}$ to a small error in the measured value of a_0 is greater the smaller is D/W, so that $\mathcal{G}_{Ic}$ measurement accuracy decreases as D/W is decreased. It would seem that having a choice between a bend specimen (requiring lower load) and a single-edge-notched tension specimen with D/W equal to $\frac{1}{2}$ (providing better accuracy) would be sufficient without complicating the issue by considering tension specimens having other values of D/W.

Having discussed the essential features of the design of single-edge-notched tension specimens, we can now consider the $\mathcal{G}_{Ic}$ measurement capacity of this type. The criterion that we use for this purpose is that the nominal stress at the crack tip should not exceed the yield strength. This is admittedly somewhat arbitrary, but is analogous to the criterion discussed previously for the symmetrically cracked specimens, except that the maximum value of the average net-section stress was limited to $0.8\sigma_{YS}$ in that case. In the case of the single-edge-notched specimen, the decrease of nominal stress with distance from the crack tip justified using a somewhat higher limit for the nominal stress at the crack tip.

What is meant by the nominal stress at the crack tip is the tensile stress that would exist at the edge of a strip of width $(W - a)$, under an eccentric tensile load, P, acting at a distance $(D - a)$ from that edge, obviously derived from a single-edge-notched specimen by removing a longitudinal strip containing the notch without changing the position of the loading axis. This stress is given by:

$$\sigma_{\text{nom}} = P/B(W - a) + 3P(W + a - 2D)/B(W - a)^2$$

From this, together with the results from which Fig. 17 was plotted, we can formally calculate values of $E\mathcal{G}/\sigma_{YS}^2W$ that correspond to $\sigma_{\text{nom}} = \sigma_{YS}$. The three curves shown in Fig. 18 for values of D/W of $\frac{1}{4}$, $\frac{1}{3}$, and $\frac{1}{2}$ are plotted from the results of such calculations. These curves represent the dependence of the quantity $EC_{I\mathcal{G}}/\sigma_{YS}^2W$ on a/W for the three different D/W ratios, and have the same significance as the curve shown in Fig. 13 for the center-cracked specimen (with the assumption that the respective criteria on which they are based are equivalent). The shapes and relative positions of the three curves in Fig. 18 would not be changed by taking the ratio $\sigma_{\text{nom}}/\sigma_{YS}$ as having some value different from unity; only the ordinate scale would be changed in proportion to the square of this ratio; therefore, the figure shows two things. First, that the maximum efficiency depends very little on D/W, being somewhat higher the lower the value of D/W. The slight advantage in efficiency when D/W is

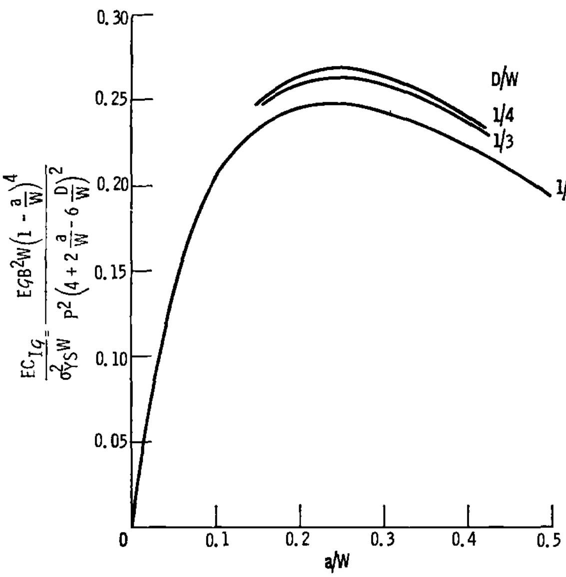

FIG. 18—Dependence of Measurement Capacity of Single-Edge-Notched Tension Specimens on a/W for Three Positions of the Load Axis (See Fig. 17).

low is unlikely to be worth the decrease in accuracy of $\mathcal{G}_{Ic}$ measurement. Second, regardless of the value of D/W, the efficiency is greatest when a/W is about 0.25, but varies only about 5 per cent in the range of a/W between 0.15 and 0.35.

With the assumption that the $\mathcal{G}_{Ic}$ measurement capacities of the center-cracked specimen type and the single-edge-notched tension specimen type are reasonably well represented respectively by Figs. 13 and 18, it is apparent that the single-edge-notched type has only a marginally greater capacity for a given width than the center-cracked type. Thus, it would appear erroneous to make the simple assumption that bisecting a symmetrically cracked specimen would result in two single-edge-notched specimens each having the same $\mathcal{G}_{Ic}$ measurement capacity as the symmetrically cracked specimen. Actually, the analysis we have just presented is open to question, and it will probably require considerable experimental work to arrive at good estimates of the $\mathcal{G}_{Ic}$ measurement capacities of the various types of specimens. In the interim, in order to have some basis for deciding upon specimen dimensions, we make use of this and similar analyses that appear to be predicated upon reasonable assumptions.

There is no reason to suppose that the limitation imposed by thickness would be different for the single-edge-notched type than for the center-cracked type of specimen. Hence we deduce that the optimum range of B/W for the single-edge-notched type should be about $\frac{1}{4}$ to $\frac{1}{8}$ as contrasted to $\frac{1}{5}$ to $\frac{1}{10}$, which were derived earlier for the center-cracked type.

Notched Bend Specimens—The notched rectangular section bend specimen was one of the earliest types of specimen to be used for fracture toughness testing. It was not at first appreciated that it was necessary to provide a notch that terminated in an actual crack, nor that the specimen, while suitable for $\mathcal{G}_{Ic}$ testing by pop-in measurement, was not suitable for accurate $\mathcal{G}_c$ testing under circumstances where the fracture was not predominantly square. Consequently, many of the early data obtained with notched bend bars are only useful in a semiquantitative sense.

There is no essential distinction between a notched rectangular section bend specimen and a single-edge-notched plate specimen tested in tension. The notched rectangular section bend specimen is simply the extreme case of the single-edge-notched plate specimen when the loading results from a couple without any additional tension component. For one of several practical reasons, it may be more convenient to test specimens in bending rather than in tension, and, in particular, the load needed to measure a given value of $\mathcal{G}_{Ic}$ is less for a bend specimen than for any other type. On the other hand, it is to be expected that the accuracy of $\mathcal{G}_{Ic}$ measurement is inherently lower for the bend specimen than for any other type because the sensitivity of the calculated value of $\mathcal{G}$ to a small error in a_0 is greater than for any other type.

Recommended dimensions for bend specimens are shown in Figs. 30(*b*) and (*c*). The symbol, W, is used for the beam depth because this dimension corresponds with the width of a single-edge-notched tension specimen. The beam thickness is B and L is the moment arm length, that is, half the difference between the major and the minor spans, which reduces to half the span for three-point loading. The total applied load, P, is assumed to be equally distributed. The bending moment within the minor span is, therefore, $PL/2$.

The most general dimensionless factor that can be used to express $\mathcal{G}$ as a function of a/W for a bend specimen is $E\mathcal{G}B^2W^3/P^2L^2$, that is, W^2/L^2 times the less general factor, $E\mathcal{G}B^2W/P^2$, which was used for the single-edge-notched tension specimen. This simply takes into account the fact that $E\mathcal{G}B^2W/P^2$ is proportional to L^2/W^2 for bend specimens having a given value of a/W. This was deduced originally by G. R. Irwin in an unpublished note and later confirmed by a different method by B. Gross of NASA (also unpublished to date). Gross has computed tables of values of $E\mathcal{G}B^2W^3/P^2L^2$ for both three-point and four-point loading by using the procedure of boundary collocation of the Williams form of the Airy stress function, which was mentioned earlier. The expressions for $E\mathcal{G}_{Ic}B^2W^3/P^2L^2$ as cubics in a/W, which are given in Figs. 30(*b*) and (*c*) for the three-point and the four-point loaded specimens, respectively, were obtained by applying least-squares best-fit procedures to these results of Gross. It is worthy of note that Gross's results are in satisfactory agreement with published results of experimental compliance calibrations by Irwin et al (16) for three-point loading and by Lubahn (33) for four-point loading, as will be discussed in a forthcoming publication.

If the expressions for three-point and four-point loading given in Figs. 30(*b*) and (*c*) are compared, it will be seen that for a given a/W, the value of $E\mathcal{G}B^2W^3/P^2L^2$ is always less for three-point than for four-point loading, an average of about 10 per cent less. Comparison of the experimental results shows the same thing (16,33). The difference arises in the mathematical treatment because the computations for four-point loading considered the region within the minor span as subjected to a bending moment only, whereas the computations for three-point loading took into consideration the shearing stress that changes from $P/2BW$ to $-P/2BW$ at the center loading point.

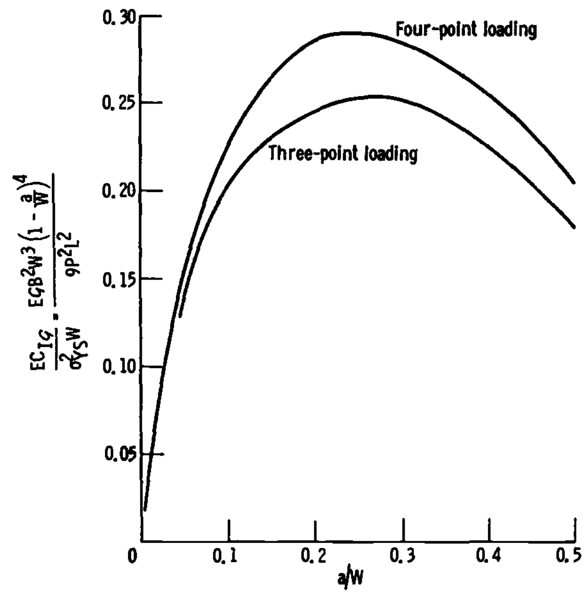

FIG. 19—Dependence of the Measurement Capacity on a/W for Bend Specimens.

The shearing stress is independent of

L, whereas $\mathcal{G}$ is proportional to L^2/W^2, as mentioned above. The influence of the shearing stress upon $\mathcal{G}$ should, therefore, diminish with increasing L/W. For this reason, it is recommended that the span of a three-point loaded specimen should not be less than $8W$, which is an unpublished estimate by G. R. Irwin. In the case of a four-point-loaded specimen, the shearing stress is zero within the minor span, but it appears desirable that the major span should not be less than $8W$ in this case also. Furthermore, it is recommended that the minor span should not be less than $2W$ on the basis that the part of the strain energy field that is appreciably affected by the crack length is contained within that part of the specimen that extends a distance W on either side of the crack. Thus, with a minor span not less than $2W$, $\mathcal{G}$ should not be appreciably influenced by either the magnitude of the shearing stress outside the minor span or by the concentrated stresses at the loading points. From these considerations, it is reasonable to expect that somewhat more accurate $\mathcal{G}_{Ic}$ measurements could be made with a bend specimen in four-point loading than with the same specimen in three-point loading.

In order to estimate the $\mathcal{G}_{Ic}$ measurement capacities of notched bend specimens, the same criterion was used as in the case of the single-edge-notched tension specimen discussed previously. Values of $E\mathcal{G}/\sigma_{YS}^2W$ corresponding to $\sigma_{\text{nom}} = 3PL/B(\text{W} - a)^2 = \sigma_{YS}$ were calculated from the expressions given in Figs. 30(*b*) and (*c*), and used to plot the curves of EC_{I_0}/σ_{YS}^2W versus a/W that are shown in Fig. 19. From these two curves it is seen that the bend specimen is apparently used more efficiently in four-point loading than in three-point loading. This, of course, is simply a reflection of the fact that the values of $E\mathcal{G}B^2W^3/P^2L^2$ are greater for four-point than for three-point loading.

From comparison of Fig. 19 with Fig. 18, it is seen that a single-edge-notched specimen loaded in four-point bending is apparently about 15 per cent more efficient than a single-edge-notched tension specimen of equal width and thickness and having D/W equal to $\frac{1}{2}$. For a specimen loaded in three-point bending, however, the efficiency is about the same as that of the tension specimen. This, of course, involves the assumption that the same limiting condition applies to both types of specimens, which appears to be reasonable in the absence of experimental data to the contrary. It should be noted that if the recommendations regarding specimen length, which are given in the Appendix, are followed, then the bend specimens would have to be about twice as long as the tension specimen of equal width.

Cracked Charpy Specimens—Considerable use has been made of cracked Charpy specimens for the intended purpose of $\mathcal{G}_{Ic}$ and even $\mathcal{G}_c$ measurement (**34**). The cracked Charpy specimen is simply a small, three-point-loaded bend specimen and is subject to exactly the same limitations as we have discussed for three-point bend specimens. The usual dimensions are as follows: W = 0.394 in., B is variable between about 0.04 and 0.8 in. (for standard Charpy specimens, it is 0.394 in.), a_0 is variable between about 0.1 and 0.2 in. (normally slightly greater than 0.1 in.), and the span is 1.574 in. The specimen is produced by machining to normal Charpy-V dimensions except that the thickness can be varied, then generating a fatigue crack at the bottom of the V-notch. It is tested either with a pendulum-type impact testing machine, in which case only the loss of pendulum energy is usually measured, or in slow bending to obtain a load-deflection record.

It would be possible to determine $\mathcal{G}_{Ic}$ values within the limitations of measurement capacity imposed by the dimensions of the Charpy specimen (C_{Iq} would be about $\sigma_{YS}^2/10E$), by measuring the pop-in load and proceeding as for any other three-point bend specimen. Although the ratio L/W is only about 2 for the Charpy specimen, rather than 4 as we recommend for three-point-loaded bend specimens, a $\mathcal{G}_{Ic}$ measurement that was accurate enough for some purposes, such as a materials screening program, might be obtained. However, this is not the way the specimen is usually treated. Instead, the loss of pendulum energy in an impact test, or the area under the load-deflection curve in a slow bend test, is measured. This energy value is usually denoted W, but here it will be called U in order to avoid confusion with the symbol for specimen width.

It is assumed that U can be equated with the energy required for the formation of new fracture surfaces only, and that no part of U is dissipated in any other way. Then a further assumption is made, essentially that the crack-extension resistance is constant during the propagation of the crack through the specimen. With these assumptions, it is concluded that $\mathcal{G}_c$, or $\mathcal{G}_{Ic}$ if the fracture is square, can be taken to be equal to U/A, where A is the area of the fractured cross section, $B(W - a_0)$. Both of these assumptions are open to considerable question, and do not appear to have been thoroughly investigated. In fact, it can be inferred from recent work by Krafft (35) that the second assumption is definitely not generally valid.

It is true that there is qualified evidence of correlation between U/A and results of some $\mathcal{G}_c$ tests to a degree that suggests that U/A may be a useful measurement for screening purposes. This is more likely to be the case when the fractures are predominantly square, and $\mathcal{G}_c$ approaches $\mathcal{G}_{Ic}$, than when the thickness is such that the fully developed fracture of a plate specimen would be predominantly slant. In any case, in the opinion of the authors the results of cracked Charpy tests should not be used for any other purpose than preliminary screening of materials, at least until such time as the interpretation of the results is much better understood than at present. It is particularly important that U/A values should not be used in an attempt to calculate critical crack dimensions for structures since this might be dangerously misleading.

Surface-Cracked Plate Specimens—Details of this type of specimen, sometimes called a part-through crack specimen, are shown in Fig. 30(*d*) (see the Appendix). It was originally introduced in order to investigate directly the effects of cracks similar to those from which fractures had often originated in service (36–38). Cracks of controlled size, approximately semi-elliptical in shape with the major axis at the surface, were formed in plate specimens by fatigue stressing (38,39), or by static stressing in a suitable environment (37). It became possible to calculate $\mathcal{G}_{Ic}$ values from the results of tests of surface-cracked specimens when Irwin (15) derived an appropriate expression for $\mathcal{G}_I$ (originally a private communication in 1960) by making use of earlier work by Green and Sneddon (40). Irwin's expression is given in Fig. 30(*d*) for the value of $\mathcal{G}_I$ in the central region of the front of a semi-elliptical surface crack that is no deeper than one half the plate thickness. The expression as given includes a plastic-zone correction term. The magnitude of $\mathcal{G}_I$ varies with position along the crack front and is greatest at the central position (15). The crack extends first in this region and the magnitude for $\mathcal{G}_I$ at other positions along the crack front is of no consequence to this discussion.

Reference (15) does not deal with the question of how narrow the plate specimen could be without appreciably influencing the value of $\mathcal{G}_I$ at the middle of the crack front. We shall assume, rather arbitrarily, that W should not be less than $6c$, where $2c$ is the surface length of the crack, assumed to be the major axis of an ellipse. This restriction is almost certainly on the safe side since the length of the pertinent central region of the crack front, where the crack first extends, is a small fraction of $2c$.

Extended discussion of the $\mathcal{G}_{Ic}$ measurement capacity of surface-cracked specimens as a function of the various dimensions of the cracked section, W, B, a, and c (Fig. 30(d)) would be unwarranted since the selection of this type of specimen would be governed by considerations other than measurement capacity. Instead we shall estimate the $\mathcal{G}_{Ic}$ measurement capacity of a selected example in which the crack dimensions are as large as the aforementioned restrictions permit, namely, $a = B/2$ and $2c = W/3$. We also assume $a/c = \frac{1}{2}$, which is a likely ratio for specimens fatigue-cracked in bending, and that the average net-section stress at instability should not exceed σ_{YS} for a valid $\mathcal{G}_{Ic}$ test. Using these conditions in the expression for $\mathcal{G}_{Ic}$ given in Fig. 30(d) gives $C_{Ig} = 1.09\, \sigma_{YS}^2 B(1 - \nu^2)/E$, which is equal to $\sigma_{YS}^2 B/E$ when Poisson's ratio is 0.3. Here, C_{Ig} is given in terms of B rather than in terms of W, as for other types of plate specimen. The reason for this difference is that it is the depth of the crack that determines the $\mathcal{G}_{Ic}$ measurement capacity of a surface-cracked specimen, and the crack depth is limited to a maximum of one half the specimen thickness.

In $\mathcal{G}_{Ic}$ tests with the surface-cracked type of specimen, it has been the usual practice to measure only the maximum load sustained in the test and the initial crack dimensions and to calculate $\mathcal{G}_{Ic}$ from these measurements. This practice assumes that instability occurs at maximum load and is not preceded by a metastable crack extension at some lower load. While the experience of the authors and examination of data obtained by others suggest this assumption is not seriously in error, at least as far as high strength materials are concerned, it ought nevertheless to be subjected to critical investigation. It is recommended that crack extension should be monitored during all tests of surface-cracked specimens, just as for other types of specimens, by using one of the methods discussed later. Results obtained without this sort of instrumentation should be regarded as somewhat uncertain, the more so the less brittle the material.

Circumferentially Notched Round Bars—Tension testing of notched round bars has an extensive history, and it was natural that this type of specimen should have been one of the earliest used for $\mathcal{G}_{Ic}$ measurement. As in the case of notched bend specimens, it was not at first appreciated that notch sharpness equivalent to that obtained by fatigue cracking was necessary for accurate $\mathcal{G}_{Ic}$ measurement, so that many of the earlier $\mathcal{G}_{Ic}$ data are of somewhat doubtful value.

There is at present no highly accurate expression for $\mathcal{G}_I$ for a round notched bar. In their contribution to this symposium, Paris and Sih discuss this case in some detail and conclude that an accurate solution would require an analysis of the type suggested by Sneddon (41). The mathematics involved in this type of approach is quite formidable. Approximate expressions for $\mathcal{G}_I$ are available from unpublished work by H. Bueckner, which are discussed by Lubahn (33) and by Wundt (42), or can be derived from stress-concentration factors as discussed in Ref (16). The results obtained by these approximate methods can be expressed conveniently in the form $E\mathcal{G}_I/(1 - \nu^2) = M\sigma_N^2 D$, where M is a dimensionless function of d/D, D is the major diameter, d is the diameter of the crack-notched section, and $\sigma_N = 4P/\pi d^2$ is the average net-section stress.

Figure 20 shows values of the dimensionless factor, M, plotted versus d/D. One set of plotted points is derived from results given in Ref (33) and the other set was obtained by the method of Ref (16). It is difficult to judge the accuracy of these values, but the extent of the agreement between them may give some indication of this. A fitted curve for using a value of d/D much different from 0.7, so that the expression for $\mathcal{G}_{Ic}$ need only be used over a very limited range of d/D. In the range of d/D from 0.65 to 0.7, the assumption that M has the constant value 0.17 is probably all that is warranted by the accuracy of the available estimates.

The value of d that should be used in calculating a value of $\mathcal{G}_{Ic}$ is less than the measured value of the initial crack diameter, d_0, by a plastic-zone correction term, $E\mathcal{G}_{Ic}/3\pi\sigma_{YS}^2$. This is equivalent to

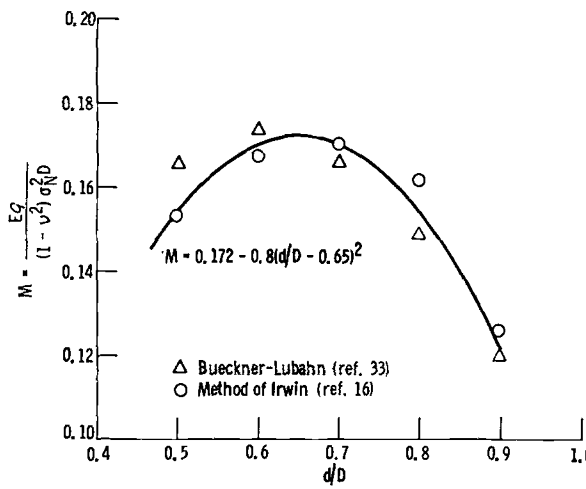

FIG. 20—Values of Dimensionless Factor, M, for Round Notched Bars Versus d/D. $E\mathcal{G}_I = M\sigma_N^2 D(1 - \nu^2)$.

corresponding to a simple expression for M is also shown in the figure. Within the range of d/D shown, which is greater than would normally be of practical interest, the simple, compact expression for M appears to fit the plotted points adequately. Consequently, in the expression for $\mathcal{G}_{Ic}$ given in Fig. 30(e), the factor M has been replaced by $[0.172 - 0.8(d/D - 0.65)^2]$. Figure 20 also shows that the most efficient value of d/D is about 0.7, which corresponds to a notched cross-sectional area equal to about one half the shank cross-sectional area. There would be no good reason increasing the initial crack depth $(D - d_0)/2$ by the same plane-strain plastic-zone correction term used for other types of specimen. It is worth mentioning that there is some arbitrariness about the choice of the value used for this term (30), which is apt to cause confusion in reading the literature unless one is aware of it. The practical effect of this, however, is negligible since it amounts to a small variation of a small correction term.

The ASTM Special Committee on Fracture Testing has recommended that the size of a round notched bar for

$\mathcal{G}_{Ic}$ measurement should be sufficient to ensure that the average net-section stress at fracture does not exceed 1.1 times the uniaxial tensile yield strength (9). The reason that the maximum recommended ratio of σ_N/σ_{YS} can be greater in this case than the ratio of σ_{net}/σ_{YS} for symmetrically cracked plate specimens is, of course, that the effective yield strength of the notched section of the round bar is correspondingly higher than σ_{YS}. A state of triaxial tension exists within the notched section and, on the basis of either a maximum shear stress or an octahedral shear stress criterion, the average net-section stress at which yielding occurs will exceed σ_{YS} to an extent depending upon d/D. For d/D equal to 0.7 or less, the effective yield strength will be high enough to justify $\mathcal{G}_{Ic}$ measurements with values of σ_N at least up to 1.1 σ_{YS}.

Applying this limitation and taking the maximum value of M as 0.17 yield the estimated $\mathcal{G}_{Ic}$ measurement capacity of a notched round bar: C_{Ig} = 0.22 $\sigma_{YS}^2D(1 - \nu^2)/E$, or 0.2 σ_{YS}^2D/E when Poisson's ratio is 0.3. This calculation takes into account the plastic-zone correction term. It is interesting to note that this estimate implies that the magnitude of C_{Ig} is just about the same for a notched round bar as for a symmetrically cracked plate specimen of width equal to the diameter of the notched round bar. The experimental results reported in Ref (22) are consistent with this conclusion, and it is also intuitively apparent if one regards a symmetrically edge-cracked plate specimen as equivalent to a longitudinal slice from the center of a round notched bar.

The round notched bar requires a considerably greater amount of material and considerably more loading capacity than any of the other types of specimen for $\mathcal{G}_{Ic}$ measurement that we have considered. To compensate for this, the potential accuracy of $\mathcal{G}_{Ic}$ measurement is probably relatively higher, but it would not be easy to attain the full potential accuracy. Apart from the need for a more accurate expression for $\mathcal{G}$ than is now available, it would be necessary to ensure almost perfect concentricity of fatigue cracking and uniformity of loading. No study has yet been made of the errors that would result from small deviations from the assumed perfectly uniform tensile loading of notched round

TABLE 1—COMPARISON OF DIMENSIONS OF VARIOUS PLANE-STRAIN CRACK TOUGHNESS SPECIMENS HAVING C_{Ig} EQUAL TO σ_{YS}^2/E.[a]

	Symmetrically Cracked Plate	Single-Edge-Notched Tension D/W = 1/2	Single-Edge-Notched Bend, three-point	Single-Edge-Notched Bend, four-point	Surface Cracked	Notched Round
Relative dimensions of initial cracks....	$2a_0/W$ = 0.3	a_0/W = 0.3	a_0/W = 0.2	a_0/W = 0.2	a_0/B = ½ $2c_0 = W/3$	d_0/D = 0.7
W or D, in...........	5.0	4.0	4.0	3.5	6.0	5.0
B, in................	0.65	0.65	0.65	0.65	1.0	
Minimum length, in...	20	16	36	32	24	20
Load/σ_{YS}, in.^{2}.......	1.8	0.8	0.14	0.16	5.4	11.2
Accuracy—order of merit.............	1	1	3	2	potentially high	potentially high

[a] Specimens of the dimensions given would be large enough to measure values of $\mathcal{G}_{Ic}$ up to σ_{YS}^2/E, according to the criteria discussed in the text. For other values of $\mathcal{G}_{Ic}$, the minimum dimensions are directly proportional, and the loads are proportional to the square of the values given in the table.

bars, but the study of single-edge-notched plate specimens discussed earlier indicates that unavoidable nonuniformity of loading could be a considerable source of error in testing notched round bars. At the present time, the best accuracy of $\mathcal{G}_{Ic}$ measurement with notched round bars is probably no better than with plate specimens.

As in the case of surface-cracked specimens, it is usually assumed that instability occurs at maximum load in a notched round bar test, and $\mathcal{G}_{Ic}$ is calculated from the maximum load and the average diameter of the initial cracked section. In this case also, the assumption ought to be subjected to adequate experimental verification utilizing crack-extension monitoring instrumentation.

Summary Comparison of Specimens for $\mathcal{G}_{Ic}$ Measurement—In selecting a particular type of specimen for $\mathcal{G}_{Ic}$ measurement, the following factors may need to be considered: (*1*) the magnitude of the highest value of $E\mathcal{G}_{Ic}/\sigma_{YS}^2$ expected among the materials to be tested; (*2*) desired accuracy of $\mathcal{G}_{Ic}$ measurement; (*3*) loading capacity of available testing machines; (*4*) economical usage of available test material; and (*5*) form of the test material.

Table 1 provides guidance regarding necessary dimensions and load requirements, and suggests an order of merit of accuracy for the various types of specimen we have considered. The proportions given for each specimen type are considered to be about optimum so far as can be estimated at the present time. The dimensions given are estimated as the smallest that could be used for determination of a value of $\mathcal{G}_{Ic}$ equal to σ_{YS}^2/E, based on the criteria discussed in the preceding sections and subject to the qualifications stated therein. These values may need to be revised when sufficient pertinent experimental data have been accumulated, but it is unlikely that the revised values will be appreciably smaller than those given in Table 1, more likely they will be greater. To estimate minimum dimensions for different values of $\mathcal{G}_{Ic}$, the linear specimen dimensions should be taken in direct proportion to the values given in Table 1, and the required load proportional to the square of the value given in the table. The safest course in deciding upon the size of specimen to be used is to overestimate substantially the largest value of $E\mathcal{G}_{Ic}/\sigma_{YS}^2$ among the materials that are to be tested and to calculate the specimen dimensions accordingly. For most purposes it is best to select from a graded series of specimen sizes, in which the linear dimensions increase by a factor of 2 from one size to the next. Following the ASTM Special Committee on Fracture Testing, one size of each type of plate specimen would be 3 in. wide. Hence, a graded series of plate specimens could conveniently have widths of 3 times 2^n in., where n has the values -2, -1, 0, 1, 2, etc.

While it is somewhat premature to be very definitive about accuracy, experience so far suggests that the best accuracy of $\mathcal{G}_{Ic}$ measurement that is likely to be achieved is of the order of ± 2 per cent. A clear distinction should be made between testing accuracy and material variability. The variance of $\mathcal{G}_{Ic}$ for a given stock of material may be of the order of 10 per cent or more, that is, the standard deviation of the results from a large number of accurate replicate tests would be of the order of 10 per cent or more of the average value. However, it is important to know the variability of the toughness of a material as well as its average toughness. In fact, a lower confidence limit is more important than the average value. For this reason, it is desirable that the $\mathcal{G}_{Ic}$

measurement precision should be substantially better than the variance of $\mathcal{G}_{Ic}$ resulting from inherent material variability. The main factors that influence the accuracy of $\mathcal{G}_{Ic}$ measurement are the accuracy of the expression used for calculating $\mathcal{G}$ and the degree of uncertainty in the estimate of the effective crack length, including the plastic-zone correction factor. The other necessary measurements can be made with relatively high accuracy (provided that the $\mathcal{G}_{Ic}$ instability is clearly defined). The authors believe that the accuracy of the expression for $\mathcal{G}$ for the single-edge-notched tension specimen (Fig. 30(*a*)) is of the order of $\pm\frac{1}{2}$ per cent when $2a_0/W$ is about 0.3 (24). This is considerably less than the ± 2 per cent suggested for best attainable $\mathcal{G}_{Ic}$ measurement accuracy, and the potentially more accurate expressions for $\mathcal{G}$ that might be obtained for the symmetrically cracked plate, the surface-cracked plate, and the notched round bar are, therefore, probably only of academic interest. The order of merit for accuracy given in Table 1 is based on these considerations and on other points discussed in connection with bend specimens.

Reference to Table 1 shows that if the loading capacity of available testing machines is the major limiting factor, a notched bend specimen will have a distinct advantage in the level of $E\mathcal{G}_{Ic}$ that can be measured with a given load. On the other hand, if material economy is of major importance because the amount of test material available is limited, then the single-edge-notched tension specimen requires only about half as much material as the bend specimen because it is proportionately shorter. It is also somewhat more accurate, but requires about five times as much load.

Both the surface-cracked plate and the notched round bar types of specimen have a considerable disadvantage in the loading capacity required to measure a given level of $E\mathcal{G}_{Ic}$. Both also require considerably more material than the other types of specimen. It is possible, though not yet established, that either the surface-cracked plate specimen or the notched round bar might be useful for $\mathcal{G}_{Ic}$ measurement in cases where definitive results could not be obtained by the pop-in measurement procedure. In this case, of course, symmetrically cracked or single-edge-notched plate specimens of sufficient thickness could also be used, but then the advantage of lower bulk would largely be lost. This is a question that has yet to be settled by careful experiment. It is of considerable practical importance in connection with materials of high toughness and low yield strength that require large specimens.

Sometimes the controlling factor in selecting a specimen type will be the form of the stock of material to be tested and its texture in relation to the directions of the nominal principal stresses in service. For a given stock of material, $\mathcal{G}_{Ic}$ may depend considerably upon the orientation of the crack in relation to the principal textural directions deriving from the ingot structure and subsequent deformation into product form. Alternatively, the measurement of toughness of welds and associated heat-affected regions may be of prime importance in a particular application. This requires very careful location of test cracks in relation to the variable structure of the weld region.

For the common case of plate stock, the nomenclature of Ref (6) is convenient in referring to the six principal systems of crack propagation. The plate-thickness direction is labeled *T*, the major rolling direction *R*, and the width direction, *W*. The six principal systems of crack propagation can then be distinguished by pairs of letters, the first letter representing the normal-to-the-crack plane and the second letter the direction of propagation. For example, *RW* would represent a crack normal to the rolling direction propagating in the width direction. It would be convenient to use either symmetrically cracked plate specimens or single-edge-notched specimens of full plate thickness for tests of either *WR* or *RW*, but surface-cracked plate specimens would be more convenient for *WT* or *RT*. Bend specimens could conveniently be used for any of these four systems of crack propagation. Tests of *TW* and *TR* present difficulties, but, fortunately, high tensile stresses in the thickness direction are usually avoided by good design. Sometimes heavy forgings may have to be used in such a way that the maximum nominal tensile stress is normal to the fibering direction, however, and in such cases it is most important to test appropriately oriented fracture toughness specimens. If necessary, extension pieces could be welded to test sections taken from the forging. In this case, the obvious precautions should be observed.

INSTRUMENTATION AND PROCEDURE

From the foregoing sections, it is clear the determination of $\mathcal{G}_c$ or $\mathcal{G}_{Ic}$ requires a knowledge of the crack length corresponding to the load at fracture instability. Essentially, two cases may be distinguished: namely, an appreciable amount of crack extension takes place before unstable fracture, or fracture instability occurs immediately from the initial crack front. The first case is frequently encountered in plane-stress testing and the method of crack detection employed must be capable of following substantial amounts of stable crack extension up to the maximum load. On the other hand, the major requirement in the second case is high sensitivity to initial crack movement as would be required in pop-in plane-strain $\mathcal{G}_{Ic}$ testing. In special circumstances, however, it may be desirable to follow crack extension from pop-in to final fracture and in such cases the instrumentation must combine adequate sensitivity with the necessary measurement range.

Before proceeding with a description of the various types of instrumentation that have been employed for crack-extension measurement, it is desirable to discuss the use of staining fluids for this purpose. In the first report of the ASTM Special Committee on Fracture Testing (5), it was suggested that a useful indication of crack length at fracture instability could be obtained by introducing a staining substance, such as India ink, into the notch or crack before starting the test. The assumption was made that the ink would follow only the stable crack extension. At fracture instability, the crack velocity would suddenly increase to a point where the ink would no longer move inward fast enough to keep pace with the crack tip. Even if this assumption could be proved correct, there are very good reasons for avoiding the use of staining agents. Thus, there is no way to determine, in advance, how much fluid must be introduced into the crack. An excess of fluid will splatter or run after fracture so that the crack length can be greatly overestimated. An insufficient amount of the staining agent will, of course, have the opposite effect. For these and other reasons, the committee no longer recommends the use of staining fluids in crack toughness tests (9).

In the following section, several crack-extension measurement methods potentially capable of yielding unambiguous results will be described. Particular attention will be given to practical applications and proper handling of the data. It should be emphasized that with the exception of cinematography, all the techniques have been recently developed and only limited data are available. For these reasons, some areas of uncertainty exist in the application of the new methods. It is also the purpose of this section to define these areas clearly.

Cinematography:

Synchronized motion-picture cameras may be used to photograph simultaneously the load dial of a tension testing machine and the plane surface of a specimen containing a through-the-thickness crack. Satisfactory resolution of the crack requires adjustment of the lighting for the particular surface conditions of the specimen being tested. Unwanted reflections can be minimized by use of polarizing screens (9). The film is examined frame by frame and the crack length directly measured. Some investigators have made this measurement to include the apparent extent of the dimple ahead of the crack with the idea of taking into account directly a plastic-zone correction; however, this procedure cannot be generally recommended since the apparent extent of the dimple will vary with the prevailing lighting conditions.

The data are generally represented as a plot of crack length and applied load (or gross-area stress) against time (or frame number). Examples of such plots are shown in Fig. 21 for wide sheets of 4330M steel provided with center fatigue cracks (unpublished data from C. F. Tiffany, The Boeing Co.). From representations of this type, the crack length at maximum gross stress may be selected for use in calculating the fracture toughness. However, some investigators select the stress at a crack length judged to correspond to the onset of "fast crack acceleration." Obviously, such a criterion for selection of crack length permits considerable latitude in the judgment when behaviors such as those shown in Fig. 21 are encountered. For this reason, it is recommended that the stress and crack length at maximum load be used in the fracture toughness calculations, in accordance with the recommendations of the ASTM Special Committee on Fracture Testing (5).

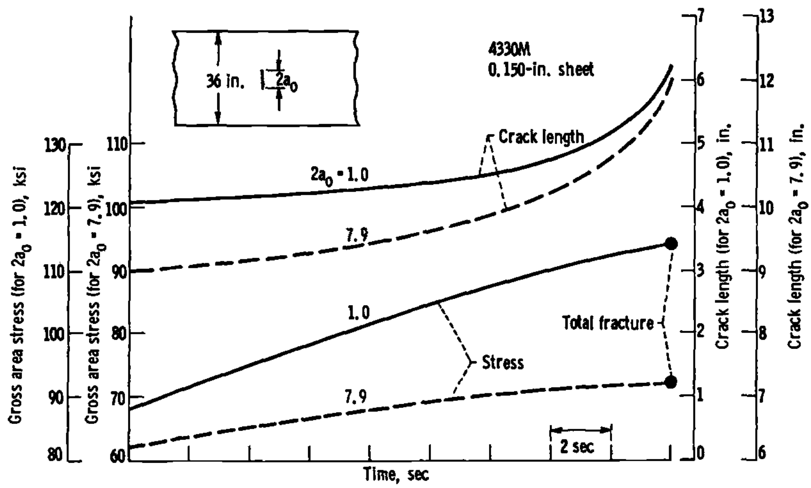

FIG. 21—Examples of Stress and Crack-Length Measurements Using Cinematography.

This photographic method has been widely employed by the aircraft industry in tests on very wide thin-sheet specimens containing long through-the-thickness slots or cracks. The materials of interest in these tests are quite tough and generally exhibit considerable stable crack extension. Under these circumstances, the technique has considerable flexibility in that it may be readily adapted to tests at both low and high temperatures provided that the specimen surface is visible. The method is unsuitable for pop-in detection, since it provides no indication of crack extension below the surface. As presently used, it is relatively insensitive to small crack extensions; however, there is no fundamental reason why considerable increase in sensitivity could not be obtained by suitable refinements in the optical system.

Electrical Potential Measurement:

If a body carrying a current contains a discontinuity, there will be a disturbance of the potential field in the region of the discontinuity. If the discontinuity is a crack, the potential difference between two fixed points spanning the crack will increase as the crack extends, provided that the total current does not decrease. This is the basis for crack-extension measurement by the electric potential method. In practice, a constant current is supplied to the specimen, and potential probes are fastened at suitable points on either side of the crack. The potential change with crack length may be measured with a double Kelvin bridge as used by Steigerwald and Hanna (43), or by electronic instruments such as the milliohmeter employed by Anctil et al (44), or a highly sensitive voltmeter amplifier described later. These electronic instruments have the advantage that an output is provided which is suitable to drive an X-Y plotter.

The potential distribution will be a function of the specimen geometry, crack size, and location of the current leads. As shown previously (44), it is possible to obtain a calibration curve that relates E/E_0 to the crack size, where E is the potential difference between the probe points measured as a function of load and E_0 is the value at no load for a specimen without a crack. A calibration curve of this type will be independent of the material and specimen size provided that all specimen dimensions are changed in proportion, including the locations of the current and potential leads. For specimens containing through-the-thickness cracks, it is convenient to make a pattern of the specimen geometry by using an electrically conductive analog paper. These paper patterns are useful not only for obtaining the calibration curve, but also for general potential mapping of a particular specimen geometry in order to determine optimum locations for the current leads and potential probes. A sufficiently constant current can be maintained if the paper is connected across a 90-v dry battery through a resistor having a value about 100 times the resistance of the paper pattern. A razor blade may then be used to cut the desired crack lengths and shapes, and a vacuum tube voltmeter employed to map the potential field. The recommended current input and probe locations as well as the calibration curves to be described were obtained in this manner.

Testing Procedure—The specimen should be electrically insulated from the tension testing machine by some suitable means, such as Teflon sheet spacers or electrical insulating tape. It is desirable to locate the current leads sufficiently far from the crack plane so that small variations in their position would not influence the results. This distance should be greater than one half the width or diameter of the practical specimen types illustrated in the Appendix. For high sensitivity to initial crack extension, the potential probes should be located as close to the crack tip as possible, the actual location depending on the method of attachment. The probe positions shown in Fig. 22 for plate specimens were established for use with a particular set of slotted yokes that span the specimen thickness and reference the specimen edges. Opposing pointed screws in each yoke serve as ternatively, wet storage cells connected in parallel can be used with a suitable ballast resistance (high relative to the specimen) in series with the specimen. If the current output drifts appreciably during a test, additional batteries should be connected in parallel to reduce the current drain per cell. The current supply cable can be connected to the specimen by clamps or by bolts through small holes. With the latter arrangement, the holes should be at least one specimen width or diameter away from the crack to avoid interaction of stress fields. The

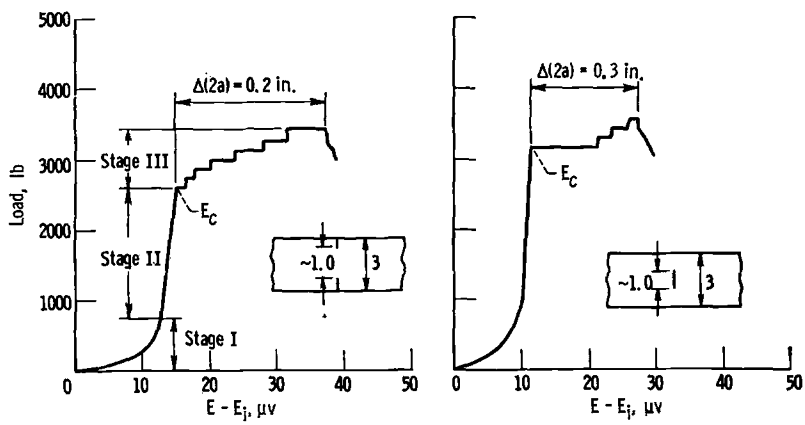

FIG. 22—Typical Load Versus Potential Records Illustrating Pop-In and Crack Extension to Maximum Load.

probes contacting the front and rear surface of the specimen. Leads from each yoke connect to the potential measuring device. It will be noted that the yokes locate the probes slightly behind the nominal initial position of the crack tip of the practical plate specimens shown in the Appendix. This horizontal location is chosen so that the tip of the shortest crack (within the expected tolerance) will be at or beyond the probe points.

The constant current may be obtained from a regulated power supply. These are commercially available in capacities up to 100 amp with high stability. Alternatively, wet storage cells connected in parallel can be used with a suitable ballast resistance (high relative to the specimen) in series with the specimen.

amount of current required for a given crack-extension sensitivity will, of course, depend on the resistivity of the specimen, its cross section, and the sensitivity of the potential measuring device employed. As an example, the authors using the potential sensing and recording equipment described below, obtain the desired sensitivity to crack extension when supplying 10 amp to a steel single-edge-notched specimen 3 in. wide and ½ in. thick.

As mentioned previously, an electronic potential measuring instrument can be used to advantage. The milliohmmeter described by Anctil et al (44) has a built-in power supply which is limited to 100 ma. This instrument, therefore, lacks sufficient sensitivity to make it generally useful in fracture testing. A recently developed (45) voltmeter-amplifier combination can be used with an external current supply such as described above and has an output of 10 v for full-scale meter deflection on any one of 13 input ranges, the most sensitive of which is 0 to 0.1 μv. Zero suppression is available up to 100 times full scale on any range. In order to minimize the influence of thermal emf, it is necessary to avoid, where possible, dissimilar metal junctions in the input circuit to the voltmeter. Difficulties due to these thermocouple effects and stray fields limit the useful working range of the voltmeter to 30 μv or higher, unless elaborate precautions are taken in the experimental setup.

Reduction of Data—If the output of the voltmeter-amplifier is fed to one channel of an X-Y recorder and the signal from a load cell to the other channel, a plot of potential against load is obtained directly. Examples of two such plots for single-edge-notched specimens are shown in Fig. 22, illustrating both a relatively small initial crack movement and a very distinct pop-in.

The initial potential, E_i, is suppressed and the potential change with load, $(E - E_i)$, may be considered as consisting of three stages. During stage I there is a rapid increase in potential at low loads due to separation of the fatigue-crack surfaces. The potential during stage II increases linearly with load and corresponds only to elastic strain. The beginning of stage III, E_c, is marked by a nonlinear increase in potential resulting from crack extension or crack-tip plasticity (the contribution of plasticity is usually considered negligible), or both. The accuracy with which the load corresponding to initial crack movement can be established depends on the sharpness of the division between stage II and stage III. In the two cases shown, this is quite distinct; however,

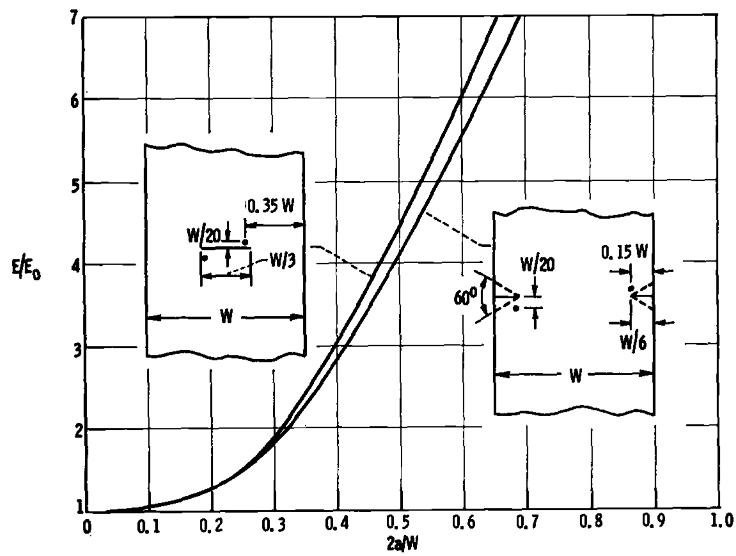

FIG. 23—Electric Potential Calibration Curves for Symmetrically Center- and Edge-Cracked Plate Specimens.

as will be discussed later (see Fig. 28), small amounts of crack extension may occur early in the test before a distinct pop-in, and, in such cases, acoustic measurements are of assistance in interpretation of the potential records. If plane-strain toughness determinations are to be made, the load at pop-in is read directly from the load-potential records and used in the appropriate $\mathcal{G}_I$ equation. Also the load-potential records may be converted to a plot of $E_i)/A$, where A is the value of E/E_i obtained from the calibration curve corresponding to the measured initial crack length and width, and E_c is the potential at crack initiation (see Fig. 22).

When calibration curves of this type are used, it is important to keep in mind certain restrictions on their application. For the probe positions and connections described, the calibration curves for symmetrically cracked plate specimens will yield the average of the

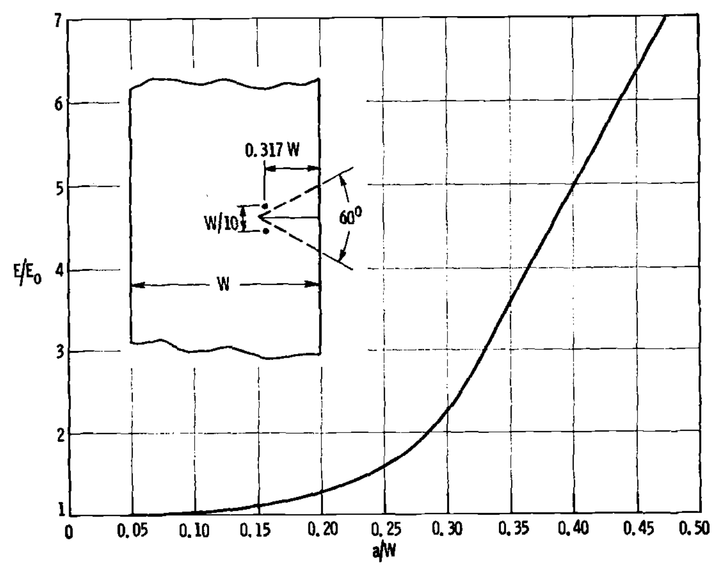

FIG. 24—Electrical Potential Calibration Curve for Single-Edge-Notched Specimen.

crack extension as a function of load by the use of calibration curves.

Calibration curves for several practical fracture toughness plate specimen types are given in Figs. 23 and 24. These have been determined for the potential probe postions shown and with the current input attachments far enough removed that the measured potential is influenced only by the crack. When these curves are used, the value of E_0 could be measured on a dummy specimen without a notch. Alternatively, E_0 for a particular test may be calculated as $E_0 = (E_c +$ crack extension occurring at each crack tip. Independent measurements are of course possible, if separate pairs of probes are used at these locations. The calibration curve corresponds to a crack front normal to the specimen surface and load axis. As discussed previously (see Fig. 6) in an actual specimen, the front is always curved and this curvature in mixed mode fractures may occupy a region about equal to the plate thickness. For this reason, crack extensions calculated from the calibration curves will closely approximate the actual values only when the curved region is a small fraction of the total crack extension. In $\mathcal{G}_c$ tests, the effect of curvature on measured crack length may be neglected if the total crack length, $2a_m$, is large in comparison with the thickness.

When studies are made of the pop-in phenomenon, it is instructive to determine the extent of crack movement increasing amounts of potential change. The specimens are then heat-tinted to outline the crack front, and broken. A plot may then be made of E/E_0 at interruption against some measured value from the heat-tinted crack indication. A few results of this type have been reported in Ref (43). Some data obtained by the authors are shown in Fig. 25 for

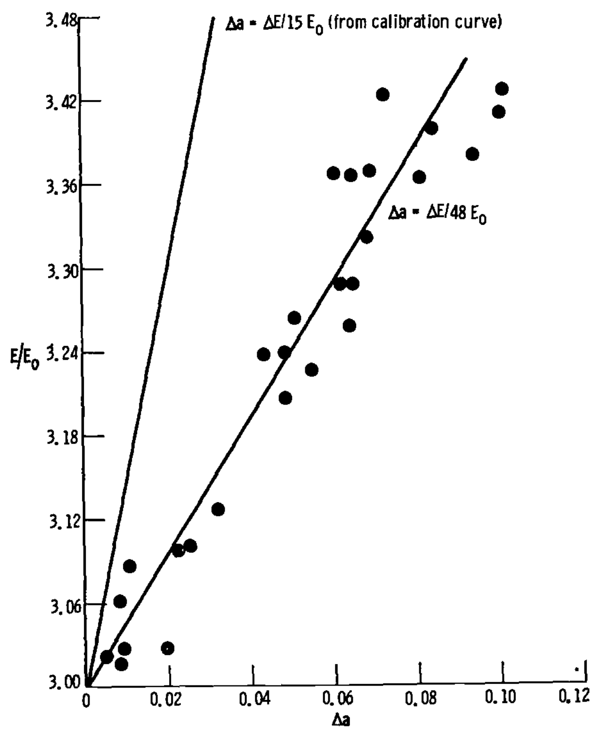

FIG. 25—Ratio of Potential Change to Initial Potential as Function of Actual Crack Extension Determined by Means of Interrupted Tests.

associated with a given indication of pop-in (for example, the magnitude of a step in the loading curve). As discussed above, the calibration curves are not particularly useful in this case, since the major portion of the crack extension is occupied by the curved fracture front. To obtain a more direct indication of crack extension under these circumstances, interrupted tests of a series of specimens may be made representing single-edge-notched tests on 18Ni-Co-Mo steel aged to a wide range of strength levels. In this case, Δa represents the maximum extension from its initial position of the most advanced point on the crack front. Within the scatter, there is roughly a linear relation between Δa and E/E_0 that is useful in estimating the amount of crack extension represented by a given potential change at pop-in. The general trend of these points may be compared with the slope of the calibration curve for the particular value of a_0/W used in these tests. As might be expected, the calibration curve would give estimates of Δa corresponding to a straight crack front and therefore considerably smaller than the actual values.

Advantages and Limitations of Potential Method—This technique appears to be readily adaptable to all practical fracture toughness specimen types. The necessary instrumentation is commercially available to permit automatic recording of the potential change. Calibration curves relating potential change to crack extension may be easily determined for through-cracked specimens by use of analog paper. With optimum location of the potential probes, a very high sensitivity to crack extension may be obtained. For example, it may be reasonably assumed that 0.050-in. chart-pen movement on the X-Y recorder is easily discernible and that a gain of 100,000 is possible through the voltmeter-amplifier with good stability. This corresponds to a sensitivity of 0.5 μv. With this sensitivity, a crack extension of 0.0025 in. is obtained from the calibration curve for an aluminum center-cracked specimen ($W = 3$ in. and $B = \frac{1}{2}$ in.) provided with 50 amp.

The current requirements can constitute a definite limitation on the use of the method. Thus, the resistivity of most metals decreases very rapidly at temperatures below about -300 F, and at liquid-hydrogen temperature, the current required for normal specimen sizes would be prohibitively large. At elevated temperatures, the resistivity increases but appreciable thermoelectric effects become difficult to avoid. The speed of testing is limited by the response of the potential measuring device employed. When the high sensitivity electronic voltmeter described above is used, the maximum response speed is of the order of $\frac{1}{2}$ sec. The use of an oscilloscope is apparently not possible because input amplifiers are not available that have sufficient gain combined with fast response, high stability, and low noise.

Displacement Gages:

The displacement per unit load between two points spanning a crack will increase with crack length. For elastic loading, this ratio is defined as a compliance and, for given specimen dimensions, depends only on the distance between the points (gage length) and the elastic modulus of the material. Measurement of displacement is the basis for use of so-called compliance gages in measuring the crack extension in fracture toughness specimens. In practice, a test specimen is provided with a gage that measures the displacement as a function of applied load as the crack extends. It is usually assumed that the compliance corresponding to any point on the curve may be obtained from the slope of a line connecting this point to the origin.

The crack length at a given load is then determined with the aid of a calibration curve. For example, in the case of symmetrically loaded plate specimens, this curve gives the ratio of $2a/W$ as a function of C/C_0, where C is the assumed compliance corresponding to a particular point on the load extension curve, and C_0 is the compliance at zero crack length. The value of C_0 may be calculated from the elastic modulus as is described later. The calibration curve in this form will apply to any material, provided that all dimensions of the specimen under test and the gage length are proportioned to the calibration specimen. Calibration curves are obtained by machining progressively longer slots (simulating the crack) into a calibration specimen and determining the compliance for the selected gage length at each known slot size for conditions of elastic loading.

This method of determining crack extension is well suited to tension-loaded plate specimens containing through-the-thickness cracks, although in principle it applies to any specimen. However, application to other specimen types offers as yet unresolved problems either in the experimental procedure or in the interpretation of the results. For example, the method has been applied to circumferentially notched round bars as described in Ref (33) and more recently by Van der Sluys (46). The data obtained indicate that the change in compliance with crack extension is relatively small for this specimen type and that eccentricities of loading (which are difficult to avoid) can have an appreciable effect on the accuracy.

Before proceeding to a discussion of the practical application of displacement-gage techniques for crack-extension measurement, it should be mentioned that the strain energy release rates can be determined from the rate of change of compliance with crack length. This technique for determining $\mathcal{G}$ values for a particular specimen geometry was suggested in Ref (32) and was used in Ref (33) to obtain an experimental relation between strain energy release rate and crack depth in bend specimens and circumferentially notched round bars. A more recent publication (24) describes a very precise method for measuring the compliance of tension-loaded plate specimens as a function of crack length and gives results for a single-edge-notched specimen.

Gage Types and Testing Procedures—The requirements for a displacement gage to be used in $\mathcal{G}_c$ tests are somewhat more difficult to meet than those for $\mathcal{G}_{Ic}$ testing. For the former application, it would be desirable to use a single calibration curve for a given specimen type. This requires that the gage length be adjustable to accommodate various specimen sizes. This, in turn, requires the signal output as a function of displacement to be linear over a sufficiently wide range to accommodate the largest displacements anticipated. On the other hand, the main requirement of the displacement gage in $\mathcal{G}_{Ic}$ testing is that of high sensitivity to initial crack movement. For either type of testing the gage length should be as short as possible as an aid in obtaining maximum sensitivity.

Linear response to displacement combined with high sensitivity and adequate range for $\mathcal{G}_c$ testing is provided by linear differential transformers. A recent paper by Boyle (47) describes a fixed gage length (2 in.) adapter that permits the use of a standard releasable extensometer for displacement measurements between gage points spanning the center notch in plate specimens. A magnification factor of 2 is provided by a lever system with spring-loaded knife edges. The adapter is not completely separable, and the gage points suffer rather badly when testing hard specimens to fracture. It is difficult to construct a trouble-free displacement gage with a variable gage length. A design of this type for center-notched specimens used by Jones and Brown (48) consists of an upper and lower split yoke. These are attached independently to the specimen so that the gage is completely separable. One yoke contains the differential transformer and the other serves as a reference surface for the transformer core. The yokes are provided with gage points that span the notch at the specimen center. A particular gage length is established by use of a positioning jig that is removed after clamping the yokes to the specimen. This gage is adaptable to any specimen thickness and, in principle, could be made to accommodate a range of specimen widths. In order to permit its use on specimens having an appreciable bow, an additional linear differential transformer should be incorporated so that the strains on the two flat surfaces of the specimen may be averaged. In an arrangement used by Bulloch and Ferguson (49) a linear differential transformer and a suitable reference surface are types of transformer are used in the displacement gage, additional circuits may be required to obtain the desired magnification factor. If the transformer output is to be fed to an X-Y recorder, it is necessary to employ a suitable converter.

As indicated previously, requirements

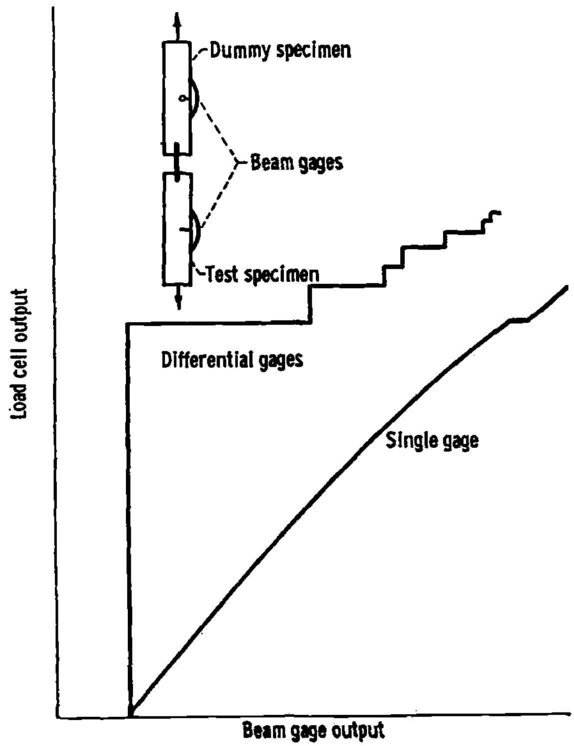

FIG. 26—Load-Displacement Records for Single-Edge-Notched Specimen Obtained by Using Single Beam Gage and Differential Beam Gage.

fastened to the specimen by means of pins fitted through small holes. This method of direct attachment appears to be limited to situations where the specimen thickness is sufficient to support the pins; however, it does have the advantage of flexibility.

It is possible to drive the load-strain recorder of some tension testing machines directly from a linear differential transformer output. However, when some

regarding the measuring range and linearity of output may be relaxed in $\mathcal{G}_{Ic}$ testing. Relaxation of these requirements gives more freedom in the design of displacement gages that are frequently optimized for a particular specimen type. The linear differential transformer gages described above are, in general, also suitable for $\mathcal{G}_{Ic}$ testing. In the case of single-edge-notched specimens, a standard releasable or separable extensometer may be clamped at the specimen edge across the notch; however, an extensometer used in this way can be damaged if the specimen halves are allowed to rotate freely about the loading pins after fracture. Excessive rotation can be prevented by placing soft metal blocks in the yokes under the specimen ends. For bend tests, Romine (50) has described the use of a conventional deflectometer to measure deflections at the point of load application.

Frequently, it is possible to use a relatively simple beam gage (or clip gage) that consists of a metal strip with wire resistance or foil strain gages on opposite faces. The beam gage is then bent to bear against two reference surfaces at the extremes of the gage length. Sensitivity of a beam gage increases with the ratio of beam thickness to length and the ratio of gage length to beam length. A description of highly sensitive gages of this type is given in Ref (24). Beam gages are readily adaptable to a variety of testing situations. For example, the gage may be located by edge grooves machined on either side of the notch in single-edge-notched specimens. Krafft (51) has used pins glued to the surface to position a beam gage across the center notch of a plate specimen. The output of a beam gage will be a nonlinear function of its end deflection; however, this is of no particular consequence in $\mathcal{G}_{Ic}$ testing, where a pop-in indication is the only information required.

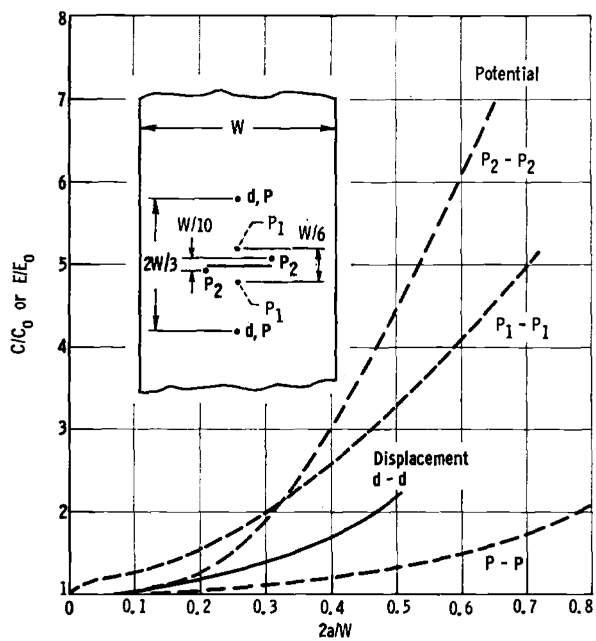

FIG. 27—Comparison of Displacement-Gage Calibration Curve with Several Calibration Curves Obtained by Using Electric Potential Measurements Illustrating Influence of Gage Length.

A differential beam gage is under development by the authors to detect pop-in in single-edge-notched specimens. The principle is to buck out that part of the gage output that is not due to a change in crack length. The arrangement used in Fig. 26 consists in loading the test specimen in tandem with a dummy.

Both specimens are provided with beam gages spanning the edge cracks, the output of these gages being opposed in a suitable bridge arrangement. The dummy specimen is identical to the test specimen except that its edge slot is terminated in a hole rather than a fatigue crack, so that no crack extension in the dummy occurs during the test. A schematic X-Y recorder plot of gage output versus applied load, shown in Fig. 26 for a single-edge-notched specimen, illustrates results obtained with a differential beam gage and a single gage. Two advantages of the differential beam gage as compared with a single gage are evident. Because the differential gage output is obtained only with crack extension, pop-in indications will be more distinct and considerably higher gain may be used without exceeding the limits of the chart paper before pop-in occurs.

The instrumentation necessary for beam gages is the same as that normally employed with wire resistance strain gages. The gage outputs can be used to drive conventional tension testing machine load-strain recorders either directly or through commercially available adaptors. If an X-Y recorder is used, the gage bridge output may be connected directly to one axis with the output from a load cell bridge on the other.

Reduction of Data—If plane-strain toughness determinations are to be made, the load at pop-in is determined from records such as those shown in Fig. 26 and used with the appropriate $\mathcal{G}_{Ic}$ equation (see Appendix). If the load-strain record has been determined with gages designed for $\mathcal{G}_c$ testing, the deflections may be converted to crack lengths by using a suitable calibration curve. A calibration curve given in Ref. (47) for center-notched specimens is shown in Fig. 27, along with some curves for the same specimen geometry obtained by the previously discussed potential method. The displacement-gage calibration is given as C/C_0 versus $2a/W$, where C is the compliance corresponding to any point on the load-displacement curve and C_0 is the compliance for zero crack length. This calibration curve applies to all center-notched specimens provided that the displacement gage used has a gage length of $2W/3$ and is located symmetric to the crack plane at the specimen centerline. Under these conditions, $C = e/P$, where e is the total measured deflection at the load, P. The value of C_0 for this gage length may be calculated as $C_0 = 2/3EB$, where B is the thickness and E is the elastic modulus of the test specimen.

This procedure for use of the calibration curve assumes that the unloading line corresponding to any given amount of crack extension on a load-displacement curve will be linear and will pass through the origin. Actually, as shown in Ref (47), the unloading curves are not exactly linear and do not pass through the origin. This is attributed to the action of a crack-tip plastic zone that acts to prop open the crack on unloading. By adjusting the unloading curve to pass through the origin, it is assumed that this propping effect is subtracted out and that the "true" compliance at load is determined.

It should be noted that the displacement measurements will be increased by crack-tip plasticity as well as by crack extension. For this reason, it has been suggested that the crack lengths calculated from the displacement-gage calibration curves be used directly in the $\mathcal{G}_c$ equations since, in effect, they already contain a plasticity correction. While this procedure should probably be followed, it is difficult to establish it on a firm basis due to the previously discussed complexities introduced by the nonideal unloading curve behavior.

When interpreting displacement-gage data in terms of crack extensions, it should be remembered that, at best, only average values can be determined unless the crack extension is large in comparison with the thickness. Measurement errors associated with small crack extensions due to the curved nature of the crack front were previously discussed in connection with data reduction from potential measurements.

Advantages and Limitations of Displacement Gages—This method in principle is adaptable to a wide variety of testing situations, but the particular gage design will depend on both the specimen type and the testing conditions. If linear differential transformers are employed, the gage may be immersed directly in a cryogenic bath. The authors have used differential transformers at liquid-hydrogen temperatures with no difficulty, provided that the transformer windings were sealed against moisture. By employing conventional extensometer extension-arm arrangements, linear differential transformer displacement gages could be used for high-temperature tests.

A beam-displacement gage for $\mathcal{G}_c$ testing at high temperatures with center-notched plates was described by Morrison et al (52). The gage is mounted between extension arms that contact the edges of the specimen near the heads and extend out the sides of a split infrared lamp furnace. Because of the fact that the gage points are far removed from the crack, this gage has rather low sensitivity. Beam gages with foil-resistance sensing elements could be used at cryogenic temperatures. A discussion of the most suitable types of foil gages for use in liquid hydrogen and special precautions regarding their application has been presented by Kaufman (53,54).

The beam-displacement gage is particularly well suited to $\mathcal{G}_{Ic}$ testing at high strain rates because the output may be easily displayed on conventional oscilloscopes. The authors have used these gages on single-edge-notched specimens fractured in the order of a few milliseconds. Care must be taken to design the gage and arrange the mounting so that the rapid application of load does not cause resonance vibration in the beam.

There appears to be no inherent limitation to the application of displacement gages in fracture toughness testing. As compared with the electrical potential technique, however, the method of adapting the sensing element to the specimen is frequently more difficult. This is particularly true of the linear gages desirable for $\mathcal{G}_c$ testing, which may require carefully machined and sometimes complex mounting and linkage systems. Another disadvantage lies in the fact that unwanted bending deflections will cause nonlinear response and require the use of double sensing elements to cancel the bending effects.

Sensitivity of Displacement Gages—Before leaving the subject of displacement gages, some comment should be made regarding their sensitivity. It has been generally assumed that this crack-measurement method is inferior to the electrical potential technique regarding the sensitivity available. This observation is probably based on the rather large apparent difference in slopes between the calibration curves that have been published for these two methods. In order to define more clearly such differences, a calibration curve for the center-notched plate displacement gage described in Ref (47) is compared (Fig. 27) with calibration curves obtained for the same specimen type by using potential measurements. From this representation it is quite evident that the slope of the calibration curves depends on the gage length and position selected.

In this respect, the potential measurement has an advantage since the probes can be located very close to the crack tips; however, it should be noted that, for identical locations and gage lengths, Boyle's displacement-gage calibration curve has a definitely greater slope than that obtained by electric potential measurements. From this displacement-gage calibration curve, an estimate was made regarding the absolute sensitivity to crack extension that could be obtained in a typical case.

The case selected as an example is represented by a load-deflection curve given in Ref (47) for a 7075-T6 center-notched specimen $\frac{3}{16}$-in. thick and 3 in.-wide. With the assumption that a chart-pen deflection of 0.050 in. is easily discernible at a magnification of 2000, a total crack extension of 0.006 in. should be detectable at the pop-in load, which was about 16,000 lb. This may be compared with the 0.003-in. crack-extension sensitivity previously mentioned for the electrical potential method when used on an aluminum single-edge-notched specimen and assuming the same minimum pen deflection for a pop-in indication. These calculated sensitivities, of course, are not directly comparable in a quantitative sense and should not be taken as limiting values. They do indicate, however, that both the displacement-gage and potential method can have very high sensitivity to crack extension.

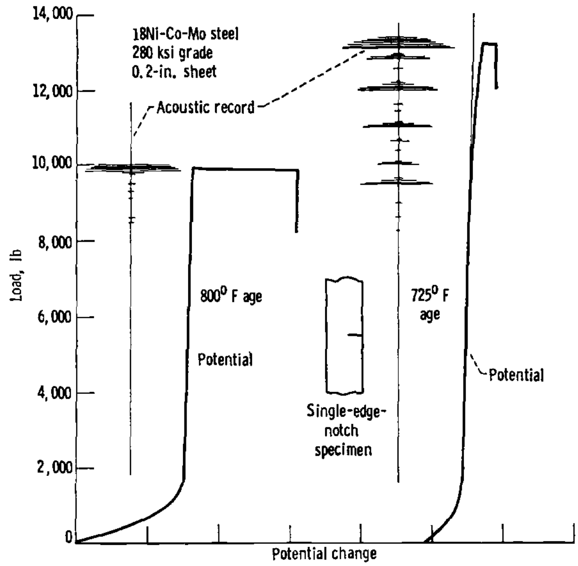

FIG. 28—Load-Potential and Acoustic Records from Single-Edge-Notched Specimens Illustrating Different Pop-In Behaviors.

Acoustic Method:

Disturbances within a material that result in the sudden release of elastic energy can frequently be detected by using a transducer that will convert an elastic vibration into an electrical signal. Thus, if a piezoelectric crystal is placed in contact with a specimen containing a propagating crack, the crystal will produce signals that may be amplified and recorded or used to drive a loud-speaker. The acoustic method of detecting crack propagation has been described in a paper by Romine (55) and in Ref (48).

The latter paper contains a detailed description of the method including the electronics required for recording load and crack sounds.

In practical application, a crystal transducer such as a slightly modified phonograph pickup is clamped to the specimen or to the loading train. A tape recording is made of the load and specimen acoustic output simultaneously on separate channels. The tape record may then be transferred to a recording oscillograph or simply audited with the tape load channel working a counter. The method is extremely sensitive to small crack extensions and may give definite indications of crack movement before either an electrical potential or a displacement gage gives a discernible output. While the amplitudes of the acoustic signals probably increase with the amount of material involved in a given increment of crack movement, there is no known way of estimating the amount of crack extension from acoustic records. For this reason, the acoustic technique is best used in conjunction with either potential measurements or displacement gages. Employed in this way, it provides additional information concerning the initial stage of the crack propagation process.

Examples of Data—As shown in Ref (48), the acoustic method is capable of indicating pop-in loads that agree well with those obtained by using displacement gages. In some cases, the acoustic method may also be helpful as an aid in interpreting a load-potential or displacement record. In order to illustrate this point, two examples are shown in Fig. 28 for single-edge-notched tests on an 18Ni-Co-Mo steel aged at 725 and 800 F. In this representation, load-potential records are given along with corresponding indications from oscillograph traces of the acoustic output. These tests were interrupted at the point indicated, heat-tinted to outline the fracture area, and then pulled to failure. Two rather different behaviors are represented by these tests.

The specimen aged at 800 F exhibited an abrupt large potential change at about 10,000 lb, and this corresponds to a large burst of sound. Preceding this burst, there were very weak acoustic indications possibly due to crack movement in fatigue-damaged metal. Approximately 0.1-in. total crack extension was represented by this pop-in, and the plastic-zone size at pop-in was less than one tenth the thickness. Under these circumstances, there seems to be little doubt that the load at fracture instability in the opening mode has been measured.

The behavior of the specimen aged at 725 F appears more complex. There is a distinct step in the load-potential curve at about 13,400 lb, and this corresponded to about 0.025-in. total crack extension. The plastic-zone size at this pop-in was approximately one eighth the specimen thickness. It will be noted that rather strong acoustic indications start at about 9500 lb and continue with increasing load. Using the acoustic indications as a guide makes it possible to detect a slight departure from linearity in the potential record also starting at about 9500 lb. Apparently, a substantial portion of the 0.025-in. total crack extension at pop-in took place at considerably lower loads. There is a question as to whether the pop-in load observed for the specimen aged at 725 F can be used to calculate a K_{Ic} having the same meaning as that calculated from the pop-in obtained from the specimen aged at 800 F.

Advantages and Limitations of Acoustic Method—The major advantage of the acoustic method lies in its relative simplicity and adaptability to a variety of specimen types and testing situations. For example, if the specimen is enclosed in a furnace or low-temperature bath, the pickup may be mounted on some part of the loading train external to the specimen enclosure. Special precautions must be taken, however, to eliminate the introduction of extraneous sounds that might mask or be confused with crack-movement indications. As a general rule, it is desirable to establish independently the background-noise character and level before conducting a series of tests. Frequently, this may be accomplished by loading a smooth specimen under the same conditions as to be used for the notch tests. As mentioned previously, a major disadvantage of the acoustic method is the fact that there is as yet no way of quantitatively relating the signal characteristics to the extent of crack movement.

Continuity Gage:

A recent paper by Kemp (56) describes the use of a "continuity" gage to measure crack extension. Essentially, this is a special type of foil-resistance strain gage and is constructed in the same general way. It consists of regularly spaced metal ribbon elements all connected in parallel and is applied to the specimen surface so that the elements are normal to the direction of crack propagation. The elements are longer the farther they are from the notch tip. This arrangement provides approximately linear resistance change as successive elements are fractured by the extending crack.

In its present form, each gage is about $\frac{1}{2}$ in. wide and has 20 elements with a spacing of approximately 0.01 in. If crack extensions beyond 0.2 in. are expected, additional gages are placed in the line of crack extension. Conventional strain-gage instrumentation may be used with each gage being part of a bridge circuit. The output of the bridge is recorded on a light-beam galvanometer oscillograph along with a load trace from a load-cell-bridge circuit. A step appears in the output for each ribbon element fractured and the crack length at maximum load can be determined by counting these steps.

The main advantage to this type of gage is its adaptability to crack-growth studies in tank tests at cryogenic temperatures. The gages are rather expensive and, of course, are not re-usable.

APPENDIX

PRACTICAL FRACTURE TOUGHNESS SPECIMENS—DETAILS OF PREPARATION, TESTING, AND DATA REPORTING

This section presents a convenient summary of the geometries of the recommended practical fracture toughness test specimens. Included also will be comments on specimen preparation, testing precautions, and data reporting.

The various practical fracture toughness test specimens are shown in Figs. 29–30. The proportions given are those developed in previous sections of this paper. Relations for $\mathcal{G}$ and K are given in the usual closed form for symmetrically cracked tension specimens (Figs. 29(*a*) and (*b*)), and for the surface-cracked plate specimen (Fig. 30(*d*)). Polynomial expressions in a/W are shown in Fig. 30(*a*–*c*) for the single-edge-notched plate and bend specimens. The sources of these expressions are discussed in the text. It will be noted that the factor $(1 - \nu^2)$ has been used in the equations relating $\mathcal{G}$ to K for plane strain. This factor is an approximation in relation to the stress state in an actual plate specimen. This point was discussed further in the text, and as mentioned, it is difficult to judge the accuracy of the published approximate solutions for $\mathcal{G}_I$ for circumferentially notched round bars. The form shown in Fig. 30(*e*) represents an average of several results in the d/D range between 0.55 and 0.9.

Specimen Machining:

The most critical features of specimen machining are concerned with the preparation and location of the fatigue crack starter notches and the means for transmitting the load to the specimen. Details of the starter notches for plate tension specimens are shown in Fig. 31. The dimensional limits given will ensure that the influence of the shape of the notch does not extend to the tip of the fatigue crack. The angle at the slot end is not critical and the notch-tip radius shown may be easily produced by slightly extending the $\frac{1}{16}$-in. slot with a 0.010-in. jeweler's saw. If the starter notches shown in Fig. 31 cannot be accommodated because of insufficient specimen width, it is best to produce narrow slots by using an electric-discharge machining process. An indentation made with a sharp chisel having a rounded end will serve as a crack starter for the surface-cracked specimens. Alternatively, a surface notch may be produced by an electric-discharge process. The V-notch in the circumferentially notched round bar should have as sharp a tip radius as possible in order to minimize the stress necessary to produce fatigue cracks in a reasonable length of time.

Where loading pinholes are shown, these should serve as reference surfaces for machining the crack starter notches. In this way, symmetry of the notches about the loading axis is easiest to achieve. It should be noted that the pinhole position in relation to the width is an important parameter in the single-edge-notched plate specimen and that the $\mathcal{G}_I$ expression shown applies to the $W/2$ position with the limits indicated. No means for gripping the surface-cracked plate specimen or the circumferentially notched round bar are shown in Fig. 30(a–e). Pin-loading of the surface-cracked specimen will require a head wider than the test section, or the use of doubler plates around the pinholes. Alternatively, the specimen may be gripped in the tension testing machine jaws. The circumferentially notched round bar is normally provided with buttonheads although, as described in Ref (8), a threaded specimen with special alignment surfaces may be used. In either case, precision machining of all cylindrical surfaces is necessary to ensure that the notch section is perpendicular to and concentric with the loading axis.

The edges of the plate tension specimens do not have to be machine-finished unless they serve as locating surfaces for positioning

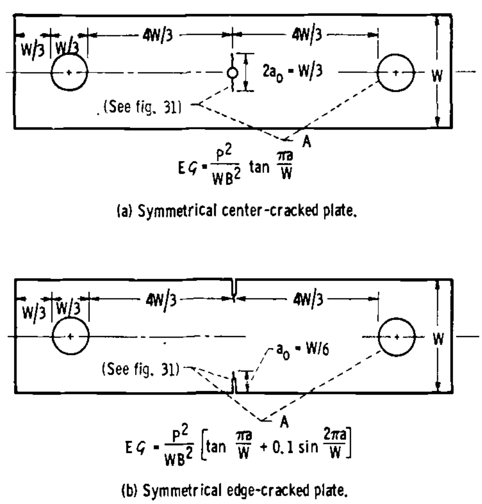

For $\mathcal{G}_c$ tests	For $\mathcal{G}_{Ic}$ tests
$16 < W/B < 45$	$5 < W/B < 10$
$E\mathcal{G} = E\mathcal{G}_c = K_c^2$	$E\mathcal{G} = E\mathcal{G}_{Ic} = (1 - \nu^2)K_{Ic}^2$
$a = a_m + \frac{E\mathcal{G}_c}{2\pi\sigma_{YS}^2}$	$a = a_m + \frac{E\mathcal{G}_{Ic}}{6\pi\sigma_{YS}^2}$

A - Surfaces must be symmetric to specimen centerline within W/1000

FIG. 29—Practical Fracture Toughness Specimen Types. Specimens for General Use. (The Factor $(1 - \nu^2)$ Is an Approximation. See Text of Appendix.)

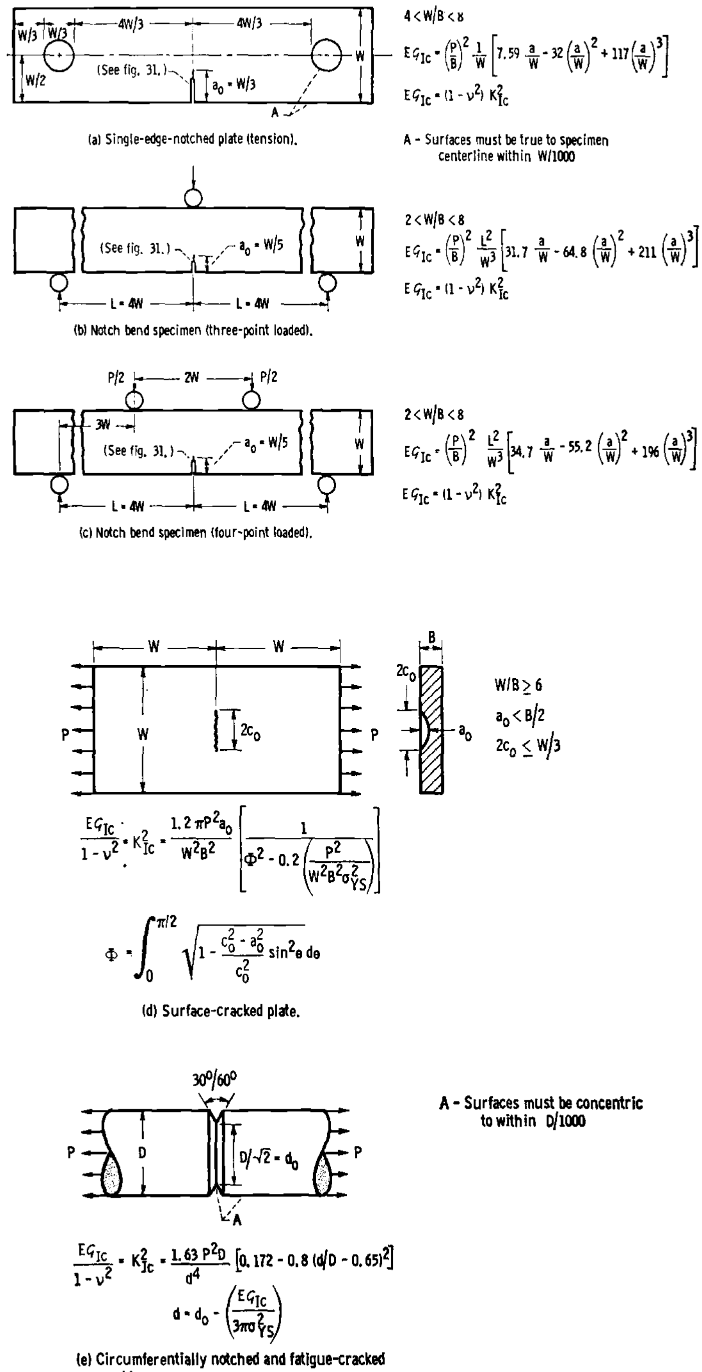

FIG. 30—Practical Fracture Toughness Specimen Types. Plane-Strain Tests. (For All Specimens $a = a_0 + E\mathcal{G}/6\pi\sigma_{YS}^2$; the factor $(1 - \nu^2)$ Is an Approximation. See Text of Appendix.)

of the notches and pinholes. The flat surfaces of these specimens are machined only when necessary to remove warping or to eliminate an unwanted surface layer. Rectangular cross-section bend specimens (Figs. 30(*b*) and (*c*)) should provide no special machining problems whatsoever. Surfaces in contact with the loading and support pins should be ground to reduce friction. These surfaces can then serve for reference purposes when machining the fatigue crack starter notch.

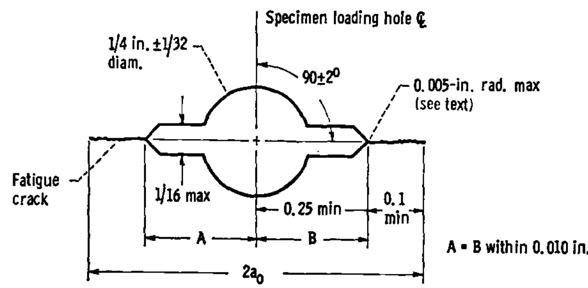

(a) Fatigue crack starter for center-cracked plate specimens (W ≥2 in.).

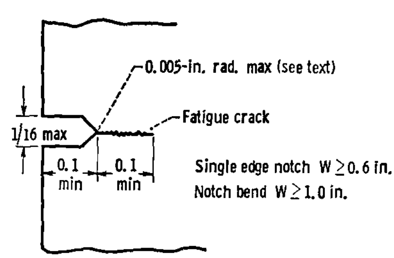

(b) Fatigue crack starter for edge-notched plate specimens.

FIG. 31—Fatigue-Crack Starter Notches for Center-Cracked and Edge-Notched Plate Specimens.

Fatigue Cracking and Heat Treatment:

Details concerning the fatigue cracking of the symmetrically cracked tension specimens (Figs. 29(*a*) and (*b*)) and the circumferentially notched round bar (Fig. 30(*e*)) have been given in Refs (**5**,**8**). It was recommended that tension-tension loading be used to produce fatigue cracks in the symmetrically center-cracked specimens; however, some investigators have cracked this type of specimen in bending with the moments perpendicular to the sheet plane. This method produces "wing cracks" starting from the surface and joining at the center of the thickness. These cracks are sometimes difficult to keep in one plane and form a crack front with considerable curvature. Further studies of these crack shapes are required before this method of producing fatigue cracks can be recommended.

Surface fatigue cracks may be produced by cantilever bending of the specimen over a support that tapers to a point. Details of this technique are given in Refs (**38**,**39**). Cracks are initiated more easily and may be located at the desired spot on the specimen surface if a small sharp indentation is provided as a crack starter. As mentioned previously, this starter notch may be produced by a chisel or by electric-discharge machining. The surface cracks produced by this method are semi-elliptical in shape with the ellipticity usually increasing with the depth; however, it is possible to control the crack shape if the starter notch is produced by electric-discharge machining by using specially contoured electrodes.

Fatigue cracking of single-edge-notched plate specimens may be conveniently accomplished by cantilever bending with the bending moment in the plane of the specimen. The stress at the notch tip is kept in tension with the minimum stress set just sufficient to ensure smooth operation of the fatigue machine and satisfactory alignment during the fatigue cycling. This method poses no special problems, and the cracks are relatively easy to control since they are running into a decreasing stress field.

There are very few data regarding the effect of the maximum stress used in producing fatigue cracks on the measured fracture toughness. Some results given in Ref (39) for surface-cracked specimens of a brittle steel indicate no significant difference in average K_{Ic} values for nominal bending stresses of about 30, 40, and 60 per cent of the yield strength. The scatter of data, however, appeared to be greater as the nominal bending stress increased. In view of these results, it would seem best to keep the nominal net-section stress below 50 per cent of the yield strength when fatigue cracking.

The question of whether heat-treating should precede or follow fatigue cracking is difficult to resolve with the limited amount of data now available. The center-crack strength of a relatively brittle steel (5) was the same whether sheet specimens were heat-treated before or after fatigue cracking. The results of a few surface-crack tests (38) appear to confirm this behavior. It would seem reasonable to assume that any differences in fracture toughness due to the cracking and heat-treating sequence would tend to be minimized by stable crack extension. For this reason, the effects of this sequence should be more pronounced in $\mathcal{G}_{Ic}$ than in $\mathcal{G}_c$ tests. In this respect, recent experiments in the authors' laboratory showed that more distinct pop-in indications were obtained for 18Ni-Co-Mo single-edge-notched tests when specimens were aged after fatigue cracking rather than before. In the absence of more definite information, it would seem reasonable to heat treat after fatigue cracking where possible. This procedure should assist in reducing any effects that might arise from differences in the fatigue stressing conditions; however, as pointed out in Ref (8), when preparing circumferentially notched round bars, it may be necessary to finish machine and fatigue crack after full heat-treatment in order to correct for warpage and to avoid quench cracks. These considerations may also be important for thick plate specimens.

Testing Procedure:

Testing procedures for symmetrically cracked sheet tension specimens and circumferentially notched round bars have been discussed in Refs (5) and (8). As described in these publications, special care should be taken to minimize eccentricity of loading by using pin-yoke assemblies for sheet specimens and by using special loading devices for notched round bars. Details concerning a concentric buttonhead loading fixture for notched rounds are given in a paper by Jones and Brown (57). When testing thick pin-loaded specimens in tension, it is advisable to make use of double pin yokes in order to minimize bending moments acting both perpendicular and parallel to the sheet plane. These yokes must be carefully machined so that they do not in themselves introduce bending due to misalignment of the pinholes. When pin yokes are used, it is desirable to lubricate the pinholes with molybdenum disulfide.

As mentioned previously, surface-cracked specimens, if pin-loaded, will require a head larger than the test section or the use of doubler plates around the pinholes. By using the tension testing machine jaws for gripping, a uniform width and thickness specimen may be employed. It might be expected that loading in the jaws of a tension testing machine would introduce considerable eccentricity, which would vary from test to test and produce excessive scatter. However, data from a large number of replicate tests on jaw-loaded surface-cracked specimens of a brittle steel have been reported (39) and these data exhibit very small scatter. In addition, a few results (38) for pin-loaded specimens indicate that surface cracks eccentric with respect to the specimen centerline do not result in lower strengths. On the basis of the data available, it would appear that jaw loading for this type of specimen is permissible. However, the data should be examined for scatter that could be attributed to variation in eccentricity from test to test.

In the case of heat-treated martensitic steels, crack extension can occur due to stress corrosion under a constant load in the presence of water vapor. Plane-strain fracture toughness values for such materials can be influenced by the amount of water vapor in the air and this effect will depend on the testing speed. Results are given in Ref (46) for circumferentially notched round bars of SAE 4340 (σ_{YS} = 225,000 psi) tested at three levels of relative humidity using normal loading rates. Because of the limited amount of data available from this investigation and the scatter encountered, no quantitative relation could be established between the amount of moisture present and the fracture toughness; however, the notch strength decreased with increasing relative humidity. In view of the uncertainties involved, it is not possible to make any recommendations at this time concerning control of the humidity during a test; however, when testing low-alloy tempered martensites or other alloys subject to stress corrosion in the presence of water, the temperature and relative humidity of the air surrounding the specimen should be recorded.

Data Reporting:

The usefulness of fracture toughness data depends not only on the selection of proper testing techniques, but also on the proper identification of the reported data. All too frequently fracture toughness information appearing in the published literature and in company reports is so poorly identified that no judgment can be made concerning its validity nor its applicability to the particular problem at hand. It must be remembered that fracture testing and fracture mechanics analysis are new approaches to a very complicated problem and that in the formative stages of any engineering science it is necessary to provide the maximum amount of information to the person attempting to use the data. With this in mind, the Fifth Report of the ASTM Special Committee on Fracture Testing (9) listed required supplementary information that should be reported with fracture toughness data.

Care should be exercised to avoid using the designation "fracture toughness" or the symbols $\mathcal{G}$ or K in connection with data that do not meet the basic requirements for fracture toughness testing. A particularly dangerous practice is the reporting of calculated critical flaw sizes as a function of applied stress when the calculations are based on poorly established fracture toughness data. Information of this type should always be carefully qualified regarding the basis of calculation and the manner in which the fracture toughness parameters were obtained.

REFERENCES

(1) C. F. Tipper, "The Brittle Fracture of Metals at Atmospheric and Sub-Zero Temperatures," *Metallurgical Review*, Vol. 2, No. 7, 1957, pp. 195–261.

(2) C. F. Tipper, "Testing for Brittleness in Structural Steels," *Report P3*, Admiralty Advisory Comm. on Structural Steel, Her Majesty's Stationery Office, 1962.

(3) W. S. Pellini and P. P. Puzak, "Fracture Analysis Diagram Procedures for the Fracture-Safe Engineering Design of Steel Structures," *Report 5920*, U.S. Naval Research Lab., March, 1963.

(4) W. S. Pellini and J. E. Srawley, "Procedures for the Evaluation of Fracture Toughness of Pressure Vessel Materials," *Report 5609*, U.S. Naval Research Lab., June, 1961.

(5) ASTM Special Committee on Fracture Testing of High-Strength Metallic Materials, "Fracture Testing of High-Strength Sheet Materials," *ASTM Bulletin*, January, 1960, pp. 29–40, and February, 1960, pp. 18–28.

(6) ASTM Special Committee on Fracture Testing of High-Strength Metallic Materials, "The Slow Growth and Rapid Propagation of Cracks," *Materials Research & Standards*, Vol. 1, No. 5, May, 1961, pp. 389–393.

(7) ASTM Special Committee on Fracture Testing of High-Strength Metallic Materials, "Fracture Testing of High-Strength Sheet Materials," *Materials Research & Standards*, Vol. 1, No. 11, November, 1961, pp. 877–885.

(8) ASTM Special Committee on Fracture Testing of High-Strength Metallic Materials, "Screening Tests for High-Strength

Alloys Using Sharply Notched Cylindrical Specimens," *Materials Research & Standards*, Vol. 2, No. 3, March, 1962, pp. 196–203.

(9) ASTM Special Committee on Fracture Testing of High-Strength Metallic Materials, "Progress in Measuring Fracture Toughness and Using Fracture Mechanics," *Materials Research & Standards*, Vol. 4, No. 3, March, 1964, pp. 107–119.

(10) A. E. H. Love, *A Treatise on the Mathematical Theory of Elasticity*, fourth ed., Cambridge Univ. Press, Cambridge, 1927, Ch. IV, Art. 83.

(11) G. R. Irwin, "Fracturing and Fracture Mechanics," *Report 202*, Dept. Theoretical and Applied Mech., University of Illinois, October, 1961.

(12) G. R. Irwin, "Fracture Testing of High-Strength Sheet Materials Under Conditions Appropriate for Stress Analysis," *Report 5486*, U.S. Naval Research Lab., July 27, 1960.

(13) J. M. Krafft, A. M. Sullivan, and R. W. Boyle, "Effect of Dimensions on Fast Fracture Instability of Notched Sheets," *Proceedings*, Crack Propagation Symposium, College of Aeronautics, Cranfield (England), September, 1961, Vol. I, pp. 8–28.

(14) J. E. Srawley and C. D. Beachem, "Crack Propagation Tests of High-Strength Sheet Materials. Part IV—The Effect of Warm Pre-Straining," *Report 5460*, U.S. Naval Research Lab., April, 1960.

(15) G. R. Irwin, "Crack-Extension Force for a Part-Through Crack In a Plate," *Journal of Applied Mechanics*, (*Transactions*, Am. Soc. Mechanical Engrs.), Ser. E, Vol. 29, No. 4, December, 1962, pp. 651–654.

(16) G. R. Irwin, J. A. Kies, and H. L. Smith, "Fracture Strengths Relative to Onset and Arrest of Crack Propagation," *Proceedings*, Am. Soc. Testing Mats., Vol. 58, 1958, pp. 640–660.

(17) J. I. Bluhm, "A Model for the Effect of Thickness on Fracture Toughness," *Proceedings*, Am. Soc. Testing Mats., Vol. 61, 1961, pp. 1324–1331.

(18) G. R. Irwin, *Fracture*, Vol. VI of *Encyclopedia of Physics*, edited by S. Flugge, Springer, Berlin, 1958, pp. 551–590.

(19) G. R. Irwin, *Fracture Mechanics. Structural Mechanics*, Pergamon Press, New York, 1960, pp. 557–594.

(20) G. R. Irwin and J. E. Srawley, "Progress in the Development of Crack Toughness Fracture Tests," *Materialprüfung*, Vol. 4, No. 1, January, 1962, pp. 1–11.

(21) J. E. Srawley and C. D. Beachem, "Resistance to Crack Propagation of High-Strength Sheet Materials for Rocket Motor Casings," *Report 5771*, U.S. Naval Research Lab., May 31, 1962.

(22) R. W. Boyle, A. M. Sullivan, and J. M. Krafft, "Determination of Plane Strain Fracture Toughness with Sharply Notched Sheets," *Welding Journal* (Research Supplement), Vol. 41, No. 9, September, 1962, pp. 428s–432s. (See also *ASME Paper 62-MET-13*, 1962.)

(23) Bernard Gross, John E. Srawley, and William F. Brown, Jr., "Stress-Intensity Factors for a Single-Edge-Notch Tension Specimen by Boundary Collocation of a Stress Function," *TN D-2395*, NASA, Aug., 1964.

(24) John E. Srawley, Melvin H. Jones, and Bernard Gross, "Experimental Determination of the Dependence of Crack Extension Force on Crack Length for a Single-Edge-Notch Tension Specimen," *TN D-2396*, NASA, Aug., 1964.

(25) D. H. Winne and B. M. Wundt, "Application of the Griffith-Irwin Theory of Crack Propagation to the Bursting Behaviour of Disks, Including Analytical and Experimental Studies," *Transactions*, Am. Soc. Mechanical Engrs., Vol. 80, 1958, pp. 1643–1655.

(26) E. J. Ripling, S. Mostovoy, and R. L. Patrick, "Measuring Fracture Toughness of Adhesive Joints," *Materials Research & Standards*, Vol. 4, No. 3, March, 1964, pp. 129–134.

(27) H. M. Westergaard, "Bearing Pressures and Cracks," *Journal of Applied Mechanics*, Vol. 6, No. 2, 1939, pp. A-29–A-53.

(28) J. A. Kies, "Aircraft Glazing Materials—A Method for Evaluating the Shatter Resistance of Aircraft Canopy Materials," *Memorandum Report 237*, U.S. Naval Research Lab., November, 1953.

(29) Martin Greenspan, "Axial Rigidity of Perforated Structural Members," *Journal of Research*, Nat. Bur. Standards, Vol. 31, No. 6, December, 1943, pp. 305–322.

(30) G. R. Irwin, "Plastic Zone Near a Crack and Fracture Toughness," *Proceedings*, Seventh Sagamore Ordnance Materials Conference, Syracuse University Research Institute, August, 1960.

(31) A. M. Sullivan, "New Specimen Design for Plane-Strain Fracture Toughness Tests," *Materials Research & Standards*, Vol. 4, No. 1, January, 1964, pp. 20–24.

(32) G. R. Irwin and J. A. Kies, "Critical Energy

Rate Analysis of Fracture Strength," *Welding Journal* (Research Supplement), Vol. 33, 1954, pp. 193s–198s.

(33) J. D. Lubahn, "Experimental Determination of Energy Release Rates for Notch Bending and Notch Tension," *Proceedings*, Am. Soc. Testing Mats., Vol. 59, 1959, pp. 885–915.

(34) G. M. Orner and C. E. Hartbower, "Sheet Fracture Toughness Evaluated by Charpy Impact and Slow Bend," *Welding Journal* (Research Supplement), Vol. 40, September, 1961, pp. 405s–416s.

(35) J. M. Krafft, "Fracture Toughness of Metals," Report of NRL Progress, U.S. Naval Research Lab., November, 1963, pp. 4–16.

(36) C. D. Beachem and J. E. Srawley, "Fracture Tests of Surface Cracked Specimens of AMS 6434 Steel Sheet," *Memorandum Report 1097*, U.S. Naval Research Lab., September, 1960.

(37) J. E. Srawley and C. D. Beachem, "Fracture of High Strength Sheet Steel Specimens Containing Small Cracks," *ASTM STP 302, Symposium on Evaluation of Metallic Materials in Design for Low-Temperature Service*, Am. Soc. Testing Mats., 1962, pp. 69–83.

(38) C. S. Yen and S. L. Pendleberry, "Technique for Making Small Cracks in Sheet Metals," *Materials Research & Standards*, Vol. 2, No. 4, November, 1962, pp. 913–916.

(39) J. E. Srawley, "Small Fatigue Cracks as Fracture Origins in Tests of High-Strength Steel Sheet," *Proceedings*, Am. Soc. Testing Mats., Vol. 62, 1962, pp. 734–741.

(40) A. E. Green and I. N. Sneddon, "The Distribution of Stress in the Neighborhood of a Flat Elliptical Crack in an Elastic Solid," *Proceedings*, Cambridge Philosophical Soc., Vol. 46, January, 1950, pp. 159–163.

(41) Ian N. Sneddon, "Crack Problems in Mathematical Theory of Elasticity," *Report ERD-126/1*, North Carolina State College, May 15, 1961.

(42) B. M. Wundt, "A Unified Interpretation of Room-Temperature Strength of Notched Specimens as Influenced by Their Size," *Paper 59-MET-9*, Am. Soc. Mechanical Engrs., 1959.

(43) E. A. Steigerwald and G. L. Hanna, "Initiation of Slow Crack Propagation in High-Strength Materials," *Proceedings*, Am. Soc. Testing Mats., Vol. 62, 1962, pp. 885–913.

(44) A. A. Anctil, E. B. Kula, and E. DiCesare, "Electric-Potential Technique for Determining Slow Crack Growth," *Proceedings*, Am. Soc. Testing Mats., Vol. 63, 1963, pp. 799–808.

(45) J. Praglin, "A Milli-Microvoltmeter," *Keithley Engineering Notes*, Vol. 8, No. 4, Keithley Instruments, Cleveland, Ohio, July, 1960.

(46) W. A. Van der Sluys, "Effects of Repeated Loading and Moisture on the Fracture Toughness of SAE 4340 Steel," *T & AM Report 245*, University of Illinois, May, 1963.

(47) R. W. Boyle, "A Method for Determining Crack Growth in Notched Sheet Specimens," *Materials Research & Standards*, Vol. 2, No. 8, August, 1962, pp. 646–651.

(48) M. H. Jones and W. F. Brown, Jr., "Acoustic Detection of Crack Initiation in Sharply Notched Specimens," *Materials Research & Standards*, Vol. 4, No. 3, March, 1964, pp. 120–129.

(49) D. F. Bulloch and R. Ferguson, "Thick Section Fracture Toughness, Exhibit B," *Quarterly Progress Report 1*, Boeing-North American, Los Angeles, Calif., October, 1963.

(50) H. E. Romine, "Plane Strain Fracture Toughness Measurements of Solid Booster Case Materials," *RTD-TDR-63-4048*, Third Maraging Steel Project Review, AF Materials Lab., November, 1963, pp. 185–211.

(51) J. M. Krafft, Unpublished note to the ASTM Committee on Fracture Testing of High Strength Metallic Materials, Aug. 29, 1963.

(52) J. D. Morrison, P. C. Jenkins, and J. R. Kattus, "An Investigation of the Crack-Propagation Resistance of High-Strength Alloys and Heat-Resistant Alloys," Summary Technical Report, Dec. 23, 1960–Oct. 23, 1962, Southern Research Inst., Nov. 21, 1962.

(53) Albert Kaufman, "Performance of Electric-Resistance Strain Gages at Cryogenic Temperatures," *NASA TN D-1663*, 1963.

(54) A. Kaufman, "Investigation of Strain Gages for Use at Cryogenic Temperatures," *Experimental Mechanics*, Vol. 3, No. 8, August, 1963, pp. 177–183.

(55) H. E. Romine, "Determination of the Driving Force for Crack Initiation from Acoustic Records of $\mathcal{G}_c$ Tests on High Strength Materials for Rocket Motor Cases," *NWL Report 1770*, U.S. Naval Weapons Lab., Oct. 4, 1961

(56) R. H. Kemp, "Characteristics and Application of Foil Strain Gages at −423° F."

Paper presented at Western Regional Strain Gage Conference, Denver (Colo.), Sept. 30–Oct. 1, 1963.

(57) M. H. Jones and W. F. Brown, Jr., "An Axial Loading Creep Machine," *ASTM Bulletin*, No. 211, January, 1956, pp. 53–60.

DISCUSSION

W. W. GERBERICH[1]—The amount of information presented in this paper is too extensive to comment on in detail so I will limit my remarks to two points.

First, I was very interested in the determination of maximum energy release rate measurement capacity, C_g, as typified in Fig. 13 since this approach is practically identical to the one I presented in a relatively uncirculated report.[2] The only difference should be the utilization factor which stems from using $\sigma_{net} = 0.8\ \sigma_{YS}$ as an upper limit for accurate measurements. However, my results are still 20 per cent higher even with the inclusion of the 0.64 factor. For example, at the maximum which occurs at $2a/W$ of about 0.35, Fig. 13 gives a value of 0.21, whereas I obtained a value of about 0.25. This later value agrees with the maximum value obtained by Irwin[3] if the 0.64 factor is included. Although this discrepancy is small, I wonder if the authors have some explanation for this difference? In general, this approach can be very useful in specimen design and the authors are to be congratulated in extending it to a number of test specimens and formulae.

Secondly, the point that accurate measurements of $\mathcal{G}_c$ should be limited to cases where the σ_{net}/σ_{YS} ratio is less than or equal to 0.8 is very realistic. When the plastic-zone size becomes much greater than the plate thickness, the energy absorbed by plastic deformation becomes significantly large, so that it cannot be estimated using elastic considerations. Using experimental stress analysis techniques,[4] it has been strongly indicated that the plastic energy release rate exceeds the modified Griffith-Irwin energy release rate at a value of σ_{net}/σ_{YS} somewhere between 0.8 and 1.0. To be conservative, the 0.8 value is a valid limitation for obtaining exact quantitative design information.

J. D. MORRISON[5]—I simply wish to congratulate the authors on their excellent presentation, which so effectively summarizes the current state of development and the significance of fracture toughness testing in terms of fracture mechanics. The further refinement of methods for evaluating plane-strain fracture toughness, continuing at the authors' laboratory, is certainly to be applauded. It is to be hoped that those individuals engaged in the design of highly stressed structures, and those developing "new" structural materials for such applications, will follow the evolution of these methods and will apply them in terms of the recommendations of the ASTM Special Committee on Fracture Testing of High-Strength Metallic Materials.

A. A. WELLS[6]—As an exposition of linear fracture mechanics from the view-

[1] Research Laboratories, Aeronutronic, Div. of Philco Corp., Newport Beach, Calif.

[2] W. W. Gerberich, "Theoretical and Practical Aspects of Correlating Percent Shear-Lip to Relative Plastic Zone Size in Brittle Fracture," *TR 32-112*, Jet Propulsion Lab., California Institute of Technology, September, 1962.

[3] G. R. Irwin, "Advanced Fracture Strength Measurement Techniques," Contributions to 1959 Lecture Series of Washington, D. C., Chapter of ASM, 1959.

[4] W. W. Gerberich, "Current Trends in Testing Methods, Design, and Material for Fracture Toughness," presented at Joint ASM-ASTME Meeting, March, 1964 and to be published in *Metals Engineering Quarterly*.

[5] Research Metallurgist, Southern Research Institute, Birmingham, Ala.

[6] Dept. of Civil Engineering, The Queens University, Belfast, Ireland.

point of its technological exploitation, the paper by Srawley and Brown offers an exceptionally well-balanced judgment. It gives loyal support to the ASTM presentation, while indicating fully and with care the uncertainties and weaknesses. It will be widely read abroad and may favorably influence the committal of opinion there, where the pioneering achievements of ASTM have been watched so far with great interest but also, it may be said, without widespread committal.

In view of the qualifications so expertly presented, there is little to criticize in the paper. It might, however, be useful to add a qualification which relates to the sources of variance of fracture toughness with crack length, and of the plane-strain values in particular. I refer to the influence of triaxiality, which may most succinctly be described in terms of the prevailing superimposed uniform stress field in the direction of crack travel, as foreshadowed many years ago by Irwin in his elucidation of crack-tip stress fields.

Effects of this type have been highlighted by our recent work in the United Kingdom, aimed at the extension of linear fracture mechanics into the general yielding range, for the benefit of utilizing the tougher low-strength materials. Readers of the paper will recognize that experiments based on low-strength steels require use of large specimens, and in their analysis one is hemmed in with boundary effects. The triaxiality variations in these experiments are mainly exposed by the magnifying effect of the temperature transition, and its movement up or down by changing other dimensions than the plate thickness.

Unfortunately, the analytical tools for the assessment of triaxiality variations under partly or fully plastic conditions are as yet rather crude, although the presence of these triaxiality variations is clearly revealed in the plastic rigid analyses for plane strain. As far as the experiments are concerned, the results obtained on 36 by 3-in. edge-notched, mild steel tension specimens may be of interest (see Table 2). For the purpose of this comparison the crack-opening displacement at fracture, δ, may be taken as proportional to fracture toughness, $\mathcal{G}_c$. The method of determining the plastic stress-intensification or triaxiality factor is described in a paper to the recent Royal Society Symposium in London which is to be published. The highest triaxiality and lowest δ values for each temperature arise at 3-in. notch depth, the over-all variation corresponding with a transition temperature shift of 20–40 C. There is reason to believe that the triaxiality falls right off for shallow notches. Of these results, most were at general yield, but the 3-in. notch result at -40 C gave a low stress fracture. Thus one would expect to see these effects in high-strength steels too.

TABLE 2.

Notch depth, in.	1½		3		6	
Test temperature, deg C	−10	−40	−10	−40	−10	−40
Crack-opening displacement at fracture, δ, mils	20.5	9	17	3	28	17
Observed plastic stress-intensification factor	2.14		2.22		2.10	

It is tentatively suggested that the ASTM Special Committee might consider the encouragement of linear mechanics investigations into this field.

J. E. SRAWLEY AND W. F. BROWN, JR. (*authors*)—The authors wish to thank the discussers for their comments. With regard to the first point raised by Mr. Gerberich, the apparent discrepancy that he finds results from an understandable oversight on his part. The value of C_0 is an implicit one, not an explicit one. The factor, $\tan(\pi a/W)$, is equal to $\tan(\pi a_m/W + EC_g/2\pi\sigma_{YS}^2)$ where a_m is the measured crack half-length and $EC_g/2\pi\sigma_{YS}^2$ is the value of the plastic-zone correction term when $\mathcal{G}$ is equal to C_g. Values of C_g have to be calculated by graphical or iterative procedures, just as do other $\mathcal{G}$ values. When this is done there is no discrepancy between our values of C_g for a utilization factor of 0.64 and Gerberich's or Irwin's for a utilization factor of unity. On his second point, we are encouraged to know that Mr. Gerberich has obtained additional evidence which supports the choice of a utilization factor of 0.64 as being realistic and conservative. There is a definite need for information of this sort which will permit us to make more confident estimates of specimen-size limitations.

We will follow with interest Mr. Wells's efforts at using crack-opening displacement measurements in toughness evaluation of low-strength (high-toughness) constructional steels, and we look forward to studying his discussion of triaxiality effects in the paper to be published by the Royal Society.[7]

Mr. Morrison hopes that those engaged in the design of highly stressed structures, and those developing new materials for such structures, will apply fracture toughness test methods. In the authors' experience there is a steadily increasing demand for this type of testing and most alloy producers are now set up to make one or more of the tests described in our paper as a matter of routine.

[7] Further discussion of these subjects appears in the panel discussion, see p. 373.

STP381-EB/Apr. 1965

EVALUATION OF PROPOSED RECOMMENDED PRACTICE FOR SHARP-NOTCH TENSION TESTING

By R. H. Heyer[1]

Synopsis

The objectives and limitations of the proposed recommended practice for determining sharp-notch strength of high-strength sheet materials are given. Two specimen designs are used: 3 in. wide with sharply machined edge notches, and 3 in. wide with a center slot extended in both directions by fatigue cracking. Evaluation test results are reported for sharp-notch strength of four materials: aluminum alloy 7075-T651, titanium alloy 4Al-3Mo-1V, maraging steel 18Ni-9Co-5Mo, and precipitation-hardening stainless steel PH 14-8 Mo.

Test data from seven laboratories are analyzed for differences among laboratories and between the two specimen designs. Agreement among laboratories is generally satisfactory considering inherent difficulties in preparing sharply notched specimens to the close tolerances required. Data from specimens out of tolerance after machining or after fatigue cracking were rejected. Center-cracked specimens have significantly higher sharp-notch strengths than edge-notched specimens in tests on the aluminum alloy and the precipitation-hardening stainless steel.

Test specimens 8 in. long are suggested as alternates for the recommended 12-in. long specimens when insufficient material is available. Significant differences in test results were obtained for the two lengths of specimens.

A proposed Recommended Practice for Sharp-Notch Tension Testing has recently been drafted by the ASTM Special Committee on Fracture Testing of High-Strength Metallic Materials. The present paper is a report on evaluation tests made according to the procedures given in the proposed recommended practice.

The sharp-notch strength of an appropriate specimen is determined by dividing the maximum load sustained in a slow tension test by the initial area of the supporting cross section in the plane of the notches or cracks. This is analogous to the ultimate tensile strength of a standard tension-test specimen, which is based on the area of the specimen before testing.

Sharp-notch tension tests were proposed as screening tests in the first committee report.[2] The effects of notch angle, notch radius, width, and thickness were considered in the design of the test specimens. The specimen width of 1 in. has been increased to 3 in. in the recommended practice. This has been found to be necessary to reduce the tendency to yield plastically on the notched section

[1] Supervising research metallurgist, Armco Steel Corp., Middletown, Ohio.

[2] "Fracture Testing of High-Strength Sheet Materials," *ASTM Bulletin*, No. 244, pp. 18–28 (1960).

when testing the newer alloys having improved toughness.

The objectives and limitations of the recommended practice are further defined in the scope as follows:

1.1 This recommended practice covers apparatus, specimens and procedures for the determination of a comparative measure of the resistance of sheet materials to unstable fracture originating from a very sharp stress-concentrator or crack. It relates specifically to fracture under continuously increasing load and excludes conditions of loading which produce creep or fatigue. The quantity determined is the sharp-notch strength of a specimen of particular dimensions, and this value is determined by these dimensions as well as by the characteristics of the material.

1.2 This recommended practice is restricted to one specimen width which is generally suitable for evaluation of high strength materials (yield strength to density ratio above 700,000 psi/lb. in.$^{-3}$. The test will discriminate differences in resistance to unstable fracture when the sharp-notch strength is less than the tensile yield strength, and the discrimination increases the lower the notch strength is with respect to the yield strength.

1.3 This test is restricted to sheet materials not exceeding 0.25 in. in thickness. Since the notch strength may vary with the sheet thickness, comparison of various material conditions must be based on tests of specimens having the same nominal thickness.

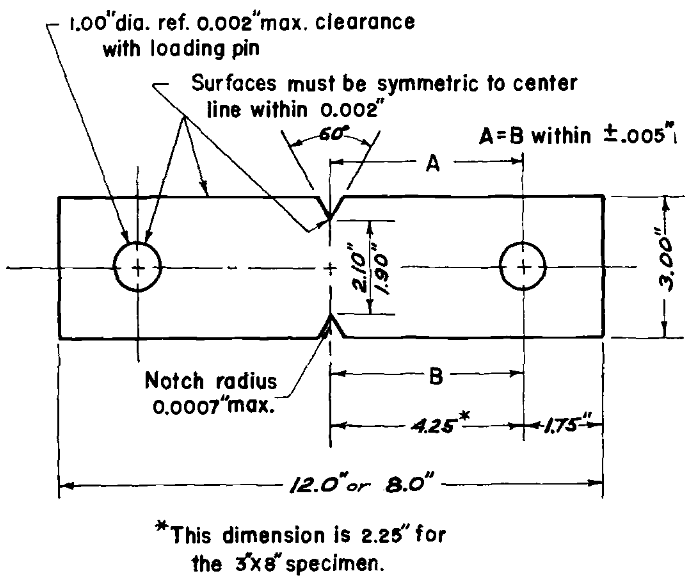

FIG. 1—Machined Sharp Edge-Notched Specimen (EN).

1.4 The sharp-notch strength may depend strongly upon temperature within a certain range depending upon the characteristics of the material. The recommended practice is suitable for use at any appropriate temperature. However, comparisons of various material conditions must be based on tests conducted at the same temperature.

The test is intended to serve the following purposes:

1. In research and development of materials, to study the effects of the variables of composition, processing, heat treatment, etc.

2. In service evaluation, to compare

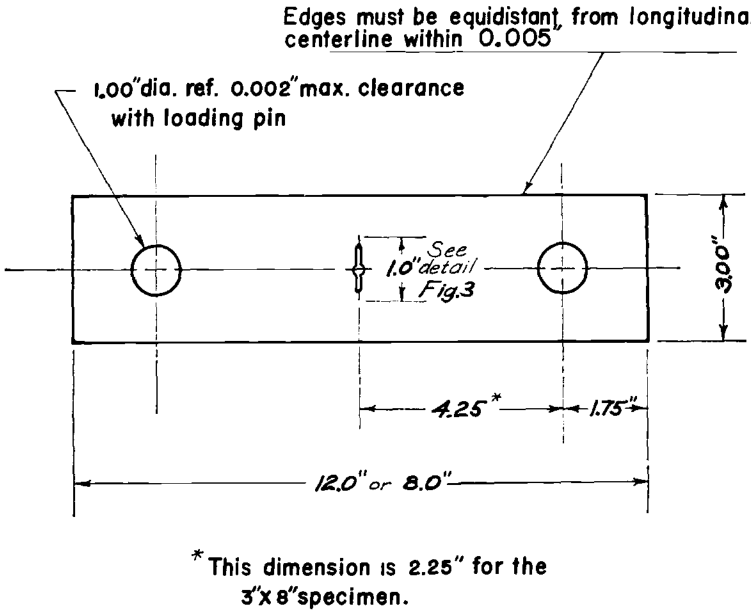

FIG. 2—Fatigue Center-Cracked Specimen (CC).

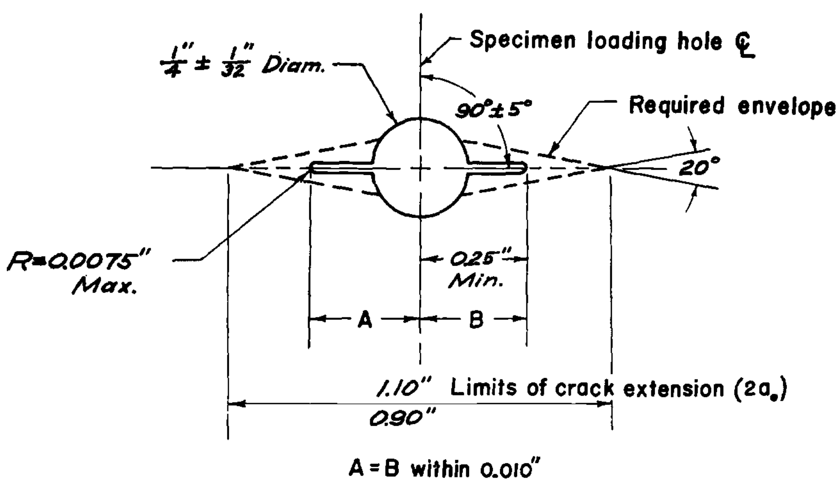

FIG. 3—Suggested Design for Center Fatigue-Crack Starter.

the relative crack-propagation resistance of a number of materials which are otherwise equally suitable for an application, or to eliminate materials when an arbitrary minimum acceptable sharp-notch strength can be established on the basis of service-performance correlation, or some other adequate basis.

3. For specifications of acceptance and manufacturing quality control when there is a sound basis for establishing a minimum acceptable sharp-notch strength. Detailed discussion of the basis for setting a minimum in a particular case is beyond the scope of this recommended practice.

TEST SPECIMENS

Two specimen designs are used. The machined, sharp-edge notch specimen (EN) is shown in Fig. 1, and the fatigue center-crack specimen (CC) in Fig. 2. The preferred length is 12 in.; however, 8-in. specimens are also provided so that tests transverse to the rolling direction may be made in laboratory-rolled sheet, which is often limited in width.

It is important to meet the notch-radius specification of 0.0007 in. maximum for the EN specimen. A method of machining these specimens has been published by March et al.[3]

The CC specimen requires machining of suitable crack-starter notches. Various methods are permissible provided the cuts are contained within the envelope shown in Fig. 3. The machining may be done before heat treating, and the cyclic stressing to extend the center cracks may be done after heat treating; however, this order of operations is not mandatory.

Both specimens are pin-loaded. Clevis-type loading devices and reinforcing plates which may be required to prevent cracking at the pinholes are illustrated in the proposed recommended practice. Methods for temperature control in tests at other than room temperature are also given.

TABLE 1—TRANSVERSE TENSILE PROPERTIES OF MATERIALS USED IN ASTM TEST PROGRAM FOR EVALUATION OF PROPOSED RECOMMENDED PRACTICE FOR SHARP-NOTCH TENSION TESTING.

Material	Thickness, in.	Lab. No.	Tensile Strength, psi	Yield Strength, psi	Elongation in 2 in., per cent
A—Aluminum alloy 7075-T651......	0.25	1	84 800	74 200	13.0
		3	84 000	74 200	13.0
		5	85 200	75 900	10.0
			84 700	74 800	12.0
B—Titanium alloy Ti-4Al-3Mo-1V..	0.062	1	176 000	156 500	8.0
		3	179 400	158 800	6.8
		5	175 700	162 800	6.1
			177 000	159 400	7.0
C—Maraging steel 18Ni-9Co-5Mo...	0.100	1	319 700	311 700	3.0
		3	324 800	312 000	3.0
		5	326 800	323 600	1.0
			323 800	315 800	2.3
D—Precipitation-hardening stainless steel PH 14-8 Mo..............	0.090	1	242 300	215 400	8.0
		3	236 800	217 000	5.5
		5	247 500	233 300	4.7
		7	236 400	212 200	6.5
			240 800	219 500	6.2

PROCEDURE

The test is conducted in a similar manner to an ordinary tension test, at a loading speed such that the increase of nominal stress in the notched or cracked section does not exceed 100,000 psi per minute. The maximum load is recorded.

[3] J. L. March et al, "Machining of Notched Tension Test Specimens," *ASTM Bulletin*, No. 244, p. 52 (1960).

TABLE 2—SHARP-NOTCH STRENGTH.
(Values are given in ksi.)

Edge-Notched (EN) and Center-Cracked (CC) specimens taken transverse to the rolling direction. Specimen length is 12 in. except for indicated tests on 8-in. long specimens.

Material	Lab 1	Lab 2		Lab 3		Lab 4		Lab 5	Lab 6		Lab 7	Tests on 8-in. Long Specimens	
	EN	EN	CC	EN	EN	CC	CC	CC	EN	CC	CC	EN	CC
												Lab 3	
A....	36.0	35.4	38.1	35.8		39.9	37.7	39.9				31.4	
	33.9	33.7	40.4	34.2		39.8	40.0	39.8				32.2	
	36.7	33.8	42.6	35.1		41.3	41.9	40.3				31.6	
	32.7	34.3	37.5	36.7		41.6	42.0	40.1				33.6	
	32.9	36.4	38.0	32.5		40.9	40.0	40.4				31.5	
							40.3						
	34.4	34.7	39.3	34.9				40.1				32.1	
							40.5						
												Lab 6	
B....	80.1	76.1	64.8	68.3	68.1		69.4	59.9	65.7	75.0		55.1	55.8
	59.0	81.4	72.1	70.3	77.6		67.8	77.9	66.4	73.5		52.9	68.0
	68.0	87.3	68.8	62.6			77.1	70.3	86.7	73.0		48.9	58.5
	66.2	80.0	79.8	62.0	67.1		58.0	73.1	81.3	66.5		44.7	69.7
	67.7	78.9	70.3	60.9			64.6	76.7	54.4	67.5		55.6	69.5
							75.4						
	68.2	80.7	71.2					71.6	70.9	71.1		51.4	64.3
							68.7						
C....	100.0	102.9	89.1	92.1			90.7	86.6	85.6	104.8		78.4	106.1
	97.5	88.0	91.5	90.3			98.5	84.4	88.0	94.0		84.2	105.2
	96.2	107.3	90.1	92.7			90.9	91.3	87.2	89.0		84.7	99.7
	96.8	92.0	92.6	93.2			98.6	88.7	89.0	92.4		83.0	100.5
	86.7	111.6	90.8	89.2			89.5		80.3	95.0		82.7	98.6
				87.1				87.8					
	95.4	100.4	90.8				93.6		86.0	95.0		82.6	102.0
				90.8									
												Lab 7	
D....	154.1	155.0	164.9	145.2			162.0	144.7			155.6		169.7
	158.6	154.5	164.5	141.1			156.6	157.3			157.0		171.0
	154.2	158.8	164.2	144.1			158.2	153.8			158.6		171.8
	150.7	158.6	161.5	145.1			157.3	153.7			159.3		172.5
	151.1	161.4	162.1	139.7			155.7						
								152.4			157.6		171.2
	153.7	157.7	163.4	143.0			158.0						

The net cross-sectional area of the EN specimen is determined from the distance between notch-root radii measured before testing. In the case of the CC specimen, the width of the net section is determined after fracture by subtracting the distance between the most advanced points of the fatigue cracks from the specimen width. It should be noted that the net sections are based on the area of uncracked metal before testing, and do not take into account possible reduction in this area due to slow crack growth before fracture.

The proposed recommended practice outlines a procedure for estimating and reporting fracture appearance.

The tensile yield strength is de-

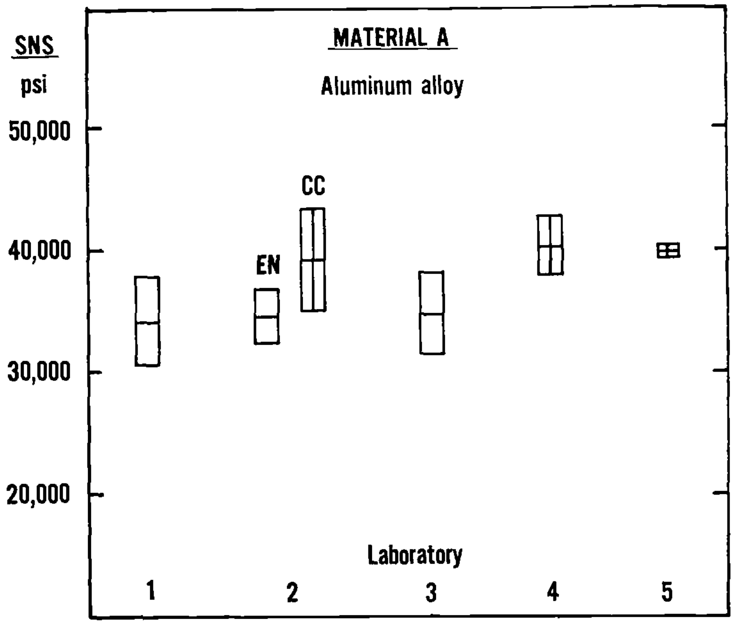

FIG. 4—Comparison of Sharp-Notch Strength Tests of Material A.

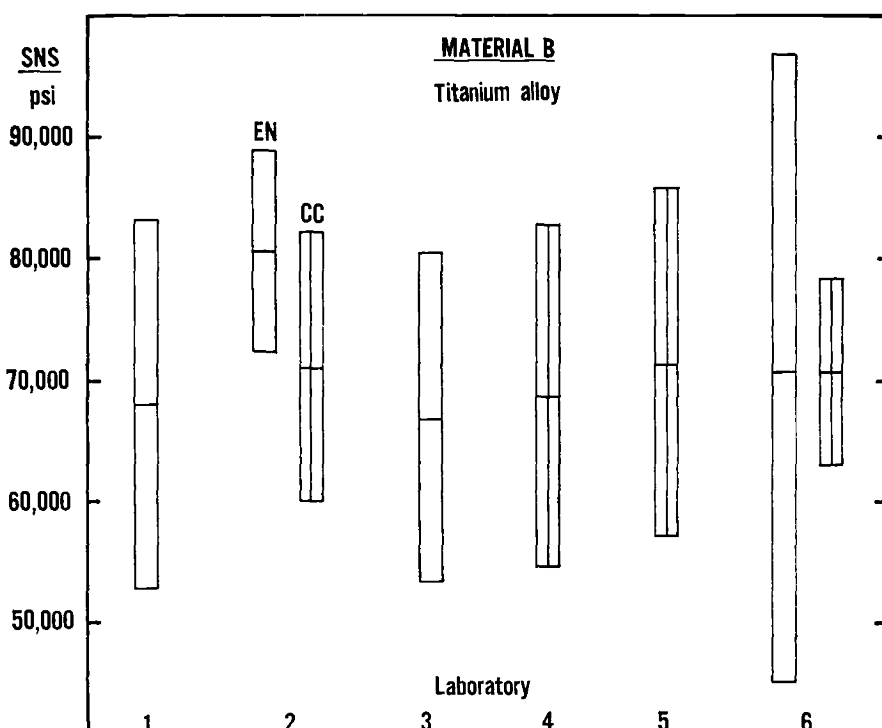

FIG. 5—Comparison of Sharp-Notch Strength Tests of Material B.

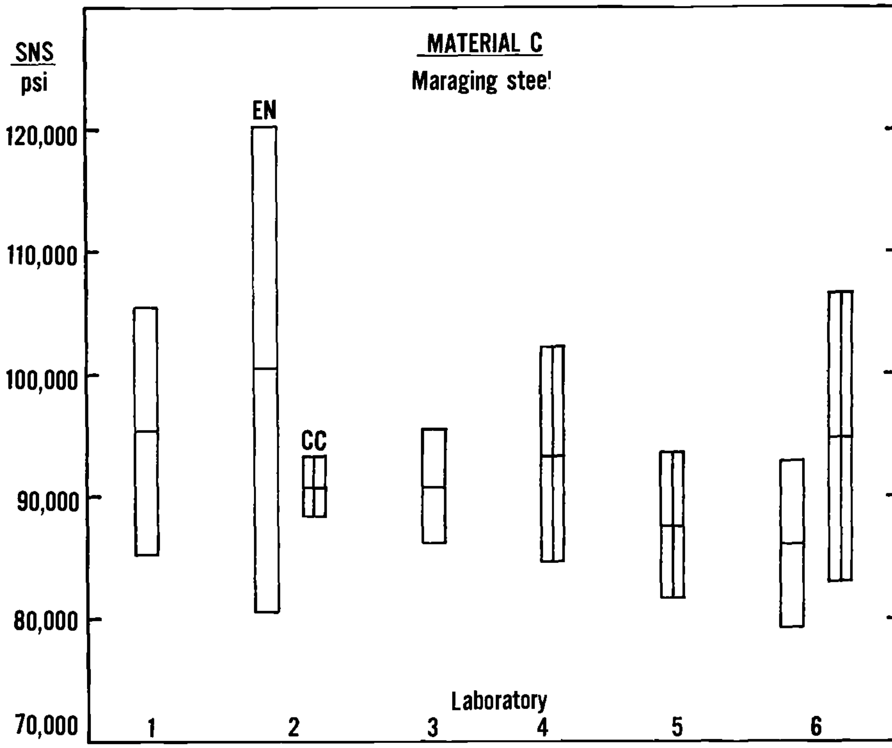

FIG. 6—Comparison of Sharp-Notch Strength Tests of Material C.

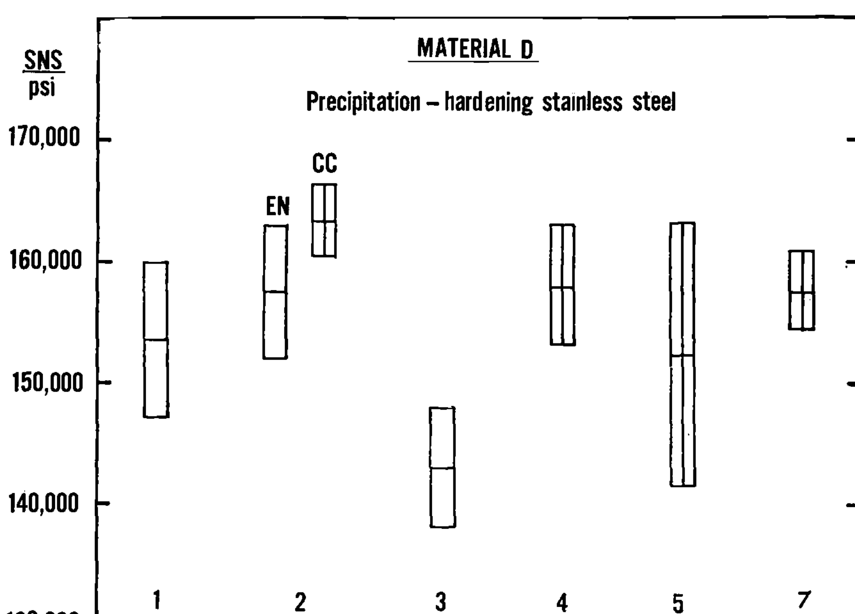

FIG. 7—Comparison of Sharp-Notch Strength Tests of Material D.

termined using a standard tension-test specimen processed in the same manner as the sharp-notch specimen. The ultimate tensile strength, the yield strength, and the ratio of the sharp-notch strength to the tensile yield strength are reported.

EVALUATION TESTS

The test materials and their standard tensile properties are given in Table 1 and the sharp-notch strength data are listed in Table 2. The aluminum and titanium alloys were sent to the cooperating laboratories in the hardened condition. The steels were supplied as solution-annealed. The maraging steel was aged by the testing laboratory, while the precipitation-hardened steel was returned to the supplier for heat treatment after machining. All tests were made in the transverse-to-rolling direction.

Specimen preparation for sharp-notch tension testing is inherently more difficult than for conventional tension testing, and the test results are more sensitive to deviations from standard tolerances. Three sets of test results, two edge-notch and one center-cracked, were rejected because the specimens were out of tolerance, either in machined dimensions or after fatigue cracking. This was the first attempt by most of the participating laboratories to produce these specimens, and the number of successful tests indicates that the procedure can be carried out and useful results obtained.

The data for the 12-in. long specimens are represented in Figs. 4–7 as mean values $\pm 2\ \sigma$ limits. The mean sharp-notch strengths and standard deviations of the four test materials are summarized in Table 3. The ratios of sharp-notch strength to yield strength are also given in the table. All of the materials were heat-treated to a relatively high strength for the grade, and the sharp-notch strengths are well below the yield strengths.

Data for each material were tested for differences in precision and in mean values among laboratories, and for differences between the means of EN and CC specimens.

TABLE 3—MEAN SHARP-NOTCH STRENGTHS (SNS) AND STANDARD DEVIATIONS (σ).
(Values are given in ksi.)

Material	EN		CC		Pooled	Ratio,
	Mean	σ	Mean	σ	σ	SNS/YS
A.............	34.7	1.6	40.1	1.4[a]	1.5	0.50
B.............	71.2	8.1	70.5	6.1	7.2	0.44
C.............	93.0	5.8[a]	92.0	4.1	5.1	0.29
D.............	151.5	2.9	158.2	3.0	3.0	0.70

[a] There were significant differences in precision among laboratories.

Significant differences in precision, using the chi-square test, or in means, using the Student's t test, could not be established at the 95 per cent confidence level except for the instances cited below.

Material A:

The precision of the CC tests of Laboratory 5 is higher than for other tests of this material, or for tests of any of the materials. The mean values of EN tests are lower than those of CC tests (see Table 3).

Material B:

The precision of the EN tests of Laboratory 6 is lower than for other tests of this material. The mean value of the EN tests of Laboratory 2 is higher than the grand mean (80,700 compared to 71,300).

Material C:

There are differences in precision among laboratories making EN tests (also for CC tests at the 90 per cent confidence level). The mean values of EN tests of Laboratories 2 and 6 are different from the grand mean (100,400 and 86,000 compared to 93,000).

Material D:

The mean value of the CC tests of Laboratory 2 is higher than the grand mean (163,400 compared to 158,200).

TABLE 4—SHARP-NOTCH STRENGTH TESTS OF 12-IN. AND 8-IN. SPECIMENS.
(Values are given in ksi.)

Material	Specimen Type	12-in. Length		8-in. Length		Difference	Confidence Levels[b]
		Mean	σ	Mean	σ		
B.........	CC	71.1	±3.8	64.3	±2.1	−6.8	98
C.........	CC	95.0	±5.9	102.0	±3.4	+7.0	90
D.........	CC	157.6	±1.7	171.3	±1.2	+13.7	99
A.........	EN	34.9	±3.4[a]	32.1	±0.9[a]	−2.8	80
B.........	EN	70.9	±13.0[a]	51.4	±4.6[a]	−19.5	95
C.........	EN	86.0	±3.4	82.6	±2.5	−3.4	80

[a] Significant difference in variance.
[b] The differences between 12-in. and 8-in. tests are significant at the indicated confidence levels.

The mean values of the EN tests of Laboratories 2 and 3 are different from the grand mean (157,700 and 143,000 compared to 151,500).

The mean values of the EN tests are lower than for the CC tests (see Table 3).

All Materials:

There were no significant differences in precision between EN and CC tests; however, the CC test results are higher than the EN for Materials A and D.

More deviation in test values was observed in tests of Materials B and C than for tests of Materials A and D (see Table 3).

Tests on the proposed alternate 8-in. long specimen and the 12-in. specimen are compared in Table 4. In some cases the differences are small and are significant only at reduced confidence levels, as low as 80 per cent.

These differences are believed to be related to stress-distribution patterns as influenced by pin loading. In the case of the EN specimens, relatively higher stresses would be expected in the vicinity of the notches of the shorter specimens, resulting in lower sharp-notch strength. In the case of the CC specimens, relatively lower stresses would be expected in the central region of the shorter specimens, resulting in higher sharp-notch strength. An exception to this pattern is the data for CC tests of Material B. It is interesting to note that the variance for the 8-in. tests is smaller than for the 12-in. tests in every case. However, only in two instances were these differences in variance shown to be significant at the 95 per cent confidence level.

SUMMARY

The general agreement among laboratories in determining the sharp-notch strength of four typical high-strength materials is quite satisfactory. It was not expected that the precision or the accuracy of the test would be equal to that of conventional smooth-bar tension tests, and the results obtained in this first trial of a new test specimen are gratifying.

On the other hand, not all laboratories were able to prepare the specimens within the proposed tolerances. While no action has been taken by the committee, the task group will recommend that the proposed specimens and procedures be used as a recommended practice without substantial modification until more experience is gained.

A statement should be added to the recommended practice noting that differences may be expected between results of EN and CC tests. It is stated in the draft copy that the 8-in. long specimen should be used only as an expedient when insufficient test material is available for the 12-in. specimen.

Acknowledgment:

The evaluation tests were made in the laboratories of the following companies: Allegheny Ludlum Steel Corp., Aluminum Company of America, Armco Steel Corp., The Boeing Co., Douglas Aircraft Co., Titanium Metals Corp., Thompson Ramo Wooldridge Inc., and at Lewis Research Laboratories of NASA.

DISCUSSION

J. G. KAUFMAN.[1]—At the Alcoa Research Laboratories, we use edge-notched tension specimens of the design in Fig. 8 for sharp-notch tension tests of aluminum alloy sheet and ¼-in. thick plate. This design meets all of the requirements of the ASTM specimen (Fig. 1, EN), but has wider grip ends so that it may be loaded through a single pin at each end, without the need for the stiffener plates and without fear of fracture at the loading holes. Data obtained with the two designs of specimen are given in Table 5. There is no significant difference in values of notch tensile strength.

We wish to emphasize the point made by Mr. Heyer that the results of sharp-notch tension tests are extremely dependent upon the thickness of the material. For example, data in Fig. 9 for 7075-T6, -T651 and 7079-T6, -T651, show the magnitude of the effects over the thickness range from 0.063 to 0.250 in. Therefore, for valid comparisons of different compositions or tempers of sheet or thin plate, the thickness should be maintained constant, or when this is not possible, the thickness should be considered a variable in the tests.

R. H. HEYER (*author*).—The Alcoa sharp-notch tension specimen, Fig. 8, is

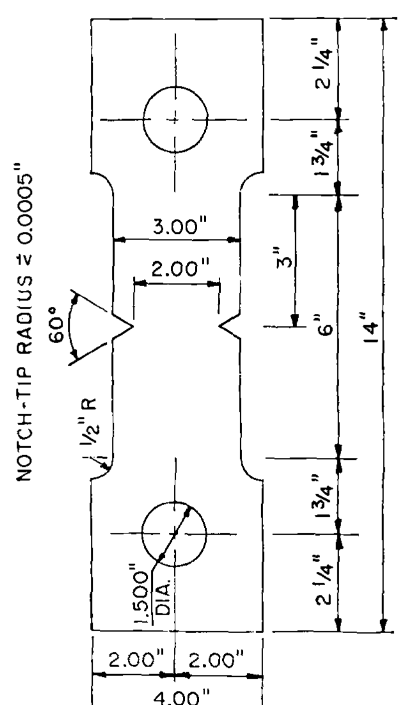

FIG. 8—Sharp-Notch Tension Specimen.

[1] Assistant chief, Mechanical Testing Div., Alcoa Research Labs., New Kensington, Pa.

TABLE 5—SHARP-NOTCH TENSILE STRENGTH, psi.

ARL Design, Fig. 8	ASTM Design, Fig. 1, EN
36 200	35 800
34 600	34 200
34 300	35 100
32 400	36 700
34 200	32 500
34 300	34 900

distribution at the notch. On the other hand, tests by Laboratory 3 on aluminum alloy 7075-T651 using the short specimen (8-in. length) were 8 per cent lower than for the regular (12-in. length) specimen, as shown in Table 2. The short specimen will not be designated as a standard specimen in the recommended practice.

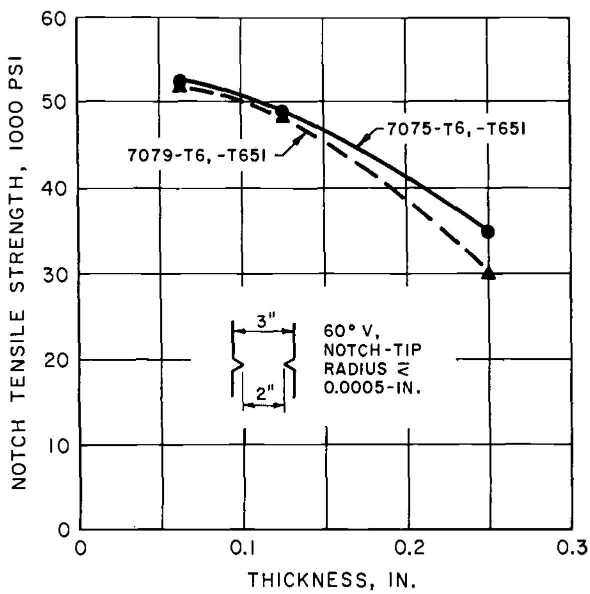

FIG. 9—Effect of Thickness on Notch Tensile Strength of 7075-T6, -T651, and 7079-T6, -T651 Sheet and Plate.

longer over-all and between loading holes than the regular 12-in. long specimen used in the committee's evaluation program. Since no difference in test results was obtained using the two specimen designs, the 12-in. specimen appears to be sufficiently long to give good stress

The effect of specimen thickness on sharp-notch strength was not included as a variable in the evaluation program. We appreciate Mr. Kaufman's data, Fig. 9, which call attention to this important variable in sharp-notch tension testing.

STP381-EB/Apr. 1965

ELECTRON FRACTOGRAPHY—A TOOL FOR THE STUDY OF MICROMECHANISMS OF FRACTURING PROCESSES

BY C. D. BEACHEM[1] AND R. M. N. PELLOUX[2]

SYNOPSIS

Uses of the electron microscope for the study of fracture surfaces and the subsequent formulation of models of fine-scale fracture mechanisms are demonstrated. Electron fractography is shown to be a valuable tool in obtaining a better understanding of fracture and in the analysis of service failures.

Various types of fracture surfaces produced by single-cycle overload and by fatigue in various materials are discussed in order to indicate the usefulness of this relatively new tool.

The scope of application in the general field of fracture research is indicated.

Visual and low-magnification observations of fracture surfaces have for a long time aided engineers in their fracture analyses. The "rock-candy" appearances of burnt steel, the concentric growth rings of fatigue, and the chevron markings of brittle fractures are examples of the use of low-power optical microscopy in the study of fracture surfaces. A powerful means of investigation has recently been added with the advent of the use of the electron microscope.

The electron microscope has shown conclusively that the large majority of materials, including engineering materials, fracture by the nucleation and growth of minute submerged free surfaces (cracks or voids) to form incremental advances of fracture. It is frequently the properties of, and conditions at, the tiny volumes of material associated with each increment of fracture which determine the resistance to fracture. The strength of interfacial bonds between constituent particles and between grains, the cleavage strength of intermetallics, the residual stresses around constituent particles, and the location, shape, size, density, and properties of constituent particles and grains are a few of the factors that determine what will occur at the tip of a crack. To understand fracture, one must be able to measure and predict all the forces and properties in the entire system, whether they be such large-scale factors as the stiffness of the testing equipment, intermediate scale factors such as stress concentration at the root of a notch, or fine-scale factors such as the forces necessary to move dislocations.

Research work with simple materials such as ionic crystals and metallic single crystals has resulted in some understanding of the basic mechanisms of fracture. On another scale, numerous

[1] Head, Micromechanical Metallurgy Section, Physical Metallurgy Branch, Metallurgy Div., U.S. Naval Research Laboratory, Washington, D. C.

[2] Head, Materials and Processes Unit, Turbine Div., The Boeing Company, Seattle, Wash.

mechanical tests of engineering materials have been done by engineers in order to evaluate and select materials for the design of useful structures. Thus research is progressing at both ends of the presently known spectrum—from bonding strength between two atoms to plane-strain fracture toughness. Though progress is being made in both the metal physics and the continuum mechanics approaches, researchers in the two fields have not been able fully to benefit from each other's results. This is partly due to the microstructural complexities of the structural materials investigated in fracture mechanics and partly because there is a large difference in scale (size) between some of the factors investigated in the two approaches.

Observations and studies of fracture surfaces at high magnification with the electron microscope (often called electron fractography) include studies of the relationships between the surface topography and the microstructure, as well as studies of the chronological order of fine-scale events taking place during fracture. The use of this new technique shows promise of helping bridge the gap between the metal physics and continuum mechanics approaches by providing qualitative assessments of micron-scale fracture processes and quantitative measurements of some of the fracture variables that are not measured in either of the above approaches.

USES OF ELECTRON FRACTOGRAPHY

Fracture surfaces are usually studied by using the following procedures: (*1*) observing cross sections of the fracture to relate the fracture surface to the structure of the underlying metal; and (*2*) observing the fracture surface along a direction normal to the macroscopic plane of fracture. Though both methods are necessary for the study of some aspects of fracture, the second method provides a much more general and complete view of the features of the fracture surface. For instance, if one wishes to determine the relative proportions of intergranular and transgranular fracture, it would be far easier to observe the fracture at an angle normal to the macroscopic plane of the fracture than it would be to make a large number of fracture-profile studies. The difference in amount of time and work necessary to find out the shape, size, and distribution of intergranular constituents on an intergranular fracture is even more striking.

The electron microscope—with a large depth of field, a high resolving power, and a large range of magnification—is an ideal tool for use in the study of fracture surfaces. Fractures should be studied on all scales, and electron fractography does not replace optical microscopy or observations with the unaided eye. An electron fractograph by itself, for instance, cannot always indicate whether the macroscopic fracture was brittle or ductile. Electron fractography, then, should be considered as a complementary tool for fracture studies and failure analyses.

Two types of electron microscopes are presently being used to study fracture surfaces. The scanning microscope permits, with limited resolution, the direct study of the fracture surface itself. This has the advantage that one can observe changes on the fracture surface as they occur. For instance, Jacoby[3] has described the ionic etching of fatigue fractures in the scanning microscope while the surface was being observed. The conventional electron microscope has a higher resolving power than the scanning microscope, but has the disadvantage that the fracture itself is not directly

[3] Private communication from Gerhard Jacoby, Institut für Festigkeit, Mülheim/Ruhr, Germany.

observed. Very thin replicas of the fracture surface must be prepared and transferred into the microscope for study. Though there are some inherent disadvantages to such an indirect method of study, replica techniques offer so many advantages that they are used almost exclusively in electron fractography.

One of the main advantages of the replica technique results from shadowing. In order to have a better contrast, the replicas used in electron microscopy are shadowed with a heavy metal evaporated under a low angle with respect to the fracture surface. This shadowing brings out the relative heights and depths of the features of the fracture surfaces. When a detailed study of the three dimensions of the fracture features is needed, stereo pairs of photomicrographs can be taken. After enlargement, the stereo pairs are studied at leisure with a stereo viewer.

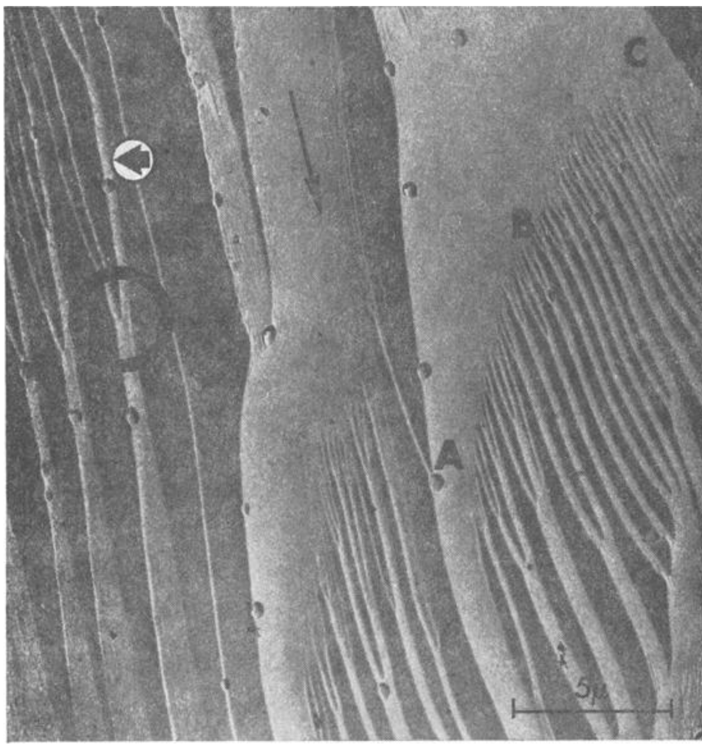

FIG. 1—Cleavage Fracture in an Alnico Alloy. A Typical Cleavage Step Is Indicated by the Horizontal Arrow.

The circle shows where two steps converge to form part of a river pattern. The river markings along *ABC*, probably originating at a twist-boundary, are clearly due to cleavage along a secondary cleavage plane. Local propagation direction is shown by the upper arrow. Two-step replica. (Reprinted from Ref (2).) 6000×. Reduced one-third in reproduction.

During the preparation of the replicas, the direction of shadowing can be selected in such a way as to coincide with the macroscopic direction of crack propagation. In this manner, the orientation of each micrograph with respect to the

FIG. 2—Cleavage Fracture Surface of a Low-Carbon Steel Broken by Impact at 78 K.

ABC is a grain boundary; *BD* is a typical river marking. The long arrows indicate local crack-propagation directions and the circled arrow indicates a cleavage step. The facet *F* is due to cleavage along a deformation twin. Direct carbon replica. (Reprinted from Ref (2).) 5500×. Reduced one third in reproduction.

general direction of crack propagation will always be known.

Finally, in many cases the replicas can be prepared in such a way as to extract *in situ* some of the second-phase particles present on the fracture surface. With these extraction replicas it is possible to analyze by electron diffraction the nature of the second-phase particles responsible for the local initiation and propagation of the fracture.

When fracture surfaces are observed at increasingly higher magnifications, the extremely complex nature of the fracture features becomes more and more apparent. Electron fractographs show clearly that structural materials generally cannot be considered as homogeneous

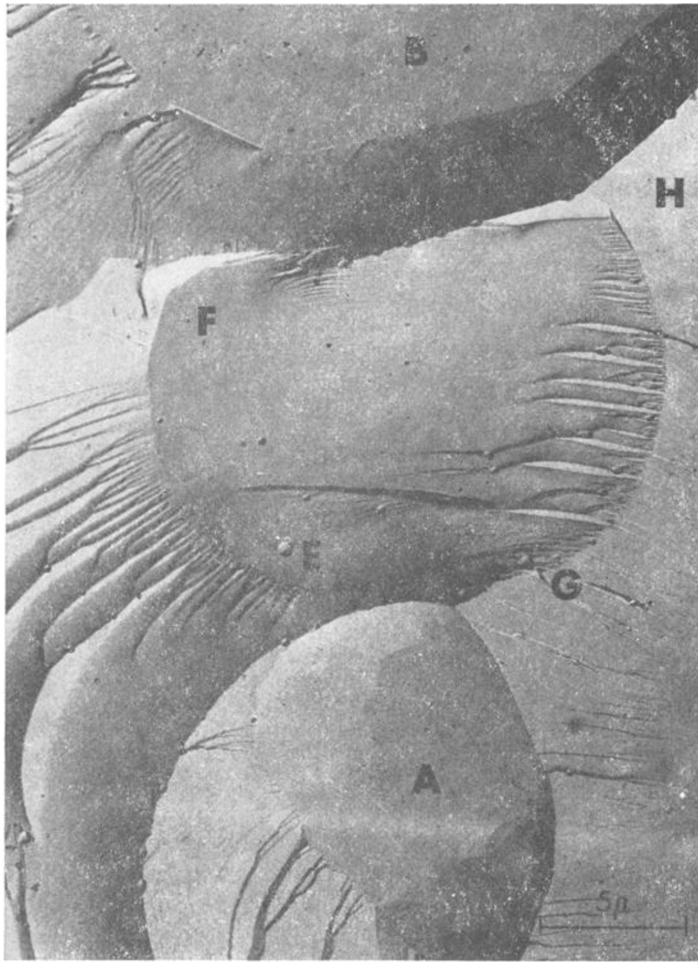

FIG. 3—Typical Cleavage Fracture Through Many Grains of an Alnico Alloy.

The grain boundaries *EF* and *GH* are clearly at the origin of the formation of cleavage steps. In grains *A* and *B*, fracture was intercrystalline. Two-step replica. (Reprinted from Ref (**2**).) 5600× Reduced one third in reproduction.

continual and that no simple dislocation models can by themselves entirely explain the fracture processes. However, in spite of the complex appearance of a fracture surface, it is possible to see, at high magnification, that a given mechanism of fracture is associated with a certain number of characteristic fracture features (**1**).[4] So far, the major part of the work done by electron fractography has been to study and classify the fine-scale features present on the fracture surfaces of known materials broken under controlled conditions. It is not possible, in general, to account for the formation of these features in terms of the simple models of fracture. However, the topography of the fracture surface and the fine-scale features can frequently be related to the microstructure of the

[4] The boldface numbers in parentheses refer to the list of references appended to this paper.

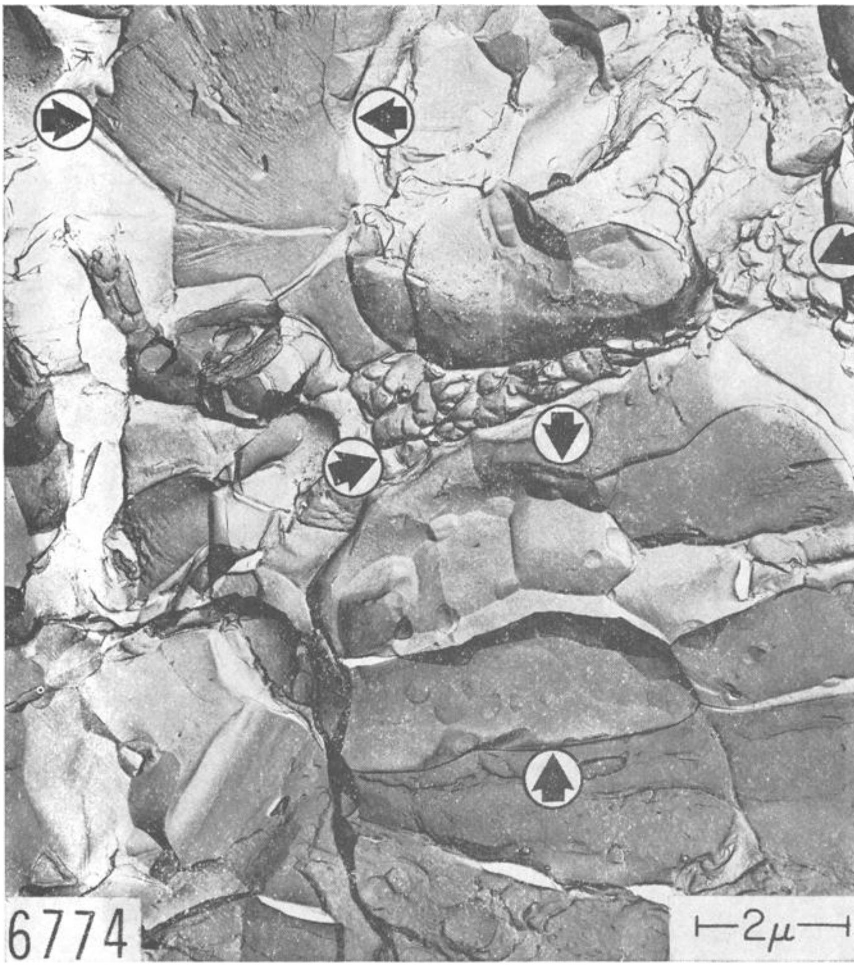

FIG. 4—Overload Fracture in a 7075-T6 Aluminum Alloy, Showing Cleaved Intermetallic Between Horizontal Arrows, Dimples Between Oblique Arrows and Intergranular Fracture Through Intermetallic Particles (vertical arrows). Direct Carbon Replica. 15,000×. Reduced One Third in Reproduction.

material. Since the fracture path is the path of least resistance, a close study of the fracture surface should reveal some of the structural weaknesses of the materials. This type of systematic study of the local origin of fracture shows the importance of electron fractography in the analysis of service failures. It is presently one of the major applications of this new tool. An example will be given later.

FRACTURE MECHANISMS STUDIED BY ELECTRON FRACTOGRAPHY

As observations are made at varying magnifications, specific features become either less or more prominent. Just as an astronaut in orbit may see a whole mountain range while a prospector on foot may see the types of minerals contained in individual rocks, unaided visual observations of fracture surfaces reveal some features not seen in the electron microscope. Of course the same is true in reverse, since many of the features discovered in the electron microscope cannot be resolved at lower magnifications. Various materials and various fracture terminology. The terms "silky," "woody," "fibrous," "rock-candy," "intergranular," "transgranular," "ductile," and "brittle" are still useful in describing fractures, but they are wholly insufficient

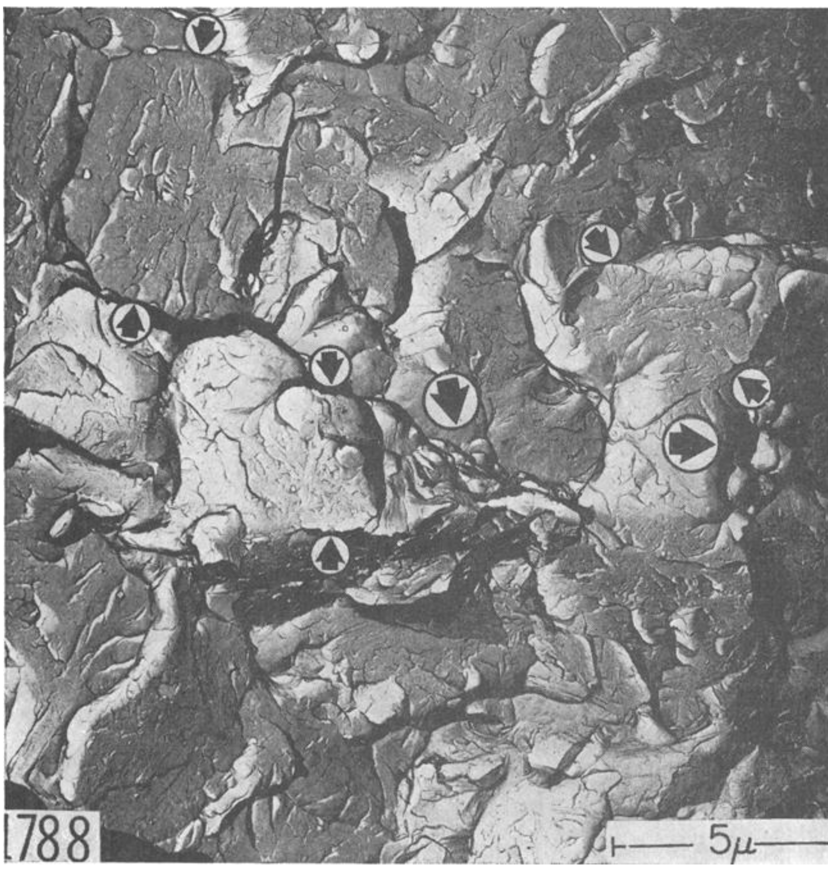

FIG. 5—Quasi-Cleavage and Dimpled Rupture in AISI Type 410 Stainless Steel, Quenched, Tempered, and Broken at Room Temperature.

Examples of quasi-cleavage facets are shown between the small arrows, and groups of dimples are indicated by large arrows. Palladium-shadowed direct carbon replica. (Reprinted from Ref (6).) 9200×. Reduced one third in reproduction.

conditions result in a large variety of different fracture-surface features. These features, viewed at higher and higher magnifications, could be differentiated again and again and classified into groups, subgroups, etc. This would lead to a complex but necessary system of to report and explain the fine-scale features of fracture surfaces. The terminology used to describe the characteristic fine-scale features of fracture surfaces has been selected after a careful consideration of what is presently known about the mechanisms of fracture.

FIG. 6—Fine-Scale Markings on a Quasi-Cleavage Facet in Quenched and Tempered Type 410 Stainless Steel Broken at Room Temperature.

The fracture-initiation region for this facet is seen just to the lower right of the center of the facet. The large arrows point out the boundaries of the facet while the small arrows indicate river patterns which lead away from the center of the facet. Palladium-shadowed two-stage carbon replica. (Reprinted from Ref (6).) 9200×. Reduced one third in reproduction.

The fracture mechanisms selected for discussion in this paper are classified as follows: (*1*) cleavage; (*2*) micro-void coalescence; (*3*) quasi-cleavage; (*4*) intergranular separation; and (*5*) fatigue.

CLEAVAGE

Cleavage is defined as the separation of a crystal along certain crystallographic planes. A typical example of a perfect cleavage fracture is the fracture of crystals of mica which split along their weakly-bonded basal planes.[5] Many other crystalline substances including metals with body-centered cubic or hexagonal structures fracture by separation along planes of high atomic density. Cleavage fracture of metal crystals is always preceded and accompanied by some plastic deformation. This means that it is not a simple process of separation along atomic planes and some of the fracture features will be related to this small amount of plastic deformation.

Examples of cleavage fracture surfaces are shown in Figs. 1–4. One might expect the two fracture surfaces created by cleavage to be perfect planes, but a single crystal is never perfect and so the cleavage crack does not follow a single plane through the entire crystal. Its actual path is usually broken up along parallel sets of cleavage planes. The steps between the parallel planes (horizontal arrows in Figs. 1 and 2) have been shown to form by cleavage along a secondary set of planes or by plastic shearing (3,4). These steps converge as the fracture propagates, and the resulting fracture surface exhibits "river patterns" which are typical of most cleavage fracture. When the steps between cleavage planes converge they usually combine to form a larger cleavage step (as shown in the circled area on Fig. 1). Screw dislocations, either present in the crystal or created by plastic deformation at the tip of the

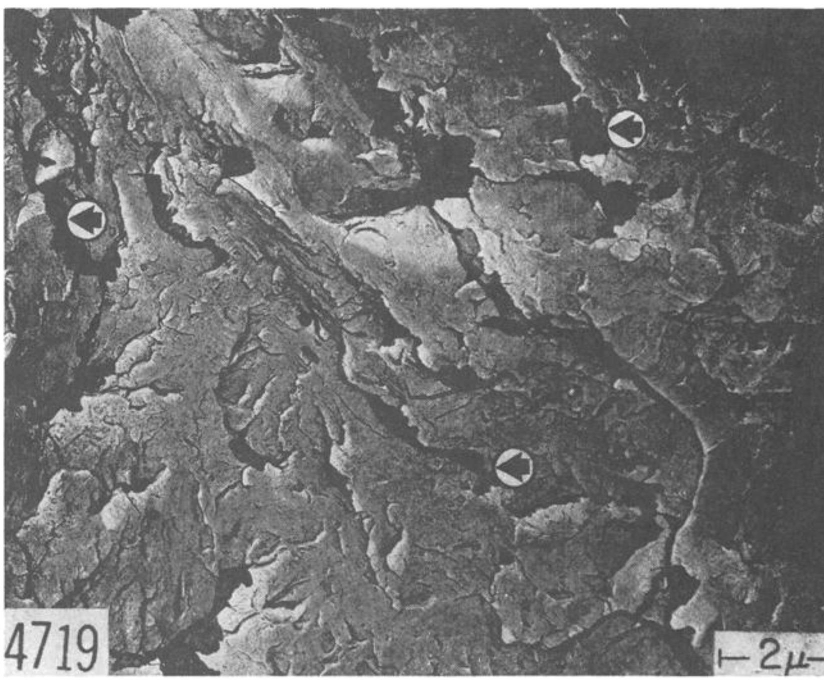

FIG. 7—Quasi-Cleavage in H-11 Steel Broken at Liquid-Nitrogen Temperature. Under Such Conditions Many Steels Fracture with a Tendency to Shatter, Producing Secondary Cracks Seen Here as Dark Bands (Arrows). (Reprinted from Ref (6).) 12,000×. Reduced One Third in Reproduction.

[5] Portions of the text and certain fractographs in this paper are taken from Ref (2).

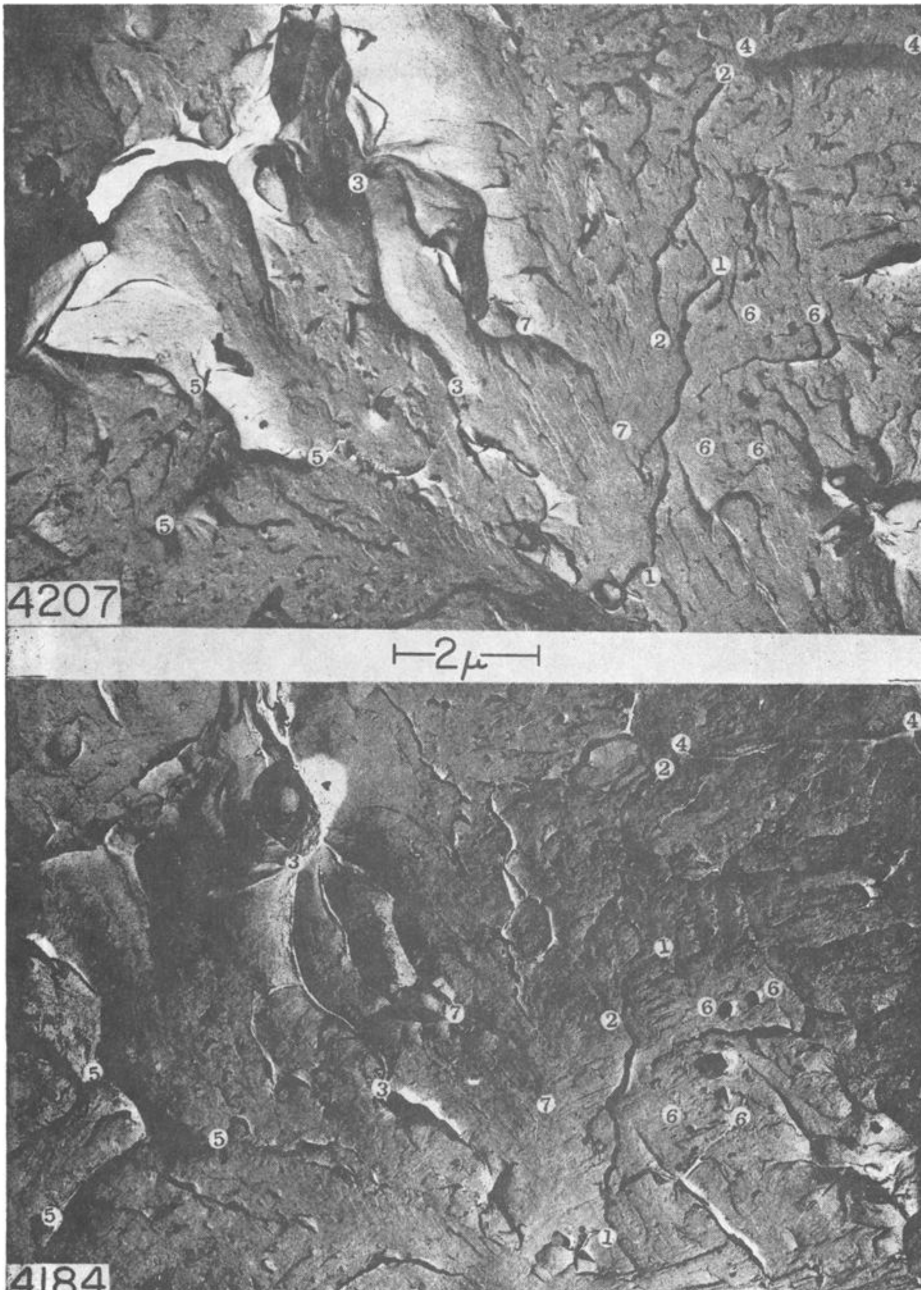

FIG. 8—Matching Quasi-Cleavage Facets from the Two Halves of a Hardened and Tempered AISI 410 Stainless-Steel Wire Broken in Tension at 50 F.

Stereo viewing showed three features of quasi-cleavage which are indicated between numbers. Between numbers 1–1 and between numbers 2–2 are steps, similar to those in true cleavage, seen as dark lines. The numbers 3–3 and 4–4 indicate examples of tear ridges and the 5's show where three tear ridges converge. "Tongues," similar to those found in true cleavage, are seen in the regions bounded by 6's. Between the numbers 7–7 is an example of a step merging with a tear ridge. Cellulose acetate replica technique. (Reprinted from Ref (**6**).) 14,500×. Reduced one third in reproduction.

advancing crack, are considered to be responsible for the formation of cleavage steps on the fracture surface. The best illustration of this explanation is the sudden increase in the number of cleavage steps that occur when the crack crosses a region of high screw dislocation density such as at a twist boundary (line ABC in Fig. 1) or at a grain boundary.

Other features of cleavage are seen in the fan-like cleavage of, for example, the intermetallics in 7075-T6 aluminum alloy (Fig. 4) and the feather-like appearance of cleavage fracture in a tungsten single crystal (5).

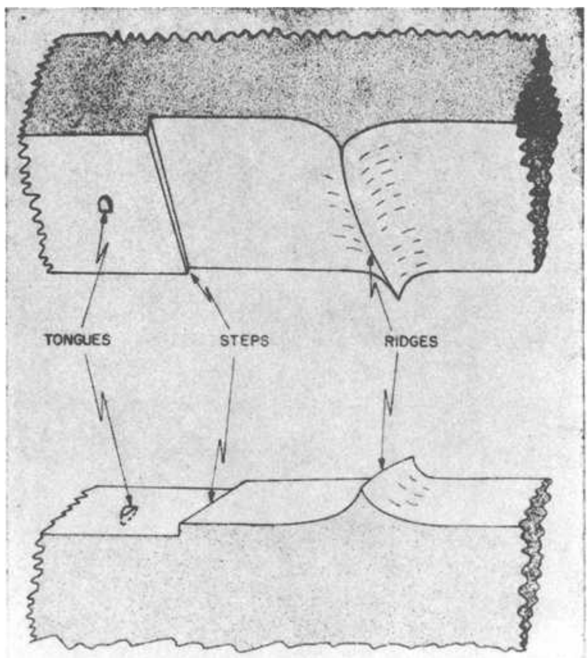

FIG. 9—Simplified Sketches of Three Distinctly Recognizable Features of Quasi-Cleavage. Mating fracture surfaces show steps and tongues which mate as in true cleavage, and tear ridges which protrude from both surfaces and therefore do not resemble true cleavage. Tear ridges are similar to the chisel edges that result from stretching apart very ductile tension specimens. (Reprinted from (Ref (6).)

QUASI-CLEAVAGE

In addition to the influence of grain boundaries and subgrain boundaries on the cleavage fracture of metals and alloys, other fine-scale features of the microstructure such as precipitates and nonmetallic inclusions, may also play an important role and can lead to rather complex mixtures of fracture modes. Thus, in quenched and tempered steels containing fine dispersions of carbide particles, several fracture modes may be distinguished.

In many of these steels, fracture surfaces created at temperatures considerably above the ductile-to-brittle transition temperature range are made up of dimples, while those created at temperatures considerably below the transition range are mainly composed of flat facets and other features that sometimes strongly, and sometimes weakly, resemble cleavage. At temperaturse within, and near, the transition temperature range, various percentages of both dimples and flat facets are found. No abrupt change in fracture mode has been found.

It has been observed that the flat facets that resemble cleavage are far larger than the discrete, fine-scale features of the tempered martensite, and that the orientation of the facets cannot definitely be related to cleavage planes in the ferrite matrix. Therefore, Srawley[6] suggested that the term "quasi-cleavage" be used to distinguish these facets from true crystalline cleavage planes. Since it is necessary to discuss the fine-scale features of low-energy fracture in quenched and tempered steels, terminology must be coined which describes adequately the newly observed features. Quasi-cleavage is admittedly unprecise, but most accurately describes this type of fracture.

In quenched and tempered martensites, quasi-cleavage is defined as a fracture mode which produces individual planar, or nearly planar, fracture facets which are transgranular with respect to the prior austenite grains. Examples are shown in Figs. 5–8,[7] and sketches of some of the features are shown in Figs. 9 and 10. Figure 5 shows a number of quasi-cleavage facets while Fig. 6 delineates the boundaries of a single facet. Figure 5 shows dimples which are often observed between facets.

Figure 6 shows river patterns which indicate that the fracture origin for this facet was within the facet rather than at the edge where fracture would originate in true cleavage. This figure provides clear indications that quasi-cleavage fractures propagate in a step-wise

[6] Private communication from J. E. Srawley.

[7] This subject is discussed more fully in Ref (**6**). Some of the illustrations here are reprinted from that reference.

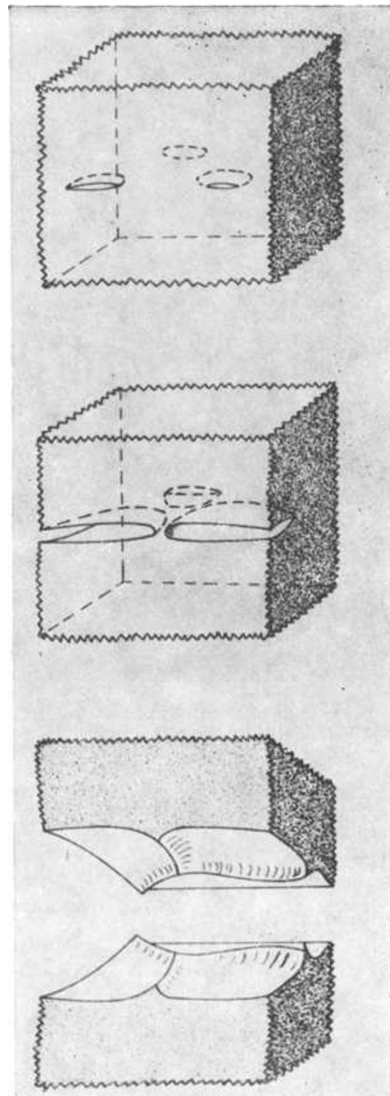

FIG. 10—Sketch of a Frequently Observed Feature of Quasi-Cleavage.

Three submerged cracks, lying in approximately the same plane, grow together from top to bottom in the sketch. Plastic deformation at their tips, as they approach one another, causes the formation of tear ridges on both fracture surfaces. Though three submerged cracks are sketched—with three resultant tear ridges intersecting one another—other configurations of joined ridges develop from other combinations of submerged cracks. (Reprinted from Ref (**6**).)

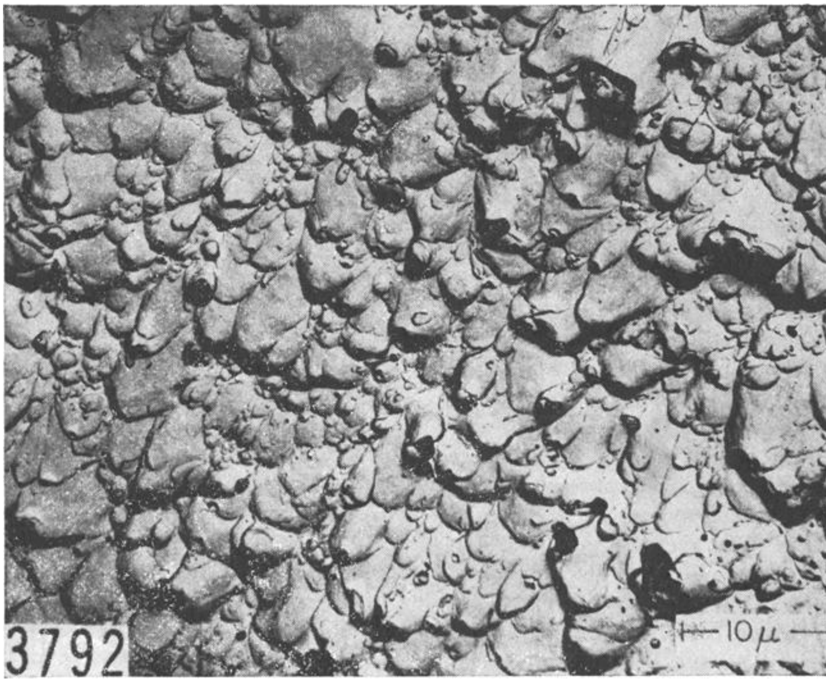

FIG. 11—Typical Shear-Rupture Dimples on Surface of Shear Lip in a Steel Specimen. 3000×. Reduced One Third in Reproduction.

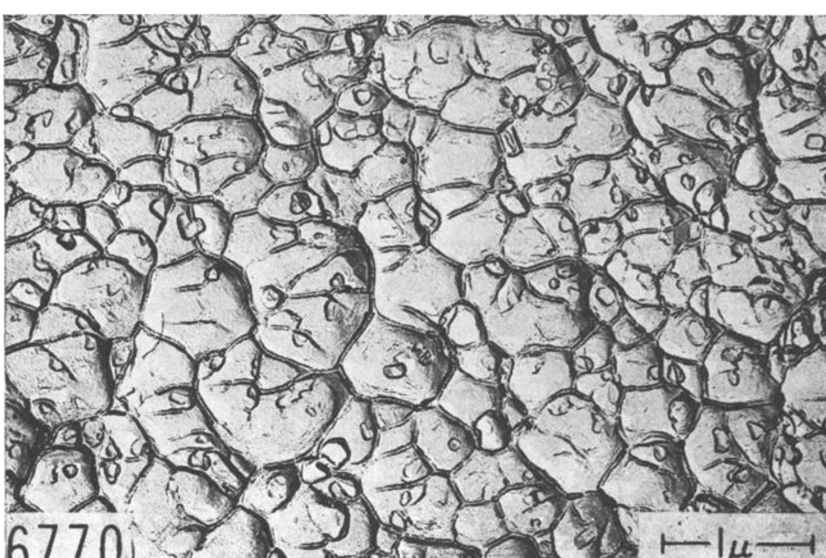

FIG. 12—Equiaxed Dimples in 7075-T6 Fracture. Direct Carbon Replica. 30,000×. Reduced One Third in Reproduction.

manner by the linking up of submerged cracks with one another or with the major fracture front. Figure 7 shows a high proportion of secondary cracks, often found in the more brittle fractures. Precisely matched fracture surfaces are shown in Fig. 8. Stereoscopic viewing of many such matching surfaces shows three distinct features which are indicated with numbers in Fig. 8. These features are as follows: steps, ridges, and tongues. They are sketched in Fig. 9. The formation of tear ridges is believed to occur by the mechanism shown in Fig. 10.

In quenched and tempered steels, quasi-cleavage exhibits some of the features of crystalline cleavage in the initiation of the facets and some of the features of plastic rupture in the linking-up of the micro-cracks. The proportion of these two modes of fracture observed in quenched and tempered steels depends upon the composition (for example, carbon content), heat treatment, and the test conditions (for example, temperature).

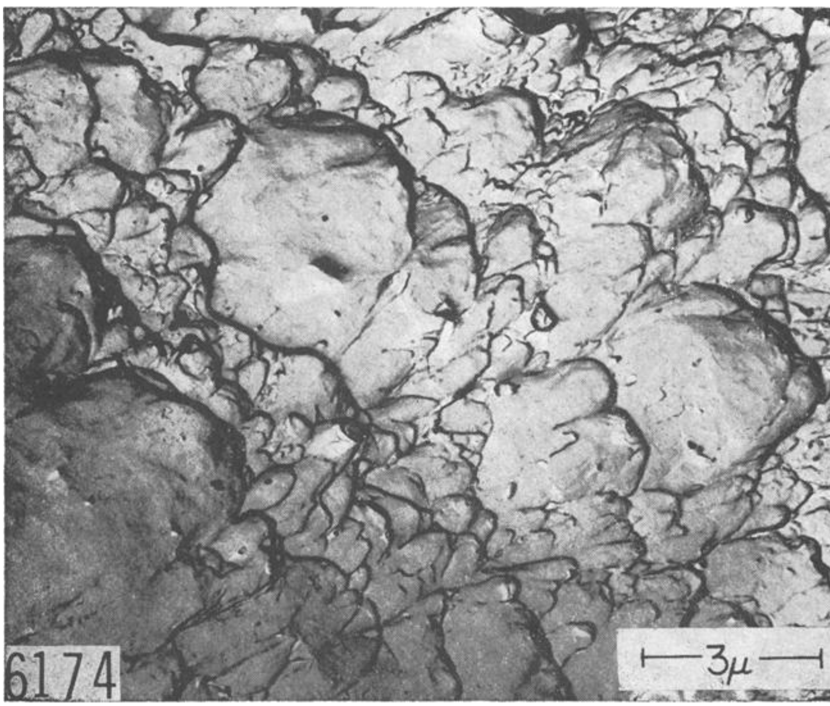

FIG. 13—Tear Dimples Formed During the Early Stages of Internal Fracture of a Necked 4340 Steel Smooth-Bar Tension Specimen. Two-Step Replica. 12,000×. Reduced One Third in Reproduction.

COALESCENCE OF MICRO-VOIDS

Fracture surfaces of many metals and alloys exhibit evidence of severe localized plastic deformation. Tear ridges in quasi-cleavage fracture already have been mentioned. However, in most ductile or tougher materials, another fracture mode involving the formation and coalescence of internal micro-voids is of major importance (7–11). The initiation of the micro-voids is dependent upon

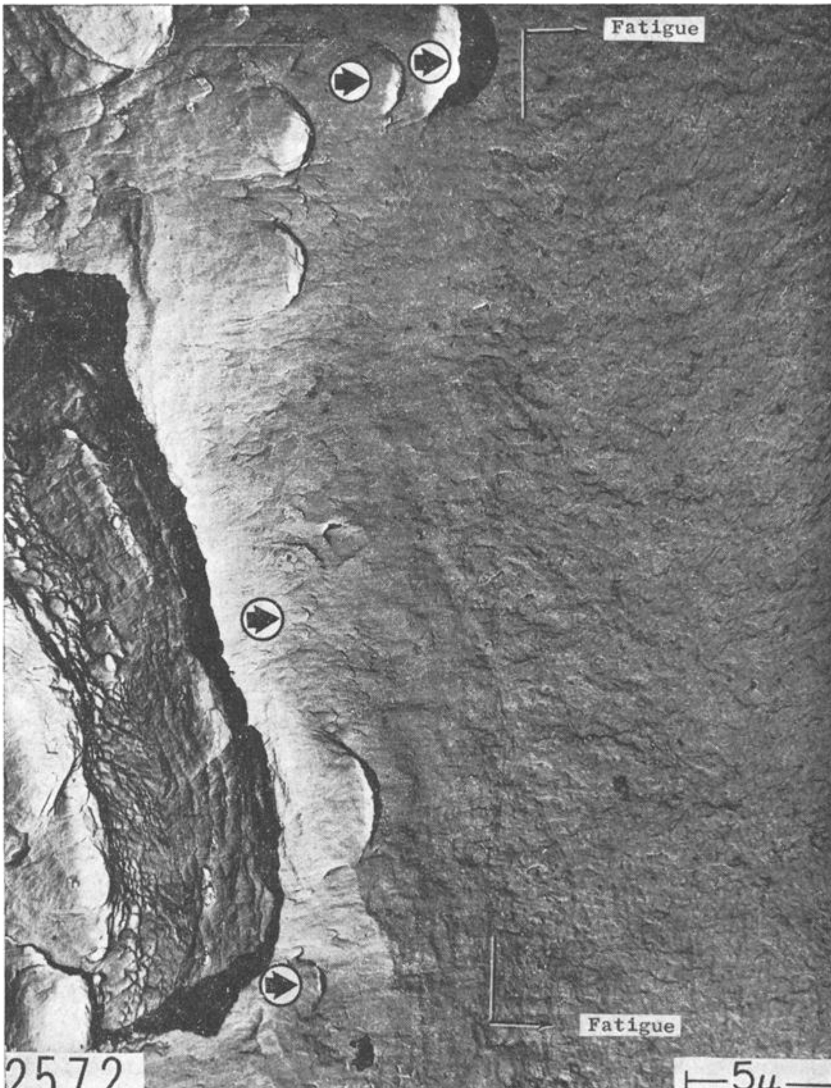

FIG. 14—Tearing at the Root of a Fatigue Crack in a Ti-2.5Al-16V Specimen.
The fatigue crack was intentionally introduced as a stress raiser for the later crack-propagation test. The tear dimples (arrows) were formed in the early stages of crack growth during the test. The fracture progressed from right to left. Palladium-shadowed direct carbon replica. (Reprinted from Ref (6).) 6000×. Reduced one third in reproduction.

the existence of some heterogeneities or defects originally present in the material or created during plastic deformation. For example, during plastic deformation and as a result of differences in elastic and plastic properties between the matrix and second-phase particles, micro-cracks or free surfaces are created at the interface between the particles and the matrix.

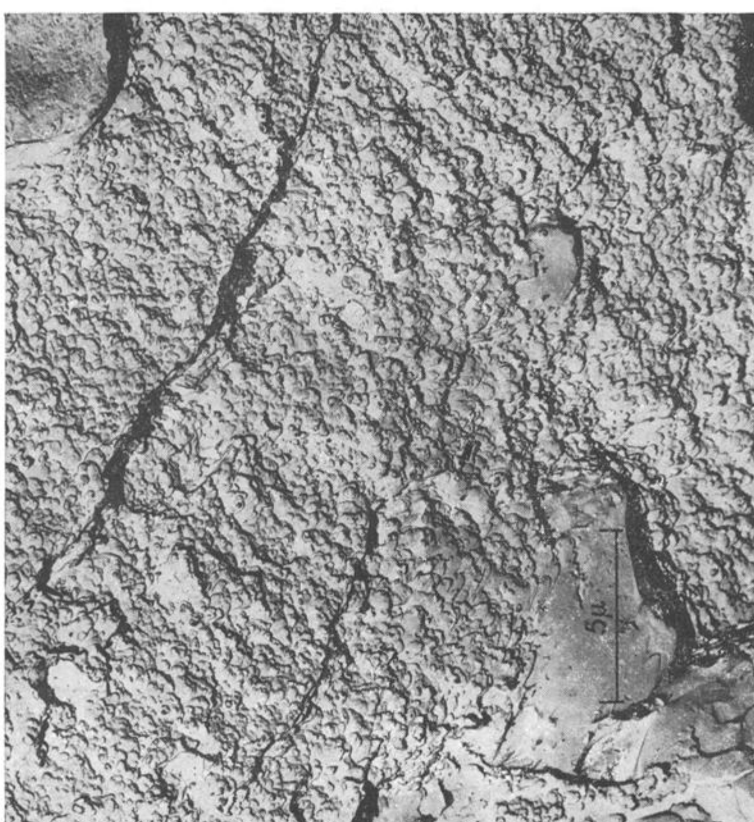

FIG. 15—Dimpled Rupture Surface in a 7078 Aluminum Alloy. Two-Step Replica. (Reprinted from Ref (2).) 6600×. Reduced One Third in Reproduction.

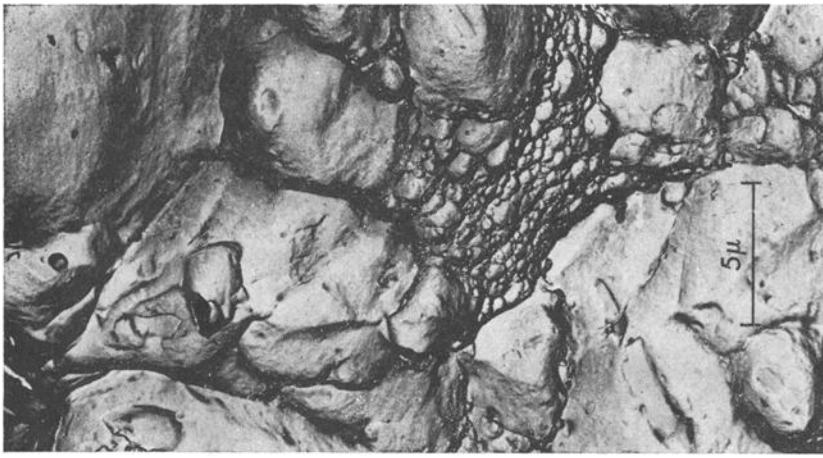

FIG. 16—Dimples on a Fracture Surface in a 2219 Aluminum Alloy. Note the Range of Sizes of the Dimples. Two-Step Replica. (Reprinted form Ref (2).) 6000×. Reduced One Third in Reproduction.

The highly complex mechanics of plastic flow during the growth of these internal free surfaces is not fully understood. It is known that the free surfaces tend to develop into rounded holes as they grow. Each one of the holes, or voids, is a fracture surface in itself, initially completely isolated from the other voids. During increasing plastic flow these voids continue to grow. If a void is near another free surface it may grow until the material between the two free surfaces thins down and separates by rupturing; this is termed coalescence. The fracture surfaces created by the coalescence of voids is made up of rounded concave depressions as shown in Figs. 11–17.

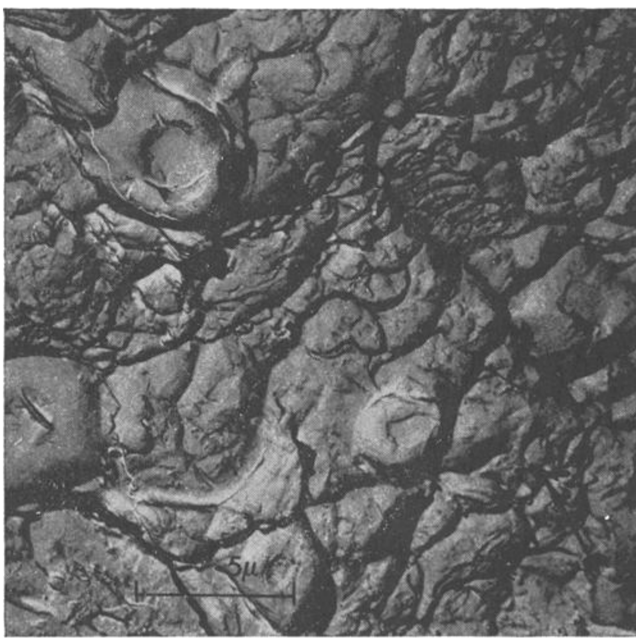

FIG. 17—Example of Dimples in a Maraging Steel. Two-Step Replica. (Reprinted from Ref (2).) 6400×. Reduced One Third in Reproduction.

The half-voids are easily divided into two distinctly different groups according to their shape: (*1*) those that are roughly hemispherical or equi-axed and were called "cupules" by J. Plateau et al; and *2*) those that have parabolic shape and-(were called "dimples." The term "dim ples" has come to be used in reference to all such half-voids on fracture surfaces. Examples of equi-axed dimples are shown in Figs. 12, 16, and 17, and they are sketched in Fig. 18(*a*). The parabolic dimples can form in two different manners: (*1*) by shear rupture (Fig. 18(*b*)); and (*2*) by tearing (Fig. 18(*c*)). Examples of shear-rupture dimples are shown in Figs. 11 and 15, and tear dimples are shown in Figs. 13 and 14. Parabolic dimples resulting from a shear fracture are practically always present on all of the shear surfaces that one sees with the unaided eye, such as on shear lips and the sides of cup-and-cone fractures. Tearing frequently occurs at the tip of sharp cracks that are opening up under tension. Unfortunately no characteristic features have yet been recognized that enable one to distinguish between tear dimples and shear-rupture dimples. However, it is evident that tear dimples, once they are identified, can be used to determine the local direction of crack propagation, just as in the case of the river patterns in cleavage.

The size of dimples is determined primarily by two factors: (*1*) the size of the initial internal free surface; and (*2*) the amount of plastic growth permitted before the void coalesces with another free surface. The first factor is determined primarily by the size of the inclusions, precipitate particles, etc. The second factor is mainly dependent upon the distance between neighboring voids which in turn is frequently determined by the density of precipitate particles. However, there is not necessarily formation of a micro-void at each

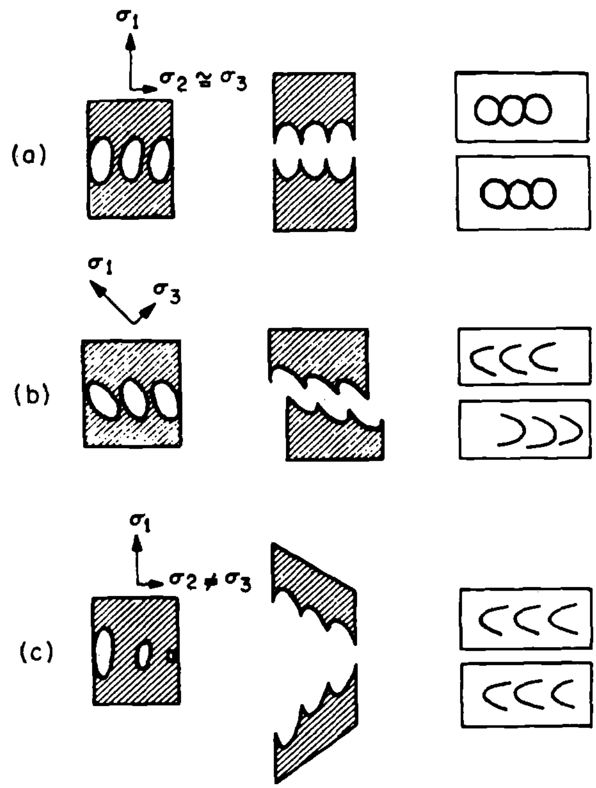

FIG. 18—Three Observed Basic Modes for the Coalescence of Voids.

For each mode the sketches show, from left to right: (1) material stressed almost to the point of local rupture; (2) local rupture; and (3) the directional sense of dimples on the rupture surfaces. (*a*) Normal rupture; coalescence under the influence of uniform plastic strain in the direction of the applied stress. (*b*) Shear rupture; coalescence under the combined influences of plastic strain in the direction of the applied stress and shear strain on a plane of maximum shear stress. (*c*) Tearing; coalescence under the influence of nonuniform strain in the direction of the applied stress. Plastic strain is greatest on the left side of the element. (Reprinted from Ref (**6**).)

precipitate lying along or near the fracture surface. In general, the density of precipitate per unit of fracture surface is much larger than the number of dimples observed on the same surface.

The work-hardening behavior of the surrounding matrix probably plays an important role in controlling the amount of plastic growth which can take place

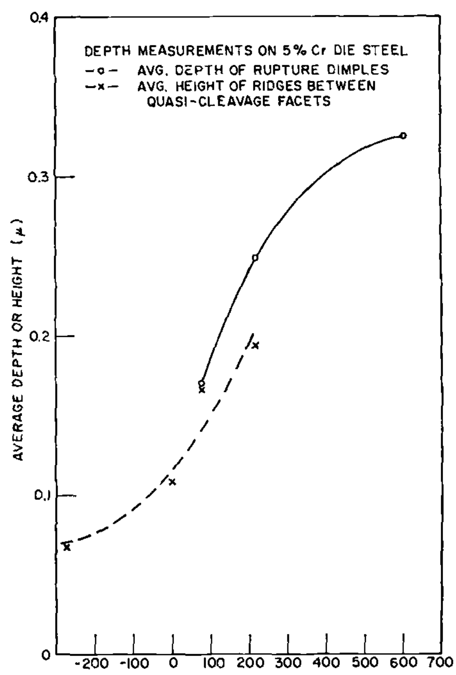

FIG. 19—Plot of Average Depth of Dimples and Height of Tear Ridges Between Quasi-Cleavage Facets as a Function of Temperature in H-11 Steel. (Reprinted from Ref (12).)

before coalescence of the micro-voids. In this connection it has been found that the depths and sizes of dimples increase with the testing temperature in several materials. For example, Fig. 19 shows the variation of dimple depth versus temperature for H-11 steel (12).

INTERGRANULAR SEPARATION

Fracture due to static overload, fatigue, hydrogen embrittlement, liquid-metal attack, quenching stresses, and stress corrosion in the presence of gases and liquids sometimes has been observed to propagate along grain boundaries in a large number of metals and alloys.

Lattice irregularities at and near grain boundaries will in general have a tendency to make these boundaries inherently weaker than the grain interiors. In addition, grain boundaries are often favorable sites for the segregation of various impurity or alloying elements to form either composition gradient zones or precipitate particles (or continuous films) of secondary phases. The presence of these segregated zones or the second phases cause the mechanical, physical, and chemical properties of the grain-boundary regions to be different from those of the grain interiors.

If the constituent particles are numerous enough or large enough and possess properties that are sufficiently different from the grain interiors, fracture may nucleate or propagate along the grain boundaries to produce intergranular fractures.

Some alloys that contain extensive brittle grain-boundary constituents may fail entirely along the grain boundaries. However, a lower amount of grain-boundary constituents may result in failures which are partly intergranular and partly transgranular.

Depending upon how much the adjoining grains deform during intergranular fracture, the exposed grain facets may vary from quite flat to somewhat convex or concave in over-all shape.

The electron microscope has permitted detailed studies of intergranular fracture surfaces and a number of interesting features have been found. Depending upon the shape, size, distribution, and properties of the weak phases which initiate local internal free surfaces along a single grain boundary, and depending

FIG. 20—Intergranular Fracture, due to Micro-void Coalescence, in a 2219 Alloy.
The difference in orientation of the grain-boundary facets is well marked and the shear direction is given by the direction of elongation of the dimples. Two-step replica. (Reprinted from Ref (2).) 5500×. Reduced one third in reproduction.

upon the test conditions, the two separated grain facets may exhibit no markings (flat and featureless as in Fig. 4), dimples (Figs. 20 and 21), cleavage steps (Fig. 22), fatigue markings (Fig. 23), various corrosion pits and products, or other markings. At times only a few markings are seen, as in Fig. 24. Figure 25 shows a feature which is often observed in quenched and tempered steels. These markings (arrows) have been observed on static overload, stress corrosion, and hydrogen-embrittlement fracture surfaces, and are thought to be formed (13) by the thinning down and rupture of material between neighboring internal grain boundary cracks (as sketched for quasi-cleavage in Fig. 10).

The recognition of all the different kinds of fine-scale markings on grain boundary facets is by no means complete. In addition, with the present limitations of replication techniques and replica fidelity it is probable that a large number of significant markings will remain undetected.

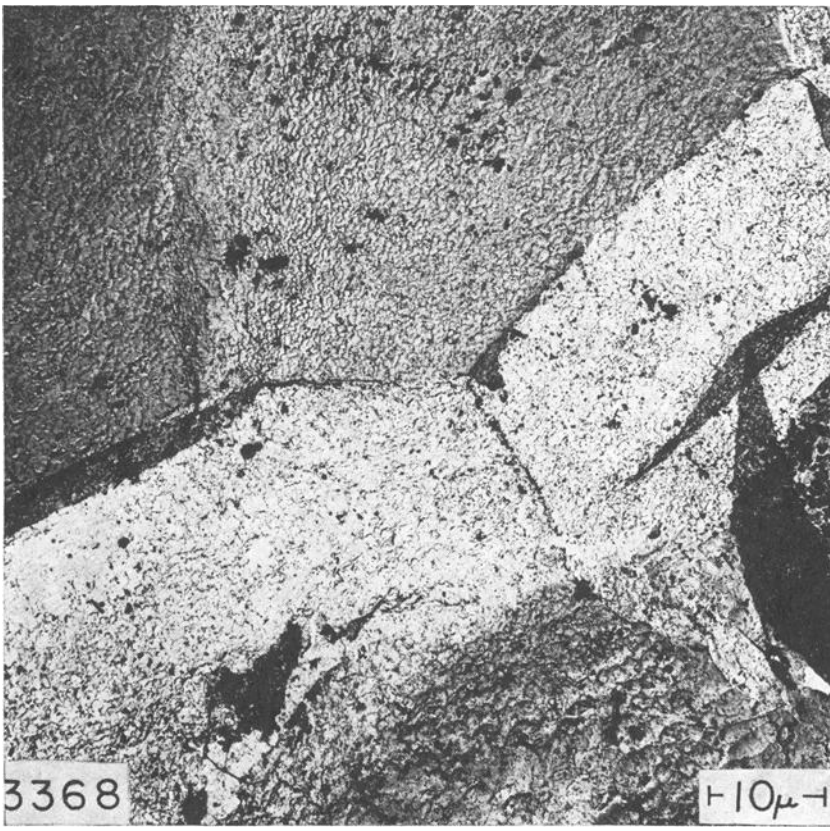

FIG. 21—Dimples Along Grain-Boundary Facets in a Weld-Heat-Affected Zone in a Steel. 2400× Reduced One Third in Reproduction.

FATIGUE

The examination of the fatigue fracture surface of an aluminum alloy by optical microscopy shows dull and bright regions. The dull zones are depressions usually with a large intermetallic particle visible at the bottom of the depression. The bright zones show a series of regular striations as illustrated by Fig. 26. The examination of the same surface by electron microscopy shows that the depressions are made up of dimples characteristic of a rapid, plastic fracture. The striations of the bright zones are clearly resolved (Fig. 27) and in the case of a fatigue test under a constant stress level, the spacing of the striations is locally very uniform. The examination of program-loaded fatigue fractures has demonstrated that each of the characteristic fatigue striations first observed by Zapffe and Worden (14) is produced by a single cycle of stress (15), thus the striations (also called crack-front arrest lines) represent the successive positions of a transgranular front at each load cycle.

Forsythe (16) has recently given an excellent survey of the mechanisms of fatigue-crack propagation in aluminum alloys. Two general types of striations have been recognized, the *brittle* and the *ductile* types. Figure 28, taken in part from Forsythe, illustrates the differences between the two types of striations. The brittle striations are connected with what seems to be a cleavage fracture along sharply defined facets. Numerous river line markings separating these facets run normal to the striations as shown on Fig. 29.

The profile of a brittle striation is

FIG. 22—Cleavage Fracture and Separation Along the Interface of a Large Particle in an Alnico Alloy.

The smooth and hexagonal steps are growth markings present on the particle before agglomeration. Two-step replica. 6600×. Reduced one third in reproduction.

shown in Fig. 28(*d*). As far as it is known, brittle striations have been observed only in high-strength aluminum alloys, and they are usually indicative of the presence of corrosive media.

The ductile striations are more common and they have also been observed in polymers which would show that their formation is not necessarily related to the crystallographic nature of metals. Figures 27 and 30 give some good examples of ductile fatigue striations. The exact mechanism of formation of these striations is not clearly understood. Figure 28(*c*) presents different profiles of fatigue striations. Smith and Laird (19) and McEvily (20) have shown that in the case of high-stress fatigue, the profiles of the two fracture surfaces do not match. Under conditions of low stress fatigue, it is not clear at this stage, whether the profiles are of the type II or type III represented on Fig. 28.

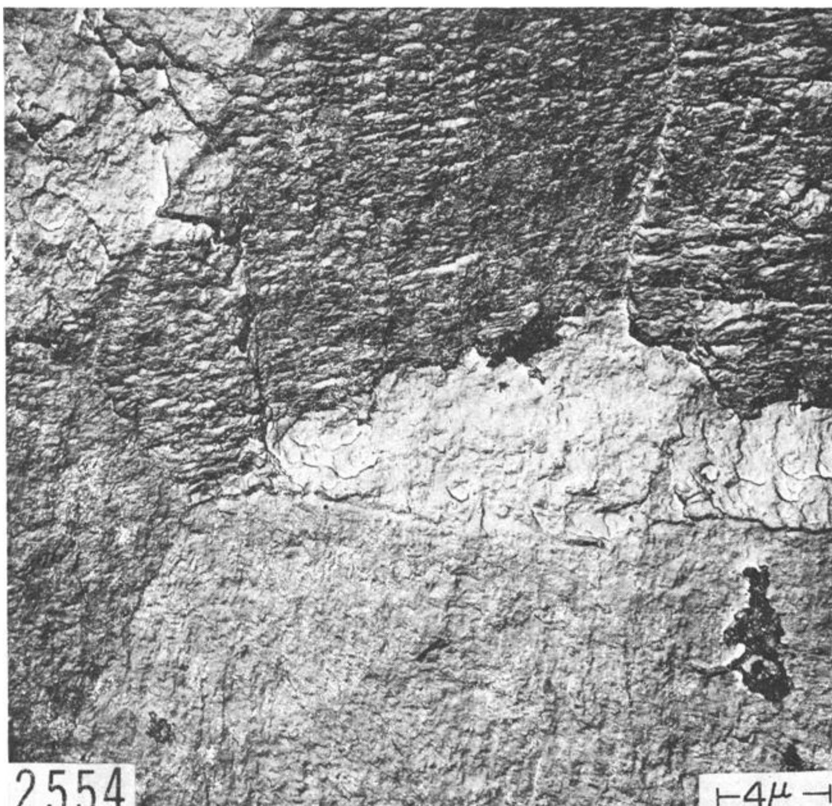

FIG. 23—Fatique Striations on Grain Boundaries in a Ti-2.5Al-16V Alloy. 6000×. Reduced One Third in Reproduction.

Grain boundaries play an important role in fatigue-crack propagation. The different figures presented here show that in aluminum alloys, the crack front is held up along grain boundaries, and the orientation of the striations changes from one grain to the other. This could be accounted for by the fact that in high-stacking fault energy materials, fatigue cracking is the result of deformation by cross slip which is more extensive inside the grains than along the grain boundaries.

the calculated crack-growth rate. However, in general, brittle fracture of intermetallic particles and ductile tear around large constituent particles result in a rapid and localized advance of the crack front. This is shown on Fig. 31(*a*) and

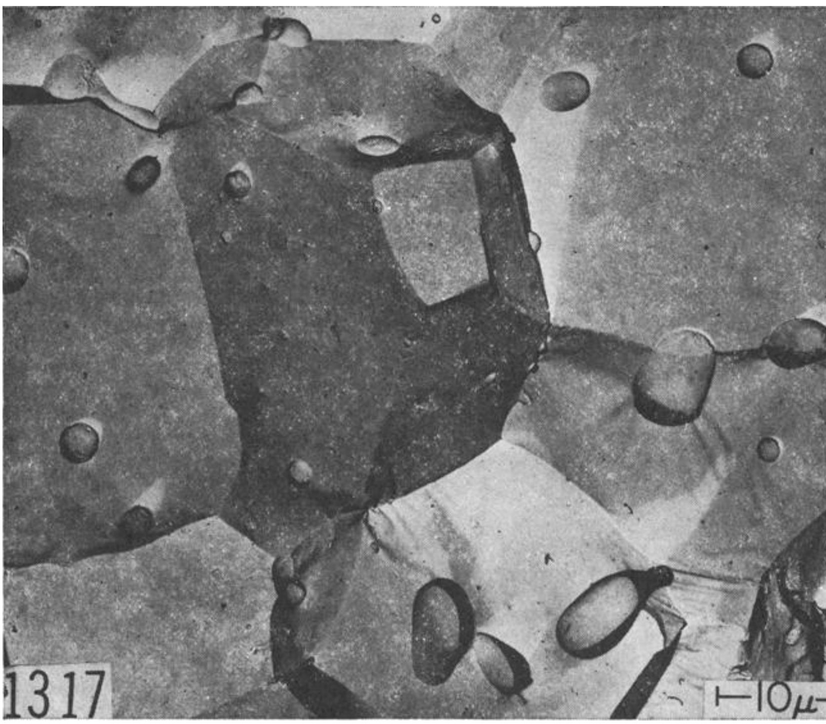

FIG. 24—Intergranular Fracture Through Sintered Tungsten. Grain Facets Have Only a Few Features Visible. 2800X. Reduced One Third in Reproduction.

Under uniform load, the height and the spacing of the striations increase with the crack length. The spacing of the striations as measured by electron microscopy is not always equal to the calculated spacing or crack-growth rate derived from macroscopic measurements of crack length *versus* number of cycles. If at each cycle the crack front does not advance in a uniform manner over its whole length, the average spacing of the observed striations will be larger than 31(*b*). Consequently, the spacing of the observed striations is, in general, smaller than the spacing expected from the macroscopic measurements of crack growth rates. Naturally the spacing of the striations is also markedly dependent on the load. Figure 32 shows that under a varying load, the spacing of the striations may vary considerably. It can also be seen from this figure that the well-defined fatigue striations provide us with an ideal marker which should be used to

FIG. 25—Intergranular Fracture in a 4340 Steel.

This intergranular fracture at the origin of a service failure was probably due to stress corrosion and hydrogen embrittlement. Note the tear ridges along the grain-boundary facets and the dimples in *A* and *B*. Two-step replica. (Reprinted from Ref (**2**).) 6000×. Reduced one third in reproduction.

FIG. 26—Optical Micrograph of a Fatigue Fracture in a 7178 Aluminum Alloy. Some Regions Are out of Focus due to the Small Depth of Field of the Optical Microscope. 3200×. Reduced One Third in Reproduction.

measure the true influence of a peak overload on the rate of crack propagation. This kind of work would be very useful in the formulation of a proper theory of fatigue damage.

discontinuous. Very often, according to the ratio of the maximum to the minimum stress, the details of the fracture surface have been destroyed by the rubbing action of the two fracture faces.

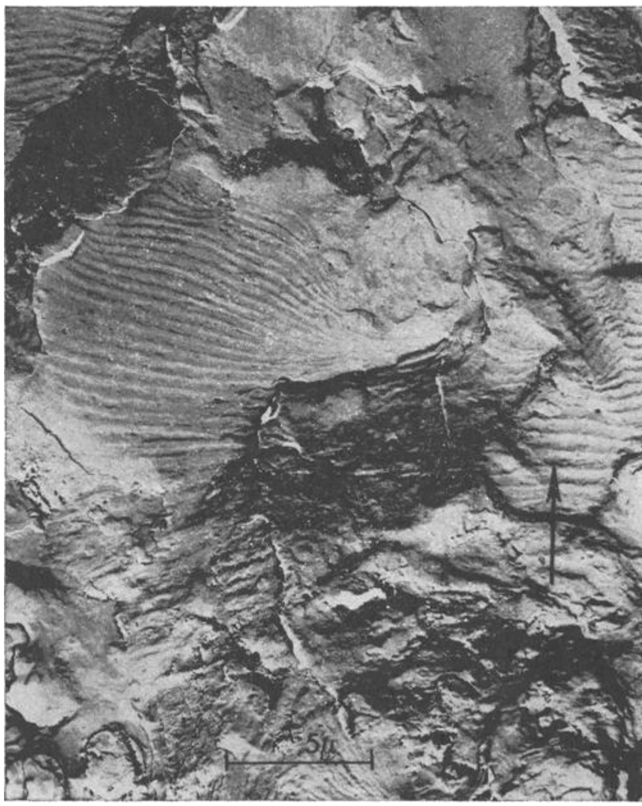

FIG. 27—Electron Micrograph of a Fatigue Fracture in a 7178 Aluminum Alloy.
By contrast with Fig. 26, this micrograph shows the larger depth of field of the electron microscope. The flat regions where the crack propagated in a cyclic manner are connected by ductile regions where fracture took place suddenly around inclusions or by shear. Two-step replica. 5800×. Reduced one third in reproduction.

Other examples of fatigue striations are shown in Figs. 33–35. In general, the striations in different materials are not as sharply defined as they are in high-strength aluminum alloys. In steels for instance, the successive positions of the crack front do not appear clearly defined; the striations are short and This is often the case with service failures where a fatigue mode of fracture is identified by the presence of a few striations on a flat surface and the absence of other characteristic fracture features. Fatigue-crack propagation is not always a transgranular mode of fracture with well-defined crack-front arrest lines. In

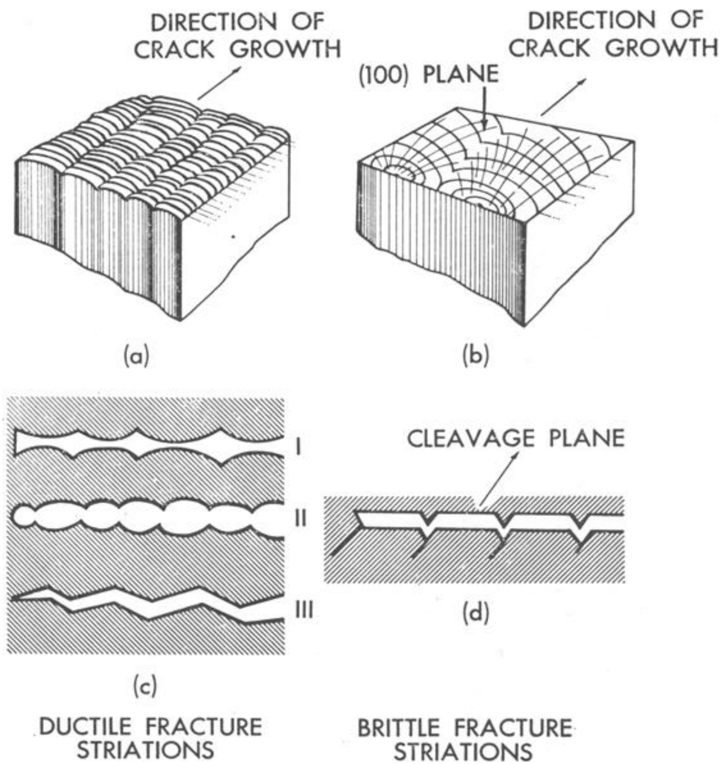

FIG. 28—Different Types of Ductile and Brittle Fatigue Striations; (*a*) and (*b*) Are Taken from Forsyth (16).

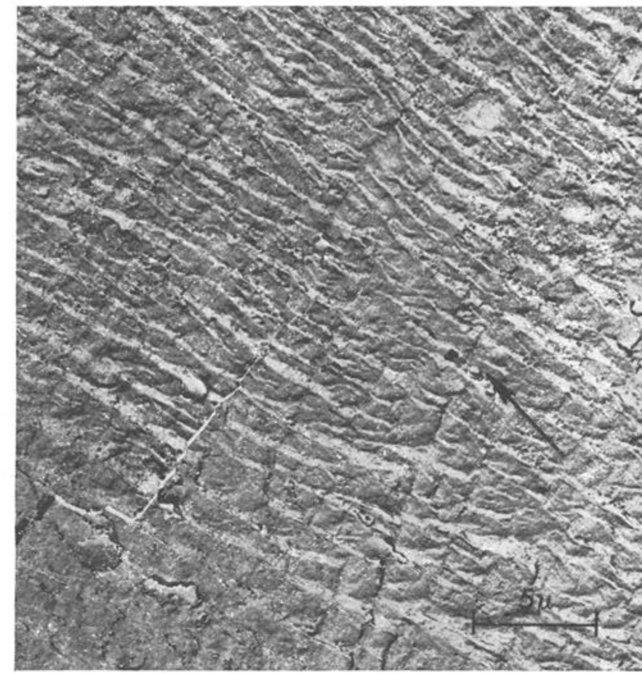

FIG. 29—Example of Brittle Fatigue Striations in a Service Failure of a 2014 Aluminum Alloy.

Note the cleavage steps running parallel to the direction of crack propagation and normal to the fatigue striations. Two-step replica. 5000×. Reduced one third in reproduction.

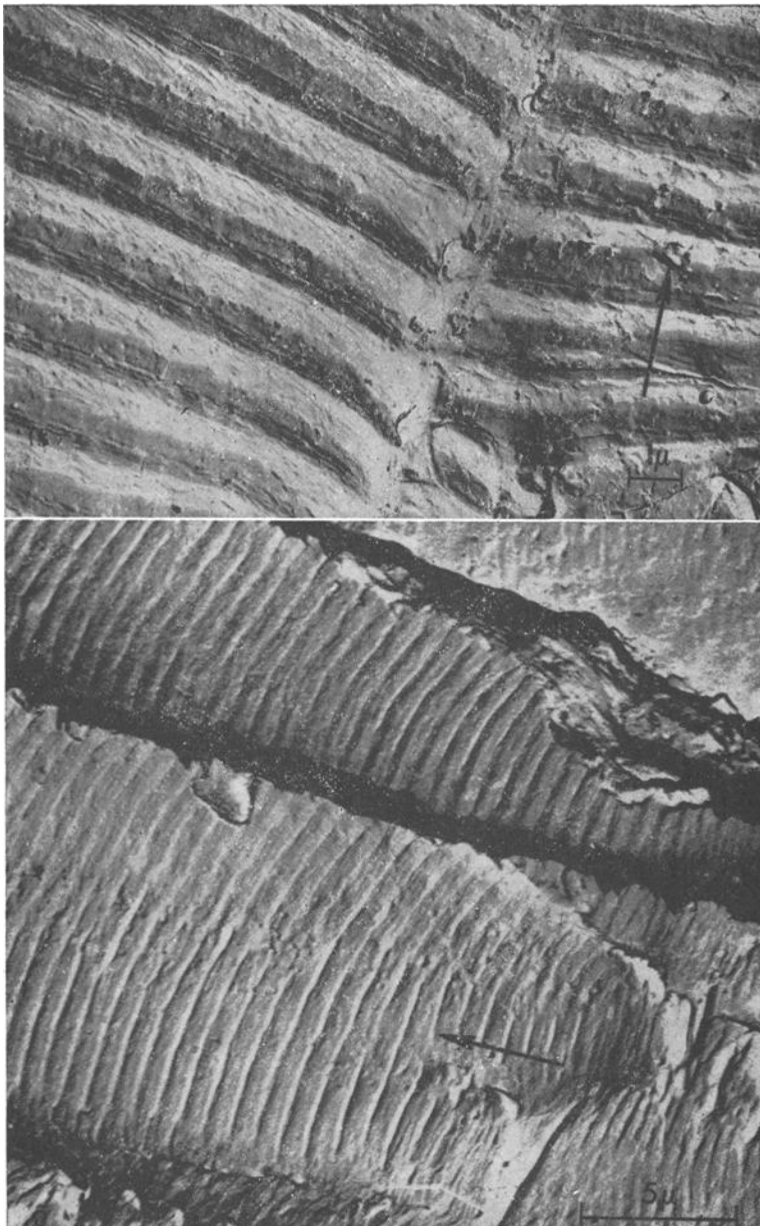

FIG. 30—Examples of Ductile Fatigue Striations in a 7178 Aluminum Alloy.

Bottom photo shows clearly the role of grain boundaries in slowing down the progression of the crack front. Two step replica. (*top*) 10,000×. (*bottom*) 6000×. Reduced one third in reproduction.

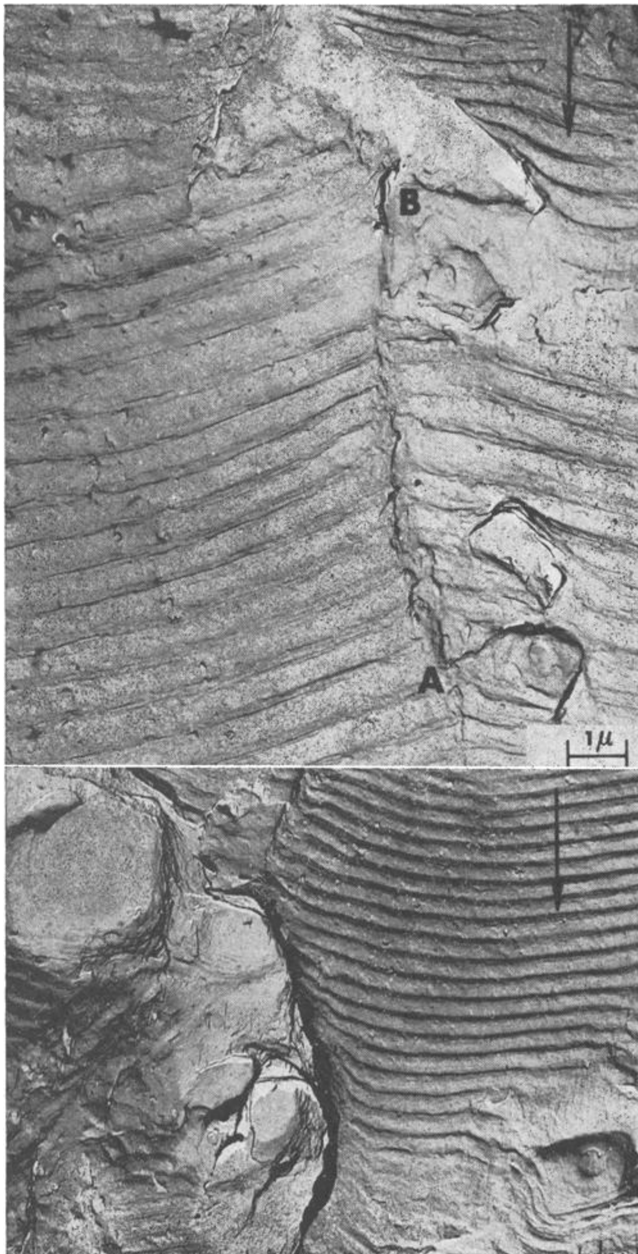

FIG. 31—Examples of Ductile Fatigue Striations and Brittle Fracture of a Second-Phase Particle in a 7178 Aluminum Alloy. Two-Step Replica. 12,000×. Reduced One Third in Reproduction.

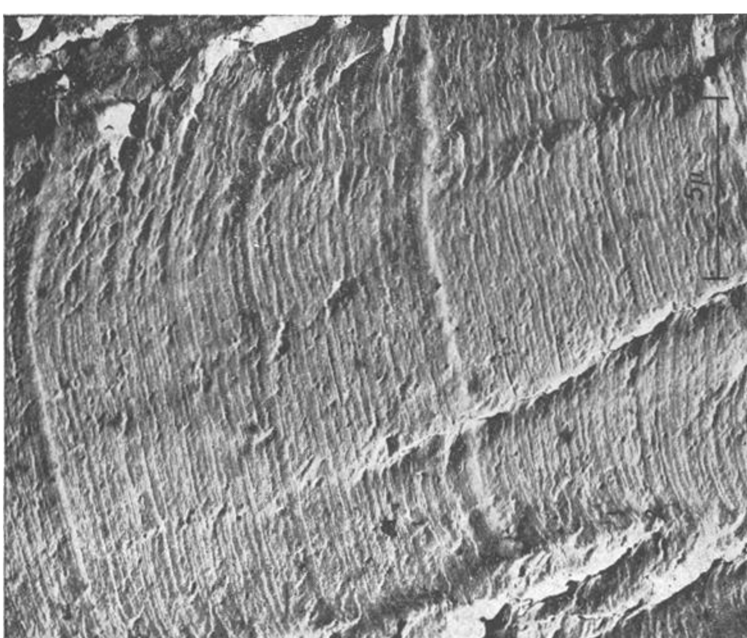

FIG. 32—Fatigue Fracture in a 7178 Aluminum Alloy.

Under a random load the spacing of the striations is not uniform. The influence of peak overloads on the rate of advance of the front are clearly indicated. Two-step replica. 7600×. Reduced one third in reproduction.

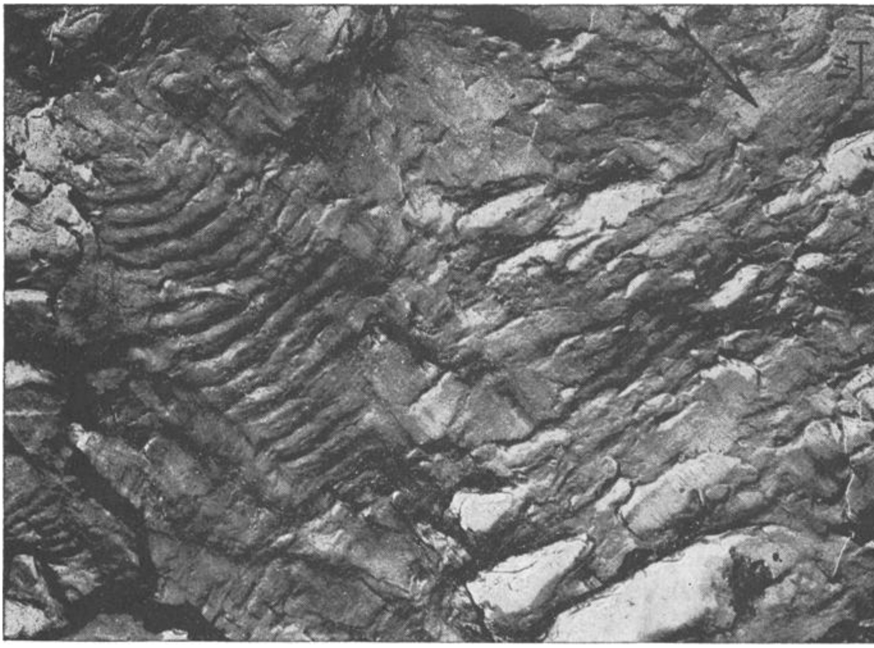

FIG. 33—Fatigue Striationsi n a 4340 Steel.

The striations are never well defined over the whole fracture surface. Two-step replica. 11,000×. Reduced one third in reproduction.

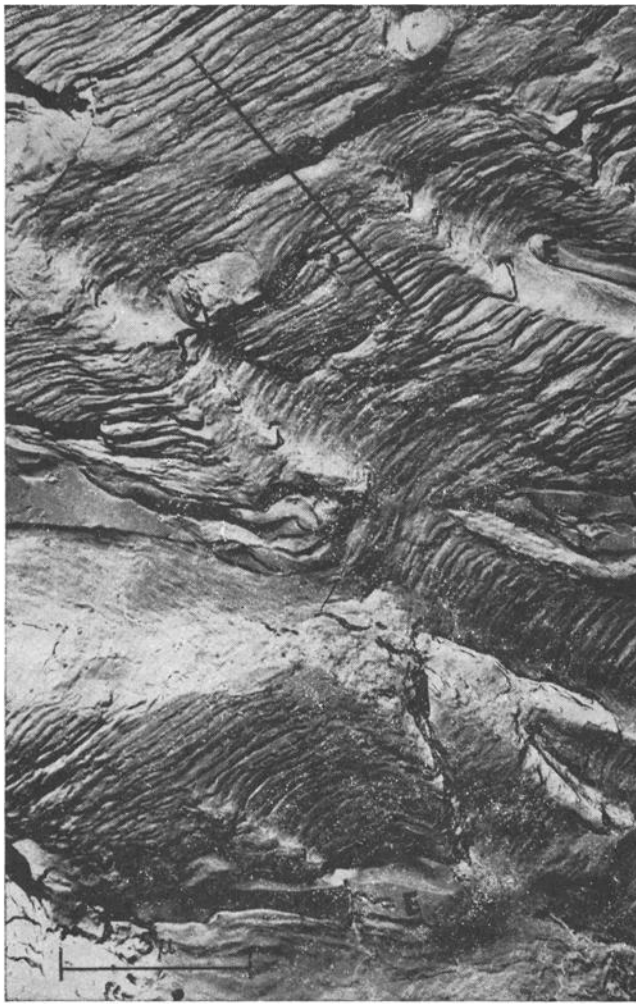

FIG. 34—Fatigue Striations in a Welded Zone of a 2219 Aluminum Alloy.

The large second-phase particles are probably eutectic particles of Al_2Cu. Two-stage replica. 6800×. Reduced one third in reproduction.

many cases, fatigue cracks propagate along grain boundaries. This type of fracture was observed in 70-30 brass by one of the authors and it also takes place in high-strength steels such as 4340.

Very often a misinterpretation of some fracture features can lead to some confusion. For instance, Wallner's lines (19) should not be confused with fatigue striations. Wallner's lines are usually observed in very brittle materials; they are the result of an interaction between the advancing crack front and an elastic wave propagating at the same time. They appear as uniformly spaced striations but with an occasional criss-crossing network of lines (Fig. 36). It also often happens that in a composite material, fracture takes place at the interface between large second-phase particles and a matrix. Such a case is shown in Fig. 22. The sharp lines and facets which are growth markings on the surface of the second-phase particles should not be confused with fatigue striations.

tions of material, stress, and environment. Successful failure analyses with this tool depend on the prior knowledge of the appearance of the fracture surfaces of a given material broken under specific

FIG. 35—Fatigue Striations in a Zirconium Alloy. Two-Stage Replica. 6400×. Reduced One Third in Reproduction.

FAILURE ANALYSES

Electron fractography has become a very useful tool in the analysis of service failures. Although it does not replace the other failure-analysis tools, it frequently permits the unambiguous identification of fatigue striations, intergranular fractures, dimples, or cleavage facets which are known to be caused by specific conditions, both in the laboratory and in service. A proper analysis of a service failure with this technique also depends on the preservation of the fracture surfaces.

As an example[8] of service failure analyses, Figs. 37 and 38 show the macroscopic and electron microscopic

[8] Unpublished work, W. R. Warke.

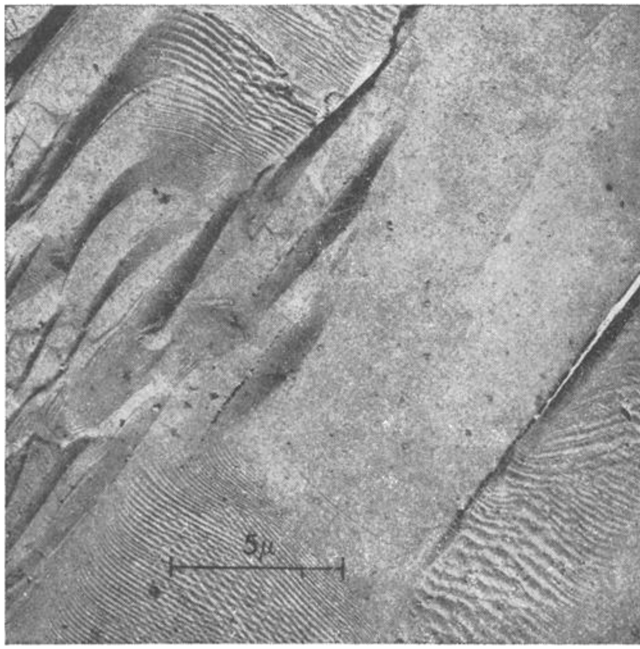

FIG. 36—Examples of Wallner's Lines Resulting from the Brittle Fracture of a Silicate Particle in an Aluminum-Silicon Alloy. Two-Stage Replica. 6800×. Reduced One Third in Reproduction.

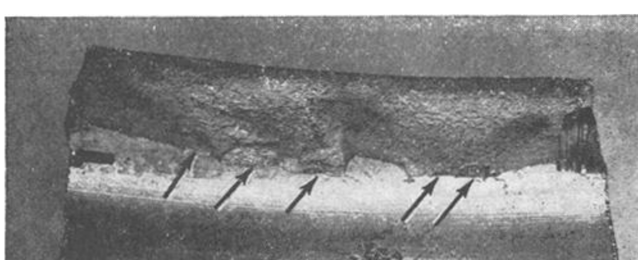

FIG. 37—Photomacrograph of a Fractured Aluminum Forging Showing Five Small Cracks Which Formed During Service. 3×. Reduced One Third in Reproduction.

features of a 2014-T6 aluminum alloy forging which developed cracks in service. The cracks were found during a routine inspection and the part was removed from service and submitted for analysis. The part was broken in the laboratory to reveal some of the cracks. Figure 38 shows the primary origin to be stress-corrosion cracking with subsequent crack growth by fatigue. In this case the techniques of electron fractography easily and quickly gave information which would have been very difficult or impossible to obtain in any other way.

SUMMARY

The direct or indirect observations of fracture surfaces at high magnification permit the study of the path of least

FIG. 38—Composite Electron Microscope Fractograph of One of the Cracks in Fig. 37 Showing Striated Fatigue Fracture Originating from a Minute Intergranular Surface Flaw. Two-Step Replica. 2400×. Reduced One Third in Reproduction.

resistance to fracture in much more detail, and much more easily, than can be done with polished cross sections. Detailed studies are revealing a new class of information which permits a fuller knowledge of the complexities of fracture and a better understanding of fracture processes. Electron fractography can help fill the research gap between continuum mechanics and mechanical metallurgy on the one hand and the metal physics approach on the other hand. It should be emphasized that the small amount of information accumulated to date is immediately useful to those who are working with high-strength engineering materials—helping them understand fracture toughness and to perform critical failure analyses.

Acknowledgment:

The authors extend their thanks to the members of the subcommittee on Fractography and Microstructure in Relation to Fracture Behavior[9] for their contributions to the body of this report and their helpful suggestions and comments concerning the text.

REFERENCES

(1) C. A. Zapffe and M. Clogg, Jr., "Fractography—A New Tool for Metallurgical Research," *Transactions*, Am. Soc. Metals, Vol. 34, 1945, p. 71.

(2) R. M. N. Pelloux, "The Analysis of Fracture Surfaces by Electron Microscopy," Boeing Scientific Research Laboratories Report D1-82-0169-R1, December, 1963.

(3) J. R. Low, Jr., "A Review of the Microstructural Aspects of Cleavage Fracture," *Swampscott Conference on Fracture*, John Wiley & Sons, Inc., New York, N. Y., 1959.

(4) J. R. Low, Jr., "Dislocations and Brittle Fracture in Metals," *Madrid Colloquium on Deformation and Flow of Solids*, IUTAM, Springer-Verlag, Berlin, 1956.

(5) E. P. Dahlberg, "Characteristics of Twinning on Fracture Surfaces of Single and Polycrystalline Tungsten," Paper J-5, *Fifth International Congress for Electron Microscopy*, Academic Press, New York, N. Y., 1962.

(6) C. D. Beachem, "Electron Fractographic Studies of Mechanical Fracture Processes in Metals," *Transactions*, Am. Soc. Mechanical Engrs., to be published.

(7) C. Crussard et al, "A Comparison Between Ductile and Fatigue Fractures," *Swampscott Conference on Fracture*, John Wiley & Sons, Inc., New York, N. Y., 1959.

( ) H. C. Rogers, "Tensile Fracture of Ductile Metals," *Transactions*, Met. Soc. Am. Inst. Mining Metallurgical Engrs., Vol. 218, June, 1960, p. 504.

(9) G. T. Hahn et al, "Initiation of Cleavage Microcracks in Polycrystalline Iron and Steel," *Swampscott Conference on Fracture*, John Wiley & Sons, Inc., New York, N. Y., 1959.

(10) C. D. Beachem, "An Electron Fractographic Study of the Influence of Plastic Strain Conditions Upon Ductile Rupture Processes in Metals," *Transactions*, Am. Soc. Metals, Vol. 56, September, 1963, pp. 318–326.

(11) P. J. E. Forsyth and D. A. Ryder, "Some Results of the Examination of Aluminum Alloy Specimen Fracture Surfaces," *Metallurgia*, Vol. 63, March, 1961, pp. 117–124.

(12) A. J. Edwards, "Depth Measurements on Fracture Surfaces," Report of NRL Progress, November, 1963.

(13) E. P. Dahlberg and D. B. Lytle, "Fatigue Crack Propagation in High-Strength 4340 Steel," NRL Memorandum Report 1471, November, 1963.

(14) C. Zapffe and C. Worden, "Fractographic Registrations of Fatigue," *Transactions*, Am. Soc. Metals, Vol. 43, 1951, pp. 958–969.

(15) P. J. E. Forsyth and D. A. Ryder, "Fatigue Fracture: Some Results Derived from the Microscopic Examination of Crack Surfaces," *Aircraft Engineering*, Vol. 32, 1960, p. 96.

(16) P. J. E. Forsyth, "Fatigue Damage and Crack Growth in Aluminum Alloys," *Acta Metallurgica*, Vol. 11, July, 1963, pp. 703–715.

(17) C. Laird and G. C. Smith, "Crack Propagation in High Stress Fatigue," *Philosophical Magazine*, Vol. 7, 1962, pp. 847–857.

(18) A. J. McEvily, R. C. Boettner, and T. L. Johnston, "On the Formation and Growth of Fatigue Cracks in Polymers," *10th Sagamore Army Materials Research Conference*, 13–16 August, 1963.

(19) H. Schardin, "Velocity Effects in Fracture," *Swampscott Conference on Fracture*, John Wiley & Sons, Inc., New York, N. Y., 1959.

[9] G. S. Ansell, Rensselaer Polytechnic Inst.; B. R. Bannerjee, Central Research Lab., Crucible Steel Co.; C. D. Beachem, U.S. Naval Research Laboratory; A. J. Brothers, Large Steam Turbine-Generator Dept., General Electric Co.; C. M. Carmen, Frankford Arsenal; R. W. Hertzberg, Lehigh University; M. Hill, Research Center, Republic Steel Corp.; M. S. Hunter, Alcoa Research Laboratories; N. A. Nielsen, Engineering Research Lab., E. I. DuPont de Nemours & Co.; G. E. Pellissier, Applied Research Lab., U.S. Steel Corp. (subcommittee chairman); R. M. N. Pelloux, Turbine Div.. The Boeing Co.; W. R. Warke, Battelle Memorial Inst.; and B. V. Whiteson, Douglas Missile and Space Systems Div.

DISCUSSION

T. G. Rochow[1]—The title and scope of your excellent paper are broad enough to include fractography of resins, polymers, and their products—amorphous as well as crystalline. Yet your observations and interpretations seem to be confined to the fractography of metallic materials. Do you mean to include resinous materials—at present or in the future?

C. D. Beachem (*author*).—We are not presently using fractography to study fracture mechanisms in resins and polymers. However, the techniques are applicable and are being used by others.

[1] Research fellow, American Cyanamid Co., Stamford, Conn.

Practical Applications

STP381-EB/Apr. 1965

APPLIED FRACTURE MECHANICS

By C. F. Tiffany[1] and J. N. Masters[1]

Synopsis

Procedures for applying fracture mechanics to typical engineering problems are reviewed. Particular emphasis is placed on plane-strain fracture of materials used in fabrication of pressure vessels and booster cases. The major areas considered are: (*1*) material selection; (*2*) the estimation of structural life; and (*3*) the determination of nondestructive inspection acceptance limits. In order to treat these items properly, a brief discussion on the character of premature structural failure is presented, followed by a discussion on the selection of a fracture toughness specimen.

In the area of material screening and selection, it is shown that the required design tool is related, not to toughness alone, but also to the design stress level and the size of the structure. In the estimation of structural life and determination of nondestructive inspection acceptance limits, emphasis is placed on the use of fracture specimen test results and the stress-intensity concept to predict critical flaw sizes and subcritical flaw growth. Both cyclic and sustained stress flaw growth are discussed and comparisons made between specimens and pressure vessels. The value of the proof test is discussed with regard to determining the maximum possible initial flaw sizes in a pressure vessel.

While the primary purpose of this paper is to review the application of fracture mechanics to the design and life prediction of structures, it appears appropriate first to provide some background as to the character of premature structural failure.

Examination of structural components which have failed during service operation typically indicates that the failure origin was a small crack or crack-like flaw. The initial flaw size may have been sufficiently large to cause fracture upon initial loading, or it may have been small enough such that the component withstood a number of load cycles and time at sustained load before the flaw attained a size sufficient to cause failure. In that the gross stress field is generally elastic at the operational loads, the failed component is normally characterized by an absence of a large amount of plastically deformed or yielded material. This is of fundamental importance and points out the danger involved in assuming that the strength and operational life of the structures can be estimated using conventional strength analyses which are predicated upon the absence of flaws and large amounts of plastic yielding prior to fracture. Clearly, it must be recognized that fabricated structures and, indeed, even the raw materials contain defects and flaws of various kinds. The lives of these structures are controlled by the flaw sizes

[1] Chief, Pressure Vessel Development Unit, and research engineer, Pressure Vessel Development Unit, respectively, The Boeing Co., Aero-Space Div., Seattle, Wash.

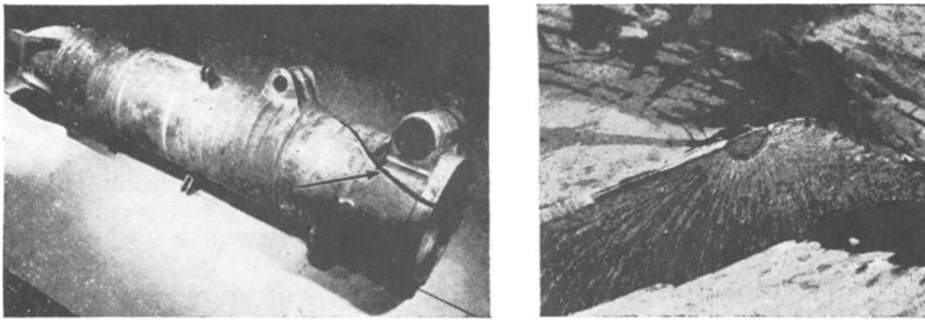

FIG. 1—Landing Gear Cylinder.

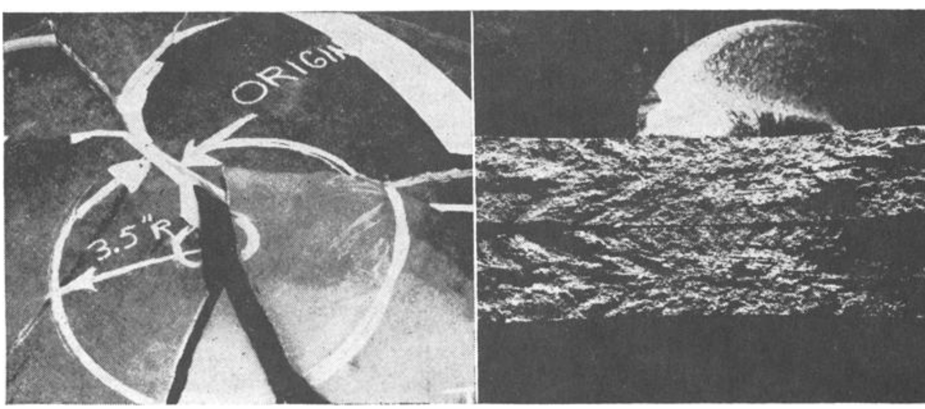

FIG. 2—Steel Pressure-Vessel Failure.

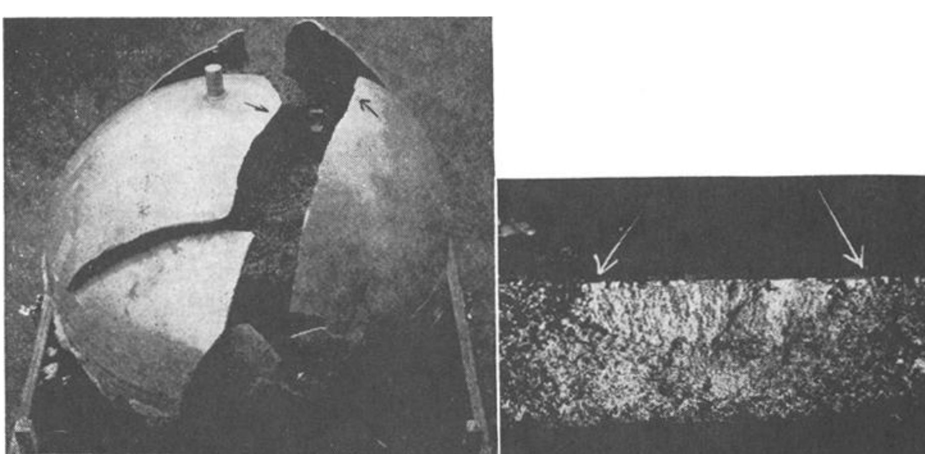

FIG. 3—Aluminum Pressure-Vessel Failure (Liquid Hydrogen Temperature).

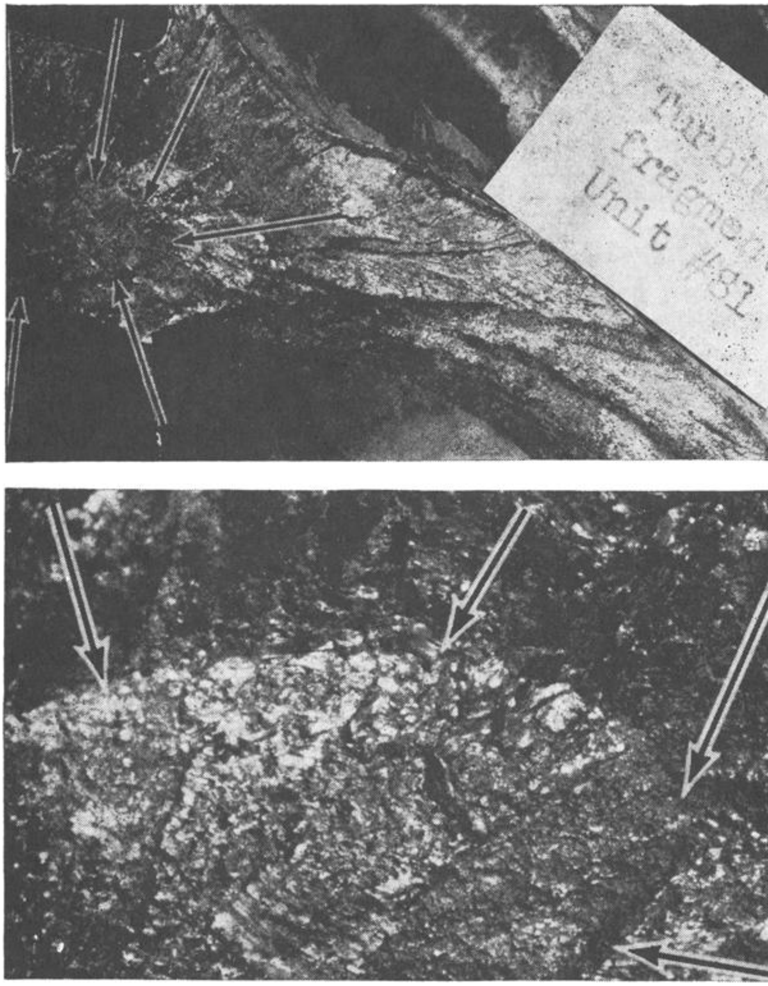

FIG. 4—Turbine-Rotor Failure.

required to cause fracture (that is, critical flaw size) at the operating stress levels, the initial flaw sizes and the sub-critical flaw-growth characteristics of the materials.

As pointed out in the fifth report of the ASTM Special Committee on Fracture Testing of High-Strength Metallic Materials (**1**),[2] the types of flaws encountered in fabricated structures can be categorized as surface flaws, embedded flaws, and through-the-thickness cracks. For surface and embedded flaws, the degree of constraint at the crack leading border is high and plane-strain conditions generally prevail. The initial flaws may or may not reach critical size prior to growing through the thickness depending upon the plane-strain fracture toughness (K_{Ic} value), the applied stress levels, and the material thickness. If the calculated critical flaw size is small with respect to

[2] The boldface numbers in parentheses refer to the list of references appended to this paper.

the wall thickness, the formation of a through-the-thickness crack prior to fracture is not likely. If fracture does occur prior to growing through the thickness, the flaw at time of fracture very often approximates an elliptical or semi-elliptical shape. This is illustrated in the fractographs of several typical component fractures shown in Figs. 1–5, and is of basic importance since the mathematical model used in predicting critical surface and embedded flaw sizes assumes this shape (1).

For through-the-thickness cracks, the mode of fracture for a given material, strength level, and test temperature is dependent upon material thickness. If the material is relatively thin, plane-stress conditions are generally predominant. With increasing thickness, the fracture appearance changes from that of full shear to an essentially flat or plane-strain fracture. Thus, for thin sections containing through-the-thickness cracks, the plane-stress fracture toughness (K_c) values are of primary importance and as the thickness is increased the plane-strain (K_{Ic}) values should be used. This is discussed in more detail in Ref (1) in conjunction with the probable types of flaw growth that can lead to structural failure.

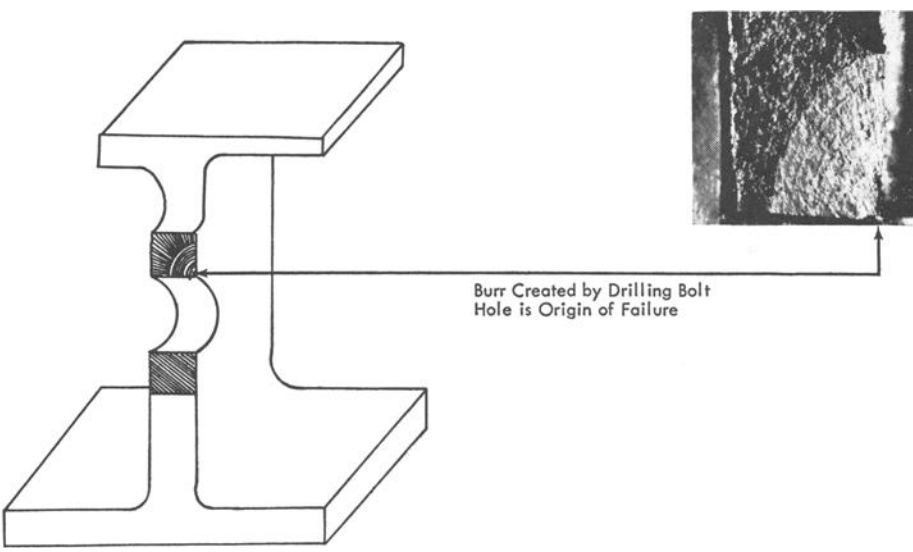

FIG. 5—Structural Stiffener Failure.

THE SELECTION OF A FRACTURE-TOUGHNESS SPECIMEN

In that Refs (1) and (2) discuss the various types of fracture specimens and the requirements for valid toughness measurements in considerable detail, it is not considered necessary to repeat them in this paper. However, it does appear appropriate to point out the significance of end-hardware application and material anisotropy on specimen selection and to show fracture-toughness correlations between several of the more common specimens.

Since conventional mechanical properties generally vary to some degree among various forms and grain directions in a given basic alloy, it is reasonable to expect that fracture toughness values

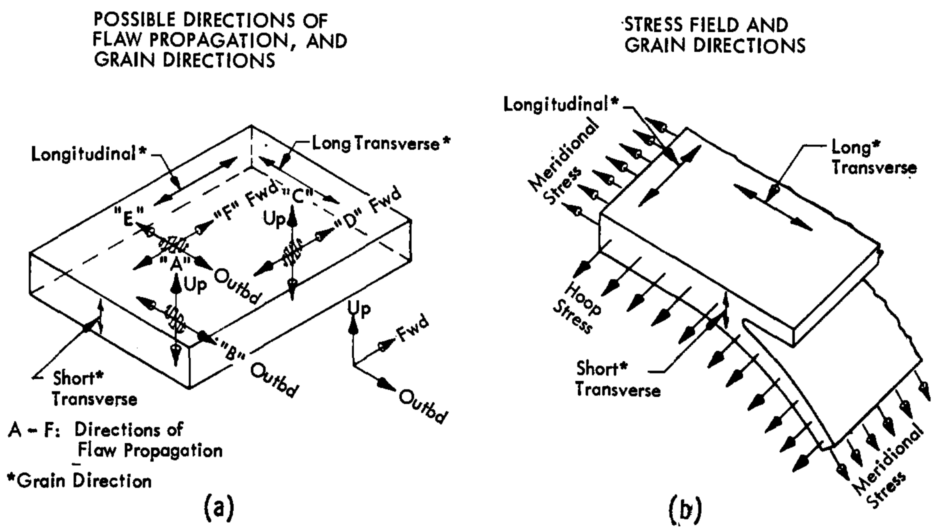

FIG. 6—Stress Field, Grain Directions, and Possible Directions of Flaw Propagation.

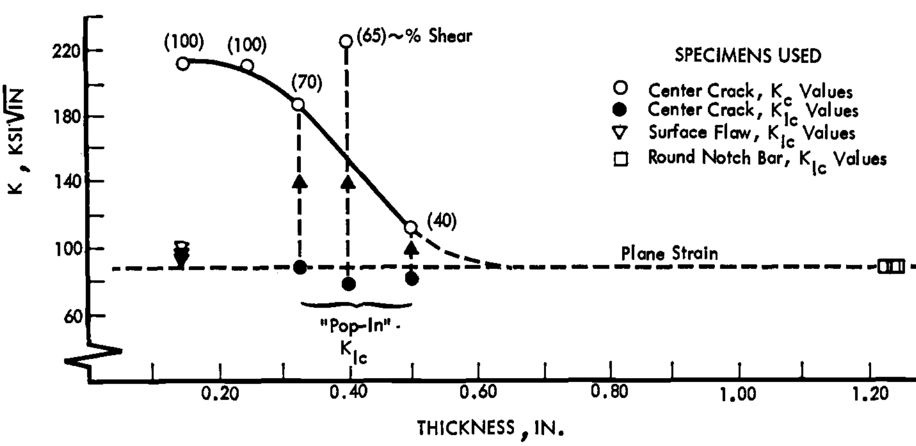

FIG. 7—Specimen Correlations, 18 Per Cent Nickel (300) Steel.

also vary. This assumption appears to be borne out by results of fracture tests performed to date on various materials.

In a rolled plate or forging, six directions of flaw propagation are possible (3), and plane-strain toughness (K_{Ic}) values may differ in each of these directions (see Fig. 6(*a*)). The need to determine the K_{Ic} values in each of these directions is directly dependent on the direction of the applied stresses in the hardware. For example, in a motor-case cylindrical shell, the stress field is biaxial in the plane of the plate. Stresses are applied in both the longitudinal and long-transverse grain directions, indicating the K_{Ic} values of interest are those relating to the *A*, *B*, *C*, and *D* directions of propagation. In such forgings as roll-forged Y rings (Fig. 6(*b*)) stress is applied in all three grain directions, thus indicating the additional need for K_{Ic} measurements in the E and F directions.

Considering the banding and delamination problems in some thick plates, it appears intuitively that the K_{Ic} values can be different between the A and B directions and, likewise, the C and D directions. This has been found to be measures the lowest of either the A or B directions, or the lowest of either the C or D directions. For material where there are no pronounced directional effects, the same toughness should be obtained regardless of which of the specimens is used. This is illustrated for 18 per cent nickel (300) vacuum-melted maraged steel in Fig. 7. Figure 8 shows a

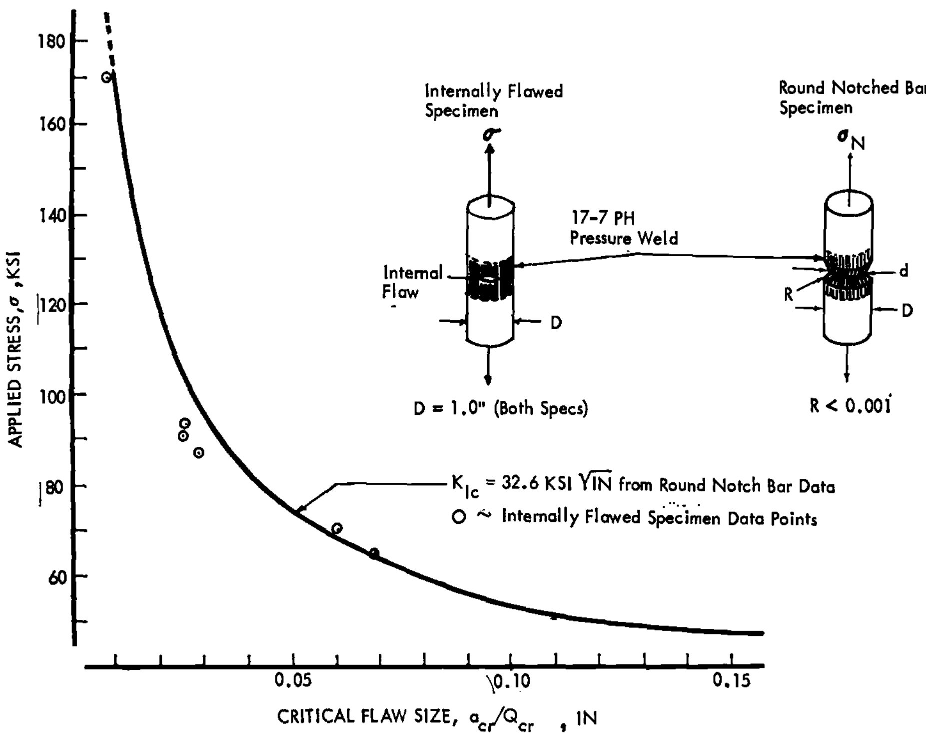

FIG. 8—Internal Flaw Correlations.

the case (4) and tends to explain the differences in K_{Ic} values obtained using surface-flawed and round notched bar or single-edge-notched fracture specimens. The surface-flawed specimen is normally used to measure the toughness in either the A or C directions, while the single-edge-notched or center-cracked (pop-in) specimens measure the toughness in the B or D directions. The round notched bar (removed so that its longitudinal axis is parallel to the plate surface) comparison of internally flawed 17-7PH steel pressure-welded specimen data with that obtained from round notched bar tests. The internal flaws were introduced by placing tungsten flakes on the edge preparation prior to welding. It is noted that in addition to illustrating specimen correlation, the data tend to support the basic relationship between failure stress and flaw size. The term, a/Q, as used to describe flaw size is discussed in Ref (1).

In the short transverse direction, there appears to be no reason for believing that there should be a significant difference in K_{Ic} values between the E and F directions; however, to our knowledge, there has been no experimental substantiation of this. Likewise, for weldments, we know of no major differences existing in K_{Ic} values for a flaw propagating parallel to the plate surface (B or D directions) as compared to a flaw propagating normal to the surface (A or C directions). However, it is known that there can be differences in fracture toughness between the weld centerline and the heat-affected zone. In addition, it is considered probable that there are differences in fracture toughness as well as subcritical flaw-growth characteristics within the heat-affected zone, and, if realistic allowable flaw sizes are to be established, the minimum K_{Ic} values must be determined.

Measurement of the actual K_{Ic} values and variations in K_{Ic}, which occur due to material anisotropy, direction of flaw propagation, and metallurgical differences, requires the use of fracture specimens designed to yield valid data. The actual specimen selection is dependent on the direction in which the K_{Ic} measurement is desired and the ability to design a large enough specimen out of the material gage to prevent general yielding prior to fracture. While round notched bar specimens might be considered to be desirable because they automatically obtain the lowest toughness value in either the A or B directions, or the lowest in either the C or D directions, it may not always be possible to use the specimen type because of material thickness limitations (that is, the specimen diameter needed to get a valid K_{Ic} value exceeds the hardware wall thickness).

In such a case, the single-edge-notched specimen might be used to obtain the toughness in the B and D directions and the surface-flawed specimen in the A and C directions. The arbitrary use of a very large diameter round notched bar fabricated from material other than that to be used in the hardware is questionable because of possible differences in toughness between the specimen material and the hardware material.

In short, it is the authors' opinion that there is no single "best fracture specimen" to use in all situations where toughness values are needed—nor is such a specimen required. Of primary importance is that the specimen selected provide toughness data which are representative of the toughness of the material as it is used in the hardware application. As such, the toughness values must not be obscured by specimen-size effects, specimen-preparation effects, and loading procedures which are unique to the laboratory test.

THE APPLICATION OF FRACTURE MECHANICS

In the selection of a material and the design of a tension-loaded structure such as a pressure vessel, one must consider the following questions:

1. What are the critical flaw sizes (that is, sizes required to cause failure) in the various portions of the vessel at the expected operational stress levels?
2. What are the maximum initial flaw sizes that are likely to exist in the vessel prior to its being placed into service?
3. Will these initial flaws grow to critical size and cause failure during the expected service life of the vessel?

Quite obviously, the answers to these questions are heavily dependent upon the inherent fracture toughness and subcritical flaw-growth characteristics of the pressure-vessel materials, but in addition, are dependent upon such items as design-safety factors, proof-test fac-

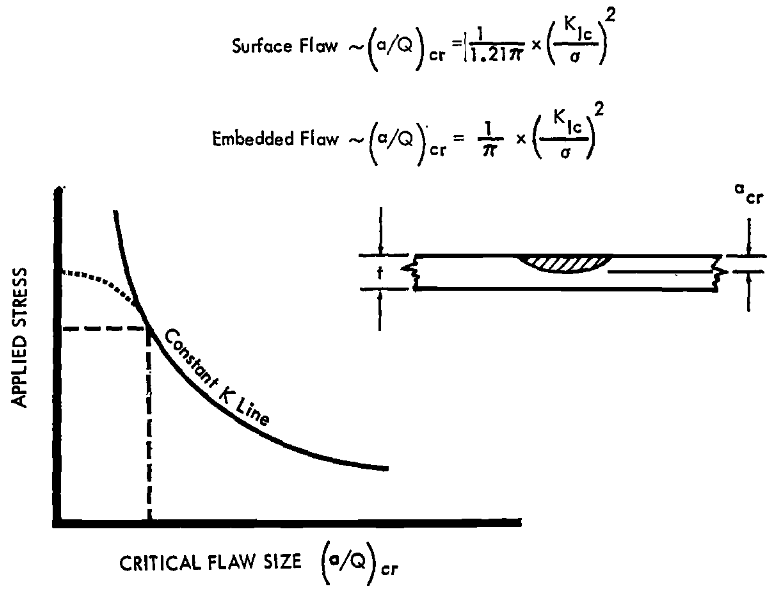

FIG. 9—Applied Stress Versus Critical Flaw Size.

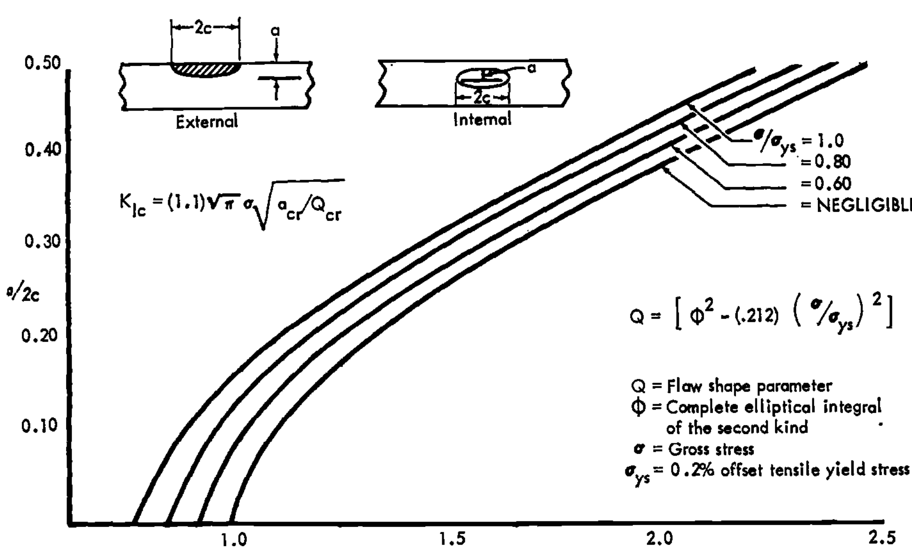

FIG. 10—Flaw-Shape Parameter Curves for Surface and Internal Cracks.

tors and the nondestructive inspection procedures that are used.

The use of fracture-toughness data and fracture mechanics analysis in predicting critical flaw sizes, evaluating subcritical flaw growth, and estimating structural life have been discussed in some detail in Ref (1). Also, Ref (1) points out the use of the conventional proof test as a means of determining the

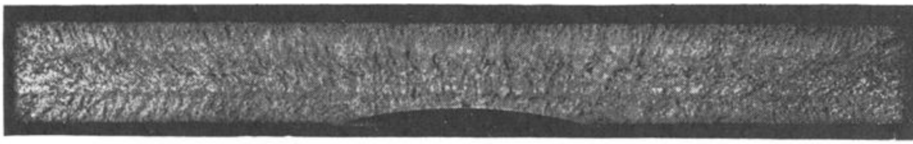

SPECIMEN 1

$a_{cr} = 0.114$ in.
$2c_{cr} = 1.441$ in.
$Q_{cr} = 0.803$
$\sigma_{Fail.} = 30.6$ ksi

$K_{Ic} = 22.6$ ksi in.$^{1/2}$ *

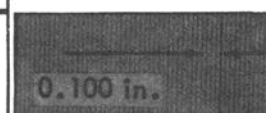

$a_{cr}/Q_{cr} = 0.142$

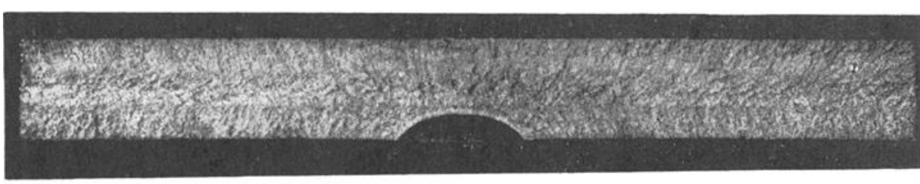

SPECIMEN 2

$a_{cr} = 0.188$ in.
$2c_{cr} = 0.749$ in.
$Q_{cr} = 1.22$
$\sigma_{Fail.} = 30.8$ ksi

$K_{Ic} = 23.5$ ksi in.$^{1/2}$ *

*May be slightly low since $\sigma/\sigma_{ys} > 1.0$

$a_{cr}/Q_{cr} = 0.154$

FIG. 11—The Significance of Flaw Shape.

maximum possible initial flaw size in a pressure vessel. In the following paragraphs a portion of the Ref (1) discussion is repeated, but expanded to include additional experimental data and to point out the significance of fracture toughness data in material selection and the use of fracture mechanics to arrive

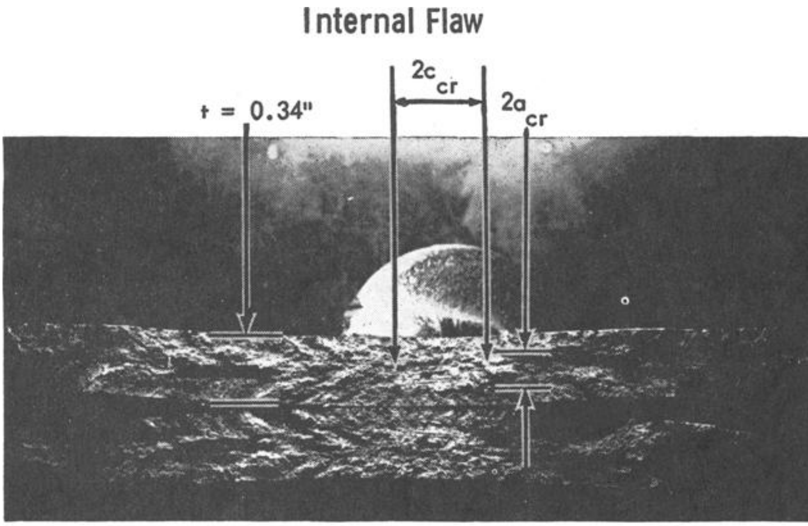

17-7 PH FORGED TANK
FAILURE ORIGIN

$\sigma_{Failure}$ = 116,000 psi
σ_{Yield} = 165,000 psi

ALL VALUES ARE YIELD CORRECTED

MEASURED FLAW SIZE DATA	MEASURED FROM TANK		PREDICTED FROM ROUND NOTCH BAR	
	K_{Ic}	a_{cr}/Q_{cr}	K_{Ic}	a_{cr}/Q_{cr}
$2a_{cr}$ = 0.1670 In. a_{cr} = 0.0835 In. $2c_{cr}$ = 0.355 In. Q_{cr} = 1.32	51,300	0.0632	48,700	0.0564

FIG. 12—Comparison of Measured and Predicted Critical Flaw Size.

at rational nondestructive inspection acceptance limits. Primary emphasis is placed upon surface and embedded flaws which can attain critical size prior to growing through the thickness. This is the most dangerous condition in that both the subcritical flaw growth and final critical flaw size are controlled by plane-strain conditions and in the case of high-pressure tanks, there is no ad-

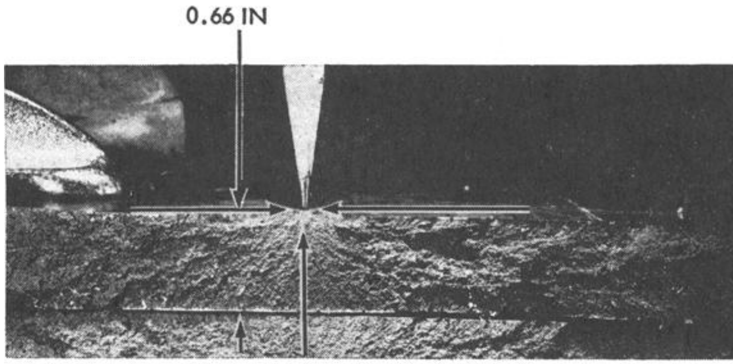

17-7 PH FORGED TANK
FAILURE ORIGIN

σ Failure = 153,000 psi
σ Yield = 160,000 psi

ALL VALUES ARE YIELD CORRECTED

FLAW SIZE DATA	MEASURED FROM TANK		PREDICTED FROM ROUND NOTCH BAR	
	K_{Ic}	a_{cr}/Q_{cr}	K_{Ic}	a_{cr}/Q_{cr}
a_{cr} = 0.075 In. $2c_{cr}$ = 0.15 In. Q_{cr} =2.26	54,000	0.033	53,000	0.031

FIG. 13—Comparison of Measured and Predicted Critical Flaw Size.

vance warning (such as leakage) of failure.

The Prediction of Critical Flaw Sizes and Their Role in Material Selection:

As noted in the previous sections, K_{Ic} values can be obtained from several types of specimens. Having developed valid data for a given material form (that is, plate, forging, weldment, etc.), heat-treat level, and test temperature, the critical flaw size can be calculated for a given hardware operating stress. For convenience, the relationship of flaw size to stress is usually plotted as shown in Fig. 9. Note that we have elected to use the term, a/Q, to describe flaw size as is discussed in Ref (1). The plot of Q versus the depth-to-length ratio $(a/2c)$ of surface and embedded flaws is given in Fig. 10. With regard to this point, it is noted that a considerable amount of data has been published in which surface-flaw sizes have been

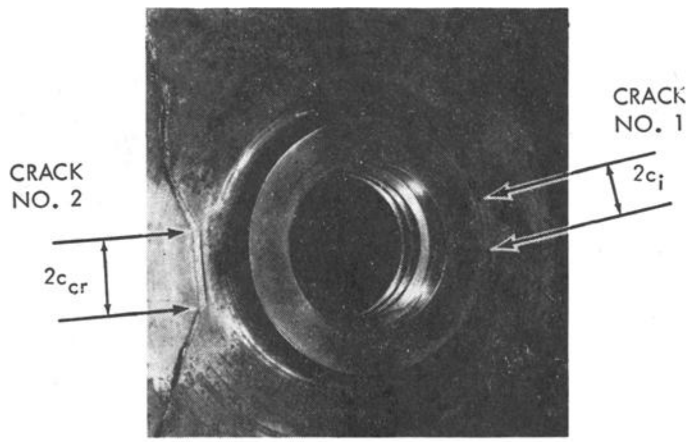

17-7 PH-FORGED TANK HEAD

σ Failure = 108,000 psi
σ Yield = 165,000 psi

ALL VALUES ARE YIELD CORRECTED

MEASURED FLAW SIZE DATA		MEASURED FROM TANK		PREDICTED FROM ROUND NOTCH BAR	
CRACK NO. 1	CRACK NO. 2	K_{Ic}	a_{cr}/Q_{cr}	K_{Ic}	a_{cr}/Q_{cr}
a_i = 0.041 In. $2c_i$ = 1.02 in. Q_i = 0.9 a_i/Q_i = 0.0414 In.	$a_i = a_{cr}$ = 0.045 In $2c_i = 2c_{cr}$ = 0.99 In. $Q_i = Q_{cr}$ = 0.9 $a_i/Q_i = a_{cr}/Q_{cr}$ = 0.0454 In.	44,900	0.0454	49,500	0.055

FIG. 14—Comparison of Measured and Predicted Critical Flaw Size (External Artificial Semi-Elliptical Flaw).

plotted in terms of flaw length, depth, or area versus gross failure stress. While such data can have a useful meaning if the $a/2c$ ratios are held constant, the $a/2c$ values are usually absent in the published reports.

The fallacy of such a presentation is obvious after reviewing the test data shown in Fig. 11. Here, two specimens with different flaw depths, lengths, and areas were tested, yet both failed at approximately the same stress. Both had approximately the same a/Q ratio, and thus the same K_{Ic} values.

The engineering usefulness of the basic stress-intensity concept in the prediction of critical flaw sizes and the use of a/Q to describe flaw size has been supported by a number of hardware correlations. Some such correlations are

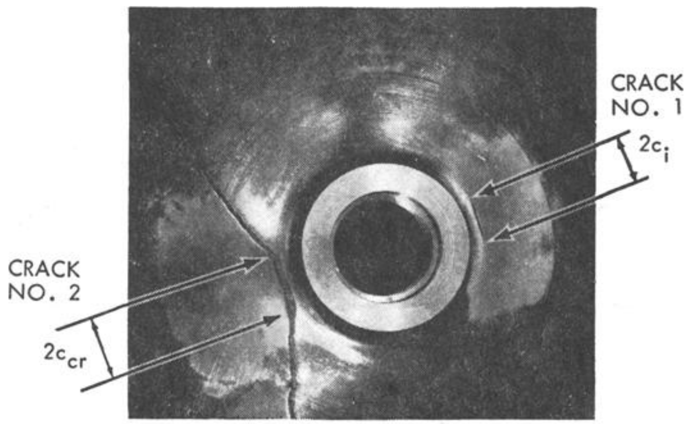

17-7 PH FORGED TANK HEAD

$\sigma_{Failure}$ = 110,000 psi

σ_{Yield} = 162,000 psi

ALL VALUES ARE YIELD CORRECTED

MEASURED FROM TANK FLAW SIZE DATA				PREDICTED FROM ROUND NOTCHED BAR	
CRACK NO. 1	CRACK NO. 2	K_{Ic}	a_{cr}/Q_{cr}	K_{Ic}	a_{cr}/Q_{cr}
a_i = 0.05 In. $2c_i$ = 1.05 in. Q_i = 0.93 a_i/Q_i = 0.0538 In.	$a_i = a_{cr}$ = 0.05 In. $2c_i = 2c_{cr}$ = 1.20 in. $Q_i = Q_{cr}$ = 0.90 $a_i/Q_i = a_{cr}/Q_{cr}$ = 0.055 In.	50,500	0.055	53,200	0.058

FIG. 15—Comparison of Measured and Predicted Critical Flaw Size (External Artificial Semi-Elliptical Flaw).

shown in Ref. (1) and in Figs. 12 through 15 of this paper.

From the equations shown in Fig. 9, it can be readily seen that the critical flaw size is equally as dependent upon applied stress level as upon the material fracture toughness. This is of basic importance when selecting a material or a heat-treat strength level, or both, for a given structural application and should be recognized when evaluating K_{Ic} data.

For the purpose of screening several materials for an end-product application K_{Ic} data are often plotted as shown in Fig. 16(a). This is a simple and useful plot showing the general trends in toughness with increase in strength level in the aluminum, titanium, and steel alloys. However, such a comparison can be misleading. For instance, a designer may reach for higher and higher material strength levels by noting the minor

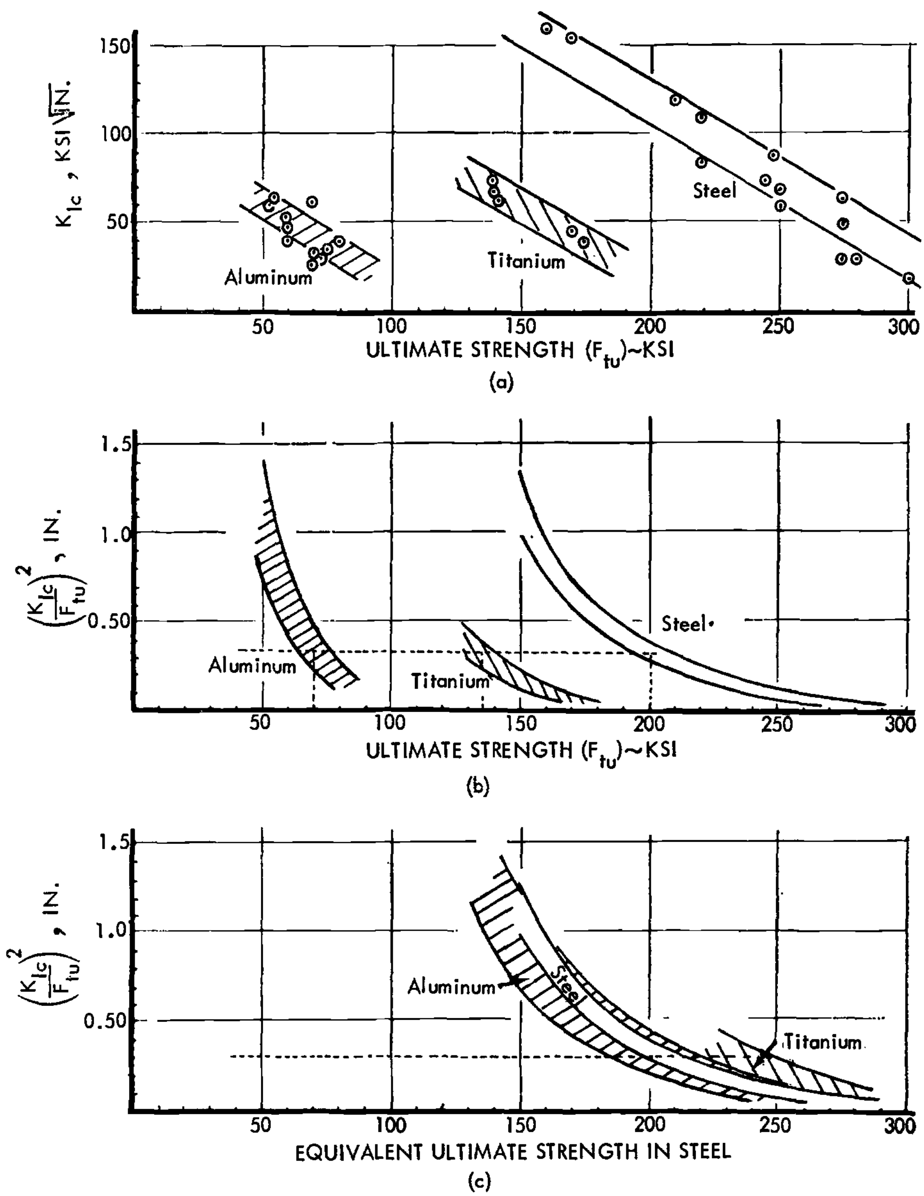

FIG. 16—Material Comparisons (Base Metal, Room-Temperature Trends).

reduction of toughness corresponding with such strength level increases.

Recognizing that the operating stress levels in structures are generally controlled to a fixed percentage of the unflawed tensile strength by the design factor of safety (that is, the actual factor of safety is often specified by the procuring agency), the data shown in Fig. 16(*a*) might more appropriately be plotted as shown in Fig. 16(*b*). The ordinate of Fig. 16(*b*) is directly proportional to the critical flaw size, thus placing the influence of varying material strength levels into better perspective. For example, an increase in ultimate strength level from 50 to 60 ksi in aluminum shows a rather nominal drop in K_{Ic} from approximately 60 ksi $\sqrt{\text{in.}}$ to 50 ksi $\sqrt{\text{in.}}$; however, in terms of critical flaw size, the use of the higher strength material represents a major decrease. The critical flaw size using the 60-ksi strength level material is

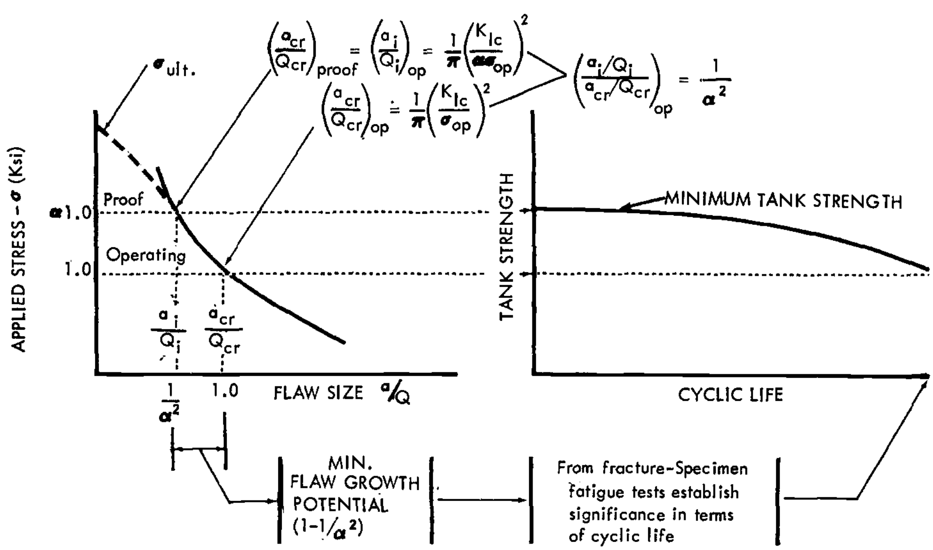

FIG. 17—Significance of Proof Testing in Estimation of Minimum Tank Life.

only one half the value obtained with the 50-ksi material. Also, from Fig. 16(*b*) the three materials can be compared upon the basis of equal critical flaw size. For example, pressure vessels designed from a 200-ksi steel, a 135-ksi titanium, and a 70-ksi aluminum would all have approximately the same critical flaw size at a given operating pressure (that is, operating stress which was a fixed percentage of the material tensile strength).

Considering the effect of structural weight, one might wish to make the further comparison shown in Fig. 16(*c*). From this figure it can be seen that the titanium should provide a somewhat lighter tank on the basis of equal critical flaw size.

Certainly such comparisons provide guidance during initial material screening; however, one must not forget that material anisotropy and variations in material forms cause differences in toughness throughout the structure, and likewise, the applied stress levels generally vary. Consequently, the critical flaw sizes in various portions of the structure will be different. In pressure vessels, weldments and base material loaded in the short transverse direction are particularly prone to low toughness and when combined with pre-existing initial defects and high applied stresses they are potentially dangerous. Weldments and the short transverse parent metal should not be ignored during the initial material screening. Also, the susceptibility of the material to subcritical flaw growth in the expected service environment should not be ignored.

While it is desirable that the material selected for a given structural application have large critical flaw sizes at the operational stress levels, low subcritical flaw-growth rates, and low probability of flaw occurrence (that is, good fabricability), actual material selection will generally involve a compromise.

The material screening program should provide sufficient insight into these items to allow a rational compromise.

The Estimation of the Life of Pressure Vessels Subjected to Cyclic and Sustained Stresses:

With pressure cycles and time at stress, an initial flaw or defect in a pressure vessel (or any other structure) will grow in size until it attains the critical size at the applied operating stress level and failure will result. The flaw-growth potential (in inches) is equal to the critical size minus the initial size. The life of the vessel is directly dependent upon this flaw-growth potential and the subcritical flaw-growth characteristics of the tankage materials.

Determination of the initial flaw sizes generally relies upon the use of nondestructive inspection procedures; however, as discussed in Ref (1), the conventional proof test can be considered to be one of the most positive inspection procedures available. A successful proof test actually defines the maximum possible initial flaw size that exists in the vessel. This results from the functional relationship between stress level and flaw size as defined by the critical stress intensity (K_{Ic}) and as illustrated earlier in Fig. 9. This is illustrated in Fig. 17. As seen in this figure, the ratio of maximum initial flaw size to critical flaw size, $(a/Q)_i/(a/Q)_{cr}$ is equal to $1/\alpha^2$, where α is the proof-test factor. Similarly, the ratio of maximum initial stress intensity to critical stress intensity, K_{Ii}/K_{Ic}, is equal to $1/\alpha$. Both are independent of the actual proof stresses, and the actual material toughness values. This is significant, since the actual proof stresses may be different because of design or manufactured discontinuities, and because the toughness values will likely vary between base metal, weldments, and forgings.

Also, as noted in the figure, the minimum flaw-growth potential in the tank, $(a_{cr}/Q_{cr} - a_i/Q_i)$, is equal to $(1 - 1/\alpha^2)$.

Probably the most predominant types of subcritical flaw growth are fatigue growth resulting from cyclic stress and environmentally induced sustained stress growth. Also, growth may occur even in the absence of severe environmental effects if the initial flaw size approaches the critical flaw size.

The technique used for predicting the subcritical cyclic or sustained stress flaw growth makes use of fracture specimen testing and the stress-intensity concept. It has been shown (1,7) that the time or cycles to failure at a given maximum applied gross stress level depends on the magnitude of the initial stress intensity at the flaw tip, K_{Ii}, compared to the critical stress intensity, K_{Ic} (that is, cycles or time to failure $= f(K_{Ii}/K_{Ic})$. Also, it is seen that the ratio of initial flaw size to critical flaw size is related to the stress-intensity ratio as follows:

$$\left(\frac{K_{Ii}}{K_{Ic}}\right)^2 = \frac{a_i/Q_i}{a_{cr}/Q_{cr}}$$

Thus, if cyclic or sustained stress fracture specimens are used to obtain experimentally the K_{Ii}/K_{Ic} versus cycles or time curves for a material, the cycles or time required for any given initial flaw to grow to critical size can be predicted. Conversely, if the required life of the structure is known in terms of stress cycles or time at stress, the maximum allowable initial flaw size can be determined.

The growth of through-the-thickness cracks with repeated stress cycles can and has been investigated (5) with relatively little difficulty since this growth can be visually observed and measured. With surface or embedded flaws (plane-strain condition), measurement of the actual growth is restricted because of the inability to make such visual observations.

What normally is obtained from a plane-strain fracture specimen cyclic test are the initial flaw size, the critical size as measured from the fracture face, the cycles it took to grow from initial to critical size, and the initially applied cyclic stress. From these data, the initial stress intensity, K_{Ii}, and the critical stress intensity, K_{Ic}, can be calculated.

In our plane-strain cyclic flaw-growth investigations, the round notched bar and the surface-flawed specimen are used as the primary experimental tools. For each material investigated, several specimens are statically tested to failure to obtain K_{Ic} values. Additional specimens are then loaded to various percentages of the critical stress intensity and cycled to failure. For round notched bars, the initial stress intensities (K_{Ii}) are calculated by substituting the maximum net-area cyclic stress in place of the net-area fracture stress, σ_N. As cycling progresses, the notch deepens under plane-strain conditions (in the same manner as a flaw grows in a tank under cycling load) and for the specimen, by virtue of the ever-increasing stress on the net area, the stress intensity increases from the initial value, K_{Ii}, to the critical value, K_{Ic}, at which time failure occurs. For surface-flawed specimens, the initial and critical stress intensities are calculated, using straightforward measurements of initial and critical flaw sizes, and gross stress. Since flaw area is controlled to a small percentage of gross area, the increase in net-area stress with cycles is negligibly small.

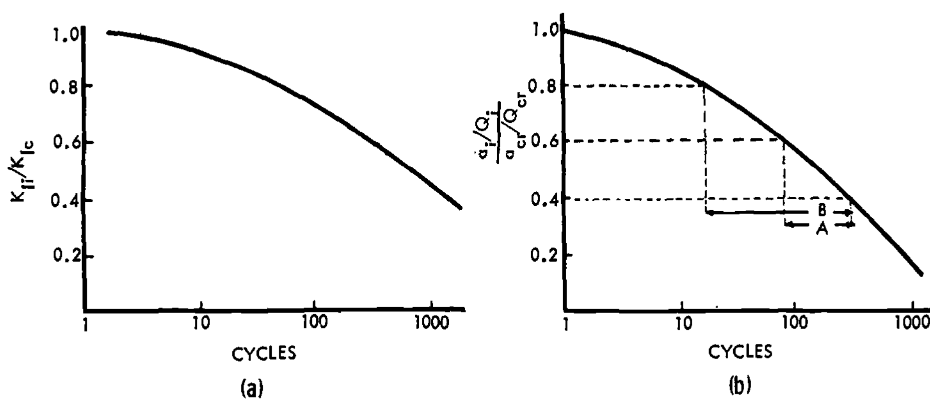

FIG. 18—Schematic Representation of Cyclic Flaw Growth.

The cyclic flaw-growth data are plotted in terms of stress-intensity ratio, K_{Ii}/K_{Ic}, versus log of cycles as shown schematically in Fig. 18(*a*). By squaring the ordinate value, the plot of the ratio of initial flaw size to critical flaw size versus the log of cycles (shown in Fig. 18(*b*)) can be obtained. With knowledge of the initial flaw size and the calculated critical flaw size, the total

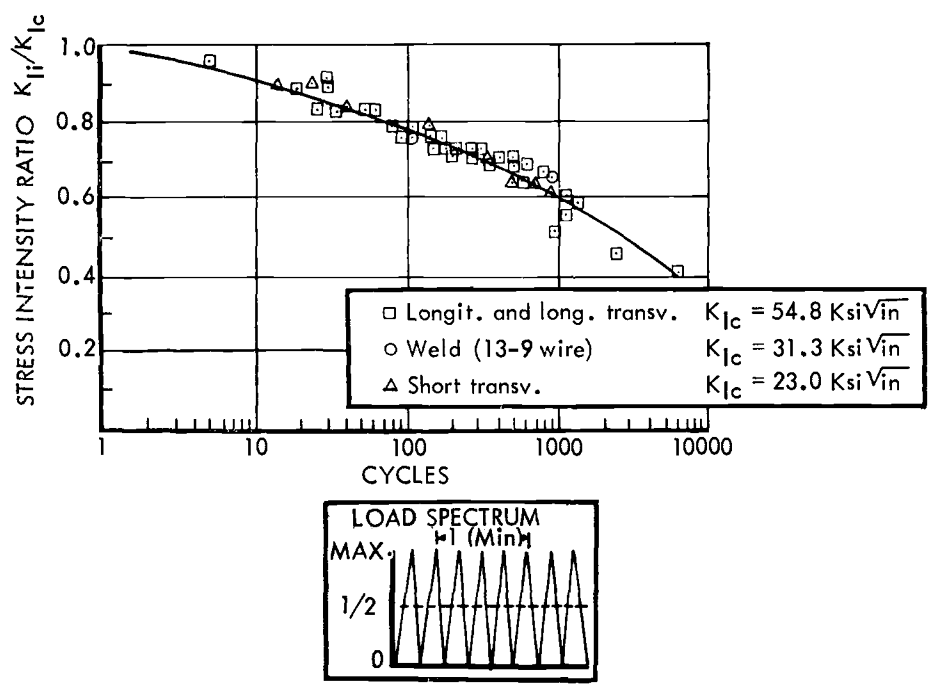

FIG. 19—Round Notched Bar Fatigue Data for 17-7PH Steel (Plate Forging, Room Temperature).

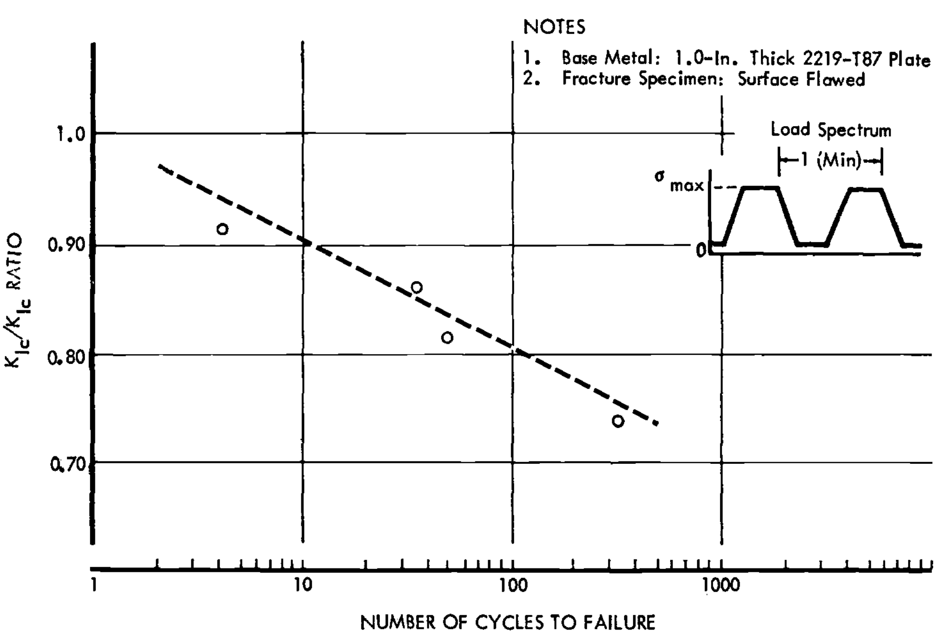

FIG. 20—Base Metal Cyclic Flaw-Growth Data (−320 F, Longitudinal Grain).

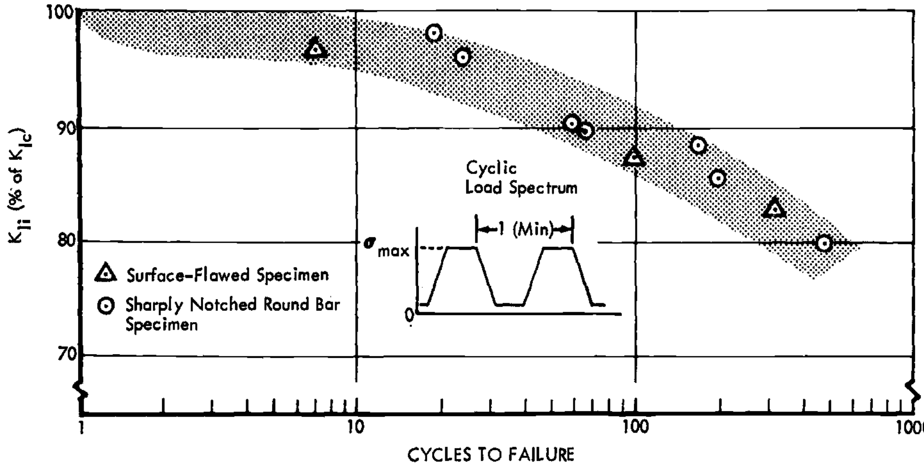

FIG. 21—Cyclic Flaw-Growth Data of 6Al-4V Titanium Plate Tested at −320 F.

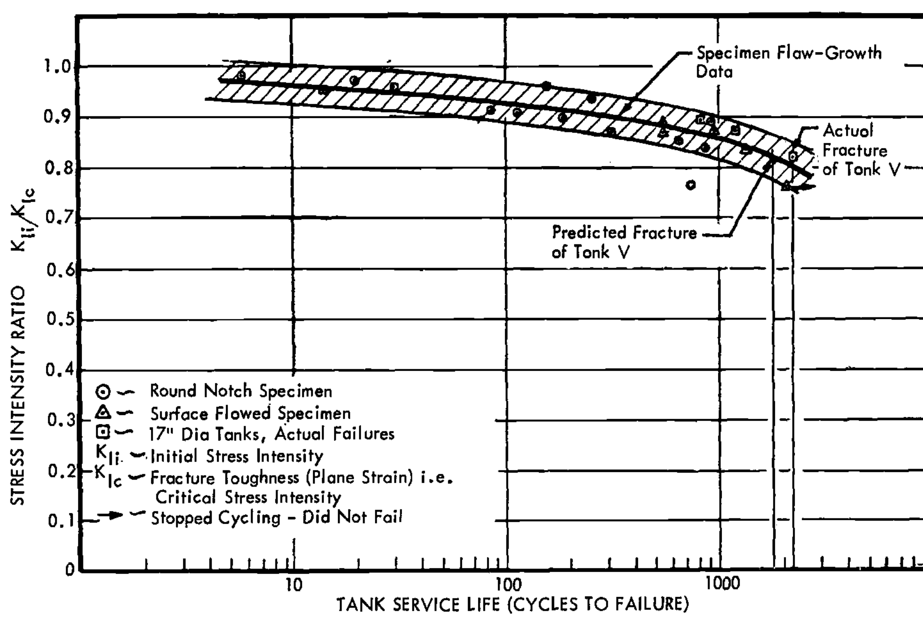

FIG. 22—Prediction and Verification of Tank Service Life from Specimen Flaw-Growth Data.

cycles to failure can be obtained directly from the plot. If the proof test is used, $1/\alpha^2$ can be entered on the ordinate and the minimum cycles to failure read off the abscissa. It should also be recognized that flaw size can be determined after any incremental number of cycles. For example: if the initial flaw-size ratio was 0.40, in A cycles the flaw would have grown, increasing the ratio to 0.6; in B cycles, it would have grown to 0.8, etc.

Cyclic flaw-growth data have been obtained on a number of materials using round notched bar and surface-flawed

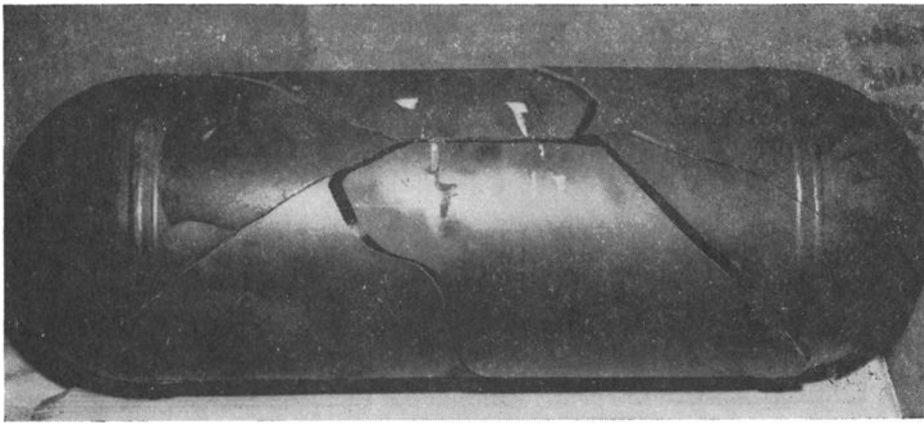

FIG. 23—Over-All View of Preflawed Tank.

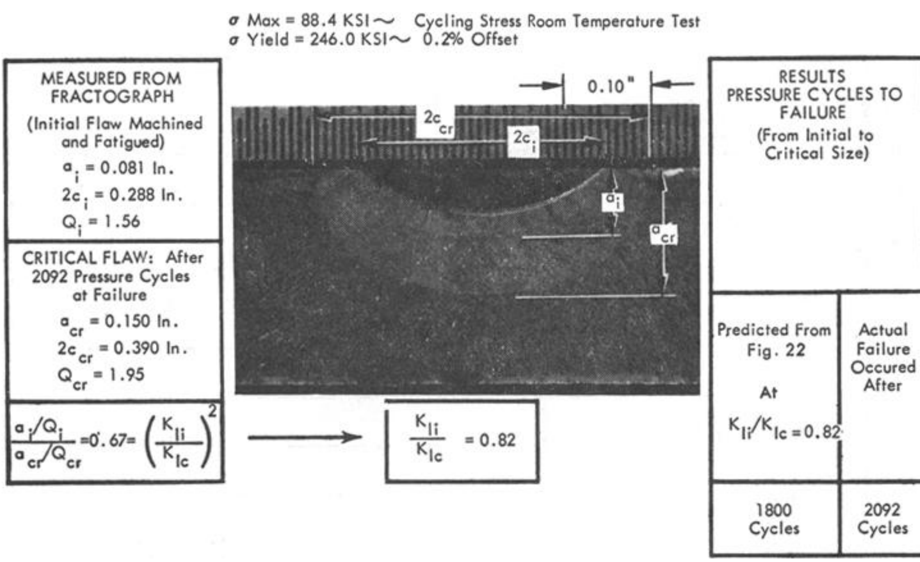

FIG. 24—Tank V, Origin-of-Failure Fractograph (17-in. Diameter Ladish D6AC Steel Tank).

specimens. Some such data are shown in Figs. 19–22. It is noted that in Fig. 21, both round notched bar and surface-flawed fracture specimen data are shown; in Fig. 22, round notched bar, uniaxial surface-flawed specimen, and preflawed tank data are shown. These data have recently been obtained on Air Force Contract AF 33(657)-10251. The purpose of this program was to verify the applicability of fracture mechanics to the prediction of low cycle pressure-vessel failures and consisted of fatigue testing a number of fracture specimens and preflawed tanks. The initial flaws were introduced in the tanks using an electrical discharge machine (EDM) and extended a small amount by low stress

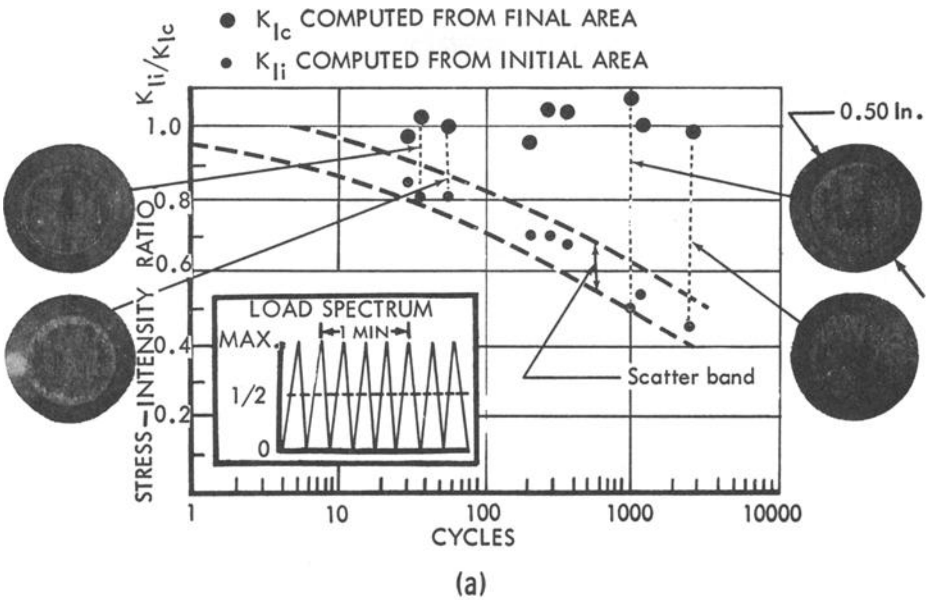

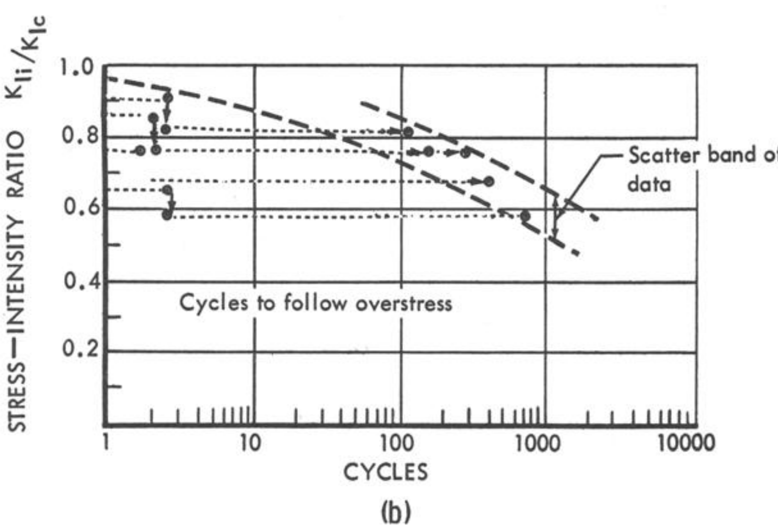

(*a*) Effect of cycling on K_{Ic} in a room-temperature test of 17-7PH steel (longitudinal and long-transverse plate and forging).

(*b*) Effect of initial overstress on subsequent cycles to failure for a 17-7PH steel (longitudinal grain forging).

FIG. 25—Effect of Cycling and Overstress.

and high-cycle fatigue (that is, pressure cycling). The tanks were then subjected to the operational cycles (0–100 per cent –0 pressure) until failure. The maximum gross-area stress during the operational cycles was approximately 100 ksi. The material yield strength was 247 ksi. After failure, both the initial and critical flaw sizes were measured and the initial and critical stress intensities computed. A photograph of a failed pressure vessel (17 in. in diameter and approximately 0.25 in. in wall thickness) is shown in Fig. 23. Figure 24 shows a typical fractograph of one of the failure origins.

Although the question may arise as to the possible effect of cycling stress on K_{Ic} due to metallurgical changes in the material, the experimental data on several alloys indicate that K_{Ic} remains essentially constant. This is illustrated in Fig. 25(*a*), where the K_{Ic} values were computed from the fatigued specimens. As seen from the figure, the notch deepening is quite large when the applied initial stress intensity is low. For these cases, the round notched bar specimen equation of Ref (6) is not strictly applicable for computation of K_{Ic} values. The 0.233 coefficient in the equation decreases with decreasing d/D. The coefficient was modified in accordance with Ref (6) in the computation of K_{Ic} values where the net area at failure was sufficiently small.

To determine whether an initial overstress (that is, the proof test) has any major influence on cyclic growth at a lower stress, a number of round notched specimens were given a two-cycle 10 per cent overstress prior to cycling to failure. As expected, there was no significant effect. This is shown in Fig. 25(*b*). It should be recognized that the effects of gross overloads (as in random loading profiles) might influence growth rates on subsequent cycles. It has been noted by several investigators (8,9) in cyclic crack-growth tests of center-cracked sheet specimens that there is a marked reduction in cyclic growth rate after an initial high overstress.

In the 17-7PH steel specimen tests shown previously in Fig. 19, the cyclic speed was varied between 20 min per cycle to 32 cycles per minute with little apparent effect on the cyclic growth

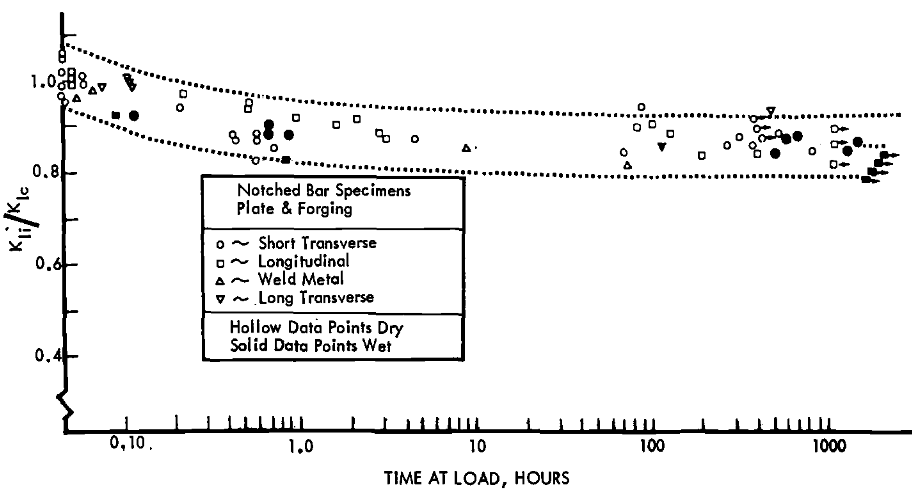

FIG. 26—Sustained Stress Data for Room-Temperature Tests of 17-7PH Steel.

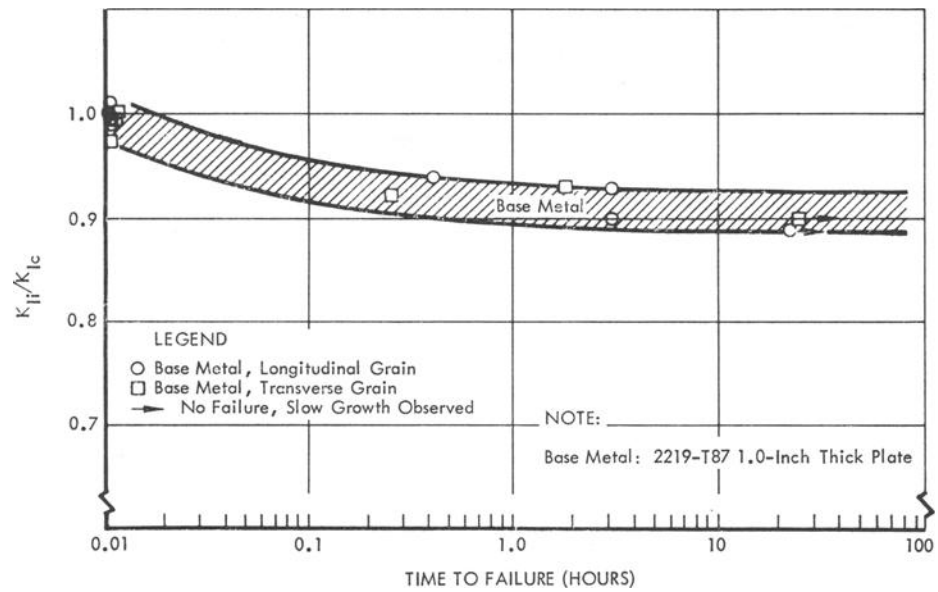

FIG. 27—Sustained Stress Flaw-Growth Data Obtained at −320 F.

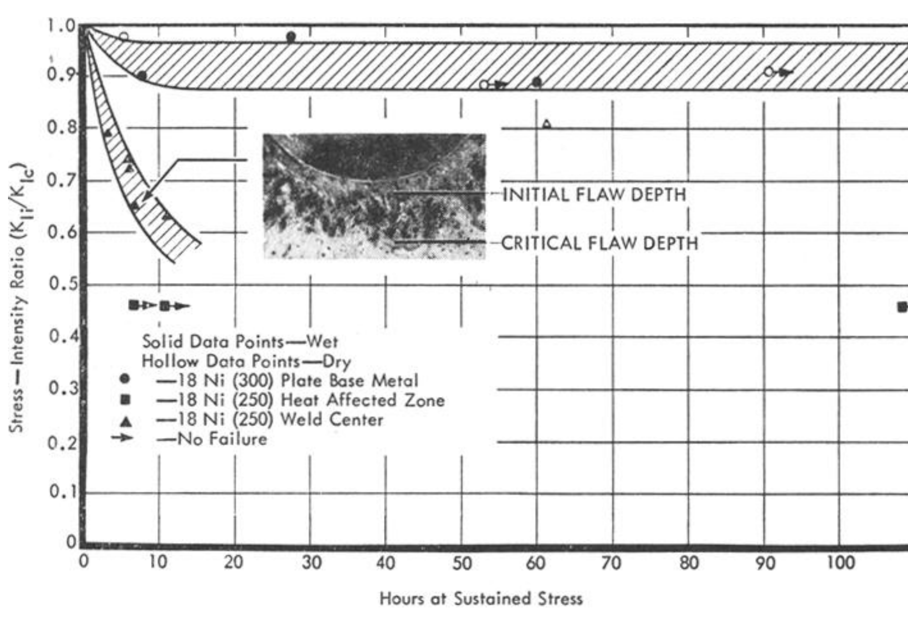

FIG. 28—Effects of Environment on Flaw-Growth Characteristics in Room-Temperature Tests.

rates until the initial stress intensity became very high with respect to the critical value. At the high stress intensities there was an apparent interaction between sustained stress and cyclic growth, causing the specimens cycled at slow speeds to fail early. This will be discussed further in subsequent paragraphs. At much higher cyclic speeds (approximately 500 cycles per minute) the flaw-growth rates decreased.

The application of fracture-specimen testing to define the effects of sustained load on flaw growth is essentially the same as used in defining cyclic flaw growth. A constant load is applied to either a round notched bar or surface-flawed specimen such that the initial stress intensity is less than the critical value and the time to failure is recorded. The K_{Ii}/K_{Ic} values are computed and the K_{Ii}/K_{Ic} ratio plotted versus log of time to failure. Reference (1) shows such sustained stress flaw-growth data for annealed 6Al-4V titanium and points out that there appears to be a threshold stress-intensity level below which sustained stress growth does not occur. Also, these data indicated that the K_{Ic} was not significantly altered by the subcritical growth mechanisms.

The existence of a threshold stress-intensity level is further supported by the data in Figs. 26 and 27 of this paper. Figure 26 shows round notched bar test data for 17-7PH steel tested in both dry and wet environments and Fig. 27 shows surface-flawed specimen data for 2219-T87 aluminum tested in liquid nitrogen. In neither case does it seem that the environment played an important role in the sustained stress growth. In both cases the apparent threshold stress-intensity levels are quite high. As noted in Fig. 28, water had a significant effect on the sustained stress flaw growth of

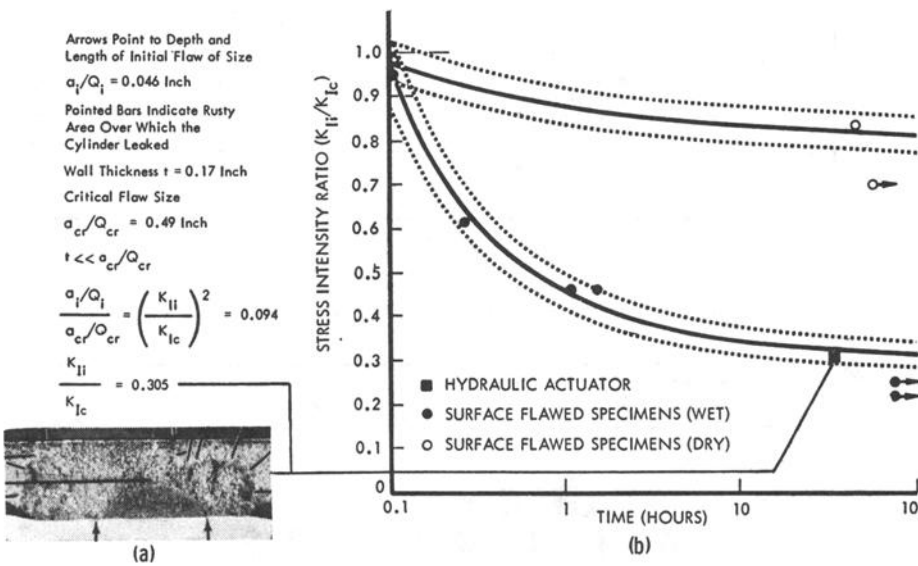

(*a*) 4330M steel actuator cylinder.
(*b*) Surface-flaw specimen test, sustained stress, 4330 steel actuator material.
FIG. 29—Analysis and Verification of Cylinder Failure.

welded 18 per cent nickel (250) steel. However, there are insufficient test data to define a threshold stress-intensity level. Likewise, for the 4330M steel shown in Fig. 29, water had a significant effect and in this case the threshold stress-intensity level appears to be approximately 30 per cent of the critical value. Also shown in Fig. 29 is a fractograph of the fracture origin of a 4330M steel hydraulic actuator (wall thickness, t = 0.17 in.) used in a ground-support the time of fracture. From the results of testing sustained stress surface-flawed specimens in water and from the magnitude of the initial stress intensity in the cylinder (K_{Ii}/K_{Ic} = 0.305), it is apparent that the subcritical growth and subsequent leakage experienced might have been expected.

Let us now consider the significance of sustained stress flaw growth and specifically the threshold stress-intensity concept on the estimated total cyclic life of

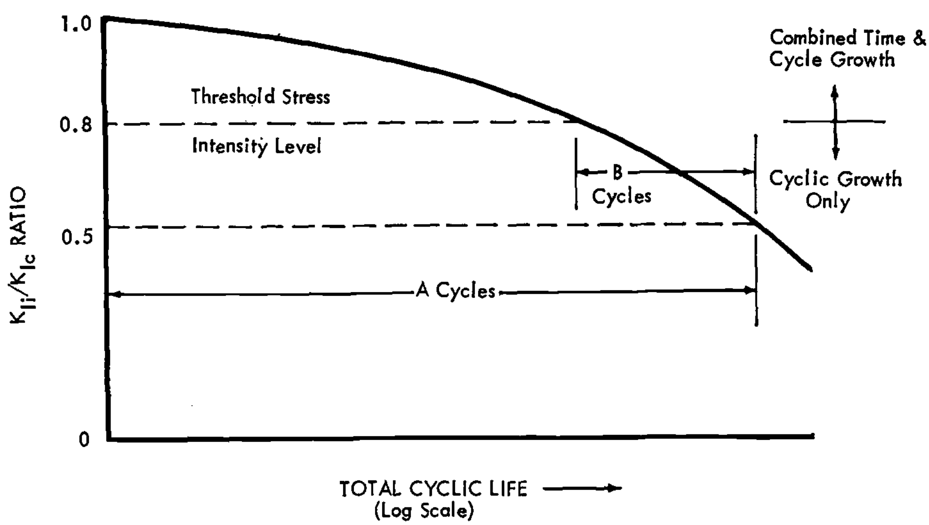

FIG. 30—Combined Cyclic and Sustained Stress Flaw-Growth Schematic Interpretation.

system. In addition to illustrating sustained-stress growth, it also illustrates a leak-before-failure condition. The actuator leaked after 32 hr at a sustained stress of approximately 72.8 ksi. The critical flaw size, based on the measured K_{Ic} of the material (approximately 100 ksi $\sqrt{\text{in.}}$) and the applied stress of 72.8 ksi, is a_{cr}/Q_{cr} = 0.49 in. This exceeded the wall thickness. The initial flaw size (a pre-existing crack) was measured to be a_i/Q_i = 0.046 in., and the initial stress intensity was 30.5 ksi $\sqrt{\text{in.}}$ Since rust was apparent on the fracture surface, it appeared that moisture was present at a tension-loaded structure containing an initial crack or crack-like flaw. To illustrate this, the schematic representation of the K–N curve is reconstructed in Fig. 30, but superimposed on this curve is a horizontal line at K_{Ii}/K_{Ic} = 0.80. This is assumed to be the threshold stress intensity as determined from sustained stress fracture tests as discussed in the previous paragraphs. Now consider the situation where the initial flaw size and applied cyclic stress result in an initial stress intensity equal to 50 per cent of the critical value. From the curve, it is seen that it would take a total of A cycles to grow this initial flaw to critical size and cause failure. However, in B cycles, the initial flaw would have increased in size enough to cause the stress intensity to reach the threshold value of $K_{Ii}/K_{Ic} = 0.80$. With additional cycles, the stress intensity would further increase and, if the stress were sustained sufficiently long, it appears possible that failure could occur on the $(B + 1)$ cycle.

If, on the other hand, the cycles were applied with little time at maximum cyclic stress, it appears that the total of A cycles could be realized. It is hypothesized that below the threshold K-value, the time at sustained stress has little or no effect on cyclic life. Above the threshold value there will be an interaction such that failure could occur anywhere within the range of $(B + 1)$ to A cycles, depending on the time the maximum stress is held during each cycle. The development of the exact time-cycle interaction curves above the threshold value would be a complex and expensive task and, as applied to most tankage structure, may not be of great importance. It appears more rational to determine the basic cyclic data and the threshold-intensity values and then verify (through prolonged-time specimen cyclic tests) that time at load is not of major significance below the threshold value. In application of the data to fatigue-life estimation, the maximum allowable stress intensity would be limited to the threshold value as determined for the material in question and for the applicable service environment. If the threshold value is very low, as is the case for the wet 4330M steel

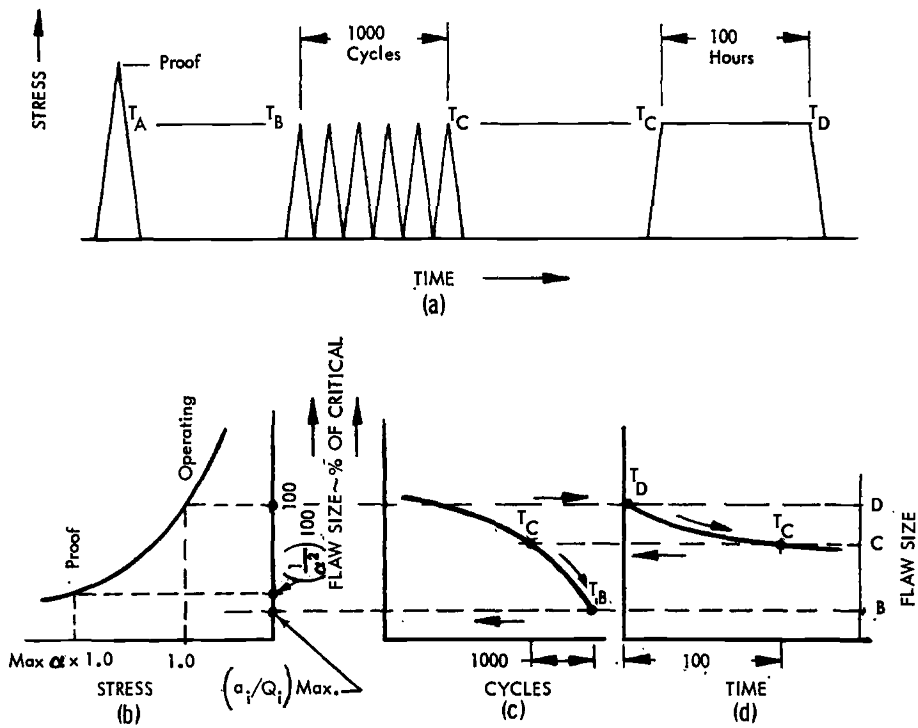

FIG. 31—Structural Life Prediction.

shown in Fig. 29, steps should certainly be taken to protect the material from the environment.

The Determination of Nondestructive Inspection Acceptance Limits:

The information presented in the preceding paragraphs can now be used to discuss the problem of establishing nondestructive inspection acceptance limits if the service-life requirements are known. This might best be illustrated by selecting a hypothetical pressure vessel that is expected to encounter a rather complex loading history. The problem then is to determine the maximum flaw size that can be allowed to exist before the initial pressure cycle and still guarantee that the vessel will not fail during service operation.

As illustrated in Fig. 31(*a*), the assumed service requirement consists of one proof-test cycle (at a stress level of α times the operating stress) followed by 1000 cycles and then 100 hr, both at a constant operating stress level of (σ = 1.0). To define the minimum inspection standards required before the vessel is placed into service, it is necessary to consider the critical flaw size (a_{cr}/Q_{cr}) at the end of service and work backwards, evaluating all portions of the loading profile that can cause flaw growth. The necessary data are shown in Figs. 31(*b*), (*c*), and (*d*). Figure 31(*b*) represents a dimensionless presentation of the relationship of stress to flaw size shown earlier. The ordinate now is plotted in terms of percentage of critical flaw size, at operating stress. Figures 31(*c*) and (*d*) are abstracted from the type of flaw-growth data also shown previously.

The approach is as follows: from Fig. 31(*b*), the critical flaw size at operating stress is represented as 100 per cent of critical, and is the maximum allowed at time, T_D (or at the end of the service life). The effect on flaw growth of the 100-hr sustained time (T_C to T_D) can be read in Fig. 31(*d*). The maximum allowable flaw size at time T_C is then shown by point C and represents the maximum allowable flaw size at the start of the 100-hr sustained stress period. The effect of the cyclic loading is seen in Fig. 31(*c*), by moving 1000 cycles from T_C to T_B. Point B then represents the maximum allowable size at time T_B, or at the start of the 1000-cycle period. This size is also the maximum allowable size before the vessel is placed into service. (Compared to the chosen service life, it can be shown that the previous one-cycle proof test generally has a negligible effect on flaw growth.) Note that in this schematic illustration, the maximum allowable flaw size is less than that which could have been present during a successful proof test, and thus the proof test could not guarantee successful fulfillment of the service-life requirement.

It should be noted that, in terms of "percentage of critical," flaw size is completely independent of actual stress and toughness values. It is obvious that the determination of finite maximum allowable flaw sizes requires a detailed knowledge of applied stresses in the various locations in the tankage, and of the fracture toughness of the materials used.

Additionally, the foregoing example was simplified for purpose of illustration. Actual application would require consideration of the effects of service environment which, depending upon the material, might significantly alter the flaw-growth rates assumed.

When establishing an allowable initial flaw size for inspection purposes, the limitations of the inspection techniques should be recognized, and allowance should be made to account for lack of specific knowledge of flaw geometry and orientation. When there is this lack of definition, the worst possible flaw geometry and orientation might be assumed. For example, the length (L) of an indication seen in X-ray inspection could be assumed to be the minor axis of an elliptically shaped internal flaw where the major axis is large with respect to the minor axis (that is, $L = 2a$, $Q \approx 1.0$).

Also, in arriving at acceptance limits, one must consider allowable spacing for internal or surface flaws (that is, aligned flaws in weldments). An approximate analytical solution for the interaction of elliptically shaped coplanar flaws has been obtained by Kobayashi and Hall (10). The results are shown in Fig. 32 along with experimental results on several Ladish D6AC steel specimens containing two coplanar semi-elliptical surface flaws. These flaws were introduced in the specimens using an electrical discharge machine and extended a small amount by low-stress fatigue.

The curves are plotted in terms of stress-intensity magnification (K_1/K_2) versus flaw spacing. Probably the most significant point is that there is very little interaction between coplanar flaws unless they are surprisingly close together.

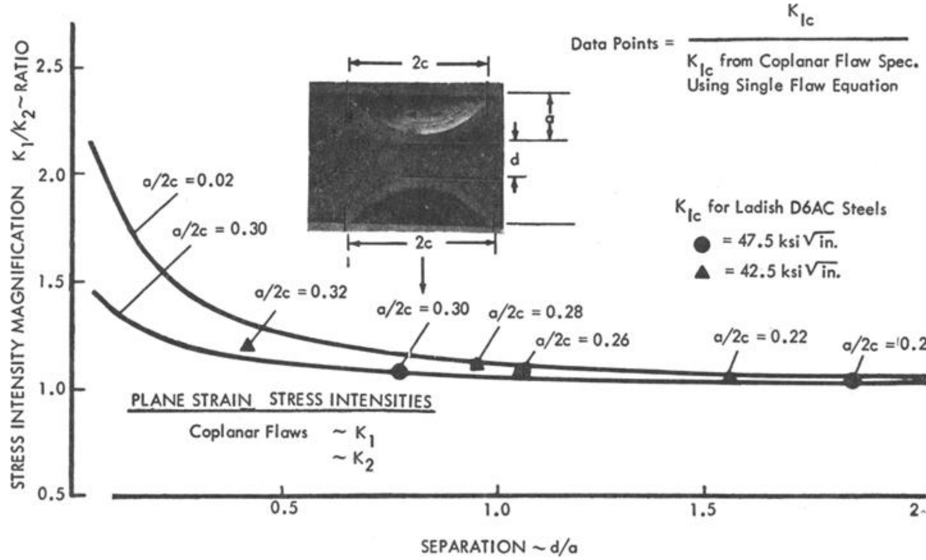

FIG. 32—Stress-Intensity Magnification for Two Coplanar Elliptical Flaws.

CONCLUSIONS

The approach presented for applying fracture-specimen testing to practical engineering problems is based upon the premise that failures of complex tension-loaded structures generally originate at small cracks or crack-like flaws, and that the lives of these structures are dependent upon the initial flaw sizes, the critical flaw sizes, and the flaw-growth characteristics of the materials involved. Primary emphasis has been placed on thick-walled pressure vessels where the critical flaw size is relatively small with respect to the wall thickness (that is, flaw depth $\leqq$ approximately one half the wall thickness).

In view of the supporting experimental data, it is concluded that critical flaw sizes can be predicted with a reasonable degree of accuracy and the stress-intensity concept can be effectively used in the evaluation of subcritical flaw growth. It has been shown that nondestructive inspection requirements (allowable initial flaw sizes) can be established using fracture-specimen test data, and in addition it has been suggested that, for pressure vessels, the conventional proof test can be a powerful inspection tool.

Presently there are limitations and areas of uncertainty in the application of fracture mechanics. Typical areas requiring further research are the determination of stress-intensity magnification associated with deep flaws (that is, flaw depths greater than one half the wall thickness) and the associated effects on subcritical flaw growth, the effects of cyclic spectrums and speeds on flaw growth, and the effects of combined shear and tension stresses on both critical flaw size and subcritical growth. Additionally, the problems of environmental influence and strain-rate sensitivity are certainly deserving of more attention.

REFERENCES

(1) ASTM Special Committee on Fracture Testing of High-Strength Metallic Materials, "Progress in the Measurement of Fracture Toughness and the Application of Fracture Mechanics to Engineering Problems," *Materials Research & Standards*, Vol. 4, No. 3, March, 1964, p. 107.

(2) J. E. Srawley and W. F. Brown, Jr., "Fracture Toughness Testing," see p. 133.

(3) Second Report of ASTM Special Committee on Fracture Testing of High-Strength Metallic Materials, "The Slow Growth and Rapid Propagation of Cracks," *Materials Research & Standards*, Vol. 1, No. 5, May, 1961, pp. 389–393.

(4) G. E. Pellissier, "Some Microstructural Aspects of Maraging Steel in Relation to Strength and Toughness," *Technical Documentary Report RTD-TDR-63-4048*, AF Materials Lab., Wright-Patterson Air Force Base, Ohio, November, 1963.

(5) W. E. Anderson and P. Paris, "Evaluation of Aircraft Material by Fracture," *Metals Engineering Quarterly*, Vol. 1, May, 1961, pp. 33–44.

(6) G. R. Irwin, "Notes for May 1961 Meeting of ASTM Committee for Fracture Testing of High-Strength Metallic Materials," U.S. Naval Research Laboratory, Washington, D.C., May, 1961.

(7) C. F. Tiffany and F. A. Pall, "An Approach to the Prediction of Pressure Vessel Minimum Fatigue Life Based Upon Applied Fracture Mechanics," *Boeing Document D2-22437*, March, 1963.

(8) R. H. Christensen and P. H. Denke, "Crack Strength & Crack Propagation Characteristics of High Strength Metals," *ASD Document ASD-TR-61-207*, January, 1962.

(9) C. M. Hudson and H. F. Hardarth, "Effects of Changing Stress Amplitude on the Rate of Fatigue Crack Propagation in Two Aluminum Alloys," *NASA Technical Note D-96*, Nat. Aeronautics and Space Administration, September, 1961.

(10) A. S. Kobayashi and L. R. Hall, "On the Correction of Stress Intensity Factors for Two Embedded Cracks," *Boeing Structural Development Research Memorandum No. 9*, The Boeing Co., 1963.

DISCUSSION

B. G. JOHNSON[1]—My comments pertain to the stress-intensity ratio concept for predicting sustained load failure where the subcritical flaw growth mechanism might involve surface absorption and subsequent diffusion to the crack front. It has been postulated, for example, that surface-corrosion reactions remote from a crack can result in a crack grown by liberation of hydrogen which diffuses to the crack front. For such mechanisms, one might expect geometrical effects such as surface area and volume to affect correlation between test specimens and the actual part.

[1] Research engineer, The Boeing Co., Airplane Div., Wichita, Kans.

C. F. TIFFANY AND J. N. MASTERS (*authors*)—One of the most important areas of uncertainty in the application of the stress-intensity concept is the influence of environmental effects on subcritical flaw growth. In the case of hydrogen cracking we agree that specimen volume and surface area could be significant factors. This point is discussed in more detail in the panel discussion included in this symposium.[2]

[2] See p. 373.

STP381-EB/Apr. 1965

FRACTURE TOUGHNESS TESTING IN ALLOY DEVELOPMENT

By R. P. Wei[1]

Synopsis

In the past five years, fracture mechanics has been used as a basis for the evaluation of the fracture toughness of high-strength steels and other high-strength alloys. Some of the considerations involved in the selection of plane-strain fracture toughness as the most appropriate and significant parameter for ultrahigh-strength alloy steel development are discussed in this paper.

The contribution of fracture mechanics to steel research and development is illustrated by brief reviews of three investigations: (1) a study of the relationships between microstructure and toughness in quenched and tempered low-alloy ultrahigh-strength steels, (2) an investigation of the effect of sulfur level on the fracture toughness of AISI 4345 alloy steel, and (3) a study of the influence of banding on fracture toughness anisotropy in a maraging steel.

During the past few years, the demand for steels with increasingly higher strength and mechanical reliability has accentuated the need for a sound and practical basis for quantitative evaluation and comparison of the fracture toughness of high-strength metallic materials. Mechanical property information of a conventional and empirical nature is no longer adequate as a guide in planning and in assessing the results of research and development programs in the field of high-strength alloys. Unlike the situation for the lower-strength steels that have been in use for many years, sufficient service experience in the high-strength steels is not available to support translation of mechanical property data into terms of design requirements and expected service performance for various types of applications. Thus, it is essential that the basis and derived methods of fracture toughness evaluation be capable of providing information that can be utilized in design considerations and in performance prediction.

In 1959, a program was undertaken by the U.S. Steel Corp. to investigate the effects of chemical composition, microstructure, and processing variables on the mechanical properties and toughness of existing ultrahigh-strength steels (>200 ksi yield strength) and to develop new and improved steels to meet the growing demands. As part of this program, investigation of methods of fracture toughness testing, based on the Griffith-Irwin fracture mechanics analysis (1)[2] was initiated. During the ensuing five years, the evaluation and utilization of fracture toughness testing procedures, as well as their improvement and extension, has constituted an important phase of the alloy steel development

[1] Senior technologist, Applied Research Laboratory, U.S. Steel Corp., Monroeville, Pa.

[2] The boldface numbers in parentheses refer to the list of references appended to this paper

effort. Fracture testing procedures were evaluated and utilized in certain parts of this program; the prospect of extending the range of application of these procedures to other strength levels is now being considered.

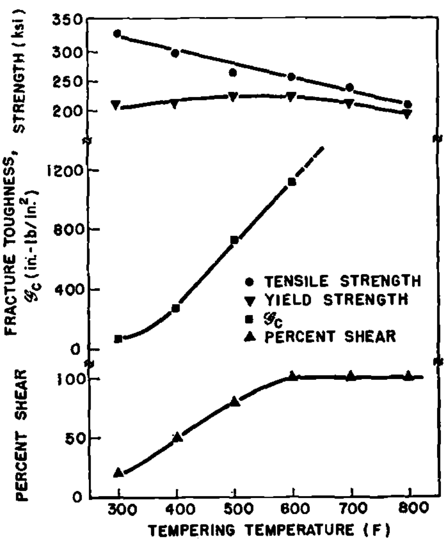

FIG 1.—Effect of Tempering Temperature on Strength and Fracture Toughness of 0.10-In.-Thick CEVR AISI 4340 Steel.

TABLE 1—MECHANICAL PROPERTIES *versus* FRACTURE TOUGHNESS OF 0.10-IN.-THICK CEVR AISI 4340 STEEL.

Tempering Temperature, deg F	Yield Strength, ksi	Tensile Strength, ksi	$\mathcal{G}_c$, in-lb/in.^{2}	β_c	Per cent Shear
300	211	330	75	0.47	20
400	214	296	275	1.80	50
500	223	263	730	4.40	80
600	222	256	1120	6.82	100
700	212	238	>1700[a]	$>2\pi$	100
800	193	208	>1400[a]	$>2\pi$	100

[a] $\mathcal{G}_c \geqq (0.38\, \sigma_{YS}{}^2 W)/E$.

SELECTION OF FRACTURE TOUGHNESS PARAMETER AND TEST METHODS

For very practical reasons, fracture testing during the first two years was devoted mainly to fracture toughness (K_c or $\mathcal{G}_c$) evaluations of ultrahigh-strength steels in the form of sheet ranging in thickness from 0.050 to 0.125 in. Figure 1 and Table 1, which show the effects of tempering treatment on strength and toughness of a CEVR AISI 4340 steel, illustrate the type of data obtained.[3] The $\mathcal{G}_c$ values correspond to different fracture modes (Fig. 2) ranging from nearly plane-strain fracture (for 300 F tempering treatment) to plane-stress fracture (for 600 F and above), as determined either by per-

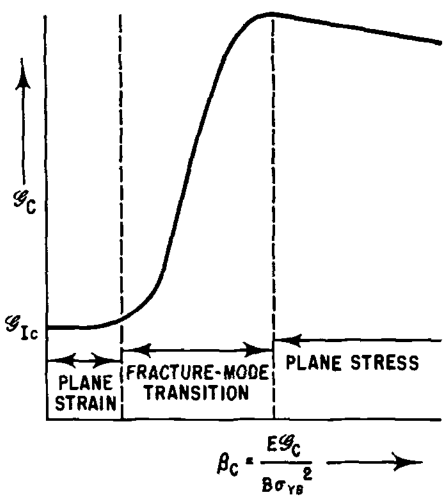

FIG. 2—Effect of Thickness and Fracture-Mode Transition.

centage of shear estimates or by calculation of the relative plastic-zone size β_c (2,3) from the expression

$$\beta_c = \frac{1}{B}\frac{E\mathcal{G}_c}{\sigma_{YS}{}^2}$$

where:

E = Young's modulus,
$\mathcal{G}_c$ = fracture toughness or critical strain energy release rate,
σ_{YS} = 0.2 per cent offset yield strength, and
B = specimen thickness.

[3] Unpublished data, R. P. Wei and F. J. Lauta, Applied Research Laboratory, U.S. Steel Corp.

A transition in fracture mode occurs in the range $1 < \beta_c < 2\pi$ (2,3).

$\mathcal{G}_c$ measurements, however, are of very limited utility in general alloy steel development for the following reasons:

1. Because of the variation in fracture mode discussed above, a uniform basis for comparison is not present. Adjustment of specimen thickness for each heat treatment so as to obtain a prescribed fracture mode or β_c value is considered to be rather impractical.

2. $\mathcal{G}_c$ values are valid only for the thickness tested. Translation of this information to other thicknesses is not possible at the present time.

3. $\mathcal{G}_c$ values are not constant but depend on the size of the crack.

On the other hand, plane-strain fracture toughness (K_{Ic} or $\mathcal{G}_{Ic}$), which characterizes crack-growth resistance under the most severe conditions of practical importance, appeared to be more suitable for use in alloy development programs. The conditions under which measurements are made are specific and readily controlled. The significance of $\mathcal{G}_{Ic}$ has been established (1) and confirmed (4). A considerable amount of effort, therefore, has been devoted to the development of valid procedures for plane-strain fracture toughness evaluation.

Several procedures for plane-strain fracture toughness evaluation are currently in use at the Applied Research Laboratory:

1. Tension testing of circumferentially notched round specimens,
2. Tension testing of single-edge-notched (SEN) specimens (5) and
3. Slow-bend testing of SEN specimens.

The last two procedures utilize the notch pop-in technique proposed by Krafft, et al (4). These procedures are complementary in that they permit $\mathcal{G}_{Ic}$ evaluation on steels over a wide range of thickness. Correlations among test results

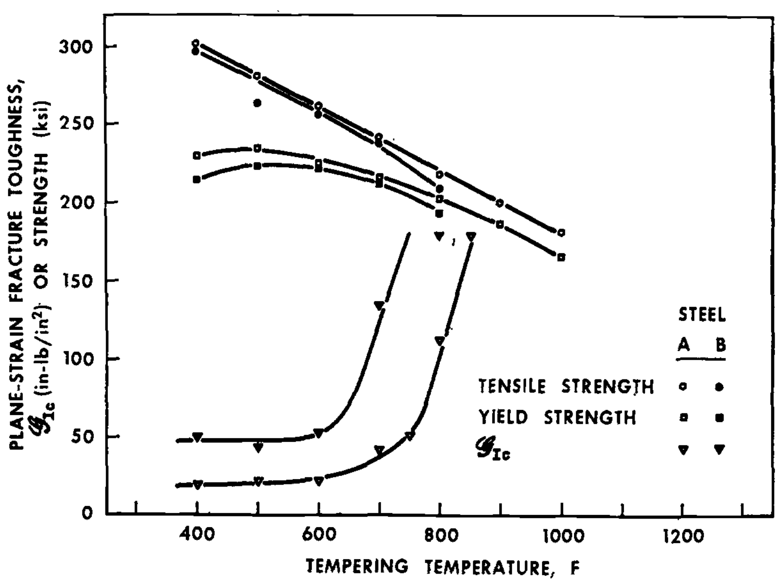

FIG. 3—Effect of Tempering Temperature on Strength and Fracture Toughness of Steels A and B.

obtained by the various procedures have been made and will be reported separately (6).

FRACTURE TESTING IN ALLOY DEVELOPMENT

The contribution of fracture mechanics to alloy development may be considered in terms of some specific examples.

Relationships Between Microstructure and Toughness in Quenched and Tempered Low-Alloy Ultra-High-Strength Steels:

Quenched and tempered low-alloy steels, with carbon content in the range 0.3 to 0.5 per cent, have been thoroughly investigated for possible application in high strength-to-weight structures. The effects of tempering treatment on plane-strain fracture toughness ($\mathcal{G}_{Ic}$) in this class of steels are similar. Figures 3 and 4 show typical examples of this behavior. For each steel, fracture toughness remains low at low tempering temperatures but abruptly increases in a critical tempering temperature range that is characteristic of the particular steel composition. The actual level of fracture toughness at low tempering temperatures depends on the individual steel composition and impurity level

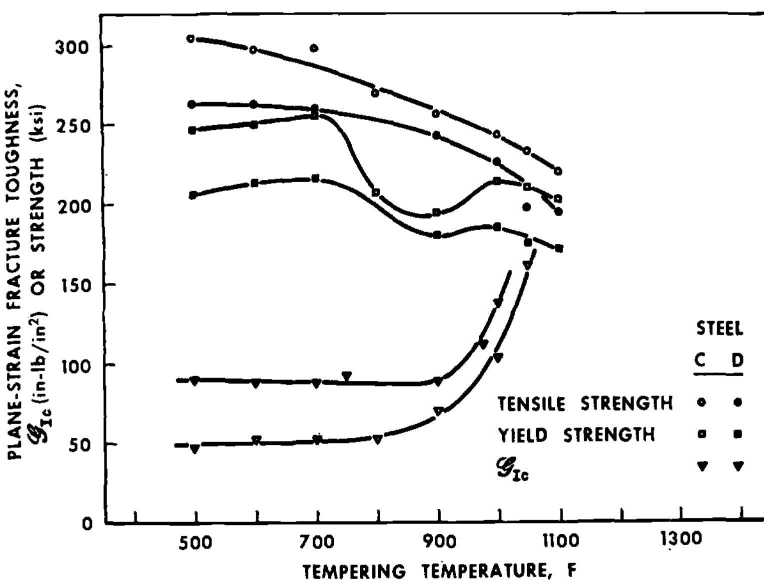

FIG. 4—Effect of Tempering Temperature on Strength and Fracture Toughness of Steels C and D.

TABLE 2—CHEMICAL COMPOSITION OF STEELS INVESTIGATED, WEIGHT PER CENT.

Steel	C	Mn	P	S	Si	Ni	Cr	Mo	V	Al
A (4340 commercial)	0.39	0.74	0.019	0.026	0.27	1.79	0.89	0.26	...	...
B (4340 CEVR)	0.43	0.77	0.009	0.008	0.27	1.16	0.73	0.26	...	0.03
C (300M CEVR)	0.42	0.74	0.005	0.006	1.60	1.87	0.83	0.37	0.10	...
D (experimental heat)	0.31	0.84	0.007	0.009	1.59	2.04	2.04	0.51	0.055	0.055

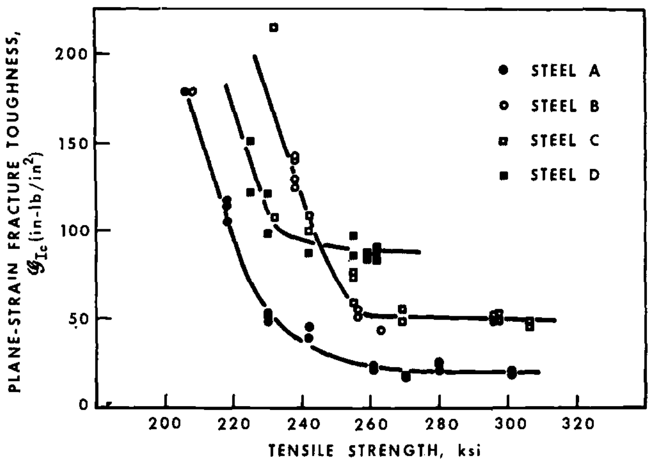

FIG. 5—Relationship Between Plane-Strain Fracture Toughness ($\mathcal{G}_{Ic}$) and Tensile Strength for Four Steels.

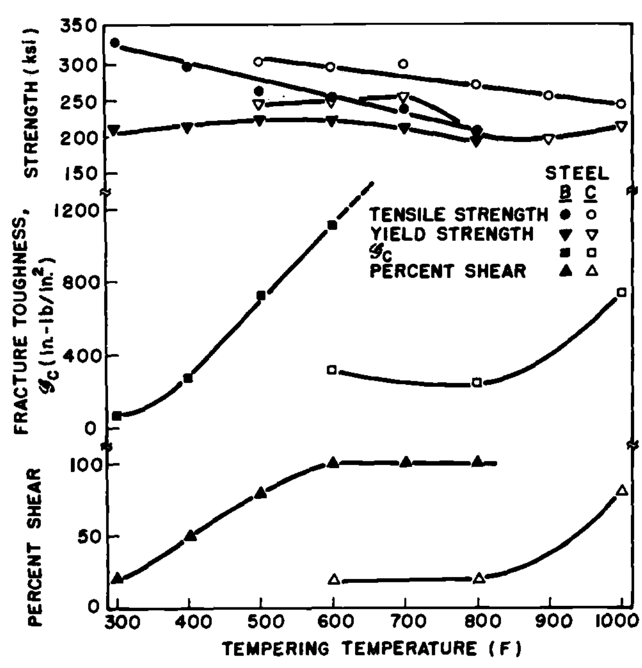

FIG. 6—Effect of Silicon on Strength and Fracture Toughness of 0.100-In.-Thick Ultrahigh-Strength Steels.

(see Table 2). Those with lower carbon (Steel D versus Steel C) and lower phosphorus and sulfur contents (Steel A versus Steel B) have a higher level of toughness. Compared at equal tensile strength levels (Fig. 5), the abrupt change in fracture toughness behavior is again apparent: above a tensile

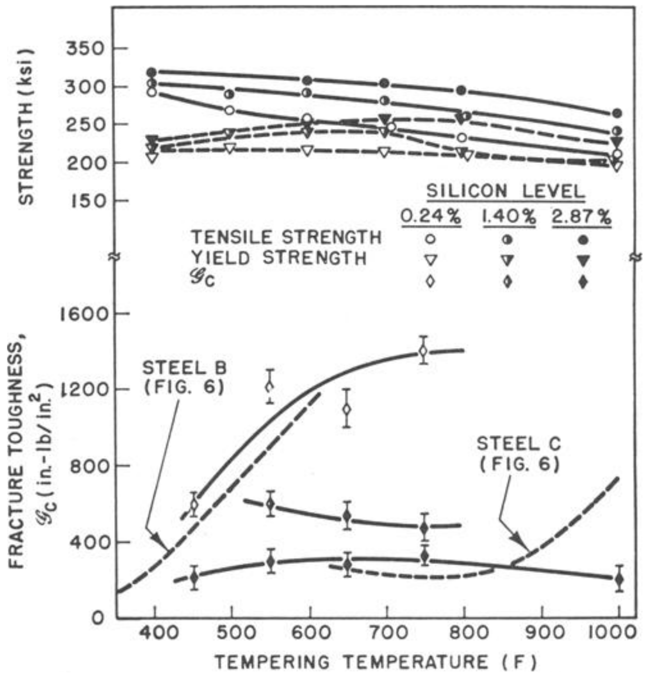

FIG. 7—Effect of Silicon on Strength and Fracture Toughness of 0.070-In.-Thick AISI 4340 Type Ultrahigh-Strength Steels.

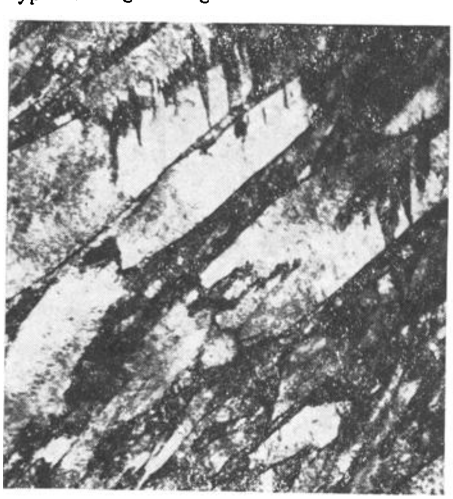

FIG. 8—Electron Micrograph of a Steel D Specimen Tempered 1 Hr at 600 F (×25,000).

FIG. 9—Electron Micrograph of a Steel D Specimen Tempered 4 Hr at 1050 F (×25,000)

strength level of about 240 ksi, the steels have low fracture toughness, whereas at lower tensile strengths the toughness increases rapidly. Comparison of Steels B and C shows that the plane-strain fracture toughness at a given tensile strength level is not improved by the addition of silicon. This had been observed previously for the fracture toughness of 0.100-in.-thick[3] and 0.070-in.-thick[4] ultrahigh-strength sheets (Figs. 6 and 7).[5]

The systematic relationships shown in Fig. 5 created interest in the associated microstructural changes, and consequently a transmission-electron metallographic study was made of these steels after various tempering treatments, both above and below the critical tempering temperature range. It was found that fracture toughness is sensitively related to microstructure changes (7). In the region of low fracture toughness, the martensite has a predominantly plate-like morphology. Two types of lattice defects are present in the martensite plates, namely, a high dislocation density and many microtwins. There is an almost continuous film of ϵ-carbide at the martensite and twin boundaries, Fig. 8. These films appear to act as preferred paths for crack propagation through the structure either by providing adjacent weak zones in the matrix or by fracturing themselves, which would qualitatively account for the low fracture toughness. Good fracture toughness develops only when certain important microstructural changes have occurred: (*a*) the elimination of embrittling carbide films at the boundaries by spheroidization, and (*b*) the redistribution and removal of lattice-defect structure by recovery processes (Fig. 9). Increasing the tempering resistance of these steels by utilizing increased amounts of certain alloying elements, such as silicon, does not lead to improved fracture toughness at a given strength level (Fig. 5, Steels B and C), because the microstructural changes essential for improvement of toughness are inhibited; although higher strengths can be retained at higher tempering temperatures, the balance between strength and toughness is not improved.

However, attractive combinations of strength and fracture toughness can be obtained in these quenched and tempered low-alloy steels by tempering at temperatures higher than conventionally used to obtain maximum yield strength. For example, by tempering Steel B at 800 F rather than in the range of 400 to 600 F, the plane-strain fracture toughness ($\mathcal{G}_{Ic}$) is increased almost four times with an attendant sacrifice in yield strength of only 15 per cent; thus $\mathcal{G}_{Ic}$ values of nearly 200 in-lb/in.^{2} can be achieved at a yield strength level of about 200 ksi.

On the basis of this study, it was concluded that carbon strengthening alone has limited potential in the development of very-high-strength steels (>220 ksi yield strength) with good toughness. Therefore, other strengthening mechanisms, and combinations of mechanisms, are being actively investigated.

Effect of Sulfur on Fracture Toughness of AISI 4345 Steels:

An adverse influence of sulfur on the toughness of steels is generally recognized, and the previous discussion has already indicated the combined effects of sulfur and phosphorus on the fracture toughness of the ultrahigh-strength steels. However, the detailed mechanisms by which sulfur affects fracture behavior are not known. Therefore, an investigation[6] has been undertaken to examine this problem in a more systematic manner. A series of experimental

[4] Unpublished data, F. J. Lauta, Applied Research Laboratory, U.S. Steel Corp

[5] $\mathcal{G}_c$ results on 0.100-in.-thick material were obtained on 3-in.-wide centrally notched (fatigue-precracked) sheet specimens. Slow crack extension was determined with a compliance gage. $\mathcal{G}_c$ results on 0.070-in.-thick specimens were obtained on 3-in.-wide centrally notched (ρ = 0.0007 in.) sheet specimens. Slow crack extension was estimated empirically from percentage shear (see Footnote 3 and Ref (2)).

[6] Unpublished data, G. E. Pellissier, Applied Research Laboratory, U.S. Steel Corp.

AISI 4345 steels, containing four different levels of sulfur, was especially prepared for this study. By using high-purity starting materials, and carefully controlled melting procedures,[7] the chemical compositions and residual impurity levels of these steels were carefully controlled (see Table 3). Charpy V-notch impact test results[6] at room temperature as a function of tensile strength (or tempering treatment) for the four steels are shown in Fig. 10. It is evident that the Charpy V-notch impact test is not capable of delineating the influence of sulfur on toughness unambiguously and sensitively at all strength levels for these steels. On the other hand, K_{Ic} results[6] (Fig. 11) clearly show an influence of sulfur over the whole range of tensile strengths.

Sulfur is present in these steels in the form of isolated inclusions or grain boundary films, or both. The amount, distribution, and location of the sulfur-containing particles or films is believed to be controlled primarily by the sulfur level, but other factors, such as oxygen level and solidification pattern, also may exert important influence. Electron metallographic examination of the microstructures and fracture surfaces are now being performed in the Applied Research Laboratory of the U.S. Steel Corp. and

TABLE 3—CHEMICAL COMPOSITION OF EXPERIMENTAL AISI 4345 STEELS, WEIGHT PER CENT.

Sample No.	C	Mn	S	Si	Ni	Cr	Mo
B-1	0.43	0.27	0.008	0.24	2.05	1.48	0.43
B-2	0.45	0.26	0.016	0.25	2.04	1.49	0.44
B-3	0.46	0.25	0.025	0.24	2.04	1.48	0.43
B-4	0.46	0.24	0.049	0.22	2.04	1.47	0.44

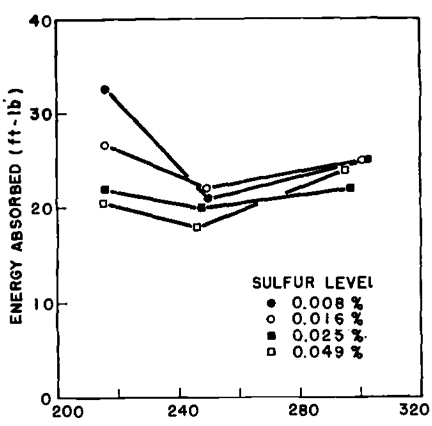

FIG. 10—Effect of Sulfur Level on Charpy V-Notch Impact Energy of AISI 4345 Steel at Room Temperature.

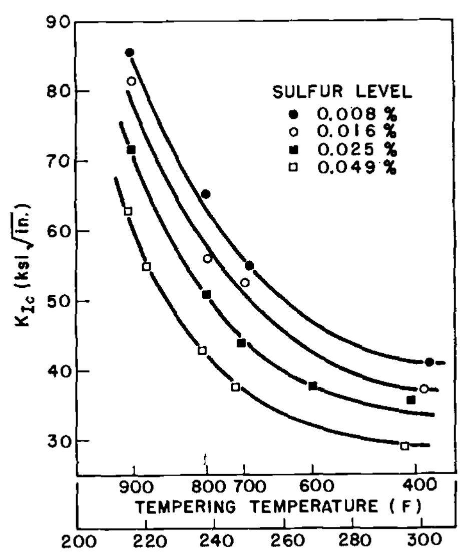

FIG. 11—Influence of Sulfur Level on Plane-Strain Fracture Toughness of AISI 4345 Steel.

[7] Steels prepared for the U.S. Steel Corp. by the Illinois Institute of Technology Research Inst.

by various members of the Fractography Subcommittee of the ASTM Special Committee on Fracture Testing of High-Strength Metallic Materials. The results of this study in conjunction with the fracture toughness test results should provide quantitative information that will contribute to a better understanding of fracture in this type of steel.

Fracture Toughness Anisotropy in a Maraging Steel:

Evidence that has been accumulating indicates that the level of plane-strain fracture toughness of the 18 per cent nickel - cobalt - molybdenum maraging steels calculated from surface-crack test results is greater (about 30 per cent) than that measured in circumferentially notched round specimen tests or in through-thickness-crack toughness tests (8). This rather consistent discrepancy has raised a question as to whether the two types of tests accurately determined the identical toughness parameter. Irwin[8] suggested that the discrepancy is not inherent in differences in the methods of test and that it is rather a reflection of anisotropy of the material, since the two types of test provide measurements of fracture toughness in two different principal directions in a rolled sheet or plate.

To test this hypothesis experimentally, fracture toughness measurements were made for the four principal planes of fracture in a maraging steel plate (8). One type of specimen was used in this study, namely, SEN tension test specimens. Test specimens were cut from $1\frac{1}{8}$-in.-thick plate of a maraging (250) steel (laboratory heat) which had been

TABLE 4—CHEMICAL COMPOSITION, HEAT TREATMENT, AND TENSILE PROPERTIES OF AN EXPERIMENTAL 18Ni-Co-Mo MARAGING STEEL.

COMPOSITION, WEIGHT PER CENT

C	Mn	P	S	Si	Ni	Cr	Mo	Ti	Al (total)	N	B	Co	Fe
0.013	0.083	0.002	0.006	0.069	17.7	0.026	4.60	0.47	0.060	0.004	0.0038	7.71	balance

HEAT TREATMENT

Solution-annealed for 1 hr at 1500 F + air cooled + aged for 3 hr at 900 F + air cooled.

TENSILE PROPERTIES (AVERAGES OF TWO TESTS)

	0.2 per cent Offset Yield Strength, ksi	Tensile Strength, ksi	Elongation in 2 in., per cent	Reduction in Area, per cent
Longitudinal	230	244	9.5	48
Transverse	231	244	7.0	35

ORIENTATION	$\mathcal{G}_{nc}$, in.-lb/in.^{2}
A	245
B	230
C	310
D	150

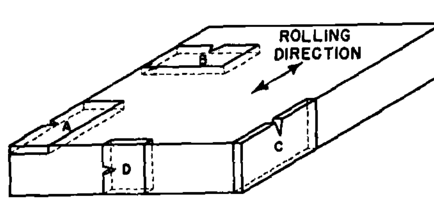

FIG. 12—Orientations of Fracture Toughness Specimens Cut From $1\frac{1}{8}$-In.-Thick Plate of Maraging (250) Steel.

[8] Private communication from G. R. Irwin to G. E. Pellissier.

solution-annealed for 1 hr at 1500 F and aged for 3 hr at 900 F. Chemical composition and tensile properties are shown in Table 4.

Specimen orientation and fracture toughness results ($\mathcal{G}_{nc}$)[9] for the four different orientations are shown in Fig. 12. The $\mathcal{G}_{nc}$ values for the *A* and *B* orientations (longitudinal and transverse) are not very different, in conformance with previous information, but the *C* orientation is greater by about 25 per cent. $\mathcal{G}_{nc}$ for the *D* orientation is only about 60 per cent of that of the longitudinal orientation. This anisotropy in fracture toughness in the maraging steel is associated with chemical segregation "banding" in the material (8). This anisotropy is believed to explain reasonably the observed discrepancies between through-thickness and surface-crack test results for the maraging steels.

SUMMARY

Fracture toughness testing, based on fracture mechanics, has made some useful contributions to quantitative metallurgical investigations at the Applied Research Laboratory of the U.S. Steel Corp.

At the present time, it is believed that these test procedures provide the only means for consistent and reliable assessment of the fracture toughness of ultra-high-strength alloy steels. This fracture toughness parameter appears to be fundamentally related to microstructure and basic mechanical behavior and may be utilized in structural design and performance prediction. Consequently, these methods of toughness evaluation have become an integral part of the Laboratory's ultra high-strength steel development programs.

Because of practical limitations, such as specimen size and test-machine capacity, it is very difficult to utilize the present test procedures for obtaining valid fracture toughness measurements for steels having yield strengths below about 200 ksi. Because the fracture mechanics method of assessing fracture toughness provides a unified basis for fracture toughness evaluation, effort is currently being made to extend the range of application of the method to yield strengths as low as 100 ksi. For this purpose, a notched slow-bend test utilizing the crack pop-in technique shows considerable promise.

Acknowledgment:

The author wishes to thank F. J. Lauta and G. E. Pellissier for permission to use their unpublished results, and A. J. Baker for furnishing the micrographs.

[9] $\mathcal{G}_{nc}$ determined by pop-in technique (4,5).

REFERENCES

(1) G. R. Irwin, "Fracture Mechanics," in *Structural Mechanics*, Pergamon Press, Oxford, 1960.

(2) ASTM Special Committee on Fracture Testing of High-Strength Materials, "Fracture Testing of High-Strength Sheet Materials," *ASTM Bulletin*, January, 1960, p. 29, and February, 1960, p. 18.

(3) G. R. Irwin, "Fracture Testing of High-Strength Sheet Materials Under Conditions Appropriate for Stress Analysis," U.S. Naval Research Lab. *Report 5486*, July 27, 1960.

(4) R. W. Boyle, A. M. Sullivan, and J. M. Krafft, "Determination of Plane-Strain Fracture Toughness with Sharply Notched Sheets," *Welding Research*, Vol. 27, No. 9, September, 1962, p. 428.

(5) A. M. Sullivan, "New Specimen Design for Fracture Toughness Tests," *Materials Research & Standards*, Vol. 4, No. 1, January, 1964, p. 20.

(6) R. P. Wei and F. J. Lauta, "Plane-Strain Fracture Toughness Evaluation Using

Carbonitrided SEN Specimens," to be published in *Materials Research & Standards*.

(7) A. J. Baker, F. J. Lauta, and R. P. Wei "Relationships Between Microstructure and Toughness in Quenched and Tempered Ultrahigh-Strength Steels," *Structure and Properties of Ultrahigh-Strength Steels*, *ASTM STP 370*, Am. Soc. Testing Mats., 1965

(8) G. E. Pellissier, "Some Microstructural Aspects of Maraging (250) Steel in Relation to Strength and Toughness," Third Maraging Steel Review Conference, WADD, Dayton, Ohio, 1963.

STP381-EB/Apr. 1965

FRACTURE TOUGHNESS TESTING AT ALCOA RESEARCH LABORATORIES

By J. G. Kaufman[1] and H. Y. Hunsicker[1]

Synopsis

At Alcoa Research Laboratories, fracture toughness determinations are made on commercial and promising experimental alloys and tempers with center-cracked specimens, single- and double-edge-notched specimens, and notched round specimens. Compliance techniques are usually used to detect the initiation of unstable crack growth. Kahn-type tear tests and sharp-notch tension tests are used as screening tests to supplement fracture toughness testing in the evaluation of the effects of composition, fabrication procedure, temper, and environment on the fracture characteristics of aluminum alloys. Tear tests have the advantage that direct measures of the relative amounts of energy required to propagate a crack can be obtained even for the toughest of aluminum alloys; furthermore, the unit propagation energy from the tear test is directly correlated with the valid values of K_c and K_{Ic}. Sharp-notch tension tests are economical and, particularly when general yielding is not obtained, the ratio of notch strength to yield strength provides a meaningful measure of relative toughness. Specific examples are given of instances in which these techniques have been used to: (*1*) determine which series of aluminum alloys shows the most promise for the development of high-toughness alloys; (*2*) establish optimum compositions and fabricating procedures for specific alloys; (*3*) develop optimum tempers; and (*4*) indicate the outstanding alloys for cryogenic applications.

The commercial aluminum alloys used in most structural applications are so tough that low-ductility fracture, that is, unstable or self-propagating crack growth in elastically stressed material, is nonexistent. However, the development of alloys having higher and higher strengths for aircraft and missile applications, where their high strength must be used to the maximum advantage, has resulted in situations where the possibility of catastrophic low-ductility failure must be considered. As a result, a need developed for procedures for evaluating the toughness of these materials and, ultimately, for designing the toughness into critical structures.

To be able to provide reliable fracture information, Alcoa Research Laboratories (ARL) have been active for many years in the fracture testing field. It is the purpose of this presentation to relate: (*1*) the development of fracture-testing techniques at ARL; and (*2*) examples of the uses to which they have been put in alloy-development efforts.

Tear Tests

After an initial survey of the problems related to evaluating the fracture char-

[1] Assistant chief, Mechanical Testing Div., and Chief, Physical Metallurgy Div., respectively, Alcoa Research Laboratories, New Kensington, Pa.

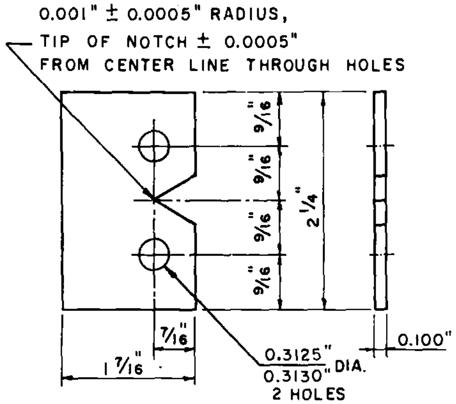

FIG. 1—Kahn-Type Tear Test Specimen.

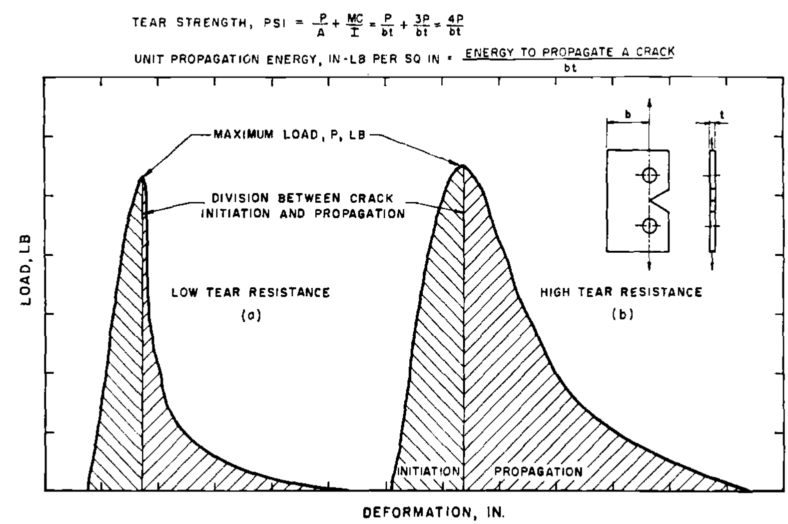

FIG. 2—Tear-Test Load-Deformation Curves.

acteristics of aluminum alloys, ARL elected to make use of a modification of the Kahn-tear test (1)[2] to measure tear resistance and obtain relative toughness ratings of the alloys (2). By this test procedure, the energy required to initiate and propagate a crack in a specimen of the design in Fig. 1 was determined by measuring the areas under portions of the autographic load-deformation curve obtained during the test. Schematic representations of the curves are shown in Fig. 2, with the areas considered to be associated with initiation and with propagation of the crack indicated. Also indicated are the most useful parameters developed from the test—tear strength (the maximum nominal combined direct-and-bending stress); and unit propagation energy.

This particular design of specimen was selected for several reasons. First, the specimen is small enough to be taken from several orientations within almost any aluminum alloy product, including forgings, extrusions, and castings, as well as sheet and plate. Also it can conveniently be tested at different temperatures or in various environments. A very sharp notch is used, in place of the keyhole notch used by Kahn, because it facilitates the initiation of the crack at relatively low energy levels, increasing the ability to measure accurately the energy required to propagate the crack. The large amount of energy required to initiate a crack with a relatively blunt notch overshadows and, on the

[2] The boldface numbers in parentheses refer to the list of references appended to this paper.

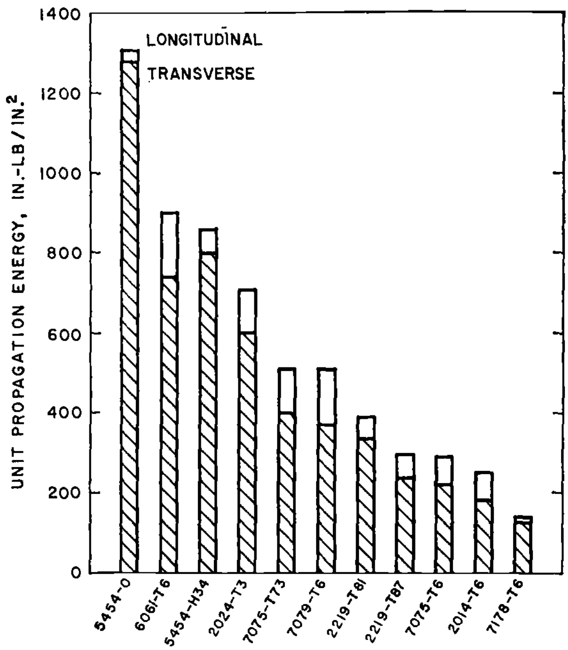

FIG. 3—Tear Resistance of 0.063-In. Thick Aluminum Alloy Sheet.

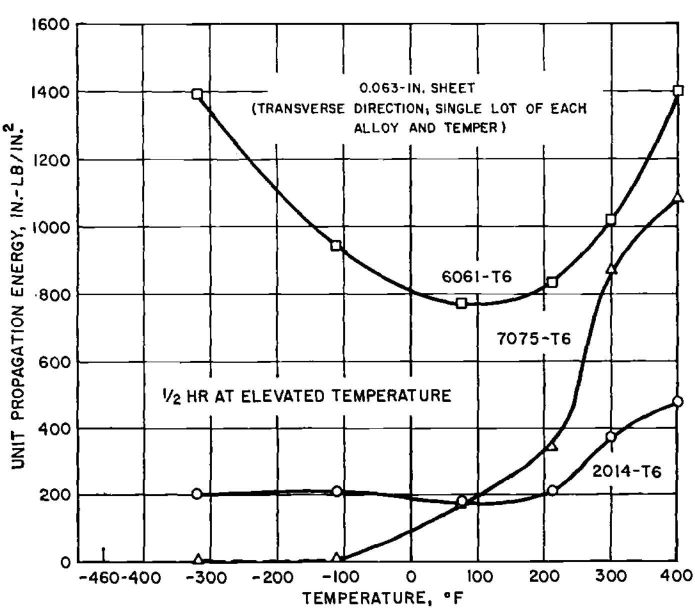

FIG. 4—Unit Propagation Energies of Some Aluminum Alloys at Various Temperatures.

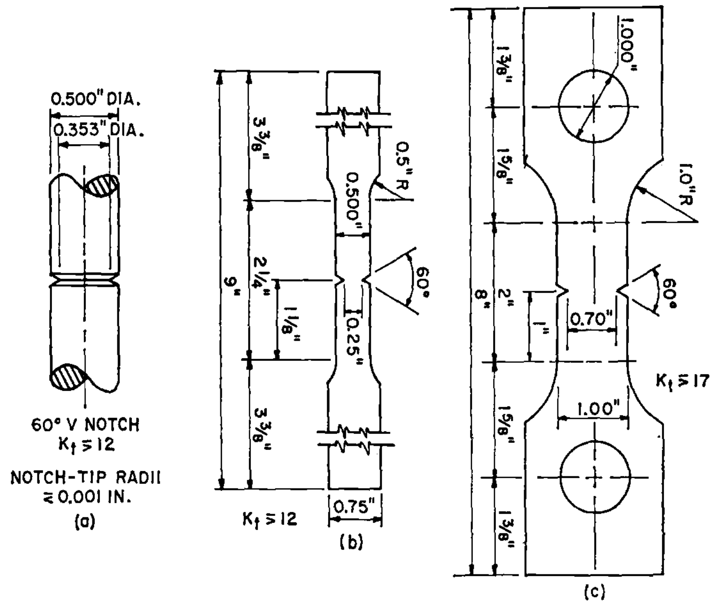

FIG. 5—Sharp-Notched Tension Specimens.

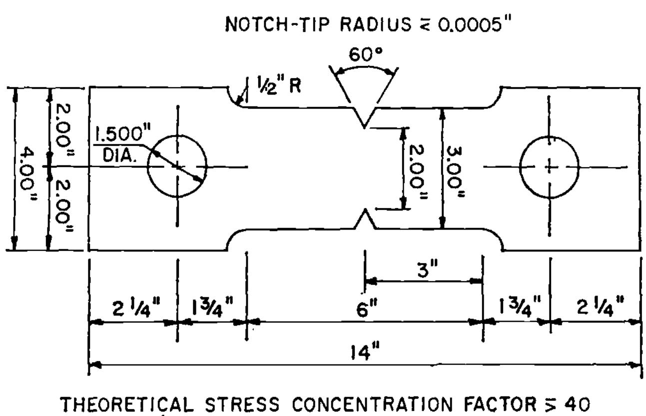

FIG. 6—Sharp-Notched Tension Specimen.

autographic chart, obscures the energy to propagate the crack.

The results of tear tests are greatly dependent upon specimen size, although, with specimens of the design in Fig. 1 and of thicknesses in the range from about 0.063 to about 0.1 in., comparable values of tear strength and unit propagation energy are obtained.

Unit propagation energy is used as the primary measure of toughness from the tear test. It takes into account both the strength and the ductility of the material. Tear strength is used in much the same way as notch tensile strength would be used, that is, on the basis of ratios of tear strength to tensile strength and to yield strength, particularly the latter.

The tear resistances of aluminum alloys determined in this manner provide a means for merit rating of alloys and tempers, even the most ductile combinations. For this purpose, comparisons may be shown in the form of bar graphs of unit propagation energy, as in Fig. 3. They also indicate the effects of temperature, as shown by the representative data in Fig. 4.

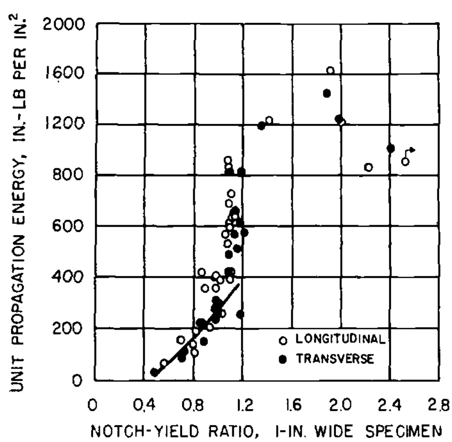

FIG. 7—Relationship Between Notch Yield Ratio and Unit Propagation Energy, 0.063-In. Sheet.

SHARP-NOTCH TENSION TESTS

The results of tension tests of sharply notched specimens have also been used to determine the relative fracture characteristics or notch toughness of aluminum alloys. In most cases, notched round specimens of the design in Fig. 5(*a*) and notched sheet-type specimens of the designs in Figs. 5(*b*) and 5(*c*), or, more recently, Fig. 6 are used. Very sharp notches (notch-tip radii <0.001 in.; $K_t > 12$) are used to simulate the most detrimental kind of stress concentrator—a crack—and the other dimensions were chosen to provide the greatest ability to discriminate among materials.

Evaluation of the data is made through the comparison of the net strength of the notched specimen to the tensile properties of the material. Although many investigators use the notch-strength ratio as a basis for evaluation, the notch-yield ratio (ratio of net strength of notched specimen to yield strength of material) provides a more meaningful measure of the ability of a material to deform plastically in the presence of a severe stress concentrator. In addition, this ratio generally provides much more consistent relative ratings when data are compared for various notch geometries (3). The ASTM Special Committee on Fracture Testing of High-Strength Metallic Materials has supported this stand by citing the notch-yield ratio as the criterion to be used in evaluating relative toughness in screening tests of sharply notched tension specimens.[3]

The notch tension test, like the tear test, can be used for a wide range of alloys and tempers, but when general yielding takes place, the results are less definitive than those of the tear tests as shown by the data in Fig. 7. When general yielding does not take place (notch-yield ratio ≤ 1.0), there is little scatter in the relationship between notch-yield ratio and unit propagation energy.

FRACTURE TOUGHNESS TESTS

Tests of wide center-slotted tension specimens were made at ARL almost twenty years ago (4), but it was only after publication of the first report (5) of the ASTM Special Committee on Fracture Testing of High-Strength Me-

[3] R. H. Heyer, "Evaluation of Proposed Tentative Method for Sharp Notch Tension Testing," see p. 199.

tallic Materials in January and February, 1960, that ARL began to take an active interest in the use of fracture toughness testing for the evaluation of aluminum alloys. The test had the

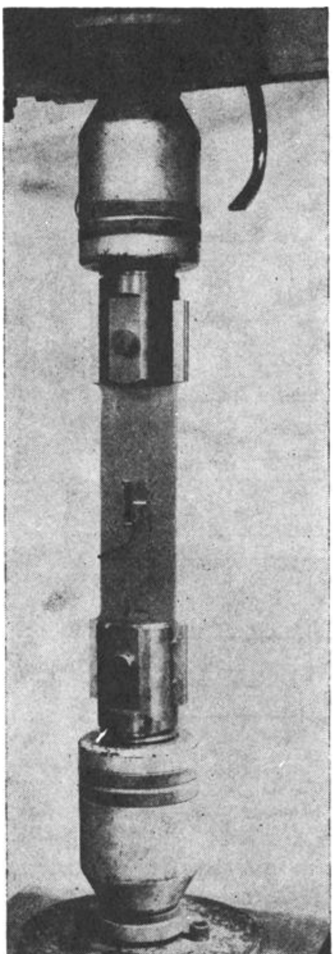

FIG. 8—Fracture Toughness Specimen in Place for Test with SR4 Gage Units for Compliance Measurement.

obvious advantage over any of the other tests available in that it provided not only a qualitative means for the merit rating of materials, but also supplemental design data for the situations where rapid crack propagation could be a potential service problem with high-strength alloys.

Initial development centered on the use of a center-notched specimen having essentially the dimensions given in Fig. 1 of the first report of the ASTM Special Committee (5). The emphasis at that time was upon the measurement of the fracture toughness at the critical situation, that is, at the onset of rapid crack propagation. Early tests were made with the ink-staining technique to measure slow crack growth. This procedure was perfected to a rather high level by the use of special combinations of drawing and plotting inks, to provide the proper combinations of fluidity and stability. Later the compliance-gage technique, in which SR-4 electrical resistance strain gages were mounted as clip-gages on the specimens or on gage-length extensions as in Fig. 8, replaced the ink-stain method of following crack growth.

Studies were made to establish the effect of specimen width, thickness, and notch-tip radius on values of critical strain-energy release rate for aluminum alloy sheet. Concurrently with other investigators, it was established that uniform values of the critical fracture parameters for aluminum alloys could be established provided that: (*1*) the notch-tip radius was equal to or less than $\frac{1}{20}$ of the radius of the plastic zone (about 0.002 in. for 7075-T6); and (2) the size of the specimen was such that the rapid fracture took place at nominally elastic stresses. The same values of the critical strain-energy release rate were obtained with fatigue-cracked and very sharply machine-notched specimens. Because of the relative ease with which aluminum alloys could be sharply notched, it appeared unnecessary to fatigue-crack specimens.

Experiments at ARL, in agreement

with findings of other laboratories (5), showed that the critical stress-intensity factor, K_c, decreased with increase in specimen thickness (Fig. 9), approaching a minimum value associated with fracture under wholly plane-strain conditions. It was also noted that the initiation of slow crack growth frequently was associated with a short burst of unstable crack growth (pop-in) at a stage where the crack driving force was the same as that for plane-strain fracture. Thus if pop-in was noted in a test of a center-notched specimen, the plane-strain parameters as well as the critical parameters could be determined from the test. Because of this, interest in the center-notched specimen continues at ARL.

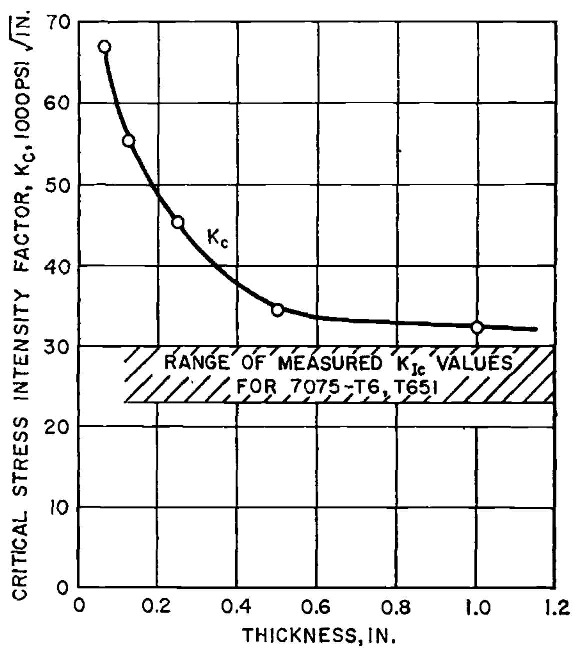

FIG. 9—Fracture Toughness of 7075-T6, -T651 Sheet and Plate (Transverse).

Attention has been given to other techniques suggested primarily for measuring plane-strain toughness. The single-edge-notched specimen and the notched round specimen are used, in addition to the center-cracked specimen. The single-edge-notched specimen appears to have the greatest versatility and has the advantage that a well-documented calibration is available (6,7). Notched round specimens provide an economical way of determining K_{Ic}, but the analysis leading to the fracture parameters is not well documented.

Even more than in measurements of the critical fracture toughness, the crack-tip radius has been found to be a very important factor in the determination of plane-strain toughness (8). Whereas machined notches with radii in the range of 0.0005 in. or less seem to provide valid values of the critical parameters, fatigue cracking consistently provides lower plane-strain parameters, as shown by the data in Table 1. Examples of the load-deformation curves obtained for center-notched specimens with and

TABLE 1—RESULTS OF FRACTURE TOUGHNESS TESTS OF ¼-IN. THICK 7075-T651 PLATE (TRANSVERSE SPECIMENS).

Type of Specimen	Notch-Tip Preparation	K_{Ic}, psi $\sqrt{in.}$
Double-edge-notched[a]	As-machined[d]	30 400
		31 400
		30 900
Center-notched[b]	As-machined[d]	32 800
		30 100
		28 300
		28 000
		29 800
	Fagitue-cracked[e]	23 000
		24 500
		25 700
		24 200
		23 100
		24 100
Single-edge-notched[c]	As-machined[d]	32 600
		30 800
		29 700
		31 000
	Fatigue-cracked[e]	24 300
		25 900
		25 100

[a] 3 in. wide.
[b] 3 in. wide; 1-in. center slot.
[c] 3 in. wide; 1.05-in. deep slot.
[d] Notch-tip radii ≦ 0.0005 in.
[e] Axial-stress ($R \approx 0.1$), maximum stress ≦ 20 per cent of yield strength.

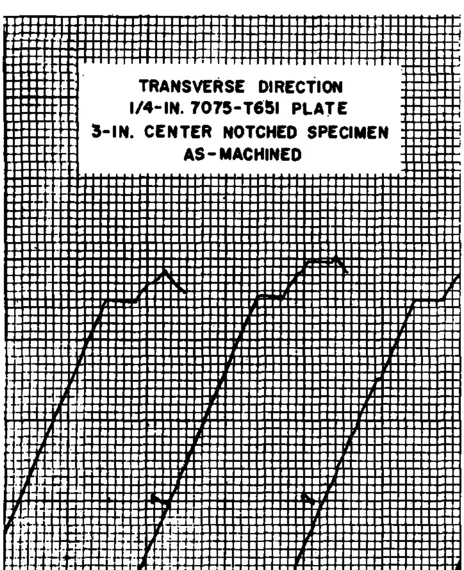

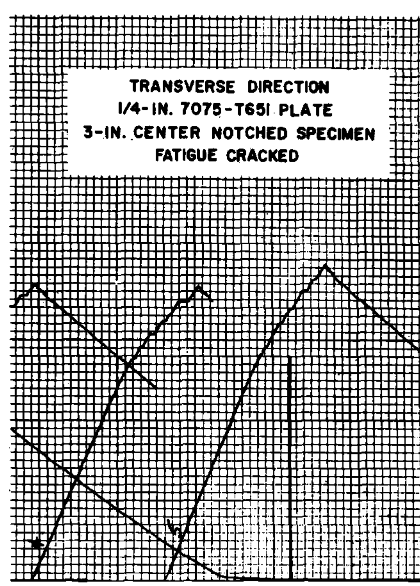

FIG. 10—Representative Load-Deformation Curves from Fracture Toughness Tests.

without fatigue cracks are shown in Fig. 10. With the as-machined notch (Fig. 10(*a*)), some initial unstable crack growth is indicated by a marked pop-in before slow crack growth continues. With fatigue-cracked specimens, the initial unstable crack growth is not as pronounced and comes at a lower stress level, indicating a lower true value of plane-strain toughness. Thus, the commercial alloys and promising experimental alloys, the test has not been extensively used for alloy development. Cost is, of course, one factor, but there is a more basic problem. It is extremely important in all fracture toughness testing that fracture take place at nominally elastic stresses, that is, in the absence of general yielding. Many aluminum alloys are too tough to de-

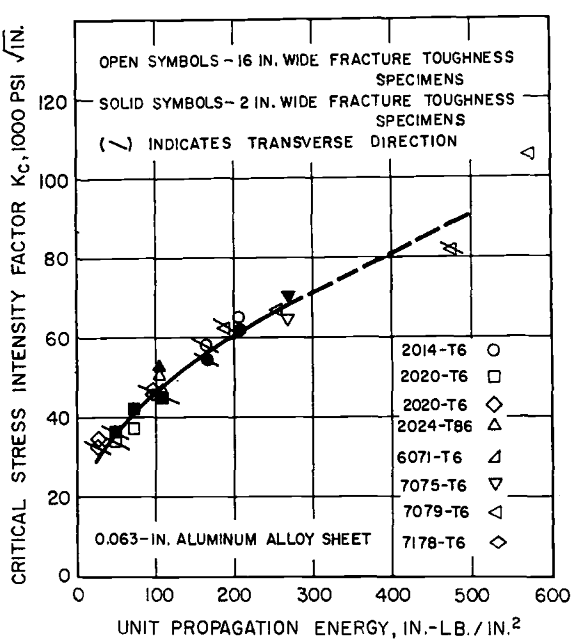

FIG. 11—Critical Stress-Intensity Factor, K_c, Versus Unit Propagation Energy.

use of fatigue-cracked specimens increases the problems of detecting the initial unstable burst of crack growth. However, there seems little doubt that fatigue cracking is necessary in determining the plane-strain toughness even of aluminum alloys, and now almost all K_{Ic} determinations at ARL are made with fatigue cracked specimens.

Despite the wide use of these various fracture toughness tests at ARL to establish the fracture parameters for velop unstable crack growth in moderately sized specimens. Variations in compositions, fabrication procedures, and temper frequently result in toughnesses that fall into this range. Furthermore, with increase in temperature, the toughness of all aluminum alloys increases, placing even the least ductile of the commercial alloys outside the range where precise fracture toughness testing would be useful in establishing toughness at elevated temperatures.

CORRELATION BETWEEN TEAR TESTS AND FRACTURE TOUGHNESS TESTS

The inherent difficulties with the use of the fracture toughness test for evaluating a wide range of alloys, plus the background of information accumulated with the Kahn-type tear test, made it attractive to determine whether a correlation exists between data from the two types of test. The first series of tests to establish the extent of correlation was conducted in the time period when center-notched specimens were being tested, with the ink-stain technique to measure crack growth. The results of the study are shown in Fig. 11, indicating a direct correlation between critical stress-intensity factor, K_c, for a given thickness of sheet, and unit propagation energy (2). Because of the thickness dependency of K_c, the correlation would differ for each thickness. Recent testing established that there is also a direct relation between unit propagation energy and plane-strain toughness as shown in Fig. 12.

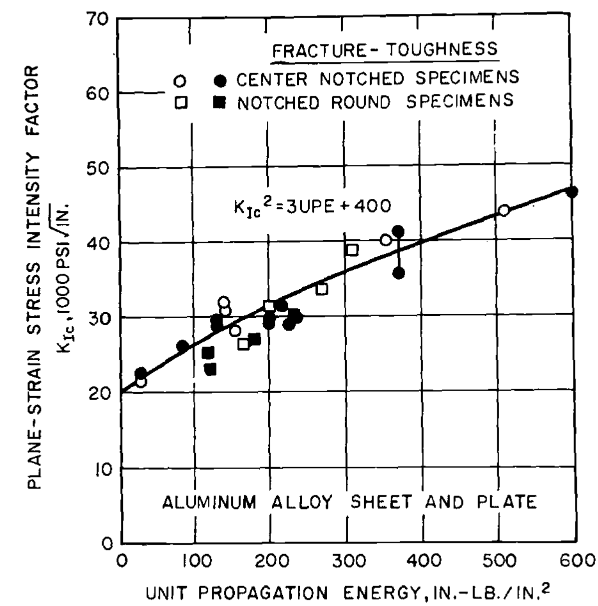

FIG. 12—Relation Between K_{Ic} and Unit Propagation Energy.

These findings had the double effect of: (*1*) increasing confidence that the tear test provides meaningful ratings for the alloys; and (*2*) providing a means for estimating the values of fracture toughness parameters from tear-test results. This added confidence, plus the problems in using the fracture toughness tests on tough materials, resulted in the concentration of alloy-development screening work on the tear test rather than the fracture toughness test.

ALLOY DEVELOPMENT

From an alloy-development viewpoint, it is essential to establish a broad understanding of the effects of numerous metallurgical variables on strength and toughness to serve as a guide in achieving improved combinations of these mechanical properties. To do this, it is necessary to be able to establish a reliable direct comparison of the toughnesses of a wide range of alloys and tempers, from low-strength very high-toughness materials to high-strength low-toughness materials. This has been greatly facilitated by the use of tear tests, which permit evaluation of the effects of composition, cold work, and heat treatment over a wide range of toughnesses and allow the relationships among these variables to be established. These tests have been supplemented for various purposes by other types of fracture tests. Some examples of the kinds of information obtained and relationships established are cited.

Strain-Hardening Alloys:

As an example of the influence of solid solution and strain-hardening effects the yield strengths and unit propagation energy values for four commercial alloys of the Al-Mg-Mn 5000 series are illustrated in Fig. 13 in relation to the magnesium contents for both the annealed (-O) and cold rolled, stabilized (-H34) tempers. It is apparent that although the resistance to deformation, as measured by yield strength, increases continuously over this range

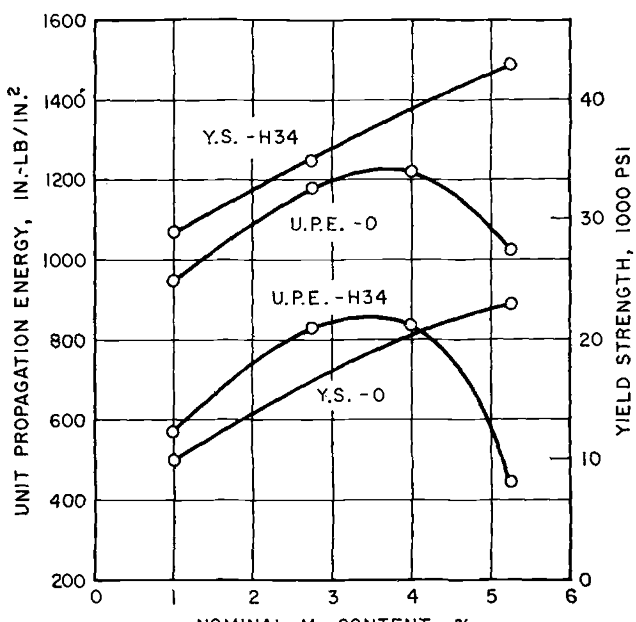

FIG. 13—Yield Strengths and Unit Propagation Energy Values of Commercial 0.063-In. Sheet of Four Aluminum–Magnesium–Manganese Alloys in Annealed (-O) and Strain Hardened, Stabilized (-H34) Tempers as a Function of Nominal Magnesium Content.

with increasing magnesium, the toughness, as measured by unit-propagation energy, achieves a maximum at an intermediate strength level and diminishes sharply at the higher levels of yield strength. A further reflection of decreasing toughness with increasing strength is found in comparing the cold-worked versus the annealed tempers. The effect of increasing degree of strain hardening on the properties of the commercial alloy 5154 (nominally 3.5

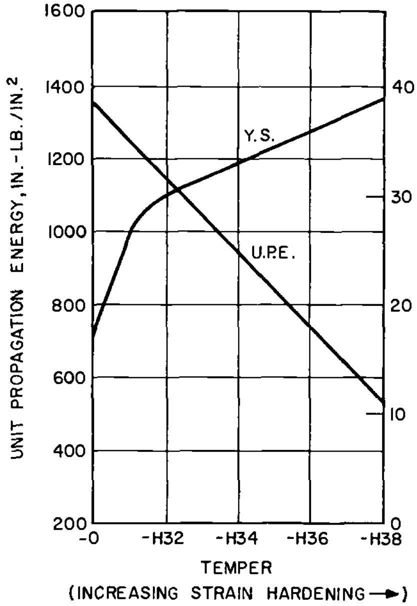

FIG. 14—Unit Propagation Energy of Commercial 5154 Alloy 0.063-In. Sheet as a Function of Temper (Increasing Strain Hardening).

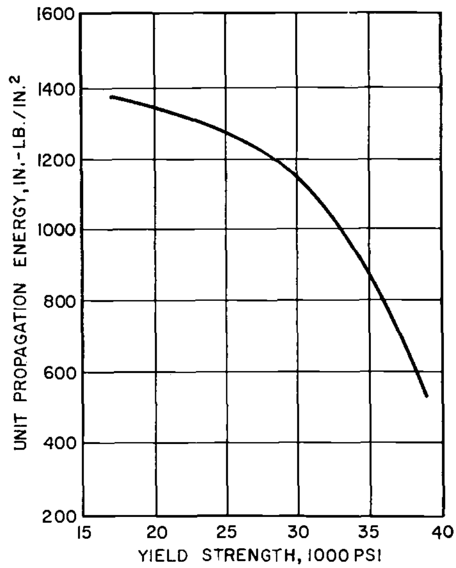

FIG. 15—Relation Between Unit Propagation Energy and Tensile Yield Strength of Commercial 5154 Alloy 0.063-In. Sheet in Several Tempers.

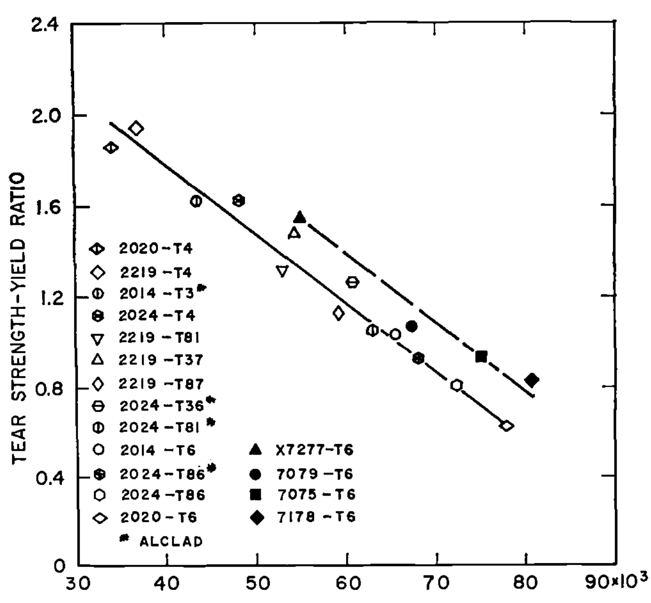

FIG. 16—Tear Strength to Yield Strength Ratio Versus Tensile Yield Strength for Commercial lauminum Alloys.

per cent magnesium, 0.25 per cent chromium) is demonstrated by the data for the various commercial tempers in Fig. 14. The unit propagation energy values decrease in an approximately linear manner with increasing amounts of strain hardening. The relationship between unit propagation energy and yield strength for this material as influenced by extent of cold working is illustrated in Fig. 15.

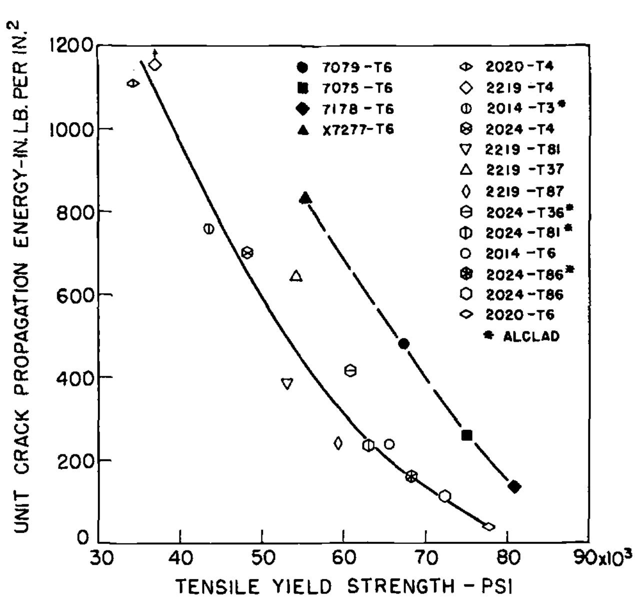

FIG. 17—Unit Propagation Energy Versus Tensile Yield Strength for Commercial Aluminum Alloys.

These data disclose that high levels of toughness prevail at intermediate contents of the solid solution-forming alloy element magnesium. They are also indicative of little probability that combinations of strength and toughness superior to those exhibited by the commercial alloys of this type can be achieved by increasing magnesium contents only, or by introducing greater amounts of strain hardening.

Precipitation-Hardening Alloys:

The aluminum alloys that are capable of developing the highest strengths are of the precipitation-hardening type, and those of greatest interest are the Al-Cu 2000 series and Al-Zn-Mg 7000 series. To obtain some guidance concerning which of these two alloy types might have greater promise for high strength and toughness at room temperature, data from tear tests of a number of the alloys in different tempers were plotted as shown in Figs. 16 and 17. These data clearly indicate that at room temperature the 7000 series alloys have a distinct advantage over those of the 2000 series, and that variations in temper for the latter merely shift the combination of yield strength and toughness one direction or the other along the curves for the 2000 series alloy (9).

Specific attention was given to the effects of variations in artificial aging treatment. For 2014 for example, the tear resistance of sheet samples was determined after natural aging (T4 temper) and after various amounts of artificial aging to develop different strength levels up to and including those of the maximum strength T6 temper; additional specimens were overaged to a series of strength levels lower than that of the T6 temper. The results of these tests are summarized in Fig. 18 in which the unit propagation energies are related to the yield strengths attained during aging. The curves illustrate that

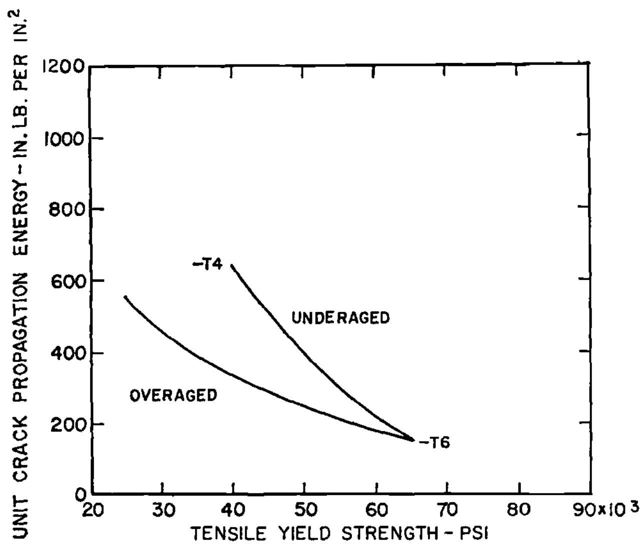

FIG. 18—Effects of Artificial Aging on Unit Propagation Energy 2014 Alloy.

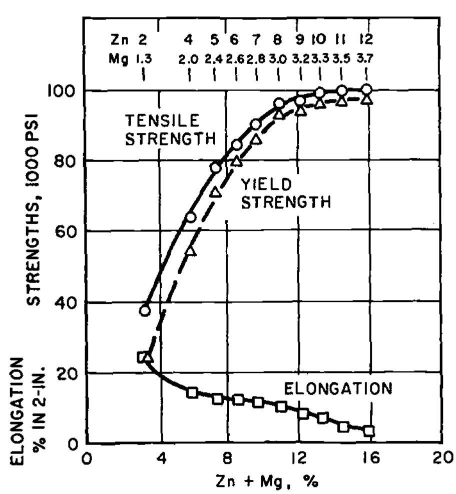

FIG. 19—Tensile Properties of Experimental Aluminum Alloy Series Containing Zinc, Magnesium, 0.8 per cent Copper, 0.2 per cent Chromium, 0.12 per cent Manganese in Relation to Sum of Zinc and Magnesium Content. Laboratory-Fabricated 0.063-In. Sheet, Heat-Treated to T6 Type Temper, Tested in Longitudinal Direction.

the strength-to-toughness relationship differs for the underaged and overaged conditions. For a specific yield strength lower than that of the T6 temper, underaging provides a higher degree of toughness than does overaging. Information of the type illustrated has assisted in establishing and selecting conditions of thermal treatment for various alloys to achieve desired strength and toughness combinations. Although these mechanical property comparisons favor the naturally aged, intermediate artificially aged, and fully aged tempers, other characteristics such as resistance to corrosion or stress corrosion, may influence the ultimate selection of temper.

High-Strength Aluminum-Zinc-Magnesium-Copper Alloys:

Experimental work was undertaken to provide information upon which the

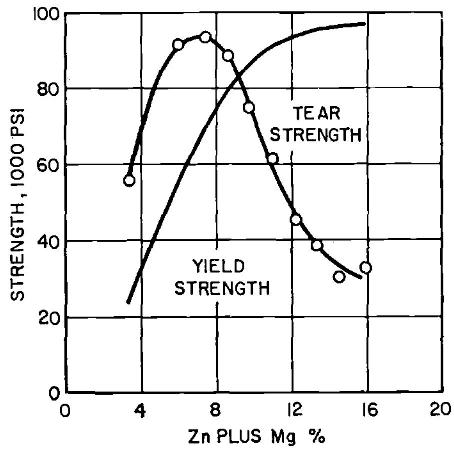

FIG. 20—Tear and Yield Strength Values for Experimental Alloys.

throughout the series. The material was laboratory-fabricated 0.064-in. sheet, heat-treated by practices designed to develop essentially maximum strengths.

The tensile properties are plotted in Fig. 19 as functions of the sum of the zinc plus magnesium contents and increase progressively with increasing alloy content. Tear tests were conducted with specimens prepared from the same panels as the tension specimens. As shown in Fig. 20, the tear strengths increased with increasing alloy content for the first three compositions but declined progressively with further increase in alloy concentration. The ratio of tear strength to yield strength of

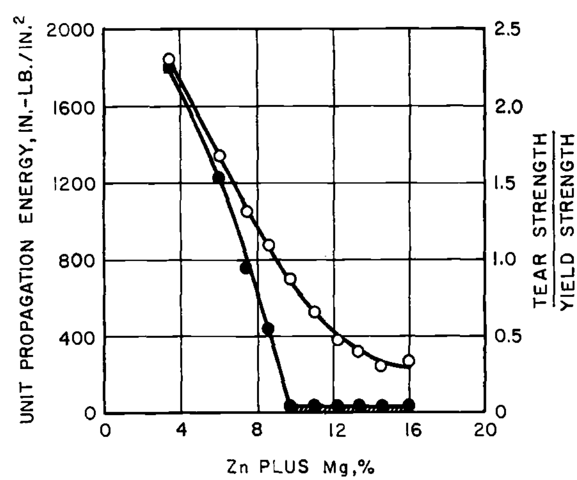

FIG. 21—Unit Propagation Energy Values and Tear Strength–Yield Strength Ratios for Experimental Alloys.

development of specific alloys having improved strength and fracture-propagation characteristics might be based. In one phase of this work, a series of alloy compositions was produced from high-purity aluminum with progressively increasing amounts of the precipitation-hardeners, zinc and magnesium (9). Supplementary alloying additions of copper, chromium, and manganese were maintained at constant percentages these alloys decreased continuously with increasing alloy content as shown in Fig. 21. The highest unit crack-propagation energy was associated with the lowest strength, highest elongation, and lowest alloy content composition of the series. The propagation-energy values declined sharply with increasing alloy content. At a zinc plus magnesium content of about 10 per cent and higher, the elastic energy in the specimens was sufficient to propagate the crack to failure so that quantitative values of energy were not obtained, but they are estimated to be less than 50 in-lb/in.^{2}. Although no differences in unit-propagation energy values could be measured among the alloys in this range, the tear-yield ratios provided some discrimination. K_c values were determined for several alloys of the series having yield strengths of 85,000 psi and higher. The results of these tests showed a fairly direct correlation between K_c and tear-yield ratio. The values ranged from K_c = 54,000 psi $\sqrt{\text{in.}}$ at a yield strength of 86,000 psi and tear-yield ratio of 0.76 to K_c = 26,000 psi $\sqrt{\text{in.}}$ at a yield strength of 94,000 psi and tear-yield ratio of 0.41.

In order to illustrate further the relationship between alloys of the nonheat-treatable and heat-treatable types and the broad range of toughness over which the tear test can provide useful information, another series of alloys was prepared and tested. This alloy series contained 3.4 per cent magnesium which, from the information presented previously, may be associated with high values of crack-propagation energy in annealed or cold-worked tempers. The alloys of this series also contained uniform contents of copper, chromium, and manganese, but zinc contents varied from 0 to 8 per cent. The yield strengths and unit-crack propagation energy values of these alloys after a heat treatment of the T6 type are plotted in Fig. 22 in relation to the zinc content. Since the alloys with 2 per cent zinc or lower

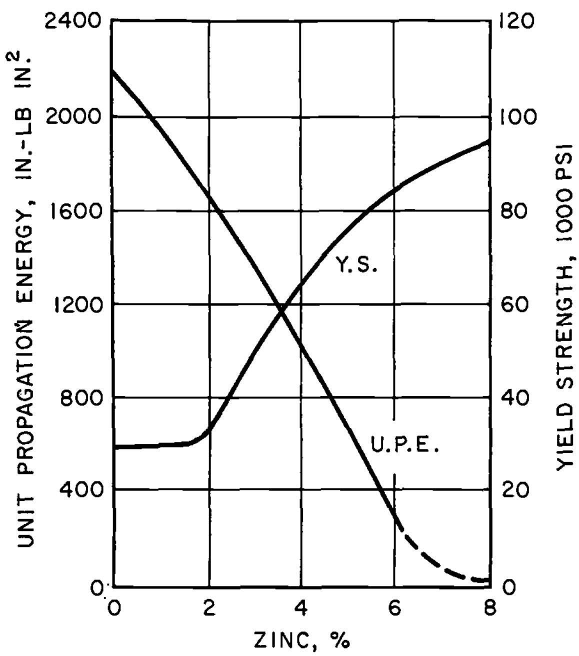

FIG. 22—Effect of Zinc Content on Yield Strength and Unit Propagation Energy of Laboratory-Fabricated 0.063-In. Sheet Containing 3.4 per cent Magnesium, 0.8 per cent Copper, 0.20 per cent Manganese, and 0.12 per cent Chromium, Solution Heat-Treated and Artificially Aged (-T6 Type) Longitudinal Direction.

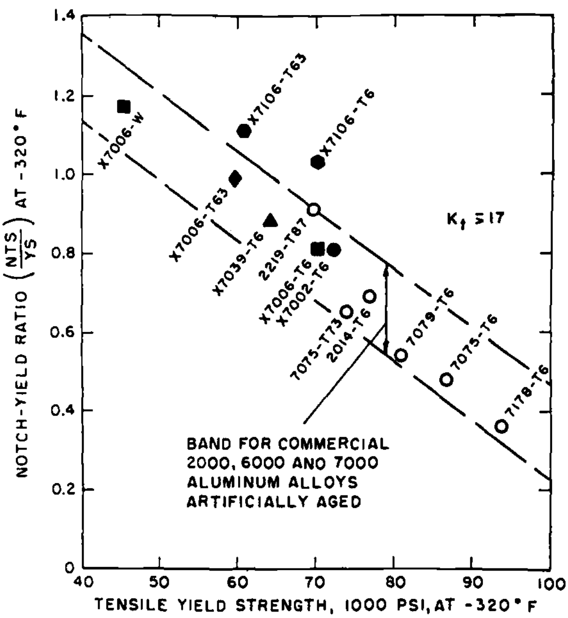

FIG. 23—Relationship Between Notch-Yield Ratio and Tensile Yield Strength at −320 F 0.063-In. Thick Sheet; Transverse.

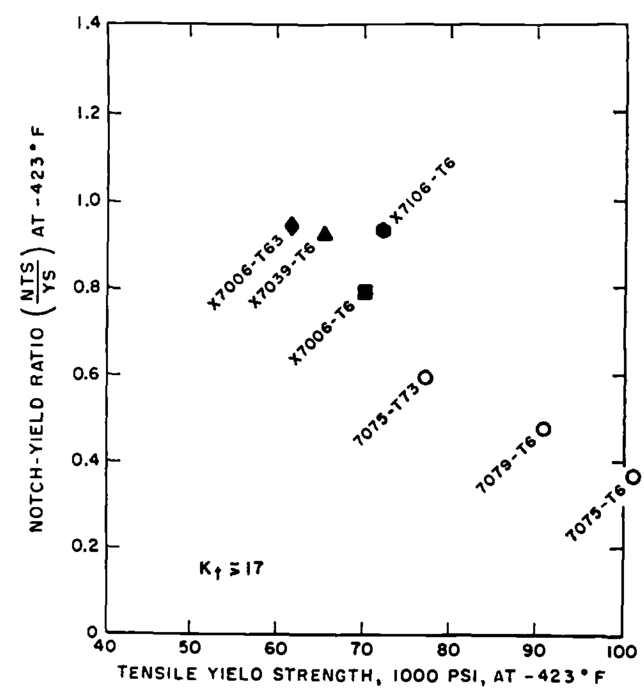

FIG. 24—Relationship Between Notch-Yield Ratio and Tensile Yield Strength at −423 F, 0.063-in. Thick Sheet; Transverse.

showed little or no precipitation-hardening with this heat treatment, their properties corresponded approximately to those of the annealed temper. With increased zinc contents, however, the heat treatment provided higher strengths. The unit crack propagation energy values decreased progressively with increasing zinc content. The results obtained from this alloy series as well as that previously discussed illustrate the merit of tear tests in comparative evaluation of aluminum alloys ranging from those that are most resistant to fracture propagation to those which have the highest strengths currently attainable by conventional processing. The information from such tests is being used in current research programs having as their objective the improvement and development of high-strength alloys for minimum weight structures.

Alloys for Cryogenic Applications:

Tension tests of smooth and sharply notched specimens were made of a series of aluminum–zinc–magnesium alloys at room temperature, −112, −320 and −423 F (10). The notched specimens were of the design shown in Fig. 5(*c*), coinciding with the recommendations in the First Report of the ASTM Special Committee (5). Notch-yield ratios from these tests were plotted as a function of tensile yield strength at −320 and −423 F as shown in Figs. 23 and 24. At −320 F, the data points for all but one of these alloys fall into a rather narrow band with data for a number of other commercial aluminum alloys. The data points for the one exception, in the two tempers tested, plotted well above the rest. This suggested a superiority of this particular alloy, X7106, at the lower temperatures. Confirmation of this trend by other series of tests of this alloy and of related alloys resulted in a new series of zirconium-bearing aluminum alloys for cryogenic applications where high toughness is required.

SUMMARY

The Alcoa Research Laboratories have been active in fracture testing of aluminum alloys for many years. Fracture toughness determinations are made on commercial and promising experimental alloys and tempers with various designs of specimen, using the compliance-gage technique to detect the initiation of unstable crack growth. Kahn-type tear tests and sharp-notch tension tests have been used to supplement fracture toughness testing in the evaluation of the effects of composition, fabrication procedure, temper, and environment on the fracture characteristics of aluminum alloys. Tear tests have the advantage that direct measures of the relative amounts of energy required to propagate a crack can be obtained even for the toughest of aluminum alloys; furthermore, the unit propagation energy from the tear test is directly correlated with K_c and K_{Ic}. Sharp-notch tension tests are economical and, in the absence of general yielding, the ratio of notch strength to yield strength provides a meaningful measure of relative toughness.

REFERENCES

(1) N. A. Kahn and E. A. Imbembo, "A Method of Evaluating the Transition from Shear to Cleavage-Type Failure in Ship Plate," *Welding Journal*, Vol. 27, 1948, pp. 169-s–182-s.

(2) A. H. Knoll and J. G. Kaufman, "Kahn-Type Tear Tests and Crack Toughness of Aluminum Alloy Sheet," *Materials Research & Standards*, Vol. 4, April, 1964, pp. 151–155.

(3) E. W. Johnson and J. G. Kaufman, 'The Use of Notch-Yield Ratio to Evaluate the Notch Sensitivity of Aluminum Alloy Sheet," *Proceedings*, Am. Soc. Testing Mats., Vol. 62, 1962, pp. 778–793.

(4) K. O. Bogardus, G. W. Stickley, and F. M. Howell, "A Review of Information in the Mechanical Properties of Aluminum Alloys at Low Temperatures," *NACA TN 2082*, May, 1950.

(5) Reports of Special ASTM Committee on Fracture Testing of High-Strength Metallic Materials:

First Report—"Fracture Testing of High-Strength Sheet Materials: A Report of A Special ASTM Committee," *ASTM Bulletin*, No. 243, January, 1960, pp. 29–40; No. 244, February, 1960, pp 18–28.

Second Report—"The Slow Growth and Rapid Propagation of Cracks," *Materials Research & Standards*, Vol. 1, No. 5, May, 1961, pp. 389–393.

Third Report—"Fracture Testing of High-Strength Sheet Materials," *Materials Research & Standards*, Vol. 1, No. 11, November, 1961, pp. 877–885.

Fourth Report—"Screening Tests for High-Strength Alloys Using Sharply Notched Cylindrical Specimens," *Materials Research & Standards*, Vol. 2, No. 3, March, 1962, pp. 196–204.

Fifth Report—"Progress in Measuring Fracture Toughness and Using Fracture Mechanics," *Materials Research & Standards*, Vol. 4, No. 3, March, 1964, pp. 107–118.

(6) J. E. Srawley, M. H. Jones, and B. Gross, "Experimental Determination of the Dependence of Crack Extension Force on Crack Length for a Single-Edge-Notch Tension Specimen," *NASA TN D-2396*, Nat. Aeronautics and Space Administration, August, 1964.

(7) B. Gross, J. E. Srawley, and W. F. Brown, Jr., "Stress Intensity Factors for a Single-Edge-Notch Tension Specimen by Boundary Collocation of a Stress Function," *NASA TN D-2395*, Nat. Aeronautics and Space Administration, August, 1964.

(8) M. H. Jones and W. F. Brown, Jr., "Acoustic Detection of Crack Initiation in Sharply Notched Specimens," *Materials Research & Standards*, Vol. 4, No. 3, March, 1964, pp. 118–128.

(9) J. A. Nock, Jr. and H. Y. Hunsicker, "High-Strength Aluminum Alloys," *Journal of Metals*, Vol. 15, No. 3, March, 1963, pp. 216–224.

(10) W. A. Anderson, J. G. Kaufman, and J. E. Kane, "Notch Sensitivity of Aluminum-Zinc-Magnesium Alloys at Cryogenic Temperatures," *Advances in Cryogenic Engineering*, Vol. 9, 1964, pp. 104–111.

DISCUSSION

JOSEPH I. BLUHM[1]—At the U.S. Army Materials Research Agency we had the occasion to make some slow tearing tests on wide sheets (12 in.) of aluminum alloys. We found that the unit-propagation energy reached a stable level only after the crack had propagated some distance. Furthermore, the unit-propagation energy varied considerably from its steady-state value. Hence, any technique of taking the *total* area under the load-deformation curve would surely include some errors due to these boundary effects. At this Agency, we continually determined the unload slope of the load-deformation curve at various crack lengths and were thus able to get the instantaneous rate of propagation energy.[2]

[1] Chief, Applied Mechanics Research Laboratory, U.S. Army Materials Research Agency, Watertown, Mass

J. G. KAUFMAN AND H. Y. HUNSICKER (*authors*)—The authors appreciate Mr. Bluhm's comment and agree with him that values of unit propagation energy determined in Kahn-type tear tests are not absolute measures of the steady-state rate at which energy is utilized. As stated in the text of the paper, it is recognized that values of unit propagation energy are specimen-size dependent. However, their primary value is for merit rating alloys and the excellent correlation between unit propagation from the tear tests and K_c or K_{Ic} from fracture toughness tests provides adequate confidence of their ability to indicate realistic ratings.

[2] See discussion of paper by Klier et al, "A Study of Certain Factors Which Modify Slow Crack Propagation in High Strength Sheet Metal," *Proceedings*, Am. Soc. Testing Mats., Vol. 64, 1964.

STP381-EB/Apr. 1965

THE APPLICATION OF FRACTURE TOUGHNESS TESTING TO THE DEVELOPMENT OF A FAMILY OF ALLOY STEELS

By J. S. Pascover,[1] M. Hill,[1] and S. J. Matas[1]

Synopsis

The use of fracture toughness in the development of the 9Ni-4Co alloy system[2] is described in this paper. The primary concern during this study was the delineation of metallurgical trends rather than the generation of quantitative data. Thus, screening tests have been employed.

The particular test chosen for any study should have four characteristics:

1. be compatible with previous data
2. be reasonable in cost
3. reflect the section size anticipated for eventual service
4. have sufficient sensitivity to define the effects of thc variables investigated.

High-strength steels were screened effectively with center fatigue precracked specimens. The thickness of the specimens was adjusted to fit a given toughness level. The sensitivity was greatest when the ratio of the nominal notch strength to the yield strength was between 0.4 and 0.8.

For tough materials at strength levels of 200 ksi and lower, the determination of valid plane-strain toughness values in the early stages of alloy and process development is impractical due to the large size of the required specimens. Precracked and standard Charpy impact specimens appeared to define usefully qualitative trends. However, in the final optimization programs, plane-strain fracture toughness specimens were used to obtain absolute fracture toughness numbers compatible with the best known state of the art.

The past few years have seen a substantial increase in the need for ultrahigh-strength materials. However, ultrahigh strength *per se* has little practical significance since a material must also show resistance to crack propagation. Although such properties as fatigue strength, stress-corrosion resistance, and ease of fabrication must also be considered in any application, only fracture toughness will be discussed herein.

The need for materials with high strength and toughness has been met in part by the development of several new alloy systems. One such series of alloys, the 9 per cent nickel - 4 per cent cobalt steels, was developed at the Republic Steel Research Center (**1–8**).[3] This paper will describe some of the experience gained in the use of fracture toughness testing during the alloy development phase of the 9Ni-4Co alloy system research. The examples described in this paper were chosen for the most part to illustrate areas of use

[1] Research metallurgists and supervisor, respectively, high strength steels, Republic Steel Corp., Research Center, Cleveland, Ohio.

[2] The 9 per cent nickel-4 per cent cobalt steels, which are designated as HP 9-4-X steels, are proprietory steels of Republic Steel Corp.

[3] The boldface numbers in parentheses refer to the list of references appended to this paper.

for fracture toughness testing where the determination of the metallurgical trends was considered more important than adherence to the rigor of fracture mechanics. Specifically, the use of fracture toughness testing in studies of the effects of heat treatment, alloy composition, melting practice, and special processing will be described.

TEST METHODS

Selection of the specific test method was related to the anticipated use of data and to the capability of the test to provide information on the toughness of the material easily and economically. This is discussed in the next two sections.

Anticipated Use of Data:

From our experience in alloy development it became apparent that testing at three levels of sophistication are required. These are:

(*a*) the use of fracture toughness testing in the initial stages of alloy and process development;

(*b*) the use of fracture mechanics in the late stages of the development; and

(*c*) the use of fracture mechanics by the user in order to determine parameters which are of help to design engineers.

In many cases the latter type of testing involves "personalized" procedures which are tailored to specific hardware applications. Although this type of testing is extremely useful to the manufacturer, it is too limited in application for the supplier who is primarily interested in establishing the potentials of an alloy or process.

The use of fracture mechanics in the late stages of development of an alloy system or process involves determination of a limited number of absolute fracture toughness parameters by rigorous techniques. A direct comparison can then be made with data from other sources.

Much of the literature describes the use of fracture mechanics in its "rigorous" sense. The aim of this paper, however, is not to contribute to the science of fracture mechanics, but rather to describe our experiences in the use of fracture toughness testing in the early stages of alloy development.

Selection Criteria:

No single test was found which would be universally applicable. Therefore the type of test used was tailored to our needs, and selected on the basis of its capability for delineating metallurgical trends.

The final selection of the testing procedure followed several guide posts:

1. The data obtained should be compatible with those previously accumulated.
2. The state of art of the testing method should be far enough advanced.
3. The test chosen should be consistent with the toughness of the material.
4. The cost of the testing program should be reasonable.

APPLICATION OF SELECTION CRITERIA

Testing of Sheet Materials at Ultrahigh-Strength Levels:

When the 9Ni-4Co program was started, emphasis was given to very high strength (250 ksi and higher). Two types of sheet specimens were available for testing these high-strength materials: One, a symmetrical edge-notched specimen;[4] the other, a center fatigue precracked specimen. The latter was chosen for its simplicity and adaptibility to the available equipment at the Research Center.

These specimens were primarily designed to measure plane-stress fracture toughness parameters; although, in

[4] Presently, this specimen is invariably fatigue precracked (**11**).

TABLE 1—NOTCH TOUGHNESS[a] OF HP 9-4-45 AS AFFECTED BY TEMPERING.
(Heat 3950701)

Dimensions of Center Fatigue Precracked Specimen[b]	Tempering Temperature,[c] deg F	Yield Strength, ksi	Net Fracture Toughness Strength, ksi	Nominal Notch Strength, ksi	K_c, ksi $\sqrt{\text{in.}}$	Gross Stress, ksi	$2a$, in.	Shear, per cent	Ratio of Notch Strength to Yield Strength
0.080 by 2 by 8 in.	400	245.0	260	153.2	207[d]	25.67	1.25	100	0.63
$2a_0$ = 0.75 in.	500	232.0	255	188.0	210[d]	114.4	1.10	100	0.81
	600	220.0	241.0	183.0	217[d]	114.7	1.05	100	0.83
0.180 by 3 by 12 in.	400	245.0	166.0	106.2	177.3	67.3	1.70	75	0.43
$2a_0$ = 1.05 in.	500	230.0	248.5	136.8	264.6[d]	88.9	1.93	100	0.59
	600	225.0	250.0	180.0	272.0[d]	117.0	1.58	100	0.80

[a] Values represent averages of more than two specimens.
[b] The definition of the fracture toughness parameters is given below:

where: P_m = maximum load
W = width
t = thickness
$2a_0$ = original crack length
$2a$ = original crack length plus length of slow moving crack which was determined by ink-staining technique.

Net fracture toughness strength $= \dfrac{P_m}{t(W - 2a)}$

Nominal notch strength $= \dfrac{P_m}{t(W - 2a_0)}$

Gross stress $= \dfrac{P_m}{tW}$

[c] All specimens were normalized at 1600 F, austenitized at 1450 F, oil-quenched, refrigerated at −120 F, and tempered at the indicated temperatures.
[d] The ratio of net fracture toughness strength to yield strength exceeded 1.0.

some instances, plane-strain fracture toughness parameters were obtainable. The determination of K_c and K_{Ic} require a knowledge of the crack length corresponding to the load at fracture instability. Initially it was suggested that a useful indication of the crack length at fracture instability could be obtained by introducing a staining substance such as India ink into the notch or crack before starting the test (9). At the Research Center, however, it was found early in the testing program that this method of determining crack instability was inaccurate and nonreproducible and presently, the use of staining fluids is no longer recommended (10). Since other methods for detecting crack instability were at their infancy at the time this particular work was done, the determination of K_c values was abandoned. Furthermore, in alloy and process development, it was found that the range where K_c can be accurately calculated was very small, as can be seen in Table 1. It is also apparent that it was difficult to obtain K_c for specimens in most heat-treated conditions because of the high toughness of the alloy system. Thus, because of K_c's limited use it was decided to use other toughness parameters which could be calculated from the same type of specimen. The use of the net-notch strength as a parameter was not considered as it is subject to the same objections as that of K_c. However, the use of nominal notch strengths looked more promising. This parameter indicates the load-carrying capacity of the material in the presence of a sharp notch, and does not require the knowledge of the length of the crack at instability. Thus, it was easily determined experimentally. Furthermore, it extended the range of discrimination as is seen in Table 1 for the 0.080-in. thick specimens. At a ratio of notch strength to yield strength

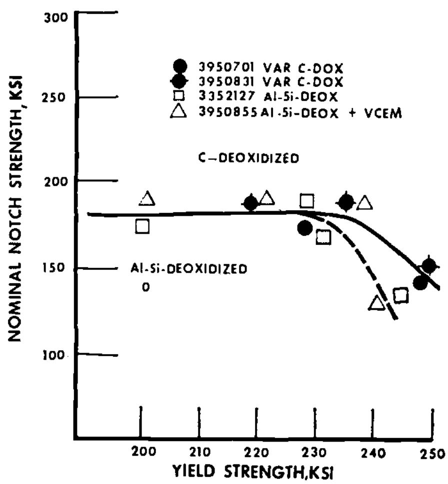

FIG. 1—The Effect of Deoxidation Practice on the Strength-to-Toughness Relationship in HP 9-4-45 Steel Sheet. Center Fatigue Precracked Specimens, Longitudinal 0.080-in. Sheet (20).

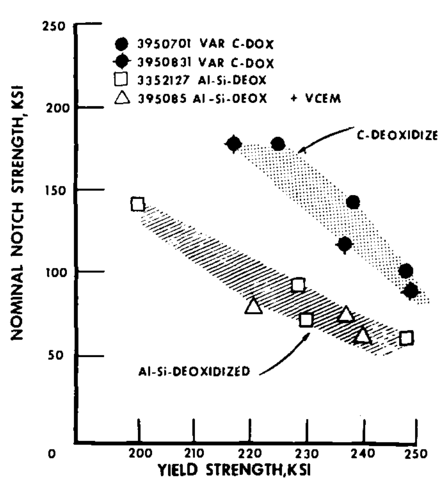

FIG. 2—The Effect of Deoxidation Practice on the Strength-to-Toughness Relationship in HP 9-4-45 Sheet. Center Fatigue Precracked Specimen, Longitudinal 0.180-in. Sheet (20).

greater than 0.8, the accuracy of this parameter also diminished. To circumvent this difficulty, one simply used a thicker specimen. As can be seen in Table 1. the ranges of sensitivity were extended to higher toughness levels when a 0.180-in. thick specimen was used instead of a 0.080-in. thick specimen.

Another example, which shows the advantage of testing specimens with two section thicknesses, is presented in Fig. 1. This example involves the study of the effect of deoxidation practice on the toughness of HP 9-4-45 steel. It is apparent that the 0.080-in. thick specimens are unable to define the effects of different melting practices. There are some indications of the difference at the higher strength, that is, lower toughness. On the other hand, the 0.180-in. thick specimens showed a significant difference between the vacuum carbon-deoxidized product and aluminum-silicon deoxidized and vacuum remelted product (Fig. 2). The use of only one type of specimen could have been misleading in this instance.

TABLE 2—THE DIRECTIONALITY OF NOTCH PROPERTIES OF SILICON-ALUMINUM DEOXIDIZED[a] HP 9-4-45 STEEL. (Heat 3352127)

Thickness of Center Fatigue Precracked Specimen, in.	Tempering[b] Temperature, deg F	Direction	Ratio of Notch Strength to Yield Strength
0.080....	400	longitudinal	0.56
		transverse	0.35
0.080....	600	longitudinal	0.80
		transverse	0.50
0.180....	400	longitudinal	0.25
		transverse	0.24
0.180....	600	longitudinal	0.39
		transverse	0.38

[a] Double slag, basic electric furnace practice. Deoxidized by addition of silicon and aluminum.

[b] All specimens were normalized at 1600 F, austenitized at 1450 F, oil-quenched, refrigerated at −120 F, and tempered at indicated temperatures.

Under very brittle conditions, it was found that the nominal notch strength of the material is so low that the test is again unable to discriminate between variables (see Table 2). These data would imply that no difference in transverse and longitudinal toughness exists in the three heats. This example suggests that the test has a lower limit of sensitivity at which point it loses its value. On the basis of these and similar data, it was decided to set a lower and upper bound for a given symmetrical center fatigue precracked specimen. The lower limit of the ratio of nominal notch strength to yield strength (NS/YS) was chosen at about 0.40, with an upper limit at about 0.80. When the data fell outside this range, the thickness of the specimen was changed. Although this may be costly (see Appendix I for cost analysis of different fracture toughness specimens), this type of testing procedure offered a reliable means of defining some of the metallurgical variables in our alloy and process development work.

Testing of Tough Materials:

Tough alloys, such as HP 9-4-25 steel, were developed in anticipation of their application in heavy sections. For such applications, one would like to determine plane-strain fracture toughness (K_{Ic}). Unfortunately, such testing often requires specimens of large size and involves great expense. To illustrate the specimen sizes, for example, the required over-all diameter of the smallest circumferentially notched round bar of HP 9-4-25 steel heat-treated to a 170-ksi yield strength level and having an anticipated K_{Ic} value of the order of 150 ksi $\sqrt{\text{in.}}$ is of the order of 4 in. in diameter. The minimum thickness of a surface-cracked specimen is on the order of $1\frac{1}{2}$ to 2 in. The minimum dimensions of the slow bend single-edge-notched specimen would be on the order of $1\frac{1}{2}$ in. square and about 12 in. long (11).

Thus, in the early stages of screening alloys and processes, the use of these plane-strain fracture toughness specimens is a rather impractical procedure from a material standpoint. In order to get an idea of the response to heat treatment of a given new composition, one needs at least five different heat-treating conditions. Thus, if one uses duplicates, this will amount to ten specimens per heat which would involve about 100 lb of material (assuming that one needs a specimen with the following minimum dimensions—$1\frac{1}{2}$ by $1\frac{1}{2}$ by 12 in. equal to about 8 lb). This would amount to about 150 lb of raw material for this type of testing per heat. In the development of a new alloy system, one usually tests close to a hundred heats.

Notwithstanding the amount of material as such, the other problem is that one cannot make a laboratory heat of 150 lb and expect valid results on $1\frac{1}{2}$-in. thick plate. To obtain the necessary amount of hot working, one must start with larger ingot cross sections than are feasible in a laboratory.

To suggest an idea of the cost of certain of the specimens required to obtain quantitative data, a cost analysis was prepared and appears in Appendix I. The cost analysis shows that the cheapest K_{Ic} specimen is at least two times as expensive as the Charpy V-notch specimen.

In view of the above considerations, the most efficient way to screen alloys in the early stages at the 200-ksi strength range would be to use Charpy V-notch specimens. This, of course, was the procedure followed during the early stages of the development of an ultra-tough 200-ksi yield-strength material. However, by the introduction of a fatigue crack into the specimen, the sensitivity of the test can be significantly increased at small additional cost. Such specimens, referred to as precracked Charpy specimens (12), are also very useful in determining directionality of small forgings and heavy plate because of their small size.

The suggested plane-strain specimens are of benefit in the late stages of development (10,11). The next section shows the evolution of our experience and will elaborate on some of the underlying reasons for our action.

SPECIFIC EXAMPLES OF THE USE OF FRACTURE MECHANICS IN ALLOY AND PROCESS DEVELOPMENT

The contribution of fracture mechanics to alloy and process development may be

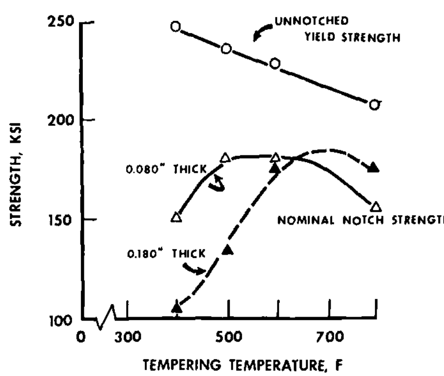

FIG. 3—The Influence of Tempering Temperature on the Strength and Toughness of HP 9-4-45 Steel (Heat 3950701). Nominal Notch Strength Determined with Center Fatigue Precracked Notched Specimens.

considered in terms of some specific examples. For the most part those examples were selected which would show the usefulness of qualitative instead of quantitative fracture mechanics testing. The advantage derived from such a qualitative study is the fact that it can describe metallurgical trends expediently and inexpensively. Only in the late stages of alloy and process development were all the "rigors" of fracture mechanics applied to obtain accurate quantitative fracture toughness parameters (or at least to the accuracy of the contemporary state of art).

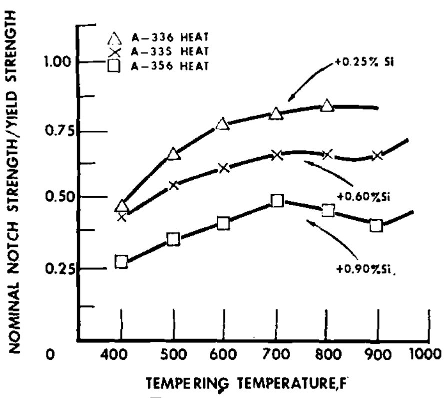

FIG. 4—The Effect of Silicon on the Ratio of Notch Strength to Yield Strength at Various Temperatures, for Air-Induction Melted 9Ni-4Co-45 C Type Steels (20).

the tempering temperature is increased, there is a continuous decrease in strength and a corresponding increase in toughness. This is in contrast to other carbon-strengthened steels and in particular to chromium-molybdenum-nickel steels, which show a discontinuous change of toughness with tempering temperatures (14–17).

This discontinuous change in toughness, commonly known as 500-F embrittlement, has been attributed by some to a change in carbide structure (14,15) and by others to the presence of certain impurities (18,19). Although, at first analysis, such a conspicuous absence

TABLE 3—TOUGHNESS OF BAINITICALLY TRANSFORMED HP 9-4-45 STEEL. (Heat 3950831)

Dimensions of Center Fatigue Precracked Specimen	Transformation Temperature,[a] deg F	Yield Strength, ksi	Nominal Notch Strength, ksi	Ratio of Notch Strength to Yield Strength
0.180 by 3 by 12 in.	500	220	202.2	0.92
	600	187	170.9	0.92
	700	138	156.7	1.13
0.250 by 4 by 16 in.	500	220	200	0.91
	550	210	191	0.91

[a] All specimens were normalized at 1600 F, austenitized at 1450 F, transferred to salt, and held for 8 hr at indicated temperatures.

of the 500-F embrittlement range could be attributed to lack of sensitivity of the test, this would not explain the results shown in Fig. 4. Additions of small amounts of silicon not only caused a drastic drop in the general toughness level of the steel but also showed an introduction of this embrittlement. Thus, it is more reasonable to assume that a 500-F embrittlement in HP 9-4-45 steel is not pronounced and only when embrittling agents such as silicon are introduced into the steel does the embrittlement become apparent.

It is interesting to note that, in a general study of the effect of alloy composition on the toughness of these high-strength steels, the effect of carbide-

Study of Thermal Treatments on Strength and Toughness of HP 9-4-45 Steel:

The characteristics of the 9Ni-4Co steels were described in great detail in a variety of publications (1–8). Herein, the use of fracture mechanics in establishing the role of heat treatment in determining the toughness of HP 9-4-45 steel will be described.

Effect of Tempering on the Strength and Toughness of HP 9-4-45 Steel—The influence of thermal treatment on the toughness[5] of the martensitic structure of HP 9-4-45 steel is shown in Fig. 3. As

[5] Center fatigue precracked specimens of two thicknesses were used to determine the toughness of the material. The fracture toughness parameter used was nominal notch strength.

forming elements was related to the toughness[6] of the steel. It was found that increasing the total amount of carbide-forming elements decreased the toughness of steels having carbon contents from 0.40 to 0.45 per cent and which were heat-treated to a 240–250-ksi yield strength level. Thus, the amount of carbide-forming elements in HP 9-4-45 steel was kept to a minimum (2,6,20). Furthermore, as described above, silicon was also shown to be detrimental to toughness and is therefore kept to a minimum in HP 9-4-45 steel.

Effect of Isothermal Transformation of Austenite to Bainite on Strength and Toughness of Sheet and Plate of HP 9-4-45 Steel—Steels heat-treated to bainitic structures were reported to have better toughness characteristics at a given strength level than when they were heat treated to tempered martensitic structures (21). To check whether a similar improvement can be realized in HP 9-4-45 steel, 0.180-in. center fatigue precracked specimens were prepared. The results are given in Table 3. The notch strength above a transformation temperature of 500 F consistently decreased with increasing reaction temperature. The drop in notch strength was not associated with a drop in toughness but with a decrease of the yield strength of the material. The material was too tough and exceeded the upper bound of the test. To return to the range of usefulness of the test, the section thickness was increased to ¼ in. Again the ratio of notch strength to yield strength exceeded 0.8, indicating that the material was too tough for this test. There was little advantage in going to ½-in. thick specimens, because of cost and because no similar data were available on tempered martensitic structures.

In a sense, we regressed when we went back to Charpy impact test specimens. The results are reproduced in Fig. 5. The data clearly show the superior toughness of the bainitic structure as compared to martensitic structures. To insure greater sensitivity, fatigue precracked Charpy specimens were also

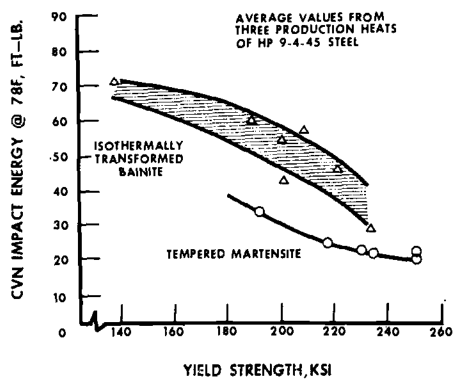

FIG. 5—The Relation between Strength and Impact Toughness of ½-in. Thick Plate of HP 9-4-45 Steel Heat-Treated to Bainitic and Tempered Martensitic Structures (6).

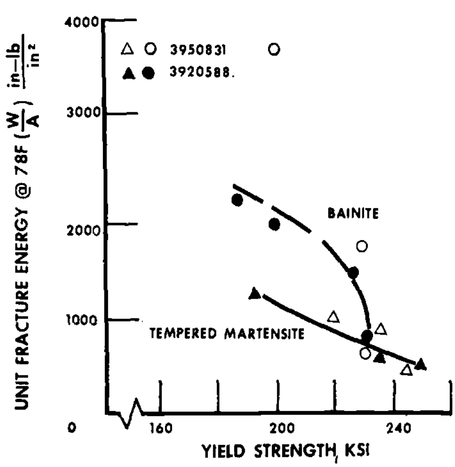

FIG. 6—A Comparison of the Unit Energy Absorption Characteristics of HP 9-4-45 Steel Heat-Treated to Various Strength Levels (6).

[6] Again, center fatigue precracked specimens were used to determine the toughness of the material.

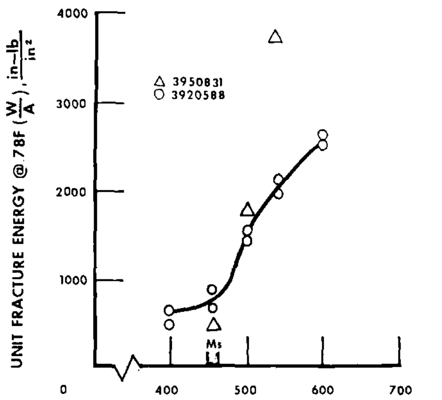

FIG. 7—The Effect of Transformation Temperature on Unit Energy Absorption of the HP 9-4-45 Steel at Room Temperature. (Specimens were Austenitized and Transformed at Temperatures Indicated (6).)

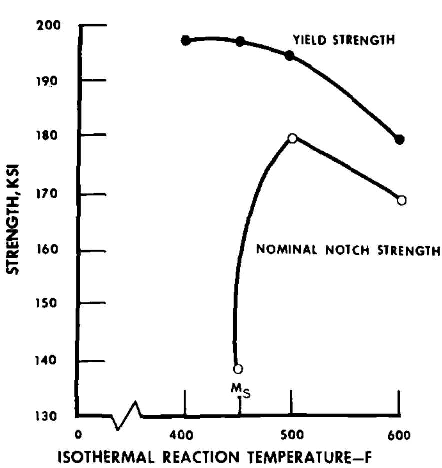

FIG. 8—The Effect of Duplex Structures on the Notch Properties of a 9Ni-4Co-38C Steel (Heat 3950704). Longitudinal Center Fatigue Precracked Notched Specimens of 0.180-in. Thickness (6).

tested. The results are shown in Fig. 6; in general, they show the same trends. However, the discontinuous change around the martensite transition (Ms) temperature was disconcerting. This can be seen better in Fig. 7, when the precracked Charpy data were replotted as a function of the transformation temperature of bainite. A re-examination of 0.180-in. thick center fatigue precracked specimens showed an even greater discontinuity as shown in Fig. 8. Although the test was of no value above the 500-F transformation temperature, it was of great value at lower transformation temperatures because the test was within its sensitivity range. This re-emphasizes the fallacy in using any single test to evaluate metallurgical phenomena. For example, if the experiment had been conducted only with Charpy impact specimens, no such embrittlement range would have been detected (compare Fig. 5 with Figs. 6–8). This is what happened, in fact, with the earlier results on AISI 4340 steel (21).

The use of plane-strain fracture toughness tests was out of the question because of the toughness of the material (Charpy impact energy = 70 ft-lb; W/A value = 2000 in-lb/in.^{2}). At the high transformation temperature, 600 F, the K_{Ic} was expected to be of the order of 140 ksi $\sqrt{\text{in.}}$, which would involve a specimen size of at least $1\frac{1}{2}$-in. thickness and material with a maximum size of 1-in. thickness was available. Slow bend single-edge-notched specimens 0.875 in. square exhibited substantial general yielding.[7]

The Effects of Anisotropy:

Another important aspect to be considered in the evaluation of a material or process is the amount of variation in toughness with orientation in the final product. Since failure will often occur along planes and directions of weakness, it is mandatory that the anisotropy of crack-growth resistance be explored.

Sheet—A typical example of such studies on sheet material can be made of a study on hot-cold-worked product of HP 9-4-45 steel. This process consists of

[7] Unpublished research, Republic Steel Corp.

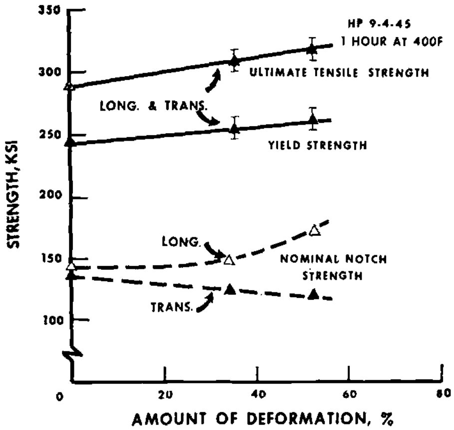

FIG. 9—The Influence of the Amount of Hot-Cold Working on the Anisotropy of Strength and Toughness of HP 9-4-45 Steel (25).

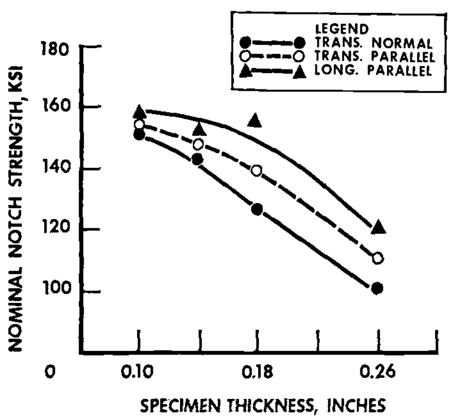

FIG. 10—Nominal Notch Strength as a Function of Specimen Thickness and Orientation in a Forged Slab (4 by 16 by 30 in.) of 18Ni-Co-Mo (250) Maraging Steel. Nominal Notch Strength was Determined on Center Fatigue Precracked Notched Specimens (see footnote 8).

the deformation of austenite prior to transformation and is similar in some respects to the so-called ausforming procedure. Much has been written on the mechanism of the property changes resulting from this procedure and some controversy still exists (22–24). It is clear, however, that when the deformation is unidirectional, a significant amount of grain refinement and distortion occurs as a result of this process. The amount of toughness variation consequent to this grain distortion is obviously of commercial and scientific importance. Figure 9 shows the effect of deformation on strength and toughness (25). It is apparent that anisotropy does exist and is a function of the amount of deformation.

Center fatigue precracked specimens were selected on the basis of convenience, the state of art, and the then-prominent hope that design data could be obtained in such a fashion.

Plate and Forgings—The anisotropy observed in heavy sections is often more severe than that seen in sheet product. Two studies of such an effect performed with different testing procedure are reported below:

18Ni-Co-Mo Maraging (250) Slab Material—The effects of directionality on the toughness of an 18Ni-Co-Mo (250) slab of dimensions 4 by 16 by 30 in. were evaluated using center fatigue precracked specimens of varying thickness.[8] Figure 10, in which nominal notch strength is plotted versus specimen thickness for three crack-growth directions, shows the results of this study. From a metallurgical standpoint, it appears that such anisotropy does exist, a finding which has recently been confirmed by Pellisier et al (26).

For the purposes of this paper, however, these data display several rather interesting characteristics. First, the ability of the test to differentiate between directions is a function of specimen thickness with this capability impaired at both the high and low toughness extremes. Furthermore, in order to obtain specimens of valid size, the original material had to be of a size which was completely inconsistent with the plane-

[8] Private communication from W. F. Barclay, Republic Steel Research Center.

stress specimen used. Stated in other terms, the results of the tests were not applicable to hardware which might utilize such 4 by 16 by 30-in. sections and the material used had a significantly different metallurgical history than that which prevails in sheet product. A more recent investigation of similar effects was carried out on a proprietory Republic alloy currently designated "Republic 9-4-20 (Cr, Mo)"[9] (7).

Republic 9-4-20 (Chromium-Molybdenum) Plate and Billet Product—In this case, material from production-sized heats of this experimental alloy was evaluated with respect to variation of toughness with product-section size and specimen orientation. The results of this study, carried out with precracked Charpy impact specimens, are quoted in Table 4. The strength data are not yet available; however, hardness checks indicate that a completely martensitic structure was maintained regardless of section size (the specimens were taken from heat-treated, quasi-infinite plates).

TABLE 4—THE TOUGHNESS OF REPUBLIC 9-4-20 (Cr, Mo) STEEL AS INFLUENCED BY SECTION SIZE, POSITION, AND ORIENTATION.
(Heat 3930785)

Section Thickness, in.	Orientation[a]	Position[b]	W/A[c] in.-lb/in.^{2}
0.550 plate	RW	surface	3150
	WR	surface	1900
1.00 plate	WR	surface	1750
2.25 plate	RW	surface	3540
	WT	surface	2973
	WR	surface	2949
	TR	surface	3035
	RW	center	3233
	WT	center	3263
	WR	center	3159
2.25 by 2.25 forged square billet	longitudinal	surface	3636
	transverse	surface	2480
	longitudinal	center	3255
	transverse	center	2724
4 by 4 forged square billet	longitudinal	surface	3574
	transverse	surface	2338
	longitudinal	center	3458
	transverse	center	2414

[a] Orientation symbol key:
First letter = specimen axis direction
Second letter = direction of crack propagation, where:
R = rolling direction
W = width direction
T = thickness direction
[b] Specimen notch location.
[c] W/A is the energy absorption per unit area of the fracturing surface (13).
NOTE: All specimens, except 0.550-in. thick plate, were oil-quenched as quasi-infinite plates or forgings.

[9] Experimental grade. The HP designation will be used when this grade becomes commercial.

The results, with the exception of the 1-in. plate, show an insensitivity to section size which is of obvious commercial importance. Furthermore, no consistently large variation with position or orientation is apparent.

The selection of the precracked Charpy was again predicated on cost and convenience. The material is too tough to be validly tested for K_{Ic} in section thicknesses of less than at least 0.875 in.[2] The length of slow bend single-edge-notched specimens, the most economical of material of the K_{Ic} specimens, would forbid testing in the short transverse direction. The precracked Charpy specimens, on the other hand, are inexpensive, easily prepared, and give information sufficient to suggest that the more rigorous procedures are, in any case, probably unnecessary.

Welding Studies:

In the manufacture of large structures such as missile cases, the weldability of a candidate material takes on an importance equal to that normally attached to strength and toughness. As the HP 9-4-25 steel alloy has been shown to provide an attractive base metal with K_{Ic} values of the order of 120 to 140 ksi-$\sqrt{\text{in.}}$ (3,7,20), work was initiated on the development of a filler metal-welding parameter system capable of producing high strength - high toughness welds with a minimum of pre- and post-heating (8). During the course of this study, some 125 experimental weldments were prepared at various section thicknesses (0.50 to 2.25 in. thick) and under varying degrees of restraint (unrestrained to "Navy Torture Test" conditions). Because of the large number of tests required, the toughness of the several metallurgical structures present in an as-welded plate, that is, base, heat-affected, and weld metal, was evaluated with standard Charpy and later. precracked Charpy specimens. When a near optimum was reached, weldments were prepared under conditions which seemed to approximate the conditions encountered in the shop fabrication of a large missile case. These results are given in Table 5.

TABLE 5—PLANE-STRAIN FRACTURE TOUGHNESS OF HP 9-4-25 1-IN. THICK WELDMENTS.[a]

Joint Design	Imposed Restraint	K_{Ic}, ksi $\sqrt{\text{in.}}$[b]	Ratio of Notch Strength to Yield Strength
Single U, flat back	none	119.3	1.4
Double U	none	116.8	1.4
Single U, V back	backup clamps	118.6	1.4

[a] The weldments were joined with the tungsten inert gas process (TIG). The filler-wire composition approximated that of the parent metal.

[b] Testing was done with slow bend single-edge-notched specimens, 0.875 by 0.875 by 4 in., with crack depths of 0.25 in. The crack was located in the center of the weld-metal deposit.

Since these tests were made to provide data as nearly applicable to design as the state of the art of testing allows, s ow bend single-edge-notched K_{Ic} specimens were selected to evaluate the weld toughness. Since the notch strength exceeded the yield strength by about 40 per cent, rigorous values were not obtained; however, it did appear that the value of 120 ksi$\sqrt{\text{in.}}$ obtained may be considered as conservative estimates of the actual toughness. This has since been confirmed under testing conditions in which valid K_{Ic} values of 130 ksi$\sqrt{\text{in.}}$ were obtained.[10]

[10] Private communication from D. Lovell, Boeing Aircraft Co.

This example serves again to emphasize the underlying philosophy of our research efforts. When rigor can be sacrificed to cost and expediency without loss of effect, qualitative tests are employed. When comparison with laboratories other than our own is required or where data which may be used in design are desired, standard and rigorous test procedures are applied.

SUMMARY AND CONCLUSIONS

The use of fracture toughness testing in an alloy research program at the Republic Steel Research Center was described. It was found that careful selection of a testing method may lead to valid comparisons on the basis of toughness without the considerable cost which may be involved in testing with absolute rigor using sophisticated plane-strain fracture toughness tests. The validity of this approach was demonstrated by the development of the HP 9-4-X alloy steels.

In general, it is suggested that for optimization programs in which internal comparisons are the prime objectives, less attention need be paid to rigor if such a situation is desirable for purely pragmatic reasons. On the other hand, where the resulting data are to be used in design criteria or for comparisons with other materials, selection of standard and rigorous tests is mandatory.

Acknowledgment:

The authors wish to express their appreciation to W. F. Brown, Jr., of the National Aeronautics and Space Administration for invaluable advice in preparing the manuscript. The authors also wish to express their appreciation to K. J. A. Kundig and S. W. Poole of the Research Center of the Republic Steel Corp. for their cooperation and assistance.

REFERENCES

(1) S. J. Matas, M. Hill, and H. P. Munger, "Current and Future Trends for Steels with High Strength and Toughness," *ASM Metals Engineering Quarterly*, Vol. 3, No. 3, August, 1963, p. 7.

(2) T. E. Perry, S. W. Poole, and S. J. Matas, "Development and Melting of an Ultrahigh Strength 9%Ni-4%Co Steel," *Electric Furnace Proceedings*, Vol. 20, 1962, p. 308.

(3) *Aerospace Materials Handbook*, Vol. 1, *Ferrous Alloys*, Syracuse University Press, Syracuse, N.Y., 1964.

(4) "Manufacturing Process Development for High Strength Steels", Republic Steel Corp., ASD Project No. 8-157, Contract AF 33(657)-1127, Interim Progress Report I, July, 1963–September, 1963.

(5) "Manufacturing Process Development for High Strength Steels," Republic Steel Corp., ASD Project No. 8-157, Contract AF 33(657)-1127, Interim Progress Report II, September, 1963–November, 1963.

(6) J. S. Pascover and S. J. Matas, "Some Relationships Between Structure and Properties in the 9Ni-4Co Alloy System," *Structure and Properties of Ultrahigh-Strength Steels*, *ASTM STP 370*, Am. Soc. Testing Mats., 1965.

(7) J. S. Pascover and S. J. Matas, "Properties of HP 9-4-X Alloy Steels," Fourth Maraging Steel Project Review Conference, WADC, Dayton, Ohio, 1964.

(8) G. D. Ries and S. W. Poole, "Welding of 9Ni-4Co Alloy Steels," Fourth Maraging Steel Project Review Conference, WADC, Dayton, Ohio, 1964.

(9) ASTM Special Committee on Fracture Toughness Testing of High-Strength Metallic Materials, "Fracture Testing of High-Strength Sheet Materials," *ASTM Bulletin*, No. 243, January, 1960, pp. 29–40; *ASTM Bulletin*, No. 243, February, 1960, pp. 18–28.

(10) ASTM Special Committee on Fracture Testing of High-Strength Metallic Materials, "Progress in Measuring Fracture Toughness and Using Fracture Mechanics," *Materials Research & Standards*, Vol. 4, No. 3, March, 1964, pp. 107–119.

(11) J. E. Srawley and W. F. Brown, Jr., "Fracture Toughness Testing," see p. 133.

(12) G. M. Orner and C. E. Hartbower, "Sheet

Fracture Toughness Evaluated by Charpy Impact and Slow Bend," *Welding Journal*, (Research Supplement), Vol. 40, September, 1961, p. 4055.
(13) G. M. Orner and C. E. Hartbower, "Precracked Charpy Fracture Toughness Correlations," presented at the symposium but not published.
(14) L. J. Klingler, W. J. Barnett, R. P. Frohmberg, and A. R. Troiano, "The Embrittlement of Alloy Steel at High Strength Levels," *Transactions*, Am. Soc. Metals, Vol. 46, 1954, p. 1557.
(15) B. J. Lement, B. L. Averbach, and M. Cohen, "Microstructural Changes on Tempering Iron-Carbon Alloys," *Transactions*, Am. Soc. Metals, Vol. 46, 1954, p. 851.
(16) G. B. Espey, M. H. Jones, and W. F. Brown, Jr., "The Sharp Edge Notch Tensile Strength of Several High Strength Steel Sheet Alloys," *Proceedings*, Am. Soc. Testing Mats., Vol. 59, 1959, p. 837.
(17) S. B. Espey, M. H. Jones, and W. F. Brown, Jr., "Effect of Carbon Content and Melting Practice on Room Temperature Sharp-Edge-Notch Tensile Characteristics of H-11 Modified and 300 M Sheet Steels," *Proceedings*, Am. Soc. Testing Mats., Vol. 60, 1960, p. 761.
(18) A. C. Haynes and W. Stevens, "The Temperature of Formation of Martensite and Bainite in Low-Alloy Steels; Some Effects of Chemical Composition," *Journal of the Iron and Steel Inst.*, Vol. 183, 1956, p. 349.
(19) J. M. Capus and G. Mayer, "The Mechanical Properties of Some Tempered Alloy Martensites," *Journal of the Iron and Steel Inst.*, Vol. 196, 1960, p. 149.
(20) S. J. Matas, "Influence of Impurities and Related Effects on Strength and Toughness of High-Strength Steels," *ASM Metals Engineering Quarterly*, Vol. 4, No. 2, May, 1964, p. 48.
(21) R. F. Hehemann, V. J. Luhan, and A. R. Troiano, "Influence of Bainite on Mechanical Properties," *Transactions*, Am. Soc. Metals, Vol. 49, 1957, p. 409.
(22) J. C. Shyne, V. F. Zackay, and D. J. Schmatz, "The Strength of Martensite Formed from Cold-Worked Austenite," *Transactions*, Am. Soc. Metals, Vol. 52, 1960, p. 346.
(23) R. A. Grange and J. B. Mitchell, "Strengthening Steels by Deforming Austenite," *ASM Metals Engineering Quarterly*, Vol. 1, 1961, p. 41.
(24) C. W. Marschall, "Hot-Cold Working of Steel to Improve Strength," *DMIC Report 192*, Battell Memorial Inst., Oct. 11, 1963.
(25) S. J. Matas, M. Hill, and H. P. Munger, "Ausforming and Hot-Cold Working—Methods and Properties," *Mechanical Working of Steel 1*, Metallurgical Soc. Conferences, Gordon and Breach, New York, N.Y., 1964, Vol. 21, p. 143.
(26) G. E. Pellissier, "Some Microstructural Aspects of Maraging (250) Steel in Relation to Strength and Toughness," Third Maraging Steel Review Conference, WADC Dayton, Ohio, 1963.

APPENDIX I

COST OF VARIOUS TYPES OF SPECIMENS

During the last several years over 10,000 test specimens have been prepared, tested, and evaluated. As a result of this program, information on the relative costs of the various tests was obtained and is tabulated in Table 6. Data are given on each aspect of the test procedure from initial material and rough-blank preparation to test evaluation in terms of the appropriate parameters.

The costs do not include estimates of professional personnel time spent in planning the initial work or interpreting the results. The values given are relative rather than dollar costs. In other words, a 2-in. wide center-notched specimen costs approximately twice that of a conventional Charpy. Accordingly, if past experience indicates that a single Charpy test cost XX dollars, a 2-in. wide-center notch will cost approximately 2(XX) dollars.

The figures given are subject to the following assumptions:

1. That sufficient specimens are prepared to permit efficient machining.
2. That the test procedure, regardless of how complex or painstaking, has become substantially routine.

TABLE 6—FRACTURE TOUGHNESS SPECIMENS AS EMPLOYED AT THE REPUBLIC STEEL RESEARCH CENTER.

Type of Specimen	Total Specimen Cost / Total Charpy Specimen Cost	Itemized Relative Costs: Rough	Heat Treatment	Finish	Test Preparation	Test	Evaluation	Total
0.252-in. round tension....	1.4	1.6	0.3	1.8	0.3	1.0	0.5	5.5
½-in. flat tension.........	2.5	2.0	0.4	2.0	0.3	1.0	0.5	9.8
Standard Charpy.........	1	0.8	0.3	0.8	0.6	1.0	0.5	4.0
Precracked Charpy.......	1.1	0.8	0.3	0.8	0.9	1.0	0.5	4.3
Center Fatigue Precracked Specimens								
2-in. wide.............	2.2	0.6	0.4	1.8	4.0	1.0	1.0	8.8
3-in. wide.............	2.3	0.8	0.4	2.0	4.0	1.0	1.0	9.2
4 in. wide.............	2.5	1.0	0.4	2.4	4.0	1.0	1.0	9.8
8-in. wide.............	5.2	4.0	0.8	6.0	6.0	3.0	1.0	20.8
12-in. wide............	7.7	6.0	0.8	10.0	8.0	5.0	1.0	30.8
Single-Edge-Notched Tension								
1½-in. wide...........	1.9	0.6	0.4	0.7	4.0	1.0	1.0	7.7
3-in. wide.............	2.2	0.8	0.4	1.8	4.0	1.0	1.0	9.0
4-in. wide.............	2.4	1.0	0.4	2.1	4.0	1.0	1.0	9.5
0.505-in. notched round..	3.1	1.6	0.4	2.4	6.0	1.0	1.0	12.4
Slow Bend Single-Edge-Notched								
½-in. square...........	1.5	0.8	0.4	0.8	2.0	1.0	1.0	6.0
⅞-in. square...........	1.8	1.6	0.4	1.2	2.0	1.0	1.0	7.2
Surface-cracked..........	1.8	0.6	0.4	1.0	3.0	1.0	1.0	7.0
Drop-Weight Tests								
3-in. Am. Gas Assn.....	1.1	2.0	0	0.2	1.0	1.0	0.3	4.5

TABLE 7—CHEMICAL COMPOSITIONS OF HP-9-4-X STEELS DISCUSSED IN THIS PAPER.

Type of Alloy	Heat No.	Melting Practice[a]	Size of Heat	Composition, Weight per cent							
				C	Mn	Si	Ni	Cr	Mo	V	Co
Republic 9-4-20 (Cr-Mo)	3930785	VAR-CDOX	10,000 lb	0.19	0.25	0.01	6.79	1.01	1.15	0.09	4.03
HP 9-4-45	3352127	Si-Al E.F.	70-ton	0.41	0.22	0.26	8.25	0.26	0.13	0.10	3.60
HP 9-4-45	3950855	Si-Al + VCEM	20,000 lb	0.42	0.09	0.28	8.10	0.23	0.15	0.10	3.65
HP 9-4-45	3950831	VAR-CDOX	20,000 lb	0.43	0.02	0.01	8.00	0.09	0.08	0.09	3.80
HP 9-4-45	3950701	VAR-CDOX	20,000 lb	0.40	0.11	0.01	8.84	0.32	0.32	0.08	3.82
HP 9-4-45	3720588	VAR-CDOX	10,000 lb	0.41	0.21	0.03	8.00	0.34	0.28	0.12	4.00
HP 9-4-25		Typical Composition		0.27	0.20	0.10 max	8.00	0.45	0.45	0.10	4.00
HP 9-4-45		Typical Composition		0.43	0.20	0.10 max	8.50	0.25	0.25	0.10	4.00
Republic 9-4-20 (Cr-Mo)		Typical Composition		0.21	0.30	0.10 max	7.25	1.00	1.00	0.10	4.00

[a] E.F. = Electric furnace (air-melted and silicon aluminum deoxidized); VCEM = vacuum consumable electrode-melted; VAR-CDOX = vacuum arc re-melt and carbon deoxidized.

DISCUSSION

J. E. CHARD.[1]—When Ray Decker and I were asked to prepare a paper on the role of fracture toughness testing in alloy development, we contacted a number of individuals in various research laboratories and they were most cooperative in replying to a questionnaire which we prepared. However, after putting this information together and drawing some general conclusions, we felt that the resultant summary did not justify presenting a technical paper but that the findings could be better presented as a short contribution to the discussion at the symposium.

In every case history of alloy development for which we obtained details, there was a realization from the beginning that some form of test was required to give an index of fracture toughness performance to supplement the conventional tension test data. However, there appeared to be an almost universal tendency to employ some relatively simple test at least during the earlier stages of development, the more sophisticated fracture toughness tests for determination of K_c value being employed only in the later stages. We feel that this is a very realistic approach from the point of view of keeping the expenditure in man-hours to a minimum.

In the initial stages of evaluating the potentials of a new and promising alloy system, comparatively simple tests provide sufficient discrimination to enable the best compositions to be selected for further work. To carry out K_c determinations at this stage would obviously be wasteful and unnecessary.

In the development of PH 14-8 Mo stainless steel, D. C. Perry of Armco Steel Corp. found the Allison instrumented bend test most useful until, as development progressed, the steel became so tough that this test was no longer definitive, at which stage a precracked sheet Charpy test was employed. Fatigue-cracked center-notched specimens for K_c determination were employed only in the later stages.

In the development of high-strength titanium alloys, E. F. Erbin of Titanium Metals Corporation of America used the NASA edge-notched specimen for screening and investigating variables and the fatigue-cracked center-notched specimen for K_c determinations.

In the development of improved low-alloy steels for heavy forgings, S. Yukawa of General Electric Co., found that the Charpy V-notch fracture appearance transition temperature was a useful index of effect of metallurgical parameters; at a later stage, slow bend tests having a fatigue-cracked or a nitrided notch were employed and, as a final stage, notched disk specimens were used for spin-bursting tests.

G. K. Bhat of Mellon Institute employed the fatigue-cracked center-notched sheet specimen and a round notched tension specimen at all stages in the development of MX-2 (a low-alloy cobalt modified 4135 ultrahigh-strength steel), and Rocoloy 270, (a low-alloy cobalt-silicon modified 4340 ultrahigh-strength steel). A biaxial cup test was

[1] Research Laboratory, International Nickel Co., Inc , Bayonne, N. J.

also employed for sheet. Small 3.5-in. diameter deep drawn (seamless) spin-closed pressure vessels, 18 in. long, were also used for study of crack growth at specified stress levels, crack tolerance, and biaxial stress enhancement. For investigating $\frac{1}{2}$- to $\frac{3}{4}$-in. thick plates, a three-point loaded notched slow bend test was found useful. The part-through-thickness surface-notched tension test was also used. Fatigue-cracked notches were employed throughout.

W. F. Brown, Jr., of NASA has found the machined, edge-notched specimen very satisfactory for studies involving the optimization of composition, and for the investigation of melting, processing, and heat-treatment variables.

At Inco, in the development of improved zerolled stainless sheet alloys by trace-element control, the machined, edge-notched sheet specimen was used throughout and proved a satisfactory means of evaluation. In the development of maraging steels, a round notched tension specimen (0.300 in. in major diameter, 0.212 in. in minor diameter, with a root radius of 0.0006 in.) was found to be a simple and effective test. There were considerable advantages in time-saving and economy in working with round bar stock in the early stages; and the ratio of notched to smooth tensile strength was found to be a useful index in evaluating the effect of compositional and processing variables. At a later stage, sheet was rolled from the more promising alloys and evaluated using the machined, edge-notched tension test. For the lower-strength compositions (below about 200-ksi yield strength) the standard Charpy V-notch impact test appears to be a satisfactory means of evaluation. The work of Puzak and Pellini has established that the Charpy V-notch impact energy is quite reliable in predicting edge drop-weight tear energy and explosive tear energy.

To sum up the situation as we see it, relatively simple and inexpensive test methods are adequate for indicating fracture toughness characteristics during the early stages of alloy development. For the final evaluation of sheet alloys, the fatigue-cracked center-notched sheet specimen is well established. However, some general agreement on the best way of measuring slow crack growth and on the relative merits of compliance gages and electrical resistance methods would be helpful. The situation for evaluation of heavier plate material is far less satisfactory at the present time. Much active development is proceeding on a variety of tests such as those utilizing notched plate tension specimens having a single notch on one edge only; notched slow bend tests; and the part-through-thickness surface-cracked plate specimens. However, there appears as yet to be no universal acceptance of any one of these tests and some question as to the relative merits of acoustical and electrical methods for following the progress of the crack. It is believed that the present symposium should serve a most useful purpose in clarifying this situation.

J. S. PASCOVER, M. HILL, AND S. J. MATAS (authors).—The authors wish to thank Mr. Chard for his interesting discussion to our paper. It is, of course, gratifying to see confirmation of our testing philosophy by so many independent organizations as was indicated in Mr. Chard's questionnaire.

STP381-EB/Apr. 1965

FRACTURE TESTING OF WELDMENTS

By J. A. Kies,[1] H. L. Smith,[1] H. E. Romine,[2] and H. Bernstein[3]

Synopsis

A new and improved apparatus has been designed and built for three-point loading of bend bars. A new formula for K_{Ic} independent of Young's modulus has been derived which fits experimental calibrations and calculations by B. Gross with satisfactory accuracy. A formula is provided by which the requirements for specimen size and notch depth can be calculated for measuring K_{Ic} for a given yield strength of material. A number of comparisons are shown for the effect of rolling direction on K_{Ic} for base plate and for several different kinds of welding. The effect of notch position on K_{Ic} is shown. The slow bend test has advantages of adaptability and simplicity for the purpose at hand.

It seems noteworthy that the effect of directionality on K_{Ic} in the base plate is in the same direction but magnified in tests of the welds in the 250-ksi yield-strength grade. For some welding procedures the K_{Ic} for some positions in welds was better than for the base plate with no deficiency of hardness. Significance tests were applied to the differences between average values of K_{Ic}. From the K_{Ic} numbers listed one may calculate the largest tolerable surface crack corresponding to a given stress applied. The center of the weld presents the lowest toughness of any position.

Techniques for measuring the fracture toughness of weldments are not unique or different from those for testing base plate except for simple considerations of adequate sampling and for studying metallurgical variables not present in the base plate. In this investigation, use of $\mathcal{G}_{Ic}$ (or K_{Ic}) toughness numbers was helpful because. from current evidence, these numbers do not vary significantly with specimen geometry. Thus the specimens could be efficiently planned from an expense viewpoint. The present paper contains a description of a bend-test procedure and neglects others only because our immediate concern is with steels for large solid propellant booster rockets in which the yield strength and the plate thicknesses are both high enough to make the use of bend tests convenient. A list of the detailed reasons for choosing the three-point loading bend test for the immediate purposes is given in the Appendix. For other applications, other tests might be preferred. In choosing a specimen for a given task in measuring fracture toughness, a few simple rules should be observed as follows:

(*a*) The plastic-zone size at critical load should be small compared with the

[1] Head, Ballistics Branch, and head, Fracture Studies Section, respectively, U.S. Naval Research Laboratory, Washington, D. C.

[2] Metallurgist, Warhead and Terminal Ballistics Lab., U.S. Naval Weapons Laboratory, Dahlgren, Va.

[3] Assistant head, Advanced Development Plans, Special Projects Office, Bureau of Weapons, Dept. of the Navy, Washington, D. C.

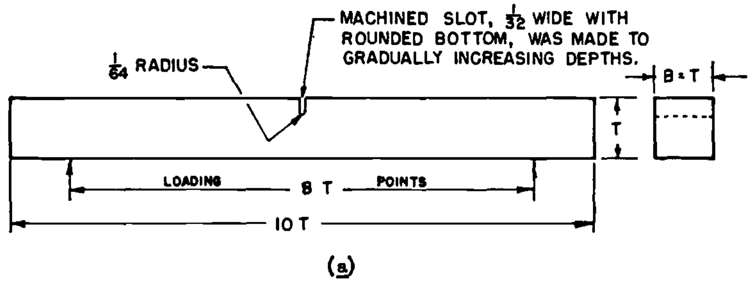

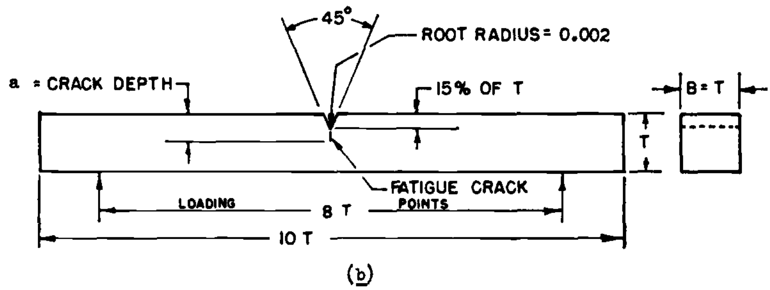

(*a*) Calibration bar for determining spring constants.
(*b*) Test bar for $\mathcal{G}_{Ic}$ values.
FIG. 1—Bend-Test Specimens.

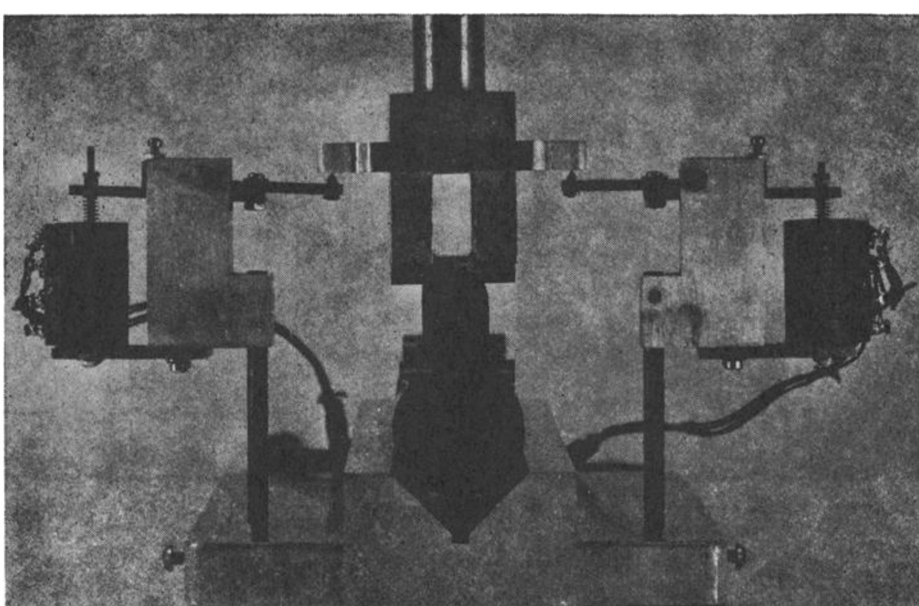

FIG. 2—Assembly of Bend-Test Specimen and Fixtures. The Transducers Were Adapted from a High-Magnification Averaging Compressometer. Opening Above Upper Loading Point Was Intended for Deflectometer Arm Formerly Used to Measure Displacement.

crack depth and with the unbroken ligament.

(*b*) The computed nominal stress disregarding stress-concentration factor should not exceed 1.1 times the nominal tensile yield strength.

THE BEND SPECIMEN AND TESTING FIXTURES

The bend specimen chosen for convenience in testing the plate is shown in Fig. 1. The testing fixturing was especially designed to provide self-align-

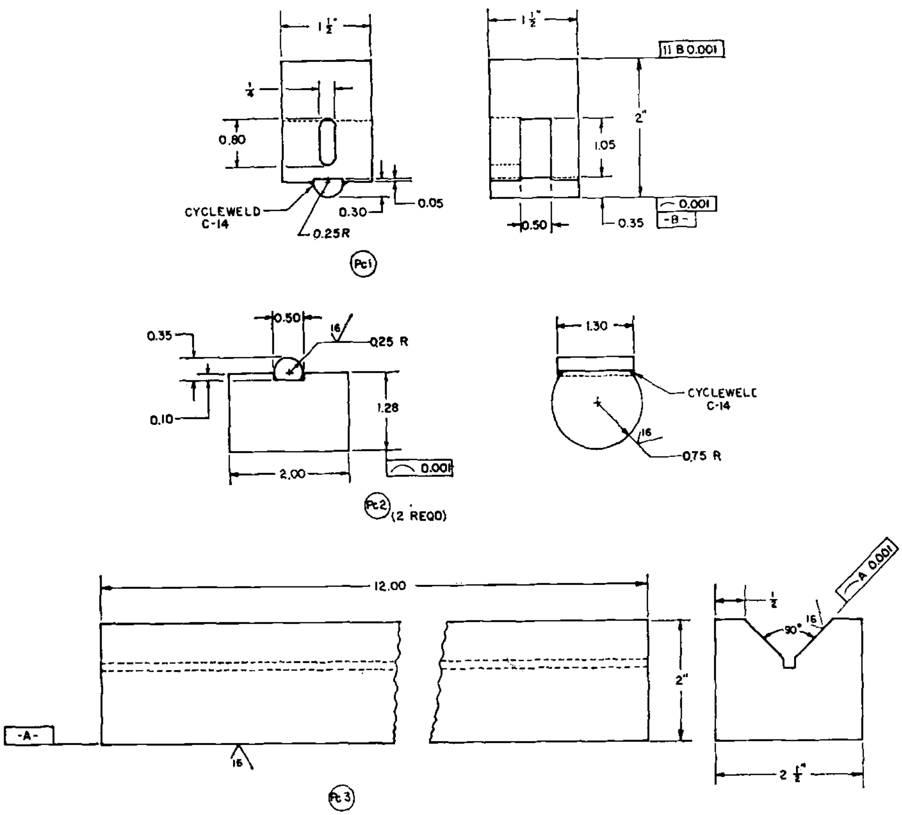

FIG. 3—Details of Parts for Bend-Test Apparatus. The Loading Bars Were 4340 Steel Hardened to 48 Rockwell C. The Other Parts Were Machined from Quenched and Tempered Alloy Steel with a Hardness of about 26 Rockwell C (STS Armor Steel). Loading Bars Were Cemented in Place with Cycleweld C-14 Adhesive (Chrysler Corp.) or Equivalent.

(*c*) The machined notch should be terminated or extended by a real crack, most conveniently a fatigue crack.

(*d*) Testing arrangements should provide reproducible load-deflection relations not disturbed by variable warpage in the specimen or insecure seating of the test fixture.

(*e*) A closed formula for *K* is highly desirable.

ment and security from tilting during load application. Figure 2 shows an assembly of specimen and fixture in the testing machine. Further details are provided by Romine.[4]

In order to satisfy testing condition

[4] H. E. Romine, "Plane Strain Fracture Toughness Measurements of Solid Booster Case Materials," *U.S. Naval Weapons Laboratory Report No. 1884*, Sept. 13, 1963.

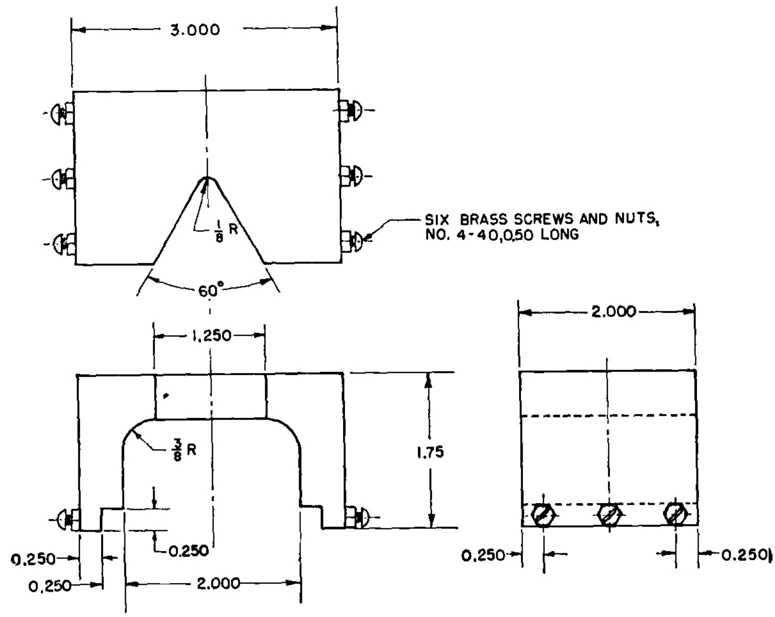

FIG. 4—Sliding Guides for Axially Centering the Test Bar. Material, 2024-T4 Aluminum Alloy.

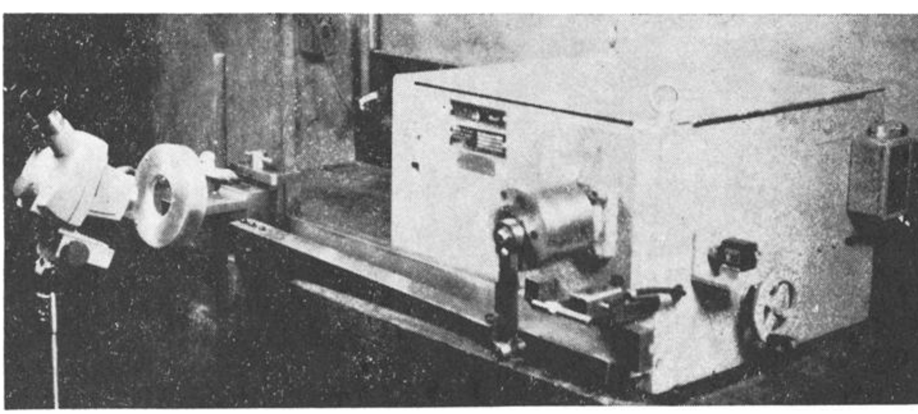

Plate fatigue machine adapted to introduce fatigue crack at root of machined notch in bend-test bars. Machine is stopped at intervals to inspect progress of fatigue crack. A zoom microscope and ring fluorescent light are shown in position to inspect front edge of crack. Microscope is racked in and a small first-surface mirror is held in position to inspect crack at back of notch.

FIG. 5—Fatigue Apparatus for Introducing a Crack at the Bottom of the Notch.

(*d*) above, a considerable effort was expended to provide a stable fixture easily lending itself to alignment and proper centering. Details of parts for the bend test apparatus are shown in Fig. 3 and sliding guides for axially centering the test bar are shown in Fig. 4.

Special attachments were made for use in fatiguing the notched bars so as to introduce a real crack. Figure 5 shows the fatigue apparatus and the test specimen. Figure 6 shows the construction of the special lever arm used for gripping the specimen.

FORMULAS AND CALIBRATION

In general, if we can measure loads and deflections with sufficient accuracy we can write for P, total load, and A, total crack area:

$$\mathcal{G} = \frac{P^2}{2}\frac{d(1/M)}{dA} \qquad \text{(1)}$$

where $1/M$ is the compliance such that the elastic deflection, δ, is P/M. Here we wish to consider bend bars of width, B, and depth, D. Then

$$\mathcal{G} = \frac{P^2}{2}\frac{d(1/M)}{B\,da} \qquad \text{(1a)}$$

where a is crack depth. If we choose to normalize with respect to plate thickness, we can write

$$\mathcal{G} = \frac{1}{2}\left(\frac{P}{B}\right)^2 \frac{d(B/M)}{da} \qquad \text{(1b)}$$

Mast[5] has postulated that for the Irwin $\mathcal{G}$ factors, $\mathcal{G}_p$ and $\mathcal{G}_m$ (strain-energy release rates), acting independently on a crack and due to tensile and bending loads, the total, $\mathcal{G}$, is

$$\mathcal{G} = \mathcal{G}_p + \mathcal{G}_m \qquad \text{(2)}$$

In this case the total K or stress-intensity factor is not obtained by stress analysis, but is given by:

$$K_I^2 = \frac{E}{(1-\nu^2)}(\mathcal{G}_{I_p} + \mathcal{G}_{I_m}) \qquad \text{(2a)}$$

for plane strain. From the experimental point of view, the derivatives of the compliance with respect to crack size would have to be independent for Eq 2 to be correct. In case these are not independent, then the total stress due to all loads would be obtained and the resulting total, K, or stress-intensity factor determined accordingly. There would be no point in determining K_p and K_m separately. If $\mathcal{G}_p$ and $\mathcal{G}_m$ are not independent, then K_p and K_m would have no usefulness as separate quantities.

In the present paper, $\mathcal{G}_p = 0$ for the bend bars and there is no ambiguity.

Mast[5] obtained approximate expressions for K_p and K_m for deep notches. His expression for K_m is:

$$K_m = \frac{2Pe}{B\pi^{1/2}l^{3/2}} \qquad \text{(3)}$$

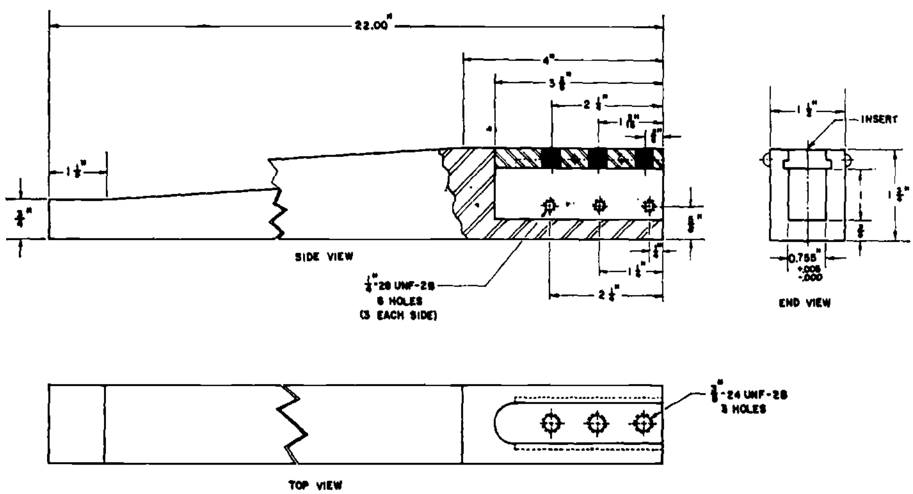

FIG. 6—Extension Bar for Fatigue Machine. Material, 4340 Steel.

[5] P. Mast, private communication.

where Pe is the bending moment, m, on the unbroken ligament

$$K_m = \frac{2m}{B\pi^{1/2}l^{3/2}}$$

and

$$\mathcal{G}_I = \frac{(1-\nu^2)}{E}\frac{4m^2}{B^2\pi l^3} \qquad (4)$$

where:

$$a + 2l = D$$
$$\alpha = 2l/D$$
$$da = -2\,dl$$
$$D\,d\alpha = -da$$

The second term within the bracket of Eq 6 assures that $\mathcal{G} = 0$ for $a = 0$ without changing the dimensions of the bracket. The choice of exponent 3 on l

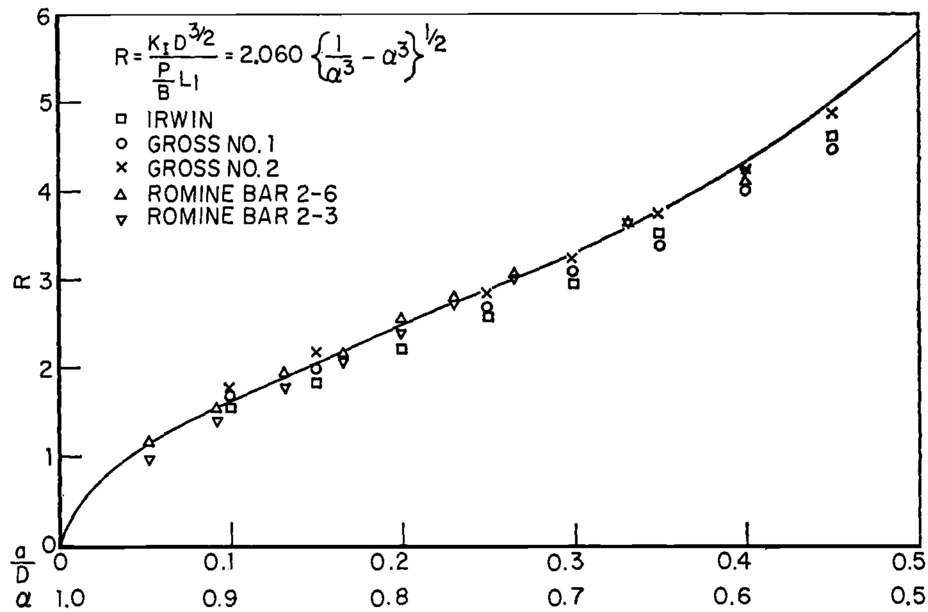

FIG. 7—Equation 10 Compared with Experimental Calibrations and Calculations.

For three-point loading as used in our experiments, $m = PL/4$ and

$$\mathcal{G}_I = \frac{1}{2}\left(\frac{P}{B}\right)^2 \frac{(1-\nu^2)L^2}{2E\pi l^3} \qquad (4a)$$

$$\frac{d(B/M)}{da} = \frac{(1-\nu^2)L^2}{2E\pi l^3} \qquad (5)$$

However, simple dimensional considerations permit us to adapt this to shallow as well as deep notches by rewriting Eq 5 as

$$\frac{d(B/M)}{da} = \frac{(1-\nu^2)L^2}{2\pi E}\left[\frac{1}{l^3} - \frac{l^3}{(D/2)^6}\right] \qquad (6)$$

was made to correspond with calibration data of Romine and calculations of B. Gross[6] except that for the Irwin calibration the second term, $[l/(D/2)^4]$, a first-power correction, provided a much better fit. D is the total beam depth. Equation 6 may be rewritten as Eq 7 with the insertion of a factor, S, needed to include the 1.2 Irwin factor for surface notches[7] and other effects.

[6] B. Gross, private communication.

[7] G. R. Irwin, "The Crack Extension Force for a Crack at a Free Surface Boundary," *NRL Report 5120*, U.S. Naval Research Laboratory, Apr. 15, 1959.

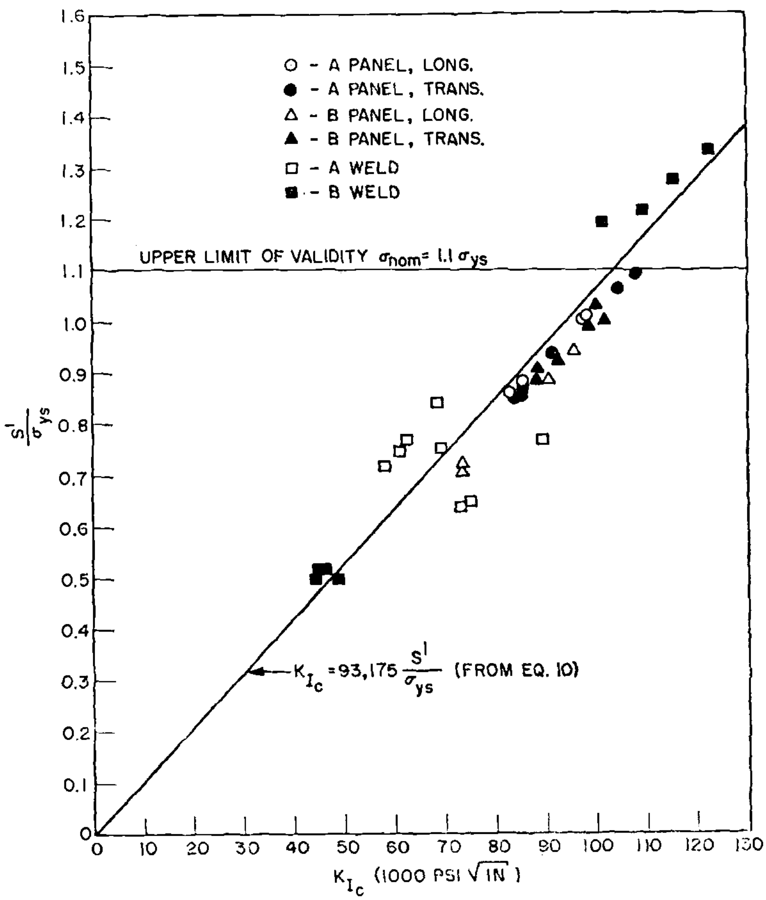

FIG. 8—Linearity Between K_{Ic} and Nominal Stress.

$$\frac{d(B/M)}{da} = \frac{4S(1-\nu^2)L^2}{\pi ED^3}\left[\frac{1}{\alpha^3} - \alpha^3\right] \quad (7)$$

and

$$\frac{B}{M} = \frac{2S(1-\nu^2)L^2}{\pi ED^2}\left[\frac{1}{\alpha^2} + \frac{\alpha^4}{2}\right] + \text{constant} \quad (8)$$

Then

$$\mathcal{G}_I = 2\left(\frac{P}{B}\right)^2 \frac{S(1-\nu^2)L^2}{\pi ED^3}\left[\frac{1}{\alpha} - \alpha^3\right] \quad (9)$$

Since

$$\mathcal{G}_I = \frac{1}{2}\left(\frac{P}{B}\right)^2 \frac{d(B/M)}{da},$$

then for $L = 2L_1$ and $S = 1.667$,

$$R = \frac{K_I D^{3/2}}{PL_1/B} = 2.060\left\{\frac{1}{\alpha^3} - \alpha^3\right\}^{1/2} \quad (10)$$

The selection of $S = 1.677$ was done for the purpose of fitting the Romine and other calibration data as shown in Fig. 7. This figure also shows that Eq 10 fits the values of R as calculated by Gross[6] well within experimental uncertainties in calibrations.[8] Equation 10 is the same for symmetrical four-point

[8] Good agreement between Eq 10 and a corrected version of a formula by Bueckner of General Electric Co. (see footnote 11) has also been reported in a private communication by Carl Hartbower, Aerojet-General Corp.

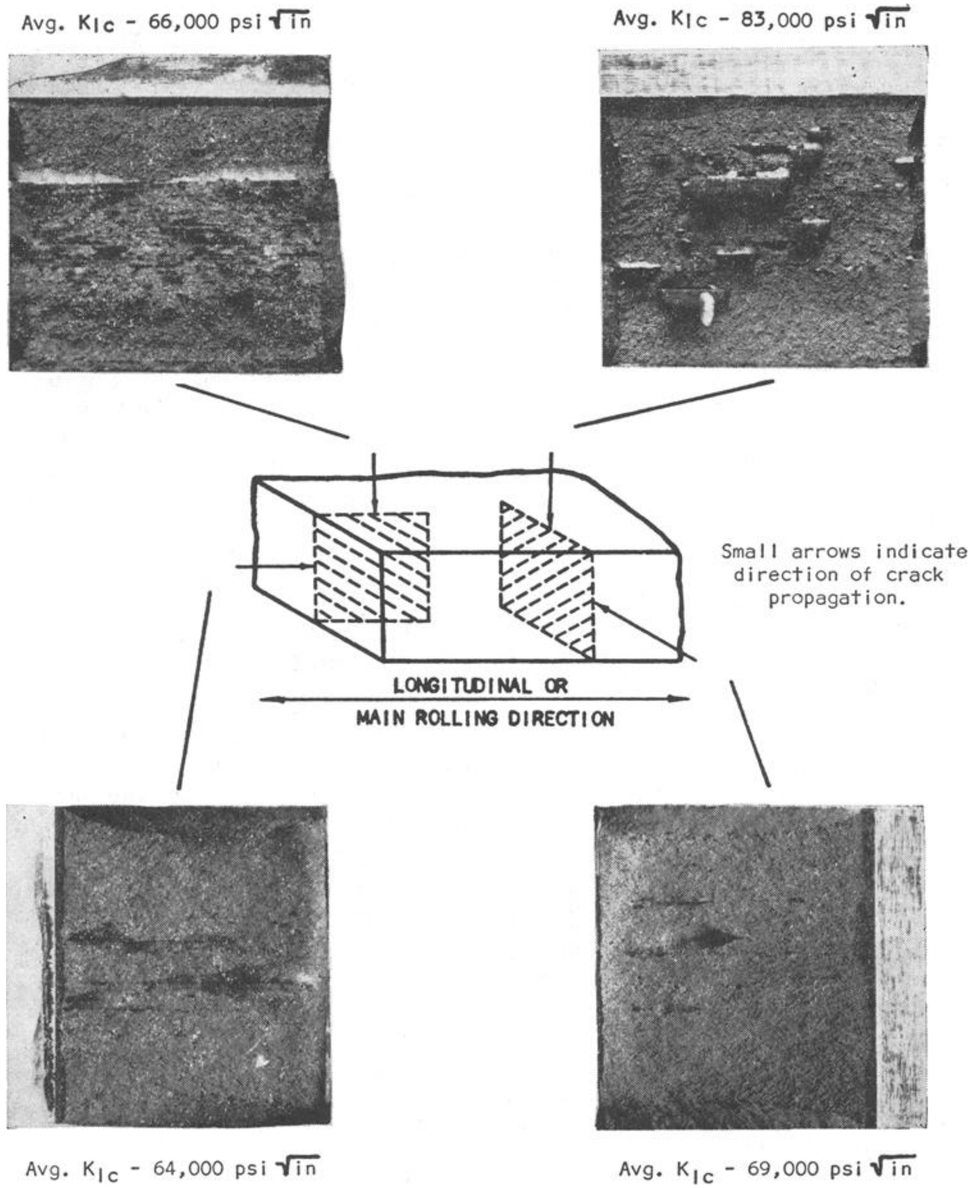

FIG. 9—Effect of Crack-Propagation Direction on Fracture Appearance and K_{Ic}, Source A.

bending except that L_1 then is the distance between outer and next inner load points. We have no experimental data at present for checking Eq 10 for four-point loading. In obtaining R experimental for the Romine calibration bars 2-3 and 2-6, the values of $E = 27 \times 10^6$ psi, $\nu = 0.25$, $D = 0.750$ in., and $L_1 = 3$ in. were used. For purposes of entering the Romine data on Fig. 7,

$$R = 0.824 \left[\frac{d(B/M)}{da} \right]^{1/2} \times 10^3,$$

where $d(B/M)/da$ was experimentally determined.

PLASTIC-ZONE LIMITATIONS

Thus far Eqs 9 and 10 for $\mathcal{G}_I$ and K_I do not include plastic-zone corrections. Introduction of this correction complicates the formula considerably and it is suggested that this is not necessary provided that the nominal fiber stress at the root of the notch is kept below 1.1 times the yield stress. The estimated plane-strain plastic-zone size, $2r_y$, when $\sigma_{nom} = 1.1\,\sigma_{YS}$ is about 0.04 in. Use of the plasticity correction would, at the extreme, increase K by about 10 per cent.

DEMONSTRATION OF LINEARITY BETWEEN K_{Ic} AND NOMINAL FIBER STRESS

A demonstration of the necessary linearity between K_{Ic} (for fixed span and approximately fixed notch dimensions) and nominal fiber stress may be seen in Fig. 8. These data points are for maraging steel bars from a heat different from that for the bulk of this report. Only specimens containing surface notches are shown. $\mathcal{G}_{Ic}$ values were computed using an equation based upon a compliance calibration. K_{Ic} values were then computed from the equation

$$K_{Ic}^2(1 - \nu^2) = E\mathcal{G}_{Ic} \quad \text{........(11)}$$

If one computes K_{Ic} using Eq 10 for these data points, the relationship between K_{Ic} and the load, P, is:

$$K_{Ic} = 27.95\,P \quad \text{...........(12)}$$

By converting the load to maximum fiber stress at the notch root, S', and dividing by the yield strength of the material, the expression for K_{Ic} becomes

$$K_{Ic} = 93{,}175 \left(\frac{S'}{\sigma_{YS}} \right) \quad \text{.......(13)}$$

The straight line through the origin representing this equation in Fig. 8 shows good agreement with Romine's results. Part of the scatter shown by the open squares may be expected on the basis of microstructural variability in welds; however, the rest of the data shows the required linearity. Variations in S'/σ_{YS} for a given K_{Ic} value reflect variations in notch depth. Variations larger than 10 ksi $\sqrt{\text{in.}}$ in the K_{Ic} reflect real changes in toughness. Within a fixed type of material (base metal, for example) the K_{Ic} toughness variations are believed to be due to delaminations. Romine's data for plate surface-notched specimens range in notch depth only from 0.10 to 0.14 in. Within this range, no special correlation of K_{Ic} with notch depth was observed.

LIMITATIONS ON SPECIMEN SIZE AND NOTCH DEPTH

In forecasting the required specimen size and notch depth, it is necessary to know in advance how high K_{Ic} will be.

Assuming that at the root of the notch the nominal fiber stress is

$$\sigma_{nom} = \frac{ml}{I} \quad \text{............ (14)}$$

$$\sigma_{nom} = 3\,\frac{PL_1}{B\alpha^2 D^2} \quad \text{.........(15)}$$

then

$$K_I = \sigma_{nom}(D)^{1/2} 0.687(\alpha - \alpha^7)^{1/2} \quad \text{...(16)}$$

If the upper limit of validity is for

$$\sigma_{nom} = 1.1\,\sigma_{SY}$$

$$K_{I\,lim} = 0.756\sigma_{YS}(D)^{1/2}\{\alpha - \alpha^7\}^{1/2} \quad \text{..(17)}$$

For the limiting case, $K_{Ic} = K_{Ic\,lim}$,

$$\Delta a_{lim} \cong \frac{K_{Ic\,lim}^2}{4(2)^{1/2}\sigma_{YS}^2}$$

or

TABLE 1—COMPARISON OF EDGE-NOTCHED TEAR TESTS WITH BEND TESTS.

Bar No.	K_{Ic}, from Compliance Bend Test, ksi $\sqrt{in.}$	K_{Ic}, Eq 10, ksi $\sqrt{in.}$	K_{Ic}, Single-Edge-Notched, ksi $\sqrt{in.}$	
2	79	81.2	82	Source B Steel
3	80	81.5	81	
Avg	79.5	81.3	81.5	

Bend Bar No.	⊥ or ∥	K_{Ic}, Eq 10, ksi $\sqrt{in.}$	Specimen No. Edge-Notch Tear	⊥ or ∥	K_{Ic}, ksi $\sqrt{in.}$
	Plate 1			Plate 2	
1-31-2	⊥	67.5	VII BA-2	⊥	73.0
1-31-3	⊥	67.2	VII BA-3	⊥	72.0
1-31-4	⊥	66.1	VII BA-4	⊥	69.0
1-31-5	⊥	68.8			
Avg		67.4			71.3
	Plate 2			Plate 1	
2-31-2	∥	68.8	VII AA-2	∥	72.0
2-31-3	∥	67.0	VII AA-3	∥	75.0
2-31-4	∥	68.5			
2-31-5	∥	68.3			
Avg		68.1			73.5

TABLE 2—COMPARISON OF EDGE-NOTCH TEAR TESTS AND BEND TESTS.
(U. S. Steel Corp. Tests)

K_{Ic}, 3-in. Wide Central Notch, ksi $\sqrt{in.}$	K_{Ic}, Single-Edge Notch, ksi $\sqrt{in.}$	K_{Ic}, Eq 10, ksi $\sqrt{in.}$	K_{Ic}, Bend Test by Bueckner Formula, ksi $\sqrt{in.}$
77.0	77.0	85.0	82.5
	79.8	83.8	82.5
	Avg 78.4	Avg 84.4	Avg 82.5

$$\Delta a_{\lim} = 0.101D(\alpha - \alpha^7) \qquad (18)$$

$f_2(\alpha) = (\alpha - \alpha^7)$ has a maximum at $a/D = 0.28$, or $\alpha = 0.72$. Thus the most favorable notch-depth ratio is about 0.28. However, the term $(\alpha - \alpha^7)$ changes by only 0.2 per cent in going from an a/D value of 0.25 to a value of 0.30. So within this range of notch-depth ratios, one may simply use the equation

$$K_I = 0.540\sigma_{nom}(D)^{1/2} \qquad (19)$$

Comparison of Plane-Strain Fracture Toughness by the Slow Bend Test and by the Single-Edge-Notched Test

Tests were made on 18 per cent nickel (250,000-psi strength level) maraging steel plates from $\frac{3}{4}$-in. thick, air-melted stock. The bend tests were made with three-point loading using $\frac{3}{4}$ by $\frac{3}{4}$ by 7.5 in. specimens while the single-edge-notched specimens were 3 by 12 by 0.75

TABLE 3—ANALYSIS OF TEST MATERIALS.
(¾-Thick Plate, 18 Per Cent Nickel Maraging Steel)

A. MATERIALS COMPOSITIONS

Element	Composition, Plates, Weight %	
	Heat X14636	Heat X53013
C	0.03	0.02
Mn	0.06	0.02
P	0 005	0.006
S	0.010	0.009
Si	0.10	0.04
Ni	18.37	17.59
Mo	4.70	4.80
Co	8.49	8.06
Ti	0.42	0.49
Al	0.13	0.07
Cu	...	0.12

B. MECHANICAL PROPERTIES OF THE PLATES

Aged Properties, 915 F for 4 hr	Heat X14636	Heat X53013
Hardness, R_c	50 to 53	50 to 53
0.2 per cent offset yield	263 ksi ‖	258 ksi ‖
	248 ksi ⊥	268 ksi ⊥
Ultimate tensile strength	272 ksi ‖	265 ksi ‖
	259 ksi ⊥	275 ksi ⊥
Elongation in 2 in., per cent	4.0 ‖	4.7 ‖
	4.6 ⊥	4.0 ⊥
Reduction area, per cent	30 ‖	35 ‖
	33 ⊥	27 ⊥
Annealed, 1550 F for 1 hr:		
Hardness, R_c	32.8	32.3

C. WELD ROD COMPOSITION

C	0.02%	Mo	4.62%
Si	0.02%	Al	0.09%
Mn	0.03%	Ti	0.45%
S	0.005%	H_2	1.5 ppm
P	0.004%	O_2	14.0 ppm
Ni	18.24%	N_2	25.0 ppm
Co	7.90%		

NOTE—Identical weld rod composition for TIG, MIG, and short arc welding. Weld rod drawn to different diameters.

D. CORRESPONDENCE BETWEEN PLATE AND HEAT NUMBERS, WELD METHOD, AND ROLLING DIRECTION

NRL Plate No.	Weld Method	Plate No. (U. S. Steel Co.)	Heat No. (U. S. Steel Co.)	Rolling Direction Orientation	
				Weld Bead	Bar Length
1	TIG	42298	X14636	⊥	‖
2	TIG	42298	X14636	‖	⊥
5	MIG	42298	X14636	⊥	‖
6	MIG	156872	X53013	‖	⊥
11	short arc	156872	X53013	⊥	‖

in. in size, loaded in tension with pinholes at the $W/2$ position. Results are given in Table 1.[9] The material used in this comparison was previously received from an outside source different from the one for which the bulk of the data are presented in this paper.

Earlier work by the U.S. Steel Corp.[10] on 0.16-in. thick 18 per cent nickel maraging steel of the 280,000-psi yield strength level gave the results shown in Table 2. The single-edge-notched specimens were loaded in tension with the pinholes at $w/3$ position. $K_{Ic} = E\mathcal{G}_{Ic}/(1 - \nu^2)$ where $E = 27 \times 10^6$ psi and $\nu = 0.3$. The bend-test values shown here are based on analytical results obtained by B. M. Wundt from work by Bueckner.[11]

TABLE 4—NRL PLATES 1 AND 2.
(K_{Ic} Values for Base Plate, Eq 10, and Visual Notch Depth, a, Used.)

Plate 1, Bars ⊥ to Rolling Direction, Base Plate			Plate 2, Bars ‖ to Rolling Direction, Base Plate		
Bar No.	a, in.	K_{Ic}, ksi $\sqrt{\text{in.}}$	Bar No.	a, in.	K_{Ic}, ksi $\sqrt{\text{in.}}$
1-1	0.16	83.7	2-1	0.06	87.2
1-2	0.15	78.1	2-2	0.05	79.2
1-3	0.14	79.7	2-3	calib.	
1-4	0.12	74.1	2-4	0.07	79.5
1-5	0.14	93.1	2-5	0.05	9.15
1-6	0.15	69.5	2-6	calib.	
1-7	0.15	80.1	2-7	0.06	84.7
1-8	0.14	76.2	2-8	0.05	82.2
1-9	0.13	74.2	2-9	ultrasonic test	
1-10	0.14	73.1	2-10	0.05	87.3
1-11	0.13	77.0	2-11	0.07	88.0
1-12	0.15	79.6	2-12	0.05	84.9
1-13	0.13	72.6	2-13	calib.	
1-14	0.14	75.8	2-14	0.07	81.5
1-15 }	calib.		2-15	0.08	88.5
1-16 }			2-16	0.07	89.5
1-17	0.15	75.3	2-17	0.07	84.8
1-18	0.14	75.5	2-18	0.08	79.8
1-19	0.14	82.2	edge fracture		
1-20	0.14	76.9	2-20	0.20	85.0
1-21	0.13	77.9	2-21	0.16	84.9
1-22	0.14	76.1	2-22	0.17	86.3
1-23	calib.		2-23	0.15	88.0
1-24	calib.		2-24	0.15	82.2
1-25	0.13	73.3	2-25	0.07	80.7
1-26	0.15	71.9	2-26	calib.	
1-27	0.14	79.9	2-27	0.05	75.4
1-28	0.13	76.2	2-28	0.14	87.2
1-29	0.13	75.7	2-29	0.05	81.1
1-30	0.13	73.5	2-30	0.07	84.7
Avg		77.0	Avg		84.3

[9] H. E. Romine, "Plane Strain Fracture Toughness by the Slow Bend Test and Through-Thickness Tensile Properties of Unwelded 18 Ni (250) Maraging Steel Plate ¾-inch Thick being Studied for Use in Large Solid-Propellant," NWL Report, to be published.

[10] U.S. Steel Corp. letter of Feb. 11, 1963, to J. M. Krafft.

[11] D. H. Winne and B. M. Wundt, "Application of the Griffith-Irwin Theory of Crack Propagation to the Bursting Behavior of Disks Including Analytical and Experimental Studies," *ASME Paper No. 58A-249*, presented December, 1957.

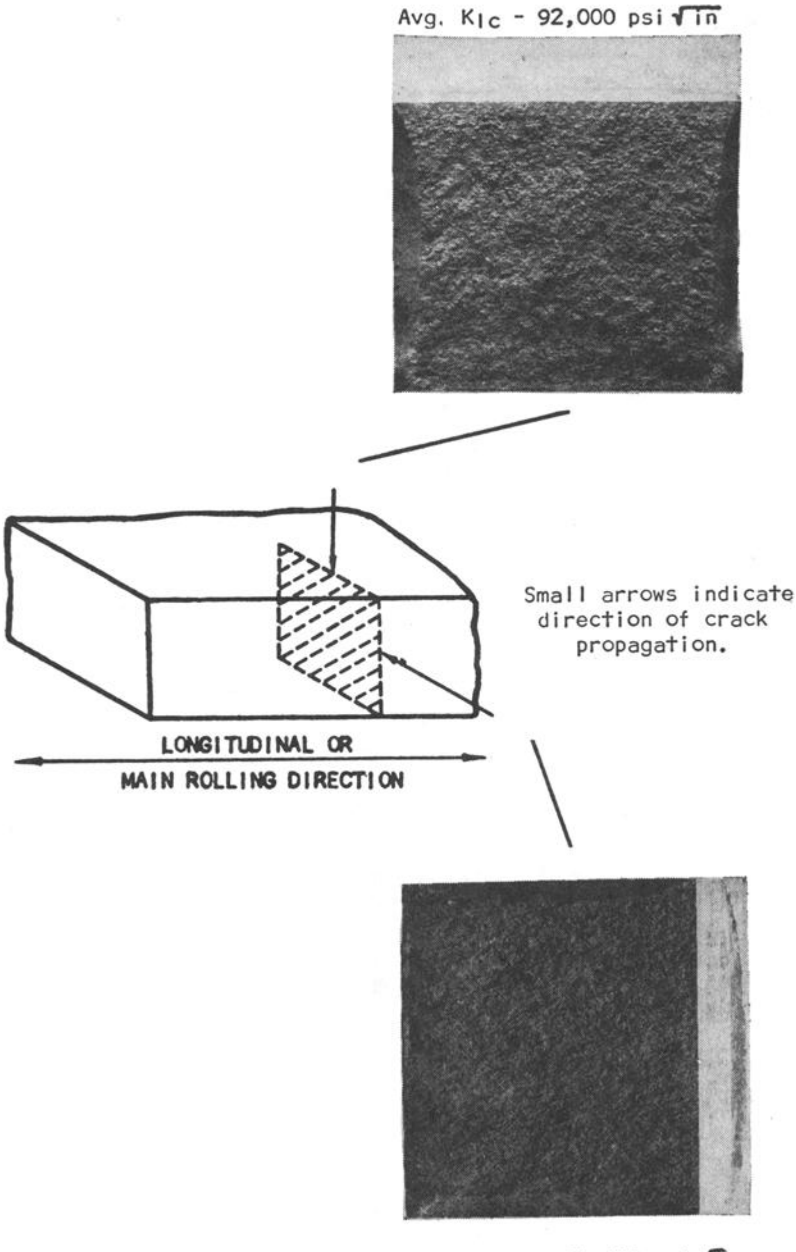

FIG. 10—Effect of Crack-Propagation Direction on Fracture Appearance and K_{Ic}, Source B.

It is tentatively concluded from Tables 1 and 2 that K_{Ic} obtained in bend tests using Eq 10 gives good agreement with single-edged pop-in tests. Further testing is in progress.

MATERIAL AND K_{Ic} TEST RESULTS FOR $\frac{3}{4}$-IN. THICK PLATE OF 18 PER CENT NICKEL MARAGING STEEL SHOWN IN TABLES 3 THROUGH 13

Compositions and heat numbers are shown in Table 3 for materials tested and results shown in Tables 4 to 13, inclusive.

Table 4 shows K_{Ic} values obtained on base plate using bars cut perpendicular to and parallel with the rolling direction. Conditions are three-point bending. K_{Ic} is computed from Eq 10 and visual notch depth.

It is noteworthy that all of the tests in Table 4 were made with the notch on the plate surface so as to simulate expected cracking in rocket cases. This direction is conducive to crack arrest by delamination or diversion of fracture path. The dependence of K_{Ic} on direction of crack propagation has been previously investigated by Romine.[9] Average K_{Ic} for plate surface notches was reported as 83 ksi $\sqrt{\text{in.}}$ versus 69 ksi $\sqrt{\text{in.}}$ for edge-wise propagation in base bars cut in the rolling direction in the earlier tests. For bars cut transverse to the rolling direction, the effect was in the same direction but less pronounced; average K_{Ic} values were 66 and 64 ksi $\sqrt{\text{in.}}$, respectively, for the same plate.

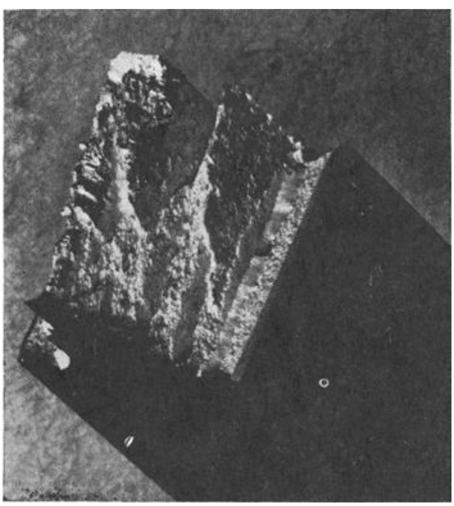

FIG. 11—Appearance of Crack Propagation Through the Thickness and Across the Rolling Direction in NRL Plate 2.

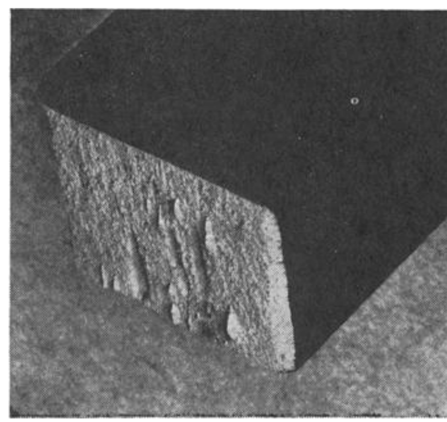

FIG. 12—Appearance of Crack Propagation from an Edge Notch Propagating Across the Rolling Direction in NRL Plate 2.

Typical fracture appearances for bend bars in which the notches are on the plate surface and plate edge are shown in Figs. 9 and 10 for plates from two different sources not represented in Tables 4–13. It is clear that the orientation of the notch has an influence on the toughness of the base plates. Similar differences according to crack-propagation direction are illustrated for NRL plate 2 in Figs. 11 and 12.

TUNGSTEN INERT GAS WELDS

Tungsten inert gas welding was investigated. The typical sequence of passes is indicated by an etched cross

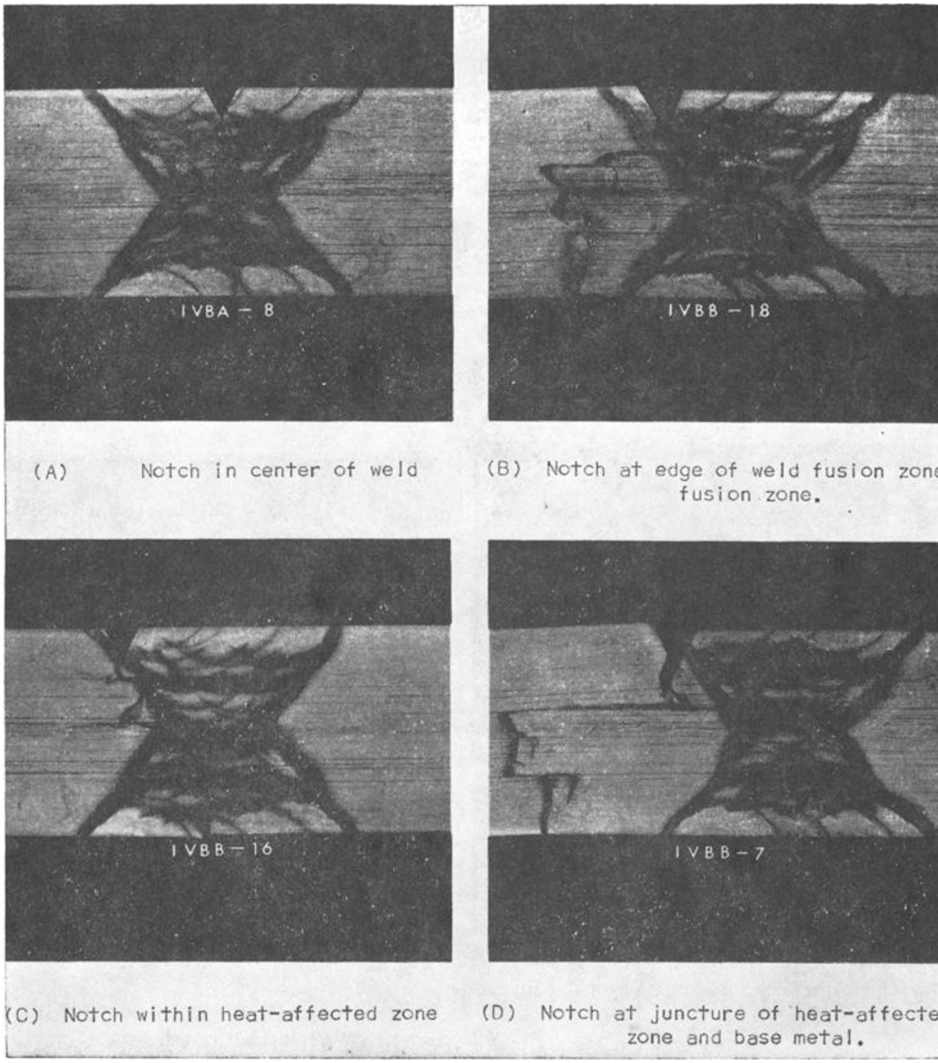

FIG. 13—Etched Bars Showing TIG Lay-Up and Position of Notches in NRL Plate 6.

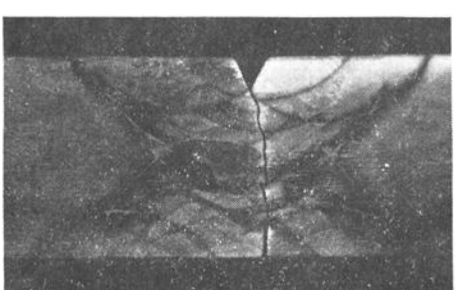

FIG. 14—Etched Bar Showing MIG Lay-Up and Position of Notch in NRL Plate 2.

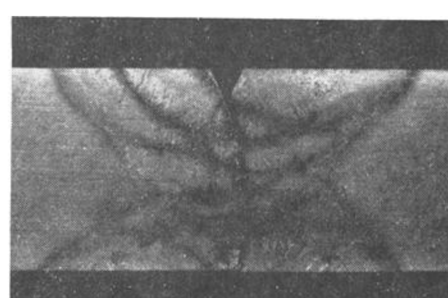

FIG. 15—Etched Bar Showing Short Arc Weld Lay-Up and Position of Notch in NRL Plate 11.

TABLE 5—K_{Ic} NUMBERS FOR NOTCHES IN THE CENTER OF TIG WELDS.
(Welds are run transverse to the bars.)

Plate 2, Bar Lengths ⊥ to Rolling Direction			Plate 1, Bar Lengths ∥ to Rolling Direction		
Bar No.	Visual a, in.	K_{Ic}, ksi $\sqrt{in.}$	Bar No.	Visual a, in.	K_{Ic}, ksi $\sqrt{in.}$
IV BA-1	0.17	66.9	IV AA-1	0.15	88.8
2	0.13	57.2	2	0.13	80.1
3	0.16	70.6	3	0.16	87.5
4	0.15	61.0	4	0.15	91.2
5	0.17	68.7	5	0.16	103.1
6	0.18	57.8	6	0.14	93.3
7	0.14	60.3	7	0.20	113.8[a]
8	0.15	67.6	8	0.15	90.3
9	0.14	79.5	9	0.16	69.8
10	0.14	68.0	10	0.15	74.5
11	0.16	77.0	11	0.15	60.3[a]
12	0.15	82.4	12	0.15	85.7
13	0.18	80.2	13	0.15	74.2
14	0.14	59.4	14	0.15	80.9
15	0.16	81.0	15	0.15	75.9
16	0.15	75.3	16	0.16	64.1
17	0.16	68.2	17	0.18	91.0
18	0.16	72.3			
Avg.		69.6	Avg.		83.8
c.v.[b]		0.12	c.v.		0.15

[a] The large difference between K_{Ic} for bars IV AA-7 and IV AA-11 was attributable to microstructure. Bar 7 was fine-grained and Bar 11 coarse-grained at the root of the starting crack. This will receive more detailed study by metallography.
[b] Coefficient of variation.

TABLE 6—K_{Ic} FOR THE FUSION ZONE TIG WELDS.

Plate 2, Bar Lengths ⊥ to Rolling Direction			Plate 1, Bar Lengths ∥ to Rolling Direction		
Bar No.	Visual a, in.	K_{Ic}, ksi $\sqrt{in.}$	Bar No.	Visual a, in.	K_{Ic}, ksi $\sqrt{in.}$
IV BD-4	0.15	77.3	IV AD-1	calibration bars	
5	0.15	87.0	2	calibration bars	
6	0.15	76.2	3	calibration bars	
7	0.19	82.3	4	0.19	106.7
8	0.15	89.6	5	0.16	97.3
9	0.15	81.7	6	0.17	100.8
IV BB-18	0.17	80.5	7	0.19	109.3
			8	0.15	90.0
			9	0.16	103.9
			10	0.16	92.0
Avg.		82.1	Avg.		100.0
c.v.[a]		0.06	c.v.		0.07

[a] Coefficient of variation.

section shown in Fig. 13. K_{Ic} values for plates TIG welded are given in Tables 5 to 8. The orientation of the bars perpendicular and parallel with the rolling direction is indicated. The weld beads were transverse to the bars and the position of the notch is coded as follows:

C.W. = center of the weld
F.Z. = fusion zone where base plate is melted

H.A.Z. = heat-affected zone in the base plate
D.B. = dark band just outside H.A.Z.

The typical TIG weld lay-up and the positions of the notches are shown in verify the position of the bottom of the fatigue crack below the notch. Although some uncertainty remained, the position code was assigned in accordance with the etched appearance, not always the

TABLE 7—K_{Ic} FOR THE HEAT-AFFECTED ZONE TIG WELDS (H.A.Z.).

Plate 2, Bar Lengths ⊥ to Rolling Direction			Plate 1, Bar Lengths ‖ to Rolling Direction		
Bar No.	Visual a, in.	K_{Ic}, ksi $\sqrt{in.}$	Bar No.	Visual a, in.	K_{Ic}, ksi $\sqrt{in.}$
IV BB-8	0.18	87.6	IV AB-9	0.14	101.9
9	0.18	66.8	10	0.14	88.6
10	0.17	71.1	11	0.14	82.3
11	0.15	59.5	12	0.14	82.3
12	0.19	73.2	13	0.15	104.0
13	0.14	90.0	14	0.14	102.7
14	0.19	60.7	17	0.16	103.1
15	0.15	76.3	18	0.16	91.6
16	0.15	85.8			
17	0.17	75.9			
Avg		74.7	Avg		94.6
c.v.[a]		0.14	c.v.		0.10

[a] Coefficient of variation.

TABLE 8—K_{Ic} FOR THE DARK BAND AT THE JUNCTION OF BASE PLATE AND HEAT-AFFECTED ZONE TIG WELDS (D.B.).

Plate 2, Bar Lengths ⊥ to Rolling Direction			Plate 1, Bar Lengths ‖ to Rolling Direction		
Bar No.	Visual a, in.	K_{Ic}, ksi $\sqrt{in.}$	Bar No.	Visual a, in.	K_{Ic}, ksi $\sqrt{in.}$
IV BB-1	0.15	62.3	IV AB-1	0.15	90.3
2	0.17	62.0	2	0.13	99.8
3	0.16	59.8	3	0.17	117.0
4	0.16	63.5	4	0.13	82.6
5	0.15	76.5	5	0.14	97.9
6	0.13	72.1	6	0.13	106.4
7	0.16	71.8	7	0.16	83.0
			8	0.15	102.2
			19	0.14	95.1
			20	0.15	91.9
Avg		66.9	Avg		96.6
c.v.[a]		0.09	c.v.		0.10

[a] Coefficient of variation.

Fig. 13. The weld bead lay-ups for MIG and short arc welds are shown on etched bend bars in Figs. 14 and 15, respectively.

The K_{Ic} results for the fusion zone or edge of the fusion zone in TIG welds are shown in Table 6. Each specimen was etched on the sides prior to testing to same as the original intended position. The code letters assigned were in accordance with Fig. 16. The notch-position assignments were the best that could be done on this basis and within the authors' ability to distinguish etched structures with the usual visual aids.

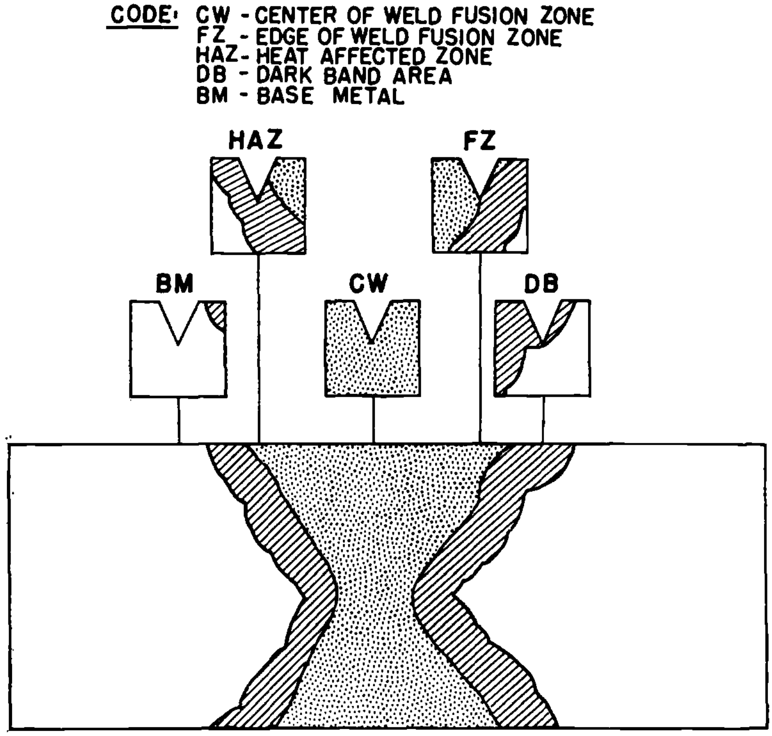

FIG. 16—Cross Section of Weld Area Showing Different Locations of Starting Notch Tipped with Fatigue Crack.

TABLE 9—K_{Ic} FOR MIG WELDS NOTCHED IN THE CENTER OF THE WELD (C.W.).

NRL Plate 6, Bar Lengths ⊥ to Rolling Direction			NRL Plate 5, Bar Lengths ∥ to Rolling Direction		
Bar No.	Visual a, in.	K_{Ic}, ksi $\sqrt{in.}$	Bar No.	Visual a, in.	K_{Ic}, ksi $\sqrt{in.}$
II BA-1	0.15	70.2	II AA-1	0.14	72.0
2	0.15	74.1	4	0.13	71.8
3	0.15	62.6	6	0.13	70.7
4	0.20	54.4	7	0.14	64.4
5	0.14	70.5	8	0.13	85.9
6	0.15	63.2	10	0.12	71.4
7	0.14	70.6	11	0.12	75.8
8	0.14	71.8	13	0.15	80.1
9	0.15	67.0	15	0.14	60.4
10	0.13	87.3	16	0.13	71.4
11	0.14	74.1	17	0.13	102.7
12	0.13	86.9	18	0.14	105.7
13	0.15	84.4			
14	0.14	83.0			
15	0.15	81.8			
16	0.14	78.8			
17	0.13	85.3			
18	0.14	74.3			
19	0.13	71.4			
Avg.		74.3	Avg.		77.7
c.v.[a]		0.12			

[a] Coefficient of variation.

TABLE 10—TOUGHNESS IN THE HEAT-AFFECTED ZONE MIG WELDS (H.A.Z.).

NRL Plate 6, Bar Lengths ⊥ to Rolling Direction			NRL Plate 5, Bar Lengths ∥ with Rolling Direction		
Bar No.	Visual a, in.	K_{Ic}, ksi $\sqrt{\text{in.}}$	Bar No.	Visual a, in.	K_{Ic}, ksi $\sqrt{\text{in.}}$
II BB-2	0.13	90.8	II AB-1	0.15	85.0
3	0.15	91.8	3	0.12	87.4
4	0.14	93.2	4	0.13	92.6
5	0.13	89.8	6	0.11	105.1
6	0.13	102.3	7	0.13	105.7
7	0.14	93.4	8	0.15	78.4
			9	0.16	81.6
			10	0.16	86.7
			11	0.14	99.0
Avg		93.6	Avg		91.3
c.v.[a]		0.10	c.v.		0.10

[a] Coefficient of variation.

TABLE 11—SHORT ARC WELD TOUGHNESS DATA FOR CENTER OF THE WELD (C.W)

Plate 7, Bar Lengths ⊥ to Rolling Direction			Plate 11, Bar Lengths ∥ with Rolling Direction		
Bar No.	Visual a, in.	K_{Ic}, ksi $\sqrt{\text{in.}}$	Bar No.	Visual a, in.	K_{Ic}, ksi $\sqrt{\text{in.}}$
V BA-1	0.150	3.5	V AA-1	0.15	64.1
2	0.120	75.4	2	0.14	75.9
3	0.155	60.0	3	0.14	73.3
4	0.140	48.0	4	0.14	72.8
5	0.155	53.5	5	0.15	68.6
6	0.160	52.6	6	0.14	61.5
7	0.145	69.0	7	0.13	67.4
8	0.150	59.0	8	0.14	65.2
9	0.155	51.5	9	0.13	89.1
10	0.160	56.5	10	0.14	79.3
			11	0.14	69.7
			12	0.14	74.7
			13	0.12	71.4
			14	0.15	72.4
			15	0.17	77.8
			16	0.13	75.9
			17	0.14	75.8
			18	0.12	79.1
			19	0.14	69.4
Avg		56.9	Avg		72.8
c.v.[a]		0.16	c.v.		0.09

[a] Coefficient of variation.

In order to get valid K_{Ic} numbers, say for F.Z. or H.A.Z., it is not necessary for the propagation to proceed more than a very small distance in the specified structure. The load at *initiation* of the fracture is hopefully the only load recorded. The pop-in must produce an offset of at least $\frac{1}{16}$ in. on the record which corresponds to 0.0004-in. deflection of the specimen. This corresponds to an increment in crack depth of 0.004 in. The records indicate that the load at pop-in is never appreciably different from that after this amount of pop-in.

The center-of-weld toughness was found to be less than that at any other position.

The microstructural details existing

TABLE 12—K_{Ic} TEST RESULTS FOR NOTCHES TERMINATING IN THE HEAT-AFFECTED ZONE, SHORT ARC WELDS.

Plate 7, Bar Lengths ⊥ to Rolling Direction			Plate 11, Bar Lengths ‖ with Rolling Direction		
Bar No.	Visual a, in.	K_{Ic}, ksi $\sqrt{in.}$	Bar No.	Visual a, in.	K_{Ic}, ksi $\sqrt{in.}$
V BB-2	0.120	92.5	V AB-1	0.12	113.3
4	0.130	96.5	2	0.13	96.4
5	0.140	89.5	3	0.11	103.2
7	0.140	85.5	4	0.12	111.3
8	0.130	86.5	5	0.14	101.1
			6	0.14	101.1
			7	0.14	120.4
			8	0.14	116.2
			9	0.14	116.9
			10	0.14	98.1
			11	0.15	109.9
			12	0.15	98.7
			13	0.14	102.4
			14	0.14	113.4
			15	0.14	106.8
			16	0.12	115.6
			17	0.13	104.5
			18	0.15	92.6
Avg		90.1	Avg		106.8
c.v.[a]		0.04	c.v.		0.07

[a] Coefficient of variation.

TABLE 13—SUMMARY OF K_{Ic} AVERAGE VALUES AND THEIR COEFFICIENTS OF VARIATION.

Table No.	Orientation of Bar with Rolling Direction	Kind of Weld	Location of Notch	K_{Ic} Average, ksi $\sqrt{in.}$	Coefficient of Variation	Heat No.
4	⊥	base plate	...	76.96	0.060	X14636
4	‖	base plate	...	84.33	0.041	X14636
5	⊥	TIG	C.W.	69.63	0.116	X14636
5	‖	TIG	C.W.	83.79	0.152	X14636
6	⊥	TIG	F.Z.	82.08	0.057	X14636
6	‖	TIG	F.Z.	100.00	0.068	X14636
7	⊥	TIG	H.A.Z.	74.69	0.139	X14636
7	‖	TIG	H.A.Z.	94.56	0.098	X14636
8	⊥	TIG	D.B.	66.86	0.089	X14636
8	‖	TIG	D.B.	96.62	0.104	X14636
9	⊥	MIG	C.W.	74.30	0.117	X53013
9	‖	MIG	C.W.	77.69	0.054	X14636
10	⊥	MIG	H.A.Z.	93.55	0.101	X53013
10	‖	MIG	H.A.Z.	91.28	0.104	X14636
11	‖	short arc	C.W.	72.81	0.088	X53013
12	‖	short arc	H.A.Z.	106.77	0.074	X53013

TABLE 14—$P(t)^a$ VALUES FOR STUDENT'S t TEST OF THE SIGNIFICANCE BETWEEN MEAN K_{Ic} VALUES.

			Base Plate		TIG Welds								MIG Welds				Short Arc Welds			
			⊥	∥	⊥				∥				⊥		∥		⊥		∥	
					C.W.	F.Z.	H.A.Z.	D.B.	C.W.	F.Z.	H.A.Z.	D.B.	C.W.	H.A.Z.	C. W.	H.A.Z.	C.W.	H.A.Z.	C.W.	H.A.Z.
Base Plate	⊥		. . .	<0.01 H.S.	<0.01 H.S.	0.015 H.S.	>0.03 N.S.	<0.01 H.S.	. . .	. . .	. . .	. . .	0.21 Po.S.	>0.01 H.S.	. . .	. . .	<0.01 H.S.	<0.01 H.S.	. . .	. . .
	∥				. . .	. . .	. . .	. . .	>0.03 N.S.	<0.01 H.S.	<0.01 H.S.	>0.01 H.S.	. . .	. . .	>0.01 N.S.	0.04 S.	. . .	. . .	<0.01 H.S.	<0.01 H.S.
TIG Welds	⊥	C.W.				<0.01 H.S.	0.178 Po.S.	>0.3 N.S.	<0.01 H.S.	. . .	. . .	. . .	0.093 Pr.S.	<0.01 H.S.	. . .	. . .	<0.01 H.S.	<0.01 H.S.	. . .	. . .
		F.Z.					0.123 Pr.S.	<0.01 H.S.	. . .	<0.01 H.S.	. . .	. . .	0.05 S.	<0.01 H.S.	. . .	. . .	<0.01 H.S.	0.014 H.S.	. . .	. . .
		H.A.Z.						0.107 Pr.S.	. . .	. . .	<0.01 H.S.	. . .	>0.3 N.S.	<0.01 H.S.	. . .	. . .	<0.01 H.S.	<0.01 H.S.	. . .	. . .
		D.B.							. . .	. . .	<0.01 H.S.	. . .	0.059 S.	<0.01 H.S.	. . .	. . .	0.032 S.	<0.01 H.S.	. . .	. . .
	∥	C.W.								<0.01 H.S.	0.07 S.	0.016 H.S.	. . .	. . .	0.262 N.S.	0.157 Po.S.	. . .	. . .	<0.01 H.S.	<0.01 H.S.
		F.Z.									>0.3 N.S.	>0.3 N.S.	. . .	. . .	<0.01 H.S.	0.074 S.	. . .	. . .	<0.01 H.S.	0.073 S.
		H.A.Z.										>0.3 N.S.	. . .	. . .	0.015 H.S.	>0.3 N.S.	. . .	. . .	<0.01 H.S.	<0.01 H.S.
		D.B.											. . .	. . .	<0.01 H.S.	0.28 N.S.	. . .	. . .	<0.01 H.S.	0.026 S.

										<0.01 H.S.	>0.3 N.S.	. . .	<0.01 H.S.	<0.01 H.S.	. . .	. . .	C.W.	⊥	MIG Welds
											. . .	>0.3 N.S.	<0.01 H.S.	0.24 Po.S.	. . .	. . .	H.A.Z.		
												0.03 S.	. . .	. . .	0.22 Po.S.	<0.01 H.S.	C.W.	∥	
													. . .	. . .	<0.01 H.S.	<0.01 H.S.	H.A.Z.		
														<0.01	<0.01	. . .	C.W.	⊥	Short Arc Welds
															. . .	<0.01 H.S.	H.A.Z.		
																<0.01 H.S.	C.W.	∥	
																. . .	H.A.Z.		

[a] $P(t)$ is the probability of a random variation in average K_{Ic} which would equal or exceed the difference shown between two average values of K_{Ic}.

NOTE:

H.S. = Highly Significant, $P(t)$ <0.024.
S. = Significant, $P(t)$ 0.025 to 0.074.
Pr.S. = Probably Significant, $P(t)$ 0.075 to 0.14.
Po.S. = Possibly Significant, $P(t)$ 0.15 to 0.25.
N.S. = Not Significant, $P(t)$ >0.26.

at the tips of the cracks were not investigated. This will be the subject of a future investigation aimed at offering guidance for future materials improvement.

The K_{Ic} test results for the heat-affected zone (H.A.Z.) are shown in Table 7 for TIG welds.

The K_{Ic} test results for dark band at the junction of the base plate and heat-affected zone are given in Table 8 for TIG welds.

TABLE 15—NRL CHEMICAL ANALYSES, CENTER OF WELD.

Element	Rod	Center of Weld		
		Short Arc	MIG	TIG
Carbon	0.02	0.02	0.02	0.02
Manganese	0.03	0.03	0.03	0.03
Phosphorus	0.004	0.002	0.003	0.004
Sulfur	0.005	0.005	0.005	0.005
Silicon	0.02	0.03	0.04	0.02
Nickel	18.24	18.2	18.0	18.0
Molybdenum	4.62	4.60	4.60	4.60
Cobalt	7.90	7.79	8.28	7.67
Titanium	0.45	0.43	0.43	0.43
Aluminum	0.09	0.09	0.10	0.11

METAL INERT GAS WELDS

A photograph of the etched cross section of a typical MIG weld is shown as Fig. 14. Toughness numbers for such welds notched in the center of the weld are given in Table 9.

K_{Ic} results for notches terminating in the heat-affected zone of MIG welds are shown in Table 10.

K_{Ic} test results for notches terminating in the center of the weld and heat-affected zones for short arc welds are shown in Tables 11 and 12, respectively.

SUMMARY OF THE TEST RESULTS

The average K_{Ic} values and their coefficients of variation are shown for the different weld methods, bar orientations, and notch positions in Table 13. The coefficients of variation are of about the same magnitude usually reported by other authors and for other test procedures. On this basis the bend-test method is not appreciably better or worse than other tests such as the edge-notched tear test. The significances of the differences between average K_{Ic} values are shown in Table 14. The levels of significance are assigned on the basis of the probability function of t in the usual t test. $P(T)$ is the probability that in another set of tests the average values being compared would overlap because of scatter in the results. Qualitative terms used in Table 14 are as follows for designating the differences between averages:

H.S. = highly significant, $P(t) < 0.024$

S. = significant, $P(t)$ 0.025 to 0.074

Pr.S. = probably significant, $P(t)$ 0.075 to 0.14

Po.S. = possibly significant, $P(t)$ 0.15 to 0.25

N.S. = not significant, $P(t) > 0.26$

CONCLUSIONS

1. K_{Ic} values from the bend tests agreed well with those from edge-notched tear tests.

2. A new K_{Ic} closed formula for bend tests was obtained which is independent of Young's modulus of elasticity.

3. There were highly significant effects of rolling direction on K_{Ic} for both heats of the 250 grade steel.

4. For TIG welds in bars cut parallel with the rolling direction, the average K_{Ic} values were higher by highly significant amounts than for bars cut perpendicular to the rolling direction. This was true for all four notch positions in the weld. The margins of superiority were magnified over that in the base plate. We have no explanation.

5. For MIG welds, no comparison was available between directions perpendicular and parallel with the rolling direction.

6. For short arc welds, the greatest average K_{Ic} was found in the heat-affected zone. For the 250-ksi yield strength steel, the directionality effect in the base plate was reflected in the welds.

7. Where a comparison was available, the TIG welds were more consistent and generally better than for the other types of welds investigated.

8. Where marked superiority of K_{Ic} for shallow (versus deeper) notches in base plate was found, this could be explained on the basis of finer grain size and fewer carbide precipitates.

9. Where wide differences in K_{Ic} were found between different bars but in the center of the weld at equal depths, the difference correlated with microstructure. Coarse-grained weld deposits with dendrites aligned mainly along the fracture path showed less toughness than fine dendrites randomly oriented.

Conclusions 8 and 9 are tentative and will be given additional study.

Acknowledgments:

The authors are greatly indebted to the following:

R. G. Hayes and A. S. Jennings of the U.S. Naval Weapons Laboratory and W. E. Anderson of the Naval Research Laboratory, for mechanical testing.

F. Stonesifer and Karl McKinney of the Naval Research Laboratory, for calculations.

W. Cohen and N. Mayer of NASA Headquarters, for the financial support of this research and testing program.

APPENDIX

FAILURE ANALYSIS EXAMPLE—WELD FLAW

Figure 17 shows an enlarged view of a fracture origin in a 156-in. diameter test chamber made of H-11 steel. The prior crack was heat-colored and presumably occurred during welding. It was situated at the edge of a longitudinal weld in the cylindrical section. At hydrotest failure (early in 1964), the hoop stress was 77,000 psi. The prior crack was not a very perfect semi-ellipse and the bottom of the prior crack was poorly delineated. The following data and conclusions illustrate a rather typical situation. Many similar hydrotest failures were encountered in the Polaris steel motor case development program.

Flaw depth, $a = 0.130 + 0.020$ in.

Plate thickness $t = B = 0.38$ in.

$2c = L$ = prior crack length at the surface = 0.500 in.

$a/2c = 0.260$

σ_{YS} = uniaxial yield strength = 203,000 psi

$\sigma_{\text{hoop}}/\sigma_{YS} = 0.378$

$$Q = [\Phi^2 - 0.212\ (\sigma/\sigma_{YS})^2] = 1.45$$

by the Tiffany chart

$$K_{Ic}^2 = [3.77\ (77000)^2\ (0.13)]/1.45$$

$$K_{Ic} \cong 45 \text{ ksi } \sqrt{\text{in.}}$$

This is the indicated value of K_{Ic} if instability or pop-in occurred at $a = 0.130$. This low value is not uncommon in and near welds in H-11 steel of this thickness.

There is no proof that instability really occurred at $a = 0.130$. It is conceivable that some slow growth extended the crack deeper. If the slow extension had carried the crack all the way through the thickness, the length of the crack would have been $2a_c \cong 1.0$ in. as judged from the photograph. Uncertainty in this number seems to be ± 15 per cent and is quite subjective. The fracture still contains almost no shear lip so that K_{Ic} is still the determining toughness for possible arrest. For the through crack:

$$K_I^2 = \frac{\pi \sigma^2 a_c}{1 - 0.5\left(\dfrac{\sigma}{\sigma_{YS}}\right)^2}$$

$$K_{Ic} \cong 100 \text{ ksi (in.)}^{1/2}$$

This is higher than we have reason to believe is characteristic of the material.

Conclusions:

1. Instability and hydrotest failure were completely determined before the surface crack had penetrated through the thickness.
2. The K_c for H-11 could not tolerate a $2t$ or $2B$ crack even at 77,000 psi hoop stress for $t = B = 0.38$ in.
3. The crack depth at instability seems to have been at the initial black-walled prior crack border, but this is not a matter of absolute certainty and depends on subjective judgment of the fracture appearance.
4. We did not have adequate data to predict the K_{Ic} or a_{crit} for such a crack. A considerable uncertainty in a_{crit} exists.
5. The important thing here is that the crack should have been detected and repaired. Failure prevention is better than failure analysis.

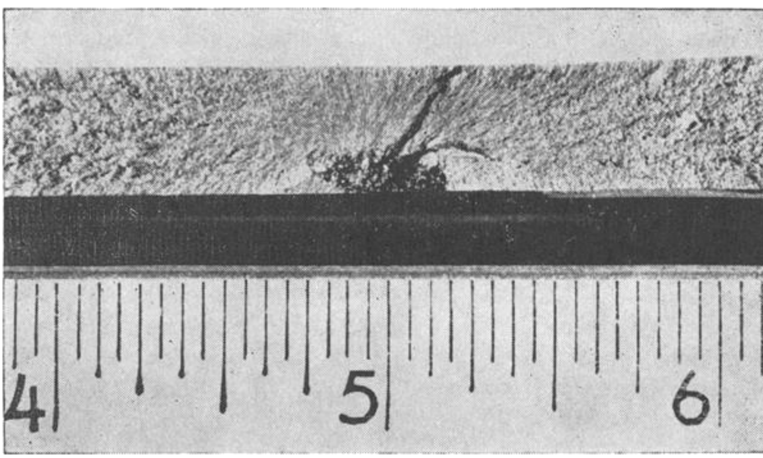

FIG. 17—Enlarged View of a Fracture Origin in a 156-In. Diameter Test Chamber Made of H-11 Steel.

Choice of Specimen Type (Three-Point Bend Test):

There are favorable points as well as objectionable points to each type of specimen which one might choose to use in making plane-strain fracture toughness measurements. The application in mind will generally dictate one's choice. For the work reported here, it was necessary to evaluate plates with a nominal thickness of $\frac{3}{4}$ in., since the application was the 260-in. solid booster motor case. Further, the material to be evaluated was the 18 per cent nickel maraging steel which has been subject to a certain amount of banding. It was also desirable to study cracks propagating in the thickness direction (short transverse) as the more likely concern from a practical application standpoint.

Because of the reasons listed here, our choice of specimen was narrowed to either the partially through surface crack in tension or the notch bend test. It was decided that different areas of the weld could be better discriminated using the flat bottom notch of a bend bar rather than the curved perimeter of an elliptical surface notch. It would require from three to four times as much material for a surface notch specimen as that required for a bend specimen.

Three-point loading rather than four-point loading was selected largely because of convenience. The deflections for a given load are larger in three-point loading, requiring less magnification of strain measurements. Further, one bend test setup is sufficient to test a wide range of specimen sizes in three-point loading.

Use of K Values Computed from an Equation:

Difficulties not previously experienced were found in this investigation, such as austenite segregation and carbide precipitates which result in varying amounts of banding throughout each plate. These variations result in an indeterminate modulus, E. One could avoid this difficulty by notching bend bars in the thickness direction. However, the resulting direction of crack propagation might be unrealistic in relation to the type of failure expected in an actual motor case.

If one measures the compliance, C, of a bend bar as a function of notch depth, the ratio of load to deflection, at the point of interest, determines the effective notch depth for use in calculating $\mathcal{G}$. However, one must know E in order to relate load to crack size. If E is indeterminate, the relation of load to crack size is indeterminate. For this reason, it was found convenient to represent EC as a function of relative crack depth in equation form and to use this representation and a visual determination of critical notch depth. The resulting K values may scatter and be somewhat altered due to delaminations, but such a procedure establishes a K value for each test which represents a relationship between load and notch depth independent of modulus. Such values are believed to be more useful than the $\mathcal{G}$ values.

DISCUSSION

CARL E. HARTBOWER[1] AND LEOPOLD ALBERTIN[1]—Results obtained from Eq 10 for computing the plane-strain stress-intensity factor from slow bend tests have been compared with results obtained from equations derived by H. Bueckner and G. Irwin using computer programs at Aerojet-General Corp.

Equation 10 is:

$$K_{Ic}\frac{D^{3/2}}{PL/B} = 2.060\left[\frac{1}{\alpha^3} - \alpha^3\right]^{1/2} \ldots (20)$$

where $\alpha = 1 - a/D$, D = depth of beam, P = load, L = span/2, B = width of beam, and a = notch plus crack depth.

Dr. Irwin's equation[2] is:

$$\mathcal{G}_{Ic} = \tfrac{1}{2}(P/B)^2\, d(B/M)/da \ldots\ldots (21)$$

where P/B is the bending load at fracture (or pop-in) per unit width of bar, and $d(B/M)/da$ is the slope of the experimental curve for reciprocal of the spring constant at notch depth, a, as determined from calibration data.

Dr. Bueckner's equation[3] is:

$$\mathcal{G}_{Ic} = \frac{(1 - \nu^2)}{E} F_n{}^2 h f(a/D) \ldots\ldots (22)$$

where $F_n = 3PL/Bh^2$, ν = Poisson's ratio (0.32), E = Young's modulus (27×10^6), h = depth below the notch, and $f(a/D) = 0.0126 + 1.9762\,(a/D) -$

[1] Research engineering specialist and metallurgical engineer, respectively, Aerojet-General Corp., Solid Rocket Operations, Sacramento, Calif.

[2] G. R. Irwin, J. A. Kies, and H. L. Smith, "Fracture Strengths Relative to Onset and Arrest of Crack Propagation," *Proceedings* Am. Soc. Testing Mats, Vol. 58, 1958, p. 646.

[3] B. M. Wundt, "A Unified Interpretation of Room Temperature Strength of Notched Specimens as Influenced by Their Size," *ASME Paper 59 MET 9*, 1959.

TABLE 16—COMPARISON OF SLOW BEND FRACTURE TOUGHNESS TESTS OF 18 PER CENT NICKEL MARAGING STEEL PLATE, REPORTED BY ROMINE, (TABLE 3)[a] USING THE SPRING-CONSTANT AND BUECKNER METHODS.

Bar No.	Notch Location	Direction Relative to Rolling	Measured Fatigue Crack Depth, in.	Effective Crack Depth, in.	P/B Unit Load To Fracture, lb/in.	Romine, $\mathcal{G}_{Ic}$, in.-lb/in.^{2}	Bueckner, $\mathcal{G}_{Ic}$, in.-lb/in.^{2}
A-1	parallel to plate surface at top center of weld	across weld	0.12	0.12	4514	173	157
A-3			0.10	0.08	5247	127	162
A-7			0.10	0.08	5486	138	176
A-9			0.10	0.08	5624	145	105
						Av. 146	Av. 170
A-11	parallel to plate surface at top edge of weld	across weld	0.10	0.02	6198	211	227
A-12			0.11	0.02	7326	295	361
A-13			0.12	0.11	5326	170	218
A-14			0.10	0.02	6039	201	213
						Av. 219	Av. 255
A-2	perpendicular to surface at side center of weld	across weld	0.14	0.13	3653	125	135
A-4			0.14	0.12	3775	123	143
A-8			0.15	0.13	3379	108	129
A-10			0.13	0.12	3508	106	109
						Av. 116	Av. 129
B-1	parallel to plate surface at top center of weld	across weld	0.10	0.06	3533	75	98
B-3			0.11	0.07	3312	77	100
B-7			0.10	0.06	3396	69	90
B-9			0.10	0.06	3776	86	112
						Av. 77	Av. 100
B-11	parallel to plate surface at top edge of weld	across weld	0.10	0.07	7621	(378)[b]	(453)
B-12			0.11	0.10	7320	(549)	(485)
B-13			0.10	0.08	7420	(440)	(433)
B-14			0.11	0.09	7362	(488)	(486)
						Av. (464)	Av. (464)
B-2	perpendicular to plate surface at side center of weld	across weld	0.13	0.09	3217	104	123
B-4			0.12	0.08	3312	99	114
B-8			0.12	0.10	3270	119	112
B-10			0.13	0.12	3073	122	110
						Av. 111	Av. 115

[a] H. E. Romine, "Plane-Strain Fracture Toughness Measurements of Solid Booster Case Materials," *Naval Weapons Lab. (Dahlgren) Report No. 1884*, Sept. 13, 1963.

[b] Values in parentheses are uncertain because net-section fiber stress exceeded yield strength.

2.1713 $(a/D)^2$. The equation for $f(a/D)$ was obtained by a least-squares computer program using corrected coordinates (private communication from H. Bueckner dated Mar. 2, 1964).

In using Eq 21, the usual experimental procedure is to establish a calibration curve for each heat of material investigated. Dr. Romine, in his study of vacuum-arc remelted grade-250 18 per cent nickel maraging steel, established calibration curves, not only for each heat but also for each weld, and notch and specimen orientation. Unfortunately, in order to obtain reliable spring constants, calibration involves several preliminary tests made under exacting conditions. Therefore, as the authors have pointed out, there is a real advantage in equations such as 20 and 22 which do not require calibration experiments.

heat treatment *B*, where the results of Bueckner's equation generally were more conservative than those obtained from the spring constant. One of the advantages of the spring-constant method is

TABLE 17—COMPARISON OF SLOW BEND FRACTURE TOUGHNESS TESTS OF 18 PER CENT NICKEL MARAGING STEEL PLATE, 200 GRADE MATERIAL, HEAT 3960524, APPLYING BUECKNER AND KIES EQUATIONS.

Aging Cycle		Specimen Orientation	Width, b, in.	Depth, d, in.	Proportional Limit Load, lb	Measured Crack Depth, in.	$\mathcal{G}_{Ic}$ (Kies et al), Fracture Toughness, in.-lb/in.^{2}	$\mathcal{G}_{Ic}$ (Bueckner), Fracture Toughness, in.-lb/in.^{2}
deg F	hrs							
900	4	longitudinal	0.600	0.750	10 200	0.232	590	605
			0.600	0.750	9 000	0.271	607	638
			0.599	0.751	8 700	0.270	562	590
			0.600	0.750	8 200	0.301	626	666
							Av. 596	Av. 625
900	4	transverse	0.600	0.751	11 500	0.171	472	457
			0.600	0.750	9 450	0.228	492	502
			0.600	0.750	10 400	0.270	511	513
			0.600	0.752	10 600	0.207	525	526
							Av. 500	Av. 499
900	16	longitudinal	0.599	0.751	10 100	0.228	560	572
			0.599	0.750	8 700	0.275	586	617
			0.600	0.751	10 700	0.222	600	610
			0.601	0.751	10 500	0.216	551	558
							Av. 574	Av. 589
900	24	longitudinal	0.600	0.750	8 900	0.246	497	514
			0.600	0.750	9 800	0.236	560	576
			0.599	0.751	10 450	0.213	538	543
			0.600	0.750	10 450	0.206	512	514
							Av. 527	Av. 537
900	24	transverse	0.600	0.750	9 200	0.240	508	524
			0.600	0.750	10 450	0.215	547	553
			0.599	0.750	10 800	0.199	521	519
			0.600	0.750	9 900	0.211	477	480
							Av. 514	Av. 519

The data presented in Table 16 are from Romine, together with recalculated values of $\mathcal{G}_{Ic}$ using Bueckner's Eq 22. A comparison of the fracture toughness data obtained by the two methods shows that Bueckner's equation gave approximately the same $\mathcal{G}_{Ic}$ values as those determined from the spring constant except in the case of

that an effective crack depth is obtained which includes the plastic zone formed at the tip of the crack. Thus, the effective crack should be larger than the measured depth of notch plus fatigue crack. Table 16 contains anomalous data in this regard, presumably the result of insufficient calibration data or inherent complications in testing inhomogeneous weld deposits, or both. Note that specimens B1–7 had measured crack depths of 0.10 to 0.11 in. and effective crack depths calculated from the spring constant of only 0.06 to 0.07 in.

Comparisons also have been made at Aerojet-General Corp. between the results obtained from Eqs 20 and 22 in forty groups of five replicate slow notch bend (SNB) specimens of vacuum-arc remelt grade-200 18 per cent nickel maraging steel, representing two orientations of a specimen aged at 850–950 F for times ranging from 4 to 24 hr. The slow notch bend specimen was 4 in. long (3-in. span), 0.6 in. wide, and 0.75 in. deep. Representative computer-run fracture toughness data are tabulated in Table 17. Note that Eqs 20 and 22 provided by the authors and Bueckner respectively gave approximately the same $\mathcal{G}_{Ic}$ values.

From the data presented in Tables 16 and 17, it is concluded that calculation of plane-strain fracture toughness from the slow bend test can be accomplished using either Bueckner's or the authors' equations, thus avoiding the expense (in materials and manhours) of the calibration experiment.

STP381-EB/Apr. 1965

INCORPORATION OF FRACTURE INFORMATION IN SPECIFICATIONS

By W. F. Payne[1]

Synopsis

Fracture tests for material and process specifications involving high-strength alloys are necessary to insure adequate inspection standards for material and hardware acceptance. Proper specimen design is necessary to produce useful toughness information, especially a specimen size adequate to avoid general yielding prior to fracture. Evidence of significant toughness variation in commercial alloys is presented. The paper illustrates the use of present analytical expressions to determine inspection standards for isolated defects of various geometry and for linear arrays of multiple defects. Specific rejection criteria for multiple defects are suggested.

The selection of a test, including proper specimen size and design, for a given specification and for the most useful application of data produced for nondestructive inspection limits is the final step in the engineering application of fracture mechanics. Selection of an inappropriate specimen or one of inadequate size reduces the ability to apply test data in the design and quality control aspects of the fracture-analysis cycle. Considerable attention is therefore directed toward criteria for specimen selection and proper use of the fracture data. Specifications also require treatment of multiple defects; therefore, a simplified analysis is included to illustrate the ability of present fracture mechanics methods to treat crack-geometry variations and crack-interaction effects.

[1] Metallurgist, Solid Rocket Division (RPMB), Air Force Rocket Propulsion Laboratory, Edwards Calif.

Specimen Selection

A review of specimens and appropriate stress-intensity expressions is provided in this symposium by Paris and Sih[2] and Srawley and Brown.[3] The relationship of specimens to practical application of fracture mechanics is discussed by Tiffany and Masters.[4] For specification use, a specimen must satisfy several requirements:

1. The configuration should be convenient to use for the product involved. For example, a notched tension test specimen is convenient for bar stock.
2. Cost must be reasonable.
3. Test technique and interpretation must be simple and insensitive to technique variation common to a testing laboratory.

One factor affecting convenience and

[2] P. C. Paris and G. Sih, "Stress Analysis of Cracks," see p. 30.

[3] J. E. Srawley and W. F. Brown, "Fracture Toughness Testing," see p. 133.

[4] C. F. Tiffany and J. Masters, "Applied Fracture Mechanics," see p. 249.

cost is the minimum specimen size that can properly measure the toughness in the material without encountering net-section yielding prior to rapid crack propagation. Figure 1 shows the minimum size estimates for specimens capable of measuring two plane-strain toughness levels (expressed as the K_{Ic}/σ_{YS} ratio) using the criteria discussed by Srawley and Brown[3] and Payne (1).[5] As toughness levels increase, the necessary specimen size quickly becomes very large.

Requirements for tensile load capacity and material volume of various specimens are also of practical interest. Comparative values of these parameters are given in Table 1. The advantage of the single-edge-notched specimen is evident. The bend specimen compares

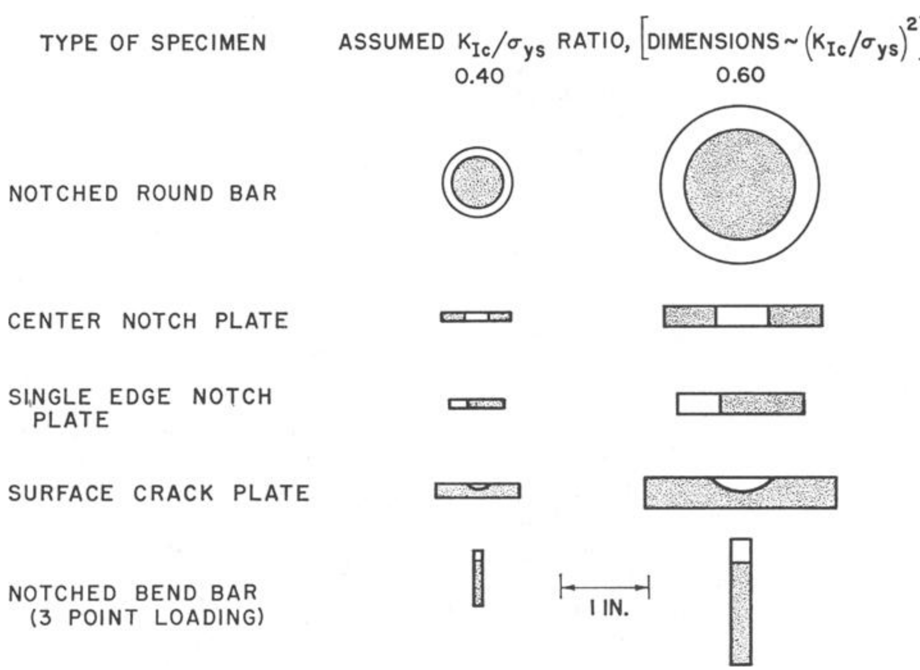

FIG. 1—Minimum Specimens for Valid K_{Ic} Measurement.

TABLE 1—RELATIVE LOAD REQUIREMENT OF VARIOUS SPECIMENS FOR EQUAL K_{Ic}/σ_{YS} MEASUREMENT.

Specimen	Load Capacity	Volume
Single-edge-notched (W = 6B)	1.0	1.0
Center-notched pop-in (W = 8B)	2.25	1.57
Notched round bar (d/D = 0.7)	14	9.0
Surface-cracked plate (W = 6B)	6.75	3.5
Notched three-point-loaded bend bar (W = 6B)	0.175	2.25

favorably on a load-requirement basis, although the material-volume requirement is greater. The bend specimen is convenient for tests with any notch orientation (surface or side notch) which is important for plate evaluation.

The plane-strain fracture toughness is calculated using the maximum load and initial crack dimensions for the circumferentially notched round bar and the surface-cracked specimens. Pop-in load

[5] The boldface numbers in parentheses refer to the list of references appended to this paper.

values are frequently used to calculate K_{Ic} for plate specimens when the specimen size is insufficient to produce a plane-strain fracture at maximum load. The conditions necessary for accurate and reproducible pop-in load measurements have not been established. Specification tests cannot be effective if the results can be influenced by personal interpretation of the test record or insensitive instrumentation. Sufficient information to design a test specimen of minimum size, free from interpretation problems, does not exist for most materials of interest. Some prior satisfactory testing experience by the testing organization seems essential before final specimen selection.

Progress toward widespread testing ability capable of giving reproducible results seems pitifully slow. Until fracture values and techniques are established, incorporation of fracture tests in material specifications on a reporting basis appears to be the only practical approach.

TABLE 2—VARIATION IN K_c TOUGHNESS OF Ti-6Al-4V SHEET.[a]

Heat	Specimen	Panel Size, in.	Grain Direction	K_c,[b] ksi $\sqrt{\text{in.}}$
D5256...........	DD22	24 × 72	L	164.7
	DD23	24 × 72	L	163.6
	DD26	24 × 72	L	169.2
	DD27	24 × 72	L	172.0
	DD29	24 × 72	L	182.1
				avg. 170.3 (L)
	DD24	24 × 72	T	149.4
	DD30	24 × 72	T	186.8
	DD38	8 × 24	T	175.2
				avg. 170.4 (T)
D5257...........	DD4	24 × 72	L	157.7
	DD9	24 × 72	L	193.0
	DD10	24 × 72	L	179.9
				avg. 176.9 (L)
	DD5	24 × 72	T	163.3
	DD6	24 × 72	T	165.7
	DD11	24 × 72	T	176.5
	DD12	24 × 72	T	165.1
	DD21	8 × 24	T	160.6
				avg. 166.2 (T)
D2963...........	248	8 × 24	T	128.5
	250	8 × 24	T	124.5
				avg. 126.5 (T)
D2382...........	283	8 × 24	T	121.9
	285	8 × 24	T	125.9
				avg. 123.9 (T)

[a] Sheet thickness, 0.050 in., center-notched specimen; $2\,a/w = 0.25$; room temperature; loading-rate effects negligible.
[b] Calculated with original crack size.

THE USE OF SUBSIZE SPECIMENS

The literature contains descriptions of many extensive test programs using arbitrarily fixed specimen geometries. These specimens are often smaller than the minimum size necessary for quantitative measurement of K_{Ic} values. The use of a subsized specimen produces tensile instability prior to general yielding, and gives a lower limit for the crack toughness—a conservative estimate of the true K_{Ic} value. This approach is satisfactory to eliminate material of toughness levels inferior to the toughness value the specimen is capable of measuring; the toughness of materials exceeding this toughness value goes essentially unmeasured. The ability to relate product test data to proper inspection criteria is reduced.

An example of misinterpretation of fracture data is the use of notch-strength analysis for surface-crack data, as shown in Ref (1). A number of investigators have defined the critical surface-crack size as a crack sufficient to reduce the notch strength (net fracture stress) to a value equal to the yield strength. This definition can lead to optimistic estimates of crack tolerance if test data are obtained with specimens of inadequate size. The influence of specimen size on the error associated with notch-strength analysis is shown in Appendix I. For example, using the smallest surface-cracked specimen allowed by the criteria in Ref (2), a 23 per cent overestimate of crack tolerance occurs with notch-strength analysis.

TABLE 3—VARIATION IN K_c TOUGHNESS OF Ti-6Al-4V SHEET.[a]

Heat	Specimen No.	Panel Size, in.	Grain Direction	K_c,[b] ksi $\sqrt{\text{in.}}$
D4949	DD51	24 × 72	L	335.7
				avg. 335.7 (L)
	DD54	8 × 24	T	137.9
				avg. 137.9 (T)
M5900	203	8 × 24	T	168.3
	194	8 × 24	T	186.6
	205	8 × 24	T	177.2
	202	8 × 24	T	170.3
				avg. 175.6 (T)
D2963	225	8 × 24	T	103.4
	218	8 × 24	T	120.4
	239	8 × 24	T	119.8
	226	8 × 24	T	117.9
				avg. 115.4 (T)
	252	8 × 24	L	104.4
	253	8 × 24	L	102.7
	254	8 × 24	L	107.5
				avg. 104.7 (L)
D2133	263	8 × 24	T	112.8
	264	8 × 24	T	99.7
	273	8 × 24	T	110.9
	259	8 × 24	T	101.9
				avg. 106.3 (T)

[a] Sheet thickness 0.025 in.; center-notched specimen; $2a/w = 0.25$; room temperature; loading-rate effects negligible.
[b] Calculated with original crack size.

Toughness Variations in Commercial Mill Products

Do we need another evaluation test in material specifications? It is reasonably simple to demonstrate that the toughness properties of commercial alloys are subject to considerable variation. It is not simple to find examples of such variation free from the confounding influence

TABLE 4—TOUGHNESS VARIATION IN 18 PER CENT NICKEL-COBALT-MOLYBDENUM (300) MARAGING STEEL AGED 900 F FOR 3 Hr.

Heat No.	Thickness, in.	Tensile Yield Strength, ksi	K_{Ic},[a] Surface-Cracked Specimen, ksi $\sqrt{in.}$	K_{Ic}, Center-Cracked Specimen, ksi $\sqrt{in.}$	Notch Strength, Center-Cracked Specimen, ksi
1..........	0.14	295 (3)[b]	125	113 (4)	193 (4)
2..........	0.14	294 (2)	95	73 (5)	146 (3)
A.........	0.25	284 (2)	115	...	...

CHEMICAL COMPOSITION

Heat No.	Ni	Co	Mo	Ti	Al	C	Si	P	S
1........	18.63	9.00	4.66	0.66	0.070	0.013	0.045	0.004	0.005
2........	17.80	8.96	4.85	0.63	0.065	0.027	0.084	0.005	0.010
A.......	18.43	8.71	4.06	0.70	0.065	0.011	0.045	0.006	0.008

[a] Author's best estimate from reported test data.
[b] Number of replicate tests.

TABLE 5—IMPACT TOUGHNESS VARIATION FOR AISI 4340 STEEL.[a]

Vendor	Heat	Average Impact Energy, ft-lb: Billet	Forging: Base	Forging: Cap	Standard Deviation, per cent: Billet	Forging: Base	Forging: Cap
			AIR MELT				
A.........	1	10.7	...	16.5	16.7	...	4.42
	2	13.2	15.9	...	12.9	1.12	...
	3	13.3	17.3	...	16.6	1.54	...
B.........	1	14.5	20.5	23.8	13.7	8.1	24.5
	2	14.9	26.0	28.6	12.2	10.6	11.9
	3	16.8	25.3	29.5	5.5	13.4	12.4
	4	...	19.5	26.0	...	12.0	18.6
	5	...	22.0	...	...	7.8	...
	6	...	...	27.3	...	...	...
			VACUUM REMELT				
C.........	1	...	...	13.6	...	...	12.0
	2	...	...	13.8	...	...	9.6
	3	...	18.5	...	...	6.8	...
	4	...	18.6	...	...	7.5	...
D.........	1	19.0	26.8	34.4	17.2	19.7	14.0

[a] Specimens normalized at 1650 F for 1 hr and air cooled, austenitized at 1550 F for 1 hr, oil-quenched and double-tempered at 950 F for 1 hr and oil quenched. All specimens transverse and tested at −40 F.

of testing variables. Several examples of toughness variation are included to show that control of strength and chemistry is not sufficient for control of material toughness.

Center-cracked panel tests of aircraft sheet materials have revealed K_c toughness variation between heats. Tables 2 and 3 show results obtained on annealed Ti-6Al-4V sheets of 0.050- and 0.025-in. thickness, respectively. The average K_c values vary from 125 to 175 ksi $\sqrt{in.}$ (These values were calculated using initial precrack length,

TABLE 6—CHEMICAL ANALYSIS (PERCENTAGE BY WEIGHT) AND VENDOR.

Vendor	Heat	C	Mn	Si	P	S	Cr	Ni	Mo
A.....	1	0.41	0.75	0.31	0.009	0.014	0.83	1.98	0.25
	2	0.42	0.76	0.30	0.007	0.016	0.75	1.84	0.22
	3	0.39	0.77	0.30	0.009	0.012	0.78	1.98	0.26
B.....	1	0.41	0.71	0.28	0.011	0.015	0.76	1.82	0.24
	2	0.40	0.69	0.28	0.010	0.009	0.78	1.79	0.24
	3	0.41	0.73	0.30	0.008	0.009	0.78	1.83	0.23
	4	0.41	0.75	0.30	0.010	0.005	0.82	1.86	0.25
	5	0.40	0.73	0.30	0.009	0.007	0.77	1.75	0.23
	6	0.41	0.75	0.30	0.010	0.005	0.82	1.86	0.25
C.....	1	0.39	0.72	0.31	0.010	0.006	0.85	1.90	0.24
	2	0.38	0.70	0.31	0.012	0.005	0.85	1.90	0.24
	3	0.38	0.70	0.27	0.009	0.006	0.85	1.86	0.27
	4	0.39	0.71	0.27	0.009	0.005	0.87	1.88	0.26
D.....	1	0.38	0.62	0.28	0.006	0.007	0.89	1.90	0.24

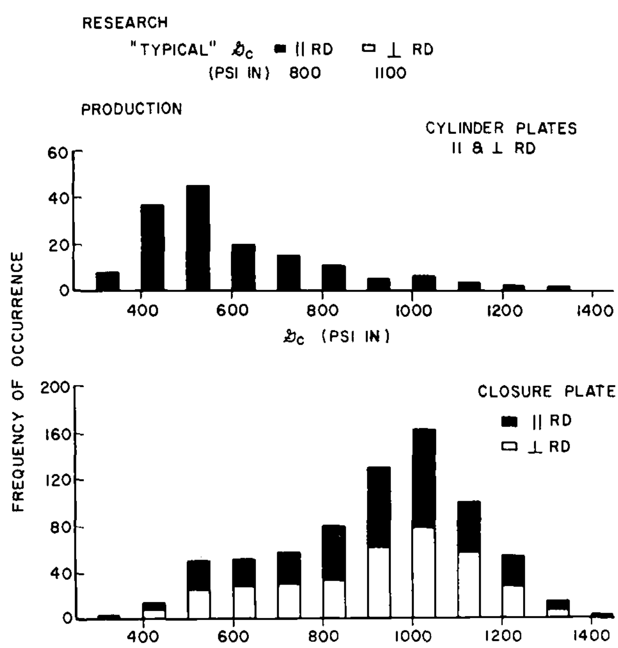

FIG. 2—Crack Toughness (K_c) Distribution Curves for AMS M-255 Low-Alloy Steel.

rather than final crack length at fracture.)

Melville (3) reported fracture toughness variations among several heats of 18 per cent nickel-cobalt-molybdenum (300) maraging steel which could not be explained with chemistry or strength variations. The two specimens employed were a 2.25- by 12-in. center-cracked plate and a 1 by 8-in. surface-cracked specimen. Table 4 shows the toughness levels in three heats, including K_{Ic}

values from surface-cracked specimens, pop-in with the center-cracked specimen, and notch strength for the center-cracked specimen (reflecting plane-stress toughness behavior).

Table 5 is a summary of impact toughness data on AISI 4340 low-alloy steel obtained in a forging procurement program by Watertown Arsenal. Toughness variation from vendor to vendor is most significant, followed by heat variation and location in the forging. The chemical analysis is given in Table 6 and is very uniform except for sulfur content of the first four heats.

In the Polaris program, research studies by Aerojet on AMS M-255 low-alloy steel plate (hardened to a minimum yield strength of 190 ksi) indicated $\mathcal{G}_c$ values of 800 and 1100 in-lb/in.^{2} for the direction parallel to and perpendicular to the rolling direction, respectively.[6] Under production conditions, closure plates (135 plates from 28 heats) gave an average toughness ($\mathcal{G}_c$) of 1000 in-lb/in.^{2} with no directionality. Cylinder plates (29 plates from 13 heats) were also checked and gave an average $\mathcal{G}_c$ value of 500 in-lb/in.^{2} with no directionality. The actual toughness distribution curves are shown in Fig. 2. These pronounced toughness differences between the closure and cylinder plates could not be correlated with chemistry or strength level.

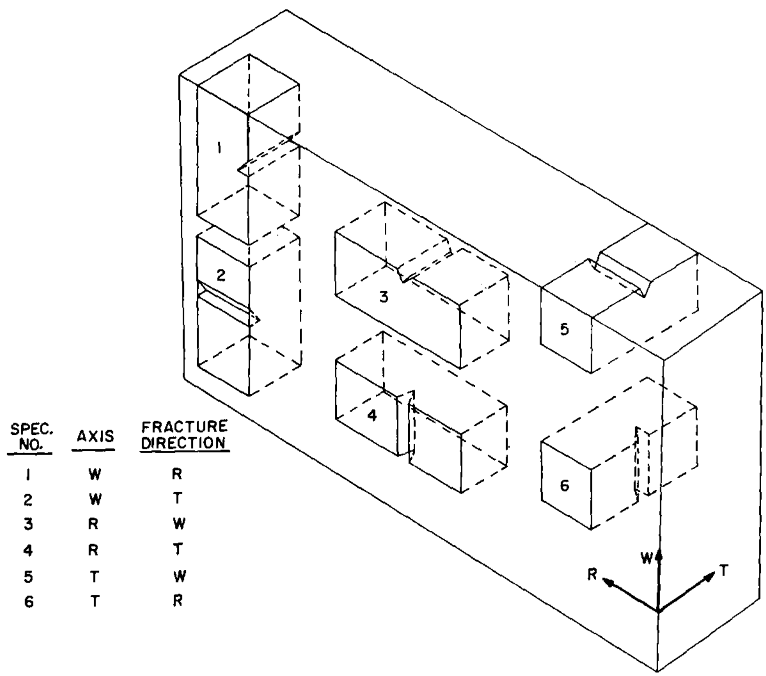

FIG. 3—Crack-Propagation Directions in Plate.

The possible directionality of tough-

[6] Measured with center-cracked specimens 2.5 in. wide with 30 per cent notch and notch radius less than 0.001 in. formed by elox machining. The notch was not fatigue-cracked, but the radius was about $\frac{1}{60}$ of the plastic-zone radius and may have been satisfactory for valid K_c values.

ness in the mill products must be considered, for various specimens often measure the toughness of different directions. In a three-dimensional body, there are six potentially different fracture directions as shown in Fig. 3, although there are only three different axes. For sheet products, a center-notched or single-edge-notched specimen would measure crack toughness in the *WR* and *RW* orientation (Nos. 1 and 3 of Fig. 3). A surface-cracked specimen would measure the toughness of the *WT* and *RT* directions (Nos. 2 and 4 of

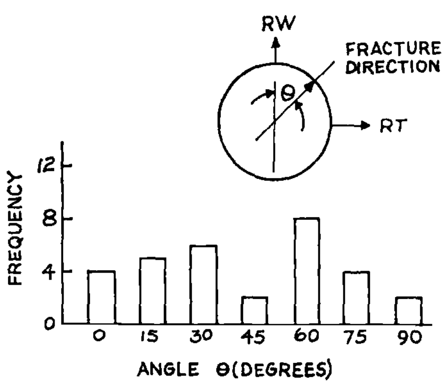

FIG. 4—Frequency Distribution of Propagation Angle in Notched Round Bar Tests on D6AC Low-Alloy Steel.

Fig. 3). A precracked round tensile bar would measure the lowest toughness orientation for a given axis direction. With thick plate, single-edge-notched or surface-cracked specimens can be sliced through the thickness, which allows evaluation of any orientation of the *W* and *R* directions. A bend specimen can usually be used to measure any orientation of the *W* and *R* direction. Testing in the short-transverse (*T*) direction is usually difficult or impossible on finished mill products.

Pellisier (4) has reported $\mathcal{G}_{Ic}$ values for 1-in. plate of 18 per cent nickel-cobalt-molybdenum (250) maraging steel. The values were 310, 245, 230, and 150 in-lb/in.^{2} corresponding to orientations *RT*, *RW*, *WR*, and *TW*, respectively. This toughness variation arises from chemical banding and preferential orientation of impurities by the rolling operation. If toughness tests are used to control the laminar banding, specimens with orientation *WR* or *RW* should be used. Use of specimens with a *WT* or *RT* orientation would be misleading because the indicated toughness would improve as the banding became more severe. For sheet and thin plate, surface-cracked specimens would be misleading and single-edge-notched, center-notched, or possibly notched bend tests would be necessary. Occurrence of any splitting in a fracture surface with *WT* or *RT* orientation should suggest additional tests in the *WR* or *WT* orientation.

The precracked round bar tension specimen can propagate in any direction in the plane of the notch. Tiffany and Lorenz (5) measured the propagation direction in notched bars of D6AC low-alloy steel by careful fracture-surface analysis. The distribution curve for propagation direction relative to grain direction is shown in Fig. 4. In this example, the toughness value did not vary significantly for the different propagation angles involved.

Sufficient data have been included to show the toughness variation that can be encountered in commercial mill products, including variation among heats, among grain directions, and among propagation directions for a specific grain direction. Proper attention to the source of toughness variation is necessary in a fracture evaluation program. In previous attempts to compare toughness values from different specimens, the difference in measured values has often been associated with material orientation variables rather than specimen variables.

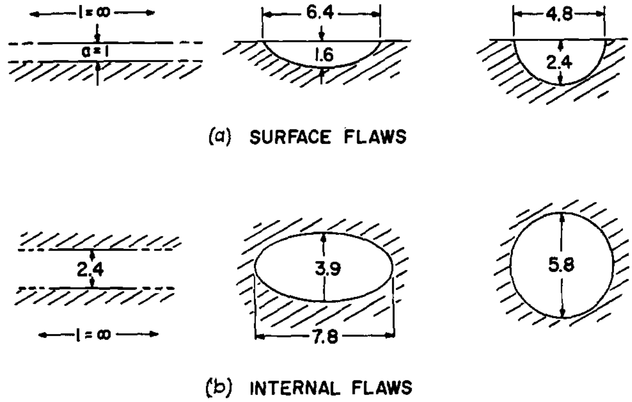

FIG. 5—Equivalent Flaw Geometry for Single Cracks.

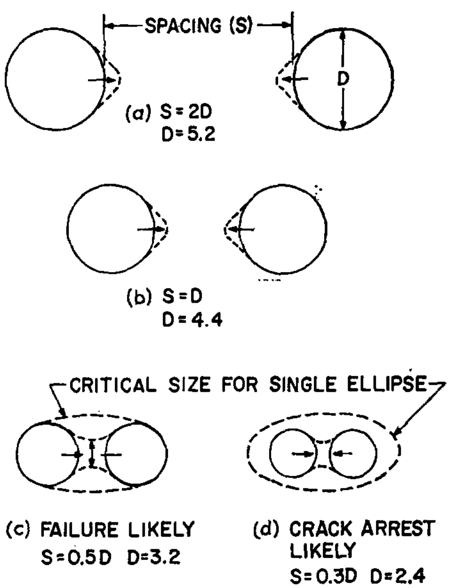

FIG. 6—Equivalent Flaw Geometry for Two Cracks.

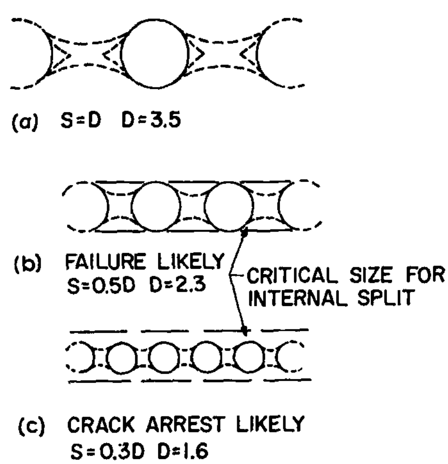

FIG. 7—Equivalent Flaw Geometry for an Array of Cracks.

EFFECT OF FLAW GEOMETRY AND MULTIPLE FLAW INTERACTIONS

Specifications must establish allowable defect levels for many possible combinations of flaw shape, location, and frequency of occurrence (multiple defects). Fracture mechanics can help establish these defect limits. The simplified model used consists of a structural member containing cracks sufficiently large to induce elastic fracture prior to general yielding but small compared with structural thickness. (Most real problems are nonideal and should be handled individually.) Crack orientation is taken as perpendicular to the principal load. This simple model is used to illustrate that present knowledge can be employed usefully in specifications.

Available stress-intensity expressions

were used to determine various arrangements of flaw size, shape, location, and interactions which should produce an equivalent "effective crack size" and therefore equal fracture strength. A plane-strain fracture mode is assumed, and size units given are relative to a long surface crack with assumed depth of one unit. The calculations made are included in Appendix II. The effect of crack shape for surface cracks and internal cracks is shown in Fig. 5. The effect of crack size and separation for two flaws and a linear array of flaws are shown in Figs. 6 and 7, respectively. Careful interpretation of the flaw-interaction effect is required, because the analysis is based on stress-intensity magnification *between* the cracks rather than around the entire crack surface. The magnification effect between cracks tends to initiate fracture of the ligament between the cracks. As the crack edges get close together, the magnification effect becomes unlimited and the joining of these flaws would be certain. However, general propagation to total fracture would be questionable if the crack size after joining were significantly smaller than the critical single-flaw size of appropriate geometry. For example, the two flaws of Fig. 6(*c*) could join together and form an ellipse of nearly critical size which would probably propagate to complete fracture, as indicated in the figure. However, the two flaws in Fig. 6(*d*) could join together and still require considerable crack growth before critical size and general fracture occurred. Propagation of these defects to failure seems unlikely and crack arrest would be expected. Similarly, the connection of cracks in a linear array would be expected to induce total fracture only if the resulting crack width approached the critical crack width for a long internal crack as shown in Fig. 7(*a*). Smaller cracks would join to form stable subcritical cracks as shown in Fig. 7(*b*) and 7(*c*). The interaction of two coplanar elliptical surface flaws was discussed by Tiffany and Masters.[4] Very little interaction was found unless the separation became less than the flaw depth. Especially noteworthy is the confirmation of predicted behavior by experimental results, as evident in Fig. 32 of their paper.

The results of these crack-interaction predictions may be summarized as follows:

1. Cracks separated by more than three crack lengths may be considered as independent flaws.
2. For two adjacent flaws, diameters less than 40 per cent of critical single-flaw diameter may be neglected.
3. For a linear array of flaws, diameters less than 30 per cent of the critical single-flaw diameter may be neglected.
4. For a two-dimensional array (estimated only), diameters less than 20 per cent of the critical single-flaw diameter may be neglected.
5. For two coplanar surface flaws, interaction may be neglected if the separation distance exceeds two crack depths.

These relative crack-geometry effects should be generally valid for any homogeneous material. The actual crack sizes will be dictated by specific values of crack toughness, applied stress, and secondary influences such as plastic-zone corrections.

Quantitative Inspection Limits

Establishing sound engineering inspection criteria requires more than accurate toughness measurements on raw material and analytical expressions relating flaw size and crack toughness to fracture strength. To establish initial inspection limits that would insure a successful service life requires several additional steps:

1. Evaluation of toughness and

strength changes during manufacturing operations such as forming, welding, and heat treatments.

2. Evaluation of subcritical crack growth during service.

3. Establishing an inspection safety factor to protect against inspection limitations and unknowns or changes in service conditions.

The pronounced effects of operations such as heat treatment and welding are well known. The influence of forming operations should also be considered. For example, Sernka (6) has reported that direct aging after shear spinning of 18 per cent nickel-cobalt-molybdenum (300) maraging steel reduced the K_c toughness from 150 to 80 ksi $\sqrt{\text{in.}}$ The proper crack toughness value for establishing hardware acceptance limits may be different from the values characteristic of the as-received mill product.

Preliminary attempts to evaluate subcritical crack growth for pressure-vessel applications are discussed by Tiffany and Masters.[4] Even for this simple application, uncertainties exist in crack-growth predictions and additional safety margins must be employed until growth kinetics is better understood.

Uncertainties also exist with any inspection method. Most nondestructive inspection methods can fail to detect cracks or defects that are tight or in an inconvenient orientation. Human error must also be expected. Additional uncertainties, such as residual stresses and local material heterogeneities, make precise analysis of growth kinetics and fracture behavior difficult. It is clear that final hardware acceptance criteria, based on nondestructive inspection, must contain an engineering judgment on the proper safety margin to accommodate these unknowns.

It is possible to include this judgment factor in the analytical expressions presented during this symposium. For example, the critical diameter, D, for an internal circular flaw (Q of 2.2) under plane-strain conditions, with an applied stress, σ, can, by neglecting plastic-zone corrections, be written as $D = 1.4 (K_{Ic}/\sigma_{YS})^2$. We can define a general factor, f, as the "inspection safety factor," having a value between 0 and 1. The f factor reflects both subcritical crack-growth allowance and safety margin selected to account for uncertainties in service conditions and inspection operations. This would produce the form $D = 1.4f(K_{Ic}/\sigma_{YS})^2$. Such representation would help separate and communicate the analytical estimates and engineering design judgments used to produce final inspection limits from initial crack-toughness and strength-level information.

CONCLUSIONS

Fracture tests as part of material specifications are necessary and should be used even though testing problems still exist. The principal problems are specimen selection, test interpretation, lack of assured reproducibility between specimens, and uncertain toughness variation with orientation. A period of joint user and supplier trial testing effort on a report-only basis is suggested to minimize these problems.

Present fracture mechanics methods can aid in establishing rejection standards for various crack geometries and interaction of multiple cracks. This type of analysis is essential for nondestructive inspection limits and material review board actions on specific material and hardware discrepancies.

The inherent ability of fracture mechanics analysis effectively to integrate the frequently divergent disciplines of materials, manufacturing, and quality control operations should be recognized.

Acknowledgment:

The impact-toughness information in Table 5 was taken from information supplied by D. E. Driscoll of Watertown Arsenal. The Polaris M-255 data were provided by H. Bernstein of the Special Project Office, Department of the Navy. The assistance of C. F. Tiffany and P. C. Paris in many discussions on the application problem is gratefully acknowledged.

REFERENCES

(1) W. F. Payne, "Analysis of Surface Crack Fracture Toughness Information," *Fourth Maraging Steel Project Review, Volume 1, ML-TDR-64-225*, USAF, Wright-Patterson Air Force Base, Ohio, July, 1964, pp. 307–367.

(2) "Progress in Measuring Fracture Toughness and Using Fracture Mechanics," *Materials Research & Standards*, Am. Soc. Testing Mats., Vol. 4, No. 3, March, 1964, pp. 107–119.

(3) A. Melville, "Metallurgical Evaluation of 18% Nickel Maraging Steel (300 ksi Strength Level)," *Third Maraging Steel Project Review, RTD-TDR-63-4048*, USAF, Wright-Patterson Air Force Base, Ohio, November, 1963, pp. 327–368.

(4) G. E. Pellisier, "Some Microstructural Aspects of Maraging Steel in Relation of Strength and Toughness," *Third Maraging Steel Project Review, RTD-TDR-63-4048*, USAF, Wright-Patterson Air Force Base, Ohio, November, 1963, pp. 407–428.

(5) C. F. Tiffany and P. M. Lorenz, "An Investigation of Low-cycle Fatigue Failures Using Applied Fracture Mechanics," *ML-TDR-64-53*, USAF, Wright-Patterson Air Force Base, Ohio, May, 1964, p. 26.

(6) R. F. Sernka, "Some Considerations in Shear Spin Processing," *ASM Technical Report No. W4-1.1*, Am. Soc. Metals, March, 1964.

APPENDIX I

COMPARISON OF CRITICAL CRACK-SIZE DETERMINATION WITH GROSS- AND NET-STRESS CRITERIA FOR SURFACE-CRACKED SPECIMEN

Use of net stress, rather than gross stress, has unfortunately been adopted by many investigators. The use of net stress to determine crack tolerance can lead to incorrect (optimistic) estimates of crack tolerance. The following analysis was performed to indicate when such estimates would be significantly in error.

The critical crack size, a_{cr} is defined as the minimum surface-crack size sufficient to initiate rapid fracture in a surface-cracked flat tension specimen subjected to a given tensile load or gross stress. For this study, the specific critical crack size of interest is the a_{cr} value for a gross strength equal to the 0.2 per cent offset yield strength, usually the highest conceivable design strength for material. Crack size will be represented in the "normalized" form, a/Q, which is equivalent to crack-depth or crack-length representation when the a/Q ratio is constant. Figure 8 shows the fracture-stress versus crack-size relationship predicted by the Irwin analysis. The fracture curve terminates at the yield strength (point A) and the a/Q_{cr} value for a fracture stress equal to the yield strength is given by:

$$\left(\frac{a}{Q}\right)_{cr} = \frac{1}{1.21\pi}\frac{K_{Ic}^2}{\sigma_{YS}^2} \quad \text{........(1)}$$

The apparent critical crack size determined with the net stress equal to yield-strength criterion (point B) is larger by the amount, e. The $(a/Q)_{net}$ at B can be calculated by determination of the identical value of $(a/Q)_{net}$ at point C. If $\sigma_{net} = \sigma_{YS}$, then the gross stress at C for a ratio, x, of crack area to specimen area, where $x = A_c/A_o$, must be

$$\sigma_g(c) = \sigma_{net}(1 - x) = \sigma_{YS}(1 - x) \quad \text{...(2)}$$

The ratio of σ_{net} to σ_g as a function of crack area A_c/A_o, is shown in Fig. 9. Hence, $(a/Q)_{net}$ can be found from

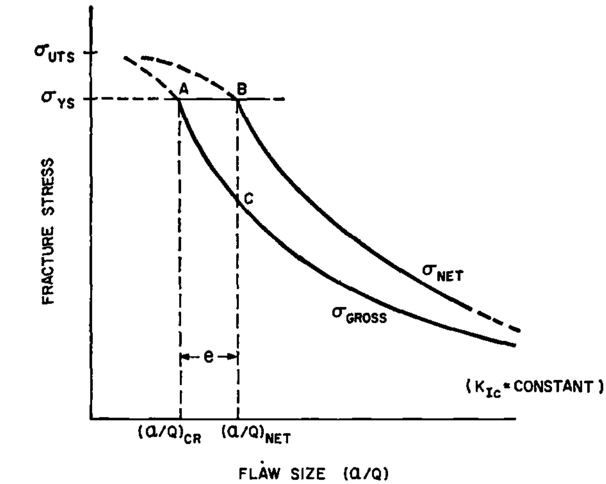

FIG. 8—Fracture-Strength Curve for Surface Cracks.

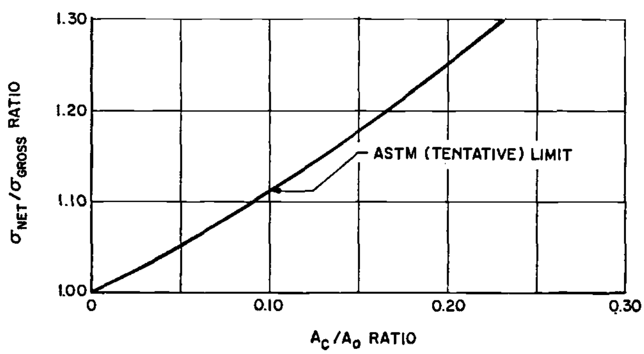

FIG. 9—Effect of Crack Area on Ratio of Net Stress to Gross Stress for a Surface-Cracked Specimen.

TABLE 7—EFFECT OF GEOMETRY ON NET STRESS AND $(a/Q)_{cr}$ USING NET-STRESS ANALYSIS.

$x = A_c/A_o$	$1 - x$	σ_{net}/σ_g	Error in $(a/Q)_{cr}$, per cent
0	1.00	1.00	0.0
0.01	0.99	1.010	2.0
0.02	0.98	1.020	4.1
0.03	0.97	1.031	6.3
0.04	0.96	1.042	8.6
0.05	0.95	1.053	10.8
0.07	0.93	1.075	15.6
0.10	0.90	1.111	23.4
0.13	0.87	1.149	32.0
0.15	0.85	1.176	38.4
0.20	0.80	1.250	56.2
0.25	0.75	1.333	77.7
0.30	0.70	1.428	104.1

$$\left(\frac{a}{Q}\right)_{net} = \frac{K_{Ic}^2}{1.21\pi\sigma_{YS}^2(1 - x)^2} \quad \ldots\ldots (3)$$

Subtracting Eq 1 from Eq 3, the error in critical crack-size determinations, using the net-stress criteria, is given by

$$e = \Delta\left(\frac{a}{Q}\right)_{cr}$$

$$= \frac{K_{Ic}^2}{1.21\pi\sigma_{YS}^2}\left[\frac{1}{(1 - x)^2} - 1\right] \quad \ldots\ldots (4)$$

$$e(\%) = 100\left[\frac{1}{(1 - x)^2} - 1\right] \quad \ldots\ldots (5)$$

Although the actual error in $(a/Q)_{cr}$ varies with the (K_{Ic}/σ_{YS}) ratio, the relative or

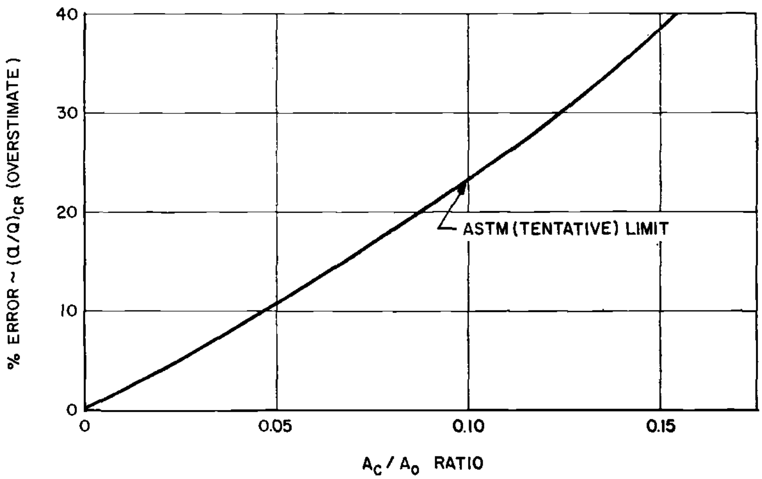

FIG. 10—Error (Overestimate) in Crack-Tolerance Estimates Caused by Notch-Strength Criteria as a Function of Surface-Crack Area.

percentage of error is only a function of the crack and specimen geometry. Calculations using Eq 5 are given in Table 7 and shown in Fig. 10.

The use of $(a/Q)_{\mathrm{cr}}$, or a_{cr} or l_{cr}, based on net-stress criteria can introduce significant errors (overestimates), especially for small cracked specimen geometries. For example, a 10 per cent error (overestimate) would be expected for a crack area of about 5 per cent, a common value for small surface-cracked specimens. The ASTM limit of $\sigma_{\mathrm{net}} \leqq 1.1\ \sigma_g$ (established for K_{Ic} calculations with σ_g only) could allow a 23 per cent overestimate of $(a/Q)_{\mathrm{cr}}$ if analyzed using net-stress criteria.

APPENDIX II

CALCULATION OF EQUIVALENT CRACK SIZE FOR VARIOUS CRACK GEOMETRIES AND INTERACTION OF MULTIPLE CRACKS

The effect of crack geometry (single cracks) can be calculated with the expressions found in the Fifth Report of the ASTM Special Committees on Fracture Testing of High-Strength Metallic Materials (2) for the plane-strain fracture mode. The calculations are made without any plastic-zone correction (which does not affect relative crack size). All size units are based on a long surface crack of a depth of one unit.

For surface cracks, all geometries must have identical (a/Q) values. For cracks of length $2c$ and depth a, see Table 8.

For internal cracks, the surface equation

TABLE 8.

Geometry	Q	Depth, a	Length, $2c$
Long crack	1.0	1.0	very long
$2c = 4a$	1.61	1.6	6.4
$2c = 2a$	2.42	2.4	4.8

TABLE 9.

Geometry	Q	Minor Axis = 2(1.21a)	c
Long internal split	1.0	2.42	very long
$c = 2b$	1.61	3.90	7.8
$c = b$ (circular)	2.42	5.85	5.85

TABLE 10—EFFECT OF MULTIPLE FLAW GEOMETRY ON ALLOWABLE DEFECT SIZE.

Number of Cracks	Assumed Separation	M_k	Diameter	Separation
1 (circular)...	...	...	5.85	...
2............	4*D*	1.02	5.6	22.4
	2*D*	1.06	5.2	10.4
	D	1.16	4.4	4.4
	0.5*D*	1.34	3.2	1.6
	0.3*D*	1.56	2.4	0.7
3............	4*D*	1.06	5.2	20.8
	2*D*	1.12	4.6	9.3
	D	1.30	3.5	3.5
	0.5*D*	1.58	2.3	1.2
	0.3*D*	1.9	1.6	0.5

is altered by elimination for the 1.21 coefficient which means the effective crack size for internal defects is 1.21 larger than the size of surface cracks. For internal defects of major axis, $2c$, and minor axis, $2b = 2\,(1.21a)$, the sizes equivalent to the surface cracks given in Table 8 are given in Table 9.

The effect of multiple cracks was estimated from the analysis for stress-intensity magnification between colinear through-thickness cracks, assuming the effects would be similar for internal cracks under plane-strain conditions. A more accurate analytical treatment may appear in the future, but no serious changes in the conclusions drawn from this engineering estimate are expected. The size for multiple cracks equivalent to an internal circular crack of 5.8 units varies inversely with the square of the magnification factor, M_k. As noted in the paper, the magnification effect only occurs between the particles. Crack propagation between multiple circular cracks of size considerably less than the critical size for a long internal split would presumably be arrested as a subcritical crack. The values obtained with these calculations are given in Table 10.

STP381-EB/Apr. 1965

DISCUSSION

J. STEPHEN PASCOVER[1]—Mr. Payne is to be congratulated on a fine paper and on his "user-oriented" approach to fracture toughness testing. The present discussion is concerned, however, with the data reported in Table 7, item 7, on the 9Ni-4Co(200) alloy. This value for K_{Ic} of 70 ksi $\sqrt{\text{in.}}$ ($K_{Ic}/YS = 0.35$) is not representative of those normally obtained in this steel. Referring to the author's source,[2] the value reported represents:

1. a nontypical composition
2. excessive net section yielding
3. the properties of the weld metal

All three of these qualifications were pointed out in the original report.

While the integrity of the data was not essential in the context of the subject paper, the tendency to quote values from such compilations out of context makes it mandatory that more representative values be pointed out. Such data appear in Table 11.

[1] Research metallurgist, Republic Steel Corp., Cleveland, Ohio.

[2] First Quarterly Progress Report on AF Contract AF33(657)-11229, Development of Welding Procedures and Filler Materials for Joining High Strength Low Alloy Steels ER 5554, October, 1953 (unpublished).

TABLE 11—PROPERTIES OF 9 PER CENT NICKEL-4 PER CENT COBALT (200) MATERIALS.

Form	Tempering Temperature, deg F	Yield Strength, ksi	Ultimate Tensile Strength, ksi	K_{Ic}, ksi $\sqrt{\text{in.}}$	Notch Strength, ksi	Ref	Remarks
1-in. plate	400	193	259.4	111	142	[a]	surface-flawed specimen 3 in. wide and 1 in. thick. a = 0.27 in., l = 0.88 in.
1 in. plate......	800	189	205.5	138	182	[a]	same specimen. a = 0.30 in., l = 0.90 in.
1-in. plate......	1000	185	195	...	195	[a]	a = 0.34, l = 1.1 in.
1-in. plate......	1000	193	202.5	139.4	300	[b]	slow bend specimen. 0.875 by 0.875 by 4 in.
Side center weld metal 1-in. plate........	as TIG welded	173.0	203.0	118.3	253	[b]	slow bend specimen as above, avg. of three weldments

[a] *Aerospace Structure Metals Handbook*, Syracuse University Press, Syracuse. N. Y., 1964 edition, Section FeUH, Code 1221.

[b] E. A. Steigerwald, TAPCO group of Thompson-Ramo Wooldridge, private communication to J. G. Hill, United Technology Center, Oct. 25, 1963.

Panel Discussion

STP381-EB/Apr. 1965

INTRODUCTION TO THE PANEL DISCUSSION

BY W. F. BROWN, JR.

During the planning for this Symposium it became quite evident that ample opportunity should be provided for those interested in fracture testing to ask questions of the authors and to make comments on their papers. Such opportunity is normally provided by a discussion period after each presentation, but this is almost always too short to be effective. It was therefore decided to devote an entire session to a panel discussion, the panel being made up of a group of people who have been closely connected with the ASTM Special Committee for Fracture Testing of High Strength Materials, and most of whom also wrote papers for the symposium. The panel discussion was based on questions submitted to the members. These related not only to information presented in the symposium papers but also included questions of general interest in fracture mechanics.

The panel was composed of the following persons:

W. F. Brown, Jr., chairman: NASA-Lewis, Cleveland, Ohio
T. J. Dolan, University of Illinois, Urbana, Ill.
G. I. Irwin, U. S. Naval Research Laboratory, Washington, D. C.
Paul C. Paris, Lehigh University and National Science Foundation, Washington, D. C.
W. F. Payne, Air Force Flight Test Center, Boron, Calif.
J. E. Srawley, NASA-Lewis, Cleveland, Ohio
C. F. Tiffany, Boeing-Aerospace Div., Seattle, Wash.
Volker Weiss, Syracuse University, Syracuse, N. Y.
A. A. Wells, Queens University, Belfast Ireland

The panel gave first attention to written questions submitted in advance of the meeting. An appropriate notice to this effect appeared as part of an article summarizing the activities of the ASTM Special Committee on Fracture Testing published in the March, 1964 issue of *Materials Research & Standards*. The response to this notice was gratifying; many pertinent and often penetrating questions were received in advance of the meeting both from persons in this country and from abroad. Questions and comments from the floor formed the basis for discussion in the last half of the session. These encompassed a broad range of experience in fracture testing, from high strength alloys to plastics. Unfortunately, time did not permit covering all of the written questions, nor was the panel able to resolve satisfactorily, in the time available, some of the points raised in the discussion from the floor.

The entire panel discussion was satisfactorily tape-recorded, and the following account is based on a transcription made from the tapes. The record is complete with the exception of those parts of the discussion from the floor which dealt with data not presented to the panel either before or during the meeting.

The panel members wish to express their appreciation to Mrs. M. A. Bishop of the Strength of Materials Branch, NASA-Lewis, for her efforts in reducing the tapes to typescript.

PANEL DISCUSSION

W. F. BROWN (*author*)—One of the authors has compared different analytical solutions for the symmetrically notched plate on the basis of solutions obtained by complex-variable techniques (conformal mapping procedures) which are stated to give very high accuracy. Mr. Paris, is there a basis for considering the accuracy of the solutions obtained by complex variable techniques to be higher than those available by other methods?

P. C. PARIS (*author*)—In my interpretation, this is strictly an elasticity problem to be solved. The accuracy of the solution of an elasticity problem can be "exact" if one satisfies the differential equations involved (that is, equilibrium, compatibility) and all of the boundary conditions of the problem with the mathematical solution. The solutions which are referred to in the question are approximate solutions, so it is a matter of judgment as to how well these approximate solutions suit each of the equations. There are some principles of theory of elasticity which help one to make these judgments. For example, if an error is made in a boundary condition which is well away from the crack tip and the error is of the nature of adding an equilibrium system of forces which has small dimensions, St. Venant's principle states that far away from that system of forces no appreciable change in stresses will be caused. Then there would be no error in stresses near the crack tip. The complex-variable methods to which the question refers are probably those used by Oscar Bowie. He uses methods of mapping of problems and he does this to a very high degree of accuracy, using very sophisticated mathematical techniques; probably his answers are well within 1 per cent. Similarly, other approximate methods, such as collocation techniques and energy methods, often give results which are equally good; but in some cases (difficult problems) the things which can be done give results only within 10 per cent. So, in summary, it is a matter of judgment on these problems, which is mainly a matter of understanding the details of mathematical analysis.

MR. BROWN—I would like to ask Mr. Paris another question. Does the mathematician have formal methods for predicting the accuracy of these solutions?

MR. PARIS—The best method is experience, as it is in many other situations. However, if you look at convergence, that is, how rapidly terms or results converge in a series, it is one means of judging the accuracy of solutions. For example, Isida has used methods in which extremely high convergence is present. Therefore, the confidence in the methods that he has used should be very high. Very often it is mainly a matter of convergence upon which the accuracy of approximate solutions are judged by the mathematician.

J. E. SRAWLEY (*author*)—May I ask Mr. Paris a related question? How accurate is the basis of comparison between the results of experimental compliance measurements of $\mathcal{G}$ and analytical calculations of K?

MR. PARIS—In theory, the compliance method is exact. But there is a question which is not quite resolved in my mind as to whether the compliance measurement should be interpreted as plane-stress or plane-strain. And, though compliance measurements should be exact, in practice they are difficult to perform. I think the compliance measurements which have been made, for example, at the Lewis Research Center of the National Aeronautics and Space Administration (NASA) have been done with extreme care, and from what I can gather should be very accurate. But let us point out one thing on this, that if the compliance measurements are plane-strain measurements, instead of plane-stress, then both Bowie's and Gross's solutions to the edge-notched plate (which we are really referring to here) are in disagreement with the compliance measurements.

MR. BROWN—Mr. Paris, I gather from what you are saying, that if we have competent mathematicians working on these problems and if their results agree, we probably have the right answer. Additional confidence is gained if we have experimental methods which check the mathematical techniques.

MR. PARIS—Well, yes. I would like to make one further comment. After going through all the papers and looking at all of the methods myself, I would be much more pleased if we could have two different analytical approaches to each problem and have them agree to within 1 per cent before we say "this is it."

MR. BROWN—That certainly would be desirable. Mr. Srawley and I have been accused of being overly concerned with the stress-analysis accuracy, considering that the reproducibility of material behavior is sometimes rather poor. Our concern stems in part from a lack of familiarity with all the mathematical solutions. However, a knowledge of this accuracy is necessary if we are properly to evaluate our fracture data. We do not demand an accuracy of 1 or 2 per cent, but we do want to know what the accuracy may be within reasonable limits. Very little attention seems to have been given to this question in the past.

J. I. BLUHM[1]—The apparent discrepancy between Bowie's results and those derived from compliance techniques is believed to stem from the fact that the specimen configuration and loading conditions for the two approaches are different. Bowie's analysis relates to a specimen with uniform distribution of stress, whereas compliance measurements are based almost without exception on pin loading. Compliance specimens generally are not long enough to permit the concentrated pin load to approach a uniform stress distribution at some section between the pin and the crack; since this would be a necessary condition for equivalence between the two approaches, the results should not be exactly comparable.

MR. BROWN—I disagree with that and would like to get Mr. Srawley's comment. He was the one responsible for these compliance measurements, and great pains were taken to avoid interaction between the stress fields of the notch and of the pins.

MR. SRAWLEY—In our compliance measurements we did establish by experiment what was a sufficient specimen length to avoid interference between the stress-field disturbance around the crack and those around the loading pin holes.[2] However, some specimen bending occurs in compliance measurement, just as in an actual crack toughness test, and this is not considered in the analytical procedures of either Bowie or Gross. The results show an increasing discrepancy with increasing crack depth between the experimental and analytical values of K. I attribute this primarily to the specimen bending effect. I would like to add that I think we have a more accurate knowledge of the dependence of $\mathcal{G}$ or K on crack length for single-edge-notched specimens, either in tension or bending, than for any other type of specimen, because we have accurate compliance data for these specimens which are in good agreement with the analytical results.

[1] Chief, Applied Mechanics Research Laboratory, U.S. Army Materials Research Agency, Watertown Arsenal, Watertown, Mass.

[2] J. E. Srawley, M. H. Jones and B. Gross, "Experimental Determination of the Dependence of Crack Extension Force on Crack Length for a Single-Edge-Notch Specimen," *NASA TN D-2396*, National Aeronautics and Space Administration, August, 1964.

MR. BROWN—I will direct the next question to George Irwin. What is meant by the onset of rapid crack extension and why does the committee equate this with the maximum load in a fracture test?

G. R. IRWIN (*author*)—The onset of gross plastic yielding of a tensile bar is usually abrupt, in a relative sense. It is natural, therefore, to use this as a measurement point to indicate the strength of the material relative to plastic yielding. In the case of fracture, the onset of rapid crack extension is abrupt to about the same degree and use of this as a measurement point for crack toughness is an equally natural choice. We cannot expect every material and test situation to provide a perfectly sharp measurement point for crack toughness. The problem here is not unfamiliar because lack of sharpness in the yield-point indication is often encountered. It is considered best to adopt such rules as are necessary so that a property characteristic of resistance to plastic yielding can be measured and recorded, and we must do the same thing for fracture. In case of measurement-point ambiguity in a crack toughness test due to lack of any abrupt starting point for onset of fast fracture, one can usually resolve the problem by selecting the place in the behavior pattern where the relationship of crack extension to load provides a nearest approach to abruptness.

The crack speed necessary to cause a maximum load point is roughly the specimen width divided by the load-rise time, which is a very small velocity. In addition, in the absence of crack extension, the load must increase until fully plastic yielding has developed. Thus, when onset of rapid crack propagation is abrupt and occurs prior to general yielding, a maximum load point occurs in coincidence with the initial acceleration of the crack speed.

MR. BROWN—I would like to refer the same question to Mr. Srawley who has been engaged in the problem of trying to measure the onset of rapid crack extension.

MR. SRAWLEY—In general, I agree with what Mr. Irwin has said. The onset of rapid crack extension is not always sharply defined, but the load at which it occurs is very little different from the maximum load recorded in the test. By taking it as occurring at maximum load, we remove any ambiguity about what load to use in calculating K_c or $\mathcal{G}_c$. The practical testing problem is not to define the load, but to define the crack length at onset of rapid crack extension, because the crack length may increase considerably in the last stage of the test while the load is almost constant. Even when a record of crack length versus time is obtained during a test, there is no apparent objective basis for choosing the point of onset of rapid crack extension—different investigators will choose significantly different values. The other thing I would say about the choice of the maximum load as the point of onset of rapid crack extension is that it is appropriate for use in connection with the concept of the crack-extension resistance curve.

I consider this a very promising basis for further exploration into the question of fracture toughness. For research purposes at least, it would be desirable to conduct tests to determine R-curves rather than simply $\mathcal{G}_c$, as elaborated in the symposium paper by Mr. Brown and me.

MR. BROWN—The next is a very practical question. Consider two materials of roughly the same yield strength and having the same fracture toughness (K_c) value, these values to be determined from the same type and size of specimen. In one case, the K_c responds to a relatively low gross-area stress combined with substantial slow crack extension, and in the other case with a higher gross-area stress but with less slow crack extension, so balanced that we get the same value in K_c. Which material is to be preferred for pressure-vessel application?

MR. IRWIN—The answer to that question depends upon the application. If the slow crack extension under consideration was due to an environment effect not present in service, then of course this particular amount of slow crack extension is not important. On the other hand, one can well recognize that there might be cases in service where the slow crack extension was quite possibly due to an environmental effect. In these cases one should consider the environmental effects when selecting materials for the service application.

MR. BROWN—I wonder if Mr. Dolan would care to comment on that? It is a practical application question.

T. J. DOLAN[3]—It seems to me that the answer depends on the individual circumstances involved. I could well visualize that if you are talking about a thin-wall pressure vessel where you were primarily concerned with getting something that would resist brittle rupture (and where it might be preferable to have a "leak before rupture" condition), the material with the slow crack growth would allow development of a crack through the wall and an obvious leak before a complete rupture of the vessel. However, if you're working with a thick-wall vessel where the wall thickness is such that the critical crack size would be reached before penetration through the wall, then you might draw the opposite conclusion. If design of the pressure vessel is based on a working stress as a fraction of the yield point, you would find that the steel which had the short crack at the critical stress condition has the larger plastic zone surrounding the tip of the crack. It is actually working in service at a stress which is a much lower fraction of the critical stress than was used to determine the K_c value; the short crack might be preferable from this viewpoint. I think perhaps the most important factor is whether or not the nature of the environment will stimulate slow crack growth to critical size.

MR. BROWN—We certainly should hear from Mr. Tiffany, because he gave the lead paper on practical application.

C. F. TIFFANY (*author*)—If the specimens contained different initial crack sizes, one might expect that the specimen with the smaller crack would fail at a high gross-stress level with only a small amount of slow growth, and the specimen with the larger crack would fail at a lower gross stress with a much larger amount of slow crack extension. In such a case, there would be no choice between the materials since one might expect them to behave in an identical fashion had the same crack size been used in both specimens.

If, on the other hand, it is specified that the initial crack sizes were the same in the two specimens, the same K_c values were obtained, and yet one material displayed a large amount of slow growth and low failure stress and the other displayed a small amount of slow growth and high failure stress, I would concur in Mr. Irwin's suspicion of an environmental effect. In that it is known that some high-strength materials are very susceptible to environmentally induced slow growth, I would be tempted to select the material which did not display the large amount of slow growth. Also, one might justify this selection merely on the fact that a higher failure stress is obtained with the material which did not have a large amount of slow growth.

MR. BROWN—Apparently the answer to this question cannot be given in any

[3] Professor and Head, Department of Theoretical and Applied Mechanics, University of Illinois, Urbana, Ill.

simple terms, but the discussion does indicate that we must always consider our fracture-test results in terms of the service conditions.

The next question is as follows: The stress analysis used for a through-crack plate specimen assumes a crack to have a straight front. However, in real situations, a crack front is usually curved. Depending on the crack length, the curved front can constitute an appreciable part of the total crack extension. At what point will this curvature introduce significant errors into the analysis?

MR. PARIS—There is a little discussion in my paper which bears somewhat on this question. If one has a straight crack front through a sheet, the stress-intensity value along that crack front will vary somewhat, since the sheet will have a local stress field which is plane-stress on the surface and plane-strain in the center. The displacements for plane strain would have to be smaller for the same K value. Consequently, displacement continuity implies that at the center there will be a tendency to have a higher stress-intensity factor than at the surface. The difference can be as much as about 5 per cent from the inside to the surface. Now that is partially the cause of the growth of the crack from the center at first, instead of from the outside. The plasticity involved also bears on this. The crack front then will become curved and a tongue will form, and when the tongue forms there will be two effects. First, the material which has not been fractured in advancing the center of the crack will tend to hold the crack closed and, by holding it closed, it will reduce the stress-intensity factor on the tip of the tongue-crack front. How much it will be reduced is a very difficult question to answer. Second, the curvature of the tip of the tongue also reduces the stress-intensity factor there.

MR. BROWN—Mr. Paris, would you care to comment on the stress-intensity factor associated with wing cracks produced by bending with the moments perpendicular to the sheet plane. As you know, these cracks intersect at the mid-thickness and produce a V-type crack front.

MR. PARIS—In that case, at the tip of the V the stress-intensity factor would be infinite, if it is a sharp tip. Slow crack extension would begin there immediately upon loading and produce a curved crack front. However, usually one should look at the gross-stress environment and not details at this fine a level. The average value of K along the crack front, which is the one given by the usual formulas, is ordinarily sufficient.

W. F. PAYNE (*author*)—Does not this curvature insure that the actual applied K at mid-thickness will be closer to the value calculated from surface-crack length? From a practical standpoint, this slight curvature would have a beneficial, rather than a detrimental, effect.

MR. PARIS—The curvature which forms is partially based on the tendency of the crack to equalize the stress-intensity factor along the crack front. But there is another complicating factor, since the surface material will be associated with plane stress and the center material with plane strain. The amounts of plasticity associated with each of these states, as well as the tendency for fracture, are different. Therefore, a higher apparent toughness at the surface leads to a higher stress-intensity factor at the surface than at the center, prior to sudden failure. Hence the curvature which occurs may overequalize and lead again to variation in K along the crack front which is difficult to estimate.

MR. IRWIN—I have two comments on the matter of crack-front curvature. First, one can consider the laboratory test in terms of how accurately it models some typical service situation. If the crack-front curvatures are similar in the laboratory test and the expected service situation, then the shape of the crack in the laboratory test should not introduce error.

The second comment concerns an interesting aspect of crack-front curvature which we noticed from examination of crack-arrest lines on adhesive-joint test specimens. In the testing arrangement used by Ripling and Mostovoy (Materials Research Laboratory), two long adherend bars, joined by the adhesive, are separated by forces acting on the bars at one end. It is essentially a stiff-adherend type of a peel test. The separating forces are quickly relaxed by crack extension. Thus a succession of onsets and arrests of crack propagation was observed as the test progressed. We noted the curvature of the arrest lines and thought this indicated an undesirable degree of plane-stress yielding influence at the side borders of the crack plane. However, when we doubled the thickness of the specimens, the curvature of the arrest lines was not significantly reduced. The reason for this can be understood if one reflects upon the anticlastic curvature of the upper and lower surfaces of a beam in simple bending.[4] Because of the anticlastic curvature tenddency, a straight crack front, extending across from one free surface face of a plate specimen to the opposite face, is not expected even in a material of extreme brittleness.

MR. BROWN—Moving on to the next question, I would like to ask Mr. Payne whether fracture toughness tests are now being incorporated into government specifications?

MR. PAYNE—Some ten years ago, J. A. Kies and others at the Naval Research Laboratory (NRL) introduced a fracture toughness requirement in the military specification on Plexiglas windshield material for aircraft. The efforts of W. S. Pellini and P. P. Puzak at NRL have resulted in certain toughness requirements for ship-plate materials, in terms of Charpy impact energy requirements supported by explosion tests and drop-weight tear-test studies. I believe the Army has also employed Charpy impact requirements in material specifications for armor-plate applications.

The Air Force has traditionally expected contractors to establish their own toughness requirements and standards. Divided thought and confusion prevail among contractors on this technical problem, and no industry-wide standards apply to Air Force procurement activities. The completion of standardization work by organizations such as the American Society for Testing and Materials will be necessary before a uniform toughness requirement is reflected by Air Force contractors. Even then, the specifications will be individual contractor specifications and will presumably vary in approach among contractors.

I can think of one example where an Air Force contractor has put in a surface-crack test in a steel-plate procurement. The specification requires three different specimen sizes and three different surface-crack lengths (sizes) per specimen size. Unfortunately, the specimen sizes relative to strength and toughness levels are such that even with the largest surface crack, one encounters general yielding. The result is a plasticity test, not an elastic fracture test. In that particular procurement, over 200 fracture tests have been conducted by the supplier and all tests have gone into general yielding. This does indicate that the toughness is somewhat more than the specimen is capable of measuring, but quantitative, elastic fracture-strength values were im-

[4] A. E. H. Love, *Mathematical Theory of Elasticity*, 4th edition, Dover Publications, N. Y., N. Y., 1944, p. 131.

possible. The end result is information of limited usefulness. Because the actual specifications are individually by the Air Force contractors, no consistent Air Force pattern to toughness in specifications can be found. In the Army and the the Navy, however, the situation is considerably different, although they use more conventional tests.

MR. BROWN—Mr. Heyer, in his symposium paper, has described a screening test procedure that seems straightforward and practical. Mr. Srawley, under what circumstances would it be necessary for the alloy developer to go beyond this and to determine actual K_c values?

MR. SRAWLEY—For screening purposes the procedure which has been developed by the ASTM Special Committee on Fracture Testing of High-Strength Metallic Materials and evaluated by round-robin program, as discussed in Mr. Heyer's contribution to this symposium, seems to me to be entirely adequate. By screening, I mean selecting the more promising from a variety of combinations of such variables as composition and heat treatment which a given organization might wish to investigate. I see no point in subjecting every conceivable variation to an elaborate fracture toughness testing program which would be much more expensive. However, when the screening program turns up what appears to be a promising material or treatment, then this should be subjected to a very thorough study of plane-strain crack toughness, covering the variables that may be important in potential applications, such as temperature, strain rate, and orientation of cracks with respect to fibering. As far as so-called plane-stress fracture toughness testing is concerned, $\mathcal{G}_c$ or K_c measurement, I do not believe that this should be done as a matter of course, but only in connection with specific applications. This point is discussed in the paper by Mr. Brown and me, in the section entitled "Variation of $\mathcal{G}_c$ with Crack Length and Specimen Width."

MR. BROWN—The study of plane-strain crack toughness becomes more difficult as the ratio of toughness to yield strength increases. For materials of low yield strength and very high toughness, very large specimens are required in order to provide crack sizes sufficiently large to cause fracture before yielding. It would seem from a practical viewpoint that there is some upper limit of crack size beyond which we need not be concerned with fracture toughness tests. Mr. Srawley, would you please give us your thoughts on this?

MR. SRAWLEY—Frankly, I have not completely resolved this question to my own satisfaction, but it does seem to me that there is a point beyond which you do not need to go in most cases. If your material is such that you need a plane-strain crack toughness specimen that contains a crack several inches long, then the contemplated structure will be able to tolerate cracks that are at least the same size. If this is not sufficient for assurance of safety, then I would suggest that consideration be given to redesign of the structure or to other measures which would guarantee that such large cracks did not occur.

MR. BROWN—Mr. Wells, would you care to comment on this matter? Your experience is primarily with lower-strength materials.

A. A. WELLS[5]—I beg to disagree with Mr. Srawley, and to suggest that thick plate structures of mild steel may need to tolerate defects inches long without fracture. They may be buried and undetected within the thickness.

---

[5] Professor, Department of Civil Engineering, Queens University, Belfast, Ireland; formerly deputy director, British Welding Research Assn., Research Station, Abington Hall, Cambridge, England.

MR. BROWN—Mr. Wells, what do you people do in the way of inspection? Some of these large defects you must be able to find by even rather crude inspection techniques. Are the vessels of such construction and put in such environments that they cannot be inspected regularly? Is that why your defects of critical size are so large?

MR. WELLS—High-temperature* and irradiated vessels cannot easily be inspected in service. Defects may also be pessimistically assumed to grow during service and between inspections. One considers particularly the possibility of fracture during cooling down after a period of service, due to the presence of one of these enlarged defects.

One can also consider the possibility of embrittled weld-heat-affected zones present in as-welded structures. Here the parent material may be capable of tolerating a long crack, but the embrittled region may not. Nondestructive testing can be of added importance in such cases. Fracture toughness testing on the embrittled material should also be worth the performance.

MR. PAYNE—Since you are concerned, there is one aerospace application I can think of that needed a large critical crack-size capability. A low-toughness aluminum alloy was used in a very large integral wing-tank structure. In my opinion, you could not effectively inspect the structure in any way except to encounter a fuel leak. This would then require a considerable critical crack length to insure leakage prior to failure.

MR. SRAWLEY—Returning to Mr. Wells's remarks, I did say that I had not completely resolved the question to my own satisfaction, and I recognize that his views and mine are colored by experiences of different kinds. He is more aware of large structures and large defects, while I am more conscious of small defects at high stress levels. I do acknowledge that there are cases where very large cracks occur, for instance, Pellini and Puzak[6] cite the case of a hydraulic press cylinder which failed from a fatigue crack which was about 16 in. long by 8 in. deep. I would like to ask Mr. Wells what he considers is a reasonable tolerable crack size.

MR. WELLS—For these situations I believe in Irwin's "leak-before-break" concept. In fact, if one can tolerate a twice-thickness crack in all parts then the structure is indeed a viable one.

MR. BROWN—Mr. Wells, do you really believe in leak-before-break calculations when applied to the low-strength heavy sections of interest to you? How do you make these calculations?

MR. WELLS—It so happens that we do not have to do the calculations. We have thick-plate testing facilities that permit us to gain experience on different types of steel at full scale. To quote some figures: a good quality 3-in. thick silicon killed steel that we use extensively (40,000 psi yield point) fractures at −10 C with a 6-in. long crack and at −40 C with a 3-in. long crack.

V. WEISS (*author*)—The difficulty in the discussion of this problem stems from the difference in viewpoints. One party may claim the absence of any danger or need to resort to sharp-crack fracture mechanics because extensive plastic flow must have occurred if the yield strength is required to fracture a part containing a 6-in. crack. Another party may insist on a solution within the sharp-crack fracture mechanics framework. This, then, requires the availability of a plasticity solution for a crack, such as McClintock and Irwin have indicated in their symposium paper. Such a solution

[6] W. S. Pellini and P. P. Puzak, "Fracture Analysis Diagram Procedures for the Fracture-Safe Engineering Design of Steel Structures," *NRL Report 5920*, Naval Research Laboratory, March, 1963.

would also considerably improve the plasticity-correction procedures now utilized for ultra-high-strength materials where sharp-crack fracture mechanics does apply reasonably well.

MR. WELLS—May I add a postscript, in view of Mr. Weiss's contribution? My quoted figures related to failure at yield-point stress, without substantial yield strain. For vessels subject to the first hydrostatic test, we are more interested in failure at $\frac{1}{2}$ per cent over-all strain with much smaller defects than 6 or 3 in., because modern design allows this amount of plastic strain at pressure-vessel nozzles and the like. Much of our effort on general yielding fracture mechanics has been to try to equate these two situations, of large defects with small applied strains, and small defects with large strains.

MR. PARIS—On to the same subject, I would like to cite the case of the skin of commercial transport airplanes, the current airplanes on which most of you flew here. In the long lives which are expected of these airplanes, sizable fatigue cracks may grow. They have to be discovered before they cause a disaster, and, as a consequence, it is current practice to design skins of the pressure cabins and wings for commercial transports so that they may sustain a very long crack; often cracks of 20 in. or more are required before a critical crack length is reached at the working stress level in these aircraft. Tests which do not simulate these conditions are not very good tests for choosing materials for this application. Though screening tests may be of initial help, programs which actually test the material at the nominal stress level involved in the airframe are most appropriate for this type of application.

MR. SRAWLEY—I would like to make it clear that my previous comments on screening tests were not intended to apply to the case that Mr. Paris has just discussed. I had in mind the use of screening tests in alloy-development laboratories. For aircraft skin applications, I would agree that fracture toughness tests utilizing appropriately long cracks are required. However, these would only be applied to materials which had already survived the screening stage.

MR. PAYNE—One application where the plane-strain fracture strength may have to be measured and analyzed empirically, rather than predicted from legitimate K_{Ic} data, is a small-diameter, thin-wall solid-propellant motor case containing surface cracks. The surface-crack expressions (as reviewed in Paris's paper) may predict too high a fracture stress for crack depths exceeding, say, half the thickness. For very deep cracks, the plastic zone extends through a significant portion of the uncracked thickness, if not entirely through the wall. The stress field is disturbed and no longer described by the linear elastic field equations.

On the other hand, crack sizes too small to propagate prior to net-section yielding are similarly outside the legitimate realm of elastic fracture mechanics. The smallest semicircular crack depth of interest would be about 0.6 $(K_{Ic}/\sigma_{YS})^2$. Hence, for thicknesses less than 1.2 $(K_{Ic}/\sigma_{YS})^2$, a semicircular crack depth sufficiently large to fail without general yielding will exceed half the thickness. The crack tip will be surrounded by a plastic-zone width of at least an additional 0.1 $(K_{Ic}/\sigma_{YS})^2$. This suggests that surface-crack tests on thicknesses less than about 1.0 $(K_{Ic}/\sigma_{YS})^2$ would have to be entirely empirical.

In 18 per cent nickel 300 maraging steel, with assumed K_{Ic} of about 100 ksi $\sqrt{\text{in.}}$ and yield strength of 300 ksi, a minimum wall thickness of 0.1 in. is required for meaningful surface-crack tests from the linear elastic analysis standpoint. The Air Force has sponsored fabrication of several 40-in. diameter cases (of the 300 maraging steel) with a design wall thickness of 0.045 in., well under the minimum 1.0 $(K_{Ic}/\sigma_{YS})^2$ thickness. Empirical fracture-test work would be required to establish flaw-size fracture strength relationships for surface cracks in this example. However, the framework of fracture analysis—especially the emphasis of gross applied stress at fracture—is useful as a guide for empirical analysis.

MR. BROWN—I have to stop discussion on that question and move on. The next question is: Has the influence of notch shape as well as depth and notch acuity been fully investigated? Mr. Srawley, will you comment briefly on this?

MR. SRAWLEY—The influence of notch shape is one of several details of fracture toughness testing which, in my opinion, have not been sufficiently explored. However, we do have some information about it which is summarized in Fig. 1. The data were obtained with single-edge-notched tension specimens of two kinds, one having a 60-deg angle notch and the other a 0.012-in. wide saw-cut slot. The specimens were ¼ in. thick and 3 in. wide, of 7075-T6 aluminum alloy. Most of the specimens had fatigue cracks extending from the slot or notch, and at the right-hand side of Fig. 1 we show a plot of the apparent K_{Ic} value versus the length of fatigue-crack extension. When the fatigue cracks are absent or very short, the apparent K_{Ic} is lower for the V-notch specimens than for the slotted specimens, but with sufficient fatigue-crack extension the results converge to a common value of K_{Ic}. Thus the effect of notch angle is negligible, provided the notch is extended by a fatigue crack of adequate length, in this case at least 0.02 in. The ASTM Special Committee recommends that specimens should always be fatigue-cracked if they are to be used for valid K_{Ic} measurement. These results give some guidance about the necessary length of the fatigue crack, but ought to be supplemented by additional data for other materials and specimen thicknesses.

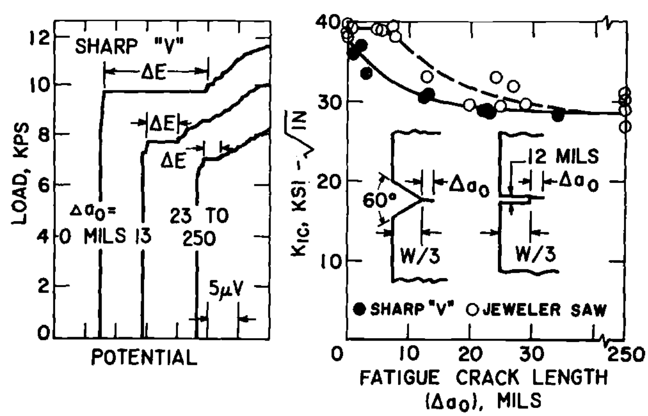

FIG. 1—Pop-in Behavior as Influenced by Fatigue-Crack Length for Single-Edge-Notched Specimens of ¼-In. Thick 7075-T6 Aluminum Alloy Plate.

There is another effect of the length of fatigue-crack extension, shown on the left-hand side of Fig. 1. With no fatigue crack, there is a very pronounced step in the record of load versus electrical potential change, indicating the sudden extension of a relatively large tongue of square fracture. With increasing length of fatigue crack, the magnitude of this initial pop-in indication diminishes, and the load at which it occurs decreases, corresponding to decreasing values of K.

MR. BROWN—I would like to ask Mr. Srawley another question which bears on this one. What is the influence of fatigue-cracking conditions such as maximum stress and resulting crack shape on the measured values of plane-strain toughness?

MR. SRAWLEY—Again, our information on this point is inadequate, but Fig. 2, taken from a previous paper of mine,[7] shows something about the effect of fatigue stress level. This shows the results of tests of surface-cracked specimens of $\frac{1}{16}$-in. thick H-11 steel sheet. The yield strength was 213,000 psi, and the specimens were fatigue-cracked in bending at three levels of the maximum nominal fiber stress, as indicated. The K value plotted in each case corresponds to the maximum load and the measured dimensions of the fatigue crack, that is, it is a K_{Ic} value if we assume that no slow crack extension occurred. There are ten points for each of the three fatigue-stressing levels, and there is no significant difference among the three average K values. However, the dispersion of the results is greater for the higher fatigue-stressing levels than for the lowest level.

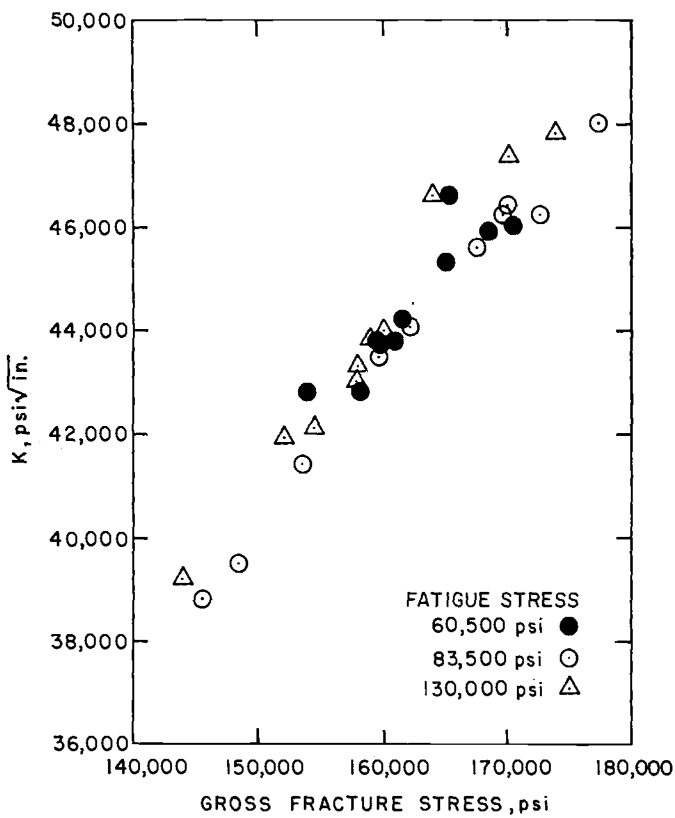

FIG. 2—Plot of K Versus Gross-Fracture Stress for Three Groups of Specimens.

[7] J. Srawley, "Small Fatigue Cracks as Fracture Origins in Tests of High Strength Steel Sheet," *Proceedings*, Am. Soc. Testing Mats., Vol. 62, 1962, pp. 734–741.

In general, we recommend that fatigue cracking should be conducted at the lowest practical nominal stress level, in no case greater than half the yield strength of the material. It should take something like 15 or 20 min to complete the fatigue cracking of a specimen at 1500 cpm. If the number of cycles is much less than 20,000, the fatigue-stressing level is too high. The crack shape is another guide as to whether the fatigue-cracking conditions were satisfactory. The broken surface of a specimen should always be examined after a test, and if the fatigue crack deviates markedly from being flat and square to the specimen surface, or if the fatigue-crack front in a single-edge-cracked or center-cracked specimen is markedly curved, then the result of the test should be regarded with some suspicion.

MR. DOLAN—There is a tendency, when people are anxious to get specimens prepared rapidly, to fatigue-crack these at rather high stresses and for very short periods of time. I was surprised that, in the Hartbower and Orner paper, they indicate that it takes only 2 min to produce fatigue cracks in their Charpy specimens. This to me seems to be abnormally short time; even if you run them at 1500 cpm, you have only about 3000 cycles to initiate and to develop the crack. To produce a sizable fatigue crack in this period of time requires a cyclic strain of at least 1 per cent, which means that the zone in advance of the tip of the crack has large plastic deformations developed which are abnormal as compared with what you would get by cracking with a low-amplitude cyclic stress. I recommend in general that fatigue cracking be done at nominal stresses much below the critical fracture stress you are expecting to reach in the subsequent test.

MR. BROWN—I think that is a good point. However, if we follow the committee's recommendation, this condition will be met for most tests. Paul Kuhn and his associates at NASA have, over the past few years, been analyzing crack-propagation data by means of a "notch analysis" based on a modified Neuber stress-concentration factor. Mr. Kuhn has prepared a written discussion which comments both on his approach and on fracture mechanics as we have been discussing it here.

P. KUHN[8]—Fracture mechanics has been and is an invaluable tool for dealing with a subject of vital importance in structural engineering. However, an increasing amount of dissatisfaction has been expressed on two main scores:

(*a*) unsatisfactory agreement between notch-toughness values obtained with different specimen configurations, and

(*b*) inaccuracy of predictions of strength of cracked structures (such as pressurized cylinders).

Most of the dissatisfaction has been expressed by engineers dealing with sheet material, and the entire following discussion is strictly confined to sheet material with through-cracks.

A critical examination of fracture mechanics and comparison with other approaches in the area indicated show that most of the trouble can be charged to the fundamental formulation of fracture mechanics, specifically, the use of the quantity, $S(a^{1/2})$, to describe the notch toughness of a material. The following discussion will give the reasoning that leads to this conclusion.

Fracture mechanics in its present form is essentially a stress-concentration approach.[9] Of basic importance in the following discussion is the range of stress-concentration factors of practical interest. Two types of application may serve as examples.

[8] Assistant Chief, Structures Div., National Aeronautics and Space Administration, Langley Research Center, Hampton, Va.

[9] "Fracture Testing of High Strength Sheet Materials," *ASTM Bulletin*, No. 243, January, 1960, p. 30.

In most types of pressure vessels, it is desired that the vessel be able to develop a hoop stress equal to the yield stress in the presence of cracks. The associated stress-concentration factor, therefore, must be less than the ratio of ultimate strength to yield strength (roughly); this ratio is usually less than 1.2 and seldom exceeds 1.5.

In the screening program for supersonic transport skin materials, the 1-in. wide ASTM V-notch specimen was used. On the basis of service experience with aluminum alloys, the rule of thumb was formulated that materials would probably be not acceptable if they had a notch-strength ratio less than 0.7, corresponding to a stress-concentration factor of 1/0.7, or 1.4.

These two examples demonstrate that many practical applications involve stress-concentration factors less than 1.5; factors substantially greater than this occur only in special applications (pressure cabins of airplanes). This writer is not aware of any practical application on metal structures involving a stress-concentration factor as large as 10 (failure at one tenth of the ultimate strength).

Consider now a wide sheet containing a transverse crack and subjected to tensile stress. The tensile stress causing failure may be defined by the formula

$$S = \frac{F_{tu}}{SCF} \quad \text{.............. (1)}$$

provided that the SCF (stress-concentration factor) is suitably calculated. For the purpose of mathematical analysis, the crack can be represented by an elongated ellipse; the theoretical stress-concentration factor for such a hole is

$$K_T = 1 + 2(a/\rho)^{1/2} \quad \text{........ (2)}$$

where a is the major semi-axis and ρ the tip radius. For cracks in actual materials (with an arbitrary amount of ductility), the stress-concentration factor can be written as

$$SCF = 1 + C_1(a)^{1/2} \quad \text{....... (2a)}$$

where C_1 is a materials constant but dependent on temperature. The method presented by Kuhn and Figge[10] shows how C_1 can be calculated from known materials' properties and shows numerous applications to aluminum alloys; other papers[11,12] show applications to titanium alloys.

Griffith, interested in developing a theory for the fracture of glass, simplified, Eq $2a$, to the form

$$SCF \approx C_1(a)^{1/2} \quad \text{......... (2b)}$$

Substitution of Eq $2b$ into Eq 1 gives

$$S = \frac{F_{tu}}{C_1(a)^{1/2}} \quad \text{............ (3)}$$

and transferring $a^{1/2}$ to the left side gives

$$S(a)^{1/2} = \frac{F_{tu}}{C_1} \quad \text{........... (4)}$$

The quantity on the left is the notch-toughness parameter used in fracture mechanics in its earlier form. Since the two quantities on the right (F_{tu} and C_1) are materials constants (at least in good approximation) it might be expected that $S(a^{1/2})$ is also a materials constant. Unfortunately, this expectation is not fulfilled because the simplified expression, Eq $2b$, for the stress-concentration factor which leads to Eq 4 is not accurate enough except in extreme cases.

The use of Eq $2b$ in place of Eq $2a$

[10] P. Kuhn and I. E. Figge, "Unified Notch-Strength Analysis for Wrought Aluminum Alloys," *NASA TN D-1259*, National Aeronautics and Space Administration, 1962.

[11] P. Kuhn, "Notch Effects on Fatigue and Static Strength," *I CAF-AGARD Symposium on Aeronautical Fatigue*, Rome, Italy, April, 1963.

[12] P. Kuhn, "The Prediction of Notch and Crack Strength Under Static or Fatigue Loading," SAE-ASME Air Transport and Space Meeting, New York, N. Y., April, 1964.

means that 1 has been omitted (or subtracted) from the stress-concentration factor. In Griffith's problem, this was permissible because he was dealing with a stress-concentration factor of about 100 (ratio of theoretical to actual tensile strength of glass). However, as noted earlier, the stress-concentration factors of interest in structural engineering are usually less than 1.5. Clearly, *an intolerable error is introduced if 1 is subtracted from a factor of 1.5.* The error introduced by subtracting 1 might be considered acceptable if the stress-concentration factor were greater than 10, but as pointed out earlier, there appear to be no cases of practical interest in this range.

The maximum error is introduced in the limiting case of vanishingly small cracks. If Eq 4 is used in reverse to predict the failing stress of such a specimen from a given value of $S\ (a^{1/2})$, an infinite stress is predicted, while the answer should, of course, be F_{tu}. This implies, furthermore, that the prediction is seriously in error for any short crack.

The method used by my associates and me[10,11,12] employs the complete Eq 2*a* instead of Eq 2*b* and correlates very successfully for one material, tests on center-cracked specimens ranging from 35 to 9 in. wide, edge-notched specimens 2.25 in. wide, and V-notch specimens 0.64 in. wide. By contrast, $\bar{K}_c = 60$ for $w = 2.25$ in., $\bar{K}_c = 90$ for $w = 12$ in., and $\bar{K}_c = 105$ for $w = 35$ in. These observations (and others) indicate that most of the width-correlation troubles experienced in fracture mechanics can be attributed to the same source—use of the simplified Eq 2*b*.

The unsatisfactory ability of fracture mechanics to correlate tests on different widths has led to the introduction of plastic-zone correction. This correction does improve the results. For instance, for specimens with vanishingly small cracks, the formula no longer predicts infinite strength. However, in some typical cases, the predicted strength is still about 50 per cent higher than the tensile strength, an error which can hardly be considered tolerable. Moreover, since the correction is tied to a physical characteristic (plasticity) of the material, while the main trouble is the algebraic one of using an unduly simplified stress-concentration factor, the correction can hardly be expected to be very successful over a wide range of widths and materials.

MR. BROWN—Thank you, Mr. Kuhn, for your comments. Before going further I would like to ask you whether or not stable crack-extension measurements were made on the wide-plate tests you referred to. Such measurements would be necessary properly to calculate K_c according to the fracture mechanics equations as presented in the reports of the ASTM Special Committee on Fracture Testing of High-Strength Metallic Materials. Also these measurements would permit calculation of the net stress at fracture instability. If this were above the yield strength, then the results would not be suitable for analysis by fracture mechanics.

MR. KUHN—In the tests that we have made and those made by many others in the airframe industry, no attempt has been made to measure stable crack extension or determine when unstable extension starts. The point that I make, and I know other people agree, is that what matters is the fracture load. It makes no difference whether at that time the crack propagates at 300 or 3000 ft/sec. As long as it fails, it fails.

MR. BROWN—Mr. Irwin wishes to reply to Mr. Kuhn.

MR. IRWIN—Mr. Kuhn suggests that the fracture mechanics approach is handicapped by neglect of the additive factor of 1 in his Eq 2*a* as compared to his Eq

2b. A large degree of equivalence exists between the stress-concentration factor approach and the fracture mechanics approach, as has been pointed out in fracture mechanics papers. However, the degree of equivalence is somewhat less than one might infer from Mr. Kuhn's discussion. He assumes we should first replace the influence of the plastic zone by an elliptical rounding of the crack shape. Next, we should derive the maximum stress at the fictitious notch root by linear elastic analysis and use this maximum stress as the fracture criterion.

Mr. Kuhn's Eq 2 is valid for a round hole in a plate ($\rho = a$). The resulting value of $K_T = 3$ is the familiar stress-elevation factor for a round hole in uniaxial tension. For biaxial tension, the added term of 1, to which Kuhn directs attention, does not apply and (for the round hole in biaxial tension) $K_T = 2$. Equations 2a and 2b from his discussion are not suitable for comparison with linear elastic fracture mechanics. Let us consider a two-dimensional crack of length $2a$ in an infinite plate with axial tension σ normal to the crack. If an elliptical boundary is constructed around but close to the crack with the ends of the crack at the focal points, the stress σ_y where the ellipse intersects the x-axis is given by

$$\sigma_y = \sigma(a/\rho)^{1/2} \qquad (5)$$

where ρ is the radius of curvature at the end region of the ellipse. From Mr. Kuhn's Eq 2, if this ellipse is regarded as a free surface, the stress, σ_y, at the same point is given by

$$\sigma_y = \sigma[1 + 2(a/\rho)^{1/2}] \qquad (6)$$

From comparison of Eqs 5 and 6, one sees that the factor of 2 multiplying $(a/\rho)^{1/2}$ corresponds to the $K_T = 2$ relationship for a round hole with biaxial tension. The added factor of 1 in Eq 2a is due to Mr. Kuhn's assumption of uniaxial rather than biaxial tension. When he draws a fictitious ellipse through the plastic zone to represent the influence of plastic-flow stress relaxation, he prefers to regard this ellipse as subject to free-surface stress conditions. This preference and the specialization of the stress state to uniaxial tension are responsible for the difference between Eqs 5 and 6 for σ_y. The stress-concentration factor approach used by Mr. Kuhn and the fracture mechanics approach are (or should be) mathematically equivalent in the representation of stresses in the elastic stress field at distances of, say, 5ρ or more from the focal points of Mr. Kuhn's ellipse. Mr. Kuhn's comment should be interpreted merely as a statement that he thinks the proper fracture criterion is a maximum stress derived in the special way indicated above, and he thinks fracture data are better represented when such a criterion is used. These opinions are based upon some experience and are deserving of respect. However, his reference to "intolerable error" in basic mathematical aspects of fracture mechanics injects an unnecessary aspect of controversy and is inappropriate. For example, it is impossible to predict a strength greater than that for general yielding, as claimed by Mr. Kuhn, unless the fracture mechanics is improperly used. We can recognize that many specialized ideas about the proper criterion for fracture exist, including Mr. Kuhn's, and these deserve trial in future research. However, the basic mathematical treatment of linear elastic fracture mechanics is quite straightforward and does not contain "intolerable" mathematical errors.

Mr. Kuhn's representation of the crack as an ellipse through the plastic zone with free surface boundaries is intended to adjust for the effect of plastic strains near the crack. The fracture mechanics adjustment for plasticity attempts to maintain both a greater degree of simplicity and a better situation for linkage to methods of elastic-plastic analysis.

As was pointed out in the McClintock and Irwin paper given in this symposium, the elementary plasticity correction thus suggested consists in adding to the crack length an amount

$$r_y = \frac{1}{2\pi}\left(\frac{K_c}{\sigma_y}\right)^2$$

This procedure, where σ_y is the uniaxial yield strength, preserves the analysis simplicity of linear elastic fracture mechanics and the one-parameter nature of the fracture criterion. More sophisticated corrections for plasticity are possible which would permit a closer representation of data in the high stress level range. However, the necessity of this for practical applications is not yet clear.

The disadvantages of the stress-concentration factor approach are primarily in terms of complexity and overspecialization. The fact that the stress-concentration factor is dimensionless tends to distract attention from the central importance of the crack-size length factor. Also the stress-concentration factor viewpoint is rather biased toward a maximum stress type of fracture criterion. In contrast, the fracture mechanics approach is sufficiently simple and unspecialized so that it is relatively easy to supplement the analysis so as to introduce criteria such as critical stress, critical strain, or critical displacement at the crack border when circumstances appropriate for these ideas seem to be present.

MR. WEISS—The stress-concentration factor approach that Mr. Kuhn has presented is indeed a very satisfactory approach for cases where one deals with mild notches. We at Syracuse, and especially George Sachs, devoted a great deal of energy to this type of work. It is a more complicated approach than the straightforward, neat, one-parameter approach of elastic fracture mechanics. It involves knowledge of the stress-concentration factor, the stress gradient, and also the stress state at the root of the notch. It is affected by the relative notch depth, by the material ductility or plasticity and it has inherent in it a dimensional material constant, the equivalent particle size, ϵ or η. All these quantities must be related to the deformation characteristics of the material because what determines fracture is not the original specimen geometry but the geometry at a point in the specimen's deformation history just prior to fracture. For example, two identical specimens, one with a large plastic zone, the other one with no plastic zone, will certainly have a different fracture behavior.

Now, while Sachs was considerably concerned with mild notches for the solution of design problems, he was also very insistent about requiring the testing of sharper and sharper notches in order to arrive at a comparative evaluation of materials. We did not consider fatigue cracks at the time, but we used the sharpest notches that could be machined. Mr. Irwin's statement is certainly correct that in some alloys it does not make too much difference whether the root radius is 0.003, 0.001, or less than 0.001 in. We have, however, tested alloys which are quite sensitive to reduction in root radius in this range down to fatigue cracks. H-11 and 300M steels heat-treated to high strengths and tested at low temperatures are cases in point. Such a situation represents an actual engineering problem and it has its root in the so-called plasticity dilemma. If the material and the notch or crack geometry just prior to the onset of fracture is represented by a low stress-concentration factor, a high ratio of notch strength to tensile strength, or a high ratio of crack strength to yield strength, then plasticity effects must have modified the original shape considerably to produce the observed effects. The development of an analytical treatment of these processes, most likely in terms of properties available from careful tension tests, is one of our ambitious goals.

The data that Mr. Kuhn reported here show the lowest K_c value for the smallest specimen and an increase with increasing size. I wonder if this is not one of the virtues of the plasticity correction as proposed by Mr. Irwin: it gives a conservative estimate for small specimens where the plastic-zone size and the specimen dimensions are comparable. In using such data, one must however, guard against a transition from plane stress to plane strain beyond the point where curve of the K_c versus size or width has levelled off.

MR. TIFFANY—I would like to comment on Mr. Kuhn's statement that I should only be interested in the failing strength of a structure with a pre-existing crack. I take exception to this. I am not so much interested in the failing strength as I am in knowing what the critical crack size is at the maximum operating or limit stress levels in the structure. Further, I am interested in knowing what initial crack size I might expect in the structure and how many load cycles and how much time at load can be encountered before this initial crack grows to critical size and failure results.

MR. KUHN—I would like to point out that calling our notch analysis a linear elastic analysis is incorrect. Although I passed over that point, I did mention that we applied two successive correlations, one for size effect and one for plasticity; we have, therefore, in effect, an engineering approximation to a nonlinear theory which involves plasticity. It is an engineering method and it does not go all the way, but it does carry considerably farther than using an elastic linear theory.

As a result of using notch analysis, we not only get a much better correlation over the full range of specimen widths (from $\frac{1}{2}$ to 35 in.), but we also avoid the complete breakdown of the formula for zero crack length and for 100 per cent crack length which is characteristic of the K_c formula. Notch analysis says that for either zero crack length or 100 per cent crack length the net-section stress is equal to the ultimate tensile strength in the case of a crack; consequently, it does not need the artificial cut-off line which says that above the yield strength or 0.8 of the yield strength the theory becomes invalid. Notch analysis is valid up to some indefinite point well above the yield—possibly up to the ultimate for cracks. I would also like to make a comment with respect to Mr. Tiffany's remark that he is not interested in the strength. This also bears on the remarks which Mr. Weiss made. The test of a fuselage costs on the order of a million dollars, and that test has to be made with a crack length specified by the Federal Aviation Administration (FAA). The designer would like to be sure that the fuselage does not blow up prematurely when FAA witnesses are standing around. Need for a second million-dollar test, damage to company prestige, and possible loss of sales are potent reasons for being interested in a good estimate of the strength of the cracked fuselage before the test is made.

I. FIGGE[13]—Several methods have been proposed to predict the residual static strength of structural parts containing cracks and notches. Other methods have been proposed which provide a useful tool for comparing materials on a notch-toughness basis. Each of the

[13] Structures Div., National Aeronautics and Space Administration, Langley Research Center, Hampton, Va.

methods has its limitations; in their present form, some are valid only for sheet specimens with through-cracks; others become invalid when the crack is short; and all appear to be questionable when the net-section stress is in the plastic range. Consequently, there is considerable difficulty in deciding which method is best to use for a specific problem. I believe it would be timely to consider defining the range of applicability of the various methods. This would probably mean a comprehensive study of such factors as the geometrical, mathematical, and loading limitations and also might include the probable percentage of error that might be expected. Such an effort would not only aid the designer in selecting the most appropriate method for his particular problem but would also give direction to future studies of fracture toughness.

MR. BROWN—Mr. Figge is correct when he suggests that systematic programs be established with the objective of defining the range of applicability of the various fracture test methods now in use. This procedure is quite obviously the most efficient and logical one to follow. However, it would require a concentrated effort lasting several years. Unfortunately, the persons and organizations best qualified for such a program are so busily engaged in trying to apply the concepts now in vogue that they are allowed insufficient time to plan and carry out long-range research programs of this type. Under these circumstances, our test specimens sometime become full-scale structures and such specimens are both difficult to analyze and rather expensive.

The remedy, I think, lies with the recognition by management that fracture testing research *per se* deserves continuous support which is completely divorced from specific hardware programs.

I am sorry to have to close this discussion that presents interesting and apparently divergent points of view. My understanding is that Mr. Kuhn will present his approach to the fracture problem at a forthcoming meeting of the ASTM Special Committee on Fracture Testing of High-Strength Metallic Materials. We certainly look forward to these further discussions.

HERSCHEL SMITH[14]—I would like to ask Mr. Tiffany whether it is feasible to lower the operating stress of a service structure with time in service in order to stay within the safe fatigue or static stress levels set by the particular fracture toughness of the material and the length to which cracks may have grown?

MR. TIFFANY—There is an actual service example for which we have done exactly that. The missile helium tank which I mentioned in my paper for this symposium is an example. This particular tank was designed so that the applied stress at maximum operating pressure was 25 per cent below the uniaxial tensile ultimate strength of the material and it was proof-tested to 1.1 times the maximum expected operating pressure. The missiles are stored with these tanks pressurized continuously except for an occasional depressurization when personnel are in the vicinity of the missile.

When these tanks were initially put into service, one helium tank failed after 21 hr at operating pressure. The failure origin was found to be a forging inclusion which had an initial size approximately 80 per cent of the critical size. During the 21 hr at stress, the flaw grew to critical size and failure resulted. As a result of this failure, an extensive investigation was performed to determine fracture toughness and subcritical cyclic and sustained stress flow growth characteristics of the tankage materials.

---

[14] Mechanics Div., Naval Research Laboratory, Washington, D. C.

Quite a bit of the data are given in the paper.

Probably the most significant outcome of this investigation was that sustained fracture specimen tests indicated that an initial flaw which was approximately 70 per cent of the critical size or greater could grow to critical size with sustained stress and that a successful proof test to 1.1 times operating could not guarantee that such a flow would not be present in the vessel when it was put into service. The successful proof test indicated that the maximum possible initial flaw size was $(1/1.1^2)$ 100, or 83 per cent of the critical size. Any tanks which actually contained flaws between about 70 and 83 per cent of critical size might then be expected to fail under sustained stress loading. Those greater than 83 per cent should fail the tank during the proof test.

It was apparent that either a higher proof pressure should be used so as to guarantee a smaller maximum possible initial flaw size, or the operating stress should be lowered, which would increase the critical flaw size and thus lower the maximum possible initial flaw size in terms of percentage of critical size. Since the proof stress using the 1.1 factor was already approaching both the material's tensile yield and ultimate strength, it was not felt that the proof stress could be increased. Consequently, it was decided to lower the storage pressure in the missile tanks and bring them up to full pressure immediately upon firing. This was accomplished by incorporating ground supply tanks in the missile shelters.

Z. P. SAPERSTEIN[15]—Perhaps this question should be addressed to Mr. Hartbower, who is interested in precracked Charpy tests, but it applies equally to other tests that we are considering. In the case of Charpy testing, the transition temperature for many materials is not well defined and covers a rather broad range. It is not one precise, single temperature. Within this transition-temperature range we frequently observe a good deal of scatter. With this thought in mind, can we use a Charpy test (or, for that matter, any other test) as a screening test when it is possible that transition-temperature ranges may overlap or be in close proximity so that we may be comparing a specimen on the tail of one transition-temperature curve with that on the plateau of another? Is it possible that in all types of fracture tests we should look at the properties over a temperature range?

C. E. HARTBOWER—It was learned many years ago that one must test over a range of temperature encompassing anticipated service conditions. If one were to test at room temperature exclusively and compare materials A and B, material A might be found to be much better than material B at room temperature; whereas, on testing at some lower temperature (sometimes as little as 10 F) both materials may be lacking in toughness. This points up one of the advantages in precracked Charpy impact testing. One can run tests at temperatures down to liquid-nitrogen temperature and up to +400 F almost as easily as at room temperature. For example, in screening 6Al-4V titanium for use in rocket-motor cases, precracked Charpy tests are made at the expected operating temperature, an intermediate temperature, and room temperature. In some heats of 6Al-V4 titanium, all bought to the same specification and all heat-treated to the same strength, the precracked Charpy test shows the toughness to be increased by a factor of 2 on raising the test temperature from room temperature to +300 F; whereas other heats show little or no change. Testing

[15] Douglas Missile and Space Systems Div., Douglas Aircraft Company, Santa Monica, Calif.

over a range of loading rates is equally as important as testing over a range of temperature in some materials. When tested in slow bend and in impact, the precracked Charpy test sometimes shows unexpected trends, as Mr. Krafft pointed out in his symposium paper. Mr. Saperstein's comment suggests that scatter may invalidate the Charpy test for purposes of screening; this is not clear. I agree that when the scatter is great in a given material condition, it is difficult to interpret the results.

Mr. WELLS—I am very interested in the Charpy test. We have tried to embrace the Charpy specimen within our treatment of cracking under fully plastic conditions, using the crack-opening displacement fracture criterion, and find on this basis that there should be proportionality between $\mathcal{G}$ and W/A. One regards Mr. Hartbower's correlation between these two quantities as satisfying because he sticks to the same thickness in his Charpy testing as in the material being examined. I think that this is important and that the transition observed in testing in this way has its counterpart in ASTM fracture toughness testing in the sense of distinguishing between plane-strain and plane-stress conditions. The scatter observed in Charpy testing, sometimes called "bimodality," is evidence of hovering on the brink of the one or the other.

However, if one performs a Charpy test with a standard thickness specimen for the purpose of assessing a thick material, the thickness of the material will also need to be taken into account, because the transitional onset of plane-strain fracture will occur at a larger W/A or fracture toughness value for the full thickness of plate. The small-specimen test under these circumstances is nonconservative.

MR. HARTBOWER—I agree with Mr. Wells that the Charpy test should be performed with a specimen encompassing the full thickness of the material, insofar as possible. The limiting thicknesses in precracked Charpy testing encompass a reasonably broad range from approximately 0.06 to 0.80 in.; that is, material in this range can and should be tested in the full thickness. Returning to the question raised by Mr. Saperstein regarding scatter in testing over a range of temperature, it is important to recognize that scatter in the Charpy test varies considerably from material to material and from heat to heat. I recall one dramatic difference in scatter from end to end of a single $2\frac{1}{2}$-in. thick plate. One end of the plate had an ASTM grain size of about 3 and the other end about 8. The material from the two ends of the plate differed widely in that the transition curve of the coarse-grain end involved a scatter band approximately 100 F wide and that of the fine-grain end was less than 20 F wide.[16] Such variation in scatter in a single plate is a special case; however, variable scatter from heat to heat is common in some materials. However, in some materials or material conditions, scatter in the precracked Charpy test is practically nonexistent. One such material was supplied by Mr. Srawley while at the Naval Research Laboratory.[17]

MR. BROWN—Regarding the thickness effect generally observed in fracture tests, to what extent is the variation of K_c with thickness thought to be a geometry effect and to what extent is it a result of metallurgical variation?

---

[16] C. E. Hartbower and W. S. Pellini, "Mechanical and Material Variables Affecting Correlation," *Welding Journal*, Vol. 29, No. 7, July, 1950, p. 356-s.

[17] G. M. Orner and C. E. Hartbower, "Sheet Fracture Toughness Evaluated by Charpy Impact and Slow Bend," *Welding Journal Supplement*, Vol. 40, No. 9, September, 1961, p. 411-s. Figure 12 shows a shift in the precracked Charpy transition curves both with thickness and melting practice, together with remarkably little scatter in the test data.

MR. BLUHM—It has been suggested that the thickness effect on fracture toughness, $\mathcal{G}_c$ (or K_c), which is generally observed at a fixed temperature, can be explained upon the basis of simple geometric considerations.[18,19] Furthermore, many data are available which tend to support this geometrically derived critical shear-lip concept. However, if temperature-transition effects are considered, then it must be emphasized that the model upon which this concept was based assumed that no metallurgical transformation occurred in the temperature ranges considered; and, further, that the crystallographic modes of shear or flat fracture, or both, did not change over these temperature ranges. It is quite conceivable (and this is suggested in the reference papers) that a flat fracture mode may change from one type to another (each being flat), but with significantly different energy-absorbing capacities. This would lead to a temperature-transition behavior which would be superposed on the geometry effect described in the basic reference.

B. G. JOHNSON[20]—My comments pertain to the stress-intensity ratio concept for predicting sustained load failure where the subcritical flaw-growth mechanism might involve surface absorption and subsequent diffusion to the crack front. For such mechanisms, one might expect geometric effects such as surface area and volume to affect correlation between test specimens and the actual part.

MR. TIFFANY—I think Mr. Johnson is referring to the fact that in a specimen test the sample being tested is generally quite small as compared to the hardware, consequently, the environmental effect may be less severe in the specimen than in the hardware. For example, in the case of hydrogen-induced crack growth the hydrogen content in the material may be dependent upon the total surface area exposed to the environment and in turn the rate of crack growth is dependent upon the hydrogen content. Also, I suppose it may be possible that surface area may play some role in stress-corrosion cracking.

All I can say to this is that I agree that specimen size may affect the results of sustained-stress fracture specimen tests. However, as I pointed out in my paper for this symposium, if such tests show a severe effect (that is, low apparent threshold stress-intensity level) when performed in the expected service environment, one should either do something to protect the material from the environment or possibly even change the material in the hardware. On the other hand, if the specimen tests show no apparent susceptibility to environmentally induced crack growth one might expect, but not necessarily guarantee, there will not be such crack growth in the hardware.

E. J. RIPLING[21]—I would like to describe a plane-stress fracture testing procedure on which our laboratory is currently working so that the panel members, particularly Messrs. Srawley and Brown, might give us their comments. The technique was initially developed for adhesive joints, but because it has some advantageous characteristics we have recently been using it on homogeneous systems, including metals and ceramics. Both the testing procedure and method of analysis, as applied to adhesives have been described.[22] Their application to solid members as opposed to joints is

[18] J. I. Bluhm, "A Model for the Effect of Thickness on Fracture Toughness," *Proceedings*, Am. Soc. Testing Mats., Vol. 61, p. 1324, 1961.

[19] J. I. Bluhm, "Geometry Effect on Shear Lip and Fracture Toughness Transition Temperature for Bimodal Fracture," *Proceedings*, Am. Soc. Testing Mats., Vol. 62, p. 914, 1962.

[20] Research engineer, The Boeing Co., Wichita, Kans.

[21] Materials Research Laboratory, Inc., Richton Park, Ill.

quite new and has not been formally disclosed as yet.

The unique characteristic of the sample is that it uses crack-line loading rather than a remotely applied load. Irwin and Kies have pointed out that for such loading the crack-extension force, $\mathcal{G}$, decreases rather than increases with crack length, a; consequently, crack extension is stable. Since a crack will propagate when $\mathcal{G}$ equals $\mathcal{G}_{Ic}$ (ignoring strain rate), stability results from the moving crack running into a region of decreasing $\mathcal{G}$, while $\mathcal{G}_{Ic}$ is constant for the material. It is this relationship between $\mathcal{G}$ and $\mathcal{G}_{Ic}$ that causes the crack to become self-arresting. For a remotely applied load, on the other hand, $\mathcal{G}$ increases with a so that once the crack begins to extend, it continues into a region of increasing $\mathcal{G}$, making crack extension unstable.

The sample shape that Sheldon Mostovoy and I have been using for adhesives is 2 in. tall, of variable thickness, and about 1 ft long. With this test specimen, we collect about 20 to 30 data points along its length so that we get a good average value of $\mathcal{G}_{Ic}$.

For homogeneous materials, the sample shapes have been more variable, ranging from 1 by 1 by 4 in. up to about the same size as used for the adhesives. A typical sample shape might be as shown in Fig. 3.

To conduct a test, a saw cut, F, is made some distance into the sample to serve as a crack starter. (We have most recently been making this cut from the two sides with a slitting cutter or abrasive wheel so that it has a winged front.) The crack starter is then extended to form a natural crack by pulling on rods that fit into loading holes, E. The crack initially jumps a considerable distance on this first pull, and we hope to minimize this distance by the use of the winged slot. After forming the natural crack, the sample is reloaded until the crack extends, it is then unloaded, and the process is repeated until the crack finally runs the full length of the sample. Each loading, of course, gives a value for $\mathcal{G}_{Ic}$.

Edge grooves are added to the sides of the sample to guide the crack. Other than this, the experimental details and analysis for homogeneous materials are identical with those described in the reference given in footnote 22 for adhesive joints.

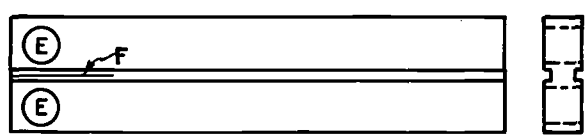

FIG. 3—Design of Fracture Toughness Specimen Using Crack-Line Loading.

This procedure for measuring $\mathcal{G}_{Ic}$ appears to have a number of advantages over those previously proposed:

1. The use of fatigue to form a sharp crack is not necessary.

2. The required loads for measuring plane-strain toughness are small.

3. The displacements for obtaining compliance are large.

4. Small samples can be used. For example, we used this test to measure the fracture toughness in the short transverse direction of 1-in. thick steel armor plate.

MR. SRAWLEY—The specimen proposed by Mr. Ripling is indeed most in

[22] E. J. Ripling, S. Mostovoy, and R. L. Patrick, "Measuring Fracture Toughness of Adhesive Joints," *Materials Research & Standards*, Vol. 4, No. 3, March, 1964, pp. 129–134.

teresting. While this specimen is mentioned in the symposium paper by Mr. Brown and me, we regarded it as a special case, appropriate for testing adhesive joints. We were not aware that it had been used successfully for homogeneous materials. However, I recollect now that there is a treatment of the cleavage of crystals by Gilman[23] that concerns a very similar sort of specimen. I am interested in the claim that there is no need for fatigue cracking of Mr. Ripling's specimen. Is this true for homogeneous materials or only for adhesive joints?

MR. RIPLING—We have not done a great deal of alloy testing, but from the little we have done there seems to be no problem. We use a 15-mil slitting saw to make a crack about 2 in. long. If the end of the crack is blunt, then it takes an appreciable amount of energy to get it to make the first jump. If you want the crack to jump only a small distance, you can put a C-clamp downstream on the sample and the crack then cannot run past it. I do not see how a crack formed in this way can differ from a running crack that we encounter in real circumstances. On the adhesive work, we use samples about 1 ft long and 2 in. deep and we get 20 to 30 data points along the length of the sample so that we get a good average on $\mathcal{G}_c$.

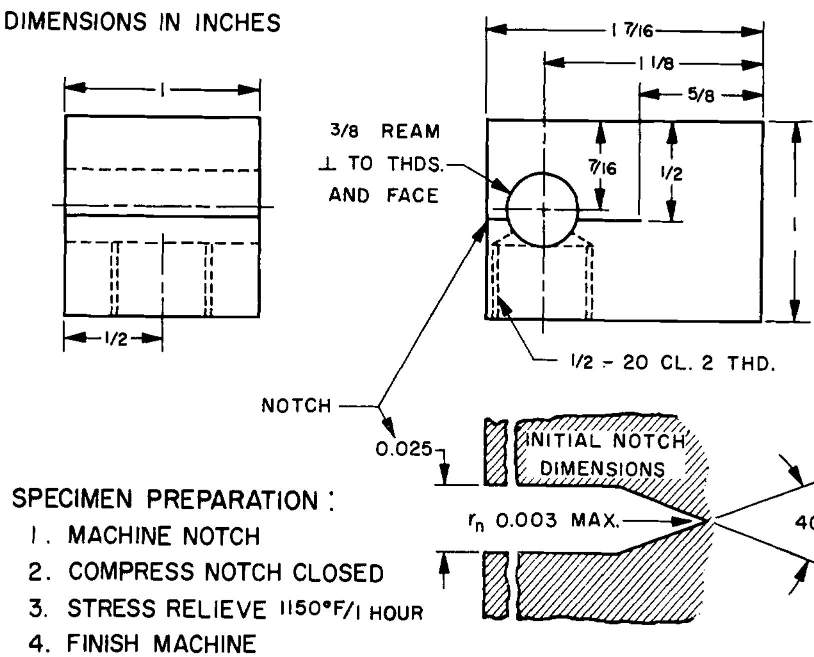

FIG. 4—Small Fracture Specimen Suitable for Use in Reactor Studies.

MR. SRAWLEY—Do you use side notches to prevent the crack from deviating from its initial plane?

MR. RIPLING—Yes, we do. And this is a modification that Mast of NRL suggested. These force the crack to remain within the plane along which you want it to run and also suppress shear lips.

[23] J. Gilman, "Cleavage and Ductility in Crystals," *Fracture*, edited by B. L. Averbach et al, Technology Press and John Wiley & Sons, Inc., New York, N. Y., 1959, p. 193.

R. E. JOHNSON[24]—A specimen similar to Mr. Ripling's was designed by Manjoine.[25] Because of its small size (see Fig. 4), it can be irradiated in a reactor core without excessive heat generation from gamma radiation. We may speculate that fracture data obtained under such loadings will, when properly analyzed, yield information as useful as that from conventional specimens. Indeed, these specimens provide flat, brittle fractures with much less expenditure of material than is required under simple tensile loading.

Such a specimen may be most applicable to the testing of tough metals. Along these lines, previous comments cast doubt on the sanity of those trying to measure the toughness of materials when critical crack sizes range in inches. In defense of this minority group, attention should be directed toward, for example, the fracture behavior of low-alloy steels in nuclear reactor pressure vessels. Given sufficient exposure to neutrons, the initially high toughness may be drastically reduced. In order to measure that change, one must have an initial value in which confidence can be placed and I submit this as a subject worthy of the panel's consideration.

MR. BROWN—Perhaps you refer to some of my previous remarks to Mr. Wells. They were not designed to test anyone's sanity, but rather to get the problem clearly fixed in the minds of those who have worried about very small cracks in high-strength alloys. I think your arguments are quite sound and, combined with those of Mr. Wells, give proper emphasis to the highly complex problem of assessing the fracture behavior of low-strength alloys.

[24] Engineer, Westinghouse Electric Corp., Pittsburgh, Penna.

[25] M. J. Manjoine, "Biaxial Brittle Fracture Tests," *ASME Preprint 64-Met-3* American Society of Mechanical Engineers, 1964.

MR. WEISS—I would like to make a comment on the type of specimen proposed by Mr. Ripling, using side notches. This specimen limits the plastic zone associated with the edge notch. If the specimen represents a design application, this is fine; however, it is not clear how one would calculate a representative K_c value or any other value which would agree with that obtained from another specimen design. We have recently obtained a few results from sheet specimens having the same crack geometry but different lengths. One might speculate that the shorter specimens would have less stored energy and, therefore, higher strength than the longer specimens. However, we found that the strength decreased substantially with a decrease in specimen length. The only explanation we have is one that might be associated with end effects. By means of compliance gages we were able to determine that the energy-release rate increases for the shorter specimen. Therefore, I think that Mr. Ripling's specimen is a conservative specimen but, since we do not know how conservative it is, a penalty may be imposed on the material that is being evaluated.

MR. IRWIN—The stress analysis of a specimen such as that described by Mr. Ripling would appear to be rather formidable since it contains side notches. However, one can use a compliance calibration to obtain an average $\mathcal{G}$ value which would represent the average across the thickness between the side notches. If the observed crack front has only moderate curvature, then there is some assurance of only a moderate variation of $\mathcal{G}$ throughout the thickness.

MR. BROWN—Messrs. Wells and Burdekin have offered to present their concepts regarding crack-opening displacement measurements. These ideas are directly related to the problems we have just been discussing concerning the evaluation of the fracture characteristics of low-strength alloys.

F. M. BURDEKIN[26]—The use of fracture mechanics concepts to predict the conditions for failure of certain materials has now become widely accepted, but the range of materials to which the straightforward ASTM treatment is strictly applicable is, of necessity, limited to truly brittle materials and those, such as high-strength steels, which fracture with only small amounts of plastic deformation localized at the tips of defects. For mild steel, however, quite widespread plastic flow may take place before the initiation of fracture even when the actual propagation is of a brittle nature (that is, exhibiting a crystalline appearance and low surface deformation). The presence of a plastic zone at the tip of a crack enables the two faces to move apart at the crack tip without increase in length of the crack. The magnitude of this separation at the crack tip has been termed the crack-opening displacement. The ASTM treatment can be extended by means of a tensile dislocation analysis to take into account this widespread plastic deformation.[27, 28]

The model for such a tensile dislocation analysis is shown in Fig. 5. This model is based on a real crack of length $2a$ in an infinite plate. Under a uniform stress, σ, applied in the y direction, a plastic zone is produced at the tip of the real crack extending to $x = \pm a_1$. This situation is represented for the purposes of analysis by a crack of length $2a_1$, which is surrounded by an entirely elastic

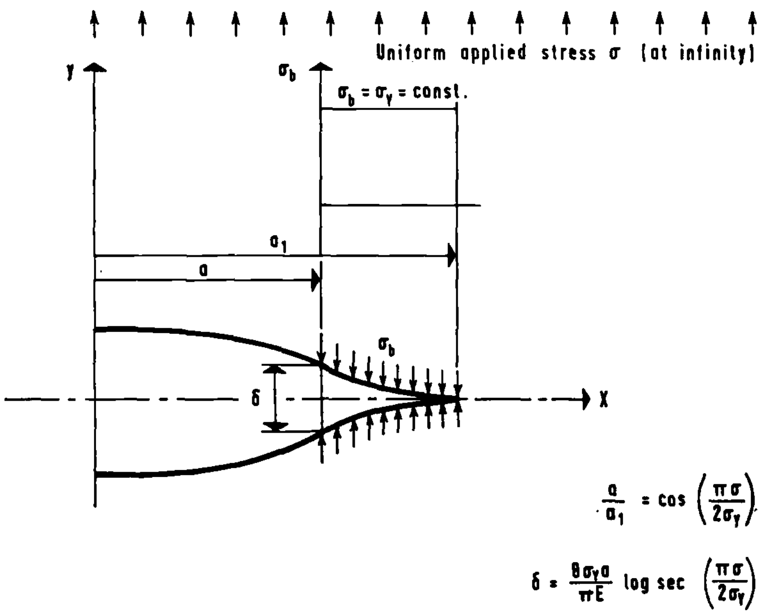

FIG. 5—Representation of Local Crack-Tip Plasticity by Tensile Dislocation.

[26] Written discussion prepared jointly by A. A. Wells, Queens University, Belfast, Ireland, and by F. M. Burdekin and D. E. W. Stone of The British Welding Research Assn., Research Station, Abington Hall, Cambridge, England.

[27] A. A. Wells, "*Notched Bar Tests, Fracture Mechanics and Strength of Welded Structures*," Houdremont Lecture, International Institute of Welding, *British Welding Journal*, Vol. 12, No. 1, Jan. 1965.

[28] F. M. Burdekin and D. E. W. Stone, "*Fracture Mechanics Progress Report C140/1, 1964*," British Welding Research Assn., 1965.

stress field when under load, but which is stressed not only by the externally applied stress, σ, but also by a series of internal tensile stresses in the y-direction of magnitude, σ_b, at $x = b$ in the region, $\pm a \leqq \pm b \leqq \pm a_1$. The stresses applied within the crack of length $2a_1$ represent the stresses in the plastic zone at the tip of the real crack and, for the purposes of this analysis, will be taken as constant and equal to the uniaxial tensile yield stress of the material, σ_y. While the assumption that plastic deformation is confined to the plane of the crack is not a rigorous plastic solution, experimentally determined plastic-strain patterns show that, for thin sheets of mild steel at least, such deformations are confined to a narrow band along the plane of the crack until the incidence of 45-deg slip lines and a general yield mechanism.

The stresses and displacements around the elastically stressed crack of length $2a_1$ can then be analyzed using the Westergaard stress-function technique and assuming plane-stress conditions. The stress function for a crack in an infinite plate under biaxial tension is well known and it is only necessary to superpose a uniform stress, $-\sigma$, in the x-direction to satisfy boundary conditions for an infinite plate under uniaxial tension. The internal stress was considered to consist of a series of internal forces of magnitude, $\sigma_b \, db$. The existing stress function for a pair of splitting forces, taken negative to represent tension, can now be integrated over the range from $b = \pm a$ to $b = \pm a_1$ to give a stress function for the internal stress system. The two stress functions for the external and internal stress systems can then be combined in any required proportion to form the final stress function. This proportion is determined by the requirement that no stresses exist in excess of the yield stress of the material, or in terms of the ASTM treatment, this may be regarded as equating the stress-intensity factors of the two individual applied stress systems. It can

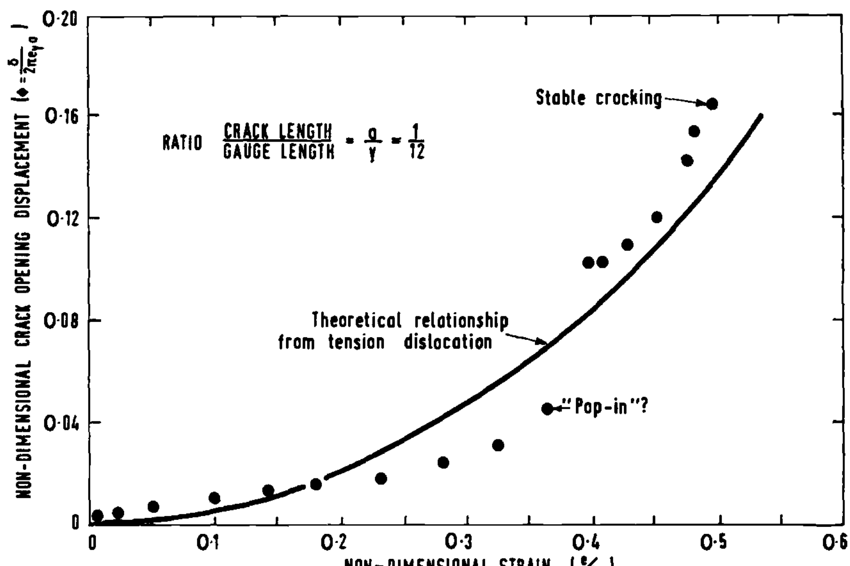

FIG. 6—Comparison of Theory and Experiment for Relationship between Crack-Opening Displacement and Over-all Strain for 7075-T6 Aluminum Alloy.

be shown that for the stresses at the point $x = a_1$ to remain finite, the relationship between the real crack length, a, and the extent of the plastic zone, a_1, is:

$$\frac{a}{a_1} = \cos\left(\frac{\pi}{2}\frac{\sigma}{\sigma_y}\right)$$

Thus a total combined stress function may be formulated from which the opening displacement at the tip of the real crack can be calculated as

$$\delta = \frac{8\sigma_y a}{\pi E}\log_e\left\{\sec\left(\frac{\pi}{2}\frac{\sigma}{\sigma_y}\right)\right\}$$

The variation of δ with the ratio of applied stress to yield stress, σ/σ_y, becomes very sensitive to small changes in this ratio as it approaches unity, and it is therefore preferred to relate the crack-opening displacement, δ, to the over-all strain, e, over a gage length, $2y$. A somewhat more complex expression may be derived from the analysis for over-all strain, and Fig. 6 shows a comparison of theory and experiment for the relationship between crack-opening displacement and over-all strain for a particular ratio of crack length to gage length plotted on a nondimensional basis. The experimental results were obtained on an aluminum alloy of low work-hardening capacity to give a true comparison with the theory which is of course based on a non-work-hardening material. The opening displacement at the crack tip was measured optically using a microscope fitted with calibrated shutters. The discontinuity in the experimental results was accompanied by a noise indicating a possible pop-in, and thus perhaps a change from plane-strain to plane-stress conditions. It must be pointed out, however, that in similar experiments on mild steel the agreement between theory and experiment was not so good, and this is believed to be largely due to strain hardening.

It is possible to relate the crack opening displacement δ to the more familiar quantity $\mathcal{G}$, the crack-extension force, to compare the analysis with the ASTM treatment for small plastic zones. This analysis makes use of the relationship, $\mathcal{G} = \sigma_y\delta$, derived by local energy arguments similar to those used to relate K and $\mathcal{G}$, to effect this comparison. By expanding the expression for δ as a series and considering the effect of the influence of successive terms, it can be seen that good agreement is obtained both with the basic ASTM expression, $\mathcal{G} = \sigma^2\pi a/E$, and with the suggested correction for small plastic zones.

$$\delta = \frac{8\sigma_y a}{\pi E}\log_e\sec\left(\frac{\pi\sigma}{2\sigma_y}\right)$$

Thus, if $\mathcal{G} = \sigma_y\delta$

$$\mathcal{G} = \frac{8\sigma_y{}^2 a}{\pi E}\log_e\sec\left(\frac{\pi\sigma}{2\sigma_y}\right) = \frac{8\sigma_y{}^2 a}{\pi E}\left\{\frac{1}{2}\left(\frac{\pi\sigma}{2\sigma_y}\right)^2 + \frac{1}{12}\left(\frac{\pi\sigma}{2\sigma_y}\right)^4 + \frac{1}{45}\left(\frac{\pi\sigma}{2\sigma_y}\right)^6 + \cdots\right\}$$

Taking only the first term in the expansion,

$$\mathcal{G} = \frac{\pi\sigma^2 a}{E} \quad \text{c.f. ASTM: } \mathcal{G} = \frac{\pi\sigma^2 a}{E}$$

Taking the first and second terms,

$$\mathcal{G} = \frac{\pi\sigma^2 a}{E}\left[1 + \frac{\pi^2}{24}\left(\frac{\sigma}{\sigma_y}\right)^2\right]$$

$$\text{c.f. ASTM: } \mathcal{G} = \frac{\pi\sigma^2 a}{E}\left[1 + \frac{1}{2}\left(\frac{\sigma}{\sigma_y}\right)^2\right]$$

Taking the first three terms,

$$\mathcal{G} = \frac{\pi\sigma^2 a}{E}\left[1 + \frac{\pi^2}{24}\left(\frac{\sigma}{\sigma_y}\right)^2 + \frac{\pi^4}{360}\left(\frac{\sigma}{\sigma_y}\right)^4\right]$$

The concept of a critical $\mathcal{G}$ for initiation of fracture of high-strength materials has proved so successful that it was logical to extend the implied critical displacement for fracture with localized plasticity to situations where the plasticity was more substantial. It was this background which led Mr. Wells to propose the hypothesis of a critical crack-opening displacement for fracture initiation, dependent only on material temperature, strain rate, and triaxiality of stress, but applicable even with extensive yielding. The critical displacement criterion is compatible with those concepts of fracture by the opening mode, which operate by the creation of a series of microcracks ahead of the crack, followed by a drawing out of the bridges between them to complete the fracture process.

This criterion has been examined experimentally in a series of tests on mild steel specimens of different sizes and geometrical configurations, and the results to date are shown in Fig. 7. The physical measurement of crack-opening displacement was made with a small probe placed in the root of the notches throughout the tests. The results shown give the values of opening displacement at fracture measured on 3-in. thick, 3-ft wide edge-notched plates in tension, and on 3- and $\frac{3}{8}$-in. square notched slow bend tests. A variety of notch depths were employed, but in all cases the tip of the notch was formed by a fine saw cut 0.006 in. thick. The first immediate impression is that the results are closely similar for the immensely different sizes of specimen employed, despite the fact that the tension tests failed around or even below general yield, and the bend specimens well after yield. Different trends are observable, however, in that there is an apparent transition indicated for each

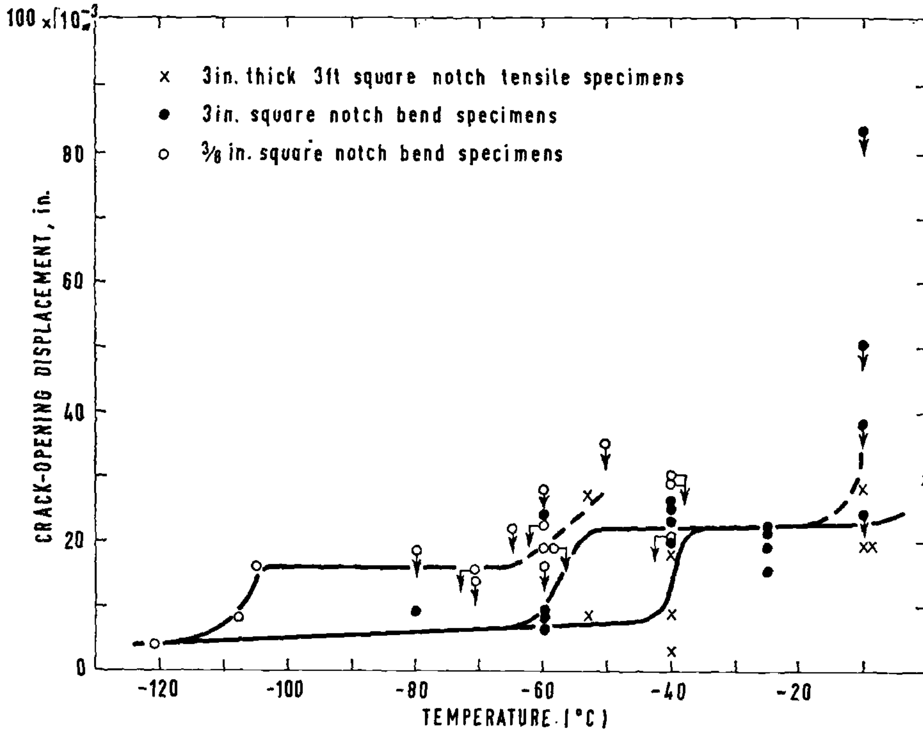

FIG. 7—Effect of Ratio of Crack Length to Plate Width on Relationship between Applied Stress and the Opening Displacement as Taken from the Tensile Dislocation Analysis.

type of specimen where there is a drop in the opening displacement at fracture with decreasing temperature.

In addition, those specimens marked with arrows showed fibrous thumbnails at the notch root. This effectively changes the depth and geometry of notch and gives a deceptively high reading for opening displacement at initiation of unstable fracture. Triaxiality effects are suspected and current work is aimed at explaining these effects more satisfactorily.

From the tensile dislocation analysis described previously, it is possible to approximate the effects of finite plate width by considering finite widths within an infinite plate. The relationship between the opening displacement, δ, and the crack length, $2a$, in a plate of width $2B$, is shown in Fig. 8 for three different ratios of net applied stress (σ_n) to yield stress (σ_y). It may be seen that failure below general yield is most likely with a ratio of crack length to plate width of about 0.3, which agrees with the suggested ratio for the occurrence of a maximum of $\mathcal{G}$. Also shown are the ratios of net stress to yield stress at fracture in some of the wide-plate tension tests previously described, and it can be seen that good agreement is obtained.

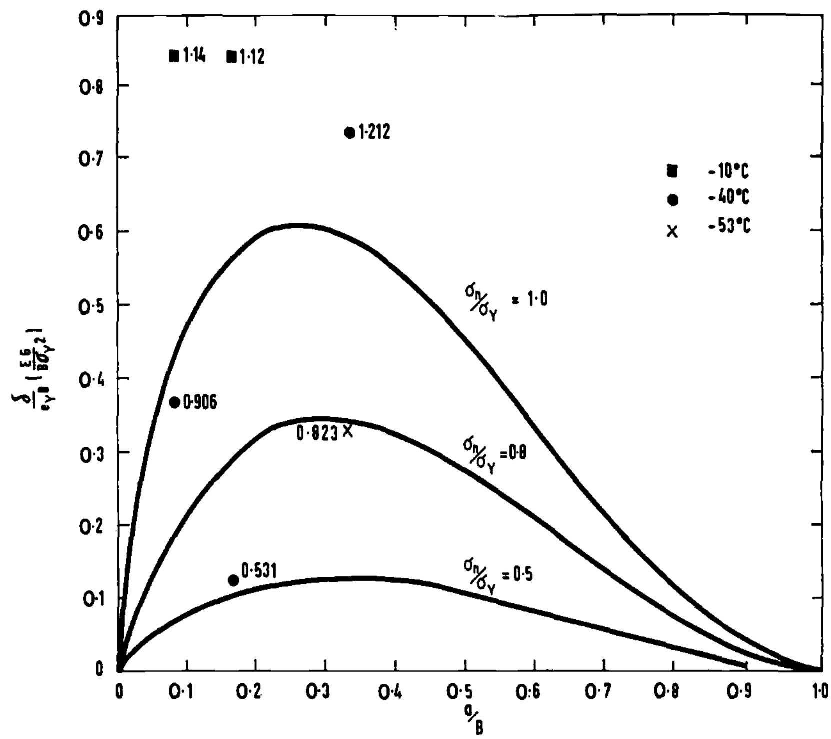

FIG. 8—Experimentally Observed Variation of Crack Opening with Temperature.

The work reviewed has been an attempt at the extension of linear fracture mechanics to materials such as mild steel having the property of substantial yielding. It is seen that this approach, employing the crack-opening displacement concept, is contiguous with the ASTM treatment of high-strength materials, and shows great promise of extending the range of applicability of fracture mechanics to yielding materials.

MR. BROWN—I would like to ask Mr. Burdekin what use he makes of these crack-opening displacements in rating materials in regard to their toughness? Do you standardize on a specimen and then measure the opening displacement?

MR. BURDEKIN—We are at a very early stage in this approach, but eventually we hope to be able to correlate results from different sizes of specimen so that the answers for full-scale behavior can be predicted from small-scale tests. Using small specimens, we would then be able to rate the toughness of the relatively low-strength materials we are working with. The first problem facing us is to sort out the effects of triaxiality on critical crack-opening displacements.

MR. BROWN—What attention are you drawing to the role of triaxiality in your test, and what is affecting the magnitude of triaxiality?

MR. BURDEKIN—I am suggesting that even under plane-strain conditions, variations in the relative magnitudes of three principal stresses may occur. With a plastic zone at the tip of a physical crack of finite root radius, the stresses at the crack tip in the x- and y-directions of the classical analyses are no longer equal, and the stress in the thickness direction will consequently be different from that of the linear elastic case, so that the ratios of the principal stresses may be different.

MR. WELLS—A particular property of the crack-opening displacement approach to fracture is that it is fully contiguous with the alternative treatment in terms of $\mathcal{G}$ or K. That is to say, a material in possession of a characteristic fracture toughness, $\mathcal{G}_c$ has a corresponding crack-opening displacement at fracture, equal to $\mathcal{G}_c$ divided by the material yield stress. Whereas $\mathcal{G}_c$ cannot be measured in specimens which yield before fracture, there is no impediment to measurement of crack-opening displacement under the same circumstances. Fracture experiments conducted at given temperatures on tensile wide plates with edge notches of a wide range of depths, leading to fracture both below and above general yield, have shown the same crack-opening displacement at fracture in both cases.

The intervention of triaxial stress effects on fracture is shown in these tests, as in established fracture toughness testing, by the exhibition of plane-strain and plane-stress fractures in different thicknesses of materials. In addition, with the additional boundary effects that arise in thick plate testing, the effects become more complex. The maximum triaxiality (lowest fracture toughness at given temperature) observed in an edge-notched tensile plate of mild steel, is higher than that seen in an equal thickness bend specimen with three-point loading. The triaxiality appears to rise with edge notch depth, in a plate of given thickness, to a maximum when the notch depth equals the thickness, and declines with deeper notches. These effects assume added importance when it is realized that they move the ductility transition temperature over an observed range of about 40 C.

It is considered that the ASTM fracture toughness testing methods for high-strength steels, now under discussion, should be re-examined for further evidence of these effects.

MR. IRWIN—When we employ linear elastic fracture mechanics analysis, inferentially this means that the terms of reference are significant and helpful to us in visualizing the physical phenomena. In the high-stress level or general yielding range, we need other viewpoints in order to provide terms of reference which are meaningful. For this purpose, the crack-opening displacement idea proposed by Mr. Wells is certainly worth a good try. I would also recommend the analysis in the McClintock and Irwin paper as worth a good try, a critical fracture strain combined with a structural-size factor.

B. M. WUNDT[29]—I would like to ask Mr. Wells to comment on the following in light of his description of crack-opening displacement measurements. It is possible to calculate, using advanced methods of elastic-plastic analysis, the strain at burst in the bore of a rotating disk. For heterogeneous materials, these strains have been found to be from 0.75 per cent to a few per cent and the stress at about the yield strength. In these cases the fracture appears to be controlled by a critical strain.

MR. WELLS—It is the object of our studies to evaluate such situations as described by Mr. Wundt, but we have not ourselves worked on the spinning disk configuration. I am of the opinion that the crack-opening displacement approach would be helpful in dealing with the problem of correlation in the plastic range between the disk results and those from smaller-notched bend and tension tests.

MR. WEISS—Fracture in ductile materials may certainly originate from a region of heterogeneity by some strain-controlled process. The paper by McClintock and Irwin shows that one needs about 20 times the elastic strain for this to happen. Neuber's relationship between true stress concentration factor, true strain concentration factor, and elastic stress concentration factor

$$((K_\sigma K_\epsilon)^{1/2} = K_{\text{elastic}})$$

suggests that such a heterogeneity would have to be equivalent to a stress concentration with a stress concentration factor between 4 and 5. Thus, it is conceivable that a relatively small inhomogeneity may nucleate a strain-controlled failure.

P. N. RANDALL[30]—I would like to refer back to the first report of the committee and ask: how do you rationalize slow crack growth in terms of linear elastic fracture mechanics? How can you do this wouthout consideration of plasticity? I raise this question because I feel there is a tendency among the uninitiated to oversell linear elastic fracture mechanics for engineering use, whereas it

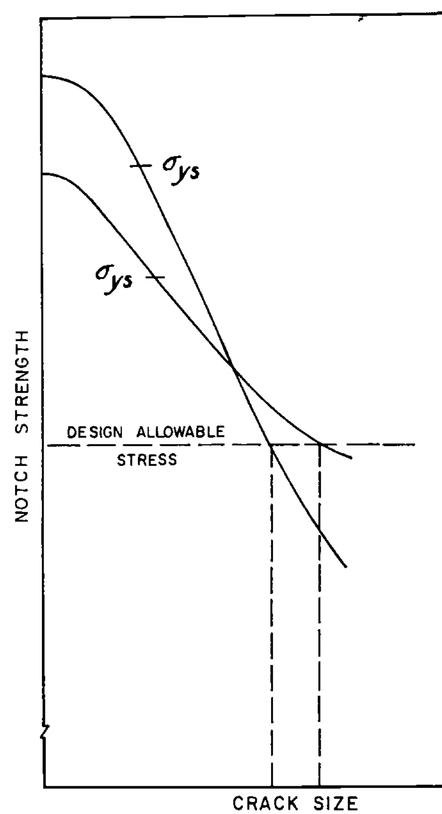

FIG. 9—Notch-Strength Versus Crack-Size Curves for Two Materials, Tested Using Surface-Cracked Specimens showing Intersection at Stresses below the Yield Strength of Either Material.

[29] General Electric Co., Large Steam Generator Dept., Schenectady, N. Y.

[30] TRW Space Technology Laboratories, Redonda Beach, Calif.

seems that one must go beyond that to explain even the common observation that crack growth can be stable.

MR. IRWIN—I had a long discussion of these matters at the November, 1963, ASME meeting.[31] Obviously, to explain any behavior aspect in the region of large nonlinear strains at the crack tip, one must have ideas beyond linear elastic fracture mechanics. Consider a length of plane-strain crack border along which the stress condition is one of plane strain. Small openings must be developing near the real border of the crack and the crack can scarcely spread forward unless these advance openings are joining laterally in the direction parallel to the crack border. A priori, the simultaneous forward and lateral joining of advance openings is a process in which the final stages through any given set of advance openings should be quite rapid. With this behavior occurring in nearly equal degree in each segment of the crack border, an abrupt forward-motion instability is expected. Why, then, do we sometimes observe slow crack extension in plane strain? In the absence of a time-dependent influence such as stress corrosion, slow growth occurs primarily as a crack-arrest behavior due to load transfer from the plane-strain region to adjacent unbroken shear lips.

MR. RANDALL—I would also like to question the use of expressions from fracture mechanics that relate the stress at failure to crack size by a single constant, K_{Ic}. Figure 9, giving typical graphs for a steel or titanium alloy heat-treated to two strength levels, shows that the curves cross, often at stresses below the yield strength. Plots of expressions from fracture mechanics have slopes proportional to K_{Ic}—the tougher material has the steeper slope—contrary to the experimental findings. There is the additional question: if K_{Ic} values are to be obtained from tests at only one crack size, how shall that size be chosen? The rating of the two materials depends on this choice.

MR. SRAWLEY—In general, a higher-strength material will have a shorter critical crack size than a lower-strength material. The curves usually intersect at a crack length less than that at which the lower-strength material could sustain loading to the yield strength before fracturing. The corresponding stress is slightly higher than the yield strength of the weaker material.

MR. PAYNE—When using surface-crack specimens, tests of several crack sizes are always desirable. The question of whether material ratings will change with crack size must be examined in light of whether or not all conditions for a valid fracture toughness test are met. It is not clear whether the curve crossing mentioned by Mr. Randall was obtained using specimens of sufficient size to avoid net-section yielding and having crack depths less than one half the thickness. I believe Mr. Randall's remarks are based on the data for Ti-6Al-4V alloy which he published early this year,[32] and not all of these data met the conditions for a valid toughness test.

MR. RANDALL—My remarks were based on data in the ASME paper plus a great deal more that were obtained by other organizations participating in the Minuteman program. Crack depths of 65 per cent of the thickness were considered permissible since the plastic zone did not appear to reach to the back face of the specimen, as evidenced by the absence of a dimple there prior to fracture.

[31] G. R. Irwin, "*Crack Toughness Testing of Strain Rate Sensitive Materials*," *Transactions*, ASME Series A, Vol. 86, p. 444, Oct., 1964. See also the present paper by J. M. Krafft and G. R. Irwin, p. 114.

[32] P. N. Randall and R. P. Felgar, "Part Through Crack Test-Relation to Solid Propellant Rocket Cases," *ASME Paper No. 63-WA 137*, Am. Soc. Mechanical Engineers, 1964.

MR. PAYNE—I recently published[33] a re-analysis of Ti-6Al-4V alloy data presented in Mr. Randall's ASME paper. If those data points are eliminated which did not have stresses above the yield strength or had crack depths greater than one half the thickness, the remaining data yielded a constant value of K_{Ic} and the crossovers were not observed. I would suggest that when unexpected behavior is observed, such as that just illustrated by Mr. Randall, larger specimens be tested to find out whether or not the behavior persists.

I would also like to make a comment on the methods used to represent surface-crack specimen data. In my opinion, a curve of gross strength versus crack size (expressed as a/Q or crack depth with a constant ratio of crack depth to length, rather than area) would be appropriate for a designer.

In hardware, net- and gross-fracture strengths are identical for practical purposes due to the large area involved. Use of net stress for laboratory surface-crack specimens simply produces artificially elevated strength values which are sensitive to actual specimen dimensions.

The use of crack area for surface cracks seems highly unrealistic. Surface-crack fractures begin at the maximum depth point, rather than randomly around the crack tip. Description of the stress distribution at fracture should apply to the region where fracture occurs. The stresses at the maximum crack depth are influenced far more by depth than by crack length, and the crack area parameter does not reflect this.

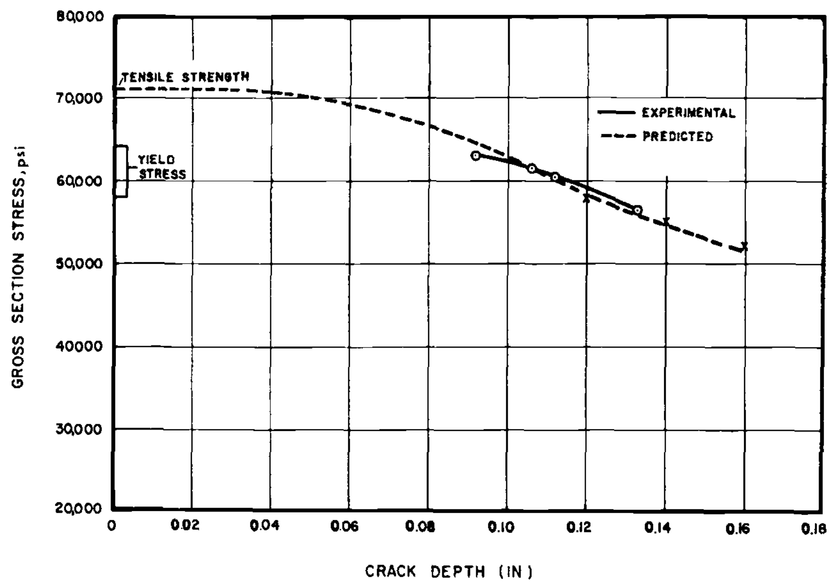

FIG. 10—Experimental and Predicted Gross-Section Stress for Semi-Elliptical Surface-Cracked Panels of 2014-T6 Alloy. (Ratio of Crack Depth to One Half the Crack Length Is 0.50.)

C. M. CARMEN[34]—I believe that our argument concerns the consistency of K_{Ic} values as measured by different techniques. For example, at Frankford Arsenal we measured the K_{Ic} values of 2014-

[33] W. F. Payne, "Analysis of Surface Crack Fracture Toughness Information," *AF Report No. ML TDR-64-225*, Vol. I, Fourth Maraging Steel Project Review, 1964, pp. 307–367.

[34] Metallurgist, Metallurgy Research Laboratory, Frankford Arsenal, Philadelphia, Pa.

T6 aluminum using a circumferentially notched round specimen. Using this K_{Ic} value, we calculated the failure stress of $\frac{1}{4}$-in. thick panels of this material having part-through cracks. These cracks were machined and fatigued so that they would all have the same geometry. The data developed are shown in Fig. 10. The agreement between the calculated and experimental breaking stresses shows good consistency in K_{Ic} values using widely different specimen geometries.

MR. BROWN—I do not think we are going to come to any definite conclusions about Mr. Randall's observations. There appears to be some question concerning the suitability of the data for a fracture mechanics analysis. Of course, to make a fair judgment on this point we would have to examine all pertinent information and we cannot do that here. However, this controversy again emphasizes the fact that judgments concerning the validity of fracture mechanics analysis require very carefully designed experiments in which all pertinent variables are systematically controlled. Perhaps this would be a suitable note on which to conclude what has been a most interesting and informative panel discussion.